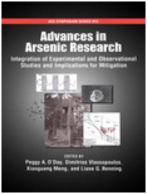

ACS SYMPOSIUM SERIES 915

Advances in Arsenic Research

Integration of Experimental and Observational Studies and Implications for Mitigation

EDITED BY

Peggy A. O'Day, Dimitrios Vlassopoulos,
Xiaoguang Meng, and Liane G. Benning

Downloaded by 217.66.152.135 on September 11, 2012 | http://pubs.acs.org
Publication Date: October 3, 2005 | doi: 10.1021/bk-2005-0915.fw001

Advances in Arsenic Research

Downloaded by 217.66.152.135 on September 11, 2012 | http://pubs.acs.org
Publication Date: October 3, 2005 | doi: 10.1021/bk-2005-0915.fw001

ACS SYMPOSIUM SERIES **915**

Advances in Arsenic Research

Integration of Experimental and Observational Studies and Implications for Mitigation

Peggy A. O'Day, Editor
University of California, Merced

Dimitrios Vlassopoulos, Editor
S.S. Papadopulos and Associates, Inc.

Xiaoguang Meng, Editor
Stevens Institute of Technology

Liane G. Benning, Editor
University of Leeds

Sponsored by the
ACS Divisions of Geochemistry, Inc., Environmental Chemistry, Inc., and Industrial and Engineering Chemistry, Inc.

American Chemical Society, Washington, DC

Downloaded by 217.66.152.135 on September 11, 2012 | http://pubs.acs.org
Publication Date: October 3, 2005 | doi: 10.1021/bk-2005-0915.fw001

Downloaded by 217.66.152.135 on September 11, 2012 | http://pubs.acs.org
Publication Date: October 3, 2005 | doi: 10.1021/bk-2005-0915.fw001

Library of Congress Cataloging-in-Publication Data

Advances in arsenic research : integration of experimental and observational studies and implications for mitigation / Peggy A. O'Day, editor ... [et al.].

p. cm.—(ACS symposium series, ISSN 0097–6156 ; 915)

Includes bibliographical references and index.

ISBN 0–8412–3913–4 (alk. paper)

1. Arsenic—Environmental aspects. 2. Arsenic—Analysis. 3. Water—Purification—Arsenic removal.

I. O'Day, Peggy A., 1962 - II. Series.

TD427.A77A38 2005
628.5'.2—dc22 2005040996

The paper used in this publication meets the minimum requirements of American National Standard for Information Sciences—Permanence of Paper for Printed Library Materials, ANSI Z39.48–1984.

Copyright © 2005 American Chemical Society

Distributed by Oxford University Press

All Rights Reserved. Reprographic copying beyond that permitted by Sections 107 or 108 of the U.S. Copyright Act is allowed for internal use only, provided that a per-chapter fee of $30.00 plus $0.75 per page is paid to the Copyright Clearance Center, Inc., 222 Rosewood Drive, Danvers, MA 01923, USA. Republication or reproduction for sale of pages in this book is permitted only under license from ACS. Direct these and other permission requests to ACS Copyright Office, Publications Division, 1155 16th Street, N.W., Washington, DC 20036.

The citation of trade names and/or names of manufacturers in this publication is not to be construed as an endorsement or as approval by ACS of the commercial products or services referenced herein; nor should the mere reference herein to any drawing, specification, chemical process, or other data be regarded as a license or as a conveyance of any right or permission to the holder, reader, or any other person or corporation, to manufacture, reproduce, use, or sell any patented invention or copyrighted work that may in any way be related thereto. Registered names, trademarks, etc., used in this publication, even without specific indication thereof, are not to be considered unprotected by law.

PRINTED IN THE UNITED STATES OF AMERICA

Foreword

The ACS Symposium Series was first published in 1974 to provide a mechanism for publishing symposia quickly in book form. The purpose of the series is to publish timely, comprehensive books developed from ACS sponsored symposia based on current scientific research. Occasionally, books are developed from symposia sponsored by other organizations when the topic is of keen interest to the chemistry audience.

Before agreeing to publish a book, the proposed table of contents is reviewed for appropriate and comprehensive coverage and for interest to the audience. Some papers may be excluded to better focus the book; others may be added to provide comprehensiveness. When appropriate, overview or introductory chapters are added. Drafts of chapters are peer-reviewed prior to final acceptance or rejection, and manuscripts are prepared in camera-ready format.

As a rule, only original research papers and original review papers are included in the volumes. Verbatim reproductions of previously published papers are not accepted.

ACS Books Department

Downloaded by 217.66.152.135 on September 11, 2012 | http://pubs.acs.org
Publication Date: October 3, 2005 | doi: 10.1021/bk-2005-0915.fw001

Downloaded by 217.66.152.135 on September 11, 2012 | http://pubs.acs.org
Publication Date: October 3, 2005 | doi: 10.1021/bk-2005-0915.pr001

Advances in Arsenic Research

Chapter 1

Advances in Arsenic Research: Introductory Remarks

Peggy A. O'Day[1], Dimitrios Vlassopoulos[2], Xiaoguang Meng[3], and Liane Benning[4]

[1]School of Natural Sciences, University of California, Merced, CA 95344
[2]S.S. Papadopulos and Associates, Inc., 815 SW 2nd Avenue, Suite 510, Portland, OR 97204
[3]Center for Environmental Engineering, Department of Civil, Environmental, and Ocean Engineering, Stevens Institute of Technology, Hoboken, NJ 07030
[4]School of Earth Sciences, The University of Leeds, Leeds LS2 9JT, United Kingdom

Downloaded by 217.66.152.135 on September 11, 2012 | http://pubs.acs.org
Publication Date: October 3, 2005 | doi: 10.1021/bk-2005-0915.ch001

Water supplies worldwide are impacted by concentrations of dissolved arsenic above acceptable health levels. These health concerns have prompted a reduction in the U.S. drinking water standard for arsenic (from 50 to 10 □g l^{-1}) and focused attention on widespread areas of the Indian-subcontinent, central and southeast Asia, and South America with large populations at risk for adverse health impacts. Although estimates vary, elevated arsenic concentrations in groundwater have the potential to adversely impact on the order of 90 million people *(1-3),* including 13 million in the U.S. *(4, 5).* Arsenic in the environment is derived from both natural and anthropogenic sources, including occurrences in sediments, soils, coal, and ore deposits, and releases from mining, coal-burning, and industrial processes. Although arsenic toxicity is not as severe at low levels as that of metals such as lead, mercury, or cadmium, natural occurrences of arsenic above background concentrations are widespread and common. Thus, cumulative effects may impact large populations, particularly in countries where unmonitored groundwater is the primary source of drinking water.

Arsenic accumulation and migration is closely tied to its chemical speciation, which is often controlled by a complex combination of abiotic and biotic processes coupled with physical transport. Arsenic is found in the environment in multiple oxidation states, with As(III) and As(V) as the most common inorganic forms. Arsenic can form methylated compounds, it occurs in an array of bioorganic substances, and it can be sequestered in a variety of oxide and sulfide minerals *(6, 7)*. Mechanisms for the removal of arsenic from water in natural settings include both adsorption and precipitation, which depend on oxidation state and local geochemical conditions. It is well established that microbial activity strongly influences, and may dominantly control, arsenic oxidation and reduction in many environments. While most microorganisms have mechanisms for detoxifying arsenic, both anaerobic respiration of As(V) and aerobic respiration of As(III) have been identified *(8-10)*. So although a toxin for most organisms, some microorganisms can take advantage of arsenic as an energy source. The numerous subtleties of arsenic chemistry and its participation in biogeochemical cycling contribute to the challenges associated with predicting the behavior of arsenic in the environment, and with developing and implementing effective and economical treatment and remediation methods.

This volume is the product of a symposium held at the 226th ACS National Meeting held in September, 2003, in New York (NY), and sponsored jointly by the ACS Divisions of Geochemistry and Environmental Chemistry. The intent of both the symposium and this volume was to foster a more unified understanding of arsenic occurrence, behavior, and mitigation by bringing together researchers from a diversity of areas to exchange new advances and information. A wide cross-section of research and application topics were presented by U.S. and international participants, including studies related to arsenic occurrence, cycling, natural attenuation, biological influences, treatment, and remediation. Although several books discussing arsenic in the environment have been published recently *(11, 12)*, the multitude of ongoing research on arsenic and rapidly developing technologies for treatment and remediation warrants timely publication of new studies.

This volume highlights a variety of new research directed at understanding the sources, distribution, and mobilization of arsenic in the environment. It includes recent efforts in the development of cost-effective treatment technologies and in approaches to natural attenuation and accelerated remediation methods. These topics are thematically organized into three sections in the volume, the first focusing on laboratory studies and theoretical modeling, the second on arsenic behavior and cycling in a range of field settings, and the third on studies associated with treatment and remediation technologies and methods. In addition to the presentation of research findings, the symposium in New York included a summary discussion of significant, unresolved issues associated with arsenic-related investigations, and symposium participants identified several key areas for further study. These included:

(1) Reduction of arsenic in water supplies worldwide: With increasing world population and the imminent prospect of significant climatic changes, groundwater represents one of the most important stable sources of drinking

Downloaded by 217.66.152.135 on September 11, 2012 | http://pubs.acs.org
Publication Date: October 3, 2005 | doi: 10.1021/bk-2005-0915.ch001

water. There is an immediate, critical need to supply arsenic-safe drinking water to large populations, and this need will continue to grow. The variability of arsenic concentrations in groundwater and its multifaceted chemical behavior necessitate a transfer of both basic scientific knowledge and optimized technology in order to supply the best available, cost-effective treatments for local populations. This is particularly true for developing nations that rely on groundwater for drinking and agriculture but lack resources for large-scale treatment systems.

(2) Improved understanding of arsenic chemistry: Despite the wealth of recent studies, there remain considerable gaps in fundamental aspects of arsenic chemistry that impact prediction of its behavior in natural systems and optimization of treatment and remediation technologies. Thermodynamic databases lack reliable, high quality data for a number of aqueous arsenic species and solid phases, particularly as a function of temperature. Our knowledge of the rates of abiotic and biologically mediated reactions that control arsenic speciation and partitioning is extremely limited, and improvements in theoretical approaches to compilation and synthesis of system kinetics are sorely needed. Research is just beginning to elucidate factors that influence competitive effects associated with arsenic adsorption on different media. More studies using *ab initio* molecular calculations, particularly coupled to experimental data, would aid in improving fundamental understanding of a range of processes. Advances in these areas would feed directly into the development of optimum treatment strategies and remediation methods that would benefit, for example, from differentiating the chemical behavior of As(III) from that of As(V) or from better quantification of competitive reactions.

(3) Improved understanding of arsenic behavior in complex systems, both natural and engineered: A striking feature of arsenic occurrence in numerous groundwater systems is its variability over hydrologically small spatial intervals (i.e., centimeters to meters). This is a reflection of the interplay among chemical, biological, and physical processes that occur at different rates in response to system changes. While studies of arsenic behavior at field sites are increasing, observations need to focus on identifying mechanisms and their relation to rates of abiotic or biologically influenced processes. Examples include cycling between oxidized and reduced conditions, the influence of organic carbon on arsenic cycling and speciation, arsenic uptake by adsorption versus precipitation or release by desorption versus dissolution, and the rates of biogeochemical processes compared to rates of physical transport. These efforts would be aided by closer integration of field studies and analogous measurements in the laboratory. Likewise, a better understanding of subsurface heterogeneity on small scales (centimeters to meters) and short times (minutes to days) and translation to larger spatial (meters to kilometers) and temporal (days to years) scales would improve predictive models. Similar issues pervade research aimed at improving remediation methods, such as the optimization of reactive and bio-enhanced barriers, or the use of monitored natural attenuation as an alternative to removal and pump-and-treat approaches. Finally, the development of

Downloaded by 217.66.152.135 on September 11, 2012 | http://pubs.acs.org
Publication Date: October 3, 2005 | doi: 10.1021/bk-2005-0915.ch001

effective and economical treatment methods would benefit from continued dialogue between basic science and technological application for topics such as optimization of filtration media and scaling from bench and pilot studies to full-scale field or plant implementation.

Acknowledgment

We thank Bob Hauserman and Dara Moore in acquisitions and Margaret Brown in editing/production in the ACS Books Department for the opportunity to publish this volume. The 2003 Symposium at 226th ACS National Meeting was supported by funding from the Petroleum Research Fund, the Geochemical Society, S. S. Papadopulos & Associates, Stevens Institute of Technology, and the and the ACS Division of Geochemistry, Inc.

Downloaded by 217.66.152.135 on September 11, 2012 | http://pubs.acs.org
Publication Date: October 3, 2005 | doi: 10.1021/bk-2005-0915.ch001

References

1. Kinniburgh, D. G.; Smedley, P. L.; Davies, J.; Milne, C. J.; Gaus, I.; Trafford, J. M.; Burden, S.; Ihtishamul Huq, S. M.; Ahmad, N.; Ahmed, K. M. The scale and causes of the groundwater arsenic problem in Bangladesh. In *Arsenic in Goundwater;* Welch, A. H.; Stollenwerk, K. G., Eds.; Kluwer Academic Publishers: Boston, 2003; pp 212-257.
2. Smedley, P. L. Arsenic in groundwater -- south and east Asia. In *Arsenic in Goundwater;* Welch, A. H.; Stollenwerk, K. G., Eds.; Kluwer Academic Publishers: Boston, 2003; pp 179-209.
3. Smedley, P. L.; Kinniburgh, D. G. A review of the source, behaviour and distribution of arsenic in natural waters. *Applied Geochemistry* **2002**, *17*, 5 17-568.
4. Welch, A. H.; Westjohn, D. B.; Helsel, D. R.; Wanty, R. B. Arsenic in the groundwater of the United States: Occurrence and geochemistry. *Ground Water* **2000**, *38*, 589-604.
5. Ryker, S. J. Arsenic in Ground Water Used for Drinking Water in the United States. In *Arsenic in Goundwater;* Welch, A. H.; Stollenwerk, K. G., Eds.; Kluwer Academic Publishers: Boston, 2003; pp 165-178.
6. Cullen, W. R.; Reimer, K. J. Arsenic speciation in the environment. *Chemical Reviews* **1989**, *89*, 713-764.
7. Francesconi, K. A.; Kuehnelt, D. Arsenic compounds in the environment. In *Environmental Chemistry of Arsenic;* Frankenberger, W. T., Jr., Ed.; Marcel Dekker: New York, 2002; pp 51-94.
8. Oremland, R. S.; Hoeft, S. E.; Santini, J. A.; Bano, N.; Hollibaugh, R. A.; Hollibaugh, J. T. Anaerobic oxidation of arsenite in Mono Lake water and by facultative, arsenite-oxidizing chemoautotroph, strain MLHE-1. *Applied and Environmental Microbiology* 2002, *68*, 4795-4802.

9. Oremland, R. S.; Stolz, J. F. The ecology of arsenic. *Science* **2003,** *300,* 939-944.
10. Stolz, J. F.; Oremland, R. S. Bacterial respiration of arsenic and selenium. *Fems Microbiology Reviews* **1999,** *23,* 615-627.
11. *Arsenic in Groundwater;* Welch, A. H.; Stollenwerk, K. G., Eds.; Kluwer Academic Publishers: Boston, 2003; p 475.
12. *Environmental Chemistry of Arsenic;* Frankenberger, W. T., Jr., Ed.; Marcel Dekker: New York, 2002; p 391.

Downloaded by 217.66.152.135 on September 11, 2012 | http://pubs.acs.org
Publication Date: October 3, 2005 | doi: 10.1021/bk-2005-0915.ch001

Chapter 2

Contrasting Sorption Behavior of Arsenic (III) and Arsenic(V) in Suspensions of Iron and Aluminum Oxyhydroxides

Janet G. Hering[1] and Suvasis Dixit[1,2]

[1]Environmental Science and Engineering, California Institute of Technology, Pasadena, CA 91125–7800
[2]Current address: Lawrence Livermore National Laboratory, Livermore, CA 94550

United Kingdom It has been widely observed that the sorption of arsenic (As) as As(III) and As(V) on iron (Fe) oxyhydroxides is comparable as is the sorption of As(V) on Fe and aluminum (Al) oxyhydroxides. However, quite different sorption behavior has been observed for As(III) on Fe and Al oxyhydroxides. Here, surface complexation modeling is used to show that recent reports of As(III) sorption onto Al oxyhydroxides are consistent with previous observations of negligible sorption under conditions relevant to water treatment. This modeling exercise also demonstrates that the level of protonation of surface species is not well constrained by commonly-reported pH edges and that the possibility of distinguishing between mononuclear and binuclear surface complexes depends on the level of surface coverage. These issues complicate the integration of macroscopic sorption studies with spectroscopic studies and molecular modeling.

In Advances in Arsenic Research; O'Day, P., et al.;
ACS Symposium Series; American Chemical Society: Washington, DC, 2005.

Introduction

The sorption behavior of arsenic (As) is crucial to both its mobility in natural waters and the efficiency of its removal by many water treatment technologies. Iron and aluminum-based sorbents are ubiquitous in natural systems (e.g., iron oxides such as goethite and hematite, aluminum oxides such as gibbsite, and aluminosilicate clay minerals) and are used in water treatment technologies as packed bed media or formed *in situ* during coagulation with hydrolyzing metal salts such as ferric chloride and aluminum sulfate (alum). The sorption of arsenic onto iron and aluminum oxides and oxyhydroxides has therefore been extensively studied (for reviews see refs. [*1,2*]).

It is a common observation in the water treatment literature [*3,4*] that alum is ineffective for the removal of As(III) from potable water but can efficiently remove As(V). Thus oxidation of As(III) to As(V), which can be accomplished by conventional disinfectants such as chlorine, is recommended if alum is to be used to treat source waters containing As(III) [*5*]. Similarly, activated alumina is not recommended as a packed bed filter media for As(III) removal [*6*]. In contrast, removal of both As(III) and As(V) can be accomplished using ferric chloride as a coagulant [*7,8*] or granular ferric hydroxide as a packed bed media [*9*]. Under conditions relevant to water treatment, better removal efficiency is achieved with ferric chloride for As(V) than for As(III) [*4,8,10*]. Though it should be noted that, under conditions nearer to surface saturation, comparable sorption of As(III) and As(V) is observed at circumneutral pH and preferential sorption of As(III) at higher pH values [*11-14*].

Recent studies, however, have demonstrated sorption of As(III) onto aluminum oxyhydroxides [*15-17*]. The results of these studies appear to conflict with those obtained under conditions relevant to water treatment but the seeming inconsistency among these results may merely reflect differences in experimental conditions. Here, our objectives are: (i) to examine consistency of these recent studies with prior work, (ii) to identify differences between iron and aluminum oxyhydroxides as sorbents for arsenic in +III and +V oxidation states, (iii) to examine constraints on surface speciation provided by macroscopic sorption studies and surface complexation modeling (SCM), and (iv) to discuss the integration of macroscopic sorption studies and SCM with spectroscopic studies and molecular modeling (which is presented in detail by Kubicki, this volume).

Background

Although a comprehensive review of the studies of As sorption/co-precipitation onto Fe and Al oxides is beyond the scope of this paper, it is worth highlighting selected evidence of the similarities and differences in the sorption behavior of As(III) and As(V) with Fe and Al oxides.

Comparability of As(III) and As(V) sorption onto Fe oxides

Numerous studies have compared the sorption of As(III) and As(V) onto Fe(III) oxides such as hydrous ferric oxide (HFO), goethite, and hematite [*11-14,18,19*]. It has been widely observed that the relative extent of As(III) and As(V) sorption is a function of pH and of the relative and absolute concentrations of the sorbent and sorbate. Since As(III) sorption is independent of pH over a broad range and As(V) sorption decreases with increasing pH, a crossover pH can be observed such that As(V) is sorbed to a greater extent than As(III) below that pH value and to a lesser extent above it (Figure 1). It should be noted, however, that, at total As and Fe concentrations where complete sorption of As(V) is observed over some pH range, the sorption of As(III) is not complete at any pH value, which indicates a greater affinity of the surface Fe sites for As(V) than for As(III). This effect becomes less significant at increasing total As concentrations.

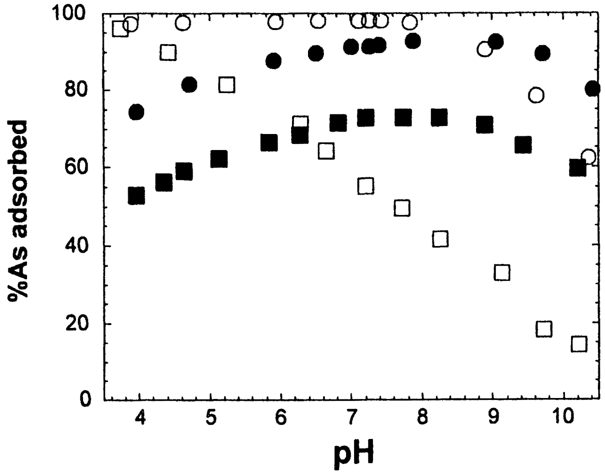

Figure 1. %As sorbed vs. pH for As(III) (closed symbols) and As(V) (open symbols) on HFO with [As]$_T$ = 10 μM (circles) and 50 μM (squares), I = 0.01, 30 mg/L HFO. Data from ref. [11].

In water treatment studies, As removal has been examined in coagulation experiments where As removal occurs concurrently with the formation of hydrous ferric oxides upon addition of a coagulant, such as ferric chloride, to test solutions. Conditions of these experiments are generally chosen to be relevant to water treatment (i.e., at low equivalent sorbent concentrations). Under these conditions, As removal (by sorption/co-precipitation) is generally observed to be more efficient for As(V) than for As(III), particularly at lower coagulant doses [*3,8*]. Similar results were observed for adsorption of As(III) and As(V) onto pre-formed HFO at comparable sorbate and sorbent concentrations [*19*].

Comparability of As(V) sorption onto Fe and Al oxides

There are apparently significant inconsistencies in the literature with regard to the affinity of As(III) for Al-based sorbents and coagulants. Several studies have reported negligible or poor removal of As(III) by alum [*3,5,7*]. A companion adsorption study [20] conducted under similar conditions of total sorbate and sorbent concentrations illustrated the striking difference between sorption of As(III) and As(V) (Figure 2).

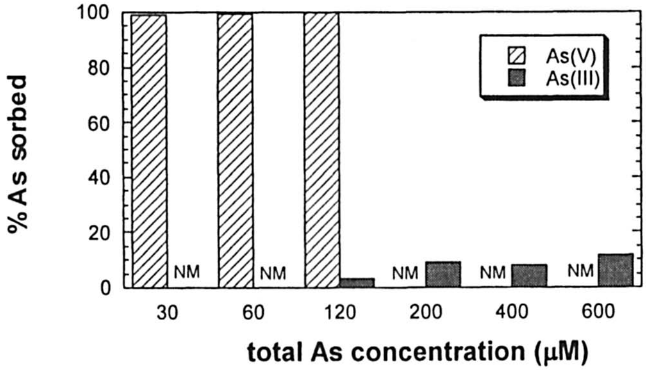

Figure 2. Sorption of As(III) and As(V) on amorphous Al hydroxide at varying $[Al]_T$ *with* $[As]_T = 1.33\ \mu M$, $pH = 6$, $I = 0.01$. *NM = not measured. Data from ref. [20].*

In adsorption studies with higher concentrations (i.e., 1-4 g/L) of activated alumina [*21*] or amorphous Al hydroxide [*15,16,22*], adsorption of As(III) has been reported with maximum adsorption at pH 8. The extent of As(III) adsorption at this pH is less than that of As(V) and the pH range over which As(III) is adsorbed onto amorphous Al hydroxide is significantly narrower than that for As(V) [*15,16,22*]. This behavior will be examined in greater detail below. Weak adsorption of As(III) on gibbsite, exhibiting some dependence on ionic strength but nearly none on pH, has been reported [*23*].

Surface species invoked in modeling macroscopic sorption experiments

In many macroscopic sorption studies, As adsorption and its effects (e.g., on electrophoretic mobility) have been interpreted in terms of chemisorption, the formation of inner-sphere complexes between As species and surface metal centers. Such surface complexation models (SCMs) may use different formalisms (e.g., constant capacitance, diffuse double layer, triple layer, etc.) to describe electrostatic interactions at the oxide surface yet have common representations of adsorbed As species. If surface species are defined merely to describe the results of macroscopic adsorption experiments, it is often sufficient to consider *mononuclear* complexes (i.e., As species bound to a single surface metal center). The level of protonation of adsorbed As species is constrained by the pH dependence of adsorption or (less often) by the observed stoichiometry of proton exchange concurrent with As adsorption [*24*]. The stoichiometry of these surface species may correspond to *monodentate* or *bidentate* complexes (i.e., binding the surface metal center through one or two coordinating ligand moieties) but this distinction is not robustly supported on the basis of only macroscopic adsorption behavior.

On the basis of spectroscopic studies, *binuclear* complexes (i.e., As species bound to two adjacent surface metal centers) have also been invoked to describe macroscopic adsorption behavior. For adsorption of As(V) and As(III) on amorphous Al hydroxide, comparable descriptions of macroscopic sorption data were obtained with only mononuclear complexes or by including binuclear complexes [*16*]. Since a unique set of surface species cannot be defined based on macroscopic adsorption data, surface species are chosen to obtain a minimum number of species [*25*] or to apply the same set of species for different conditions or solids [*11*].

For As(III), *outer sphere* as well as *inner sphere* complexes have been used in modeling. In an outer sphere complex, the As(III) anion is farther from the oxide surface due to the presence of intervening water molecules and experiences less electrostatic interaction with the surface. The triple layer model is generally used to accommodate this type of surface species. Outer sphere complexes are often invoked when a strong effect of ionic strength on adsorption is observed. However, the model fit to data using outer sphere complexes may be very poorly constrained, particularly if the constants for outer sphere complexes of major cations and anions (e.g., Na^+ and Cl^-) are used as adjustable fitting parameters.

The lack of uniqueness of surface species used to describe the adsorption of As(V) and As(III) on Fe and Al oxyhydroxides is evident in Tables I and II.

Spectroscopic evidence for surface speciation

Spectroscopic techniques, including Raman, Fourier Transform Infrared (FTIR), and Extended X-ray Absorption (EXAFS) spectroscopy, have been used

Table I. Sets of As(V) Surface Species for Metal Oxyhydroxides

surface species	*pH range*	*solid*	*reference*
$\equiv MH_2AsO_4$	4-10	HFO	[25]
$\equiv MHAsO_4^-$			
$\equiv MOHAsO_4^{3-}$			
$\equiv MH_2AsO_4$	4-10	HFO, goethite	[11]
$\equiv MHAsO_4^-$	4-10	HFO	[26]
$\equiv MAsO_4^{2-}$	4-10	HFO	[15]
	3-10	goethite	[27]
	2-10	goethite	[28]
	2-12	am-Al oxide	[15]
	3-11	gibbsite	[28]
	4-10	gibbsite	[27]
	5-8	am-Al oxide	[27]
$\equiv MHAsO_4^-$	4-11	am-Al oxide	[16]
$\equiv MAsO_4^{2-}$	3-11	am-Al oxide	[22]
$\equiv MAsO_4^{2-}$	2-11	HFO	[22]
$\equiv MAsO_4^{2-}$	4-11	am-Al oxide	[16]
$\equiv M_2AsO_4^-$			

Table II. Sets of As(III) Surface Species for Metal Oxyhydroxides

surface species	*pH range*	*solid*	*reference*
$\equiv MH_2AsO_3$	4-10	HFO	[25]
$\equiv MH_2AsO_3$	4-10	HFO, goethite	[11]
$\equiv MHAsO_3^-$	3-11	HFO	[15]
	2-11	HFO	[22]
	3-11	am-Al oxide	[22]
$\equiv MHAsO_3^-$	4-11	am-Al oxide	[16]
$\equiv MAsO_3^{2-}$			
$\equiv M_2HAsO_3$	3-11	goethite	[12]
$\equiv M_2AsO_3^-$			
$\equiv MAlO_3^{2-}$	4-11	am-Al oxide	[12]
$\equiv M_2HAsO_3$			
$\equiv M_2AsO_3^-$			
$\equiv(MOH_2^+)_2{-}HAsO_3^{2-}$	2-10	am-Al oxide*	[15]
$\equiv(MOH_2^+)_2{-}AsO_3^{3-}$			

*outer-sphere complex

to interrogate the structure of surface complexes. Direct comparison with macroscopic sorption studies is complicated by differences in experimental conditions; spectroscopic studies generally require higher concentrations of both sorbate and sorbent and also higher surface coverage than are typical for macroscopic adsorption studies. Some spectroscopic studies have also been conducted with dried solids or crystalline salts rather than with suspensions. Nonetheless, the results of spectroscopic studies have been used to constrain interpretations of adsorption studies [*16*].

Vibrational spectra of adsorbed As(V) support the assignment of inner-sphere complexes on both Fe and Al oxyhydroxides. Both Raman and IR spectra show distinct differences in frequencies associated with the arsenate anion for As(V) in solution, adsorbed to Fe or Al oxyhydroxides, and in crystalline As(V) salts [*15,29-32*]. Absorbances associated with the surface hydroxyl groups of goethite were also found to be influenced by adsorption of As(III) and As(V) [*30,31*]. Features attributable to inner sphere complexes of As(III) have been reported for Fe oxyhydroxides [*15,30-32*] but were not apparent in the case of Al oxyhydroxides [*15*].

Numerous studies have used EXAFS to probe the coordination environment of As(V) adsorbed onto various Fe oxyhydroxides, such as ferrihydrite, goethite, akaganeite, and lepidocrocite [*33-36*]. In EXAFS studies, surface structures are distinguished primarily on the basis of the observed distance between As and Fe atoms. While there is some disagreement regarding the occurrence of various surface structures, it is generally agreed that As(V) adsorbs in large part as a binuclear, bidentate complex in which As(V) is bound to apical oxygens of two adjacent, edge-sharing Fe octahedra [*33-36*]. However, other structures, specifically a mononuclear, monodentate complex [*34-36*] and mononuclear, bidentate complex [*36*], have also been proposed. The contributions of the various complexes vary with surface coverage [*34,36*].

A binuclear, bidentate complex has also been proposed for As(III) adsorbed onto goethite [*12*]. Protonation of the surface complex with decreasing pH was proposed but this would not change the As–Fe distance nor were spectra obtained below pH 6.4. A mononuclear, monodentate complex was considered but not supported by the spectroscopic evidence.

EXAFS spectra for As(V) and As(III) adsorbed onto γ-Al_2O_3(s) have also been interpreted as consistent with binuclear, bidentate complexes [*17*]. However, the X-ray Absorption Near Edge (XANES) spectrum for adsorbed As(III) indicated a contribution of an outer sphere as well as the inner sphere complex.

Using surface complexation modeling to evaluate surface speciation and consistency of experimental observations

Despite the issue of non-uniqueness discussed above, it may be instructive to use surface complexation modeling as a tool to examine the macroscopic implications of surface speciation and to integrate structural information obtained from other (e.g., spectroscopic) methods. For example, EXAFS data provide a compelling rationale for the inclusion of binuclear, bidentate complexes in modeling macroscopic adsorption data [*16*] yet this information must be integrated with constraints on surface speciation derived from macroscopic data. SCMs can also be used, with appropriate caution, to compare macroscopic data obtained under varying experimental conditions. Here, we use surface complexation modeling to compare and contrast the sorption behavior of As(III) and As(V) on Al oxyhydroxide as reported by Goldberg and Johnston [*15*].

Extraction of constants for surface complexation modeling

Equilibrium constants for inner-sphere As(III) and As(V) surface complexes on amorphous Al oxide were obtained for data reported in ref. [*15*] using FITEQL [*37*] to optimize values for the constants. Electrostatic corrections for surface species were made using the diffuse layer model (DLM). The values for total concentrations of surface sites were not optimized but rather were fixed based on the solids concentration, the reported BET surface area (209 m^2/g), and a value for surface site density of 2.31 sites/nm^2 as recommended by Davis and Kent [*38*]. The sorption data used in the fitting were obtained for $[As]_T = 1$ mM, 0.5 or 4.0 g/L solid, and I = 0.01 [*15*].

The values of the constants as optimized by FITEQL are not adjusted for ionic strength and are valid for I = 0.01. The values for the sorption constants reported in Table III have been adjusted to zero ionic strength using the Davies equation to obtain activity coefficients for dissolved species. Predictions based on these constants were made using MINEQL+, v. 4.5 [*39*]. Activity coefficients of all dissolved species (including those participating in sorption reactions) were adjusted for ionic strength in MINEQL+ using the Davies equation.

Table III lists the reactions included in the fitting and modeling exercises with the corresponding mass law expressions and intrinsic equilibrium constants. The constants for protonation and deprotonation of the surface hydroxyl groups (Table III, Rxns. 1a,b) are the same as those used in ref. [*15*], in which the constant capacitance model (CCM) was used to make electrostatic corrections. Although we applied the diffuse layer rather than the constant capacitance model, we felt that modification of the values of these constants was not necessary. As discussed by Westall and Hohl [*40*], the values of these constants are similar whether the electrostatic term is obtained with the CCM or DLM. For binuclear complexes, the mass law expressions in Table III include a squared term for the concentration of the free surface hydroxyl groups. Although there is some disagreement in the literature as to the appropriate mass law expression for binuclear complexes, Benjamin [*41*] has argued that the squared term should be included and this convention has been followed by several other researchers [*12,15,16*].

Modeling sorption of As(III) on Al oxyhydroxide

Surface complexation modeling was used, in the case of As(III) sorption onto Al oxyhydroxide, to examine two issues: the level of protonation of surface complexes and the formation of binuclear vs. mononuclear surface complexes.

Protonation of surface complexes

Model fits to the sorption data for As(III) on Al oxyhydroxide using surface species with varying levels of protonation were compared for binuclear surface complexes. As previously discussed by Manning [*16*], binuclear surface complexes were selected based on spectroscopic information obtained for As(III) surface complexes on Fe(III) oxyhydroxides. As can be seen in Figure 3, the fit obtained using only the charged surface species is only marginally improved if the uncharged surface species in included. (See Table III, Rxns. 3a,b, for stoichiometry of the surface species and corresponding equilibrium constants for surface complex formation.) When both charged and uncharged species are included in the fitting exercise, <15% of the sorbed As(III) is calculated to be present as the uncharged surface species.

It may be noted that, with either of both the charged and uncharged surface species, the model underpredicts the observed extent of As(III) sorption between pH 7 and 9. This primarily reflects the fixed value used for the maximum surface site concentration (see above).

It is apparent from the comparison of these model predictions that this data set does not provide sufficient constraints to make a robust assignment of the contributions of charged and uncharged surface species. However, for further comparison of binuclear and mononuclear complex formation, both charged and uncharged surface species were considered.

Table III. Surface reactions, mass law expressions and constants*

reaction	*mass law expression*[‡]	*log* K_{int}
(1a) $\equiv MOH + H^+ = \equiv MOH_2^+$	$[\equiv MOH_2^+][\equiv MOH]^{-1}[H^+]^{-1}\exp(F\psi R^{-1}T^{-1})$	7.42
(1b) $\equiv MOH = H^+ + \equiv MO^-$	$[H^+][\equiv MO^-][\equiv MOH]^{-1}\exp(-F\psi R^{-1}T^{-1})$	−9.13
(2a) $\equiv MOH + H_3AsO_3 = \equiv MH_2AsO_3 + H_2O$	$[\equiv MH_2AsO_3][\equiv MOH]^{-1}[H_3AsO_3]^{-1}$	2.29
(2b) $\equiv MOH + H_3AsO_3 = \equiv MHAsO_3^- + H^+ + H_2O$	$[\equiv MHAsO_3^-][H^+][\equiv MOH]^{-1}[H_3AsO_3]^{-1}\exp(-F\psi R^{-1}T^{-1})$	−4.63
(3a) $2\equiv MOH + H_3AsO_3 = \equiv M_2HAsO_3 + 2H_2O$	$[\equiv M_2HAsO_3][\equiv MOH]^{-2}[H_3AsO_3]^{-1}$	5.41**
(3b) $2\equiv MOH + H_3AsO_3 = \equiv M_2AsO_3^- + H^+ + 2H_2O$	$[\equiv M_2AsO_3^-][H^+][\equiv MOH]^{-2}[H_3AsO_3]^{-1}\exp(-F\psi R^{-1}T^{-1})$	−1.46[†]
(4a) $\equiv MOH + H_3AsO_4 = \equiv MH_2AsO_4 + H_2O$	$[\equiv MH_2AsO_4][\equiv MOH]^{-1}[H_3AsO_4]^{-1}$	11.95
(4b) $\equiv MOH + H_3AsO_4 = \equiv MHAsO_4^- + H^+ + H_2O$	$[\equiv MHAsO_4^-][H^+][\equiv MOH]^{-1}[H_3AsO_4]^{-1}\exp(-F\psi R^{-1}T^{-1})$	5.45
(4c) $\equiv MOH + H_3AsO_4 = \equiv MAsO_4^{2-} + 2H^+ + H_2O$	$[\equiv MAsO_4^{2-}][H^+]^2[\equiv MOH]^{-1}[H_3AsO_4]^{-1}\exp(-2F\psi R^{-1}T^{-1})$	−3.24

*mass law constants for zero ionic strength

[‡] in the mass law expressions, *F* is the Faraday constant, ψ is the surface potential, R is the gas constant, and T is temperature

**value of constant obtained with both charged and uncharged species; for uncharged species only, value is 6.04

[†] value of constant obtained with both charged and uncharged species; for charged species only, value is −1.26

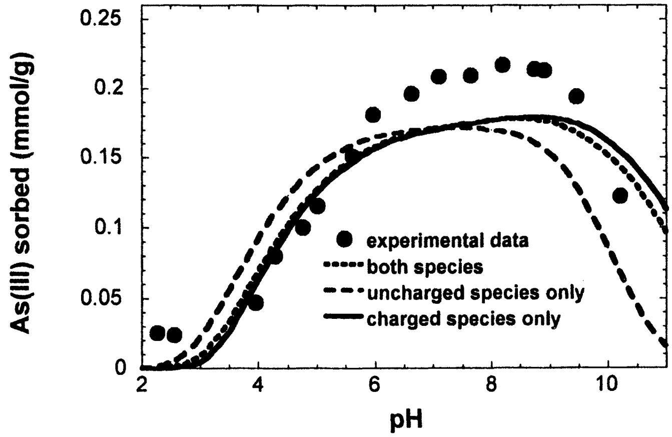

Figure 3. Comparison of data (symbols) and model predictions (lines) for sorption of As(III) on Al oxyhydroxide. Conditions $[As]_T$ = 1mM, 4 g/L solid, I = 0.01. Data from ref. [15]. See text for discussion of modeling.

Binuclear vs. mononuclear complex formation

Similar fits to the sorption data for As(III) on Al oxyhydroxide could be obtained using either binuclear or mononuclear surface complexes when both charged and uncharged surface species were included (Figure 4, Table III, Rxns. 2a,b, 3a,b). In both cases, two surface As(III) species were considered.

One important constraint that could distinguish between binuclear and mononuclear surface complexes is the maximum sorption capacity for As(III). If As(III) sorbs as a mononuclear complex, its maximum sorption density should be similar to that for simple sorbates such as fluoride or protons. This would not be the case if As(III) sorbs as a binuclear complex (i.e., occupying two sorption sites per As(III) bound). This constraint is not, however, manifest in the data set modeled here since, under those experimental conditions, the maximum sorbed As(III) concentration was only 27% of the total site concentration (as estimated from the measured BET surface area and a fixed site density of 2.31 sites/nm^2). Clearly, if the sorbed As(III) concentration is observed to exceed 50% of the total site concentration, not all the sorbed As(III) could be accommodated as binuclear complexes.

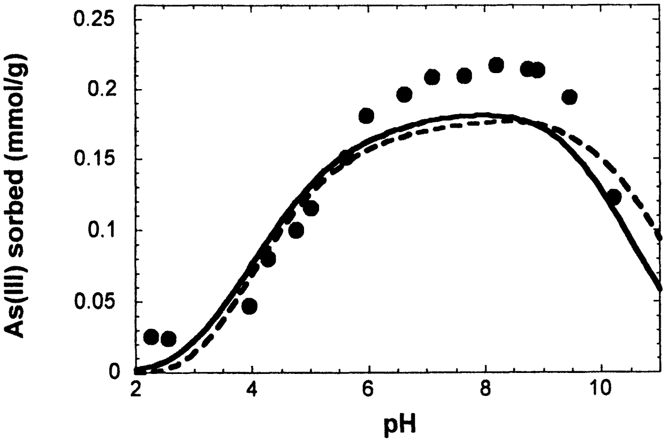

Figure 4. Comparison of data (symbols) and model predictions (lines) for sorption of As(III) on Al oxyhydroxide. Conditions: [As]$_T$ = 1mM, 4 g/L solid, I = 0.01. Data from ref. [15]. The solid line corresponds to the fit with mononuclear surface complexes and the dashed line to the fit with binuclear surface complexes.

Modeling sorption of As(V) on Al oxyhydroxide

This constraint is indeed manifest in the data for sorption of As(V) on Al oxyhydroxide where the observed sorbed As(V) concentration was actually slightly in excess of the estimated total site concentration. This is apparent in the deviation of the model prediction from the data for pH < 6.7 (Figure 5). In this case, only mononuclear complexes (Table III, Rxns. 4a,b,c) were used to fit the data since inclusion of binuclear complexes would only increase the discrepancy between the model prediction and the data.

Extrapolation to conditions relevant to water treatment

Admittedly, the extrapolation of model predictions outside the range of experimental conditions for which the model parameters were obtained is fraught with uncertainties. Nonetheless, it may be instructive to use such extrapolations to gain a sense of the level of consistency of observations made under different conditions. The constants for formation of mononuclear surface complexes of As(III) and As(V) that provide a good description of the sorption data from ref. [*15*] were used to predict the extent of As(III) and As(V) sorption onto Al oxyhydroxides under conditions relevant to water treatment. As can be seen in Figure 6, sorption of As(V) is predicted to be complete up to about pH 7 but sorption of As(III) is predicted to be negligible over the entire pH range examined. Thus this prediction is consistent with the observations of poor removal of As(III) from drinking water by coagulation with alum and negligible sorption of As(III) on Al oxyhydroxides under comparable conditions (cf. Figure 2).

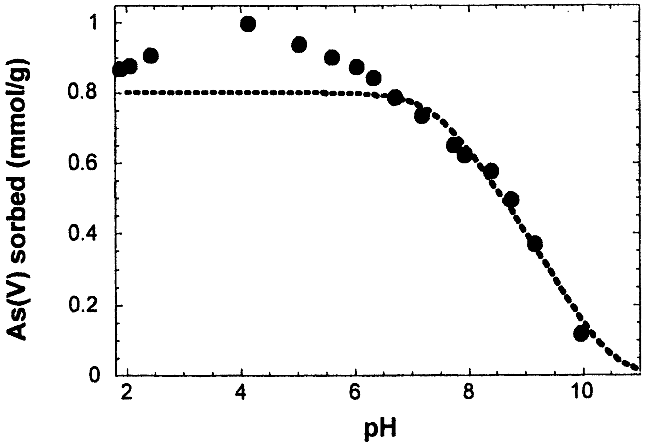

Figure 5. Comparison of data (symbols) and model predictions (dashed line) for sorption of As(V) on Al oxyhydroxide. Conditions: $[As]_T$ = 1mM, 0.5 g/L solid, I = 0.01. Data from ref. [15]. The model prediction is for three mononuclear surface complexes (see Table III, Rxns. 4a-c). Data for pH < 6.7 were not included in the fitting exercise.

Concluding Comments

Surface complexation modeling was developed to provide a description of observed (macroscopic) sorption behavior. With the increasing availability of complementary information derived from spectroscopic techniques, an obvious question is how this structural information can be related to the stoichiometries of surface complexes inferred from macroscopic sorption data. And, with the increasing application of molecular modeling to metal-ligand complexes in aqueous solution and at mineral-water interfaces, another question is how results of molecular modeling can be integrated with (or constrained by) information gained from spectroscopy and surface complexation modeling. One important caveat in making such comparisons (or applying such constraints) is that spectroscopic studies and macroscopic sorption studies are often performed under very different experimental conditions, which may lead to real differences in surface speciation.

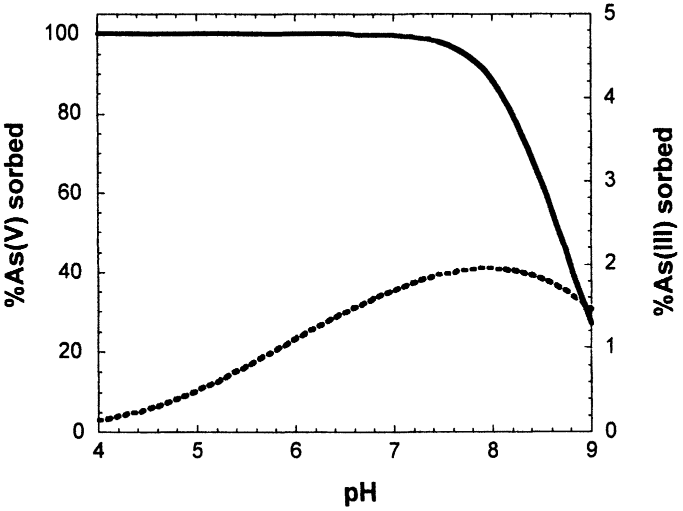

Figure 6. Prediction of the extent of sorption of As(V) (solid line) and As(III)(dashed line) on Al oxyhydroxide for $[As]_T = 0.27$ μM, $[Al]_T = 100$ μM (corresponding to 7.8 mg/L $Al(OH)_3(s)$ or $[\equiv AlOH]_T = 6.25$ μM), $I = 0.01$. Note difference in scale of right and left axes. Predictions are based on mononuclear constants listed in Table III (Rxns. 2a,b, 4a-c).

The modeling exercise performed here indicates that the level of protonation of surface complexes is not well constrained by the pH edges commonly reported in macroscopic sorption studies. Additional information on the protonation of surface species might be gained from data on proton consumption or release during sorption reactions.

The distinction between binuclear and mononuclear surface complexes is of particular interest because of the evidence provided by spectroscopic methods for binuclear complexes. In modeling macroscopic sorption data, either binuclear or mononuclear complexes can provide an adequate description of sorption data at low surface coverage. However, mononuclear complexes must be invoked when the surface coverage by the sorbate exceeds 50% of the total site concentration. Presumably, if mononuclear complexes are formed under these conditions, they must also contribute to the speciation of sorbed species at lower surface coverages.

In this modeling exercise, only inner-sphere complexes were considered in fitting sorption data. Formation of outer-sphere complexes, although not considered here, has been invoked on the basis of spectroscopic evidence and the ionic strength dependence of macroscopic sorption.

Surface complexation modeling provides a useful framework for the comparison of macroscopic sorption data obtained under varying experimental conditions. Integration of surface complexation modeling with spectroscopy and molecular modeling must account for the varying interpretations possible in these various approaches to interrogating surface structure and for the extent to which these interpretation are constrained by observations.

Acknowledgments

The authors are indebted to Dr. Sabine Goldberg (U.S. Salinity Laboratory) for providing sorption data. This work was supported in part by the National Science Foundation (BES-0201888) and by the generous support of William Davidow.

References

[1] Stollenwerk, K.G. In *Arsenic in Ground Water*, Welch, A.H. and Stollenwerk, K.G., Eds.; Kluwer Academic: Boston, MA, 2003; pp. 67-100.

[2] Smedley, P.L.; Kinniburgh, D.G. *Appl. Geochem.* **2002,** *17*, 517-568.

[3] Sorg, T.J.; Logsdon, G.S. *J. Am. Water Works Assoc.* **1978**, *70*, 379-393.

[4] Jekel, M.R. In *Arsenic in the Environment. Part I: Cycling and Characterization*, Nriagu, J.O., Ed.; Wiley-Interscience: New York, NY, 1994; pp. 119-132.

[5] Hering, J.G.; Elimelech, M. "Arsenic Removal by Enhanced Coagulation and Membrane Processes"; Report No. 90706, 1996; American Water Works Assoc. Research Fndn., Denver, CO.

[6] Clifford, D.A. In *Water Quality and Treatment*, Letterman, R.D., Ed.; McGraw-Hill: New York, NY, 1999; pp. 9.1-9.91.

[7] Hering, J.G.; Chen, P.Y.; Wilkie, J.A.; Elimelech, M. *J. Environ. Eng.-ASCE* **1997**, *123*, 800-807.

[8] Hering, J.G.; Chen, P.Y.; Wilkie, J.A.; Elimelech, M.; Liang, S. *J. Amer. Water Works Assoc.* **1996**, *88*, 155-167.

[9] Driehaus, W.; Jekel, M.; Hildebrandt, U. *J. Wat. Supply Technol.-AQUA* **1998**, *47*, 30-35.

[10] Shen, Y.S. *J. Amer. Water Works Assoc.* **1973,** *65*, 543-548.

[11] Dixit, S.; Hering, J.G. *Environ. Sci. Technol.* **2003,** *37*, 4182-4189.

[12] Manning, B.A.; Fendorf, S.E.; Goldberg, S. *Environ. Sci. Technol.* **1998,** *32*, 2383-2388.

[13] Raven, K.P.; Jain, A.; Loeppert, R.H. *Environ. Sci. Technol.* **1998**, *32*, 344-349.

[14] Jain, A.; Loeppert, R.H. J. *Environ. Qual.* **2000**, *29*, 1422-1430.

[15] Goldberg, S.; Johnston, C.T. *J. Coll. Interface Sci.* **2001**, *234*, 204-216.

[16] Manning, B.A.; Goldberg, S. *Environ. Sci. Technol.* **1997**, *31*, 2005-2011.

[17] Arai, Y.; Elzinga, E.J.; Sparks, D.L. *J. Coll. Interface Sci.* **2001**, *235*, 80-88.

[18] Bowell, R.J. *Appl. Geochem.* **1994**, *9*, 279-286.

[19] Wilkie, J.A.; Hering, J.G. *Coll. Surf. A* **1996**, *107*, 97-110.

[20] Wilkie, J.A. Ph.D. Thesis, Univ. of California, Los Angeles, CA, 1997.

[21] Ghosh, M.M.; Yuan, J.R. *Environ. Prog.* **1987**, 6, 150-157.

[22] Goldberg, S. *Soil Sci. Soc. Am. J.* **2002**, *66*, 413-421.

[23] Weerasooriya, R.; Tobschall, H.J.; Wijesekara, H.; Arachchige, E.; Pathirathne, K.A.S. *Chemosphere* **2003**, *51*, 1001-1013.

[24] Jain, A.; Raven, K.P.; Loeppert, R.H. *Environ. Sci. Technol.* **1999**, *33*, 1179-1184.

[25] Dzombak, D.A. and Morel, F.M. *Surface Complexation Modeling*; Wiley-Interscience: New York, NY, 1990; 393 pp..

[26] Hsia, T.S.; Lo, S.L.; Lin, C.F.; Lee, D.Y. *Coll. Surf. A* **1994**, *85*, 1-7.

[27] Goldberg, S. *Soil Sci. Soc. Am. J.* **1986**, *50*, 1154-1157.

[28] Manning, B.A.; Goldberg, S. *Soil Sci. Soc. Am. J.* **1996**, *60*, 121-131.

[29] Myneni, S.C.B.; Traina, S.J.; Waychunas, G.A.; Logan, T.J. *Geochim. Cosmochim. Acta* **1998**, *62*, 3285-3300.

[30] Lumsdon, D.G.; Fraser, A.R.; Russell, J.D.; Livesey, N.T. *J. Soil Sci.* **1984**, *35*, 381-386.

[31] Sun, X.H.; Doner, H.E. *Soil Sci.* **1996**, *161*, 865-872.

[32] Suarez, D.L.; Goldberg, S.; Su, C. In *Mineral-Water Interfacial Reactions*, Sparks, D.L.; Grundl, T.J., Eds.; ACS Symp. Ser. vol. 715; American Chemical Society: Washington, DC, 1999, pp. 136-178.

[33] Manceau, A. *Geochim. Cosmochim. Acta* **1995**, *59*, 3647-3653.

[34] Waychunas, G.A.; Rea, B.A.; Fuller, C.C.; Davis, J.A. *Geochim. Cosmochim. Acta* **1993**, *57*, 2251-2269.

[35] Waychunas, G.A.; Davis, J.A.; Fuller, C.C. *Geochim. Cosmochim. Acta* **1995**, *59*, 3655-3661.

[36] Fendorf, S.; Eick, M.J.; Grossl, P.; Sparks, D.L. *Environ. Sci. Technol.* **1997**, *31*, 315-320.

[37] Herbelin, A.L.; Westall, J.C. "FITEQL 4.0: A computer program for the determination of chemical equilibrium constants from experimental data"; Oregon State Univ.: Corvallis, OR, 1999.

[38] Davis, J.A.; Kent, D.B. In *Mineral-Water Interface Geochemistry*, Hochella, Jr., M.F.; White, A.F., Eds.; Rev. Mineral. vol. 23; Mineralogical Soc. Am.: Washington, DC, 1990, pp. 177-260.

[39] Schecher, W.D.; McAvoy, D.C. "MINEQL+: A Chemical Equilibrium Modeling System", Environmental Research Software: Hallowell, ME, 1998.

[40] Westall, J.; Hohl, H. *Adv. Coll. Interface Sci.* **1980**, *12*, 265-294.

[41] Benjamin, M.M. *Environ. Sci. Technol.* **2002**, *36*, 307-313.

Chapter 3

Arsenate and Arsenite Sorption on and Arsenite Oxidation by Iron(II, III) Hydroxycarbonate Green Rust

Chunming Su and Richard T. Wilkin

Ground Water and Ecosystems Restoration Division, National Risk Management Research Laboratory, Office of Research and Development, U.S. Environmental Protection Agency, 919 Kerr Research Drive, Ada, OK 74820

Iron(II,III) hydroxycarbonate green rust is a major corrosion product of zerovalent iron that is being used in permeable reactive barriers to remediate groundwater arsenic contamination. To optimize the design of iron barriers, it is important to evaluate the influence of geochemical parameters such as pH, time, and arsenic concentration on the interactions of arsenic with iron corrosion products. We synthesized iron(II, III) hydroxycarbonate green rust by neutralizing $FeSO_4$ solution with NaOH and Na_2CO_3 or $NaHCO_3$ followed by air sparging. The synthetic products were characterized with scanning electron microscopy, X-ray diffraction, and wet chemical analysis. We conducted batch sorption experiments with arsenate and arsenite in an anaerobic glovebox. The pH ranged from 7.5 to 10.7. Both arsenate and arsenite sorption increased with increasing time up to 60 days. More arsenite was sorbed at pH 7.5 than at pH 10.4. Arsenite showed much higher sorption than arsenate. Sorbed arsenite (up to 90 g kg^{-1}) was partially oxidized at the surface of carbonate green rust. Oxidation of sorbed arsenite could be advantageous because arsenate is generally less toxic and less mobile than arsenite.

© U.S. government work. Published 2005 American Chemical Society.

In Advances in Arsenic Research; O'Day, P., et al.;
ACS Symposium Series; American Chemical Society: Washington, DC, 2005.

Introduction

Arsenic (As) contamination of water resources is a worldwide problem and active remediation of contaminated groundwater is required at many sites. Zerovalent iron (Fe^0) has been shown to effectively remove both arsenate (As(V)) and arsenite (As(III)) from water in laboratory batch and column tests (*1-12*) and Fe^0 has shown to be a promising material that can be used as a medium for permeable reactive barrier (PRB) applications to remediate groundwater As contamination. The main removal mechanism seems to be surface adsorption/complexation of As with the iron corrosion products (*3, 11, 12*). Redox transformation of sorbed As at the surface of corroded iron metal also takes place (*3, 11*). Arsenite was found to be partially oxidized in the Fe^0 system even after a short time of contact; whereas, arsenate reduction was detected only after 30 days of reaction (*3*).

Green rusts (GR) are a group of iron(II, III) hydroxy compounds characterized by a layered structure made of brucite-like sheets, positively charged due to the trivalent Fe cations, $[Fe(II)_{(1-x)}Fe(III)_x(OH)_2]^{x+}$ with $x = Fe^{3+}/Fe_{tot}$, which alternate with interlayers composed of anions (e.g., CO_3^{2-}, Cl^-, SO_4^{2-}) and water molecules, to restore the overall electroneutrality. GR is a major iron corrosion product identified in pilot-scale and field-scale PRBs (*13-17*). Examination of iron corrosion in full-scale PRBs through solid phase characterization and geochemical modeling suggest that in non-mining impacted groundwater, iron(II,III) hydroxycarbonate green rust, or simply carbonate green rust (CGR) precipitates preferentially over the sulfate form in zerovalent iron systems (*18*).

Green rusts are highly reactive mineral phases found in soils, sediments, and aquifers under anoxic conditions (*19*). They are participants of redox processes and may thus control the speciation, solubility, mobility, bioavailability, and toxicity of redox sensitive elements (e.g., As, Se, Cr, U, Pu, Np, Tc) in natural environments. A recent study using micro X-ray fluorescence and micro X-ray absorption spectroscopy shows that the corrosion of Fe^0 to CGR reduces selenite to Se^0 within a time frame of < 3 months (*20*). This finding is consistent with the results of a study on abiotic selenium redox transformation in the presence of sulfate GR (*21*).

There is a lack of understanding of the interactions between inorganic As species and GR. One study shows that As(V) is not reduced to As(III) after reaction with sulfate green rust for 24 h and sorbed As(V) forms inner-sphere bidentate corner-sharing surface complexes (*22*). As far as we know, there is no reported study on the interactions between As and carbonate green rust. Because CGR is a predominant mineral in the Fe^0-based PRB environment, we focused our research on the influence of CGR on the fate of As at the time scale of hours to two months. The objectives of this study were to: (1) evaluate the extent of As sorption by CGR as a function of time, pH, and As concentration; (2) examine redox transformation of As in the CGR system; and (3) investigate possible implications of the laboratory results to field PRB applications.

Materials and Methods

Synthesis of Carbonate Green Rust

All chemical reagents used in this study were reagent or analytical grade. The synthesis of CGR was carried out by following a modified procedure from those described by Bernal et al. (*23*) and Drissi et al. (*24*). Exactly 250 mL of deionized water in a 500 mL-polypropylene bottle was purged for 30 minutes with N_2 gas to remove dissolved oxygen. A mass of 13.901 g of ferrous sulfate heptahydrate ($FeSO_4{\bullet}7H_2O$) (Sigma-Aldrich) was added to the bottle to bring the solution to 0.2 M and a stir bar was placed at the bottom of the bottle. Once the ferrous sulfate heptahydrate was well mixed in the water by a magnetic stir, a mass of 3.333 g of sodium hydroxide (NaOH) (Mallinckrodt) was added to bring the molar ratio $[Fe^{2+}/OH^-] = 0.6$. A mass of 5.300 g of sodium carbonate ($NaCO_3$) (Baker) or 4.200 g of sodium bicarbonate ($NaHCO_3$) (Baker) was then added to bring the solution to 0.2 M. The bottle was then capped and the suspension was purged with air using a small air pump (commercial fish tank bubbler) for two hours. The suspension was well mixed during air sparging using the magnetic stir bar. The gas was then turned off and the bottle was capped. The bottle was then transferred to an anaerobic glovebox (3 - 6% H_2 in N_2). A pipette was used to remove the suspension to a 250 mL-polyethylene bottle, trying to avoid mixing the red rust that had formed on the sides of the polypropylene bottle with the suspension. The pH and Eh of the suspension were measured using a combination pH electrode and a platinum redox electrode, respectively. The Eh values were reported as values relative to standard hydrogen potential.

Solid concentration of the fresh suspension was determined gravimetrically using a subsample (2.5 mL suspension) that was filtered through a 0.22 μm membrane mounted on a filter holder attaching to a syringe, rinsed with 10 mL of deionized and deoxygenated water, and dried in the glovebox for 24 h. Fresh CGR materials were used for batch As sorption experiments. The remaining CGR materials were stored inside the glovebox in bottles wrapped with aluminum foil to prevent light exposure.

SEM Examination

Particle morphology and elemental composition of CGR before and after interaction with As were examined using a JEOL JSM-6360 scanning electron microscope equipped with an Oxford Instruments energy dispersive X-ray spectroscopy (EDX) system. The atomic percentage of the elements present on the iron particles were semiquantitatively determined using EDX. Care was taken not to oxidize CGR during sample transfer from the glovebox to the SEM instrument.

X-ray Diffraction

Fresh synthetic CGR and As(V)/As(III)-treated CGR materials were examined with X-ray diffraction technique. CGR was reacted with As(V) or As(III) at an As concentration of 750 mg L^{-1} (0.05 g CGR in 18 mL of solution) for time periods up to 60 days. Chemical reagents of $NaH_2AsO_4 \bullet 7H_2O$ (Baker) and $NaAsO_2$ (Baker) were used. CGR particles in suspension were filtered through a 2.5 cm diameter 0.22 μm membrane, rinsed with deionized and deoxygenated water, and dried in the glovebox on the filter membrane for at least 3 h at 23 ± 1°C and humidity of 30 - 50%. CGR particles were mounted in the glovebox on a flat zero-background quartz slide. Approximately 20 mg of material was mixed with a drop of glycerol to form a smooth paste on the flat slide to prevent oxidation by air. The quartz slide was taken out of the glovebox and examined with a Rigaku Miniflex X-ray diffractometer at a scan rate of 0.5° 2θ min^{-1} (Fe Kα radiation; operated at 30 keV and 15 mA).

Arsenic Sorption Isotherms

Arsenic batch sorption experiments were performed inside the anaerobic glovebox at 23 ± 1°C. Duplicate samples of CGR suspensions at equivalent mass of 0.05 g were pipetted into 50 mL centrifuge tubes. Appropriate amounts of stock solutions of 2000 mg of As(V) L^{-1} or 2000 mg of As(III) L^{-1} were added to make the targeted initial concentrations of As(V) (25, 50, 100, 250, 500, and 750 mg L^{-1}) and of As(III) (50, 100, 250, 500, 750, and 1000 mg L^{-1}). The total volume of solution was 18 mL. The pH of the suspensions was generally not adjusted because the suspensions contained approximately 0.02 M $NaCO_3$ or $NaHCO_3$ in addition to 0.025 M Na_2SO_4 from CGR stock suspensions, which helped keep the final pH to the alkaline range typically found in Fe^0-based PRBs. For batch sorption experiments with target pH values lower than 10, CGR samples synthesized using $NaHCO_3$ were used and the centrifuge tube suspension pH values were adjusted with 1.0 M HCl. The tubes were capped, then wrapped with aluminum foil to prevent light exposure. The tubes were manually shaken periodically. At preset time intervals, the pH and Eh were measured in the suspension. Tubes were taken out of the glovebox and centrifuged for 30 min at 6000 rpm (2600 g). Thereafter, tubes were put back into the glovebox and 10 mL of the supernatant were filtered through 0.22 μm membranes before total As determination using Inductively Coupled Plasma-

Optical Emission Spectrometry (ICP-OES). Selected samples were also analyzed for As speciation with ion chromatography - hydride generation - atomic fluorescence spectrometry (IC-HG-AFS). As(V) and As(III) were first separated by IC, then reacted to form arsine gas through a hydride generation apparatus, and finally detected by an atomic fluorescence spectrometer using the PS Analytical Millennium Excalibur system (PSA 10.055). The quantification limit of the system was 5 μg of As L^{-1} for each As species. Total arsenic concentrations measured with ICP-OES were generally in good agreement within 10% with the sum of As(V) and As(III) from IC-HG-AFS measurements.

The Langmuir sorption isotherm, $X = KMC/(1 + KC)$, was used to describe As sorption as a function of equilibrium concentration, where X is the amount of As sorbed (mg kg^{-1}), K (L mg^{-1}) is a parameter related to the affinity of the sorbent for the sorbate, M (mg kg^{-1}) is the maximum As sorption capacity, and C is the As concentration in the equilibrium solution (mg L^{-1}). The value of X is calculated from the difference between the initially added As concentration and equilibrium As concentration as determined by ICP-OES. This isotherm is not useful for deriving sorption mechanisms. Its use is mostly for obtaining the M value because magnitude of the K value is probably devoid of any physical or chemical meaning with respect to the forces involved in sorption (*25*).

Speciation of Surface Sorbed Arsenic

At the completion of a batch As sorption experiment, the suspensions were centrifuged and supernatant solutions were removed. The solids were extracted with 18 mL of 1.0 M HCl for 24 h inside the glovebox in the dark. The extractants were then filtered through 0.22 μm membranes before As speciation was performed using IC-HG-AFS. The amount of As species on the solids was determined after gravimetrically correcting for the carry-over of As(V) and As(III) in the residual solution. In general, greater than 90% of the solids were dissolved by the 1.0 M HCl extraction. Minor amounts of magnetite were resistant to HCl extraction.

Results and Discussion

Characterization of Carbonate Green Rust

Fresh synthetic CGR suspensions typically exhibited values of pH of 10.5 and Eh of -450 mV after air sparging of the precipitates when Na_2CO_3 was used in the synthesis; and pH of 8.4 and Eh of -250 mV when $NaHCO_3$ was used. The synthetic CGR particles exhibited hexagonal platy morphology typical of GR under SEM (Figure 1). CGR particles were reacted with either As(V) or As(III) at initial As concentrations from 25 to 1000 mg L^{-1} for time periods from 2 h to

60 days, and did not show any detectable morphological changes based on SEM examination (data not shown). Although $FeSO_4$ was used in the synthesis of CGR, there is no evidence that the solid product contained any sulfate GR based on XRD examination. Measurement of dissolved sulfate concentration after CGR precipitation indicated that all added sulfate was distributed in the solution phase. CGR stored for 60 days inside the glovebox in the parent solution underwent partial decomposition to form magnetite and ferrous hydroxide [$(Fe(OH)_2$] and the suspension pH increased from 10.5 to 10.9; whereas, CGR reacted with As(V) or As(III) at initial concentrations of 750 mg L^{-1} for 60 days did not show XRD patterns other than those of CGR and trace amounts of magnetite (Figure 2). The results suggest that discrete As-containing solid phases most likely did not form under present experimental conditions. Surface precipitation may not be as important as surface adsorption with regard to bonding between As and CGR. A previous study showed that sulfate green rust reacted with a 3 mM mixture of As(V) and As(III) solution at pH 7 for 3 months resulted in the formation of crystalline parasymplesite [$Fe(II)_3(AsO_4)_2 \bullet 8H_2O$] (*26*). Because the pH in Fe^0-based PRBs is usually much greater than 7 and As concentrations are not commonly higher than the mM level, this solid phase may not be important in PRB applications.

EDX electron back scattering data (not shown) suggest that sorbed arsenic was evenly distributed over the CGR particles. There is no evidence for preferential enrichment of As on the edges of hexagonal crystals. EDX atomic ratio Fe/O for pure synthetic CGR was 0.15, lower than the ideal Fe/O ratio of 0.35, based on the commonly written formula as $Fe(II)_4Fe(III)_2(OH)_{12}CO_3 \bullet 2H_2O$.

Arsenic Sorption as Affected by Time, pH, and Arsenic Concentration

When As(V) was the initially added species, CGR suspensions were well buffered by the Na_2CO_3 inherited from the synthetic parent suspension to values close to pH 10.7; and Eh values were close to -400 mV, conditions typically found in Fe^0-based PRBs (Figure 3). As(V) sorption by CGR increased with increasing time and increasing equilibrium As(V) concentration (Figure 3). At time periods of 2 h and 1 day, As(V) sorption showed a small increase with increasing equilibrium As(V) concentration at levels greater than 250 mg L^{-1}; whereas, at longer periods of reaction time of 30 and 60 days, As(V) sorption kept increasing with increasing equilibrium As(V) concentration. The measured As(V) sorption on CGR was between 1 and 11 g kg^{-1}.

The relationship between As(V) sorption on CGR and equilibrium As(V) concentration was described satisfactorily with the Langmuir sorption isotherm (Table 1). The magnitude of the K value is probably just that of a fitting parameter. Longer reaction times (30 and 60 days) showed greater sorption capacity values than short reaction times (2 h and 1 day). It is possible that some

As(V) anions were able to migrate into the interlayers of CGR with increasing reaction time to replace carbonate ions and water molecules there; however, XRD results did not show any detectable changes in the d-spacing of CGR before and after As sorption.

There is no evidence of chemical reduction of added As(V) to form As(III) from the speciation data of dissolved As in the solution phase. Speciation of sorbed As on the surface of CGR via 1.0 M HCl extraction of CGR sorbed As also did not show any presence of As(III). Despite the low Eh reducing conditions, As(V) reduction in the CGR system did not take place even after reaction times of up to 60 days. As(V) reduction under such reducing conditions may be kinetically inhibited in the presence of CGR or is thermodynamically infeasible. Randall et al. (22) showed absence of reduction of added As(V) to sulfate green rust suspension at pH 7 for 24 h, and argued that the free energy (activity) of $H_2AsO_4^-$ is strongly decreased by formation of a stable surface adsorption complex on sulfate green rust. Our results show that As(V) reduction was not observed for reaction times even up to 60 days. This outcome could be advantageous because As(V) is less mobile and less toxic in aquatic environments.

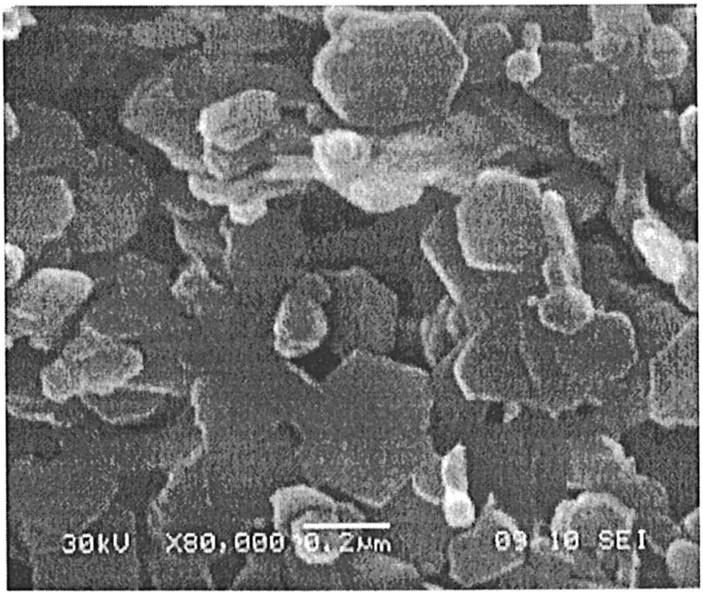

Figure 1. SEM micrograph of synthetic carbonate green rust showing mostly hexagonal platy particles.

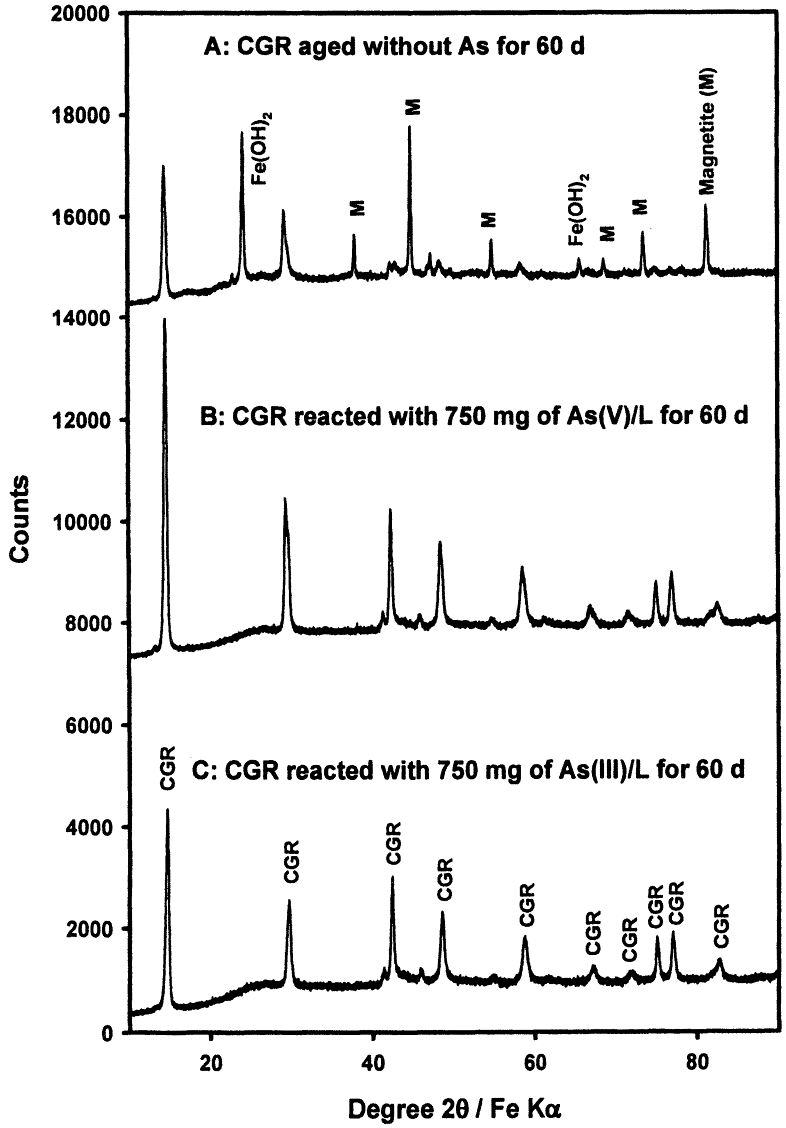

Figure 2. XRD of carbonate green rust after 60 days: (A) in the synthetic parent suspension (pH =10.9, Eh = -485 mV); (B) reacted with As(V) (pH =10.6, Eh = -417 mV); and (C) reacted with As(III) (pH = 10.4, Eh = -396 mV).

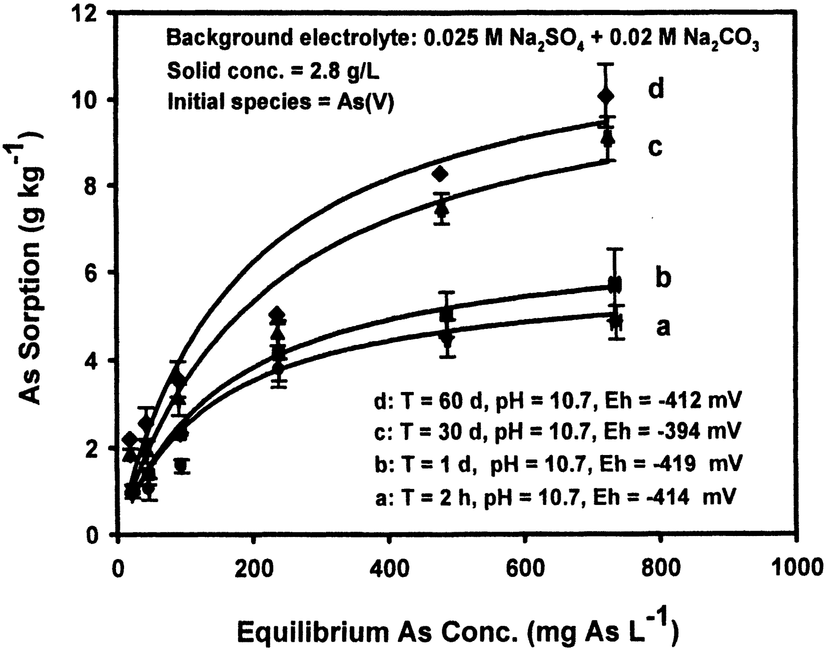

Figure 3. Arsenate sorption on carbonate green rust as a function of time and equilibrium arsenic concentration at 23 ± 1°C. Solid lines are Langmuir isotherm fits.

Measured As(III) sorption on CGR was 2 to 8 times greater than As(V) sorption at similar pH levels and initial As concentrations (Figure 4). This is consistent with the trend that shows greater sorption capacities for As(III) than for As(V) (Table 1). Our results are comparable to a recent study that demonstrated that both As(V) and As(III) have strong affinities for ferrihydrite, and that As(III) is adsorbed in much larger amounts than As(V) at pH > 7.5 or at high As concentrations in solution (*27*). Most As(III) sorption isotherms could be fit with the Langmuir equation with the exception of the 2 h (pH 10.5) batch experiment. Also, a less than satisfactory fit was observed for the pH 7.5 batch data. The striking difference in the amount of sorption between As(V) and As(III) by CGR may be partly explained by the difference of ionization behavior between arsenic acid (H_3AsO_4) and arsenious acid (H_3AsO_3). Arsenic acid undergoes stepwise dissociation to form $H_2AsO_4^-$, $HAsO_4^{2-}$, and AsO_4^{3-} with the correspondingly increasing dissociation constants ($pK_1 = 2.24$, $pK_2 = 6.96$, $pK_3 = 11.50$). At pH 10.7, about 90% of dissolved As(V) is in the form of $HAsO_4^{2-}$ and 10% in the form of AsO_4^{3-}. On the other hand, arsenious acid dissociates to form $H_2AsO_3^-$, $HAsO_3^{2-}$, and AsO_3^{3-} ($pK_1 = 9.29$, $pK_2 = 12.13$, $pK_3 = 13.4$). Dissolved As(III) in the solution of our study was mainly present in the form of $H_2AsO_3^-$ with minor amounts of the neutral species H_3AsO_3. There is no information available about the surface charge of CGR at pH ranges of 7.5 to 10.7, but we can assume that negative charge derived from dissolution of surface hydroxyl functional groups on CGR particles would increase with increasing pH. Most iron (hydr)oxides show net negative charge at pH > 10, and it is reasonable to assume that CGR particles would also be negatively charged at pH > 10. Because charge repulsion between CGR surface and the more negatively charged $HAsO_4^{2-}$ and AsO_4^{3-} anions would be greater than charge repulsion between CGR surface and the less negatively charged $H_2AsO_3^-$ anion and the neutral H_3AsO_3 molecule, less As(V) would be sorbed than As(III) by CGR at alkaline pH. Additionally, As(III) ions should have a greater tendency to migrate into the interlayers of CGR to replace carbonate ions because of the similarities between the molecular structure of $HAsO_3^{2-}$ and that of CO_3^{2-} (both have three oxygen atoms and show pyramidal molecular configuration). Further studies are needed to confirm this inference.

Table 1. Summary of Langmuir Sorption Isotherms for As(V) and As(III) on Carbonate Green Rust.

	Time	*pH*	*Eh(mV)*	*R^2*	*K(L mg^{-1})*	*M (mg kg^{-1})*
As(V)	2 h	10.7±0.1	-414±20	0.919	0.0071±0.0042	6.01±2.28
As(V)	1 d	10.7±0.1	-419±16	0.982	0.0062±0.0017	6.91±0.53
As(V)	30 d	10.7±0.1	-394±18	0.924	0.0046±0.0005	11.11±0.31
As(V)	60 d	10.7±0.1	-419±16	0.921	0.0055±0.0008	11.85±0.40
As(III)	2 h	10.5±0.2	-392±12	0.114	NA	NA
As(III)	1 d	10.4±0.2	-410±4	0.982	0.0037±0.0002	43.8±1.2
As(III)	30 d	10.3±0.2	-414±23	0.998	0.0071±0.0009	87.2±10.1
As(III)	60 d	10.6±0.2	-397±10	0.983	0.0195±0.0069	96.2±13.0
As(III)	1 d	9.3±0.1	-259±25	0.912	0.0058±0.0030	47.9±12.3
As(III)	1 d	7.5±0.3	-181±33	0.762	0.0022±0.0002	123±6

Previous studies using FTIR spectroscopy, electrophoretic mobility measurement, and proton balance determination on amorphous iron and aluminum oxide suggest that $HAsO_4$ and H_2AsO_3 are the dominant surface species (*28*). Inclusion of microscopic (ATR-FTIR) and macroscopic (sorption and electrophoretic mobility measurement) results suggest that As(V) forms an inner-sphere surface complex on both amorphous aluminum and iron oxides; whereas, As(III) forms both inner- and outer-sphere surface complexes on amorphous iron oxide and outer-sphere surface complexes on amorphous aluminum oxide (*29*). Studies on As(III) and As(V) adsorption complexes in the Fe^0 corrosion products and synthetic iron oxides (goethite, hematite, lepidocrocite, maghemite, and magnetite) by extended X-ray absorption fine structure (EXAFS) spectroscopy indicate that both As species form inner-sphere bidentate complexes (*8*). A recent EXAFS study further demonstrated that As(V) forms predominantly bidentate corner-sharing complex on the iron oxides (ferrihydrite, goethite, hematite, and maghemite) (*30*), the same complex found on sulfate GR (*22*). Further studies are needed to explore if As(III) also forms similar complexes with CGR. It will be interesting to see if similar surface complexes also exist on the surface and in the interlayer of CGR. It will also be desirable to confirm the oxidation of arsenite on CGR using spectropscopic methods such as FTIR and EXAFS.

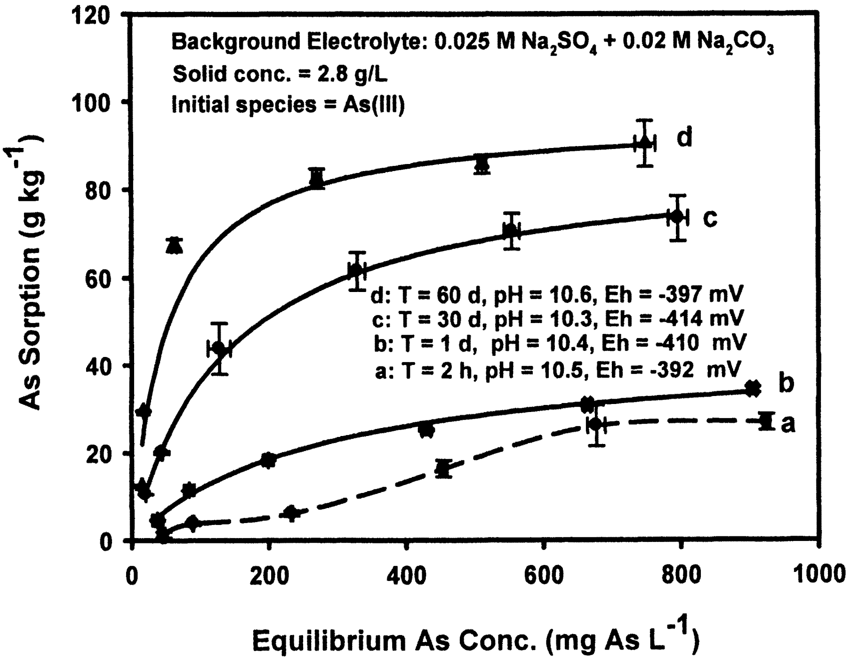

Figure 4. Arsenite sorption on and its surface oxidation by carbonate green rust as a function of time and equilibrium arsenic concentration at 23 ± 1 °C. Solid lines are Langmuir isotherm fits and broken line is a polynomial fit.

Arsenite Oxidation by Carbonate Green Rust

Preliminary tests showed that dissolved As(V) and As(III) at concentrations from 25 to 1000 mg L^{-1} in 1.0 M HCl in the absence of CGR solids are stable for at least two weeks. Therefore extraction of sorbed As on CGR by using 1.0 M HCl for 24 h should not change the As speciation for the sorbent. As(III) oxidation occurred for the one day (pH 7.5) batch test resulting in conversion of about 20% of sorbed As(III) to As(V) on the surface of CGR (Figure 5). Conversion of As(III) to As(V) also showed up in the solution for initial As(III) concentrations of less than 750 mg L^{-1} (less than 10% of total dissolved As). Because dissolved As(III) in water in the absence of CGR did not show any oxidation effect, it is concluded that As(III) oxidation must be a solid-promoted process. More As(III) oxidation (up to 80% of sorbed As(III)) took place at pH 10.4 (Figure 6) than at pH 7.5 (about 20% of sorbed As(III)) (Figure 5). More sorbed As(III) was oxidized on CGR at 60 days than at one day of reaction (data not shown).

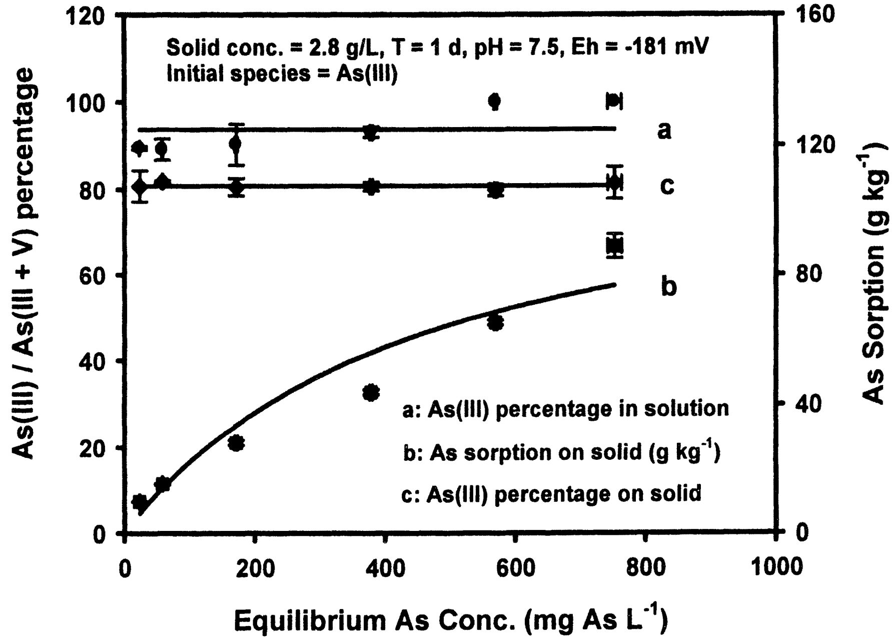

Figure 5. Arsenite sorption on and its surface oxidation by carbonate green rust at pH 7.5 as a function of equilibrium arsenic concentration.

Heterogneous oxidation of As(III) has been shown to occur in synthetic manganese oxides (*31-33*), clay minerals (*34*) and lake sediments (*35, 36*). Heterogeneous oxidation of As(III) to As(V) was observed in all four California soils studied and the recovery of As(V) from As(III)-treated soils was dependent on levels of oxalate-extractable manganese and soil texture (*37*). It was concluded that an abiotic process involving manganese oxide minerals was directly responsible for As(III) oxidation. The reagent $FeSO_4 \cdot 7H_2O$ we used to synthesize CGR contained trace amounts of Mn so that the total Mn concentration in synthetic CGR (determined from analysis of the 1.0 M HCl extract) was about 0.3 g kg^{-1}; however, this concentration was too low to explain the sole role of Mn impurity in As(III) oxidation in the CGR suspension. In addition, previous investigation of the pH dependence of As(III) oxidation by δ-MnO_2 determined that the oxidation reaction rate increases with decreasing pH (*32*). Our results showed that oxidation of As(III) by CGR increased with increasing pH, a contrary outcome as compared to the manganese oxides. A more reasonable candidate to serve as an oxidant in CGR therefore would be the ferric ion in the structure of CGR. Further studies are needed to see if ferrous iron is simultaneously produced in the process of As(III) oxidation by CGR.

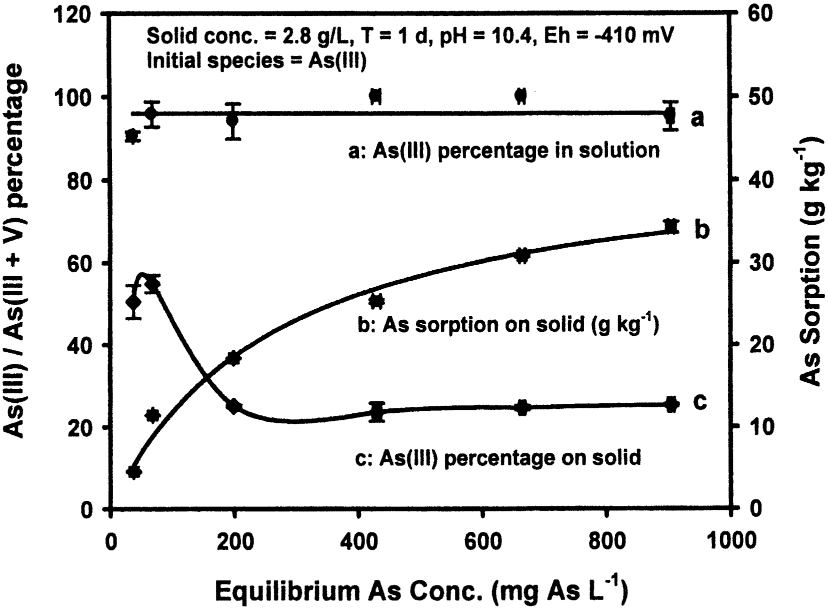

Figure 6. Arsenite sorption on and its surface oxidation by carbonate green rust at pH 10.4 as a function of equilibrium arsenic concentration.

Environmental Impacts

The stability of CGR affects the life-span and effectiveness of iron-based PRBs for groundwater arsenic remediation. Geochemical modeling for two PRB sites indicates that CGR is not the most stable iron mineral in PRBs and it eventually degrades to magnetite under anaerobic conditions (*18*); however, this study shows that sorption of anions such as As(V) and As(III) inhibits CGR degradation. Other anions such as phosphate and silicate are expected to exhibit similar effects. This protecting effect may prolong the effectiveness and longevity of a PRB for groundwater arsenic remediation as compared to a situation without these oxyanions. The green rust minerals will continue to sequester As even after the exhaustion of elemental iron. Although GR minerals are known to reduce a variety of anions such as chromate, nitrate, and selenate, this study shows no evidence of reduction of As(V) by CGR, which is a desirable outcome since As(III) is more toxic and more mobile than As(V) in groundwater systems.

Conclusions

More As(III) was sorbed by carbonate green rust than As(V) at pH values ranging from 7.5 to 10.7 under reducing conditions at ambient temperature. No reduction of As(V) was observed in CGR suspensions from 2 h to 60 days of contact. Sorbed As(III) was partly oxidized by CGR. Oxidation of sorbed As(III) increased with increasing time, increasing pH, and increasing amount of sorption. Sorbed As inhibited decomposition of CGR which may be more persistent than what may be predicted in the absence of As in the PRBs. This may have positive environmental remediation implications in that the effectiveness and longevity of Fe^0-based PRBs may be maintained for extended periods of time.

Acknowledgments

Although the research described in this report has been funded wholly by the United Sates Environmental Protection Agency, it has not been subjected to Agency review and, therefore, does not necessarily reflect the views of the Agency, and no official endorsement should be inferred. Analytical assistance was provided by Drs. Genevieve Betts, Ning Xu, and Jihua Hong with ManTech Environmental Research Services Corp.

References

1. Lackovic, J. A.; Nikolaidis, N. P.; Dobbs, G. M. *Environ. Eng. Sci.* **2000,** *17,* 29-39.

2. Khan, A. H.; Rasul, S. B.; Munir, A. K. M.; Habibuddowla, M.; Alauddin, M.; Newaz, S. S.; Hussam, A. *J. Environ. Sci. Health* **2000,** A35, 1021-1041.
3. Su, C.; Puls, R. W. *Environ. Sci. Technol.* **2001,** *35,* 1487-1492.
4. Farrell, J.; Wang, J.; O'Day, P.; Conklin, M. *Environ. Sci. Technol.* **2001,** *35,* 2026-2032.
5. Melitas, N.; Wang, J.; Conklin, M; O'Day, P.; Farrell, J. *Environ. Sci. Technol.* **2001,** *35,* 2074-2081.
6. Ramaswami, A.; Tawachsupa, S.; Isleyen, M. *Water Res.* **2001,** *35,* 4474-4479.
7. Melitas, N.; Conklin, M; Farrell, J. *Environ. Sci. Technol.* **2002,** *36,* 3188-3193.
8. Manning, B.A.; Hunt, M. L.; Amrhein, C.; Yarmoff, J. A. *Environ. Sci. Technol.* **2002,** *36,* 5455-5461.
9. Karschunke, K.; Jekel, M. *Water Sci. Technol: Water Supply.* **2002,** *2,* 237-245.
10. Wilkin, R. T.; McNeil, M. S. *Chemosphere* **2003,** *53,* 715-725.
11. Su, C.; Puls, R. W. *Environ. Sci. Technol.* **2003,** *37,* 2582-2587.
12. Nikolaidis, N. P.; Dobbs, G. M.; Lackovic, J. A. *Water Res.* **2003,** *37,* 1417-1425.
13. Gu, B.; Phelps, T. J.; Liang, L.; Dickey, M. J.; Roh, Y.; Kinsall, B. L.; Palumbo, A. V.; Jacobs, G. K. *Environ. Sci. Technol.* **1999,** *33,* 2170-2177.
14. Roh, Y.; Lee, S.Y.; Elless, M.P. *Environ. Geol.* **2000,** *40,* 184-194.
15. Philips, D.H.; Watson, D.B.; Roh, Y.; Gu, B. *J. Environ. Qual.* **2003,** *32,* 2033-2045.
16. Liang, L.; Sullivan, A.B.; West, O.R.; Moline, G.R.; Kamolpornwijit, W. *Environ. Eng. Sci.* **2003,** *20,* 635-653.
17. Furukawa, Y.; Kim, J. W.; Watkins, J.; Wilkin, R. T. *Environ. Sci. Technol.* **2002,** *36,* 5469-5475.
18. Wilkin, R. T.; Puls, R. W.; Sewell, G. W. *Long-term performance of permeable reactive barriers using zero-valent iron: An evaluation at two sites;* U.S. EPA Environ. Res. Brief, EPA/600/S-02/001, 2002.
19. Trolard, F.; Genin, J.M.R.; Abdelmoula, M.; Bourrie, G.; Humbert, B.; Herbillon, A. *Geochim. Cosmochim. Acta* **1997,** *61,* 1107-1111.
20. Scheidegger, A.M.; Grolimund, D.; Cui, D.; Devoy, J.; Spahiu, K.; Wersin, P.; Bonhoure, I.; Janousch, M. *J. Phys. IV France* **2003,** *104,* 417-420.
21. Myneni, S.C.B.; Tokunaga, T.K.; Brown, G.E. *Science* **1997,** *278,* 1106-1109.
22. Randall, S.R.; Sherman, D.M.; Ragnarsdottir, K. V. *Geochim. Cosmochim. Acta* **2001,** *65,* 1015-1023.
23. Bernal, J.D.; Dasgupta, D.R.; Mackay. *Clay Miner. Bull.* **1959,** *4,* 15-30.
24. Drissi, S.H.; Refait, P.; Abdelmoula, M.; Genin, J.M.R. *Corrosion Sci.* **1995,** *37,* 2025-2041.
25. Sposito, G. *The Chemistry of Soils;* Oxford University Press: New York, 1989.
26. Lin, Z.; Puls, R.W. *Adv. Environ. Res.* **2003,** *7,* 825-834.
27. Jain, A.; Raven, K.P.; Loeppert, R.H. *Environ. Sci. Technol.* **1999,** *33,* 1179-1184.
28. Suarez, D.L.; Goldberg, S.; Su, C. *Am. Chem. Soc. Symp. Ser.* **1998,** *No. 715,* 136-178.

29. Goldberg, S.; Johnston, C. T. *J. Colloid Interface Sci.* **2001,** *234,* 204-216.
30. Sherman, D.M.; Randall, S.R. *Geochim. Cosmochim. Acta* **2003,** *67,* 4223-4230.
31. Oscarson, D.W.; Huang, P.M.; Liaw, W.K. Hammer, U.T. *Soil Sci. Soc. Am. J.* **1983,** *47,* 644-648.
32. Scott, M.J.; Morgan, J.J. *Environ. Sci. Technol.* **1995,** *29,* 1898-1905.
33. Sun, X.; Doner, H.E. *Soil Sci.* **1998,** *163,* 278-287.
34. Manning, B. A.; Goldberg, S. *Environ. Sci. Technol.* **1997,** *31,* 2005-2011.
35. Oscarson, D.W.; Huang, P.M.; Liaw, W.K. *J. Environ. Qual.* **1980,** *9,* 700-703.
36. Oscarson, D.W.; Huang, P.M.; Liaw, W.K. *Clays Clay Miner.* **1981,** *29,* 219-225.
37. Manning, B.A.; Fendorf, S.E.; Suarez, D.L. *Am. Chem. Soc. Symp. Ser.* **2003,** *No. 835,* 57-69.

Chapter 4

Adsorption and Heterogeneous Reduction of Arsenic at the Phyllosilicate–Water Interface

L. Charlet[1], S. Chakraborty[1,2], S. Varma[3], C. Tournassat[1,4], M. Wolthers[1], D. Chatterjee[2], and G. Roman Ross[1]

[1]Environmental Geochemistry Group, LGIT-OSUG, University of Grenoble, BP 53, F–38041 Grenoble, Cedex 9, France
[2]Department of Chemistry, University of Kalyani, Kalyani 741 235, West Bengal, India
[3]Institute of Physics, Bhubaneswar 751005, India
[4]Current address: BRGM, BP 6009, F–45060 Orléans, Cedex 2, France

The Bengal Delta Plain (BDP) shallow aquifer is extensively used for public water supply but is severely polluted with naturally occurring arsenic, threatening the health of millions of people. Arsenic (III) is the most toxic and mobile aqueous arsenic species, but homogeneous reduction of As(V) is usually sluggish. Since in our study site field data indicate near equal amounts of As(III) and As(V), we investigated the heterogeneous reduction of arsenic at the muscovite-water interface, as muscovite is a mica frequently found in the BDP sediment. As(V) adsorption on muscovite was studied as a function of pH and compared to As(III) adsorption. The pH dependence for As(III) and As(V) adsorption are remarkably similar, and this similarity contrasts with the distinct reactivity of many minerals such as Fe and Mn (oxyhydr)oxides and other phyllosilicates towards the two species. The reacted muscovite samples were investigated by PIXE (Particle Induced X-Ray Emission) and XPS (X-Ray Photoelectron Spectroscopy)spectroscopy, and it was revealed that As(V) is completely reduced upon adsorption. This was also observed for muscovite flakes sampled in the upper aquifer sediment, and thus only As(III) sorption on muscovite was described

In Advances in Arsenic Research; O'Day, P., et al.;
ACS Symposium Series; American Chemical Society: Washington, DC, 2005.

using surface complexation modelling. In the presence of aqueous Fe(II), As(V) is also partly reduced to As(III) at the montmorillonite/water interface. The two investigated mineral surfaces have therefore been shown to catalyse, in different way, the reduction of As(V). Thus arsenic immobilization may be intimately linked to adsorption and electron transfer phenomena occurring at the phyllosilicate/water interface, and this may affect the transport of arsenic in anoxic groundwaters.

Introduction

The occurrence of elevated levels of As in soil and groundwater can compromise soil and water quality. For instance, over the past three decades, millions of tube-wells have been installed in the Ganges-Brahmaputra Bengale Delta Plain to provide pathogen free water for cooking and drinking. This unexpected arsenic-contaminated water is now affecting at least 30-50 million people in Bangladesh and West Bengal, India. Another 10 million people are also affected in Vietnam, Argentina, and Central America, and arsenic has now been recognized as one of the most widespread and problematic water contaminants (*1, 2*). In the environment, As(V) is present as ionic species, usually $H_2AsO_4^-$ or $HAsO_4^{2-}$, while the dominant form of As(III) species is the non-ionic $H_3AsO_3^\circ$ complex, a rather poorly sorbing and lipophyllic species.

Arsenic toxic and teratogenic effects depend strongly on this speciation. Elevated arsenic levels are likely to cause numerous cancers of the skin, liver, lungs and other internal organs (*3, 4*). The two usual ways of absorption of arsenic are by inhalation or ingestion, although there may be some degree of skin absorption of trivalent arsenic species since it is more lipid soluble than pentavalent species (*5*). Gastronintestinal uptake amounts to 60% for arsenate, 80% for arsenite and nearly 100% for methylated arsenic species (*6*). Once in the cell, As(III) may interact with specific functional groups such as protein thiol (R-SH) and sufhydryl (-SH) groups, inhibiting a variety of enzymes, e.g. in the pyruvate oxidase system (*7*). In contrast, As(V) uptake and metabolic disturbance is due to its substitution for phosphate, in particular in the glycolase reaction chain (*8, 9, 10*).

As a water contaminant, As(III) is more problematic than As(V). Previous studies seeking to understand the mechanism of arsenic mobilization have usually focused on sediment iron (oxyhydr)oxide coatings, due to the high affinity of these solids for arsenic (V) (*1, 11*). However, in the reductive conditions prevailing in the Holocene BDP shallow aquifer, little Fe (oxyhydr)oxide is found. The grey, fine- to medium-sized sand particles of this aquifer are made of quartz, feldspar and mica often coated with mixed Fe(II)/Fe(III) (oxyhydr)oxides (*12, 13, 14*). The reductive conditions prevailing in the BDP aquifer are thought to arise from oxygen consumption coupled to mineralisation of organic matter either deposited over the past 10,000 years, as sea-level rose from the previous glacial low stand (*13, 15*) or introduced in the last 50 years through irrigation and latrines (*16*). Once dissolved oxygen and nitrate supplied by recharge are consumed, further mineralisation of organic matter is thought to be coupled to the reductive dissolution of As-rich Fe (oxyhydr)oxides, particularly in river beds. This microbially-driven reduction, coupled to the release of bicarbonate and As(V) aqueous species has frequently been invoked as an arsenic mobilization mechanism (*17, 18, 16, 19*), and bacterial species involved have only recently been identified (*20, 21*); further reduction of the released As(V) to As(III) may be driven by the presence of sulfide ions.

An alternative explanation explored in the present paper is that As may be significantly reduced upon adsorption on mica and clay particles. Up to now, only few studies have investigated the adsorption and redox transformation of arsenic on aluminosilicate minerals, despite the abundance of these materials in the terrestrial environment. Kaolinite, montmorillonite and illite were shown to have higher affinities for As(V) than for As(III) (*22, 11*), and heterogeneous reduction of As(V) on phlogopite, an Fe(II) free micas, was shown to occur in the presence of Fe(II) (*23*).

By studying arsenic surface reactions on muscovite and montmorillonite, the objective of the present study was to determine if a direct link could be established between groundwater As speciation and reactions occurring at the phyllosilicate/water interface. XPS and PIXE studies were conducted with large crystals of muscovite previously reacted with As(V) solution in order to determine the localisation of As sorption and the redox speciation of As ions sorbed on the mica surfaces. The very small crystallite size of montmorillonite particles prevents any fine characterisation of the As adsorption localisation with PIXE. Furthermore, montmorillonite is not able to sorb a sufficient amount of As to be detected by XPS and PIXE. Hence, only solution chemistry experiments were performed to assess the potential of specifically sorbed Fe(II) (24) towards the reduction of As(V) in solution. The results of these experiments are compared to field data collected in Chakdaha, West Bengal, India. XPS spectra of a natural Bengal muscovite and As speciation in groundwater as a function of pe, pH and Fe concentration equilibrium conditions are discussed.

Field Site, Material and Methods

Field Site and Sampling

Field investigations were conducted on a deep, unconfined silty sand aquifer in Chakdaha, 65 km North of Calcutta, West Bengal, India. The study area covers 19 km^2 (Latitude 23° 04′ 00″ N – 23° 06′00″; longitude 88° 30′ 00″ E – 88° 33′ 00″ E) and is situated in the heart of the BDP along the Hoogly River, a main tributary of the river Ganga. The BDP encompasses an integral part of the Ganga–Brahmaputra delta, the world's largest deltatic alluvium. The Ganges and Brahamaputra River sediment load is extremely high, reaching as much as 13 million tons per day during the monsoon season. The large alluvial plain, spreading southward down to the Bay of Bengal, is formed by successions of a fining upward sequence with occasional clay layers. The Ganga has shifted from time to time to the west during the Holocene. There is a gentle gradient with an elevation difference of 2 to 4 m generally sloping towards the southeast direction. At our site, a natural levee separates the paddy-field floodplain located to the West, along the Hoogly River, from the inhabited area located to the East, along the railway (Figure 1). Most tube wells sampled throughout the study area are 20 to 25 m deep and are located in the shallow Holocene aquifer, below a 15-20 m thick silt to silty clay layer (*19*).

Water sampling was conducted in March-April 2002. Groundwater was siphoned during steady pumping using a hand-pump until pH and redox potential reading had stabilized (i.e. long enough to flush several times the 21-liters interval of a typically 20-meter deep well). Samples for chemical analysis of well waters were collected in previously acid-washed 60-ml high-density polyethylene bottles and subsamples to measure major and trace elements were immediately acidified to 1% HCl (Fisher Optima). Whenever possible, a multiprobe (multilane YSI) fitted with calibrated platinum redox and dissolved-oxygen electrodes was introduced directly into the groundwater. Chemical analytical methods are described in detail elsewhere (*19*). Briefly, samples for measurement of Fe(II) and sulfide were immediately collected with a syringe and filtered through a 0.45 μm cellulose ester filter membrane directly into pre-prepared colorimetric reagent solutions (*25*). Redox-sensitive constituents (Fe(II) and sulfide ions) were measured colorimetrically with a Hach DR 2010 spectrophotometer. Dissolved ferrous iron was measured using the O-phenantrolin method (*26*), and was found to be closed to saturation with respect to siderite, while Ca concentrations are at equilibrium with calcite (19). Calculations were made with Phreeqc2 and the Llnl.dat database. Sulfide was analysed using the method adapted from Fonselius (*27*). pH was measured on-site with a WTW 197 pH meter. To prevent any organic growth or decay, samples were refrigerated in an icebox within minutes after collection and laboratory. Sampling, sample filtration, treatment and measurement of Fe(II) and H_2S took about 2–3 h.

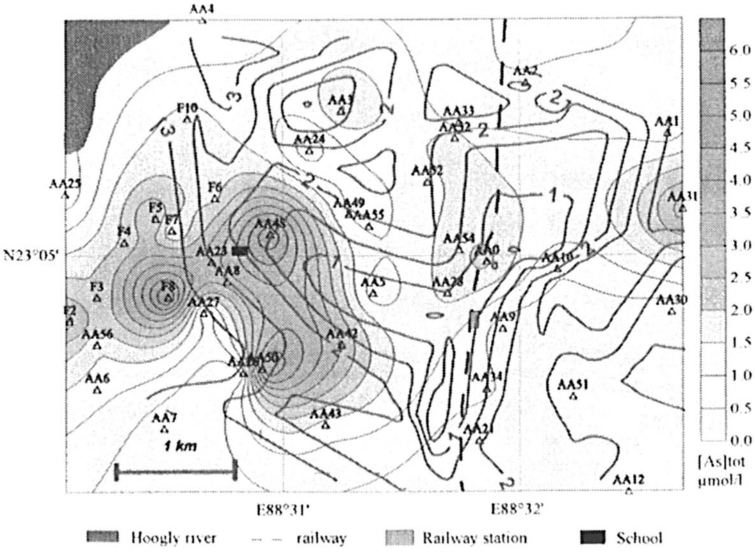
AA4
AA2
AA3
AA33
AA32
AA1
F10
AA24
AA52
AA25
F6
AA49
AA55
AA31
F5
F7
AA45
F4
AA23
AA8
AA54
AA40
N23°05'
F3
F8
AA27
AA5
AA28
AA30
F2
AA9
AA56
AA42
AA50
AA34
AA6
AA51
AA7
AA43
AA21
1 km
AA12
E88°31'
E88°32'
6.0
5.5
5.0
4.5
4.0
3.5
3.0
2.5
2.0
1.5
1.0
0.5
0.0
[As]tot
µmol/l
Hoogly river
railway
Railway station
School

Figure 1. Water table drawdown contour with well positions and groundwater total arsenic concentration at the study site, Chakdaha Block, Nadia district, 65 km north of Calcutta in West Bengal, India (data from (19)). The railway runs through the middle of the city. The black box outlines the 4 km x 5 km study area, located on the Hoogly River East bank. (See page 1 of color insert.)

An undisturbed sediment core was extracted from the 18-m-deep silty clay layer nearby the school (Figure 1). The 60-cm tube was sealed, put in a sealed bag filled with nitrogen and transported in an ice box to Grenoble, France, where the bag and the tube were opened in a glove box. Sediments were also sampled during manual drilling and collected at a depth of 12-15m. These samples were air-dried and muscovite micas were separated by hand plucking from dried sediment samples using a needle.

Mineral sorbents

The reference muscovite used in this study was obtained from Ward's Natural Science Establishment. It was ground with a pestle and mortar, to pass a <50 µm sieve, and used without any further pretreatment. Its chemical composition is $KAl_2(Si_3Al)O_{10}(OH,F)_2$. Specific surface areas of the sorbents were determined by single-point Brunauer-Emmet-Teller (BET) adsorption, and found to be equal to 14.28 m^2g^{-1}. X-ray diffraction (XRD) analysis of random powder mounts and oriented slide mounts indicated muscovite to be pure. In the discussion that follows, we refer to the (001) cleavage plane as the basal plane. For convenience we refer to the surfaces normal to (001) as the edge surfaces. In terms of the mica structure, the basal plane is parallel to the 2:1 structural layers, whereas the edge surfaces cut perpendicularly across the layers.

The montmorillonite clay sample was purified from an MX-80 bentonite sample (Wyoming bentonite, reference BF100, CETCO France) and Ca-saturated as described elsewhere (*28*). The <2 μm fraction contains trace impurities of amorphous silica, as indicated by XRD, and Fe hydroxides , as indicated by Mössbauer spectroscopy (*28*), and the various specific surface areas are described in details elsewhere (*29*). The chemical composition of the Ca-montmorillonite is $(Si_{3.98}Al_{0.02})(Al_{1.61}Fe^{3+}_{0.13}Fe^{2+}_{0.02}Mg_{0.24})\ O_{10}(OH)_2Ca_{0.14}$. (*29*).

Experimental design

Stock solutions of 15 mM As(III) or As(V) in de-ionized water (Millipore Milli-Q 18MΩ) were made from $NaAsO_2$ (Fluka) or $Na_2HAsO_4.7H_20$ (Fluka), respectively.

For XPS and PIXE measurements, large crystals of reference muscovite were shaken overnight with 10^{-3} M $NaNO_3$ (Fluka), and then As(V) stock solution (1.33 mM) was added and equilibrated for 24 hrs at room temperature (20.0 ± 1.0 °C) at pH 8.6. Muscovite samples were rinsed in a stream of deionised water, then air dried and stored in a vacuum desiccator, until XPS or PIXE measurements were performed. The XPS samples were mounted on the sample holder with double sided conducting carbon tape. One natural muscovite sample collected from an arsenic contaminated sediment and a synthetic muscovite sample reacted as described above were studied.

Batch experiments of As(III) and As(V) adsorption were performed in 40-ml polycarbonate centrifuge tubes by shaking mica suspensions containing 82.4 mg of micas in 20 mL of 13 μM As(III) or As(V)at room temperature (20.0 ± 1.0 °C) . Preliminary kinetic experiments indicated that 9 days were necessary for As concentration in solution to reach equilibrium (data not shown). Suspension pH (pH 3 to pH 8) was adjusted with 0.1 M NaOH/HCl after addition of the arsenic solutions. Ionic strength was maintained using 1.0 mM $NaNO_3$ background electrolyte. After 9 days, the tubes were centrifuged at 14400 rpm for 10 min, pH determined directly in the supernatant solutions with an Orion glass combined electrode followed by filtration with 0.22 μm cellulose acetate membranes. In these experiments, no attempt was made to exclude O_2 or CO_2.

As(V) reduction experiments were conducted in an N_2 atmosphere glove box (Jacomex) in which the pO_2 was monitored continuously by a Jacomex O_2 sensor. For these experiments, the O_2 content of the confined atmosphere never exceeded 0.5 ppm. A montmorillonite suspension (4 g L^{-1}) was prepared from

Ca-conditioned MX-80 clay fine fraction (<2 μm) and was allowed to equilibrate at 25.0 ± 1.0 °C with a Ca 0.05 mol/l solution in a 350 ml glass reactor. In order to minimize any influence of a pH change during the experiment, the suspension pH was buffered with a 0.1 M HEPPS buffer (4-(2-Hydroxyethyl)-piperazine-1-propane-sulfonic acid) and remained at a value of 5.85 ± 0.03 throughout the experiment. Then, Fe(II) was added (70 μM) to the suspension and the suspension was allowed to equilibrate for one month. At t = 0, As(V) was added to the suspension, as a Na_2HAsO_4 10 mM solution, so that the total As concentration was 8.5 μM. Redox potential and pH were monitored continuously with combined platinum and glass electrodes. Kinetics of As(V) reduction was followed by sampling the suspension, filtering the aliquots through a 0.22 μm pore size membrane, and analyzing the solution for total As and As(III) concentrations.

Arsenic Determination

Total arsenic was measured by ICP-AES (Inductively Coupled Plasma-Atomic Emission Spectrometry)(Perkin Elmer 3300 DV Optima) with a detection limit of 0.3 mmol L^{-1}, or by hydride generation atomic fluorescence spectroscopy (HG-AFS, Millenium Excalibur System, PS Analytical Ltd, Kent, UK) with a quantification limit of 1.5 nmol L^{-1}. All total As values were well above the detection limits. Spatial distribution of total arsenic concentration in the field site shallow aquifer is shown in Figure 1. To selectively analyze for As(III), we used two methods. In the analytical speciation method (*30*), aliquots from the filtered solutions were diluted at ratios between 1:500 and 1:50 into a 0.5 M Na_2H-citrate buffer. As(III) is selectively converted to AsH_3 under these conditions. It was verified that As oxidation in the citrate buffer continued only at a very slow rate. In the second method (*31*), species were separated using an anion exchange resin, which retains As(V) but not As(III). The difference between the two methods was not significant.

Speciation and Eh calculations were carried out using PhreeqC2 and Llnl.dat database (*32*). All calculations were performed using the actual groundwater temperatures measured in the field, which ranged between 26 and 29 °C.

XPS and PIXE Spectroscopy

The XPS measurements were conducted using a VG system with a base pressure of 1 x 10^{-10} Torr at the Insitute of Physics, Bubaneshwar, India. The analyzer was operated with a pass energy of 200eV for large size survey scans of 0-1000eV. For high resolution scans a pass energy of 50 or 20eV was utilized. The XPS system is equipped with dual Mg-Al anodes and a hemispherical analyzer.

Non-monochromatic Mg Kα (1253.6eV) radiation was used at 300W. The instrumental resolution is about 0.9 eV. Data were acquired at a take-off angle, that is, the angle between the sample normal and the analyzer axis, of 30°. Total analysis time ranged from 1 to 2 h, and the analytical reproducibility was 5%. Since muscovite is an insulator, we first investigated for charge corrections the C_{1s} feature in survey scans (Figure 2) and calculated the binding energy shift in this feature from the referenced value of adventitious C_{1s} value of 284.6 eV. Value of shift measured were applied to correct the binding energy position of all other peaks, observed in the high resolution regional scans (approx. 30eV wide regions with step size 0.025eV) for all the elements of interest. This method of charge correction is routinely applied in XPS for non conducting and powdered samples (*33*), while the charge neutralization method using flood gun sometimes creates differential charging in the different grains of the powdered sample.

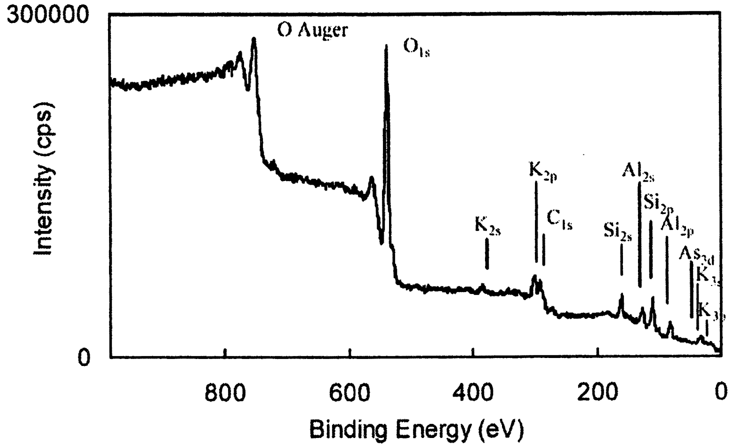

Figure 2. Survey Scan of the muscovite reference sample reacted with As

For these samples, it was of interest to specifically investigate the surface species present on both the natural as well as the synthetic muscovite. In order to increase the surface sensitivity of the XPS experiments, the sample (normal) was rotated by a polar angle, θ, with respect to the analyzer axis (considered $\theta=0^0$). In XPS, the probing depth, d, of the sample is given by $\sim 3\lambda\cos\theta$ where λ is the mean free path of the observed photoelectrons. An increased polar angle θ would have increased the surface sensitivity, but decreased the X-ray flux on the sample leading to an increase in the X-ray exposure time which was not desirable. Hence $\theta=30^0$ was chosen as an optimum parameter of our system for this experiment. With $\theta=30^0$ and $\lambda\sim10$ Å for As_{3d} electrons, the probing depth is about 25 Å.

An adequate signal to noise ratio for As_{3d} was attained in 5-10 min. With the inclusion of setup time, the samples were exposed to X-rays for a total of 15-20 min. No changes in peak position or shape were noticeable over this time interval. In fact, no change was noticeable even after 10h of exposure to the X-rays. Peak positions were referenced to the binding energy of adventitious C_{1s} at 284.6eV and compared to the NIST database, version 1.0. Background was subtracted with either a linear or a Shirley fit. The same background fitting procedure was used for each element.

PIXE spectroscopy was performed using 3.07 MeV $4He^+$ at the Laboratoire Pierre Sue nuclear microprobe facility in Saclay, France. Reacted muscovite samples were mounted on pure silica SUPRASIL slides. PIXE spectra were collected using Si(Li) X-Ray detector and they were analyzed using GUPIX data reduction software (34). Elemental mapping was obtained using a 2μm beam.The detection limit for arsenic is 10 $mgkg^{-1}$.

Modeling As Adsorption data

The constant capacitance (CC) model was used to describe the sorption of As(III) onto the muscovite surface as a function of pH. The CC model is an equilibrium surface complexation model, in which it is assumed that ion adsorption occurs by an inner-sphere ligand exchange mechanism (*34*). In a first approach, the hydrated muscovite surface is described by one surface reactive site, assumed to protonate and deprotonate according to the following surface protonation reactions:

(1) $\equiv SOH^\circ + H^+ \leftrightarrow \equiv SOH_2^+$ K_1^{app}

(2) $\equiv SOH^\circ \leftrightarrow \equiv SO^- + H^+$ K_2^{app}

where $\equiv SOH^\circ$ is the neutral surface group which can protonate (reaction 1) and deprotonate (reaction 2). K_1^{app} and K_2^{app} are the apparent proton affinities and are variable model parameters.

The pH-dependence of As(III) sorption onto muscovite was modeled by considering the simple, chemically reasonable, model given by equations (1) and (2) and an inner-sphere complexation of the neutral arsenite $As(OH)_3^\circ$ complex, the dominant aqueous As(III) species, by ligand exchange with the neutral surface site:

(3) $\equiv SOH^\circ + As(OH)_3 \leftrightarrow \equiv S\text{-}O\text{-}As(OH)_2 + H_2O$ K_{ads}^{app}

where K_{ads}^{app} is the apparent sorption constant and is a variable model parameter. The best fit by eye was obtained for the pH-dependence graphs. In each step, first the computer program MINEQL+ 4.06 (36) was used to calculate the surface speciation from estimated K values for Equations 1– 3, using the constant capacitance model with a specific capacitance of 1.0 F m^{-2} (Faraday per square meter). In modeling the As sorption data, the site concentration and the protolysis and sorption constants for As(III) sorption at the illite surface (*11*) were, in absence of muscovite titration data, taken as a first-estimate for the muscovite surface and adapted within the fitting procedure. This means that four adjustable parameters were optimized to achieve a satisfactory fit to the sorption pH-dependence data. Note that modeling was performed throughout at the actual muscovite concentration.

Results and Discussion

Arsenic Adsorption on micas

The effect of pH on the adsorption of As(III) and As(V) onto muscovite is shown in Figure 3. The similarity between the As(III) and As(V) adsorption edge curves is striking and contrasts with the edges observed on other phyllosilicates where As(V), i.e. $H_2AsO_4^-$ and $HAsO_4^{-2}$, is commonly more strongly adsorbed than As(III), i.e. $As(OH)_3^\circ$ (e.g. *11, 37*). Below, some spectroscopic evidence will be discussed, which may account for this similarity.

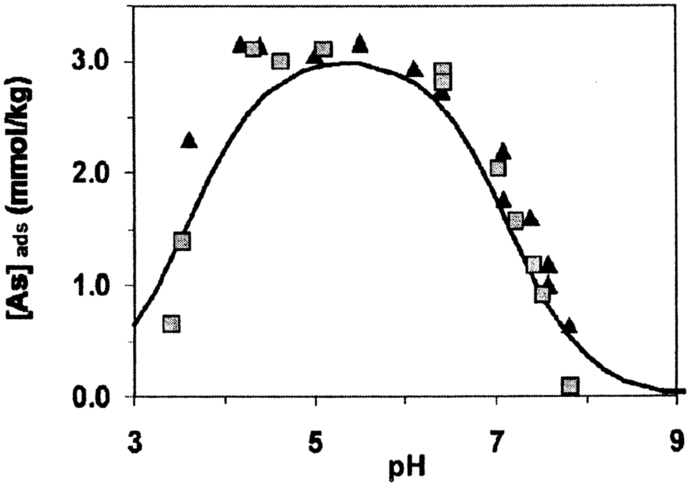

Figure 3. Effect of pH on the adsorption of As(III) (squares) and As(V) (triangles) onto muscovite, with CC model output for As(III) sorption (solid line). Reaction conditions: 4.12 ± 0.12 g L^{-1}; $[As]_o$ = 13 µM; reaction time = 9 days; ionic background: 10^{-3} M $NaNO_3$.

The result of the CC modeling of the As(III) sorption data set is shown as a line in Figure 3. The solid line shows the sorbed arsenite species from the model calculations, that is, [$\equiv$S-O-As$(OH)_2$]. This fit was obtained with the following parameters: total site concentrations $[\equiv S]_T$ = 0.0035 mol kg $^{-1}$ = 0.25 sites nm^{-2};

$\log K_1^{app}$ = -1.75 ± 1.0; $\log K_2^{app}$ = +9.0 ± 1.0; $\log K_{ads}^{app}$ = +9.3 ± 1.0. The $\log K_i^{app}$ values indicate a point of zero net proton charge (PZNPC) of 5.25, a value within the accepted PZNPC range for phyllosilicates (*11, 28*). Note that, within a certain range, equally good fits were obtained by simultaneously increasing one apparent surface acidity constant and decreasing another. This interdependence is reflected in the error given for the $\log K_i^{app}$ values.

The amount of Si released to solution could influence arsenate and arsenite adsorption, since silicate ions were shown to strongly compete with arsenic for adsorption on Fe(III) hydroxide sites (*18, 20*). In the present experiments, aqueous silicic acid concentration steadily increased from 70 to 180 µM as pH increased from 3 to 9 (data not shown), while the total arsenic concentration was constant and equal to 13 µM. Thus the Si/As ratio never exceeded 30 in the investigated pH range, a ratio required to see an impact of silicate adsorption onto As adsorption (*20*).

Heterogeneous reduction of arsenic (V) in Fe(II) containing suspensions

Figure 4 shows the result of the As(V) reduction experiments performed in Fe(II) containing montmorillonite suspension. From t = 0 hr to t = 0.8 hr, a rapid decrease of As(V) concentration in solution (from 8.5 µmol/l to 3 µmol/l) was observed.

As(III) appears in solution after less than three minutes and its concentration remains stable afterwards, at ~0.2 µmol/l. As(V) concentration decreases slightly with time and attains 1.7 µmol L^{-1} at t ~ 70 hrs. At the end of the experiment, approximately 80 % of the total As concentration present in the suspension was sorbed onto the clay particles.

Since the only possible reductant present is Fe(II), these experiments show that sorbed Fe(II) (or Fe(II) present in the clay structure) is able to reduce part of As(V) into As(III). The efficiency of this mechanism can not be accurately evaluated because no information on the As speciation in the solid is available. Indeed the As content on the solid (1.6 mmol kg^{-1} or 120 ppm) was too low to carry out XPS and XANES (X-Ray Absorption Near Edge Structure) spectroscopic experiments (*33*).

Goldberg et al. (*11, 37*) showed that As(V) is sorbed more efficiently than As(III) on a SWy-1 montmorillonite. Hence, considering the greater solute concentration of As(V) than As(III) in our experiment, we may consider that sorbed As is mainly present as As(V). However, Manning and Goldberg (*11*) also showed that As sorbed as pure As(III) initially, is partially desorbed by phosphate ions as both As(III) and As(V) (experiments were performed in air), with desorbed As(V) representing 10-20 % of total desorbed As. This oxidation occurred in a period of less than 24 hours, which is fast, compared to the oxidation half-life of 8760 hrs by oxygen in homogeneous solution (*38*). Hence, it appears (i) that the oxidation rate in the Manning and Goldberg study (*11*) and

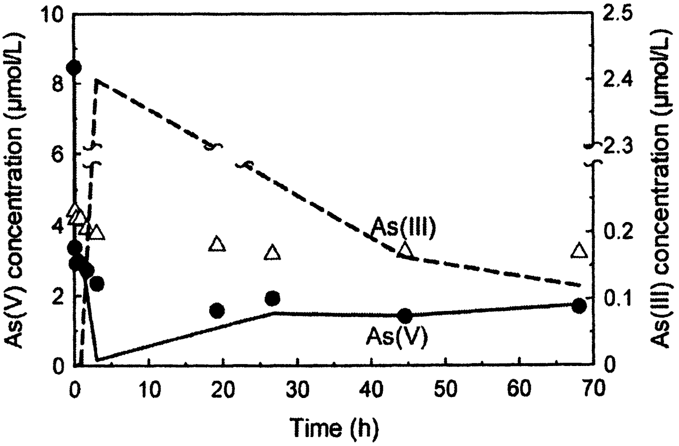

Figure 4. Results of the As(V) reduction experiment in clay suspensions in presence of Fe(II). As(III)(△) and As(V) (●) concentrations as a function of time. Dashed and solid lines show the calculated As(III) and As(V) concentrations respectively based on pe measurements and on the total As concentration (see text) Experimental conditions: 4 g clay L^{-1}; 0.05 M $CaCl_2$; pH = 5.85; $[Fe(II)]_{total}$ = 70 µM; [As]tot = 8.5 µM.

reduction rate in our study are both greatly enhanced by the presence of clay particles and (ii) that As redox speciation on the solid can not be simply inferred from As redox speciation in solution.

In our study, the redox potential was monitored with a platinum redox electrode.The As speciation in solution was calculated based on the total concentration of arsenic in solution at time t (Figure 4), on the measured redox potential of the suspension (Figure 5) and on the equation:

(4) $\frac{1}{2} H_2AsO_4^- + H^+ + e^- \leftrightarrow \frac{1}{2}H_2AsO_3^- + \frac{1}{4} H_2O \qquad K_{red} = 10^{-6.23}$

Even though the measured redox potential fluctuates strongly at the beginning of the experiment (and leads to a large overestimation of As(III) concentration, see Figure 4 and Figure 5), one can note a good agreement between measured and calculated As speciation in solution after 40h. Since Fe is more labile than As, we expect the redox electrode to be at equilibrium with the Fe(II)/Fe(III) redox couple. If this hypothesis is verified, this reduction experiment shows that the As redox speciation equilibrates with the redox potential, while the latter is fixed by the Fe composition of the suspension (Fe(II) in solution, Fe(II) on the solid, and Fe(III) in the solid) in a time period of approximately two days.

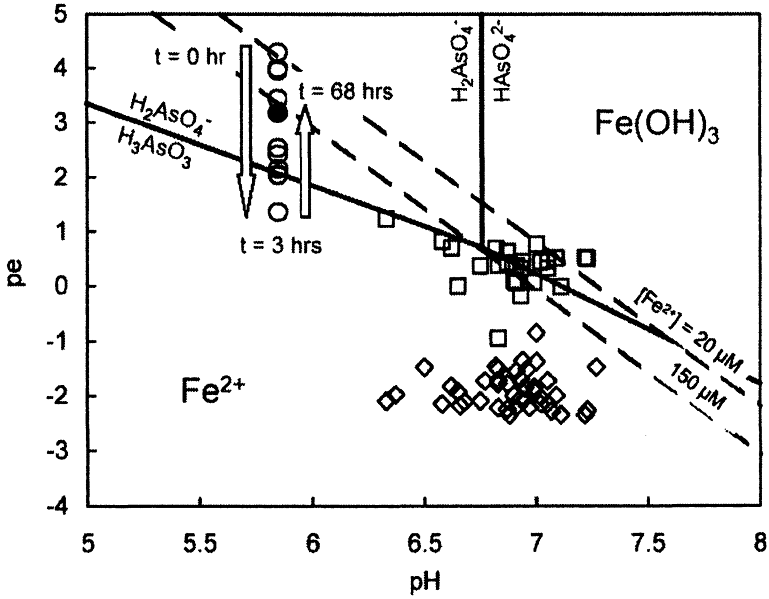

Figure 5. pe-pH diagram of arsenic and iron. Empty diamonds: redox potential measured in the field with a platinum electrode; Empty squares: redox potential given by the field As(III)/As(V) mole balance. Empty circles: redox potential measured as a function of time during the As(V) reduction experiment. Black dot is giving the redox potential at the end of the experiment. Dashed and solid lines are the limits between predominance domains of iron and arsenic, respectively. The dashed line is the limit between the $Fe(OH)_3$ *domain and the Fe(II) domain for an Fe(II) concentration in solution of 20 μM (experimental conditions) or 150 μM (field conditions) (calculations made with Phreeqc2 and the Llnl.dat database).*

Figure 5 also shows field redox potential measured in Bengal compared to redox potentials calculated using the As(III)/As(V) mole balance in groundwater.

The comparison shows a discrepancy between the values of 1.4 ± 0.3 pe units, the calculated pe being higher than the measured one. This discrepancy can be explained by three phenomena. The first one is a problem of electrode calibration and uncertainty on the measurement. The second one is kinetics, although we showed that a rapid equilibrium can be attained between the redox potential fixed by a clay-solute Fe(II) suspension and the As(III)/As(V) couple. Note that in the auifier the Fe(II) concentration is high, close to equilibrium with siderite (*19*). The third envisiaged phenomenon is the coexistence of other redox couples which are not at equilibrium with the Fe(II)/Fe(III) couple. S(-II) was always present below the detection limit (10 μmol L^{-1}). The assessed presence of S(-II) gives redox values approximately 1.5 pe units lower than measured (data not shown.) Hence, the measured pe value lies in-between values calculated with either the S(-II)/S(+VI) or the As(III)/As(V) couple. Assuming that As(III)/As(V) is a equilibrium with Fe(II)/Fe(III), this result would indicate that S(-II)/S(+VI) and Fe(II)/Fe(III) are not at equilibrium, due to the remaining presence of Fe(III) in a solid phase such as hydroxides or clay minerals for example. Mössbauer study of Fe redox state in the sediment would be useful to assess or invalidate this assumption.

Heterogeneous reduction of As in Fe(II)-free suspensions

The PIXE arsenic element map (Figure 6) shows an accumulation of As both on the mica edge, and to a lesser extent on the basal surface (to the right). However, since the PIXE pixel is about 1 µm wide, this basal surface may contain quite a few crystallographic steps. Therefore whereas sorption on the clay edge is confirmed, sorption on the basal plane could not be excluded. We therefore use in the above CC model an average surface site.

Figure 7 shows high resolution XPS scans of the reference muscovite sample reacted with As and of the natural muscovite sample. In the spectra, the presence of oxygen O_{2s} (24.95eV and 23,7 eV, respectively), potassium K_{3s} (near 33eV) and arsenic As_{3d} (near 40.8eV and 39.6 eV, respectively) was observed. The position of the O_{2s} feature is at the expected position (*33*). The K_{3s} feature indicate the presence of two components, at 31.5eV (K_1) and 33.5eV (K_2) (Figure 7 and Table I). The presence of two components of K suggests that potassium is present in two states. The K feature at 33.5eV represents the +1 state. The second peak represents a more reduced state. Indeed the exact binding energy of an electron depends on the oxidation state. Thus an atom that is in a reduced state will produce an XPS peak at a lower binding energy than that of an atom in a higher oxidation state.

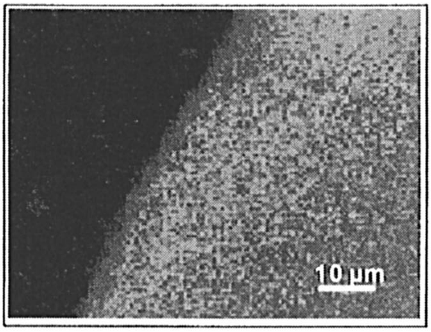

Figure 6. PIXE elemental map of a muscovite particle reacted with arsenic (V). Blue pixel: 16 mg kg^{-1} and pink pixel denoteAs concentration below detection limit (d.l. = 10 mg kg^{-1}). Reaction conditions: $[As(V)]_o$ = 1.3 mM, pH 8.6, I = 10^{-3} M $NaNO_3$. (See page 1 of color insert.)

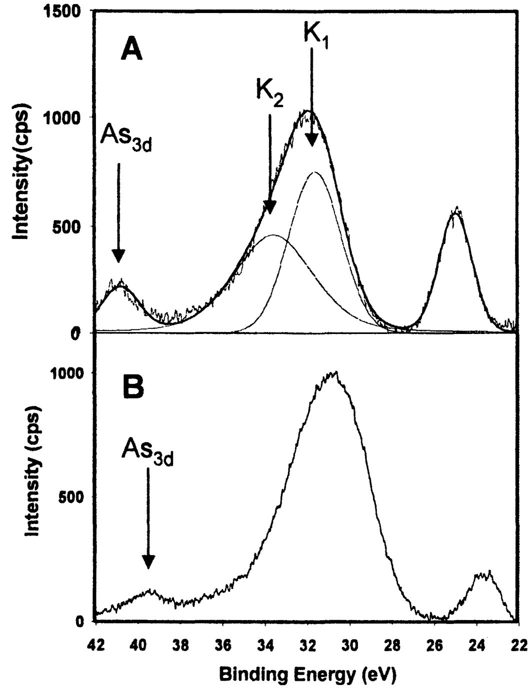

Figure 7. A. XPS spectra of muscovite basal plane after reaction with an aqueous solution containing As(V) = 1.33 X 10^{-3} M at pH = 8.6. B. XPS spectra of natural muscovite sample collected from arsenic contaminated sediment.

For instance, the position of As_{3d} should be at 44.4 eV for As(III) and 45.15 eV for As(V) (*39*). This difference in energy is of the same order as our resolution (0.9 eV), but the two peaks, if they existed, could a priori be resolved because a shoulder should appear on the prominent feature and as the overall FWHM should be bigger than for a single species.

Table-I: XPS data of the basal plane of reference muscovite and natural Bengal muscovite. Reference muscovite refers to a muscovite having been reacted with an aqueous solution containing As(V) = 1.33 mM at pH = 8.6

	Reference muscovite			Bengal muscovite		
Elements	Peak Height	Peak position	Ratio As/K	Peak Height	Peak position	Ratio As/K
As	204	40.8		105	39.7	
K_1	751	31.5	0.27	966	30.8	0.11
K_2	459	33.5	0.44	136	35.2	0.77

In our case however, the As_{3d} binding energy observed in Figure 7A is much smaller, with a 40.8 eV value similar to that observed in GaAs at ~40.7 eV (40). The As_{3d} peak observed on the natural muscovite indicates an even lower binding energy (Figure 7B). This confirms the macroscopic data (Figure 4) and represents additional supporting evidence for the reduction of arsenic at the muscovite/water interface.

Conclusion

Previous studies seeking to understand the elevated arsenic concentration in BDP groundwater have pointed out As-rich materials that occur in discrete layers in aquifer sediments, such as As-rich pyrite or Acid Volatile Sulfides (*41, 16*) and dispersed As associated primarily with iron oxyhydroxides (*42, 43*). The oxidation state of arsenic in these minerals have not been studied until now in detail. In the "oxidation hypothesis", As-rich Fe-sulfide were supposed to dissolve through oxidation driven partly by increased groundwater withdrawal. This cannot be the case at our study site, since piezometric level depression due to over pumping is only 4 meter deep (Figure 1), while wells are typically 15 to 25 meter deep and since a large excess of ferrous iron is always present in anoxic-rich groundwater and this Fe(II) would trap any dissolved oxygen (*19*). In the "reduction hypothesis", the reduction of As-rich Fe-oxides is assumed to result from increased oxygen demand possibly related to buried peat (*15, 43*), and organic matter introduction in the last twenty years by irrigation practices and latrines (*16*).

This study constitutes a reconnaissance effort designed to propose an alternative arsenic redox transformation hypothesis, i.e. to delineate the control on aqueous arsenic by the sorption and reduction of As(V) on phyllosilicate mineral surfaces. Muscovite and montmorillonite were shown to be effective in removing As(V) from aqueous solution in near neutral pH conditions. In the presence of aqueous ferrous iron, the experiments demonstrate that pentavalent arsenic is sorbed and reduced at the montmorillonite-water interface. XPS spectra of both muscovite flakes reacted with aqueous As(V) and muscovite flakes sampled in the upper sediments of the Ganges Delta Plain further demonstrate the occurrence of heterogeneous reduction of arsenic in the Bengal aquifer.

Acknowledgments

The program was partially funded by IFCPAR, ANDRA and the ACI "Eau". Exchange travels were funded by the Embassy of France in New Dehli and PROCOPE. Beamtime at ESRF and at the Laboratoire Pierre Sue, Saclay, as well as technical assistance by Hicham Kodja, Martine Lanson and Delphine

Tisserand are acknowledged. The authors thank Dr. T. Kotzer and another, anonymous, reviewer.

References

1. Smedley, P. L.; Kinniburgh, D. G. Appl. Geochem. **2002,** 17, 517 - 568.
2. Berg, M.; Hong Con Tran, R.; Thi Chuyen Nguyen, R.; Hung Viet Pham, R. S.; Chertenleib, R.; Giger, W. Environ. Sci. Technol. **2001,** 35, 2621 - 2626.
3. Smith, A. H.; Lingas, E. O.; Rahman, M. B. World Health Organ. **2000,** 78, 1093-1103.
4. Guidelines for drinking water quality, 2nd ed.; World Health Organization: Geneva, Switzerland, 1996; Vol. 2.
5. Winship, K. A. Adv. Drug React. Acute Poisoning Rev. **1984,** 3, 129-160.
6. Gebel, T. Chem.-Biol. Interact. **1997,** 107, 131-144.
7. Delnomdedieu, M.; Basti, M. M.; Otvos, J. D.; Thomas, D.J. Chem. Res. Toxicol. **1993,** 6, 598-602.
8. Dixon, H. B. F. Advances in Inorganic Chemistry **1997,** 44, 191-227.
9. Gresser, M. J. J. Biol. Chem. **1981,** 256, 5981-5983.

11. Aposhian, H. V. In Reviews in Biochemical Toxicology; Hodgson, E., Bend, J. R., Philpot, R. M., Eds.; Elsevier: New York, 1989; pp 265-299.
11. Manning, B. A.; Goldberg, S. Environ. Sci. Technol. **1997,** 31, 2005-2011.
12. Ansari, A. A. Ph. D. thesis, University of Erlangen-Nuremberg, Germany, 1997.
13. Kinniburgh, D. G.; Smedley, P. L. "Arsenic contamination of groundwater in Bangladesh," British Geological Survey and Department of Public Health Engineering (BGS/DPHE), 2001.
14. van Geen, A.; Rose, J.; Thoral, S.; Garnier, J. M.; Zheng, Y.; Bottero, J. Y. Geochim. Cosmochim. Ac. **2004,** in press.
15. McArthur, J. M.; Ravenscroft, P.; Safiulla, S.; Thirlwall, M. F. Water Resour. Res. **2001,** 37, 109-117.
16. Harvey, C.; Swartz, C. H.; Badruzzaman, A. B. M.; Keon-Blute, N. E.; Yu, W.; Ashraf Ali, M.; Jay, J.; Beckie, R.; Niedam, V.; Brabander, D. J.; Oates, P. M.; Ashfaque, K. N.; Islam, S.; Hemond, H. F.; Feroze Ahmed, M. Science **2002,** 298, 1602-1606.
17. Nickson, R. T.; McArthur, J. M.; Ravenscroft, P.; Burgess, W. G.; Ahmed, K. M. Appl. Geochem. **2000,** 15, 403-413.
18. Appelo, C. A. J.; Van der Weiden, M. J. J.; Tournassat, C.; Charlet, L. Environ. Sci. Technol. **2002,** 36, 3096-3103.
19. Charlet, L.; Chakraborty, S.; Appelo, C. A. J.; Roman-Ross, G.; Nath, B.; Ansari, A. A.; Musso, M.; Chatterjee, D.; Basu Mallick, S. Chem. Geol. **2004,** in press.

20. Thoral, S. Ph. D. thesis, Université Aix-Marseille III, Marseille, France, 2004.
21. Islam, F. S.; Gault, A. G.; Boothman, C.; Polya, D. A.; Chatterjee, D.; Lloyd, R. Nature **2004,** in press.
22. Frost, R. R.; Griffin, R. A. Soil Sci. Soc. Am. J. **1977,** 41, 53-57.
23. Charlet, L.; Bosbach, D.; Peretyashko, T. Chem. Geol. **2002,** 190, 303-319.
24. Tournassat C., Charlet L., and Greneche J. M. **2004** Geochim. Cosmochim. Acta 68 (11S): A162.
25. Lindsay, S. S.; Baedecker, M. J. Ground Water Contamination: field methods, ASTM STP 963; American Society for Testing and Materials: Philadelphia, 1986.
26. Vogel, A. I. Vogel's textbook of quantitative chemical analysis; Longman Scientific and Technical, 1989.
27. Fonselius, S. H. In Methods of Seawater Analysis; Grasshoff, M. E., Kremling, K., Eds.; Verlag Chemie: Germany, 1983.
28. Tournassat, C.; Greneche, J. M.; Tisserand, D.; Charlet, L. J. Colloid Interface Sci. **2004,** in press.
29. Tournassat, C.; Neaman, A.; Villiéras, F.; Bosbach, D.; Charlet, L. Am. Mineral. **2003,** 88, 1989-1995.
30. Kuhn, A.; Sigg, L. Limnol. Oceanogr. **1993,** 38, 1052-1059.
31. Kneebone, P. E.; Hering, J. G. Environ. Sci. Technol. **2000**, 34, 4307-4312.
32. Parkhurst, D. L.; Appelo, C. A. User's Guide to PHREEQC,U.S. Geological Survey, 1999.
33. Briggs, D.; Riviere, J. C. In Practical Surface Analysis by Auger and X-ray Photoelectron spectroscopy; 2nd ed.; Briggs, D., Seah, M. P., Eds.; John Wiley & Sons: New York, 1996; Vol. 1, p 438.
34. Maxwell, J. A.; Campbell, J. L.; Teesdale, W. J. Nucl. Instrum. Meth. B **1989**, 43, 218-230.
35. Dzombak, D. A.; Morel, F. M. M. Surface Complexation Modelling - Hydrous Ferric Oxide; John Wiley & Sons: New York, 1990.
36. Westall, J. ;Zachary, J.L. ;Morel, F. M. M. MINEQL: A computer program for the calculation of chemical equilibrium composition of aqueous systems, Massachusetts Institute of Technology: Cambridge, MA, 1976.
37. Goldberg, S. Soil Sci. Soc. Am J. **2002,** 66, 413-421.
38. Eary, L. E.; Schramke, J. A. In Chemical Modeling of Aqueous Systems II; ACS: Washington, DC, 1990; pp 379-396.
39. Nesbitt, H. W.; Canning, G. W.; Bancroft, G. M. Geochim. Cosmochim. Ac. **1998**, 62, 2097-2110.

40. Hou, T., Greenlief, C.M., Keller, S.W., Nelen, L., Kauffman, J.F. Chem. Mater **1997**, 9, 3181

41. Chaterjee, A.; Das, D.; Mandal, B. K.; Chowdhury, T. R.; Samanta, G.; Chakraborti, D. Analyst **1995**, 120, 643-650.

42. Bhattacharya, P.; Chaterjee, D.; Jacks, G. Int. J. Water Res. Dev. **1997**, 13, 79-92.

43. Nickson, R.; McArthur, J.; Burgess, W.; Ahmed, K. M.; Ravenscroft, P.; Rahman, M. Nature **1998**, 395, 338.

Chapter 5

Arsenic Uptake by Pyrite at Ambient Environmental Conditions: A Continuous-Flow Experiment

M. Wolthers[1], I. B. Butler[2], D. Rickard[2], and P. R. D. Mason[1]

[1]Faculty of Geosciences, Utrecht University, Utrecht, The Netherlands
[2]School of Earth, Ocean and Planetary Sciences, Cardiff University, Cardiff, Wales, United Kingdom

Pyrite was synthesized in the presence of arsenite, As(III), at concentrations approaching those in ambient environments, under controlled, monitored, anoxic conditions in a continuous-flow reaction system at pH 6 and 25°C. During the continuous pyrite growth in these experiments, a continued uptake of arsenic by pyrite was observed. No unequivocal effect of As(III) on the amount of pyrite or on the textures formed was observed. The results presented here demonstrate that a continuous-flow approach to experimentation allows the investigation of contaminant uptake at realistic concentrations. The net result of the reactions studied is the continued fixation of arsenic in pyrite, and the formation of arsenian pyrite. The uptake of arsenic by continuously growing pyrite strongly suggests that arsenic cannot be re-released into solution, unless pyrite is oxidatively dissolved. Furthermore, the synthesis of arsenian pyrite at ambient environmental conditions is in agreement with authigenic arsenian pyrite formed in, for example, marine sediments.

In Advances in Arsenic Research; O'Day, P., et al.;
ACS Symposium Series; American Chemical Society: Washington, DC, 2005.

Introduction

Pyrite (FeS_2) is the most stable and ubiquitous authigenic iron(II) sulfide phase in the Earth surface environment. Many different reactions for pyrite formation at ambient conditions have been suggested (e.g. *1*, *2*) but detailed mechanistic investigations are exceptional (*3–6*). A general conclusion is that the formation of the relatively oxidized S_2(–II) disulfide ion is a prerequisite step in any pyrite forming reaction (*7*). Nucleation of pyrite occurs on existing pyrite surfaces (*8*, *9*), on organic surfaces (*10*) and, possibly, on defects on the precursor FeS surface (*11*).

Extensive scavenging of trace elements by pyrite has been previously reported (*12*, *13*). Through this scavenging, pyrite plays an important role in retarding the migration of trace elements in the anoxic environment. Huerta-Diaz and Morse (*12*) found concentrations of As in marine sedimentary pyrites to be ranging up to 0.93 wt%. Their results indicated that sedimentary pyrite is an important sink for As, even if only minor pyrite formation has taken place.

In a recent study (*14*), the association of As(V) and As(III) with a nanoparticulate mackinawite (nominally FeS) was studied in batch experiments. It was shown that, with increasing initially added As(III) concentrations, the transformation of the pyrite precursor FeS to pyrite is inhibited by stabilization of the precursor mackinawite surface and (or) prevention of the essential intermediate aqueous FeS cluster complex (cf. *6*, *15*, *16*). However, batch experiments are limited by reactant concentrations and changing conditions during the experiments (*14*).

Here, the results of a pilot study making use of a chemostatic experimental approach to study dissolved As uptake in iron sulfide systems are reported. Pyrite synthesis in the presence of iron, sulphide and arsenic levels similar to those of natural anoxic sulphidic sediment pore waters (i.e., arsenic equals 0.02–4.01 µM, *17–19*) was studied under strictly controlled and monitored conditions in a continuous-flow reaction system (*9*). Arsenic was added as As(III), which is the dominant aqueous arsenic species in anoxic environments (*20–22*). The metastable persistence of mackinawite–H_2S suspensions in the absence of any other electron acceptor is well known (cf. *23*, *24*, *9*). Therefore, pyrite seeds were used to overcome the nucleation barrier and facilitate pyrite formation and As uptake (*8*). Changes in the solution chemistry were monitored *in situ* via electrodes and *ex situ* by regular sampling and ICP–MS and AAS analyses. The precipitates were characterized by scanning electron microscopy (SEM), X-ray powder diffraction (XRPD) and laser-ablation ICP–MS (LA–ICP–MS). The results are interpreted in terms of solution chemistry stability, pyrite textures formed, the effect of arsenic on, and the fate of As(III) during, pyrite formation.

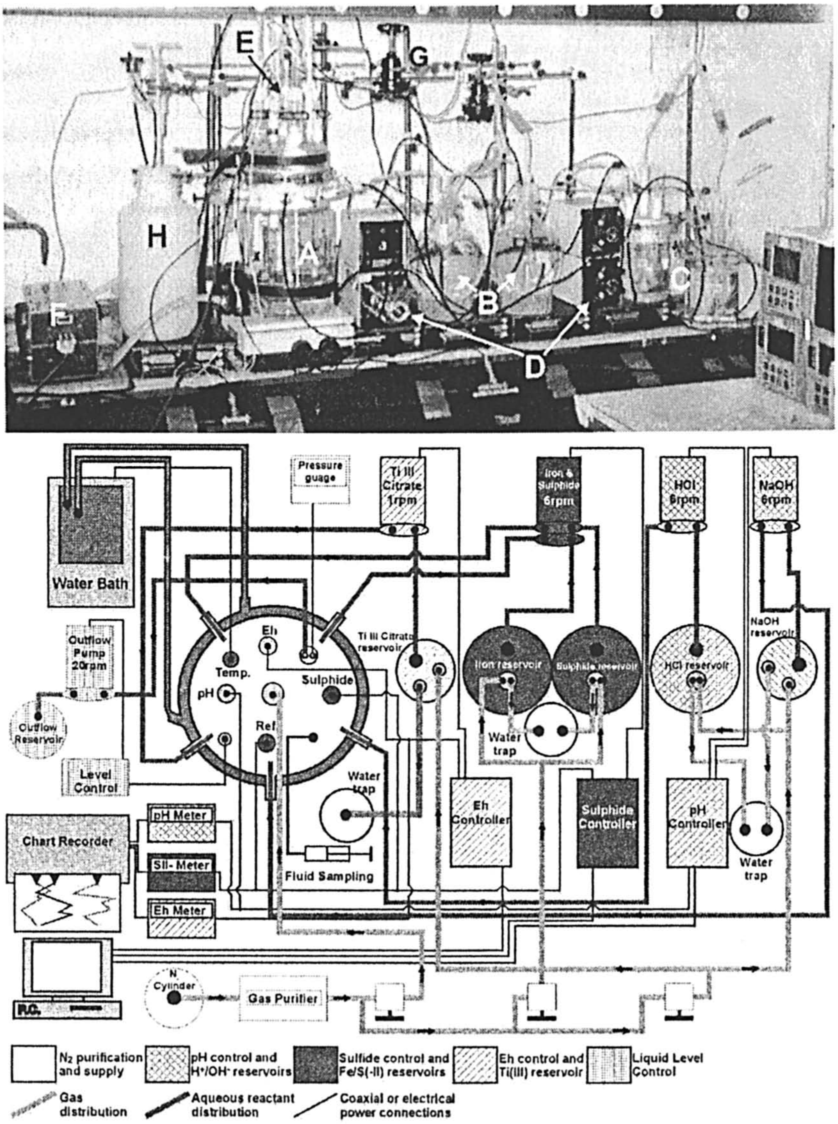
E
G
H
A
B
C
F
D
Pressure guage
Ti III Citrate 1rpm
Iron & Sulphide 6rpm
HCl 6rpm
NaOH 6rpm
Water Bath
Outflow Pump 20rpm
Outflow Reservoir
Level Control
Eh
Temp.
pH
Sulphide
Ref
Ti III Citrate reservoir
Iron reservoir
Sulphide reservoir
HCl reservoir
NaOH reservoir
Water trap
Water trap
Water trap
Eh Controller
Sulphide Controller
pH Controller
Chart Recorder
pH Meter
SII- Meter
Eh Meter
Fluid Sampling
P.C.
N Cylinder
Gas Purifier
N₂ purification and supply
pH control and H⁺/OH⁻ reservoirs
Sulfide control and Fe/S(-II) reservoirs
Eh control and Ti(III) reservoir
Liquid Level Control
Gas distribution
Aqueous reactant distribution
Coaxial or electrical power connections

Figure 1. A schematic overview (bottom) and photograph (top) of the continuous flow reaction system (after 9). (A) reaction vessel; (B) iron(II) and sulfide reservoirs; (C) acid and base reservoirs; (D) peristaltic pumps; (E) electrode entries at reaction-vessel head; (F) O_2-free N_2-gas purifier; (G) O_2-free N_2-gas flow-rate control valves; (H) outflow reservoir; (I) process controllers. See text for details.

Materials and methods

Materials

All reagents were analytical grade Fisher Chemicals and used without further purification. Solutions were prepared from 18 MΩ distilled deionized water. The background ionic medium was 0.2 M NaCl. Acid and base solutions were 0.01 M HCl and NaOH, respectively. A 2.0×10^{-3} M sulfide solution was made by dissolving $Na_2S{\cdot}9H_2O$. A 6.0×10^{-4} M Fe(II) solution was prepared from Mohr's salt ($Fe(NH_4)_2(SO_4)_2{\cdot}4H_2O$). The reaction vessel concentration of Fe(II) was controlled by the FeS solubility, while the S(-II) concentration is not controlled by the FeS solubility due to the excess addition of sulfide. A 1×10^{-2} M As(III) solution was prepared by dissolving $NaAsO_2$ in deionized water. The Fe(II) solution was spiked with As(III) by adding 0.1 mL of the As(III) solution. The As(III) reservoir concentration was 1.1×10^{-6} M. The solution in the reaction vessel was supersaturated with respect to crystalline orpiment but undersaturated with respect to amorphous As_2S_3 and other crystalline arsenic sulfides during the experimental runs (PHREEQC with the MINTEQ database and solubility data for As_2S_3(am) from *25*). Immediately after preparation, the solutions were poured into the O_2-free N_2-filled reservoirs of the chemostat (Figure 1), while vigorously purging with O_2-free N_2, and the reservoirs were sealed. Analytical grade O_2-free N_2 was passed through a Supelco high capacity gas purifier to remove traces of O_2 prior to flushing into the reservoirs and the chemostat (Figure 1). Cubic pyrite crystals, purchased at R.G. Widdowson (Scarborough, U.K.), were embedded in Epotech resin. The resin was cut into rectangles with two cm-sized pyrite cubes per block and from each cube one (001) face was exposed by carefully cutting and polishing off the resin. Before inserting the rectangular blocks into the reaction vessel, the quality of the exposed surfaces was investigated by SEM and the pyrite surfaces were cleaned by rinsing with 10% HCl and with acetone and dried. One pyrite face was covered with PTFE tape as a control face.

Continuous-flow reaction system

The custom-built continuous-flow reaction system, or chemostat, in the Cardiff laboratory was used (Figure 1). The main reaction vessel could be sealed air-tight and all connections for electrodes and tubing were air-tight clamped. Purified N_2 was delivered from a Supelco high capacity gas purifier (granular Zr at > 300°C) to the reaction vessel and reservoirs. The temperature in the reaction vessel was controlled at 40 ± 0.1° C. The solution volume was kept constant at 1.00 ± 0.02 L by a vertical float switch and controller connected to a 20 rpm peristaltic pump. The solution was kept homogenous by magnetic stirring (~60 rpm). The solution conditions in the reaction vessel were monitored using: (i) a gel-filled paper pulp combination pH electrode designed for reliability at high sulfide activity; (ii) a standard combination Pt electrode for redox potential monitoring and; (iii) a Ag/Ag_2S sulfide specific electrode with a double-junction calomel reference electrode (E in Figure 1). The pH electrode was calibrated using Hydrion pH 7.0 and 4.0 buffer solutions. The Pt electrode was checked using Zobell's solution and the sulfide electrode was equilibrated and checked in a concentrated $Na_2S{\cdot}9H_2O$ solution. The calibrations and electrode checks were performed prior to and after each experimental run. The pH controller was set to keep the pH in the reaction vessel constant at 6.0 ± 0.05 (Table I). The redox potential was not controlled, only monitored. The sulfide controller was set to a constant slow addition of reagents to the reaction vessel at 0.36 mL min^{-1} at 6 rpm via the low-flow (6 rpm) peristaltic pumps. The peristaltic-pump tubing was Masterflex LS13 Viton® tubing, which has extremely low O_2 permeability.

Continuous flow method

Before an experiment was started, the reservoirs and reaction vessel were filled and the system was purged with O_2-free N_2 for approximately 24 hours. The reaction vessel was filled with 1 litre of 0.2 M NaCl, to provide an identical electrolyte concentration to that of the reservoir solutions. After sealing the reaction vessel, internal pressure built up and pH and liquid-level control were initiated; after system stabilization, the reactant pumps were started. The As(III)-doped iron(II) solution and the sulfide solution were added via the same peristaltic pump. The initial concentration for all reactants at time zero was zero. It is ascertained that after day one, in both runs, steady state conditions for all reactants were achieved (Table I).

Sampling was done using a syringe and a tube incorporated in the wall of the vessel. Samples of ~40 mL were directly filtered through a Swinnex syringe filter-holder using a 0.2 μm cellulose nitrate membrane filter disk and a Whatman no. 4 glass-fiber prefilter. Subsamples of the filtrate were stored in a sealed glass vial at 4°C until acidification and analysis for total Fe and As. Filter disks were freeze-dried and immediately analyzed by XRPD. At the end of runs, 60 to 80 mL solution was sampled and filtered using a 0.02 μm Millipore filter under a N_2-filled hood. The solid was freeze-dried for ~24 hrs and stored at -18°C until XRPD analysis. Pyrite blocks were removed from the reaction vessel, during and at the end of runs, via a port in the lid. The blocks were washed with deionized water, freeze-dried and immediately Au-coated for SEM analyses. After coating, the blocks were stored in air-tight containers. After SEM analyses, the blocks were stored at −18°C for LA–ICP–MS analysis.

Analyses

Acidified solution samples were analyzed for total dissolved arsenic using a Perkin Elmer Elan 5000 ICP–MS. The detection limit was 6.5×10^{-9} M (blank ± $5 \times \sigma$). Total dissolved iron was measured using a Varian Spectra 300 acetylene-air-flame AAS. The detection limit was 7.4×10^{-9} M (blank ± $5 \times \sigma$); errors listed (Table I) are absolute analytical standard deviations. SEM images and energy-dispersive X-ray (EDX) analyses of the Au-coated pyrite blocks were collected on a Leica/Cambridge Instruments S360 SEM. XRPD was carried out using a Philips PW170 based diffractometer (Cu*K*α radiation, 35 kV, 40 mA). Freeze-dried samples on filter disks were loaded into a specimen holder. XRPD patterns, in the range of 3–80° 2θ, were collected under air using the following settings: 0.1 mm receiving slit, 0.4 s/0.02° 2θ counting time. Laser-ablation ICP–MS analyses of a reacted and an unreacted pyrite block surface were performed using a Micromass Platform ICP equipped with a hexapole device (collision cell) for ion focusing and a quadrupole mass analyzer. Samples were ablated with a Microlas GeoLas 193 nm laser-ablation system, which delivers a homogenized beam at the sample surface, ideal for depth analysis. The system hardware is described in more detail by (*26*). In order to work at the lowest possible ablation rate of ~0.1 μm per pulse, the laser was set to 0.03 GW cm^{-2} irradiance (*27*). The laser-crater diameter was 120 μm and the pulse repetition rate was 1 Hz.

Results

The experimental conditions during the two runs are listed in Table I. The electrode output signals were relatively stable after one day of reaction. In run 1, the sulfide electrode output was −544 ± 14 mV and in run 2 −534 ± 12 mV. The Eh closely followed the sulfide electrode signal. The total dissolved iron concentration was observed to decrease over the course of the runs, and was continuously below the iron concentration predicted from the iron monosulfide solubility product (*28*; calculated in MINEQL+ and thermo database). If it can be assumed that sulfide precipitated stoichiometrically with Fe, then the total sulfide concentration in the reaction vessel varied between 8×10^{-4} M (Fe:S = 1:1) and 4×10^{-4} M (Fe:S = 1:2). Dissolved arsenic was $(4.5 \pm 2.9) \times 10^{-9}$ M during the runs, which is ~5% of the reservoir concentration. Thus, the

Table I. Experimental conditions for runs 1 and 2. p_{rv} = pressure above ambient pressure; S(–II) and Eh are the uncalibrated raw millivolt signals from the sulfide and redox potential electrodes, respectively; $[Fe]_{aq}$ is the total dissolved iron concentration measured by AAS; $[As]_{aq}$ is the arsenic concentration measured by ICP–MS; XRPD-identifiable products; Py = pyrite, FeS = mackinawite, NaCl = Sodium chloride. Last column lists when which pyrite block was retrieved during the runs. See text for detection limits and standard deviations.

Run	*Day*	*p_{rv} (mbar)*	*pH*	*S(–II) (mV)*	*Eh (mV)*	*$[Fe]_{aq}$ ($\times 10^{-5}$ M)*	*$[As]_{aq}$ ($\times 10^{-8}$ M)*	*XRPD*	*Pyrite*
1	0	21	6.05	-123	-222				
	1	22	6.07	-530	-347				
	2	25	5.98	-535	-354	3.76 ± 0.07	2.7 ± 1.3	NaCl + FeS	
	3	23	6.03	-539	-359	3.12 ± 0.04	5.3 ± 1.3	NaCl	1A
	4	20	6.07	-548	-356				
	5	22	6.01	-547	-356				
	6	35	6.08	-558	-363	2.04 ± 0.04	2.7 ± 1.3	NaCl	
	7	27	6.02	-550	-360	2.90 ± 0.04	5.3 ± 1.3	NaCl	
	8	27	6.09	-548	-354	2.72 ± 0.06	6.7 ± 1.3	NaCl	
	9	29	6.12	-551	-350	2.15 ± 0.03	5.3 ± 1.3	NaCl + Py	1B
2	0	27	6.05	-70	-137				
	1	35	6.02	-522	-321				
	2	28	5.98	-532	-333	4.72 ± 0.06	6.7 ± 1.3	NaCl + FeS	
	3	22	6.09	-528	-334	4.83 ± 0.02	9.3 ± 1.3	NaCl	2A
	4	33	6.05	-527	-328				
	5	36	6.04	-532	-335				
	6	38	6.05	-538	-342				
	7	38	6.03	-547	-353	2.08 ± 0.01	d.l.	NaCl	
	8	37	6.05	-546	-393	2.44 ± 0.01	1.3 ± 1.3	NaCl	
	9	39	6.10	-545	-392			NaCl + Py	2B

conditions during the runs were stable and comparable between the two runs. The only significant difference was that, to keep the pH static in run 1, approximately twice the amount of acid was needed than in run 2, that is, 0.01 moles H^+ instead of 0.005 moles.

The suspended-solid concentration was generally too low to yield enough material for XRPD analyses during the runs, except at three days after reaction when the suspended FeS concentration was high enough. Usually, the only diffraction pattern observed was that of NaCl(s) (Table I) from the background ionic medium. A larger solid sample volume retrieved from the bottom of the reaction vessel after magnetic stirring was stopped, yielded enough material to show the presence of pyrite (Table I).

SEM imaging and EDX analyses confirmed the formation of pyrite on the pyrite blocks after 9 days of reaction in runs 1 and 2. In run 1 after 3 days, precipitated FeS was found within holes in the pyrite surface (*pyrite block 1A*, Figure 2a). EDX analysis of the precipitate returned Fe:S ratios characteristic of FeS. The block retrieved after 9 days displayed steps (*pyrite block 1B*, Figures 2b to 2d) and holes in the surface and the precipitate formed as a surface overgrowth consisted of subhedral sub-micrometer sized crystals (Figures 2c and d). Approximately 10% of the surface consisted of holes and cracks in the pyrite block. EDX analysis of the overgrowth (Figure 2b) returned Fe:S ratios characteristic of FeS_2. Analyses of the spherical particles formed on the overgrowth returned Na and Cl signals next to variable Fe:S ratios. Within the overgrowth, regularly shaped holes were observed (Figure 2b). In contrast, after three days in run 2, no SEM-identifiable material was formed (*pyrite block 2A*, Figure 3a). After nine days of reaction in run 2, an overgrowth of submicrometer-sized euhedral pyrite cubes on the surface of the pyrite block was formed and globular proto-framboidal pyrite formation occurred on the overgrowth (*pyrite block 2B*, Figures 3b to 3d). Less than 1% of the surface consisted of holes and cracks in the pyrite block. EDX analysis returned ratios characteristic of FeS_2 for both the microcrystalline overgrowth and the globular pyrite.

Figure 4 shows laser-ablation craters formed in the surface of reacted pyrite block 2B, which had been retrieved at the end of run 2. After approximately ten laser pulses, the boundary between the overgrowth and the underlying pyrite block was crossed (b in Figure 4). On the basis of the estimated ablation rate of 100 nm $pulse^{-1}$, this corresponds to an overgrowth thickness of ~1 μm, which agrees with the average overgrowth-thickness of ~1 μm estimated from the SEM observations (Figures 3b to 3d). Results from the depth analyses by LA–ICP–MS are plotted in Figure 5. Figure 5a shows the depth profile for the unreacted control surface of pyrite block 2B. At the start of ablation, which is marked by arrow 1 in Figure 5a, the response for $^{57}Fe^+$ rapidly increased while the response at masses (i.e., mass/charge or *m/z*) 30, 37 and notably 75 remained unchanged.

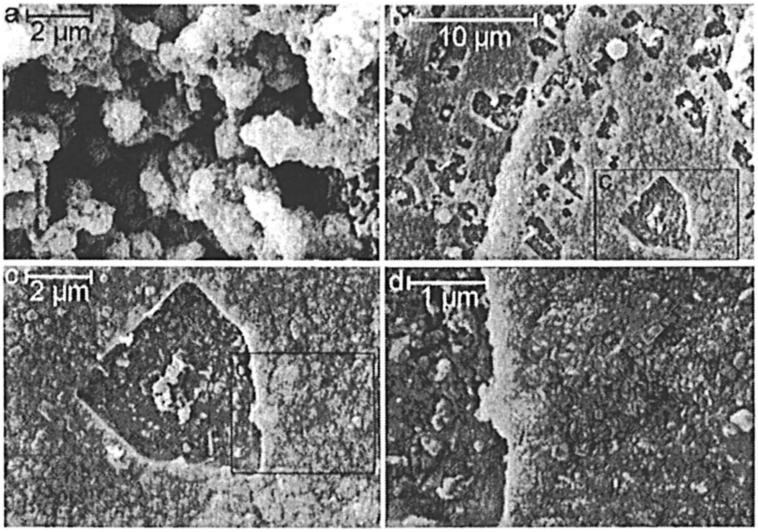

Figure 2. SEM images of (a) FeS precipitate formed on the cubic pyrite surface of pyrite block 1A after 3 days of reaction in run 1; (b) subhedral pyrite formed epitaxially on the pyrite block 1B surface after 9 days of reaction in run 1; (c) and (d) show details of (b).

This shows qualitatively that no arsenic, *m/z* = 75, was present at the surface of unreacted pyrite block 2B. At *m/z* = 30, $^{30}Si^+$ was analyzed simultaneously and the flat response for this isotope shows that no silicate inclusion was ablated. Depth analyses of reacted pyrite block 2B, showed a response- change for $^{57}Fe^+$ and $^{75}As^+$ at the start of ablation (arrow 1 in Figure 5b). With analysis-time and thus depth, the response for $^{57}Fe^+$ remained constant, while the response for $^{75}As^+$ dropped to the background level when the boundary between the overgrowth and the underlying pyrite was crossed (arrow 2 in Figure 5b). Isobaric interferences are possible at *m/z* = 75 from $^{40}Ar^{35}Cl^+$ polyatomic ion, which may be produced if the concentration of Cl in the system is high. To test this possibility, $^{37}Cl^+$ and $^{35}Cl^+$ were measured simultaneously during the analysis. Since there was no change in the $^{37}Cl^+$ signal and taking into account that $ArCl^+$ should form at 100–200 ppm level (*26*), the *m/z* = 75 cannot be explained by the production of $^{40}Ar^{35}Cl^+$. Furthermore, at *m/z* = 35, there was a small but constant increased signal after the start of the ablation which does not correlate with the signal at *m/z* = 75. This signal, which was also observed in the unreacted pyrite block (Figure 5a), is most likely due to the presence of $^{34}S^1H^+$ as seen in previous studies (*29*). The slopes of the curves as a response to concentration changes are not optimal, that is, not near-vertical (*27*). This is due to the small size of the sample chamber relative to the pyrite block. The resulting large dead volume in the sample chamber causes imperfect mixing of the ablated material and the carrier gas and thus imperfect response times to ablation.

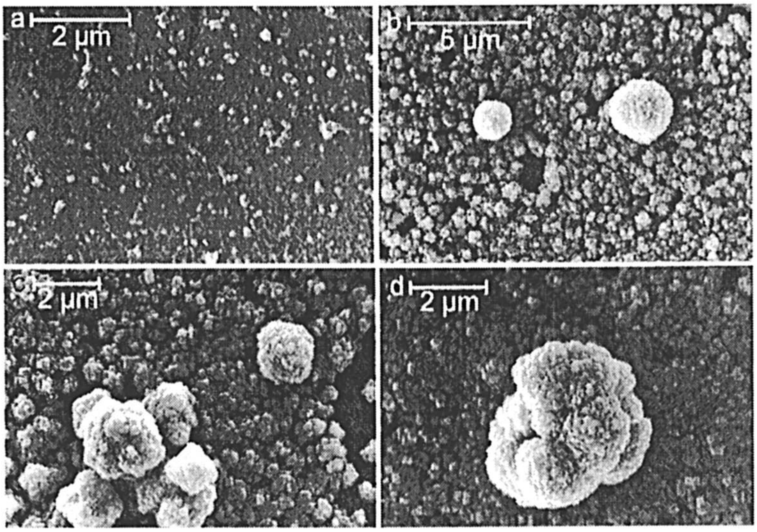

Figure 3. SEM images of products formed on (a) pyrite block 2A after 3 days and (b) – (d) on pyrite block 2B after 9 days of reaction in run 2. (a) unidentifiable precipitate formed on the still visible cubic pyrite surface; (b) euhedral cubic pyrite overgrowth, formed epitaxially on the cubic pyrite surface, and two solitary proto-framboids (cf. 5) formed on the euhedral-pyrite overgrowth; (c) solitary proto-framboid formed and proto-framboid cluster in the initial stage of forming on the euhedral-pyrite overgrowth; (d) proto-framboid cluster formed on the euhedral-pyrite overgrowth.

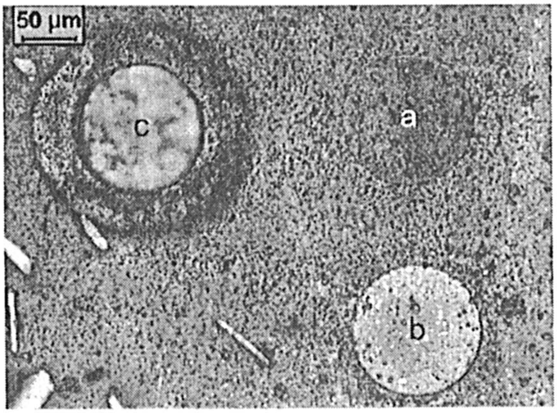

Figure 4. Laser ablation craters in the surface of pyrite block 2B (a) after 5 pulses; (b) after 10 pulses and; (c) after the analysis depicted in Figure 5b. Needle-shaped inclusions in the pyrite (bottom-left corner) are hornblende crystals.

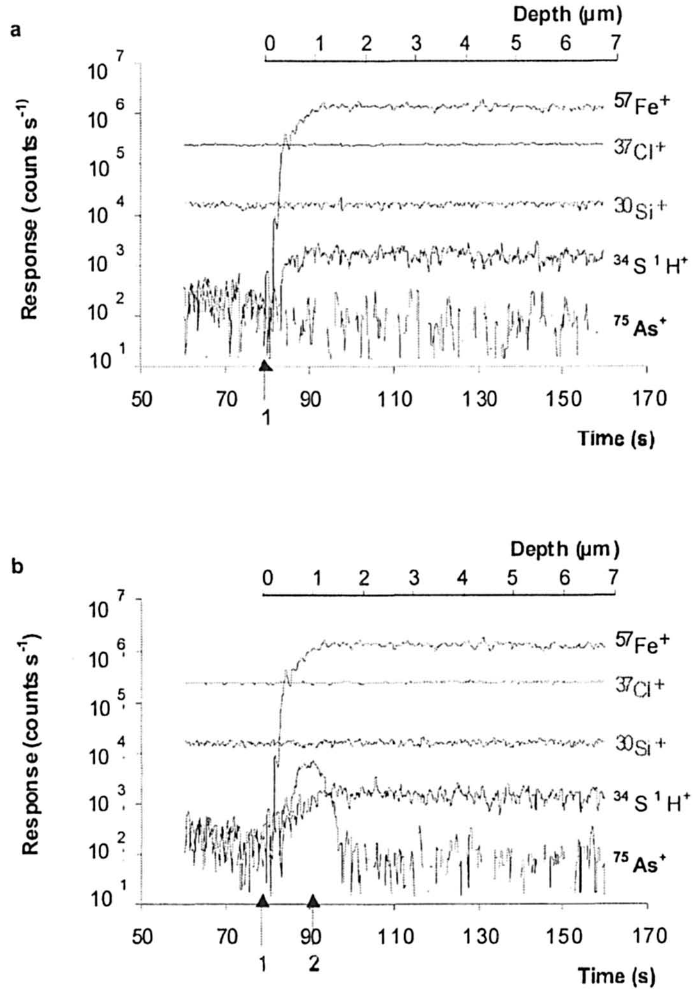

Figure 5. LA–ICP–MS depth profiles of (a) unreacted control section of pyrite block 2B and; (b) reacted section of pyrite block 2B. Arrow 1 marks the start of ablations; arrow 2 marks when the boundary between the overgrowth and the underlying pyrite was crossed. The signals were smoothed by averaging 5 points at equal weight.

However, the depth resolution of the system was sufficient to identify chemical differences between the 1 μm overgrowth and the underlying pyrite.

The results show qualitatively that arsenic was present in the overgrowth formed on the surface of reacted pyrite block 2B. Accurate quantification was not possible as laser ablation is dependent on sample matrix. Suitable matrix-matched metal sulfide standard reference materials which are homogenous at the sub-100μm scale do not currently exist (e.g. *30*). Nevertheless, a semi-quantitative calibration against NIST 612 glass, taking isotopic abundance, ionization efficiency and instrumental response into consideration gave an estimate of 200 ppm As in the FeS_2. The detection limit for As in pyrite in the EDX analyses was approximately 0.5 wt% (P. Fisher, pers. comm. to I.B.). Despite these stated problems, it can be inferred that the results of the LA–ICP–MS and EDX analyses are consistent.

Discussion

Pyrite textures

XRPD analysis showed the formation of pyrite in both runs. However, the pyrite textures formed varied between the two runs. The euhedral overgrowth and globular proto-framboidal pyrite-textures formed in run 2 after 9 days of reaction (Figures 3b to 3d) are identical to the blank runs with single crystal pyrite blocks and no arsenic present (Figure 6a and 6b, see also *9*), except for the lack of evidence for framboidal-pyrite formation. However, Butler et al. (*9*) proposed that the formation of framboidal pyrite in their experiments is partly controlled by hydrodynamics causing diffusion-limited niches in, for example, holes in the pyrite surface. The surface of block 2B was devoid of large holes in the surface, which may explain the lack of framboidal-pyrite formation. In contrast, the pyrite textures formed in run 1 are subhedral (Figures 2b to 2d). Although the subtle controls on pyrite textures developed in experimental systems are not well understood, the pyrite surface and the hydrodynamics are contributing factors controlling the pyrite textures formed (*9*). The results obtained from the present experiments provide no evidence for a specific control on the pyrite textures. Nevertheless, some important differences between the two runs were observed. After reaction, many more holes were observed at the surface of block 1B, than at the surface of block 2B. Furthermore, steps in the surface of block 1B were observed. Since they were not observed during SEM imaging of the surface prior to reaction, the steps may have formed by dissolution or growth of the pyrite block surface during run 1. Since the surface of block 1B contained more imperfections, the surface may have had more high-energy nucleation sites. This could explain the higher density of crystals formed at the surface of block 1B relative to block 2B. Through spatial constraints, this higher density would limit the size and shape of the crystals formed.

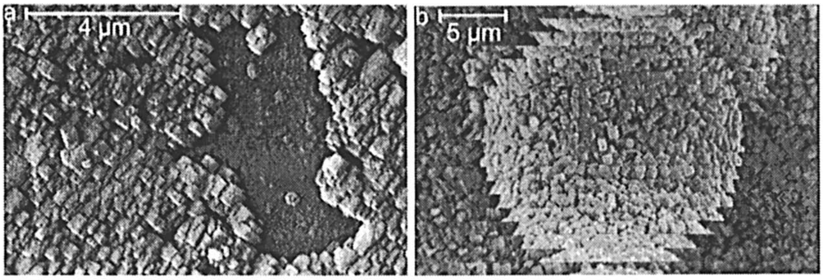

Figure 6. SEM image of the surface precipitates formed on the surface of a pyrite block after 37 days of reaction in a control run, i.e. no arsenic was present; (a) epitaxial pyrite overgrowth; (b) euhedral cubic pyrite overgrowth, formed expitaxially on the cubic pyrite surface, and a solitary framboid. Figures from (9).

In addition to the relative quality of the surfaces, one significant difference between the two runs was noted: the amount of acid needed to control the pH within the set boundaries. Approximately 0.01 mole of protons was consumed overall in run 1 and ~0.005 mole in run 2. The consumption was faster over the whole period of run 1. Since solution conditions did not vary strongly between the two runs (Table I), this proton consumption must be related to the solid phase. It could, for example, be related to dissolution of inclusions in the pyrite block. The observed steps, holes and regularly shaped "windows" in the pyrite overgrowth (Figure 2b) would support such a dissolution and indicate incomplete removal and coating of inclusions in pyrite block 1B. Other, more subtle differences between the two runs are a slightly lower redox potential as measured by the Eh electrode, and a stop of several hours in the supply of Fe(II) and sulfide on day 6 of run 1. It may be that the combination of the subtle differences with the differences in surface-quality of the pyrite blocks between runs 1 and 2 has triggered a switch from the formation of pyrite textures identical to previous experiments in the same set-up (*9*) to the formation of a subhedral texture.

Effect and fate of As(III)

Equilibrium calculations showed that the saturation index for crystalline orpiment, as defined by SI = log(I.A.P./K_{sp}), is > 13 after a steady state has been reached in the reaction vessel for both runs (PHREEQC with MINTEQ database). Modelling based on the solubility product for amorphous As_2S_3 from Eary (1992) showed that As_2S_3(am) and all other crystalline As-sulfides were strongly undersaturated. These calculations suggest that arsenic sulfide phases do not control the aqueous As concentration. It is possible that slow As-sulfide formation and continual addition of fresh aqueous arsenite lead to a steady state disequilibrium condition in the reaction vessel where aqueous As concentrations were not controlled directly by orpiment solubility for kinetic reasons. Nevertheless, no heterogeneous As distribution in the epitaxial overgrowth was observed by SEM–EDX, As was continuously below EDX detection limit, nor was a pure arsenic sulfide phase observed by XRD. So the precipitation of a pure As-sulfide mineral seems to be kinetically inhibited at these concentrations and pH, possibly due to the undersaturation with respect to As_2S_3(am) which may otherwise have served as a precursor phase.

The LA–ICP–MS data clearly showed As present in the newly formed pyrite layer. Also, the layer thickness based on ablation rate is consistent with visual observation, and the As concentration in the pyrite layer is semi-quatitatively estimated to be ~200 ppm.

In the highly supersaturated (i.e., nucleation dominated) batch experiments discussed in (*14*), a strong effect of arsenic on pyrite formation was observed. At arsenic concentrations similar to the arsenic reservoir concentration in the continuous-flow experiments, less pyrite was formed in comparison to arsenic-free control experiments. In the less supersaturated continuous-flow experiments presented here, pyrite crystal growth dominated nucleation during most of the experiment time. During the continuous pyrite growth in these experiments, a continued uptake of arsenic by pyrite is indicated by the constantly low aqueous arsenic concentration. Previously published experimental results indicate that pyrite nucleation is negatively affected by arsenic (*14*), yet the results presented here show that crystal growth is not, or not strongly, affected at similar arsenic concentrations. As discussed above, the pyrite textures varied between the runs, therefore, there is no unequivocal evidence for an effect of As(III) on the textures formed. Nevertheless, the formation of identical textures in run 2 (Figure 3) and in the blanks (Figure 6, see also *9*) suggest that As(III) at environmentally realistic concentrations used herein exerts no strong control on the textural development of pyrite.

In view of the data from LA–ICP–MS, thermodynamic modeling and observational results, uptake of As by pyrite is the simplest explanation of the experimental data. The experimental data do not permit the differentiation between adsorption or structural incorporation. Nevertheless, structural incorporation will be preceded by a sorption step and sorption onto a phase which is continuously growing, either by increasing crystal size or the formation of layer upon layer of crystals, will result in the entrapment of arsenic.

Implications

Firstly, the results presented here demonstrate that a continuous-flow approach to experimentation allows the investigation of contaminant uptake at realistic concentrations. Secondly, it is shown that As, at (sub)micromolar concentrations or less, is readily taken up by the neoformed pyrite. Thus, the net result of the reactions in the chemostat is the continued fixation of arsenic in pyrite and, hence, the formation of arsenian pyrite (that is, pyrite containing arsenic). This implies that arsenic cannot be re-released into solution, unless pyrite is oxidatively dissolved. The low solubility of pyrite means that it provides a long term stable sink, limiting As bioavailability in anoxic environments. In addition, the metastable pyrite precursor FeS dissolves to form pyrite (*5*), and so cannot be regarded as a stable sink for arsenic and other trace elements. Furthermore, the synthesis of arsenian pyrite at ambient environmental conditions is in agreement with authigenic arsenian pyrite formed in, for example, marine sediments (*12*).

Acknowledgements

Steve Grimes, Anthony Oldroyd and Sarah Goldsmith (Cardiff University), Cornelis Woensdregt, Cornelis van der Weijden (Utrecht University) and Peter van der Linde (University of Professional Education Leiden) are acknowledged. The manuscript was improved by the valuable comments of three anonymous reviewers and the associate editor. This research was supported by NWO/ALW grant 750.197.06 to M.W. and NERC grant NERLS200000611 to D.R. The Utrecht LA–ICP–MS lab was supported by the NWO/GOA. This research was conducted under the program of the Netherlands Research School of Sedimentary Geology.

References

1. Morse, J.W.; Millero, F.J.; Cornwell, J.C.; Rickard, D., The Chemistry of the Hydrogen Sulfide and Iron Sulfide Systems in Natural Waters. *Earth–Sci. Rev.* **1987,** *24*, 1–42.
2. Wilkin, R.T.; Barnes, H.L., Formation processes of framboidal pyrite. *Geochim. Cosmochim. Acta* **1997,** *61*, 323–339.
3. Rickard, D., Kinetics and mechanism of pyrite formation at low temperatures. *Am. J. Sci.* **1975,** *275*, 636–652.
4. Luther, III G.W., Pyrite synthesis via polysulfide compounds. *Geochim. Cosmochim. Acta* **1991,** *55*, 2839–2849.
5. Rickard, D., Kinetics of pyrite formation by the H_2S oxidation of iron(II) monosulfide in aqueous solutions between 25 and 125°C:The rate equation. *Geochim. Cosmochim. Acta* **1997,** *61*, 115–134.

6. Rickard, D.; Luther, III G.W., Kinetics of pyrite formation by the H_2S oxidation of iron (II) monosulfide in aqueous solutions between 25 and 125°C:The mechanism. *Geochim. Cosmochim. Acta* **1997,** *61*, 135–147.
7. Tossell, J.A.; Vaughan, D.J.; Burdett, J.K., Pyrite, marcasite and arsenopyrite type minerals: crystal chemical and structural principles. *Phys. Chem. Min.* **1981,** *7*, 177–184.
8. Harmandas, N.G.; Fernandez, E.N.; Koutsoukos, P.G., Crystal growth of pyrite in aqueous solutions. Inhibition by organophosphorus compounds. *Langmuir* **1998,** *14*, 1250–1255.
9. Butler, I.B.; Rickard, D.; Grimes, S.T.; Oldroyd, A., Nucleation and growth of pyrite on pyrite seeds. *Abstr. Pap. Am. Chem. Soc.* **2003,** *225*.
10. Grimes, S.T.; Brock, F.; Rickard, D.; Davies, K.L.; Edwards, D.; Briggs, D.E.G.; Parkes, R.J., Understanding fossilization: experimental pyritization of plants. *Geology* **2001,** *29*, 123–126.
11. Wang, Q.; Morse, J.W., Pyrite formation under conditions approximating those in anoxic sediments I. Pathway and morphology. *Mar. Chem.*, **1996,** *52*, 99–121.
12. Huerta-Diaz, M.A.; Morse, J.W., Pyritization of trace metals in anoxic marine sediments. *Geochim. Cosmochim. Acta* **1992,** *56*, 2681–2702.
13. Morse, J.W.; Luther, III G.W., Chemical influences on trace metal-sulfide interactions in anoxic sediments. *Geochim. Cosmochim. Acta* **1999,** *63*, 3373–3378.
14. Wolthers, M.., Geochemistry and environmental mineralogy of the iron–sulphur–arsenic system. PhD thesis. Geologica Ultraiectina 225. 2003.
15. Butler, I.B.; Grimes, S.T.; Rickard, D. , Pyrite formation in an anoxic chemostated reaction system. *J. Conf. Abs.* **2000,** *5*, 274–275.
16. Rickard, D.; Butler, I.B.; Oldroyd, A., A novel iron sulphide mineral switch and its implications for Earth and planetary science. *Earth Planet. Sci. Lett.* **2001,** *189*, 85–91.
17. Widerlund, A.; Ingri, J., Early diagenesis of arsenic in sediments of the Kalix River estuary, northern Sweden. *Chem. Geol.* **1995,** *125*, 185–196.
18. Yan, X–P.; Kerrich, R.; Hendry, M.J., Distribution of arsenic(III), arsenic(V) and total inorganic arsenic in porewaters from a thick till and clay-rich aquitart sequence, Saskatchewan, Canada. *Geochim. Cosmochim. Acta* **2000,** *64*, 2637–2648.
19. Sullivan, K.A.; Aller, R.C., Diagenetic cycling of arsenic in Amazon shelf sediments. *Geochim. Cosmochim. Acta* **1996,** *60*, 1465–1477.
20. Andreae, M.O., Arsenic speciation in seawater and interstitial waters: The influence of biological-chemical interactions on the chemistry of a trace element. *Limnol. Oceanogr.* **1979,** *24*, 440–452.
21. Sadiq, M., Arsenic chemistry in marine environments: a comparison between theoretical and field observations. *Mar. Chem.* **1990,** *31*, 2850–297.

22. Kuhn, A.; Sigg, L., Arsenic cycling in eutrophic Lake Greifen, Switzerland: influence of seasonal redox processes. *Limnol. Oceanogr.* **1993,** *38*, 1052–1059.
23. Schoonen, M.A.A.; Barnes, H.L., Reactions forming pyrite and marcasite from solution: I. Nucleation of FeS2 below 100°C. *Geochim. Cosmochim. Acta* **1991,** *55*, 1495–1504.
24. Benning, L.; Wilkin, R.T.; Barnes, H.L., Reaction pathways in the Fe-S system below 100°C. *Chem. Geol.* **2000,** *167*, 25–51.
25. Eary, L.E., The solubility of amorphous As_2S_3 from 25 to 90°C. *Geochim. Cosmochim. Acta* **1992**, 56, 2267–2280.
26. Mason, P.R.D.; Kraan, J.W., Attenuation of spectral interferences during laser ablation inductively coupled plasma mass spectrometry (LA-ICP-MS) using an rf only collision and reaction cell. *J. Anal. At. Spectrom.* **2002,** *17*, 858–867.
27. Mason, P.R.D.; Mank, A.J.G., Depth-resolved analysis in multi-layered glass and metal materials using laser ablation inductively coupled plasma mass spectrometry (LA-ICP-MS). *J. Anal. At. Spectrom.* **2001,** *16*, 1381–1388.
28. Davison, W.; Philips, N.; Tabner, B.J., Soluble iron sulfide species in natural waters: reappraisal of their stoichiometry and stability constants. *Aquat. Sci.* **1999**, 61, 23–43.
29. Mason, P.R.D.; Kaspers, K.; Van Bergen, M.J., Determination of sulfur isotope ratios and concentrations in water samples using ICP-MS incorporating hexapole ion optics. *J. Anal. At. Spectrom.* **1999,** *14*, 1067–1074.
30. Nesbitt, R.W.; Hirata, T.; Butler, I.B.; Milton, J.A., UV Laser Ablation ICPMS: Some Applications in the Earth Sciences. *Geostandards Newsletter* **1998**, 20, 231–243.

Downloaded by PENNSYLVANIA STATE UNIV on September 11, 2012 | http://pubs.acs.org
Publication Date: October 3, 2005 | doi: 10.1021/bk-2005-0915.ch006

Chapter 6

Transformation and Transport of Arsenic within Ferric Hydroxide Coated Sands upon Dissimilatory Reducing Bacterial Activity

Mitchell Herbel and Scott Fendorf

**Department of Geological and Environmental Sciences,
Stanford University, Stanford, CA 94305**

The mobility of arsenic in contaminated aquifers is primarily controlled by the presence of iron (hydr)oxides and sulfides. Under reducing conditions, bacteria that can alter ferric bearing phases will likely have a strong effect on the chemistry and hence the mobility of arsenic. Here we investigate how arsenic complexed with ferrihydrite is mobilized under dynamic flow conditions in the presence of anaerobic bacteria that can reduce As(V) and/or Fe(III) through dissimilatory processes. Ferrihydrite-coated sands were loaded with 200 to 300 mg Kg^{-1} As(V) or As(III) and inoculated with *Sulfurosprillum barnesii* strain SES-3. The sands were packed into columns through which a minimal ground water media was passed. In columns containing As(III)-loaded ferrihydrite and SES-3, As(III) release to the aqueous phase was most intense initially when microbial activity was high and decreased thereafter. Similar results were observed with As(V)-loaded ferrihydrite and SES-3, yet As(V) reduction to As(III) occurred prior to the onset of high Fe(II) in solution. Arsenic release into the aqueous phase is thus coincident with iron reduction and plays a critical role in dissolved arsenic concentrations.

In Advances in Arsenic Research; O'Day, P., et al.;
ACS Symposium Series; American Chemical Society: Washington, DC, 2005.

Introduction

Arsenic shares many qualities with other redox-sensitive inorganic compounds, such as NO_3, Fe, Mn, SO_4, and trace elements, such as Se, Cr, Hg, and U, in that it can exist in surface environments in multiple redox states and can complex with many inorganic and organic substances. Numerous Prokaryotes can utilize soluble and solid phase compounds of arsenic to fuel their metabolism (*1-3*). Others may alter the As speciation through detoxification mechanisms (*4, 5*). Biological activities may therefore produce soluble forms of As that can enter a region's water supply and pose health risks to humans and animals.

In surface and subsurface environments, changes in water chemistry often result in a release of arsenic from soils and sediments. Release of solid phase As may occur when incoming waters contain high concentration of ions, and in particular phosphate, that can displace adsorbed As (*6-10*). Incursion of dissolved, labile organic carbon stimulates microbial activity, and as a consequence under anaerobic conditions may enhance the dissolution of Mn(IV/III) or Fe(III) minerals that may contain As (*9, 11*). With an influx of aerobic water, oxidative dissolution of arsenic in sulfide minerals, such as arsenopyrite, realgar, or orpiment, may significantly increase aqueous phase As concentrations, yet oxidation of the released Fe(II) and Mn(II) will form Fe(III) and Mn(IV) (hydr)oxide precipitates that can attenuate soluble As (*12, 13*). Of these release mechanisms, the change from aerobic to anaerobic conditions most often correlates with high levels of aqueous As (*12*), and microbial respiratory reduction processes are paramount to bringing about this change.

Because reduction processes directly influence the stability, and hence mobility of arsenic in iron (hydr)oxide systems under hydrodynamic conditions, we chose to investigate effects of dissimilatory Fe(III) and As(V) reduction on arsenic transport under dynamic flow conditions (Figure 1). Our specific objective was to determine whether arsenic or iron reduction dominated changes in arsenic mobility within anaerobic environments. Here, we used a freshwater anaerobic bacterium, *Sulfurosprillum barnesii* strain SES-3, that reduces both Fe(III) and As(V) through dissimilatory reduction processes (*14*, *15*). Although we recognize the importance of sulfidogenesis in arsenic speciation and transport, we chose to initially focus our efforts on arsenic transport typical of many freshwater and terrestrial environments (i.e., our systems represent freshwater environments having low sulfur contents).

Downloaded by PENNSYLVANIA STATE UNIV on September 11, 2012 | http://pubs.acs.org
Publication Date: October 3, 2005 | doi: 10.1021/bk-2005-0915.ch006

Downloaded by PENNSYLVANIA STATE UNIV on September 11, 2012 | http://pubs.acs.org
Publication Date: October 3, 2005 | doi: 10.1021/bk-2005-0915.ch006

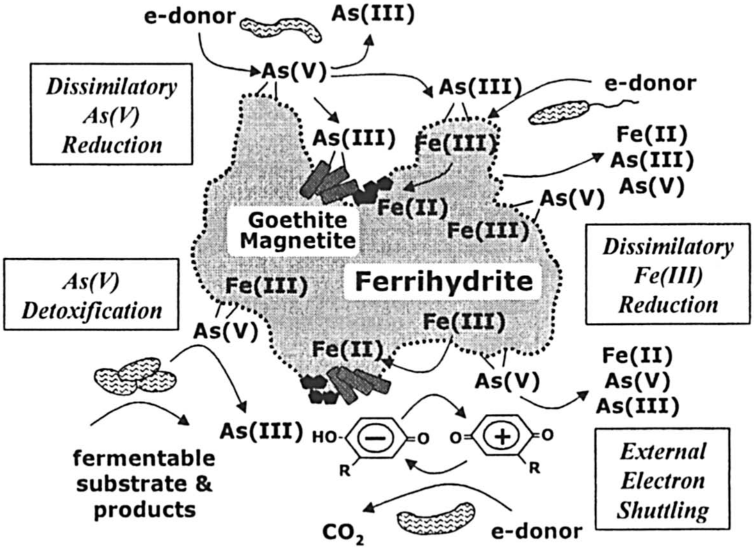
e-donor
As(III)
As(V)
As(III)
e-donor
Dissimilatory As(V) Reduction
As(III)
Fe(III)
Fe(II)
As(III)
As(V)
As(V)
Fe(II)
Goethite
Magnetite
Fe(III)
Dissimilatory Fe(III) Reduction
As(V) Detoxification
Fe(III)
Ferrihydrite
As(V)
Fe(III)
Fe(II)
Fe(II)
As(V)
As(V)
As(III)
As(III)
HO
O
O
O
R
R
fermentable substrate & products
External Electron Shuttling
CO$_2$
e-donor

Figure 1. Bacterial mobilization processes for iron oxide-complexed arsenic.

Experimental Design

Ferrihydrite coated sands were prepared using previously described methods (*16, 17*). Briefly, 2-line ferrihydrite was produced by titrating a ferric chloride solution to pH 7.5 using 1 M NaOH over a period less than 5 min, which minimized formation of akageneite or goethite. After equilibrating for 2 h, excess salts were removed from the ferrihydrite precipitate by repeatedly centrifuging and washing with distilled, deionized water. The ferrihydrite slurry was then mixed with IOTA-6 quartz sand (Unimin Corp., Spruce Pine, NC) and dried at 20°C for a period of 4 d, during which time the sands were repeatedly mixed to insure even drying. The purity of ferrihydrite was verified by XRD.

Arsenic sorption and desorption were examined by equilibrating 1.0 g ferrihydrite-coated sands with 30 mL pH 7.2 PIPES buffer prepared as above. Arsenic, as As(III) or As(V), was added to obtain 50 to 1000 μM concentrations. Samples were shaken at 75 r.p.m. for 3 d at 22°C, then centrifuged at 5000 r.p.m. for 10 min. The solutions were decanted, passed through 0.2 μm filters, and either acidified to pH < 2 with HCl or frozen for later analysis. Desorption of arsenic was tested by adding a 30 mL pH 7.2 PIPES buffer back to the ferrihydrite-coated sands and shaking for 1 d. To select samples 0.5 or 3.0 mM sodium lactate was added to examine effects of organic acids on desorption phenomenon. Soluble As(III) and As(V) concentrations were determined from hydride-generation ICP using 0.15 M $NaBH_4$/0.12 M NaOH and 6 M HCl.

After rinsing in distilled, deionized water to remove loosely bound ferrihydrite, the sands were equilibrated in a 10 mM pH 7.1 PIPES buffer with dilute KH_2PO_4 for 3 d (provides 10 mg PO_4 Kg^{-1} ferrihydrite). The buffer was then decanted, and a similar 10 mM PIPES buffer, containing ~1.5 mM As(III) or As(V) was then equilibrated with the ferrihydrite-coated sands to adsorb approximately 200 to 300 mg As Kg^{-1}. After a similar 3 d equilibration, the sands were rinsed with buffer then mixed with ~100 mL 10^8 cells/mL of *Sulfurosprillum barnesii* strain SES-3, and loaded into the 25 cm columns. A minimal nutrient artificial ground water media was then pumped into the columns at ~ 3 pore volumes per day in a reverse flow manner to minimize development of preferential flow pathways. The media consisted of 10 mM PIPES at pH 7.1, with 2.8 mM lactate as electron donor.

The chemistry of pore water, influent and effluent solutions were monitored over the next 25 d. Total dissolved iron and arsenic were measured in 0.12 M HCl acidified aliquots of aqueous sample by ICP-OES. Arsenic(V) and As(III) were measured in non-acidified samples with soluble Fe^{2+} removed by BioRad AG50W-X8 ion exchange resin prior to ion chromatography separation (*18*) and ICP-OES analyses. Organic acids were quantified using a Dionex DX-500 Ion Chromatograph using an IonPac AS9-HC column with 0.4 mM heptafluorobutyric acid eluent and suppressed ion conductivity detection.

At experiment termination, the sands from the columns were collected in 2-5 cm sections for further As and Fe speciation. Each section was mixed thoroughly, and portions were dissolved using 6 M HCl to determine total Fe and As concentrations by ICP-OES while other portions were analyzed for Fe(II) and Fe(II+III) by the ferrozine method (*17*). The remaining portion was rinsed with distilled, deionized water and dried under anaerobic conditions prior to X-ray absorption spectroscopic analysis. Arsenic XANES spectral data were collected on beam-line 13ID-C at the Advanced Photon Source at Argonne National Laboratory using similar procedures as described by Hansel et al. (*19*).

Downloaded by PENNSYLVANIA STATE UNIV on September 11, 2012 | http://pubs.acs.org
Publication Date: October 3, 2005 | doi: 10.1021/bk-2005-0915.ch006

Results

Adsorption of As(III) on ferrihydrite coated sands was approximately two-fold that of As(V) (Figure 2), which was similarly observed in studies with other hydrated or disordered Fe(III) minerals (*20, 21*). Adsorption isotherms were best modeled using Langmuir isotherms. Reaction of 1.5 mM As(III) or As(V) with the ferrihydrite coated-sands (which were then used in the column experiments) resulted in mass loadings of 318.2 mg As(III) Kg^{-1} and 201.7 mg As(V) Kg^{-1} ferrihydrite. Sorption-desorption hysteresis was observed for both As(III) and As(V) with the ferrihydrite coated sands (Figure 3). Although less As(V) was adsorbed, a greater amount was retained on the sands upon desorption than As(III). The addition of lactate to the desorbing solution did not have an appreciable effect on either As(III) or As(V) desorption (data not shown). Hysteresis results from a more rapid adsorption than desorption reaction and is indicative of the strong affinity arsenic (both arsenate and arsenite) possesses for ferric (hydr)oxides.

Downloaded by PENNSYLVANIA STATE UNIV on September 11, 2012 | http://pubs.acs.org
Publication Date: October 3, 2005 | doi: 10.1021/bk-2005-0915.ch006

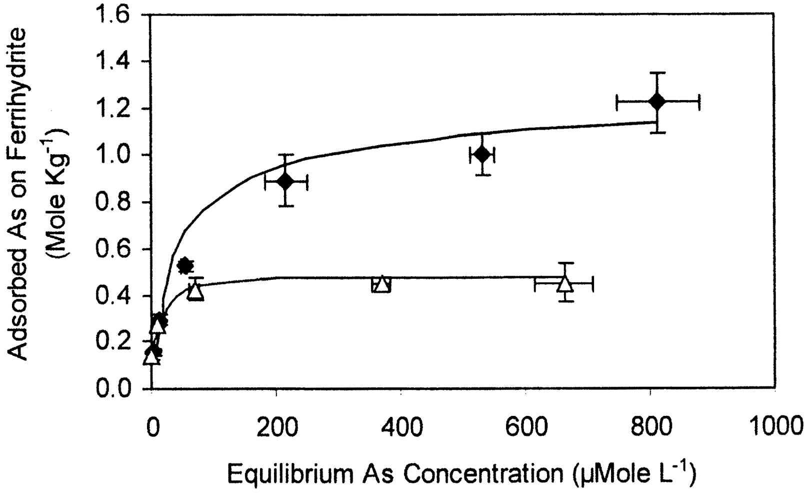

Figure 2. Adsorption isotherms for As(III) (solid circles) and As(V) (open triangles) on ferrihydrite in 10 mM PIPES buffer, pH 7.

Arsenic and Iron Release

Respiratory reduction of Fe(III) and As(V) by *Sulfurosprillum barnesii* results in an initially rapid declining release of arsenic from the ferrihydrite-coated sands under dynamic flow conditions. SES-3 quickly reduced As(V) to As(III), which was the only species eluted after 6 d. Total dissolved As in the effluent decreases rapidly from 52 μM to ~11 μM within 3 d, yet concentrations either remain near this level or slightly increased as the experiment progresses (Figure 4). Bacterial lactate oxidation initially produces a pulse of acetate within the first 3 d, diminishes at intermediate times, and then increases again after 12 d (Figure 5). The amount of acetate produced from lactate oxidation (8.3 meq) was over three times greater than that of aqueous Fe(II) and As(III) (2.6 meq) (the imbalance is rectified by considering solid-phase reduction products). In the effluent solution, Fe(II) concentrations increase (to 600 μM) after the initially rapid As(V) reduction. A cumulative 6.9% loss of initial Fe from the columns was observed during the experiment, yet only 4.1% of the initial As(V) was lost, indicating a majority of the As remained within the solid matrix of the columns.

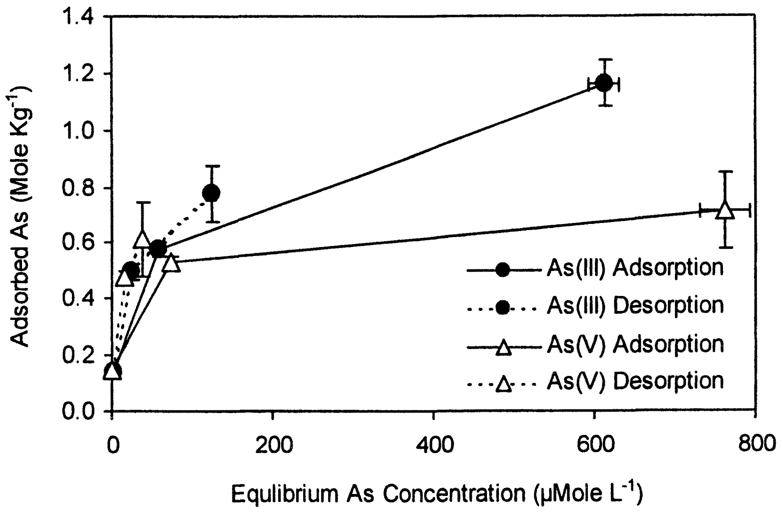

Figure 3. Arsenic adsorption-desorption hysteresis with ferrihydrite-coated sands.

Downloaded by PENNSYLVANIA STATE UNIV on September 11, 2012 | http://pubs.acs.org
Publication Date: October 3, 2005 | doi: 10.1021/bk-2005-0915.ch006

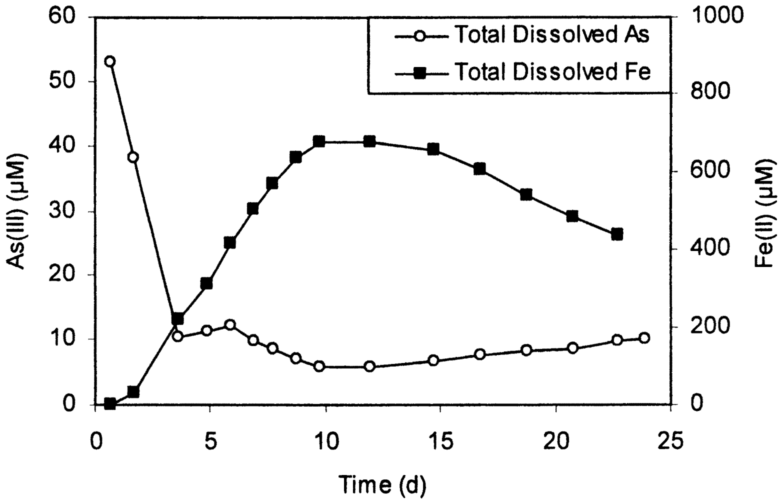

Figure 4. Total dissolved As and Fe in the effluent from ferrihydrite-coated sand column initially loaded with As(V) and Sulfurosprillum barnesii strain SES-3.

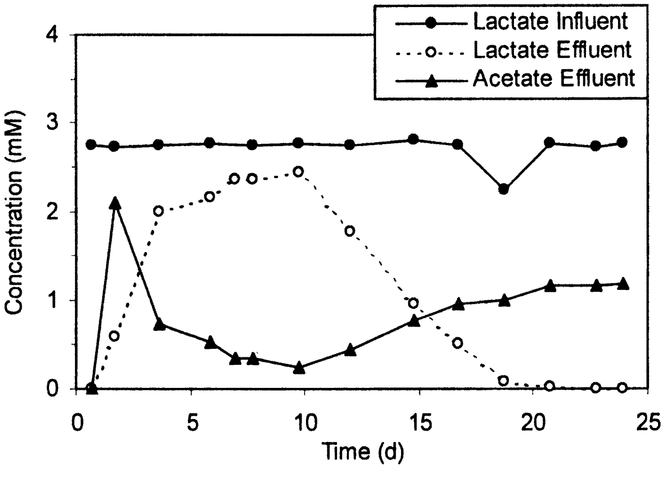

Figure 5. Lactate and acetate concentrations in the influent and effluent for the ferrihydrite-coated sand column initially loaded with As(V) and Sulfurosprillum barnesii strain SES-3.

Downloaded by PENNSYLVANIA STATE UNIV on September 11, 2012 | http://pubs.acs.org
Publication Date: October 3, 2005 | doi: 10.1021/bk-2005-0915.ch006

A larger cumulative loss of Fe (10.3%) but smaller cumulative loss of As (2.3%) was observed from the column initially loaded with As(III) (Figure 6). Soluble As in the pore waters and effluent remained as As(III) (data not shown). Elution of As(III) from the column was similarly rapid as was observed with As(V), but concentrations asymptotically decreased after 5 d to levels approaching 5 μM. The large spike in dissolved Fe(II) at 21 d reflects an intentional decrease in pH in the feed solution by 0.4 units. Concomitant with the pH change, a proton-induced release of labile Fe(II) from the surfaces of the ferrihydrite resulted in a two-fold increase in dissolved Fe(II) and a slight decrease in eluted As(III). Cumulative Fe(II) released from the As(III)-loaded ferrihydrite-sands was 2.1 meq as compared to the 5.5 meq of acetate produced (Figure 6). This disparity again is rectified by considering Fe(II) and As(III) generated/retained within the solid phase.

Discussion and Summary

The greatest release of arsenic from the ferrihydrite-coated sand columns occurs within the first 5 d after flow initiation, corresponding with the highest bacterial respiration, as represented by the rapid conversion of lactate to acetate (Figures 5 and 7). The secondary increase in lactate oxidation to acetate after 12 d, which does not correlate with a spike in arsenic release, likely results from bacterial adjustment to the geochemical and hydrodynamic conditions prevailing within the column. The initial generation of ferrous-iron induces a dramatic shift in ferrihydrite transformation to goethite and magnetite (*17*), and the resulting mineralogical shift has a profound impact on arsenic release. Furthermore, surface modification induced by Fe(II) adsorption alters the binding affinity of arsenate and arsenite, and for both ions likely diminish its retention (*8*).

After the initial release from the columns, dissolved As decreases while Fe(II) concentrations continue to increase. Diminished arsenic elution is not a result from an exhausted source; a large fraction of arsenic remains on the solid phase even at the experiments termination. Once the rapid transformation of ferrihydrite to goethite and magnetite has occurred, it appears that a secondary state is reached where, despite iron reduction, limited arsenic desorption results. Only minor darkening of the iron oxide-sands was observed after the first seven days for both columns (data not shown), indicating that changes in iron

Downloaded by PENNSYLVANIA STATE UNIV on September 11, 2012 | http://pubs.acs.org
Publication Date: October 3, 2005 | doi: 10.1021/bk-2005-0915.ch006

Downloaded by PENNSYLVANIA STATE UNIV on September 11, 2012 | http://pubs.acs.org
Publication Date: October 3, 2005 | doi: 10.1021/bk-2005-0915.ch006

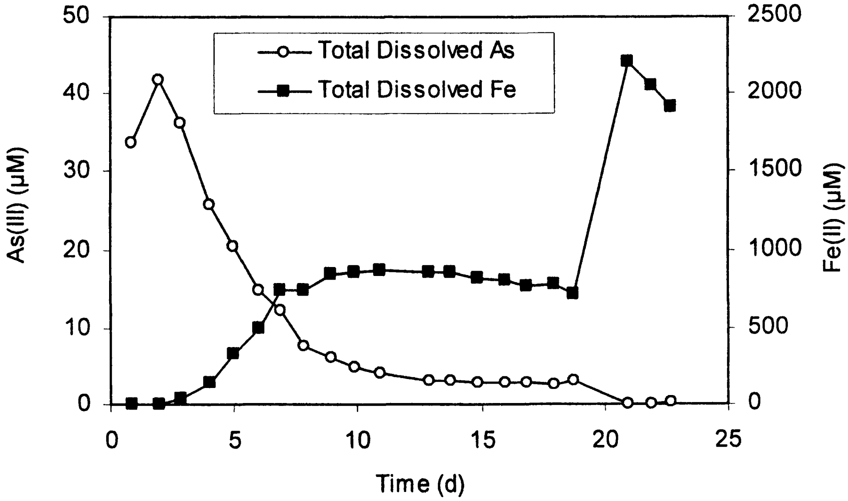

Figure 6. Total dissolved As and Fe in effluent from the ferrihydrite-coated sand column initially loaded with As(III) and Sulfurosprillum barnesii strain SES-3.

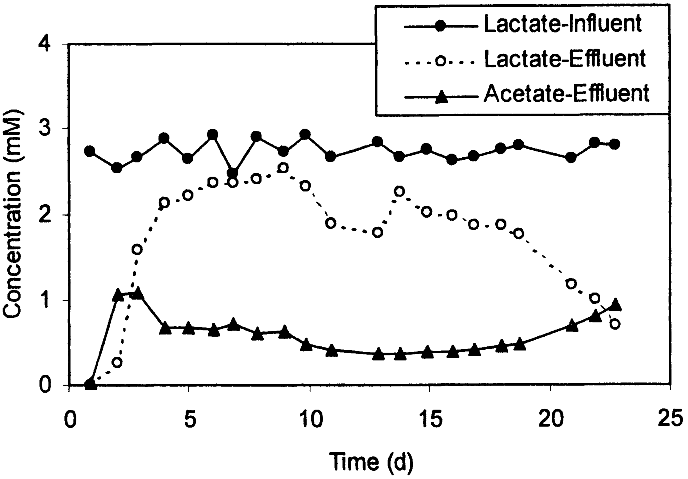

Figure 7. Lactate and acetate concentrations in the influent and effluent for the ferrihydrite-coated sand column initially loaded with As(III) and Sulfurosprillum barnesii strain SES-3.

mineralogy were minimal after this period. Owing to the high affinity both arsenate and arsenite have for most iron (hydr)oxides (*20*), inclusive of magnetite and goethite, the mineralogical shift has only one major impact on arsenic: a decrease is reactive surface area. Once the surface area adjustment has occurred, notable arsenic displacement is not observed. Undoubtedly, if the experiments were continued until the quantity of iron were limiting (near complete consumption), then obviously one would expect arsenic elution. Accumulation of As relative to Fe in the downfield portions of the column (Table I), particularly for As(III), is, in fact, a direct response to the displacement and re-adsorption induced by ferrihydrite transformation.

In contrast to the dramatic effect ferrous iron has on arsenic desorption, competitive ligand displace of arsenic by lactate is not likely, since lactate addition to the desorption experiments did not enhance arsenic release as compared to controls without lactate. Although desorption of As by organic acids and anions has been observed (*6, 10, 22-26*), it appears to be a minor effect relative to ferrihydrite transformation. The rapid release of adsorbed As(III) and As(V) into the eluent upon exposure to media with a labile carbon source (lactate) has important implications for environmental quality. In the ever changing environments of soils and sediments, the most vulnerable time period for arsenic release appears to occur immediately at the onset of reduction, when labile carbon pools are most available, leading to reduction and transformation of Fe(III) (hydr)oxides and, if present, adsorbed arsenate.

Differences in arsenic and iron release profiles for the columns are minor, but mechanistically important features may exist and may explain the 'tailing' of arsenic elution noted in each column. For the As(V)-loaded sand column, a greater proportion of As was eluted compared to Fe than in the As(III)-loaded sand column (Figures 4 and 6). Within 3 d, all the soluble As(V) was reduced to As(III), even though high concentrations of arsenate remained on the solids at the end of the 23 d experimental period (Table I). Arsenic XANES spectra indicated that for the down-gradient portions of the column the proportion of As(V) (to total As) dropped to 56-59%, revealing that the As(III) produced by bacterial respiration accumulated within the iron oxide sands. Arsenate remaining on the solid phase appears resistant to rapid bacterial reduction and is reduced only after ferrihydrite degradation. The greater amounts of Fe initially released in the As(III)-loaded sands column likely reflect that Fe(III) is the sole electron acceptor for the bacteria; under such conditions, As(III) release arises solely from changes in iron mineralogy (from high surface area ferrihydrite to lower surface area minerals such as magnetite and goethite/lepidocrocite).

Downloaded by PENNSYLVANIA STATE UNIV on September 11, 2012 | http://pubs.acs.org
Publication Date: October 3, 2005 | doi: 10.1021/bk-2005-0915.ch006

Table I. Solid phase iron and arsenic speciation at experiment termination of the ferrihydrite-coated sands initially loaded with As(V) or As(III).

Section (distance from inlet)	*Fe(II) mg/Kg (%)*	*Fe(III) mg/Kg (%)*	*As_T mg/Kg*	*As(V) (%)*†	*As(III) (%)*†	*As:Fe mol:mol*
			As(V)-Column			
15-20 cm	826.5 (23.5)	2692.2 (76.5)	64.1	59	41	0.014
10-15 cm	823.0 (24.7)	2514.3 (75.3)	161.1	57	43	0.036
5-10 cm	687.0 (22.7)	2340.3 (77.3)	149.4	NM‡	NM	0.037
0-5 cm	53.2 (1.9)	2756.0 (98.1)	93.7	74	26	0.025
Initial	NM	3973.3 (100.0)	201.7	100	0	0.038
			As(III)-Colmnn			
15-20 cm	1171.9 (21.9)	4177.1 (78.1)	194.7	0	100	0.027
10-15 cm	772.3 (15.1)	3816.6 (84.9)	358.0	0	100	0.058
5-10 cm	665.9 (16.8)	3734.2 (83.2)	466.4	0	100	0.079
0-5 cm	1297.9 (30.2)	2995.3 (69.8)	220.0	0	100	0.038
Initial	NM	4468.0 (100.0)	318.2	0	100	0.053

† - Determined by As-XANES spectra peak fitting.
‡ - Not Measured

The mechanism and site of bacterial arsenate reduction will also likely have an important role in the extent to which arsenic is released to solution. It is conceivable, albeit against current evidence, that bacteria could reduce As(V) on the ferrihydrite surfaces via enzymes on the outer membrane, thus negating the need for transport into the cell. The transfer of electrons to adsorbed As(V) (tetrahedral oxo-coordination) would convert it to As(III) (trigonal oxo-coordination), which would require a coordination change. Although As(V) and As(III) form similar bidentate, binuclear complexes with iron oxides (*27-30*), bonding rearrangements caused by changes in molecular orbital geometries upon reduction from the (V) to the (III) state may allow As(III) to temporarily

Downloaded by PENNSYLVANIA STATE UNIV on September 11, 2012 | http://pubs.acs.org
Publication Date: October 3, 2005 | doi: 10.1021/bk-2005-0915.ch006

dissociate from the iron oxide surfacen. However, ferrihydrite has a greater capacity to adsorb As(III) than As(V), and spatially the As(III) would remain very close to the surface, thus suppressing As desorption.

At present, identified enzymes responsible for dissimilatory arsenate reduction reside exclusively in the periplasmic space of gram negative bacteria (*11, 31*). As a consequence, arsenate desorption is a prerequisite to bacterial reduction. Subsequent to reduction, arsenite would then be readily released into the bulk solution and would have a greater likelihood of elution from the column. In the current experiments, the As(V)-loaded sand column continued to release higher levels of arsenic, as As(III), after the initial large release in the first 5 d compared to the As(III)-loaded column. We therefore postulate that arsenate desorbs from the iron (hydr)oxide, is transported into the periplasm of the bacterial cell, then reduced to As(III) which then transports back across the cell membrane into the external media. The expelled arsenite re-adsorbs on the iron (hydr)oxide but a measurable fraction elutes from the column, thus providing the means by which a 10 μM tailing of dissolved As(III) is maintained in the effluent at $t > 15$ d.

The effects of bacterial dissimilatory reduction on adsorbed As(V) are potentially more complex. Upon exposure to labile organic carbon, bacterial reduction of Fe(III) (hydr)oxides will release both Fe(II) and As(V) into solution. If As(V)-respiring bacteria are present, desorbed As(V) will quickly be converted to As(III). Arsenate-respiring bacteria attached to sediment surfaces may also enhance dissolution of adsorbed As(V) by transporting it across their cell membranes and releasing As(III) into solution via As(III) specific transporters.

Solid phase arsenic in sediments and soils presents a risk to drinking water supplies since it can be liberated to the dissolved phase by several mechanisms, including oxidative dissolution of arsenic sulfides and other arsenic minerals, displacement of arsenic from adsorption sites by competing ions, reduction of arsenate to arsenite, and reductive dissolution of iron and manganese (hydr)oxides that serve as adsorbents of arsenic. Here we explored the liberation and transport of arsenic induced by dissimilatory As(V) or Fe(III) reduction—a condition prevalent upon a transition from aerobic to anaerobic conditions. Our current findings reveal that indeed arsenic is mobilized during dissimilatory reduction of Fe(III) and As(V), but that the release is transient, occurring dominantly during the first few days of biological activity. Transformation of the high surface area ferrihydrite and related minerals to lower surface area, more crystalline minerals, such as goethite and magnetite, or to minerals containing higher amounts of Fe(II), such as siderite or green rust will decrease the retention capacity of soils and sediments. Hence, released arsenic will persist in the aqueous phase and can thus jeopardize the quality of aquifers or effluent waters. Reductive transformation of iron and manganese (hydr)oxides upon

Downloaded by PENNSYLVANIA STATE UNIV on September 11, 2012 | http://pubs.acs.org
Publication Date: October 3, 2005 | doi: 10.1021/bk-2005-0915.ch006

introduction of a labile carbon source and anaerobiosis leads to the displacement of arsenic and therefore represents critical processes by which the toxicity of arsenic may be expressed within natural environments.

References

1. Ehrlich, H. L. *Geomicrobiol. J.* **1999,** 16, 135-153.
2. Lovley, D. R. *Adv. Agron.* **1995,** 54, 176-217.
3. Lovley, D. *Ann. Rev. Microbiol.* **1993,** 47, 263-290.
4. Mukhopadhyay, R.; Rosen, B. P.; Pung, L. T.; Silver, S. *FEMS Microbiol. Rev.* **2002,** 26, 311-325.
5. Oremland, R. S.; Newman, D. K.; Kail, B. W.; Stolz, J. F. In *Environmental Chemistry of Arsenic*; Frankenberger, J., W T, Ed.; Marcel Dekker: New York, 2002; pp 273-295.
6. Jain, A.; Loeppert, R. H. *J. Environ. Qual.* **2000,** 29, 1422-1430.
7. Smith, E.; Naidu, R.; Alston, A. M. *Adv. Agron.* **1998,** 64, 149-195.
8. Appelo, C. A. J.; Van der Weiden, M. J. J.; Tournassat, C.; Charlet, L. *Environ. Sci. Technol.* **2002,** 36, 3096-3103.
9. Harvey, C. F.; Swartz, C. H.; Badruzzaman, A. B. M.; Keon-Blute, N.; Yu, W.; Ashraf Ali, M.; Jay, J.; Beckie, R.; Niedan, V.; Brabander, D.; Oates, P. M.; Ashfaque, K. N.; Islam, S.; Hemond, H. F.; Ahmed, M. F. *Science* **2002,** 298, 1602-1606.
10. Redman, A. D.; Macalady, D. L.; Ahmann, D. *Environ. Sci. Technol.* **2002,** 36, 2889-2896.
11. Oremland, R. S.; Stolz, J. F. *Science* **2003,** 300, 939-944.
12. Smedley, P. L.; Kinniburgh, D. G. *App. Geochem.* **2002,** 17, 517-568.
13. Hering, J. G.; Kneebone, P. E. In *Environmental Chemistry of Arsenic*; Frankenberger, J., W T, Ed.; Marcel Dekker: New York, 2002; pp 155-181.
14. Oremland, R. S.; Switzer Blum, J.; Culbertson, C. W.; Visher, P. T.; Miller, L. G.; Dowdle, P. R.; Strohmeier, F. E. *Appl. Environ. Microbiol.* **1994,** 60, 3011-3019.
15. Zobrist, J.; Dowdle, P. R.; Davis, J. A.; Oremland, R. S. *Environ. Sci. Technol.* **2000,** 34, 4747-4753.
16. Benner, S. G.; Hansel, C. M.; Weilinga, B. W.; Barber, T. M.; Fendorf, S. *Environ. Sci. Technol.* **2002,** 36, 1705-1711.
17. Hansel, C. M.; Benner, S. G.; Neiss, J.; Dohnalkova, A.; Kukkadapu, R. K.; Fendorf, S. *Geochim. Cosmochim. Acta* **2003,** 67, 2977-2992.
18. Manning, B. A.; Martens, D. A. *Environ. Sci. Technol.* **1997,** 31, 171-177.
19. Hansel, C. M.; La Force, M. J.; Fendorf, S.; Sutton, S. *Environ. Sci. Technol.* **2002,** 36, 1988-1994.

Downloaded by PENNSYLVANIA STATE UNIV on September 11, 2012 | http://pubs.acs.org
Publication Date: October 3, 2005 | doi: 10.1021/bk-2005-0915.ch006

20. Dixit, S.; Hering, J. G. *Environ. Sci. Technol.* **2003,** 37, 4182-4189.
21. Raven, K. P.; Jain, A.; Loeppert, R. H. *Environ. Sci. Technol.* **1998,** 32, 344-349.
22. Simeoni, M. A.; Batts, B. D.; McRae, C. *App. Geochem.* **2003,** 18, 1507-1515.
23. Xu, H.; Allard, B.; Grimvall, A. *Water, Air, Soil Pollut.* **1991,** 57-58, 269-278.
24. Peryea, F. J.; Kammerack, R. *Water, Air, Soil Pollut.* **1997,** 93.
25. Kim, M.-J.; Nriagu, J.; Haack, S. *Environ. Sci. Technol.* **2000,** 34, 3094-3100.
26. Grafe, M.; Eick, M. J.; Grossl, P. R.; Saunders, A. M. *J. Environ. Qual.* **2002,** 31, 1115-1123.
27. Fendorf, S. E.; Eick, M. J.; Grossl, P. R.; Sparks, D. L. *Environ. Sci. Technol.* **1997,** 31, 315-320.
28. Inskeep, W. P.; McDermott, T. R.; Fendorf, S. In *Environmental Chemistry of Arsenic*; Frankenberger, J., W T, Ed.; Marcel Dekker: New York, 2002; pp 183-215.
29. Manning, B. A.; Fendorf, S.; Goldberg, S. *Environ. Sci. Technol.* **1998,** 32, 2382-2388.
30. Waychunas, G. A.; Fuller, C. C.; Rea, B. A.; Davis, J. A. *Geochim. Cosmochim. Acta* **1996,** 60, 1765-1781.
31. Saltikov, C. W.; Newman, D. K. *Proc. Natl. Acad. Sci. U. S. A.* **2003,** 100, 10983-10988.

Downloaded by PENNSYLVANIA STATE UNIV on September 11, 2012 | http://pubs.acs.org
Publication Date: October 3, 2005 | doi: 10.1021/bk-2005-0915.ch006

Downloaded by NORTH CAROLINA STATE UNIV on September 11, 2012 | http://pubs.acs.org
Publication Date: October 3, 2005 | doi: 10.1021/bk-2005-0915.ch007

Chapter 7

Transport of As(III) and As(V) in Experimental Subsurface Systems

Tanja Radu, Jeremiah C. Hilliard, Jae K. Yang, and Mark O. Barnett*

Department of Civil Engineering, 238 Harbert Engineering Center, Auburn University, Auburn, AL 36849

The goal of this study was to investigate the adsorption and transport of As(III) and As(V) in columns with Fe-coated sand. The experiments were conducted to examine the effect of pH, pore water velocity, and phosphate on As(III)/As(V) mobility. Both As(III) and As(V) exhibited rate-dependent adsorption in the columns. An increase in pH led to a significant increase in As(III) adsorption (decreased mobility) but decreased As(V) adsorption (increased mobility). As(III) was desorbed more readily than As(V) in As-free solution. The competing effect of phosphate was examined by introducing phosphate solution to the column with adsorbed As(III)/As(V). Phosphate mobilized both adsorbed As(III) and As(V), but some As(V) remained immobile even in the presence of phosphate. In general, but not under all circumstances, As(III) adsorbed less and was more mobile than As(V). The effect of the examined parameters on mobility and recovery of As species increased in the order pH < pore water velocity < phosphate < oxidation state.

In Advances in Arsenic Research; O'Day, P., et al.;
ACS Symposium Series; American Chemical Society: Washington, DC, 2005.

Introduction

The presence of Fe oxides has a significant influence on the mobility of As in groundwater. Previous research has proven Fe oxides to be strong adsorbents for As (*1-4*). The adsorption of As(III) and As(V) was reported to occur by forming monodentate and bidentate surface complexes between Fe oxides and As species (*5*). It is influenced by the type of Fe oxide and the oxidation state of the As species (*6*). The adsorption of As on goethite is not an instantaneous process. It is rather a two phase process with initial fast adsorption (time scale of minutes) followed by a much slower phase of continued uptake for days (*1*). Phosphate, often present in high concentrations relative to As in nature, is an effective competing ion for sites on the surface of the Fe minerals (*7*). This is caused by its similar chemical behavior to that of the As species. Phosphate is available in As-contaminated agricultural areas due to the treatment of soils with fertilizers containing phosphate (*7*). The competing effect of phosphate ions is well known from previous research (*8*).

However, most of the previous research done in this area was conducted in well mixed batch experiments (*6*). In contrast, dynamic column experiments more accurately simulate a natural groundwater flow and therefore, are closer to the real situation in the field. Yet there has been limited research done with dynamic flow experiments (*9-11*). The objective of this study was to examine As(III)/As(V) interactions with Fe oxides in the dynamic environment of column experiments. The variables of main interest were pore water velocity, pH, and the presence of phosphate as a competing ion. The goal of this study was to investigate and compare the adsorption and mobility of As(III) and As(V) under various conditions in column experiments.

Materials and Methods

Materials

The adsorbent used in these experiments was synthetic goethite-coated sand. Goethite (α-FeOOH) is a common coating material for subsurface particles (*12*). The Fe-coated sand was prepared by air oxidation of $FeCl_2{\cdot}2H_2O$ in a suspension of medium quartz sand as described by Roden et al. (*13*). The extractable Fe was measured by extraction with dithionite-citrate-bicarbonate (DCB) (*14*), and the sand had an Fe content of 75 ± 1 μM Fe per gram of sand, or 4200 mg Fe per kg of sand.

Arsenic solutions were prepared using reagent grade $NaAsO_2$ and As_2O_5. A constant ionic strength of 0.01 M was achieved by the addition of $NaNO_3$. The

Downloaded by NORTH CAROLINA STATE UNIV on September 11, 2012 | http://pubs.acs.org
Publication Date: October 3, 2005 | doi: 10.1021/bk-2005-0915.ch007

desired pH values of solutions were adjusted by the addition of HCl or NaOH. The phosphate solution was prepared by use of NaH_2PO_4.

The column experiments were performed at pH values of 4.5 and 9. In this pH range, the predominant As(III) species is neutral arsenious acid, H_3AsO_3 (pKa of 9.2), while the predominant As(V) species in the same pH range are $H_2AsO_4^-$ (pH<6.98) and $HAsO_4^{2-}$ (pH>6.98).

Analytical methods

Unfiltered aqueous samples were analyzed for total As concentration by atomic absorption spectrometry. Samples were analyzed within a few hours of sample collection. Separation of As(III) and As(V) species was obtained by use of an ion exchange column containing Dowex 1X 50-100 mesh CL Form resin (*15*). The As(V) species were adsorbed to the resin while As(III) passed through the resin column. The As concentration in the column inlet solution was checked prior to each experiment as well as after the end of the experiments. In the case of As(III) experiments, only solutions containing a minimum 95% of As(III) were used.

Experimental Setup

Columns were prepared using 2.4 g of Fe-coated sand dry-packed to a depth of 2.1 cm in a one-centimeter diameter glass tube. Solutions were pumped through the column using an Acuflow Series II high performance liquid chromatography pump. Effluent was collected using a Spectra/Chrom CF-1 Fraction Collector.

The variables examined in this study were pore water velocity, pH, and phosphate concentration. The column was pre-conditioned by pumping As-free 0.01 M $NaNO_3$ solution at a pH of 4.5 or 9 for 24 hours. After pre-conditioning, a solution containing 1.33×10^{-5} M (1 mg/L) As in 0.01 M $NaNO_3$ at the same pH was introduced to the column (solution I in Figure 1). Next (solution II in Figure 1), an As-free 0.01 M $NaNO_3$ solution was pumped through the column. Finally, a 2.5×10^{-4} M NaH_2PO_4 with 0.01 M $NaNO_3$ solution was introduced (solution III in Figure 1). Each of these solutions was pumped through for 700 pore volumes. The column pore volume was determined by direct physical measurement. The resulting column effluent breakthrough curves exhibited three distinct sections corresponding to the solutions being pumped through the column. The first stage (I) of the breakthrough curve represents the As that was initially eluted out of the system (i.e., the As that was not adsorbed to the sand at the end of the input pulse). The second stage (II) was the As that was desorbed from the system by

Downloaded by NORTH CAROLINA STATE UNIV on September 11, 2012 | http://pubs.acs.org
Publication Date: October 3, 2005 | doi: 10.1021/bk-2005-0915.ch007

Downloaded by NORTH CAROLINA STATE UNIV on September 11, 2012 | http://pubs.acs.org
Publication Date: October 3, 2005 | doi: 10.1021/bk-2005-0915.ch007

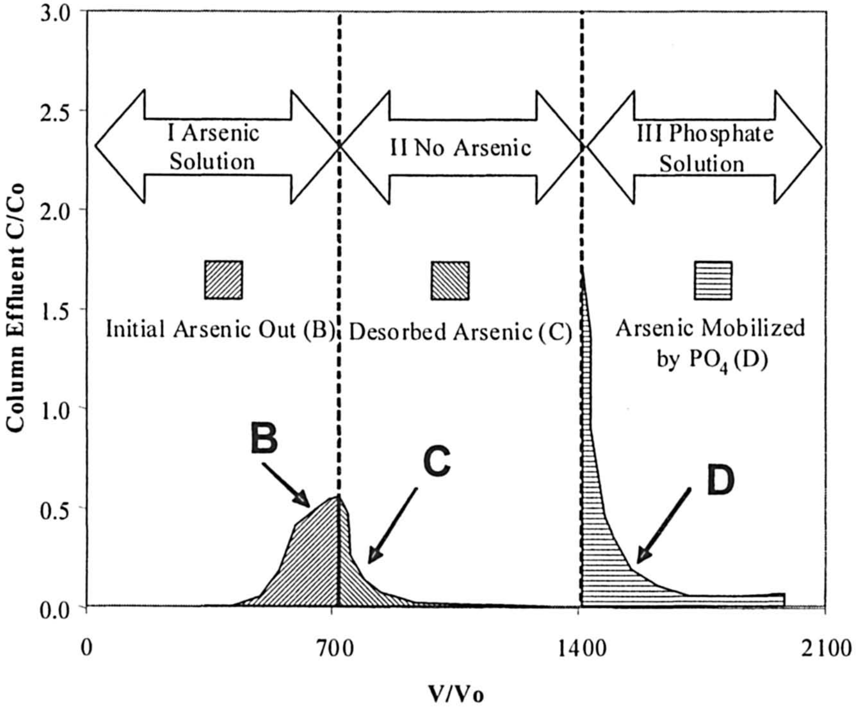

Figure 1. Schematic diagram of column outlet concentrations (C/C_0) as a function of pore volume: B- As effluent concentration (input amount minus amount adsorbed) in Phase I, C- amount desorbed in As-free solution (Phase II) and D – amount mobilized by phosphate addition (Phase III)

the As-free 0.01 M $NaNO_3$ solution. The final stage (III) measured the As that was mobilized by phosphate.

To study the effect of different groundwater velocities, the pump rate was adjusted to achieve a pore water velocity of 0.23 cm/min (low velocity) and 2.3 cm/min (high velocity). To examine the effect of pH, experiments were performed at both pH 4.5 and 9, corresponding to the approximate pH range of natural soils (*12*). Experiments were performed in duplicate.

Downloaded by NORTH CAROLINA STATE UNIV on September 11, 2012 | http://pubs.acs.org
Publication Date: October 3, 2005 | doi: 10.1021/bk-2005-0915.ch007

Quantitative Techniques for Column Comparisons

The experimental results were quantified by mass balances for the percentage of mass adsorbed, desorbed, and mobilized by phosphate as described below. These sections were constructed by integrating various portions of the effluent curves (Figure 1). The mass balances were performed on three sections (B, C, and D) of the effluent curve, and the following quantities were calculated:

$$\%\ \text{As Adsorbed} = (A\text{-}B)/A * 100\% \quad (1)$$

$$\%\ \text{As Desorbed} = C/(A\text{-}B) * 100\ \% \quad (2)$$

$$\%\ \text{As Mobilized w/}PO_4 = D/(A\text{-}B\text{-}C) * 100\% \quad (3)$$

$$\%\ \text{Total As Recovered} = (B+C+D)/A * 100\ \% \quad (4)$$

The part "A" (not shown on Figure 1) is the initial total As input to the column. A summary of the results is given in Table I.

Results and Discussion

Effect of pore water velocity

As(III)

At the pore water velocity of 0.23 cm/min, As(III) first broke through at about 200 pore volumes (Figure 2). Because of the decreased contact time between the solution and sand, it was expected that for high pore water velocity, the breakthrough curve would be shifted to the left, indicating less As(III) adsorbed with a more rapid initial breakthrough. Surprisingly, in the case of

As(III) adsorption, the initial breakthrough occurred at approximately the same pore volumes for both pore water velocities. However, the influence of different pore water velocities on the breakthrough curve can be observed in the number of pore volumes necessary to reach a C/C_0 value of 1. The breakthrough curve at high velocity was more rapid, reaching a C/C_0 value of almost 1 after 700 pore volumes, while the lower velocity experiment had only reached a C/C_0 value of 0.8 after the same number of pore volumes. The percentage of adsorbed As(III) was calculated for both pore water velocities (Table I). In the case of lower velocity, 47 ± 0.4% of the As(III) was adsorbed, while only 28 ± 10% was adsorbed in experiments at high velocity. This indicates that the pore water velocity and resulting contact time had a significant effect on As(III) adsorption in these experiments.

Downloaded by NORTH CAROLINA STATE UNIV on September 11, 2012 | http://pubs.acs.org
Publication Date: October 3, 2005 | doi: 10.1021/bk-2005-0915.ch007

Table I. Quantitative comparison of goethite coated sand experiments.

As(III)

V (cm/min)	*pH*	*% adsorbed*	*% desorbed*	*% mobilized*	*% recovered total*
0.23	4.5	47 ± 0.4	58 ± 17	68 ± 18	94 ± 8
2.30	4.5	28 ± 10	64 ± 10	100 ± 15	104 ± 4
0.23	9	59 ± 4	52 ± 4	61 ± 2	89 ± 2

As(V)

V (cm/min)	*pH*	*% adsorbed*	*% desorbed*	*% mobilized*	*% recovered total*
0.23	4.5	77 ± 7	13 ± 1	47 ± 2	64 ± 2
2.30	4.5	56 ± 5	17 ± 1	41 ± 2	73 ± 2
0.23	9	51 ± 5	24 ± 1	43 ± 2	78 ± 3

calculation based on formulas (1), (2), (3), and (4)

"±" represents standard deviation

The pore water velocity had no significant effect on As(III) desorption. There was 58 ± 17% of adsorbed As(III) desorbed at low velocity, while 64 ± 10% was desorbed at high velocity.

When introduced to the system, the phosphate ions initially replaced As(III) ions on the Fe coated sand, as indicated by the immediate peak in effluent As concentration. After this initial peak, the effluent concentrations rapidly decreased. The phosphate containing solution essentially flushed all of the

Downloaded by NORTH CAROLINA STATE UNIV on September 11, 2012 | http://pubs.acs.org
Publication Date: October 3, 2005 | doi: 10.1021/bk-2005-0915.ch007

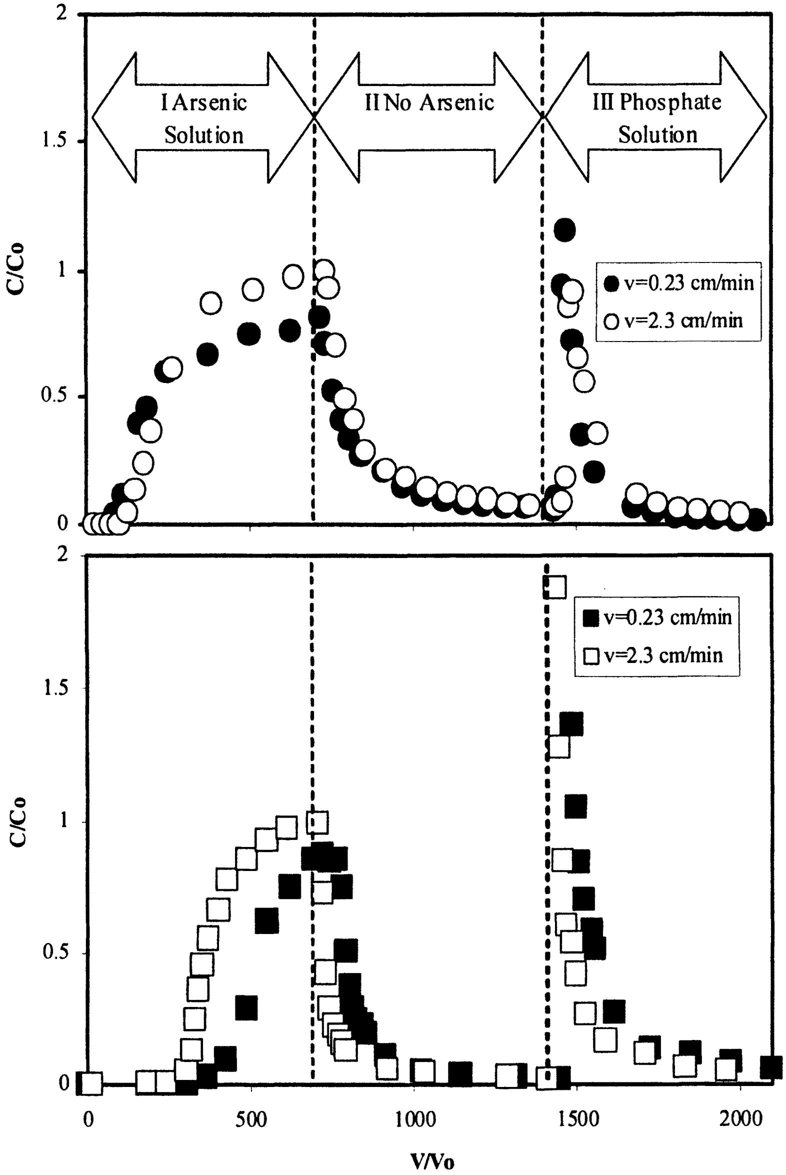

Figure 2. Breakthrough curves for As(III)(top) and As(V) (bottom) in a column of goethite coated sand; comparison of the pore water velocity effect, pH 4.5

remaining As(III) out of the system, resulting in essentially complete recovery of the As(III) introduced to the columns (Table I).

As(V)

The pore water velocity had an even more significant effect on As(V) adsorption (Figure 2). At 0.23 cm/min, As(V) first broke through ($C/C_0 > 0.02$) at about 400 pore volumes, and at 700 pore volumes, C/C_0 was equal to 0.86. If adsorption equilibrium was not instantaneous, it would be expected that at a higher flow rate, the breakthrough curve would shift to the left because of the decreased time that the As(V) has in contact with the sand. This phenomenon was observed when the bulk velocity was increased to 2.3 cm/min. With a higher flow rate, initial breakthrough ($C/C_0 > 0.02$) first occurred after only 300 pore volumes. The breakthrough curve also peaked more rapidly, reaching a C/C_0 value of 0.98 by 600 pore volumes. These experiments demonstrated that contact time has a significant effect on As(V) adsorption, transport, and breakthrough, causing less As(V) to adsorb to the sand at the higher flow rate. At the lower flow, 77 ± 7% of the input amount of As(V) adsorbed, while at high flow rate only 56 ± 5% was adsorbed.

Desorption also occurred more rapidly at the high pore water velocity. On a percentage basis, more As(V) was desorbed at the higher pore water velocity: 17 ± 1% versus 13 ± 1% for the lower pore water velocity. More As(V) was mobilized by phosphate ions at the lower flow rate than at the high flow rate because of the longer residence time. At the lower flow, 47 ± 2% of the remaining adsorbed As(V) was mobilized, while at the high rate, 41 ± 2% of the As was mobilized. For both pore water velocities, recoveries were less than 100%, 64 ± 2 for 0.23 cm/min and 73 ± 2 for 2.3 cm/min.

pH variation experiments

As(III)

The As(III) breakthrough was much more rapid at pH 4.5 than at pH 9 (Figure 3). This result agrees with previously performed batch tests (not shown) which show that As(III) adsorption is favored at pH 9. The breakthrough curve at pH 9 reached a C/C_0 value of 1 after 700 pore volumes. The effluent concentration from the experiment performed at pH 4.5 did not reach this value. There was 48 ± 0.4% of As(III) adsorbed at pH 4.5, while 59 ± 4% was adsorbed at pH 9.

Downloaded by NORTH CAROLINA STATE UNIV on September 11, 2012 | http://pubs.acs.org
Publication Date: October 3, 2005 | doi: 10.1021/bk-2005-0915.ch007

Downloaded by NORTH CAROLINA STATE UNIV on September 11, 2012 | http://pubs.acs.org
Publication Date: October 3, 2005 | doi: 10.1021/bk-2005-0915.ch007

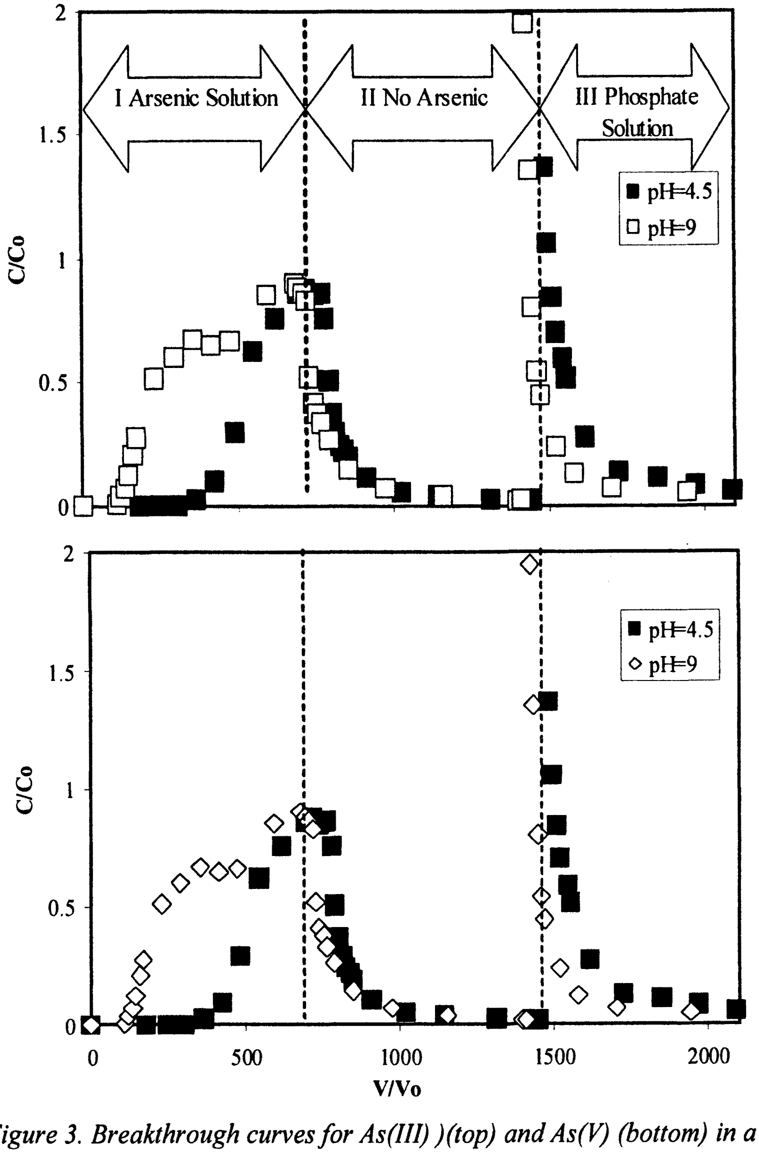

Figure 3. Breakthrough curves for As(III))(top) and As(V) (bottom) in a column of goethite coated sand: comparison of the pH effect, v=0.23 cm/min

The desorption process was similar at both pH values. Figure 3 shows an initially higher concentration in the effluent at pH 9, which is consistent with the higher adsorbed As concentration at pH 9. However, there was no significant difference in the relative As desorption at these two pH values, 58 ± 17% desorbed at pH 4.5 compared with 52 ± 4% for pH 9.

Upon the addition of 2.5×10^{-4} M phosphate, 68 ± 18% of the remaining As(III) was mobilized at pH 4.5 while 61 ± 2% mobilized at pH 9. The total recovery of As(III) in all experiments ranged from 89 to 100% .

Downloaded by NORTH CAROLINA STATE UNIV on September 11, 2012 | http://pubs.acs.org
Publication Date: October 3, 2005 | doi: 10.1021/bk-2005-0915.ch007

As(V)

As(V) showed much more rapid breakthrough and greater mobility at pH 9, in contrast to As(III) which showed the opposite effect (Figure 3). At pH 9 the breakthrough curve was not as steep, and it had an intermediate leveling for the pore volume range of 300 to 500. Less As(V) was initially adsorbed at pH 9 (51 ± 5%) than at pH 4.5 (77 ± 7%). These results can be explained from the surface charge stand point. The pH_{pzc} for goethite reported in literature varies between 7.0 and 9 (*16*). At low pH values such as pH 4.5, the goethite surface is positively charged. The increase in pH reflects a decrease in the number of protons in water, thus making the Fe surface more negatively charged. The As(V) ions were electrostatically repulsed by the negatively charged surface, and more As(V) remained in the aqueous phase. At the low pH the surface is positively charged, and it attracts $H_2AsO_4^-$ ions present in the solution at this pH (*17*). This is also the potential explanation for the lower recovery of As(V).

An increase in pH also had an effect on As(V) desorption in the sand. Approximately 24 ± 1% of the adsorbed As(V) was desorbed by the pH 9 solution, compared with only 13 ± 1% that was desorbed by the pH 4.5 solution. The phosphate solution at the lower pH was able to mobilize more As(V). In terms of mass, twice as much As(V) was mobilized by the pH 4.5 solution, but the actual percentage of mobilized As(V) calculated with respect to the initially adsorbed amount was very similar. At pH 4.5, 47 ± 2% of As(V) was mobilized compared with 43 ± 2% mobilized on pH 9. Total recovery of As(V) in all As(V) experiments mentioned above ranged from 64 to 78%. The lowest recovery corresponds to pH 4.5 where As(V) adsorption is strongest and therefore more of As(V) was retained on the sand and irreversibly adsorbed, even in the presence of phosphate.

Comparison of As(III) and As(V) data

A comparison of the collected experimental results between As(III) and As(V) is presented in Figure 4. The results confirm the greater mobility of As(III) at pH 4.5 while As(V) is more mobile at pH 9. On the other hand, As(III) has shown to be more readily desorbed in As-free solution than As(V) at both pH values. However, an interesting feature is observed in this part of the experiment. Although As(III) was more readily desorbed than As(V), a significant amount remained adsorbed even after 700 pore volumes of As-free solution. Moreover, the addition of phosphate ions easily mobilized both As(III) and As(V) ions. The addition of 2.5×10^{-4} M of phosphate remobilized the remaining As(III) and a significant fraction of As(V). However, this amount of phosphate ions was insufficient to completely remobilize As(V), since approximately 25-30% of As(V) remained adsorbed at the end of the experiments.

Downloaded by NORTH CAROLINA STATE UNIV on September 11, 2012 | http://pubs.acs.org
Publication Date: October 3, 2005 | doi: 10.1021/bk-2005-0915.ch007

Conclusions

As demonstrated in this study, arsenic adsorption and transport is dynamic and complex. It depends on both physical (flow) and chemical parameters (pH and competing ions). In this study, we conclude that the adsorption of As species is a rate dependent process. In all cases, adsorption was significantly reduced in the case of high pore water velocity because of shorter contact time. The system was also highly dependent on the pH. Our findings agree with the conclusion of previous researchers that As(III) adsorption is favored at high pH, while As(V) is more strongly adsorbed at low pH (*3*). Overall As(III) exhibited higher mobility (weaker bonding) and was desorbed from the sand more easily.

Overall we can summarize the conclusions as follows:

- Both As(III) and As(V) exhibited rate dependent adsorption;
- As(III) was desorbed more readily than As(V) in As-free solution. However, a significant amount of both As(III) and As(V) remained adsorbed even after 700 pore volumes of As-free solution;
- 2.5×10^{-4} M phosphate remobilized the remaining As(III) and a significant fraction of the As(V). However, approximately 25-35% of the As(V) was not recovered even in the presence of 2.5×10^{-4} M phosphate;
- As(III) was less strongly adsorbed and more mobile at pH 4.5 than pH 9, while As(V) was less strongly adsorbed and more mobile at pH 9.
- The overall comparison of the examined parameters on the system indicates that the effect on mobility and recovery of As species increased in the order pH < pore water velocity < phosphate < oxidation state.

Downloaded by NORTH CAROLINA STATE UNIV on September 11, 2012 | http://pubs.acs.org
Publication Date: October 3, 2005 | doi: 10.1021/bk-2005-0915.ch007

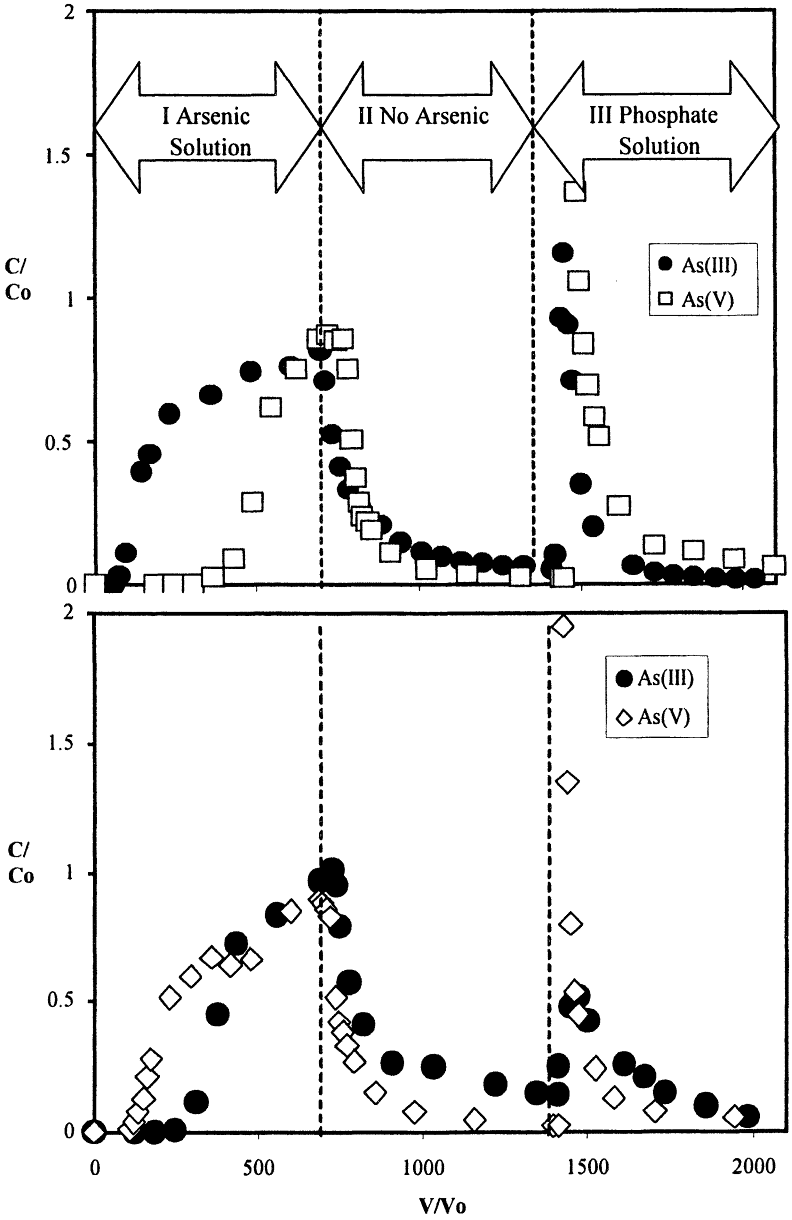

Figure 4. Comparison of the breakthrough curves for As(III)/ As(V) in a column of goethite coated sand – pH 4.5(top) and pH 9 (bottom), v=0.23 cm/min

- Simple models (e.g., K_D) of contaminant transport will not work. In order to make an accurate model, one must consider many parameters including pore water velocity (i.e., kinetic effects), pH, the presence of the competing ions, and adsorption irreversibility. Efforts to model this data are ongoing.

Aknowledgements

This research was supported in part by the Strategic Environmental Research and Development Program (SERDP) under the direction of Dr. Andrea Leeson. Also thanks to Dr. E. Roden from the University of Alabama for prepairing and supplying Fe- coated sand.

Downloaded by NORTH CAROLINA STATE UNIV on September 11, 2012 | http://pubs.acs.org
Publication Date: October 3, 2005 | doi: 10.1021/bk-2005-0915.ch007

References

1. Fuller C.C.; Davis J.A.; Waychunas G.A. *Geochim. Cosmochim. Acta.* **1993,** 57, 2271-2282
2. Melitas N.; Conklin M.; Farell J. *Environ. Sci. Technol.* **2002,** 36, 3188-3193
3. Wilkie J.A.; Hering J.G. *Colloid Surface. A.* **1996,** 107, 97-110
4. Hering J.G.; Chen P.Y.; Wilkie J.A.; Elimelech M.; Liang S. *J. Am. Water Works Assoc.* **1996,** 88(4), 155-167
5. Fendorf, S.; Eick M. J.; *Environ. Sci. Technol.* **1997,** 31(2): 315-320.
6. Dixit S.; Hering J.G. *Environ. Sci. Technol.* **2003,** 37 (18): 4182-4189
7. Smith E.; Naidu R.; Alston A.M. *Adv. Agron.* **1998,** vol 64 :149-195
8. Zhao H.S.; Stanforth R. *Environ. Sci. Technol.* **2001,** 35(24): 4753-4757
9. Vaishya R.C.; Gupta S.K. *J. Environ. Eng.* **2003,** 129(1), 89-92
10. Greenleaf J.E.; Cumbal L.; Staina I.; Sengupta A.K. *Process Saf. Environ.* **2003,** 81(2), 87-98
11. Williams L.E.; Barnett M.O.; Kramer TA,; Melville J.G. *J. Environ. Qual.* **2003,** 32 (3): 841-850
12. Bohn H.L.; McNeal B.L.; O'Connor G.A. *Soil Chemistry, 3rd edition* **2001,** John Wiley & Sons, Inc, New York, pp.145
13. Roden, E. E.; Urrutia M. M. *Appl. Environ. Microb.* **2000,** 66(3): 1062-1065
14. Mehra, O. P.; Jackson, M. L. *Clays Clay Miner.* **1960,** 7, 317-327.
15. Ficklin W.H. *Talanta.* **1983,** 35(5): 371-373
16. Gaboriaud F.; Ehrhardt J.J. *Geochim. Cosmochim. Acta.* **2002,** 67(5), 967-983
17. Raven K.P.; Jain A. *Environ. Sci. Technol.* **1998,** 32(3): 344-349

Downloaded by PENNSYLVANIA STATE UNIV on September 11, 2012 | http://pubs.acs.org
Publication Date: October 3, 2005 | doi: 10.1021/bk-2005-0915.ch008

Chapter 8

Comparison of As(III) and As(V) Complexation onto Al- and Fe-Hydroxides

James D. Kubicki

Department of Geosciences, The Pennsylvania State University, University Park, PA 16802

Ab initio hybrid molecular orbital/density functional theory (MO/DFT) calculations were performed on model aqueous and adsorbed arsenic species. As(III) and As(V) were modeled in both monodentate and bidentate bridging configurations with Al- and Fe-hydroxide dimer clusters to approximate M-OH and M-OH_2 groups (where M = Al(III) or Fe(III)) on solid surfaces. Estimates of the relative Gibbs free energy changes of adsorption were consistent with the observed preference of As(III) for hydrous ferric oxide (HFO) over Al-based phases. Calculated results were compared to interatomic distances derived from EXAFS spectra. The bidentate bridging configuration is most consistent with spectroscopic data, but the model ΔG_{ads} suggest that the monodentate configuration may be stable as a minor species on HFO surfaces.

In Advances in Arsenic Research; O'Day, P., et al.;
ACS Symposium Series; American Chemical Society: Washington, DC, 2005.

Introduction

Other chapters in this volume discuss the role adsorption of As onto mineral surfaces plays in the environment. Excellent reviews can be found in (*1*, *2*). Adsorption of As onto Al- and/or Fe-hydroxides in aquifers is one example. Another is the use of amorphous Al- and Fe-hydroxides to remove As from drinking water (*3*). This discussion will focus on a specific problem of As adsorption, namely why does As(V) adsorb to both Al- and Fe-hydroxides in similar amounts, but As(III) prefers Fe-hydroxides over Al-hydroxides (*3*)?

The literature on spectroscopic studies to determine the structure of As surface complexes (*4*) on these materials contains controversy (*5*, *6*). However, a recent paper with an analysis of EXAFS data from As(V) on Fe-hydroxides (*7*) agrees with the consensus view that a bidentate bridging mechanism predominates in this case. Studies also suggest that the same surface complex is dominant for As(V) on Al-hydroxides and for As(III) on both Al- and Fe-hydroxides. Consequently, understanding the differences in adsorption isotherms for As(III) on Al- and Fe-hydroxides is perplexing because similar structures are invoked although different surface sites may be involved (*2*). One caveat is that recent Grazing Incidence X-ray Absorption Fine Structure (GIXAFS) spectroscopic results indicate that the stable surface complex will vary with crystal face and may include tridentate species (G. A. Waychunas, pers. comm.)

Ab initio calculations can be useful in helping to interpret spectra of amorphous or disordered systems (*8*, *9*). A few studies have been conducted previously that bear on the topic at hand and on As speciation in the environment in general (*7*, *10*, *11*). Aqueous As species were modeled by Tossell (*10*) who calculated the structures and vibrational frequencies of numerous species to compare with the observed Raman spectra of Pokrovski et al. (*12*). Tossell (*13*) followed up on this line of investigation by modeling As interaction with Al-hydroxides. Accurate methods for calculating reaction energies were developed and applied to the question of which surface species - arsenate or carbonate - would be more stable on Al- and Fe-hydroxide mineral surfaces (*14*). Ladeira et al. (*11*) collected EXAFS spectra and performed DFT calculations and determined that the dominant surface complex is a bidentate, binuclear (bridging) configuration for As(V) on gibbsite ($Al(OH)_3$). Different configurations (bidentate mononuclear, monodentate mononuclear, and monodentate binuclear) were modeled with DFT calculations to help interpret and verify their interpretation of the EXAFS spectra. Sherman and Randall (*7*) published a study that included EXAFS spectroscopy and DFT calculations. Their conclusion concurred with a number of other researchers that the bidentate binuclear ("bidentate corner-sharing (^{2}C)" in their terminology) configuration

Downloaded by PENNSYLVANIA STATE UNIV on September 11, 2012 | http://pubs.acs.org
Publication Date: October 3, 2005 | doi: 10.1021/bk-2005-0915.ch008

was most stable for As(V) on Fe-hydroxides compared to monodentate mononuclear and bidentate mononuclear ("bidentate edge-sharing (^{2}E)" in their terminology). Consequently, this study has focused on the bidentate bridging configuration (Fig. 1) for As(III) and As(V) adsorption onto Al- and Fe-hydroxides. To test this assumption, calculated values of the interatomic distances are compared to EXAFS data. Some differences exist between the models used in this study and those in the papers mentioned above which are discussed below.

Downloaded by PENNSYLVANIA STATE UNIV on September 11, 2012 | http://pubs.acs.org
Publication Date: October 3, 2005 | doi: 10.1021/bk-2005-0915.ch008

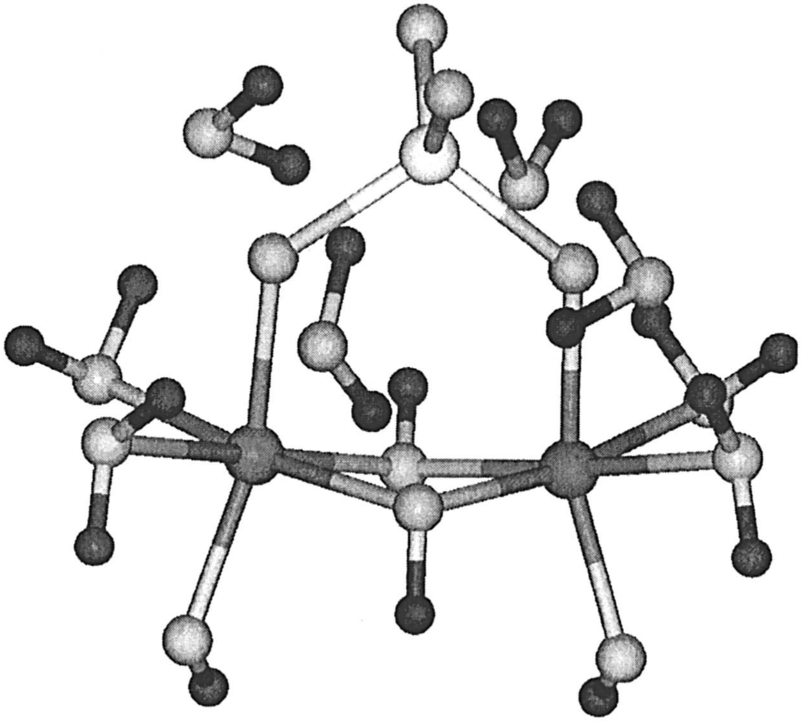

Figure 1. Bidentate briding configuration of $Al_2(OH)_4(OH_2)_4AsO_4{\bullet}4(H_2O)$ as optimized with the B3LYP/6-31G(d) method in Gaussian 98 (15). As white, H black, O light grey, Al dark grey in all figures.

Methods

Calculations were performed with Gaussian 98 (*15*), and models were constructed in Cerius^2 (*16*). Energy minimizations and frequency calculations were performed using HF/3-21G(d,p) and B3LYP/6-31G(d) basis sets (*17, 18, 19*). Structures and frequencies reported here were based on the latter method. The HF/3-21G(d,p) method was used to generate starting configurations for the more accurate B3LYP/6-31(d) calculations.

Model surface complex clusters were designed to minimize the charge because local charge buildup on the actual mineral surfaces is believed to be relatively small. Explicit hydration (addition of H_2O molecules) was included for the aqueous species, the surface M-OH groups, and the surface As complexes (Figs. 1-3). This factor can be key in accurately predicting structures and frequencies of anionic surface complexes because both are a function of the hydration state of the sample (*20, 21*). Adsorption free energies were estimated using model reaction components.

Downloaded by PENNSYLVANIA STATE UNIV on September 11, 2012 | http://pubs.acs.org
Publication Date: October 3, 2005 | doi: 10.1021/bk-2005-0915.ch008

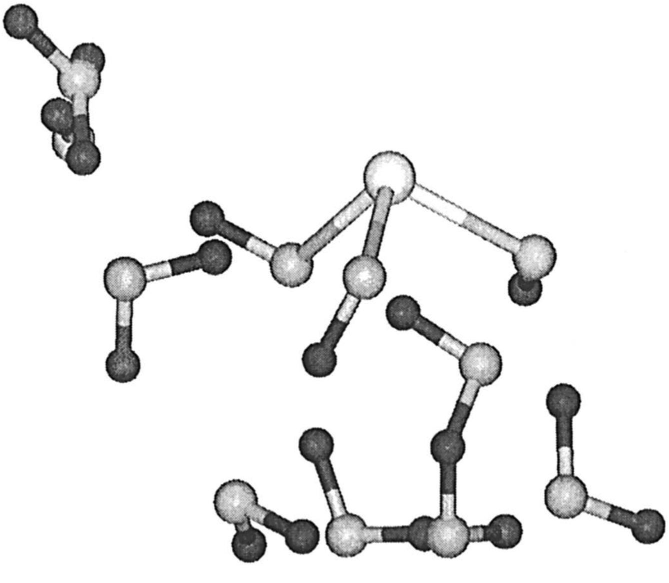

Figure 2. Model of the solvated H_3AsO_3 species after energy minimization shows that the OH groups are hydrophilic but the As(III) appears to be hydrophobic.

Downloaded by PENNSYLVANIA STATE UNIV on September 11, 2012 | http://pubs.acs.org
Publication Date: October 3, 2005 | doi: 10.1021/bk-2005-0915.ch008

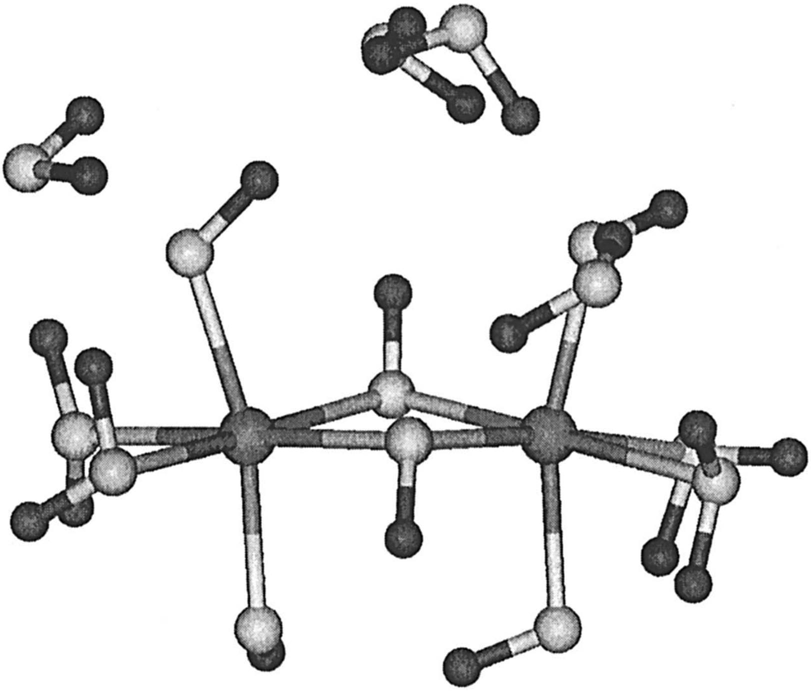

Figure 3. Model of a neutral Al-hydroxide surface site as represented by $Al_2(OH)_6{\bullet}4(H_2O$.

Gibbs free energies of each species were modeled by calculating the free energy in a polarized continuum. The Integrated Equation Formalism Polarized Continuum Model (*22*) was used to calculate the Gibbs free energy in solution. Single point energy calculations were performed with the B3LYP/6-311+G(d,p) method (*23*). The ΔG_{ads} was then estimated from stoichiometrically balanced reactions. Configurational entropy terms were neglected in this approach; hence, it is important to emphasize that these are Gibbs free energy estimates. The relative free energy changes for As(III) and As(V) adsorbed onto Al- versus Fe-hydroxides are compared, so neglect of configurational entropy will cancel out to a large degree. Interatomic distances calculated in each model surface complex were compared to As-O and and As-M distances obtained from EXAFS spectra (*7, 24*).

Results

H_3AsO_3, $H_2AsO_3^{1-}$, $H_2AsO_4^{1-}$ and $HAsO_4^{2-}$ were modeled as reactants because these will be the dominant species (H_3AsO_3 - $pK_1 = 9.2$; H_3AsO_4 – $pK_1 = 2.2$, $pK_2 = 7.0$, $pK_3 = 11.5$) present (*25*) under the pH range of interest (approximately pH 3 to 11). (Note that eight H_2O molecules were included around each molecule to account for short-range solvation effects.) The modeled adsorption reactions often result in the release of H_2O, H_3O^+ or OH^-, so the free energies of the clusters $5(H_2O)$, $H_3O^+(H_2O)_4$, and $OH^-(H_2O)_4$ were also calculated in order to account for these products in a self-consistent manner.

Surface charge on Al- and Fe-hydroxides varies as a function of pH as well as the protonation state of the As aqueous species. Negatively charged surfaces are less likely to adsorb the negatively charged As aqueous species (with the exception of the neutral H_3AsO_3). Hence, neutral and positively charged Al- and Fe-hydroxide terminal surface groups were modeled by the $[M_2(OH)_{6-z}(OH_2)_{4+z}]^{z+}$ clusters (where M is either Al(III) or Fe(III), and z is the charge on the total model cluster). Direct modeling of pH in these types of calculations is not possible; but, with this array of surface and aqueous species, reactants can be selected that represent the experimentally determined species over the pH range of interest. Again, the surfaces will be solvated prior to the adsorption reactions, so four H_2O molecules were included to account for H-bonding to the surface M-OH groups.

The protonation state of adsorbed As species is not well known, but EXAFS data indicate four relatively equivalent As-O bonds which is most consistent with no As-OH bonds because As-OH bonds are typically longer than As-O bonds (*20*). With this in mind, the surface complexes were modeled by AsO_3^{3-} and AsO_4^{3-} (Fig. 1). Adsorbed anions commonly retain H_2O molecules (*20, 21, 26, 27*) due to strong H-bonding. Four H_2O molecules were included to model this physisorbed water. Initially, the surface species modeled were $HAsO_3^{2-}$, $H_2AsO_4^{1-}$, and $HAsO_4^{2-}$ without solvation. These models are included for the sake of completeness and will be useful in comparison to the study of Sherman and Randall (*7*) who used protonated, non-hydrated model surfaces.

Comparison of EXAFS and calculated interatomic distances

The main experimental evidence for inner-sphere complexation of As on Al- and Fe-hydroxides comes from EXAFS spectra (*7, 28, 29, 30, 31, 32*). Table I

Downloaded by PENNSYLVANIA STATE UNIV on September 11, 2012 | http://pubs.acs.org
Publication Date: October 3, 2005 | doi: 10.1021/bk-2005-0915.ch008

lists the As-O, As-Al and As-Fe interatomic distances obtained from some of these studies. For the bidentate bridging configuration, the model As(III) and As(V) species on both the Al- and Fe-hydroxide model surfaces result in As-O and As-M interatomic distances in good agreement with the observed values (Table I). The agreement is fortuitously accurate for some of the As-O bond lengths as one typically expects accuracy on the order of a few hundreths of an Angstrom for this type of calculation. The As-O bond length for the Fe-As(V) complex falls outside this error bar, but the range presented in (*7*) for As-O bonds is significantly wider than that presented in other studies (*28-32*).

The calculated As-M distances are generally in error by approximately 0.1 Å. Most of this error is due to the fact that complete relaxation of the model surface was allowed in order to achieve minimum energy configurations. Mineral surface groups are restricted at least partially by the underlying crystal lattice, so full relaxation overestimates the amount of displacement the metal ion can undergo on the surface as a result of complexation to As. Without the restriction of the bulk crystal lattice, the initial model surfaces are not likely to have Fe-O bond lengths accurate to less than 0.1 Å compared to a mineral surface.

Downloaded by PENNSYLVANIA STATE UNIV on September 11, 2012 | http://pubs.acs.org
Publication Date: October 3, 2005 | doi: 10.1021/bk-2005-0915.ch008

Table I. Observed and calculated bond lengths of adsorbed arsenic species

	Distance	*Expt*	*Calc*
Bidentate bridging			
$Al_2(OH)_4(OH_2)_4AsO_3^-(H_2O)_4$	As-O	1.77(*31*)	1.77 & 1.80
	As-Al	3.21(*31*)	3.21
$Fe_2(OH)_4(OH_2)_4AsO_3^-(H_2O)_4$	As-O	1.78(*32*)	1.76 & 1.80
	As-Fe	3.38(*28*)	3.28
$Al_2(OH)_4(OH_2)_4AsO_4^-(H_2O)_4$	As-O	1.68(*31*)	1.70
	As-Al	3.11(*31*)	3.19
$Fe_2(OH)_4(OH_2)_4AsO_4^-(H_2O)_4$	As-O	1.62-1.71(*7*)	1.69 & 1.73
	As-Fe	3.2-3.35(*7*)	3.28
Monodentate			
$Al_2(OH)_4(OH_2)_5AsO_4^-(H_2O)_6$	As-O	1.68(*31*)	1.68 to 1.74
	As-Al	3.11(*31*)	3.22 & 4.37
$Fe_2(OH)_4(OH_2)_5AsO_4^-(H_2O)_6$	As-O	1.62-1.71(*7*)	1.68 to 1.74
	As-Fe	3.2-3.35(*7*)	3.32 & 4.51

The monodentate configurations generally provide good agreement with the experimental As-O and As-Al distances as well (Table I). However, an extra As-

M distance is present in the calculations at 4.4 to 4.5 Å that is not observed in the EXAFS spectra. Furthermore, current EXAFS spectra suggest two roughly equivalent As-M distances should be present, consistent with the bidentate bridging complex.

As mentioned above, protonated As surface species without explicit solvation were also modeled as surface complexes. Agreement between experiment and model can be good for many structural parameters. However, several discrepancies exist that suggest there is a problem with using these model surface species. For example, the model As-O bond lengths to the O atoms attached to the Al and Fe clusters were close to the observed values, but the As-OH bond lengths are significantly longer than the experimental values (e.g., 1.93 versus 1.77 Å in $Al_2(OH)_4(OH_2)_4HAsO_3$). The distortion of the As-OH bonds compared to As-O bonds in these model calculations is consistent with IR spectral evidence (*20*) but the opposite of that predicted in (*7*). This discrepancy will be discussed below.

Calculated reaction free energies for neutral and positive surfaces

The above discussion has focused on verifying that the model calculations resemble the actual adsorption of As(III) and As(V) onto Al- and Fe-hydroxides. The main research question, however, is to explain why As(V) binds to both Al- and Fe-hydroxides whereas As(III) has a strong preference for Fe-hydroxides over Al-hydroxides (*3*). To this end, estimates of the free energies of reaction were calculated for pairs of aqueous and surface species.

Table II lists a number of possible surface adsorption reactions. Two trends can be extracted from the results that are consistent with the observations of Hering et al. (*3*) mentioned above. First, the calculated ΔG_{ads}'s for all the As(V) bidentate complexes on Al- and Fe-clusters were within approximately ±20 kJ/mol of one another. Given the potential errors induced by the computational method and model simplifications, these values can be considered roughly equivalent to one another. When a significant discrepancy exists in the calculated values for adsorption onto Al-hydroxides versus Fe- hydroxides, then the Al-hydroxide surface complex is more commonly favored. Second, the model adsorption free energies for H_3AsO_3 can be -30 to -40 kJ/mol more favorable onto Fe- hydroxides than Al-hydroxides (Table II).

Another set of comparisons can be made to the experiments of Dixit and Hering (*33*) based on the results in Table II. The above authors noted a decrease in the percent adsorbed As(V) onto HFO and goethite as pH increased from 3.5 to 10.5. If one compares the two model reactions that should occur near pH 4 and 7 -

Downloaded by PENNSYLVANIA STATE UNIV on September 11, 2012 | http://pubs.acs.org
Publication Date: October 3, 2005 | doi: 10.1021/bk-2005-0915.ch008

Table II. Calculated Gibbs free energy of adsorption

Positively charged surface - As(V)

$H_2AsO_4^-(H_2O)_8 + Al_2(OH)_5(OH_2)_5^+(H_2O)_4 \rightarrow$
$Al_2(OH)_4(OH_2)_4AsO_4^-(H_2O)_4 + [H_3O^+(H_2O)_4] + 5H_2O = -54$ kJ/mol

$H_2AsO_4^-(H_2O)_8 + Fe_2(OH)_5(OH_2)_5^+(H_2O)_4 \rightarrow$
$Fe_2(OH)_4(OH_2)_4AsO_4^-(H_2O)_4 + [H_3O^+(H_2O)_4] + 5H_2O = -64$ kJ/mol

$H_2AsO_4^-(H_2O)_8 + Al_2(OH)_5(OH_2)_5^+(H_2O)_4 \rightarrow$
$Al_2(OH)_4(OH_2)_5AsO_4^-(H_2O)_6 + [H_3O^+(H_2O)_4] + 2H_2O = -134$ kJ/mol

$H_2AsO_4^-(H_2O)_8 + Fe_2(OH)_5(OH_2)_5^+(H_2O)_4 \rightarrow$
$Fe_2(OH)_4(OH_2)_5AsO_4^-(H_2O)_6 + [H_3O^+(H_2O)_4] + 2H_2O = -38$ kJ/mol

Neutral surface - As(V)

$H_2AsO_4^-(H_2O)_8 + Al_2(OH)_6(OH_2)_4(H_2O)_4 \rightarrow$
$Al_2(OH)_4(OH_2)_4AsO_4^-(H_2O)_4 + 2[5(H_2O)] = -120$ kJ/mol

$H_2AsO_4^-(H_2O)_8 + Fe_2(OH)_6(OH_2)_4(H_2O)_4 \rightarrow$
$Fe_2(OH)_4(OH_2)_4AsO_4^-(H_2O)_4 + 2[5(H_2O)] = -116$ kJ/mol

$HAsO_4^{2-}(H_2O)_8 + Al_2(OH)_6(OH_2)_4(H_2O)_4 \rightarrow$
$Al_2(OH)_4(OH_2)_4AsO_4^-(H_2O)_4 + [OH^-(H_2O)_4] + 5H_2O = -177$ kJ/mol

$HAsO_4^{2-}(H_2O)_8 + Fe_2(OH)_6(OH_2)_4(H_2O)_4 \rightarrow$
$Fe_2(OH)_4(OH_2)_4AsO_4^-(H_2O)_4 + [OH^-(H_2O)_4] + 5H_2O = -172$ kJ/mol

Positively charged surface - As(III)

$H_3AsO_3(H_2O)_8 + Al_2(OH)_5(OH_2)_5^+(H_2O)_4 \rightarrow$
$Al_2(OH)_4(OH_2)_4AsO_3^-(H_2O)_4 + 2[H_3O^+(H_2O)_4] = +57$ kJ/mol

$H_3AsO_3(H_2O)_8 + Fe_2(OH)_5(OH_2)_5^+(H_2O)_4 \rightarrow$
$Fe_2(OH)_4(OH_2)_4AsO_3^-(H_2O)_4 + 2[H_3O^+(H_2O)_4] = +14$ kJ/mol

Neutral surface - As(III)

$H_3AsO_3(H_2O)_8 + Al_2(OH)_6(OH_2)_4(H_2O)_4 \rightarrow$
$Al_2(OH)_4(OH_2)_4AsO_3^-(H_2O)_4 + [H_3O^+(H_2O)_4] + 5H_2O = -8$ kJ/mol

$H_3AsO_3(H_2O)_8 + Fe_2(OH)_6(OH_2)_4(H_2O)_4 \rightarrow$
$Fe_2(OH)_4(OH_2)_4AsO_3^-(H_2O)_4 + [H_3O^+(H_2O)_4] + 5H_2O = -38$ kJ/mol

$H_2AsO_3^-(H_2O)_8 + Al_2(OH)_6(OH_2)_4(H_2O)_4 \rightarrow$
$Al_2(OH)_4(OH_2)_4AsO_3^-(H_2O)_4 + 10(H_2O)] = -29$ kJ/mol

$H_2AsO_3^-(H_2O)_8 + Fe_2(OH)_6(OH_2)_4(H_2O)_4 \rightarrow$
$Fe_2(OH)_4(OH_2)_4AsO_3^-(H_2O)_4 + 10(H_2O)] = -59$ kJ/mol

Downloaded by PENNSYLVANIA STATE UNIV on September 11, 2012 | http://pubs.acs.org
Publication Date: October 3, 2005 | doi: 10.1021/bk-2005-0915.ch008

$H_2AsO_4^-(H_2O)_8 + Fe_2(OH)_5(OH_2)_5^+(H_2O)_4 \rightarrow$
$Fe_2(OH)_4(OH_2)_4AsO_4^-(H_2O)_4 + [H_3O^+(H_2O)_4] + 5H_2O = -64$ kJ/mol

and

$H_2AsO_4^-(H_2O)_8 + Fe_2(OH)_6(OH_2)_4(H_2O)_4 \rightarrow$
$Fe_2(OH)_4(OH_2)_4H_2AsO_4^+ + 2[OH^-(H_2O)_4] + (H_2O)_4 = -43$ kJ/mol,

respectively, as the surface changes from positively charged to more neutral, then a decrease in the equilibrium adsorption would be predicted. As a cautionary note, however, as the model pH moves to approximately 10, the reaction – $HAsO_4^{2-}(H_2O)_8 + Fe_2(OH)_6(OH_2)_4(H_2O)_4 \rightarrow$
$Fe_2(OH)_4(OH_2)_4AsO_4^-(H_2O)_4 + OH^-(H_2O)_4 + 5H_2O = -172$ kJ/mol
may also occur because the second pK_a for arsenic acid is 7. The model result suggests that adsorption would increase above pH 7, but this is not observed (*33*). The discrepancy may be indicating an error in the methodology for estimating the ΔG_{ads}, but the more likely explanation is that the surface is becoming negatively charged. pH 10 is above the zero-point of charge for HFO and goethite (*34*). Negatively charged surface models were not included here but should be included in future work to address this question.

The trend for As(III) adsorption onto HFO and goethite is not as strong a function of pH as for As(V), and it is in the opposite direction. The ΔG_{ads} values listed in Table II are qualitatively consistent with this trend because the values become more negative from the positively charged to the neutral model surface. However, the former predicts that adsorption should not occur to any significant degree because the ΔG_{ads} is positive albeit only by +14 kJ/mol for the Fe-hydroxide cluster. (One should also note that adsorption of As(III) onto HFO decreases at pH 10. Again, modeling a negatively charged surface would be more appropriate to compare to this experimental result because this is above the ZPC of HFO (*34*).)

Discussion

One difference between the models used in this study and those of Ladeira et al. (*11*) and Sherman and Randall (*7*) is the protonation state of the As surface species. These previous authors both chose to model the adsorbed As(V) species as $H_2AsO_4^-$ compared to the AsO_4^{3-} species. Initially, a similar configuration was used in this study as well, $M_2(OH)_4(OH_2)_4H_2AsO_4^+$. Although the protonation state of adsorbed anions is not unequivocally known, experimentalists working on similar problems pointed out (*20, 21*) that these types of anionic species tend to form XO_4-type surface complexes (e.g., PO_4, SO_4, AsO_4). ATR-FTIR spectra of phosphate on ferrihydrite, for example, have been interpreted in terms of non-protonated, bidentate binuclear complexes (*35*). In these cases, where an adsorbed anion has an oxygen atom pointed toward the

Downloaded by PENNSYLVANIA STATE UNIV on September 11, 2012 | http://pubs.acs.org
Publication Date: October 3, 2005 | doi: 10.1021/bk-2005-0915.ch008

solution, H-bonding is strong and the structure and vibrational spectrum is dependent on the hydration of the surface (*26, 27*). Consequently, the solvated $M_2(OH)_4(OH_2)_4AsO_4^-$ model should be more comparable to the actual surface complex than the $M_2(OH)_4(OH_2)_4H_2AsO_4^+$ model without any H_2O molecules. In addition, the $M_2(OH)_4(OH_2)_4HAsO_4$ and $M_2(OH)_4(OH_2)_4HAsO_3$ structures result in As-O bond lengths inconsistent with EXAFS data (i.e., the As-OH bonds are too long by 0.1 to 0.15 Å).

Another discrepancy between these results and those of (*7*) is the relative stability of the monodentate and bidentate bridging configurations for As(V). Sherman and Randall use the reaction

$Fe_2(OH)_2(OH_2)_7H_2AsO_4^{3+} \rightarrow Fe_2(OH)_2(OH_2)_6AsO_2(OH)_2^{3+} + H_2O$,

and they conclude that the bidentate configuration is -95 kJ/mol more stable than the monodentate complex; hence, the monodentate configuration will not be significant due to this energy difference. The above scheme is a good approach because the model surface complexes are compared directly which will help cancel out errors inherent in the computational methodology.

The approach described in this paper predicts that the bidentate bridging complex is only -26 kJ/mol more stable than the monodentate configuration for the reaction of $H_2AsO_4^-$ onto positively charged Fe-hydroxide (Table II). The ΔG_{ads} estimate is within computational error; hence, this result suggests that an equilibrium could exist between the two configurations. Entropic effects may favor the bidentate configuration, however, as H_2O release results in a positive entropy change. Depending on the pH, crystal faces present, etc., each configuration could predominate the surface adsorption of As on Fe-oxides and Fe-hydroxides. On the other hand, the monodentate configuration is favored by -80 kJ/mol in these calculations for adsortion onto positively charged Al-hydroxide (Table II). If this is correct, these relative thermodynamic stabilities predict different bonding mechanisms for As(V) onto Al- and Fe-hydroxides under the conditions most common in the environment (i.e., $H_2AsO_4^-$ and positively charged surfaces).

Fewer configurations of the monodentate complex were modeled here because the bidentate bridging configuration has been preferred based on EXAFS spectra. Another reason for this is that monodentate surface complex models based on the neutral surface model (e.g., $Al_2(OH)_6(OH_2)_4(H_2O)_4$ + $HAsO_4^{2-}(H_2O)_8 \rightarrow Al_2(OH)_5(OH_2)_4AsO_4^{2-}(H_2O)_6 + 7(H_2O)$) tended to undergo H^+ transfer reactions during energy minimizations. These H^+ transfer reactions were artifacts of the cluster termination process and not relevant to As surface complexation. Calculations on a periodic system could help address this issue.

Several differences exist between the Sherman and Randall (*7*) and this study that complicate comparison of the theoretical results, and these are listed below.

Downloaded by PENNSYLVANIA STATE UNIV on September 11, 2012 | http://pubs.acs.org
Publication Date: October 3, 2005 | doi: 10.1021/bk-2005-0915.ch008

1) The Sherman and Randall reaction involves protonated As species, and the monodentate equivalent of these surface complexes were not modeled here.
2) The charge on the model surface complexes in (*7*) is larger than in this study.
3) The computational methodologies are different with the previous work using pure DFT methods; this research relied upon hybrid MO/DFT calculations.
4) The effect of solvation by H_2O molecules was not included in (*7*).

Consequently, accounting for the discrepancies in the relative stabilities of the monodentate versus bidentate bridging complexes in these two studies is not possible within the time constraints for publication of these results. Future work will attempt to minimize the differences listed above between the two studies to better help constrain the stabilities of these two surface complexes.

To a first approximation, the model ΔG_{ads} values presented here are consistent with the similar behavior of As(V) on Al- and Fe-hydroxides and the dissimilar behavior of As(III) on these surfaces. The true reason behind this dissimilar behavior is not yet clear, however. Natural bond orbital population analyses (*36*) of the aqueous and surface complex models reveals relatively small changes (on the order of 0.01 electrons) in the electron configurations around the Al, Fe, and As atoms. Whether or not these small changes could be responsible for such a distinctive change in adsorption behavior is not clear.

Modeling pH effects is a difficult problem for molecular modeling. The limited number of atoms in the model system precludes a realistic treatment of a system containing 10^{-7} H^+, for example. The approach used here is to build models that mimic the protonation state of a given experimental system, and then self-consistently account for proton transfer and solvation effects among all components. Even if this were computed accurately, comparison to experiment would be complicated by the fact that a number of competing reactions may be occurring in a macroscopic system. The equilibrium behavior of the experimental system will be a combination of these reactions; but, in a model system, only one reaction is considered at a time. For this reason, the most reliable comparisons between experimental data and model results are based on comparing spectroscopic, rather than thermodynamic, parameters. This author prefers to more heavily weight the spectroscopic evidence when assigning the existence of a given surface complex. Once this assignment is made, the configuration selected can be used to constrain surface complexation modeling which does a better job of reproducing experimental equilibrium behavior. Without prior constraint, however, surface complexation modeling efforts often result in non-unique explanations for the experimental observation. Thus, a strategy of spectroscopy, molecular modeling, potentiometric experiments, and surface complexation modeling is required to constrain surface speciation.

Downloaded by PENNSYLVANIA STATE UNIV on September 11, 2012 | http://pubs.acs.org
Publication Date: October 3, 2005 | doi: 10.1021/bk-2005-0915.ch008

Acknowledgements

The author acknowledges two anonymous reviewers as well as comments by G. A. Waychunas, D. Sherman, and A. Foster. Discussions with J. Hering were critical to the initiation and progress of the study. JDK acknowledges the support of "Stony Brook-BNL collaboration to establish a Center for Environmental Molecular Sciences (CEMS)." Computations were supported, in part, by the Materials Simulation Center, a Penn State MRSEC and MRI facility.

Downloaded by PENNSYLVANIA STATE UNIV on September 11, 2012 | http://pubs.acs.org
Publication Date: October 3, 2005 | doi: 10.1021/bk-2005-0915.ch008

References

1. Oremland, R.S.; Stolz, J.F. The ecology of arsenic. *Science* 2003, *300*, 939.
2. Ng, J.C.; Wang, J.P.; Shraim, A. *Chemosphere* **2003**, *52*, 1353.
3. Hering, J. G.; Chen, P-Y.; Wilkie, J.A.; Elimelech, M. *J. Env. Eng.* **1997**, 800.
4. Foster, A. Spectroscopic investigations of arsenic species in solid phases. In *Arsenic in Ground Water: Geochemistry and Occurrence*, Welch (ed), 2002, Kluwer, p. 25.
5. Waychunas, G.A.; Davis, J.A.; Fuller, C.C. *Geochim. Cosmochim. Acta* **1995**, *59*, 3655.
6. Manceau, A. *Geochim. Cosmochim. Acta* **1995**, *59*, 3647.
7. Sherman, D.; Randall, S.R. *Geochim. Cosmochim. Acta* **2003**, *67*, 4223.
8. Tossell, J.A. Calculating the NMR properties of minerals, glasses, and aqueous species. In *Molecular Modeling Theory: Applications in the Geosciences*, R.T. Cygan and J.D. Kubicki (eds), *Rev. in Mineral. Geochem.* 2001, *42*, p. 437.
9. Kubicki, J.D. Interpretation of vibrational spectra using molecular orbital theory calculations. In *Molecular Modeling Theory: Applications in the Geosciences*, R.T. Cygan and J.D. Kubicki (eds), *Rev. in Mineral. Geochem.* 2001, *42*, p. 459.
10. Tossell, J.A. *Geochim. Cosmochim. Acta* **1997**, *61*, 1613.
11. Ladeira, A.C.Q.; Ciminelli, V.S.T.; Duarte, H.A.; Alves, M.C.M.; Ramos, A.Y. *Geochim. Cosmochim. Acta* **2001**, *65*, 1211.
12. Pokrovski, G.; Gout, R.; Schott, J.; Zotov, A.; Harrichoury, J.-C. *Geochim. Cosmochim. Acta* **1996**, *60*, 737.
13. Tossell, J.A. *Abs. Papers. Am. Chem. Soc.* **2003**, *226*, in press.
14. Appelo, C.A.J.; Van der Weiden, M.J.J.; Tournassat, C.; Charlet, L. *Environ. Sci. Technol.* **2002**, *36*, 3096.
15. Frisch, M.J. Gaussian 98, Gaussian, Inc., Pittsburgh PA, 2002.
16. Cerius^2, Accelrys Inc., San Diego, CA.
17. Hehre, W.J.; Ditchfield, R.; Pople, J.A. *J. Chem. Phys.* **1972**, *56*, 2257.
18. Becke, A.D. *J. Phys. Chem.* **1993**, *98*, 5648.
19. Lee, C.; Yang, W.; Parr, R.G. *Phys. Rev. B* **1988**, *37*, 785.

20. Myneni, S.C.B; Traina, S.J.; Waychunas, G.A.; Logan, T.J. *Geochim. Cosmochim. Acta* **1998**, *62,* 3285.
21. Hug, S.J. *J. Coll. Interface Sci.* **1997**, *188*, 415.
22. Cancès, E.; Mennucci, B.; Tomasi, J. *J. Chem. Phys.* **1997**, *107*, 3032
23. Foresman, J.B.; Frisch, Æ. *Exploring Chemistry with Electronic Structure Methods*, 1996, Gaussian Inc., Pittsburgh, PA.
24. Clausén, M.; Öhman, L-O.; Kubicki, J.D.; Persson, P. *J. Chem. Soc., Dalton Trans.* **2002**, 2559
25. Faure, G. *Principles and Applications of Geochemistry.* 1991, Prentice-Hall, Upper Saddle River, NJ, p. 120.
26. Pohle, W.; Bohl, M.; Böhlig, H. *J. Mol. Structure* **1991**, *242*, 333.
27. Persson, P.; Nilsson, N.; Sjöberg, S. *J. Coll. Interface Sci.* **1996**, *177*, 263.
28. Waychunas, G.A.; Rea, B.A.; Fuller, C.C.; Davis, J.A. *Geochim. Cosmochim. Acta* 1993, *57*, 2251.
29. Fendorf, S.; Eick, M.J.; Grossl, P.; Sparks, D.L. *Environ. Sci. Technol.* **1997**, *31*, 315.
30. Manning, B.A.; Fendorf, S.E.; Goldberg, S. *Environ. Sci. Technol.* **1998**, *32*, 2383.
31. Arai, Y.; Elzinga, E.J.; Sparks, D.L. *J. Coll. Interface Sci.* **2001**, *235*, 80.
32. Farquhar, M.L.; Charnock, J.M.; Livens, F.R.; Vaughan, D.J. *Env. Sci. Tech.* **2002**, *36*, 1757.
33. Dixit, S.; Hering, J.G. *Environ. Sci. Technol.* **2003**, *37*, 4182.
34. Dzombak, D. A.; Morel, F.M.M. *Surface Complexation Modeling - Hydrous Ferric Oxide*, 1990. p. 94.
35. Arai, Y.; Sparks, D. L. *J. Coll. Interface Sci.* **2001**, *241*, 317.
36. Breneman, C.M.; Wiberg, K.B. *J. Comp. Chem.* **1990**, *11*, 361.

Downloaded by PENNSYLVANIA STATE UNIV on September 11, 2012 | http://pubs.acs.org
Publication Date: October 3, 2005 | doi: 10.1021/bk-2005-0915.ch008

Downloaded by NORTH CAROLINA STATE UNIV on September 11, 2012 | http://pubs.acs.org
Publication Date: October 3, 2005 | doi: 10.1021/bk-2005-0915.ch009

Chapter 9

Calculation of the Interaction of Bicarbonate Ion with Arsenites in Aqueous Solution and with the Surfaces of Al Hydroxide Minerals

J. A. Tossell

Department of Chemistry and Biochemistry, University of Maryland, College Park, MD 20742 (tossell@chem.umd.edu)

Quantum mechanical calculations are used to study the stabilities of arsenite - bicarbonate and carbonate complexes and the stability of bicarbonate adsorbed onto models for Al hydroxide mineral surfaces. We identify a complex $As(OH)_2CO_3^-$, with a As-O-C linkage, which has a similar stability to the condensation dimer of $As(OH)_3$. This complex may significantly contribute to the total concentration of As in solution. The hydrated ion-pair form of this complex, $As(OH)_2CO_3Na(OH_2)_2$, is calculated to have a vibrational spectroscopic signature which may help in its identification. By contrast, the interaction of bicarbonate with the Al hydroxide mineral surface is much weaker than that of arsenite or arsenate, so that adsorbed arsenite and arsenate species will not be displaced by bicarbonate.

Introduction

High As concentrations have recently been observed in the groundwaters of Bangladesh and other regions *(1,2)*. One relatively new interpretation attributes this enrichment of As to either its displacement from the surfaces of Al and/or Fe oxyhydroxides through competition with carbonates or to the complexation of As species by carbonates *(3,4)*. Large formation constants for As - carbonate complexes were estimated by extrapolation of data for REE-carbonate complexes *(3)*. Indeed, these researchers stated that "according to these *estimates, which need to be confirmed experimentally* (our emphasis

In Advances in Arsenic Research; O'Day, P., et al.;
ACS Symposium Series; American Chemical Society: Washington, DC, 2005.

added), the carbonate complexes may be the most stable inorganic arsenic species in the aquatic environment." There are, however, no experimental structural or spectral data for arsenite - carbonate or bicarbonate complexes.

Rather than carrying out solubility or spectroscopic studies on such we approach the question of As-bicarbonate or carbonate complex formation and carbonate competition with arsenic species for adsorption sites on Al hydroxide mineral surfaces using quantum chemical computations.

The basic question to be addressed computationally is: what are the energetics for the interaction of bicarbonate and carbonate with As containing species in aqueous solution and with hydroxide mineral surfaces? In addition, the spectral properties of any stable complexes found have been calculated to help in verifying their identity. We have recently completed several such studies for various As and Sb bisulfide and hydroxide species, obtaining very good agreement between calculated and experimental reaction energies *(5)*.

Downloaded by NORTH CAROLINA STATE UNIV on September 11, 2012 | http://pubs.acs.org
Publication Date: October 3, 2005 | doi: 10.1021/bk-2005-0915.ch009

Theoretical methods used

We have used the methods of molecular quantum mechanics, specifically the Hartree-Fock (HF) method, the MØller-Plessett many body perturbation theory method to 2nd order (MP2) *(6)*, and coupled cluster theory with single, double and perturbative triple substitutions (CCSD(T)) *(7)*, All these methods are described in standard computational chemistry monographs *(8)*. The MP2 and CCSD(T) methods incorporate correlation in the motion of electrons, which is neglected at the HF level. They typically provide much more accurate bond energies and somewhat better equilibrium geometries than does the HF method. However, they are more demanding of computer time than HF. We have employed the MP2 approach as our base method because of its accuracy and efficiency. The basis sets used to expand the molecular orbitals are generally those of valence-electron only, relativistic effective core potential type *(9)*, which we designate SBK, with added polarization functions on the heavy atoms but not on H. For all the species considered we have determined equilibrium geometries in the gas-phase and have evaluated vibrational frequencies, zero-point vibrational energies (ZPE) and vibrational, rotational and translational (VRT) contributions to the gas-phase free energy at 25 °C. The necessary equations for the ZPE and VRT contributions *(10)* are incorporated into the GAUSSIAN code.

To approximate hydration energies we have used the COSMO (Conductor-like Screening MO method) *(11)* version of the self-consistent reaction field polarizable continuum method *(12)*. This is a very rapid and efficient technique which utilizes a non-spherical cavity about the solute and gives results very similar to those from older non-spherical cavity polarizable continuum models, but at much less computational cost. Nonetheless it still suffers from the main ambiguity of polarizable continuum model - the lack of uniqueness in the choice of the solute cavity. The implementation of this method in GAUSSIAN98 *(13)* also includes the calculation of several small energetic terms which are evaluated semiempirically, such as the cavitation energy and the dispersion energy. However, the implementation available in GAUSSIAN is only available for Hartree-Fock or density-functional calculations, not for more advanced approaches like MP2. It is important to realize that any polarizable continuum model of hydration involves very serious approximations and that the hydration energy differences evaluated for reactions, particularly those involving ions, are invariably much less accurate than are the corresponding gas-phase energies.

UV-visible absorption spectra have also been calculated for some of the species using the configuration interaction singles method *(14),* along with a COSMO repreesentation of the solvent, and we have used the Hartree-Fock version of the GIAO method *(15)* to calculate NMR shieldings. We used the quantum chemical software GAMESS *(16)* and GAUSSIAN98 *(13)* for the calculations.

Downloaded by NORTH CAROLINA STATE UNIV on September 11, 2012 | http://pubs.acs.org
Publication Date: October 3, 2005 | doi: 10.1021/bk-2005-0915.ch009

Results

Aqueous species

Reaction energies were calculated as sums of a gas-phase reaction energy, $\Delta E(g)$, the sum of the vibrational, rotational and translational contributions to the free energy in the gas phase, ΔG_{VRT}, and the hydration energy for the reaction obtained using the COSMO method, $\Delta\Delta G_{COSMO}$. The equation used was:

$$\Delta G(aq) = \Delta E(g) + \Delta G_{VRT} + \Delta\Delta G_{COSMO} \quad (1)$$

For our initial exploratory studies the MP2 method with a polarized SBK basis set was employed for the gas-phase calculations. We first considered reactions similar to those suggested in ref. (3), with the carbonate maximally bonded to As and some of the OH^- displaced, e.g. species such as that designated $As(CO_3)(OH)_2^-$, in which the As is bonded to two O atoms from the CO_3 group to form a ring. Such maximally bonded complexes were invariably found to be unstable with respect to $As(OH)_3$ and HCO_3^- as reactants, as indicated by the positive $\Delta G(aq)$ values in Table I (note that for the reactions in Table I we had not yet included the small ΔG_{VRT} terms, since the reactions clearly have unfavorable free energies). Our conclusion is that $\Delta G(aq)$ is highly positive for all the reactions considered above, so that formation of such maximally bonded complexes of HCO_3^- or CO_3^{-2} with $As(OH)_3$ is not favorable.

But are other only slightly different complexes more stable? Let's take a step back and try again. First, are the oxidation, oligomerization and protonation

Table I. Calculated energetics (in kcal/mol) for interaction of As(III) hydroxide species with carbonate, with gas-phase energies evaluated at the polarized SBK MP2 level and with COSMO solvation

reaction	$\Delta E(g)$	$\Delta\Delta G_{COSMO}$	$\Delta G(aq)$
$As(OH)_3 + HCO_3^- \Rightarrow$ $As(CO_3)(OH)_2^- + H_2O$	+43.0	+9.9	+52.9
$As(OH)_3 + CO_3^{-2} \Rightarrow$ $As(CO_3)(OH) + 2OH^-$	+29.2	+31.9	+61.1
$As(OH)_3 + CO_3^{-2} \Rightarrow$ $As(CO_3)^+ + 3OH^-$	+279.6	-137.0	+142.6

states chosen for the reactants reasonable? Initially we will assume that As(III) predominates (studies on As(V) complexes are in progress). In oxidic environments we can assume that $As(OH)_3$ is the predominant As (III) species, and concentrations of As are probably too low for dimerization to produce species like $(OH)_2AsOAs(OH)_2$. The pK_a's of the relevant species are 9.2 for $As(OH)_3$ and 6.3 (pK_{a1}) and 10.3 (pK_{a2}) for H_2CO_3, so near neutral pH we should have predominantly $As(OH)_3$ and HCO_3^-. Closer inspection of our results also revealed that the original geometry optimization for $As(CO_3)(OH)_2^-$ using GAMESS software had not converged sufficiently to allow us to calculate accurate vibrational properties, i.e. we had not really found a stationary point on the potential energy surface. When the GAMESS calculation was restarted and allowed to run until it had satisfied the convergence criterion of the software a qualitatively new (and considerably more stable) structure was obtained, as shown in Figure 1: In this new structure one of the As-O bonds has broken but the energy is 58.5 kcal/mol below the maximally bonded structure, which would be expected to be more stable. The species in Fig. 1 looks much like the condensation dimer of $As(OH)_3$, in which the monomers combine to form $(OH)_2As\text{-}O\text{-}As(OH)$. The difference is that we are now condensing $As(OH)_3$ and HCO_3^{-1} by splitting out the molecule of water. Apparently stable structures can be formed through such condensation dimerization reactions, with no change in number of bonds and minimal replacement of $-OH^-$ by carbonate ligands.

We then studied such species systematically at the polarized SBK MP2 level, producing the results show in Table II. In this case we have included the small ΔG_{VRT} terms, but we see they have no significant effect upon the energetics. These data indicate that the interaction of $As(OH)_3$ with HCO_3^- has similar energetics to the interaction of two $As(OH)_3$, so such a complex could have a significant concentration for large bicarbonate concentrations. Interaction of $As(OH)_3$ with a $NaHCO_3$ model for the bicarbonate species is even more favorable. On the other hand other linkages, e.g. As-O-N, are quite unfavorable. One interpretation of this fact is that O in a As-O-N linkage is overbonded in the Pauling sense, with a total bond strength sum of 2.67 rather than 2.0.

Downloaded by NORTH CAROLINA STATE UNIV on September 11, 2012 | http://pubs.acs.org
Publication Date: October 3, 2005 | doi: 10.1021/bk-2005-0915.ch009

Downloaded by NORTH CAROLINA STATE UNIV on September 11, 2012 | http://pubs.acs.org
Publication Date: October 3, 2005 | doi: 10.1021/bk-2005-0915.ch009

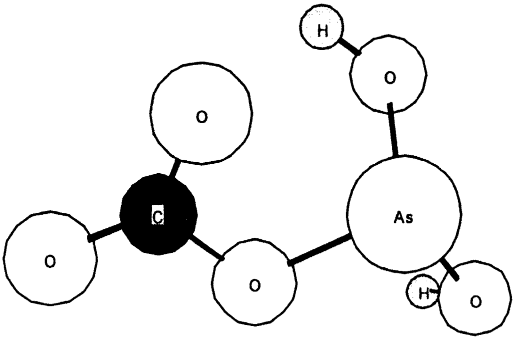

Figure 1. Structure of $As(OH)_2CO_3^{-1}$ calculated at the polarized SBK MP2 level.

Table II. Calculated energetics (in kcal/mol) for the condensation of oxyacids of B, N, P, As and C with $As(OH)_3$, with gas-phase energies evaluated at the polarized SBK MP2 level and with COSMO solvation

reaction	ΔE(g)	ΔG$_{VRT}$	ΔΔG$_{COSMO}$	ΔG(aq)
$As(OH)_3 + B(OH)_3 \Rightarrow (OH)_2AsOB(OH)_2 + H_2O$	+12.1	-1.1	-11.4	-0.4
$As(OH)_3 + HCO_3^- \Rightarrow As(OH)_2CO_3^- + H_2O$	-13.4	+1.6	+15.6	+3.8
$As(OH)_3 + NO_3^- \Rightarrow As(OH)_2(NO_3)^+ + OH^-$	+80.0	+0.7	-45.8	+34.9
$As(OH)_3 + H_2PO_4^- \Rightarrow As(OH)_2PO_2(OH)_2 + OH^-$	+87.1	+ 0.7	-59.6	+28.2
$2\ As(OH)_3 \Rightarrow (OH)_2AsOAs(OH)_2 + H_2O$	+10.3	+1.2	-7.8	+3.7
$As(OH)_3 + CO_2 \Rightarrow As(OH)_2CO_3H$	+10.3	+ 6.3	-2.6	+14.0
$As(OH)_3 + NaHCO_3 \Rightarrow As(OH)_2CO_3Na + H_2O$	-9.9	1.1	+5.2	-3.6

Table III. Calculated energies (in kcal/mol) for the gas phase reaction: $As(OH)_3 + HCO_3^- \Rightarrow As(OH)_2CO_3^- + H_2O$ using different computational methods

method	ΔE(g)
pol. SBK MP2	-13.4
6-31G* MP2	-26.4
6-31+G(2d,p) MP2	-24.3
6-31G* CCSD(T) @ 6-31G* CCD opt. geom.	-29.1

Downloaded by NORTH CAROLINA STATE UNIV on September 11, 2012 | http://pubs.acs.org
Publication Date: October 3, 2005 | doi: 10.1021/bk-2005-0915.ch009

We then focused more carefully on the $As(OH)_2CO_3^-$ species, assessing its energetics and structure at a number of quantum mechanical levels higher than that of polarized SBK MP2. The results we obtained are shown in Table III.

Although the energetic results are still not completely converged with respect to improvements in basis set and method, it is clear that larger basis sets and more highly correlated methods give an even more favorable reaction energy than do our original polarized SBK MP2 calculations. It is certainly dangerous to improve the calculation of the gas-phase energy without at the same time improving the calculation of the hydration energies, but we have no way to reliably go beyond the HF level using COSMO hydration at this time. However, based on the gas-phase energies it does appear that the reaction of $As(OH)_3$ with HCO_3^- in aqueous solution will be favorable.

We can now consider some of the properties of the $As(OH)_2CO_3^-$ (and related) complexes which might be useful in their spectral identification. Our unpublished calculations on the properties of HCO_3^- in solution indicate that a hydrated ion-pair may be the best simple model for the bicarbonate ion in $NaHCO_3(aq)$, one simple example being $NaHCO_3(OH_2)_4$. Therefore we use similar hydrated ion-pair models for the As-O-C species. For example, we use $As(OH)_2CO_3Na(OH_2)_2$, rather than the simpler $As(OH)_2CO_3^-$, to achieve better comparability with the $NaHCO_3(OH_2)_4$ model for $NaHCO_3(aq)$. First we evaluate the ^{13}C NMR shifts for selected complexes, as shown in Table IV below. We calculate the NMR shieldings, σ, in ppm and compare them with the calculated shielding for the ^{13}C reference compound TMS, $Si(CH_3)_4$.

The conclusion from the data in Table 4 is that ^{13}C carbonate shift is not modified significantly by interaction with the $-As(OH)_2$ unit, since the best models for HCO_3^- and $As(OH)_2CO_3^-$ (the Na^+ ion-pair with hydration) give almost the same ^{13}C NMR shifts.

The IR and Raman spectrum of $As(OH)_2CO_3^-$ and $As(OH)_2CO_3Na$ and their hydrated analogues have also been calculated at a number of different levels, up to 6-31G* MP2. To connect most closely to experiment, we employ the hydrated ion-pair model with standard scaling factors for the calculated frequencies (17). Results will be presented here only for $As(OH)_2CO_3Na(OH_2)_2$ at the 6-31G* HF and MP2 levels, for which the scaling factors commonly used are 0.893 and 0.943, respectively *(17)*.

Some frequencies are not much changed from the parent species, e.g. $As(OH)_3$ has a lowest energy As-O stretch calculated at the 6-31G* MP2 level of 688 cm^{-1} after scaling, while the lowest energy As-O stretch in the complex $As(OH)_2CO_3Na(OH_2)_2$ is calculated to be 669 at the same scaled 6-31G* MP2 level. However, other frequencies are more distinctive, e.g. the stretching mode involving the bridging O calculated at a scaled value of 676 cm^{-1}, as shown in Fig. 2.

Any determination of the existence of this complex using vibrational spectroscopy will probably need to examine relatively small differences between the spectra of arsenite solutions with and without bicarbonate. The vibrational properties calculated for this complex are collected in Table V.

Downloaded by NORTH CAROLINA STATE UNIV on September 11, 2012 | http://pubs.acs.org
Publication Date: October 3, 2005 | doi: 10.1021/bk-2005-0915.ch009

Table IV. Calculated ^{13}C NMR shifts (in ppm) for carbonates and As (III) oxide - carbonate complexes (using polarized SBK MP2 geometries and 6-311+G(2d,p) HF calculations of NMR shieldings)

molecule	^{13}C NMR shift (relative to TMS, σ = 189.4 ppm)
HCO_3^-	+168.8
	(exp. 163.3, 162.1)
Na HCO_3	+178.9
$NaHCO_3(OH_2)_4$	+175.3
$As(OH)_2CO_3^{-1}$	+162.3
$As(OH)_2CO_3H$	+167.6
$As(OH)_2CO_3Na$	+179.3
$As(OH)_2CO_3Na(OH_2)_2$	+174.5

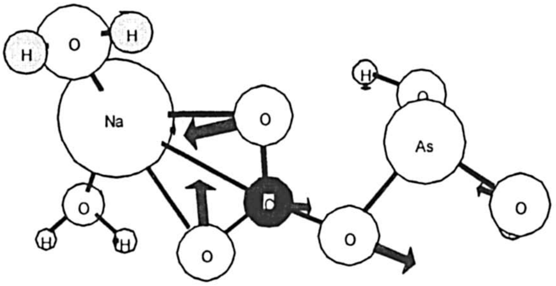

Figure 2. Bridging O stretch in $As(OH)_2CO_3Na(OH_2)_2$

Table V. Calculated As-O and C-O stretch vibrational frequencies (in cm^{-1}) for $As(OH)_2CO_3Na(OH_2)_2$, from 6-31G* calculations at HF and MP2 levels

$\nu_{HF}(cm^{-1})$	x 0.893	Rel. IR Intensity	Rel. Raman intensity	$\nu_{MP2}(cm^{-1})$	x 0.943
781	697	89	6.4	709	669
792	706	26	2.7	716	676
810	723	118	7.8	738	696
871	778	53	8.6	773	729
952	850	88	0.3	825	778
1105	987	184	1.1	1043	984
1143	1021	196	1.7	1055	995
1181	1055	82	4.9	1090	1028

We then calculated visible-UV absorption energies for some of the arsenite - carbonate complexes, using the configuration interaction singles (CIS) (14) method with a large 6-311+G(2d,p) basis set and COSMO solvation. Results are given in Table VI.

Table VI. Calculated UV absorption energies (in eV) for $As(OH)_3$ and As (III) - carbonate complexes (using polarized SBK MP2 geometries and 6-311+G(2d,p) CIS COSMO calculations of UV energies and intensities)

molecule	CIS COSMO ΔE (eV) (lowest three allowed) transitions
$As(OH)_3$	7.3, 7.3, 7.8
$(OH)_2AsOAs(OH)_2$	7.2, 7.5, 7.6
$As(OH)_2CO_3^{-1}$	7.8, 7.8, 8.4
$As(OH)_2CO_3H$	7.8, 8.1, 8.3
$As(OH)_2CO_3Na$	7.7, 8.0. 8.4

Our conclusion is that there is a blue shift in the lowest absorption energy when one of the -OH ligands of $As(OH)_3$ is replaced by carbonate, but it is fairly small, on the order of half an eV.

It is also worthwhile to address the question of whether $As(OH)_2CO_3^-$ would be the predominant arsenite - carbonate species or would it actually be protonated? We have calculated the energies for various deprotonation reactions, as shown in Table VII.

Downloaded by NORTH CAROLINA STATE UNIV on September 11, 2012 | http://pubs.acs.org
Publication Date: October 3, 2005 | doi: 10.1021/bk-2005-0915.ch009

The conclusion is that $As(OH)_2CO_3H$ is much easier to deprotonate than is HCO_3^-, so that the anionic species, $As(OH)_2CO_3^-$ will be dominant over the neutral (although as mentioned previously it may be better represented by a hydrated ion pair like $As(OH)_2CO_3Na(OH_2)_2$).

Adsorbed species

Let us now address the second possibility for the effect of carbonate concentration on the solubility of arsenites and arsenates - the interaction of HCO_3^- with coordinatively unsaturated Al hydroxide mineral surfaces. Although Fe hydroxides may well be more important in this context we presently restrict ourselves to the Al compounds.

We use a simple molecular model for the unsaturated Al hydroxide surface, as has been done by several researchers recently *(19)*, and bond various small molecules to it. For example, the interaction of $H_2AsO_4^-$ with the Al hydroxide surface is modeled by the cluster shown in Figure 3 below:

The energetics calculated for the formation of such surface complexes are shown in Table VIII below. In all cases we assume an inner-sphere bidentate corner sharing geometry as shown, consistent with previous calculations and experiment *(19)*. We have used both +4 charged models and neutral models (with four H_2O replaced by four F^-) for the mineral surface.

The conclusion is that for both the charged and neutral Al hydroxide models, HCO_3^- binds more strongly than do two waters, but much less strongly than $H_2AsO_4^-$, $H_2AsO_3^-$ or $H_2PO_4^-$. Note that the common and often studied $H_2PO_4^-$ anion binds with similar energetics to the arsenite and arsenate oxyanions Note also that the As(III) oxyanion actually bonds about as strongly as does the As(V) oxyanion. Experimental results for arsenite and arsenate binding at pH on Fe oxyhydroxide surfaces are similar *(20)),* although bulk results for the compound alum indicate that arsenate is more strongly bound than arsenite at all pH values *(21)*. Our results indicate that HCO_3^- will not effectively compete with arsenites or arsenates for sites on the Al hydroxide surface. It remains to be seen whether computational results will be similar for a Fe hydroxide surface. Of course, the energetics of adsorption depend upon solution pH, which partially determines the charge state of the adsorbing species. The above results are relevant for an environment in which each of the oxyacids exists predominantly as a mononegative ion.

Downloaded by NORTH CAROLINA STATE UNIV on September 11, 2012 | http://pubs.acs.org
Publication Date: October 3, 2005 | doi: 10.1021/bk-2005-0915.ch009

Table VII. Calculated energetics (in kcal/mol) for deprotonation reactions, using pol. SBK MP2 gas phase energies, and COSMO solvation free energies but with -269.0 kcal/mol for the free energy of the hydrated proton *[18]* (which dominates $\Delta\Delta G_{COSMO}$ for this case)

reaction	$\Delta E(g)$	ΔG_{VRT}	$\Delta\Delta G_{COSMO}$	$\Delta G(aq)$
$As(OH)_2CO_3H \Rightarrow As(OH)_2CO_3^- + H^+$	+324.0	-13.0	-314.0	-7.4
$HCO_3^- \Rightarrow CO_3^{-2} + H^+$	+498.5	-13.7	-449.9	+30.5

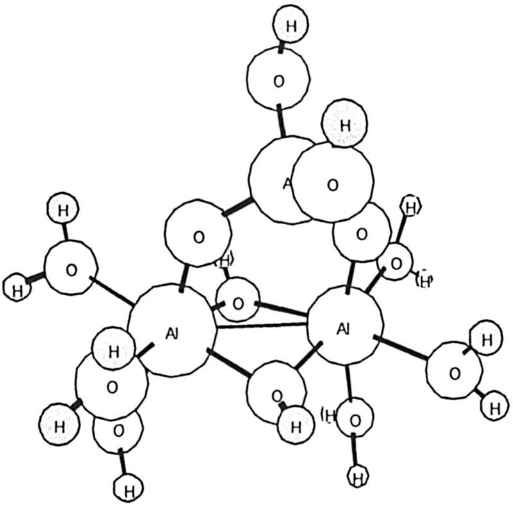

Figure 3. $Al_2(OH)_2(OH_2)_6^{+4}...H_2AsO_4^-$ complex used to model arsenate adsorbed on an Al oxyhydroxide surface

Downloaded by NORTH CAROLINA STATE UNIV on September 11, 2012 | http://pubs.acs.org
Publication Date: October 3, 2005 | doi: 10.1021/bk-2005-0915.ch009

Downloaded by NORTH CAROLINA STATE UNIV on September 11, 2012 | http://pubs.acs.org
Publication Date: October 3, 2005 | doi: 10.1021/bk-2005-0915.ch009

Table VIII. Calculated energetics (in kcal/mol) for interaction of $H_2AsO_4^-$, $HAsO_3^-$, HCO_3^- and $2H_2O$ with models for a coordinatively unsaturated Al oxyhydroxide surface, with gas-phase energies evaluated at the polarized SBK MP2 level and with COSMO solvation

reaction	ΔE_g	ΔG_{VRT}	$\Delta\Delta G_{COSMO}$	$\Delta G(aq)$
Charged models				
$Al_2(OH)_2(OH_2)_6^{+4} + H_2AsO_4^- \Rightarrow$ complex	-457.6	+14.8	+382.2	-60.5
$Al_2(OH)_2(OH_2)_6^{+4} + H_2AsO_3^- \Rightarrow$ complex	-464.0	+16.5	+379.5	-68.0
$Al_2(OH)_2(OH_2)_6^{+4} + HCO_3^- \Rightarrow$ complex	-432.2	+15.7	+377.6	-38.9
$Al_2(OH)_2(OH_2)_6^{+4} + H_2PO_4^- \Rightarrow$ complex	-460.4	+14.6	+381.3	-64.5
$Al_2(OH)_2(OH_2)_6^{+4} + 2\ H_2O \Rightarrow$ complex	-83.6	+25.5	+47.0	-11.1
Neutral models				
$Al_2(OH)_2F_4(OH_2)_2 + H_2AsO_4^- \Rightarrow$ complex	-47.5	+10.2	+28.2	-9.1
$Al_2(OH)_2F_4(OH_2)_2 + H_2AsO_3^- \Rightarrow$ complex	-70.1	+12.2	+38.5	-19.4
$Al_2(OH)_2F_4(OH_2)_2 + HCO_3^- \Rightarrow$ complex	-53.9	+13.6	+42.9	+2.6
$Al_2(OH)_2F_4(OH_2)_2 + H_2PO_4^- \Rightarrow$ complex	-46.4	+11.3	+25.1	-10.0
$Al_2(OH)_2F_4(OH_2)_2 + 2\ H_2O \Rightarrow$ complex	-33.8	+25.1	+23.2	+14.5

Conclusions

Based on these quantum calculations, rather than experiments or extrapolations of experiments, we come to the following conclusions.

1. HCO_3^- will condense with $As(OH)_3$ about as strongly as $As(OH)_3$ condenses with itself, so it may have a significant effect upon total As concentrations in solution.
2. The $As(OH)_2CO_3^-$ or $As(OH)_2CO_3Na$ species have IR/Raman and visible/UV spectra which may help in their identification.
3. HCO_3^- does not complex strongly enough with the Al hydroxide surface to displace arsenite or arsenate (but interaction with Fe hydroxide surfaces has not yet been studied).

Acknowledgements

This work was supported by NSF Grant EAR-0001031 and DOE Grant DE-FG02-94ER14467. The COSMO hydration energy calculations were performed using GAUSSIAN98 on the Carnegie Alpha Cluster, which is supported in part by NSF MRI Grant AST-9976645.

References

1. Nickson, R.; McArthur, J.; Burgess, W.; Ahmed, K. M.; Ravenscroft, P.; Rahman, M., *Nature*, **1998**, *395*, 338.
2. Smedley, P. L.; Edmunds, W. M.; Pelig-Ba, K. B., in *Environmental Geochemistry and Health: with special reference to the developing countries*, Geol. Soc. Spec. Publ. No. 113, ed. Appleton, J. D.; Fuge, R.; McCall, G. J. H., pp. 163-181, **1996**
3. Kim, M.-J.; Nriagu, J.; Haack, S., *Environ. Sci. Technol.*, **2000**, *34*, 3094.
4. Lee, J. S.; Nriagu, J. O., in *Biogeochemistry of Environmentally Important Trace Elements*, ACS Symp. Series 835, ed. Cai, Y.; Braids, O. C., pp. 33-4, **2003**
5. Tossell, J. A., *Environ. Sci. Technol.*, **2000**, *34*, 1483 ; Tossell, J. A., *J. Phys. Chem. A*, **2003**, *107*, 7804; Tossell, J. A., *Geochim. Cosmochim. Acta*, **2003**, *67*, 3347
6. Head-Gordon, M.; Pople, J. A.; Frisch, M. J., *Chem. Phys. Lett.*. **1988**, *153*, 503.
7. Scuseria, . E.; Janssen, C. L.; Schaefer, H. F. III, *J. Chem. Phys.*, **1988**, *89*, 7382.
8. Jensen, F. *Introduction to Computational Chemistry*, Wiley, New York, **1999**
9. Stevens, W. J.; Krauss, M.; Basch, H.; Jansen, P. G., *Can. J. Chem.*, **1992**, *70*, 612
10. Hehre, W. J.; Radom, L.; Schleyer, P.v.R.; Pople, J. A., *Ab Initio Molecular Orbital Theory*, Wiley, New York, **1986**..
11. Truong, T. N.; Stefanovich, E. V., *Chem. Phys. Lett.*, **1995**, *240*, 253.
12. Cossi, M.; Barone, V., *J. Chem. Phys.*, **2001**, *115*, 4708.
13. Frisch, M. J.; Trucks, G. W. ; Schlegel, H. B. ; Sciueria, G. E. ; Robb, M. A;, Cheeseman, J. R,; Zakrzewski, V. G.; Montgomery, J. A.; Stratmann, R. E.; Burant, J. C.; Dapprich, S.; Millam, J. M.; Daniels, A. D.; Kudin, K. N.; Strain, M. C.; Farkas, O.; Tomasi, J.; Barone, V.; Cossi, M.; Cammi, R.; Mennucci, B.; Pomelli, C.; Adamo, C.; Clifford, S.; Ochterski, J.; Petersson, G. A.; Ayala, P. Y.,; Cui, Q.; Morokuma, K.; Malick, D. K.; Rabuck, A. D.; Raghavachari, K.; Foresman, J. B.; Cioslowski, J.; Ortiz, J. V.; Stefanov, B. B.; Liu, G.; Liashenko, A.; Piskorz, P.; Komaromi, I.; Gomperts, R.; Martin, R. L.; Fox, D. J.; Keith, T.; Al-Laham, M. A.; Peng, C. Y.; Nanayakkara A.; Gonzalez, C.; Challacombe, M.; Gill, P. M. W.; Johnson, B. G.; Chen, W.;

Downloaded by NORTH CAROLINA STATE UNIV on September 11, 2012 | http://pubs.acs.org
Publication Date: October 3, 2005 | doi: 10.1021/bk-2005-0915.ch009

Wong, M. W.; Andres, J. L.; Head-Gordon, M.; Replogle, E. S.; Pople, J. A., GAUSSIAN 98, Rev. A.9.3, Gaussian, Inc., Pittsburgh, PA, 1998

14. Foresman, J. B, Head-Gordon, M., Pople, J. A. and Frisch, M.J., *J. Phys Chem.* **1992** *96*, 135.
15. Wolinski, K., Hinton, J. F. and Pulay, P., *J. Am..Chem. Soc.* **1990** *112*, 8251.
16. Schmidt, M. W.; Baldridge, K. K.; Boatz, J. A.; Elbert, S. T.; Gordon, M. S.; Jensen, J. H.; Koseki, S.; Matsunaga, N.; Nguyen, K. A.; Su, S. J., Windus, T. L., Dupuis, M.; Montgomery, J. A., *J. Comput. Chem.*, **1993**, *14*, 1347.
17. Pople, J. A.; Scott, A. P.; Wong, M. W.; Radom, L., *Isr. J. Chem.*, **1993**, *33*, 345.
18. Liptak, M. D. and Shields, G.C., *Int. J. Quantum Chem.* **2001** *85*, 727.
19. Ladeira, A. C. Q.; Ciminelli, V. S. T.; Duarte, H. A., Alves, M. C. M.; Ramos, A. Y., *Geochim. Cosmochim. Acta*, **2001**, *65*, 1211; Sherman, D. M.; Randall, S. R., *Geochim. Cosmochim. Acta*, **2003**, *67*, 4223.
20. Dixit, S.; Hering, J. G., *Environ. Sci. Technol.*, **2003,** *37*, 1482.
21. Hering, J. G., Chen, P.-Y., Wilkie, J. A. and Elimelech, M., *J. Environ. Eng.* **1997**, *123*, 800.

Downloaded by NORTH CAROLINA STATE UNIV on September 11, 2012 | http://pubs.acs.org
Publication Date: October 3, 2005 | doi: 10.1021/bk-2005-0915.ch009

Downloaded by STANFORD UNIV GREEN LIBR on September 12, 2012 | http://pubs.acs.org
Publication Date: October 3, 2005 | doi: 10.1021/bk-2005-0915.ch010

Chapter 10

Arsenic Reduction by Indigenous Bacteria in Shallow Aquifers from Ambikanagar, West Bengal, India

Joyanto Routh[1], Ambujom Saraswathy[2], Sisir Kanti Nag[3], S. P. Sinha Ray[3], and Gunnar Jacks[4]

[1]Department of Geology and Geochemistry, Stockholm University, 10691 Stockholm, Sweden
[2]Department of Biology, West Virginia State College, Institute, WV 25112
[3]Department of Geology, Jadavpur University, Jadavpur 700032, Kolkata, India
[4]Department of Land and Water Resources Engineering, Royal Institute of Technology, 10044 Stockholm, Sweden

Possible biological mechanisms contributing towards the transformation of arsenic (As) in aquifer sediments was investigated in Ambikanagar. Enrichment cultures indicated several As tolerant species, which actively reduced As(V) under sub-oxic conditions. High As concentrations in the microcosms increased toxicity, and hence, bacterial types and the heterotrophic plate counts declined. Bacteria isolated from enrichment cultures were *Acinetobacter johnsonii, Citrobacter freundii, Comamonas testosteroni, Enterobacter cloacae,* and *Sphingobium yanoikuyae.* On inoculating the medium with these bacteria, different growth and As(V) reduction rates occurred. A zero-order model fits the As(V) reduction data. Initial As concentration seems to affect growth and As(V) reduction rates, and these values were highest in *A. johnsonii.* In contrast, *C. testosteroni* and *S. yanoikuyae* were almost unaffected by the initial As(V) concentrations. As(V) reduction in these bacteria occurs for detoxification or respiratory purposes (e.g., *A. johnsonii*). These experiments confirm that microorganisms may result in remobilization of As from sediments, and impact groundwater treatment.

In Advances in Arsenic Research; O'Day, P., et al.;
ACS Symposium Series; American Chemical Society: Washington, DC, 2005.

Introduction

The toxic properties of arsenic (As) compounds have been known for a long time, but renewed interest in this metalloid arises from the presence of high As levels in sedimentary aquifers (*1*). Arsenic compounds pose a health hazard because they readily accumulate in living tissues or cause breakdown of oxidative phosphorylation (*2*). The As crisis is most critical in Bangladesh and India where over 70 million people are at risk from drinking As-rich water (*3*). Arsenic commonly occurs in these environments as inorganic trivalent As(III) and pentavalent As(V) species (*4*). The trivalent arsenous acid is more dominant under reducing conditions, whereas its pentavalent counterpart, in the form of arsenic acid is common under oxidizing conditions. Compared to As(V), As(III) demonstrates greater mobility. The difference in mobility results from the high affinity of As(V) for aluminum, ferric, and manganese oxides (*4*).

Several studies indicate that microbial processes involved in As transformation are many times faster than chemical conversion (*5, 6*). Microbial oxidation of As(III) to As(V) involves a detoxification pathway, but seldom involves transfer of energy (*7*). Microbial reduction of As(V) to As(III) occurs via respiration (*8*) or detoxification (*9*) reactions. These reactions involve As(V) reductases, which differ functionally and structurally (*2*). During respiration, bacteria use As(V) as the terminal electron acceptor to gain energy, whereas enzymes transcribed by the *ars operon* are used during detoxification (*2, 9*).

We focused on studying the As crisis in Ambikanagar, West Bengal. This small town has reported several chronic As poisoning cases (including a few fatalities). The primary objective is to investigate whether indigenous bacteria in these aquifers are involved in As transformation and mobilization. We isolated several pure strains of bacteria from sediments, and evaluated their growth and As(V) reduction rates. To the best of our knowledge, this is one of the first reports on microbial transformation and mobilization of As from aquifer sediments in India, and has important implications on As cycling in aquifers.

Study Area

Ambikanagar is located in the Deganga Block of North 24 Parganas in West Bengal (Figure 1). The area is a flat alluvial plain with River Hooghly to the east. The deltaic floodplains consist of numerous streams, marshlands, ox-bow lakes, and paddy fields. The underlying thick Quaternary alluvium consists of cycles of complete or partly truncated fining-upward sequences dominated by coarse to medium sand, fine sand, silt, and clay. Aquifer sediments in deep wells are mostly coarse sand, whereas shallow wells consist of fine-to-medium grained sand. The water table occurs at a depth of *ca.* 5-m. Rainfall in summer is the principal source of recharge. Groundwater in the northern and central

Downloaded by STANFORD UNIV GREEN LIBR on September 12, 2012 | http://pubs.acs.org
Publication Date: October 3, 2005 | doi: 10.1021/bk-2005-0915.ch010

Downloaded by STANFORD UNIV GREEN LIBR on September 12, 2012 | http://pubs.acs.org
Publication Date: October 3, 2005 | doi: 10.1021/bk-2005-0915.ch010

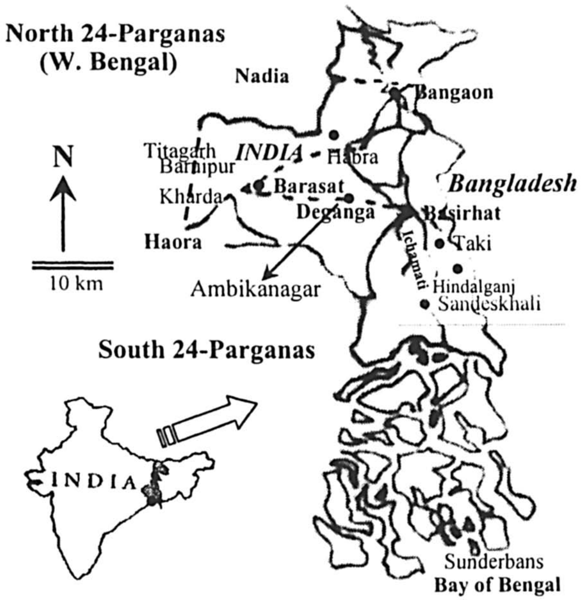
North 24-Parganas
(W. Bengal)
Nadia
Bangaon
N
10 km
Titagarh
Barnipur
INDIA
Habra
Bangladesh
Kharda
Barasat
Deganga
Basirhat
Haora
Taki
Ichamati
Ambikanagar
Hindalganj
Sandeskhali
South 24-Parganas
INDIA
Sunderbans
Bay of Bengal

Figure 1. Location of drilling site in Ambikanagar, West Bengal (India).

parts occurs under unconfined condition, whereas in the south and southeastern parts, groundwater is under confined conditions. Reconnaissance work indicates that As concentrations in the shallow wells are often above the permissible drinking water limit (50 μg/L), and it is a source of concern for the local population (*10*).

Methods and materials

In January 2003, an 18-m deep well was installed by air jet drilling, and samples were collected at 3-m intervals. About 200 g of sediment from each depth interval was stored in bags with Anaerocult A mini system (Merck EuroLab AB, Sweden). The experiments were started within four days after sampling. The microcosm experiments were a two-step process: 1) enrichment studies to isolate bacteria tolerant to high As levels, and 2) determine the As mobilization capacity using pure cultures. All chemicals used for this study were reagent grade or better, and were used, without further purification. Seven different sediment types varying in color (brownish to grayish) and grain-size (medium sand to clay) were chosen. The samples were added in duplicate to the basal salts medium. A set of two samples were set up as controls after treating them with 7.4 mM $HgCl_2$ (25% wt/vol of sediment) and 0.04% of HCHO.

Downloaded by STANFORD UNIV GREEN LIBR on September 12, 2012 | http://pubs.acs.org
Publication Date: October 3, 2005 | doi: 10.1021/bk-2005-0915.ch010

Enrichment studies

About 100-150 g of sediment sample was suspended in 500 ml glass bottles containing 250 ml of sterile minimal medium. The medium was prepared after modifying the method (*11*) by mixing three solutions: 1) solution one containing 1.4 g KH_2PO_4, 2.5 g NH_4Cl, 5 g KCl, 1.5 g $CaCl_2.2H_2O$, 5 g NaCl, and 6.2 g $MgCl_2$ in 1000 ml H_20, 2) solution two containing 0.5 mg para-amino benzoic acid in 1000 ml of H_20, and 3) solution three containing 1 mg $MnCl_2.4H_20$, 1.2 mg $Co(NO_3)_2.6H_2O$, 0.7 mg $ZnCl_2$, 0.6 mg H_3BO_3, 0.25 mg $Ni(NO_3)_2.6H_2O$, 0.15 mg $CuCl_2.2H_2O$, 0.25 mg $Na_2MoO_4.2H_2O$, and 15 mg $FeCl_2$ in 1000 ml of H_2O. Lactate (0.09 mM) was added as the carbon source. The medium was initially spiked with 0.025 mM As, but later, the As spike was increased to isolate more As resistant bacteria. Thus, sampling performed on days 7, 14, and 21 coincided with additional spikes of 0.25, 2.0, and 5.0 mM As(V), respectively to the medium. Argon was bubbled through the medium for 30 minutes and the bottles sealed tightly with butyl rubber-stoppers. The samples were incubated at room temperature in a flow through N_2-filled box. The microcosms were sampled (four sampling events in 21 days), and 50 ml of sample sacrificed periodically. During sampling, we used Orion electrodes to measure Eh (Model 91-03AP), pH (Model 96-78), and oxygen (Model 97-08). The sediment slurries extracted under aseptic conditions through the rubber septa were centrifuged

(Beckman J2-MC) at 907 G (3000 rpm) for 30 minutes. The aqueous phases were analyzed for As(III) and As(V) species, and compared to the plate counts.

Arsenic speciation

The aqueous phase was filtered through a 0.45 μm Millipore filter, and As species in the medium analyzed after modifying existing spectrophotometric methods (*12, 13*). The method involved dividing the samples into unoxidized, oxidized and reduced fractions by adding 100 μl of HCl, KI, or the cold reducing agent (mixture of sodium meta thiosulfate, sodium meta bi-sulfate, and H_2SO_4), respectively to 1200 μl of sample. Finally, 600 μl of mixed reagent (containing H_2SO_4, ascorbic acid, ammonium molybdate, and potassium antimonyl tartarate) was added to the samples. All the samples were incubated for 10 min at 78°C and cooled for 5 min at -20°C. The blue colored arseno-molybdenum complex so formed was analyzed at 865 nm (Hitachi U 2001 spectrophotometer) to determine the As concentration. As(III) was obtained as a difference of the unoxidized and oxidized sample, and As(V) was obtained as the difference of the oxidized and reduced sample. The instrument detection limit for As was ~10 μM.

Heterotrophic plate counts and identification

One ml of As enriched cultures was diluted 10-fold using a phosphate buffered saline solution (8 g of NaCl, 1.21 g of K_2HPO_4, and 0.3 g of KH_2PO_4 in 1000 ml of H_2O at pH 7.2). About 0.1 ml of sample was spread on Tryptic Soy Agar (TSA; Difco, BD Biosciences, Sweden) plates spiked with 0.45 mM As. After 72 hours of incubation at 22°C, when single colonies had similar macroscopic characteristics, a representative colony was selected and replated until pure cultures were obtained. The isolates were identified using the API and 16S rRNA techniques at the Department of Clinical Bacteriology, Göteborg University, Sweden. The 16S rRNA gene of the isolate was amplified by PCR and directly sequenced using a *Taq* dye-Deoxy terminator cycle sequencing kit (Applied Biosystems, Foster City, CA., USA) and an automatic DNA sequencer (model 373A, Applied Biosystems). For genetic identification, these sequences were retrieved from GenBank for comparison.

Arsenic mobilization capability

The bacteria were inoculated into sterile basal salts medium containing 2 mM and 5 mM As, and 0.09 mM lactate to evaluate their As mobilizing capability. The initial optical density (absorbance at 600 or 450 nm;

Downloaded by STANFORD UNIV GREEN LIBR on September 12, 2012 | http://pubs.acs.org
Publication Date: October 3, 2005 | doi: 10.1021/bk-2005-0915.ch010

spectrophotometric method) of the pure cultures was ~ 0.1. Argon was bubbled through the medium for 30 minutes, and the bottles sealed tightly with butyl rubber-stoppers. The samples were incubated at room temperature in a flow through N_2-filled box. Replicate samples were sacrificed periodically (five sampling events over a 10-days period), and biomass determined by measuring optical density and dry weight. Optical density was calibrated for each strain. Arsenic species were analyzed spectrophotometrically. Eh, pH, and oxygen levels were also measured.

Downloaded by STANFORD UNIV GREEN LIBR on September 12, 2012 | http://pubs.acs.org
Publication Date: October 3, 2005 | doi: 10.1021/bk-2005-0915.ch010

Results and discussion

Enrichment cultures

Oxygen and Eh levels decreased, whereas pH increased when measured 2-4 cm above the sediments in the bottles (Table I). The controls did not show any change in pH or oxygen levels, but Eh increased slightly. As(V) concentrations in the aqueous medium steadily decreased despite the fact, that As(V) was added to the enrichment cultures during each sampling event (Table I). This 'loss' may have resulted from As(V) being reduced to As(III) or sorption of As(V) to sediments. Although inorganic geochemical processes may result in similar changes (*14, 15*), these processes are reported to be kinetically slow (*14, 16*). Moreover, during sampling, we did not detect any H_2S odor or change in color in the sediments to suggest iron sulfides are a major component in these sediments. Interestingly, maximum As(V) reduction (21-68%) occurred on the seventh or fourteenth day, and corresponds with consistent increase in microbial counts in the different sample types. In contrast, the controls indicate low As(V) reduction (1-2%) and absence of microbial colonies in the plates. Notably, variation in sediment texture did not affect As reduction or growth (plate counts; Table 1). Microbial counts in all enrichment cultures however, decreased over the 21-days period. The decrease is most likely related to one or more reasons: 1) consumption of lactate during growth, 2) increase in As toxicity, and 3) decrease in micronutrients. These results confirm the role of *in situ* bacteria in As(V) reduction and mobilization. Another recent study in West Bengal aquifers reported similar conclusions on the role of bacteria in As remobilization (*17*).

Mass balance calculation implies a net increase in As(V) levels possibly due to sorption processes (Table I). This was not confirmed by As speciation in sediments, but sorption of As(V) by Fe and Mn oxides at sub-neutral pH is well-characterized (*4*). Moreover, sorption can simultaneously occur in conjunction with ongoing microbial processes (*18, 19*). We speculate that the increase in As(V) concentrations is closely related to the fall in microbial As(V) reduction because of As toxicity to intercellular functions (*9, 20*). Consistent with this idea, we note that decrease in heterotrophic plate counts coincided with a steady decline in different types of bacteria on the TSA plates and % As reduced in the enrichment cultures. Perhaps the decline in As(V) reduction was equally affected by the availability of electron donors (lactate or natural sedimentary organic matter in sediments) due to mutual competition (*17*). Organic matter breakdown products were not measured, but consistent increase in pH, As(III), and microbial numbers support reaction pathways involving breakdown of lactate or *in situ* sedimentary organic matter as reported in other studies (*21*, *22*).

$$\text{Lactate}^- + 2\text{HAsO}_4^- + \text{H}^+ \rightarrow \text{Acetate}^- + 2\text{H}_2\text{AsO}_3^- + \text{HCO}_3^-$$

We isolated 11 microbial strains. From these, five bacteria were selected that were morphologically most distinct from each other for subsequent identification, genetic characterization, and As mobilization experiments. These bacteria were *Acinetobacter johnsonii, Citrobacter freundii, Comamonas testosteroni, Enterobacter cloacae,* and *Sphingobium yanoikuyae.* The bacteria range from aerobic to facultative anaerobic species, and similarity of the 16S rRNA sequence with GenBank varies between 98 and 100%.

Growth and As(V) reduction

Microbial growth and As(V) reduction rate was evaluated by measuring the optical density and dry weight after inoculating the media with individual bacteria. Increase in optical density directly correlated with growth as noted in other studies (*8*, *13*). No change in As speciation was observed in the controls (Figure 2), confirming that As(V) reduction was 'biologically mediated'. In contrast, As(V) reduction was prevalent in all inoculated samples as indicated by increase in optical density. Optical density decreased sharply after the sixth day implying a decline in bacterial growth. Optical density was highest for *A. johnsonii* (0.9 in 2 mM and 0.6 in 5 mM As solutions) implying higher growth and reduction rates for this bacterium. For the remaining strains, optical densities reached 0.40-0.80 in 2 mM and 0.30-0.45 in 5 mM As(V) solutions.

The effect of As(V) concentration on bacterial growth was also evaluated. A zero-order model with respect to As(V) concentration best fits the experimental data. The kinetic model applied to evaluate As(V) reduction is similar to U(VI) reduction involving sulfate reducing bacteria (*23*). The model is represented as:

$$\text{As} = \text{As}_0 - k_0 X\,(t) \qquad (1)$$

Downloaded by STANFORD UNIV GREEN LIBR on September 12, 2012 | http://pubs.acs.org
Publication Date: October 3, 2005 | doi: 10.1021/bk-2005-0915.ch010

Table I. Change in As speciation in enrichment cultures in Ambikanagar sediments

	Microbial count cfu/ml	O_2 mM	Eh mV	pH	Spike As(V) mM	Measured conc. As(V) mM	Measured conc. As(III) mM	Loss As(V)*	Gain As(III)	As(V) sorption	%As reduced
Sediment 1: Clay											
0 Day	1.2×10^6	0.12	154	6.9	0.03	0.34	0.02				
7 Day	2.9×10^6	0.11	113	7.1	0.25	0.43	0.06	0.16	0.05	0.11	29.2
14 Day	1.1×10^5	0.11	120	7.2	1.99	0.94	0.55	1.49	0.48	1.01	36.7
21 Day	9.0×10^4	0.11	85	7.1	5.00	1.50	0.72	4.44	0.17	4.27	16.1
Sediment 2: Sandy-clay											
0 Day	1.0×10^3	0.17	156	7.0	0.03	0.05	0.02				
7 Day	5.5×10^6	0.16	123	7.0	0.25	0.19	0.06	0.10	0.05	0.06	45.5
14 Day	1.4×10^3	0.15	102	7.1	1.99	1.00	0.57	1.18	0.50	0.68	42.5
21 Day	4.4×10^4	0.13	110	7.4	5.00	1.09	1.61	4.91	1.05	3.86	21.3
Sediment 3: Fine sand											
0 Day	2.0×10^5	0.11	120	7.0	0.03	0.05	0.01				
7 Day	1.7×10^6	0.10	100	7.3	0.25	0.13	0.07	0.18	0.06	0.12	32.2
14 Day	1.2×10^5	0.08	99	7.5	1.99	0.80	0.35	1.32	0.28	1.04	21.3
21 Day	3.8×10^4	0.06	89	7.6	5.00	1.05	0.70	4.75	0.35	4.40	7.4
Sediment 4: Coarse sand											
0 Day	1.1×10^4	0.13	120	7.1	0.03	0.34	0.01				
7 Day	8.3×10^4	0.12	112	7.4	0.25	0.45	0.06	0.14	0.06	0.09	40.2
14 Day	4.0×10^4	0.10	104	7.0	1.99	0.83	0.63	1.61	0.56	1.05	34.9
21 Day	8.0×10^5	0.09	87	6.9	5.00	1.67	1.18	4.16	0.55	3.61	13.3
Sediment 5: Clay											
0 Day	6.4×10^5	0.16	296	6.5	0.03	0.05	0.01				
7 Day	2.1×10^6	0.15	178	7.0	0.25	0.03	0.19	0.27	0.18	0.09	68.0
14 Day	7.0×10^4	0.15	125	7.1	1.99	0.66	0.53	1.35	0.34	1.02	24.8
21 Day	4.6×10^4	0.14	83	7.2	5.00	0.99	0.90	4.67	0.37	4.30	7.9
Sediment 6: Medium sand											
0 Day	7.0×10^3	0.17	285	6.6	0.03	0.05	0.01				
7 Day	2.8×10^5	0.14	180	6.9	0.25	0.09	0.05	0.21	0.05	0.16	23.6
14 Day	7.2×10^5	0.12	150	7.0	1.99	0.42	0.41	1.66	0.36	1.31	21.4
21 Day	1.5×10^3	0.08	79	7.1	5.00	0.87	0.97	4.55	0.56	3.98	12.4
Sediment 7: Medium sand											
0 Day	1.0×10^2	0.16	285	6.6	0.03	0.04	0.01				
7 Day	1.2×10^4	0.12	210	6.7	0.25	0.18	0.06	0.11	0.06	0.05	53.4
14 Day	2.0×10^6	0.10	183	6.8	1.99	0.86	0.50	1.31	0.44	0.87	33.3
21 Day	2.3×10^5	0.08	141	6.9	5.00	1.65	0.99	4.21	0.49	3.73	11.6
Control 1: Coarse sand											
0 Day		0.13	296	6.4	0.03	0.05	0.00				
7 Day	-	0.13	302	6.5	0.25	0.03	0.01	0.26	0.00	0.26	0.93
14 Day	-	0.13	312	6.7	1.99	0.04	0.03	1.99	0.02	1.96	1.18
21 Day	-	0.14	305	6.8	5.00	0.06	0.05	4.97	0.02	4.95	0.45
Control 2: Clay											
0 Day		0.13	298	6.5	0.03	0.05	0.01				
7 Day	-	0.13	312	6.5	0.25	0.10	0.00	0.20	0.00	0.20	-2.20
14 Day	-	0.12	313	6.5	1.99	0.06	0.04	2.03	0.03	2.00	1.69
21 Day	-	0.12	318	6.5	5.00	0.07	0.06	4.99	0.02	4.97	0.44

* Loss in expected As(V) conc. is due to partial reduction to As(III) and sorption processes

- Samples treated with formaldehyde and $HgCl_2$; no microbial growth noted

Downloaded by STANFORD UNIV GREEN LIBR on September 12, 2012 | http://pubs.acs.org
Publication Date: October 3, 2005 | doi: 10.1021/bk-2005-0915.ch010

Downloaded by STANFORD UNIV GREEN LIBR on September 12, 2012 | http://pubs.acs.org
Publication Date: October 3, 2005 | doi: 10.1021/bk-2005-0915.ch010

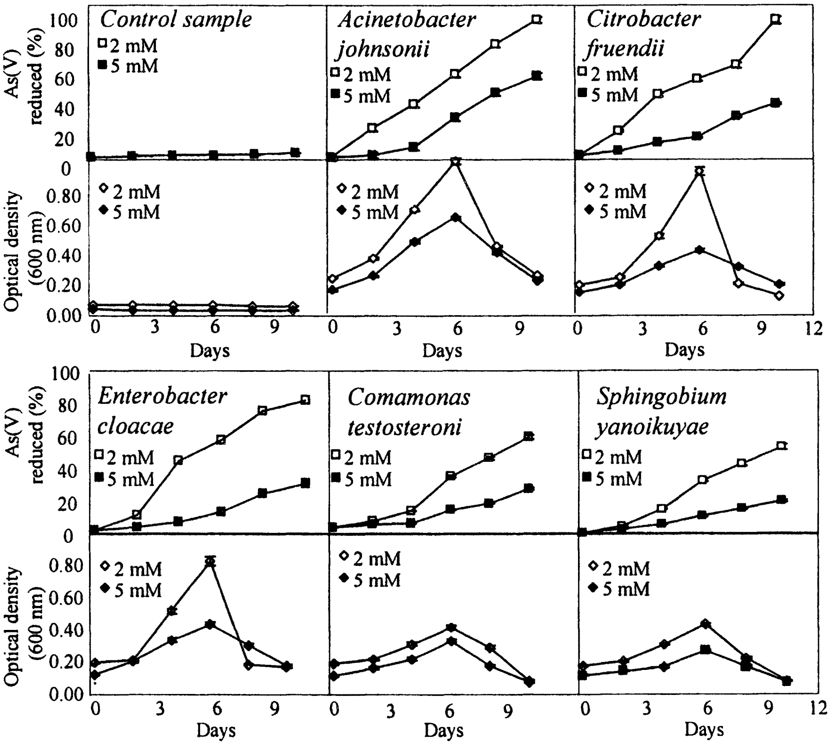

Figure 2. Optical density and As(V) reduced vs. time for As(V) spiked medium inoculated with bacteria isolated from enrichment cultures. Experiments were conducted in duplicate and error bars denote one standard deviation about the mean. As(V) reduced(%) = 100[1-As(V)/As$_{(tot)}$]

where As = is the model predicted As(V) concentration, As$_0$ = initial concentration of As(V), k_0 = maximum specific reaction rate coefficient expressed as As(V) concentration/mg (dry weight) of cells/ml/h, X = bacterial cell concentration in mg (dry weight)/ml, and t = time in hours. Figure 3 indicates the trend for modeled and fitted k_0 values for *A. johnsonii*. The zero order model is a simplification of Michaelis-Menten and Monod type kinetics at high substrate concentrations denoted by:

$$k_0 = \mu_m/Y = V_{max} \qquad (2)$$

where V_{max} = Michaelis-Menten maximum substrate utilization rate constant expressed as the As(V) concentration/mg (dry weight) of cells/ml/day, μ_m = Monod maximum specific growth rate constant/h, and Y = cell yield expressed as mass of cells in mg per mg of substrate used.

The k_0 values ranged from 20-49 ± 1 μM of As(V)/mg dry weight of cells/ml/h and 14-46 ± 1 μM of As(V)/mg dry weight of cells/ml/h for 2 and 5 mM As(V) concentration, respectively. V_{max} ranged from 0.20-0.50 ± 1 μM of As(V)/mg dry weight of cells/ml/day and 0.14-0.47 ± 1 μM of As(V)/mg dry weight of cells/ml/day for 2 and 5 mM As(V) concentration, respectively (Table II). Comparison of k_0 and V_{max} values ranked the five bacteria as: *A. johnsonii* > *C. freundii* > *E. cloacae* > *C. testosteronii* > *S. yanoikuyae*.

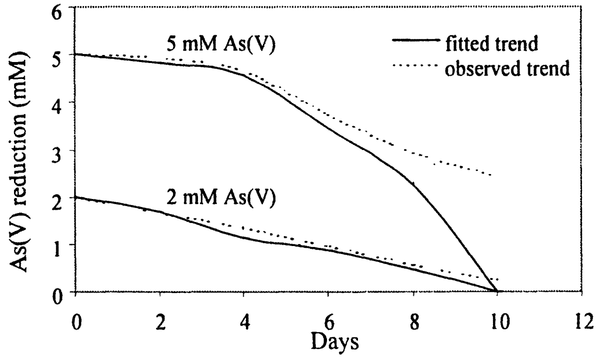

Figure 3. Time course of As(V) reduction by Acinetobacter johnsonii fit with a zero-order model. Model lines are based on the coefficients of Table 2. Data points represent at least two experiments.

The data indicated that initial As(V) concentration seemed to have little affect on growth and As(V) reduction rates in *C. testosteroni* and *S. yanoikuyae* (Figure 2; Tables II, III). Notably, the dry weight measurements remained either same or decreased during the course of the 10-days experiment. The decrease may be related to the death of bacterial cells. If the coupling of As(V) reduction with lactate oxidation was the sole energy source for these bacteria, a direct correlation between the initial As(V) concentration versus growth and biomass yields (reflected as measurements of optical density, dry weight, k_0, and V_{max} values) would be expected (*6*). Therefore, the results imply that As(V) was not used for respiration in these incubations; rather As(V) was most likely reduced involving the detoxification pathway (*6*). In contrast, the other bacteria in this study i.e., *A. johnsonii, C. freundii*, and *E. cloacae* suggested that initial As(V)

Downloaded by STANFORD UNIV GREEN LIBR on September 12, 2012 | http://pubs.acs.org
Publication Date: October 3, 2005 | doi: 10.1021/bk-2005-0915.ch010

concentrations seemed to affect both growth and reduction rates (Figure 2; Tables II, III). This was most evident in *A. johnsonii*, which indicated highest growth and As(V) reduction rates. Perhaps As(V) reduction was not restricted to detoxification, and existence of alternate As(V) reduction pathways is possible.

Table II. Maximum specific reaction rate coefficients for reducing As(V) to As(III) by bacteria in aquifer sediments from Ambikanagar

Microorganism	Initial As(V) conc. (mM)	Final As(V) conc. (mM)	Initial cell conc. (mg[dry wt]/ml)	Final cell conc. (mg[dry wt]/ml)	k_0(μM As(V)/mg [dry wt] cells/ml/h	V_{max} (μmol As(V)/mg [dry wt] cells/ml/day
Acinetobacter johnsonii	2 mM	0.23	12 ± 2	34 ± 2	49.4 ± 1	0.50 ± 0.1
	5 mM	2.43	11 ± 2	21 ± 2	46.9 ± 2	0.47 ± 0.1
Citrobacter freundii	2 mM	0.24	11 ± 2	16 ± 2	42.9 ± 2	0.42 ± 0.1
	5 mM	1.65	11 ± 2	14 ± 2	31.9 ± 2	0.31 ± 0.1
Enterobacter cloacae	2 mM	0.28	11 ± 2	16 ± 3	35.4 ± 2	0.35 ± 0.1
	5 mM	3.46	12 ± 2	13 ± 3	23.0 ± 2	0.23 ± 0.1
Comamonas testosteroni	2 mM	0.86	12 ± 2	12 ± 2	36.9 ± 1	0.37 ± 0.1
	5 mM	3.77	12 ± 2	11 ± 2	29.8 ± 2	0.30 ± 0.1
Sphingobium yanoikuyae	2 mM	0.80	13 ± 2	10 ± 2	20.0 ± 1	0.20 ± 0.1
	5 mM	3.86	13 ± 2	10 ± 2	14.7 ± 2	0.14 ± 0.1

Reduction rates

Comparisons between the bacteria indicated difference in growth and reduction rates (Figure 2; Table III). Maximum As(V) reduction occurred in *A. johnsonii*, which converted between 0.18 and 0.25 mM/day in the 2 and 5 mM As(V) spiked solutions, respectively. In contrast, *S. yanoikuyae* reduced 0.12 and 0.11 mM/day of As(V) in solutions of similar concentrations. Compared to other As(V) reducing bacteria (i.e., strict anaerobes, microaerophiles, and facultative anaerobes), microorganisms isolated in this study indicate As(V) reduction rates and growth that were low (Table III). For example, *A. johnsonii*, *C. freundii*, and *E. cloacae* indicated they were capable of reducing only 0.15-0.25 mM/day from 5 mM As(V). In this context, a notable difference between the previous studies (*8*, *24*) versus the present is that organic matter content in the enrichment and pure cultures were at low levels. This was done to represent conditions similar to those in the Ambikanagar sediments, which have carbon content < 1%. Consequently, competition for suitable electron donors may have resulted in the low As(V) reduction rates. Notably, the putative absence of strict anaerobic microorganisms in the microcosms does not imply they do not occur

Downloaded by STANFORD UNIV GREEN LIBR on September 12, 2012 | http://pubs.acs.org
Publication Date: October 3, 2005 | doi: 10.1021/bk-2005-0915.ch010

in these sediments, instead, they indicate conditions, which do not promote their growth. Nonetheless, studies such as this and others (*17*) emphasize the role of bacteria in transformation and mobilization of As in sedimentary aquifers.

Table III. As(V) reduction in various microorganisms

Microorganisms	Initial As(V) conc. mM	As(V) reduced mM/day	Carbon source	Strain, As(V) reduction pathway, and reference
Strict anaerobe	5	1.6	10 mM formate	*Desulftobacterium* respiration (29)
	7	1.4		
Strict anaerobe	1	0.15	10 mM lactate	*Desulfotomaculum auripigmentum* respiration (14)
	5	0.59		
	9	0.68		
Strict anaerobe	1	1	2 mM lactate	MIT-13 respiration (8)
	5	4		
	10	3.3		
Strict anaerobe	0.2	0.03	5 mM glucose	CN-8 (*Clostridium*?) detoxification (6)
	0.6	0.18		
Weak microaerophile	10	3.6	20 mM lactate	*Bacillus selenitireducens* respiration, detoxification (24)
Facultative anaerobe	1	0.06	0.09 mM lactate	*Arsenicoccus bolidensis* respiration, detoxification (Saraswathy, unpubl., 30)
	2	0.09		
	5	0.20		
Aerobes/ Microaerophile	2	0.18	0.09 mM lactate	*Acinetobacter johnsonii* (respiration, detoxification)
	5	0.25		
	2	0.16		*Citrobacter freundii* (respiration, detoxification)
	5	0.18		
	2	0.15		*Enterobacter cloacae* (respiration, detoxification)
	5	0.17		
	2	0.11		*Commonas testosteroni* (detoxification)
	5	0.12		
	2	0.12		*Sphingobium yanoikuyae* (detoxification)
	5	0.11		

Biochemical pathway

The results imply these bacteria are not strict aerobes (as thought), but rather, they are opportunistic; possibly some are even microaerophilic. Microaerophiles are capable of O_2-dependent growth (< 21 vol%), and can use O_2 or other terminal electron acceptor for respiration (*25*). In contrast, strict

Downloaded by STANFORD UNIV GREEN LIBR on September 12, 2012 | http://pubs.acs.org
Publication Date: October 3, 2005 | doi: 10.1021/bk-2005-0915.ch010

aerobes use O_2 as the terminal acceptor, and if they are involved in As reduction, it is strictly for detoxification purposes (*2, 9*). Recent studies suggest that presence of an enzymatic detoxification pathway does not preclude the As(V) respiration capability in bacteria (*2*). For example, both detoxifying and respiratory As(V) reductases occur in the microaerophile *Bacillus selenitireducens* (*24*) and the As(V)-respiring anaerobe *Shewanella* ANA-3 strain (*26*). Similar possibilities may exist in some of the bacteria discussed here, but needs further genetic verification (*26*).

Downloaded by STANFORD UNIV GREEN LIBR on September 12, 2012 | http://pubs.acs.org
Publication Date: October 3, 2005 | doi: 10.1021/bk-2005-0915.ch010

Environmental implications

Recent focus on providing clean and safe drinking water in As-rich areas have focused on methods that are supposed to be cost-affective, and reaches out to a larger population. Several methods are used in India and Bangladesh for groundwater treatment to reduce As (*27, 28*). The most commonly used *in situ* techniques involve maintaining aerobic conditions through aeration or use chemical oxidants to convert As(III) to the less mobile and toxic As(V) species. It is surprising many of these otherwise very successful laboratory methods (As removal rates as high as 70-95%) function poorly in the field.

Our investigations in these aquifer sediments show that microbial processes play an important role in mobilizing As under laboratory conditions. This may have important implications on groundwater treatment involving external manipulation of As redox status. If microbial As(V) reduction in these aquifers is common, then the prediction of As valence and behavior, based solely on redox status may be problematic. Moreover, chemical oxidation of As(III) to As(V) during groundwater treatment may be affected because As(V) is actively reduced to As(III) by *in situ* bacteria. Thus, it is important to assess the As reduction efficiency of these and similar bacteria in field-based pilot studies as a prerequisite.

Conclusions

Microbial processes play a role in mobilizing As by converting As(V) to the more mobile and toxic As(III) species in the Ambikanagar sediments. The sediments indicate several microbial strains that are capable of tolerating high As concentrations. Increase in As(V) spike in the enrichment cultures over a 21-days period indicate decrease in different types of bacteria growing on the TSA plates and total heterotrophic plate counts. The decline may be related to increase in As toxicity in the medium.

On inoculating the medium with bacteria from enrichment cultures, different growth and As(V) reduction rates are noted. A zero-order model fits the As(V) reduction data. Maximum growth and As(V) reduction is noted in the bacteria *A. johnsonii*, but it decreased when As concentration was increased. Compared to other As(V) reducing microorganisms, bacteria isolated in this study indicate lower reduction rates (0.11-0.25 mM/day). Although initial As(V) concentration seems to affect growth and As(V) reduction rates, it does not play a role the bacteria *C. testosteroni* and *S. yanoikuyae.* As(V) reduction in these two bacteria most probably results from detoxification processes because a direct correlation between the initial As(V) concentration, growth rate, and biomass yield is lacking. In contrast, As(V) reduction perhaps is not restricted to detoxification alone in the other bacteria (particularly *A. johnsonii*). The level of biomass *per se* correlates with As(V) metabolism in these bacteria. Because microaerophily is a viable option, existence of alternate As(V) reduction mechanisms is possible.

To the best of our knowledge, suitable on or off-site groundwater As treatment facilities remains to be set up in Ambikanagar. Because bacterial As(V) reduction occurs in Ambikanagar sediments, it is reasonable to suppose that specific conditions might favor increase in As levels in groundwater. Therefore, elucidating the important pathways responsible for As transformation and increases in the total aqueous As species would be timely and beneficial for designing appropriate groundwater treatment methods.

Downloaded by STANFORD UNIV GREEN LIBR on September 12, 2012 | http://pubs.acs.org
Publication Date: October 3, 2005 | doi: 10.1021/bk-2005-0915.ch010

Acknowledgement

Sayantan Datta helped us in the field and Birgitta Boström in the laboratory. We thank Roger Herbert for his suggestions. We appreciate the careful review by Mark Barnett and Brian Mailloux. The study was funded by SIDA-Sarec.

References

1. Nriagu, J.O. In *Environmental Chemistry of Arsenic*; Frankenberger W.T., (Ed.); Dekker, NY, **2002**.
2. Oremland, R.S., Stolz, J.F. *Science* **2003**, *300*, 939-944.
3. Bhattacharya, P.; Jacks, G.; Frisbie, S.H.; Smith, E.; Naidu, R.; Sarkar, B. In *Heavy metals in the environment*; Sarkar, B., (Ed.); Marcel Dekker, NY, **2002**, 147-215.
4. Cullen, W.R.; Reimer, K.J.. *Chem. Rev.* **1989**, *89*, 713-764.
5. Sohrin, Y.; Matsui, M.; Kawashima, M.; Hojo, M.; Hasegawa, H. *Environ. Sci. Technol.* **1997**, *31*, 2712.

6. Jones, C.A.; Lagner, H.W.; Anderson, K.; McDermott, T.R.; Inskeep, W.P. *Soil Sci. Soc. Am. J.* **2000**, *64*, 600-608.
7. Santini, J.M.; Sly, L.I.; Schnagl, R.D.; Macy, J.M. *Appl. Environ. Microbiol.* **2000**, *66*, 92-97.
8. Ahmann, D.; Roberts, A.L.; Krumholz, L. R.; Morel, F.M.M. *Nature* **1994**, *371,* 750.
9. Cervantes, C.; Ji, G.; Ramirez, J.L.; Silver, S. *FEMS Microbiol. Rev.* **1994**, *15*, 355-367.
10. Routh, J.; Sinha Ray, S.P.; Nag, S.K.; Jacks, G.; Bhattacharya, A.; Datta, S.; Bhattacharya, P. *7th International Conference on Biogeochemistry of Trace Elements, Uppsala (Sweden)* **2003**, *2*, 462-463.
11. Turpeinen, R.; Pantsar-Kallio, M.; Häggblom, M.; Kairesalo, T. *The Sci. of Tot. Environ.* **1999**, *236*, 173-180.
12. Johnson, D.L.; Pilson, M.E.Q. *Anal. Chem. Acta* **1972**, *58*, 289-299.
13. Cummings, D.E.; Caccavo, F.J.; Fendorf, S.; Rosenzweig, R.F. *Environ. Sci. Technol.* **1999**, *33*, 723-729.
14. Newman, D.K.; Kennedy, E.K.; Coates, J.D.; Ahmann, D.; Ellis, D.J.; Lovley, D.R.; Morel F.M.M.. *Arch. Microbiol.* **1997**, *168*, 380-388.
15. Rochette, E.A.; Bostick, B.C.; Li, G.; Fendorf, S. *Environ. Sci. Technol.* **2000**, *34*, 4714-4720.
16. Kuhn, A.; Sigg, L., *Limnol. Oceanogr.* **1993**, *38*, 1052-1059.
17. Islam, F.S.; Gault, A.G.; Boothman, C.; Polya, D.A.; Charnock, J.M.; Chatterjee, D.; Lloyd, J.R. *Nature* **2004**, 430, 68-71.
18. Routh, J.; Bhattacharya, A.; Saraswathy, A.; Jacks, G.; Bhattacharya, P. *Water, Air, Soil Pollut.* (in review).
19. Lagner, H.W.; Inskeep, W.P. *Environ. Sci. Technol.* **2000**, *34*, 3131-3136.
20. Saltikov, C.W.; Cifuentes, A.; Venksteswaran, K.; Newman, D.K. *Appl. Environ. Microbiol.* **2003**, *69,* 2800-2809.
21. Laverman, A.M.; Blum, J.K.; Schaefer, J.K.; Phillips, E.J.P.; Lovley, D.R.; Oremland, R.S. *Appl. Environ. Microbiol.* **1995**, *61*, 3556-3561.
22. Zobrist, J.; Dowdle, P.A.; Davis, J.A.; Oremland, R.S. *Environ. Sci. Technol.* **2000**, *34*, 4747-4753.
23. Spear, J.R.; Figueroa, L.A.; Honeyman, B.D. *Appl. Environ. Microbiol.* **2000**, *66*, 3711-3721.
24. Switzer Blum, J.; Bindi, B,A.; Buzzelli, J.; Stolz, J.F.; Oremland, R.S. *Arch. Microbiol.* **1998**, *171*, 19-30.
25. Krieg, N.R.; Hoffman, P.S. *Ann. Rev. Microbiol.* **1986**, *40*, 107-130.
26. Saltikov, C.W.; Newman, D.K. *Proc. Nat. Acad. Sci.* **2003**, *100,* 10983-10988.
27. Ahmed, M.F. Technologies for Arsenic Removal from Drinking Water. *BUET-UNU International Workshop*, **2001**, 251-269.

Downloaded by STANFORD UNIV GREEN LIBR on September 12, 2012 | http://pubs.acs.org
Publication Date: October 3, 2005 | doi: 10.1021/bk-2005-0915.ch010

28. Murcott, S. In *Arsenic Exposures and Health Effects IV*; Chappell, W.R.; Abernathy, C.O.; Calderon, R.L. (Eds.) 2001. Elsevier, Amsterdam, The Netherlands, **2001**, 419-429.
29. Niggemyer, A.; Spring, S.; Stackebrandt, E.; Rosenzweig, R.R. *Appl. Environ. Microbiol.* **2001**, *67*, 5568-5580.
30. Saraswathy, A. (unpublished).

Downloaded by STANFORD UNIV GREEN LIBR on September 12, 2012 | http://pubs.acs.org
Publication Date: October 3, 2005 | doi: 10.1021/bk-2005-0915.ch010

Downloaded by PENNSYLVANIA STATE UNIV on September 11, 2012 | http://pubs.acs.org
Publication Date: October 3, 2005 | doi: 10.1021/bk-2005-0915.ch011

Chapter 11

Arsenic Distribution and Speciation in the Mahomet and Glasford Aquifers, Illinois

Thomas R. Holm[1], Walton R. Kelly[1], Steven D. Wilson[1], George S. Roadcap[1], Jonathan L. Talbott[2], and John S. Scott[2]

[1]Illinois State Water Survey, Champaign, IL 61820
[2]Illinois Waste Management and Research Center, Champaign, IL 61820

The distribution and geochemistry of arsenic in two large aquifers in central Illinois was characterized. The areal distribution was complex; wells with high arsenic concentrations were often located less than 1km from wells with low or undetectable arsenic. High arsenic concentrations were associated with high concentrations of iron, organic carbon, bicarbonate, and ammonia, which is consistent with iron oxide reduction as the arsenic source. There was no clear pattern of arsenic concentration vs. depth and no correlation with chloride, so saline groundwater from the bedrock was not a significant source. High arsenic concentrations were also associated with low sulfate concentrations which may indicate sulfate reduction and sorption of arsenic to sulfide minerals. In most samples As(III) made up over 90% of the total arsenic, which is consistent with the redox conditions.

In Advances in Arsenic Research; O'Day, P., et al.;
ACS Symposium Series; American Chemical Society: Washington, DC, 2005.

The Mahomet Aquifer underlies a large area of east-central Illinois and serves as the water source for several communities and thousands of private homes and farms. The aquifer is a sand and gravel deposit that is up to 50m thick and partially fills the Mahomet buried bedrock valley (*1*). It is isolated from the surface by up to 70m of glacial till. The bedrock consists mostly of shale and carbonates. The Glasford Aquifer, which overlies parts of the Mahomet Aquifer, is a discontinuous sand and gravel deposit that is up to 20m thick and is separated from both the Mahomet Aquifer below and the land surface above by up to 20m of clayey till. Groundwater from some wells in both aquifers has arsenic concentrations over 10 $\mu g\ L^{-1}$ and a few wells have up to 100 $\mu g\ L^{-1}$ (*2, 3*). Arsenic concentrations in the bedrock shale, sand and gravel, and till are 5-55, 3-5, and 7-8 $\mu g\ g^{-1}$, respectively (*3*).

The likely source of arsenic to groundwater in south Asia is release to solution following iron oxide reduction (*4, 5*). Iron oxide reduction may also be a source of arsenic in the Mahomet Aquifer. Iron oxide coatings have been found on the Mahomet and Glasford sands (*6*). Most of the arsenic in sand and gravel aquifers is sorbed to iron oxide coatings. Incubation experiments with aquifer sediment from West Bengal, India have shown that microbial reduction of the iron oxide releases arsenic (*7*). The electron acceptor is natural organic matter (NOM), which may come from peat deposits (*8*) or from recharge induced by irrigation pumping (*9*). The Glasford Aquifer contains a number of paleosols and other organic-rich silts. Organic-rich zones are also found, to a lesser degree, in the Mahomet Aquifer (*10*).

Another potential arsenic source in the Mahomet Aquifer is saline groundwater from the bedrock. Chloride concentrations in the central part of the aquifer increase abruptly just west of Champaign County and bedrock groundwater has chloride concentrations 100-1000 times greater than in the overlying sand and gravel (*1*). In the same part of the aquifer, arsenic and chloride concentrations are positively correlated and arsenic concentrations generally increase with depth, although the correlation is statistically insignificant. A bedrock source of arsenic has been suggested (*3*).

In the present work, iron oxide reduction was hypothesized to be the source of arsenic in the Mahomet Aquifer. An alternate hypothesis was that the source is saline groundwater from the bedrock. The hypotheses were tested by collecting groundwater samples from wells screened in the upper, middle, and lower part of the aquifer, determining arsenic concentrations and speciation, and also performing complementary groundwater geochemical analyses. Organic matter may be more abundant in the overlying till than in the sand and gravel. If so, then the wells in the upper part of the aquifer may have a higher average arsenic concentration than wells in the middle or lower parts. If the bedrock is the source of the arsenic, then the wells in the lower part of the aquifer would have higher average arsenic values than wells in the middle and upper parts and high arsenic concentrations would be associated with high chloride concentrations.

Downloaded by PENNSYLVANIA STATE UNIV on September 11, 2012 | http://pubs.acs.org
Publication Date: October 3, 2005 | doi: 10.1021/bk-2005-0915.ch011

Materials and Methods

Approximately 50 wells each were selected in Champaign and Tazewell Counties with approximately 10% of the wells in the Glasford Aquifer and 30% in each of the upper, intermediate, and lower sections of the Mahomet Aquifer. Arsenic concentrations above 10 μg L^{-1} (0.13 μM) are fairly common in Tazewell County in the western part of the aquifer, while high arsenic concentrations in the eastern part, including Champaign County, are less common (*1*).

As part of a regional flow model of the Mahomet Aquifer, the Illinois State Water Survey (ISWS) has mapped the regional bedrock surface and aquifer thickness. Using this information, water well records on file at the ISWS were evaluated to estimate the elevation of the screened interval for each well and its vertical position within the aquifer. Plotting these data along with the aquifer thickness allowed wells to be selected within specific vertical sections of the aquifer. Private wells with 5- or 10-foot screens were selected for sampling. To strengthen the comparability of data between different aquifer vertical sections, we attempted to locate groups of wells that were in close geographic proximity and were in all three vertical portions of the aquifer. The final selection of wells depended on having driller's logs for the wells in the ISWS files, the horizontal and vertical distributions, and obtaining permission from the well owners to collect samples.

Each system (well and pressure tank) was purged while monitoring the pH, conductivity, oxidation-reduction potential (ORP), temperature, and dissolved oxygen (DO). The pH, conductivity, ORP, and temperature readings usually stabilized within 15-20 minutes and it was assumed that the system was adequately purged (*11*). The DO reading rarely stabilized, but the final readings were always below the reliable range (<0.5 mg/L), indicating anoxic conditions, by the time the other readings stabilized. Following stabilization of the readings, unfiltered samples were collected for total (dissolved plus particulate) arsenic and organic carbon and filtered (0.45 μm) samples were collected for arsenic species and other solutes. Samples for arsenic species were preserved with ultrapure HCl, while samples for total arsenic and for dissolved arsenic and metals were preserved with ultrapure HNO_3. Each day each sampling crew collected duplicate sets of samples from one well, a duplicate filtered sample from one well that was spiked with a mixture of arsenic species, and one set of blanks.

Total (unfiltered) and dissolved (filtered) arsenic concentrations were determined by ICP-MS with readings corrected for chloride (*12*). The detection limit (*13*) was 1.0 μg L^{-1} for the Champaign County samples and 0.5 μg L^{-1} for the Tazewell County samples. The concentrations of As(III), As(V), monomethylarsonic acid (MMAA), and dimethylarsinic acid (DMAA) were

Downloaded by PENNSYLVANIA STATE UNIV on September 11, 2012 | http://pubs.acs.org
Publication Date: October 3, 2005 | doi: 10.1021/bk-2005-0915.ch011

determined by HPLC with ICP-MS detection. The arsenic species all eluted before chloride so there was no chloride interference. All arsenic species determinations were completed within 24 hours of sample collection. The agreement between all duplicates was better than 10% for arsenic concentrations greater than 5 μg L^{-1}. (Relative precision is typically worse near the detection limit.) The agreement between As(III)+As(V) and dissolved arsenic was also better than 10% except near the detection limit. This gives confidence in the speciation method. The recoveries of As(III) and As(V) spiked in the field were between 80% and 120% (within typical acceptance criteria), so the arsenic speciation was stable within the holding time. Arsenic was undetectable in all blanks.

All solutes besides arsenic were determined by standard methods (*12*). Metals and other elements (Fe, Mn, Ca, Mg, Na, Si, P) were determined by ICP-MS. Anions (SO_4^{2-}, Cl^-, F^-) were determined by ion chromatography. Non-purgeable organic carbon (NPOC) was determined by persulfate oxidation and infrared detection. Alkalinity was determined by potentiometric titration. Ammonia-N (NH_3-N) was determined by automated colorimetry. All analyses were completed within established holding times (*14*).

Downloaded by PENNSYLVANIA STATE UNIV on September 11, 2012 | http://pubs.acs.org
Publication Date: October 3, 2005 | doi: 10.1021/bk-2005-0915.ch011

Results and Discussion

In Champaign County, arsenic was undetectable (<1 μg L^{-1}) in 20 wells (40% of samples), over 10 μg L^{-1} in 5 wells, and over 50 μg L^{-1} in one well (Figure 1). In Tazewell County, arsenic was undetectable (<0.5 μg L^{-1}) in 12 wells (24%), over 10 μg L^{-1} in 21 wells, and over 50 μg L^{-1} in 5 wells (Figure 2). The spatial distribution of arsenic was complex in both counties. In many cases, wells with over 50 μg L^{-1} were located less than 1 km from wells with undetectable arsenic. Large spatial variability in arsenic concentrations has also been reported in Wisconsin (*15*), New England (*16*), Mexico (*17*), Argentina (*18*), and Bangladesh (*4*).

Arsenic was detectable (with a few exceptions) in samples with alkalinity, NPOC, iron, and NH_3-N concentrations over 350 mg L^{-1}, 2 mg L^{-1}, 1.3 mg L^{-1}, and 0.7 mg L^{-1}, respectively, and mostly undetectable for lower concentrations (Figure 3). These results are consistent with the iron oxide reduction/arsenic release hypothesis (*19*). An adequate amount of organic matter was needed to serve as the reductant. Oxidation of the organic matter produced CO_2, which reacted with solid $CaCO_3$ to increase the alkalinity. The NH_3-N came from deamination of NOM. Both alkalinity (r^2=0.8) and NH_3-N (r^2=0.7) were correlated with NPOC. Reduction of a small fraction of an iron oxide coating would probably release little arsenic because the arsenic would sorb to the remaining oxide. Arsenic would only accumulate in solution when a sufficient fraction of the oxide got reduced so that the remaining oxide was saturated with sorbed arsenic. Therefore, the availability of solid organic matter may be an important factor in the observed patchy distribution of dissolved arsenic. Groundwater containing arsenic that was released in NOM-rich areas flowed to NOM-poor areas where the arsenic re-sorbed to the iron oxide.

Downloaded by PENNSYLVANIA STATE UNIV on September 11, 2012 | http://pubs.acs.org
Publication Date: October 3, 2005 | doi: 10.1021/bk-2005-0915.ch011

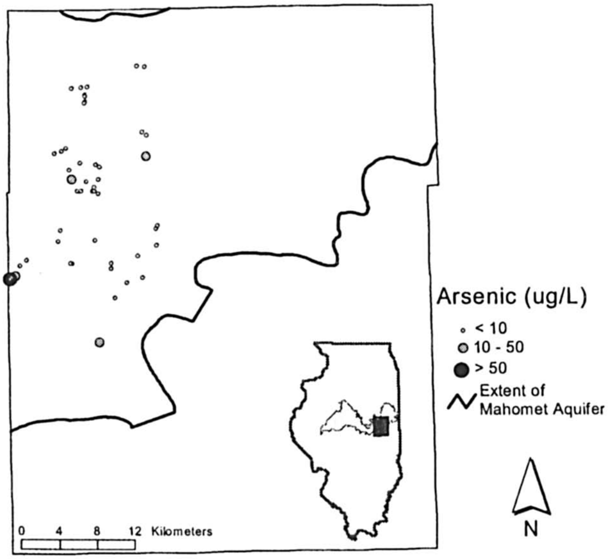

Figure 1. Dissolved arsenic concentrations in Champaign County wells. The thick solid lines show the boundaries of the Mahomet Aquifer.

Dissolved arsenic and iron were poorly correlated, but this does not disprove the iron oxide reduction hypothesis. All samples were close to saturation with siderite ($FeCO_3$) with a median saturation index of 0.2. Although ferrous iron was produced by ferric oxide reduction, it did not accumulate in solution above the siderite saturation limit. Carbonate sorbs to iron oxide (*20, 21*) and carbonate competition reduces arsenate sorption to iron oxide under some conditions (*22*). Therefore, carbonate produced by iron oxide reduction may also have inhibited resorption of any released arsenic. NOM also competes with arsenate for iron oxide sorption sites (*23*). Therefore, NOM may affect dissolved arsenic both by serving as a reductant for iron oxide and by inhibiting re-sorption to the remaining oxide.

Arsenic and sulfate were nearly mutually exclusive. If sulfate was detected (>0.25 mg L^{-1}) arsenic usually was not (Figure 4). Others have found arsenic and sulfate to be mutually exclusive (*8, 24*). Similarly, for NPOC concentrations greater than 2 mg L^{-1}, sulfate was undetectable, which is consistent with sulfate reduction in areas where NOM was abundant. Although no sulfide analyses were performed, all groundwater samples had at least 0.1 mg L^{-1} Fe, so any sulfide produced would probably have precipitated as FeS. Arsenic(III) sorbs to FeS and FeS_2 (25) and arsenic sorption/coprecipitation accompanies bacterial sulfate reduction (26). Therefore, sulfate reduction may affect the arsenic distribution in the Mahomet and Glasford Aquifers. Dissolved arsenic may have been released in areas where sulfate became depleted but re-sorbed in areas where there was active sulfate reduction.

Downloaded by PENNSYLVANIA STATE UNIV on September 11, 2012 | http://pubs.acs.org
Publication Date: October 3, 2005 | doi: 10.1021/bk-2005-0915.ch011

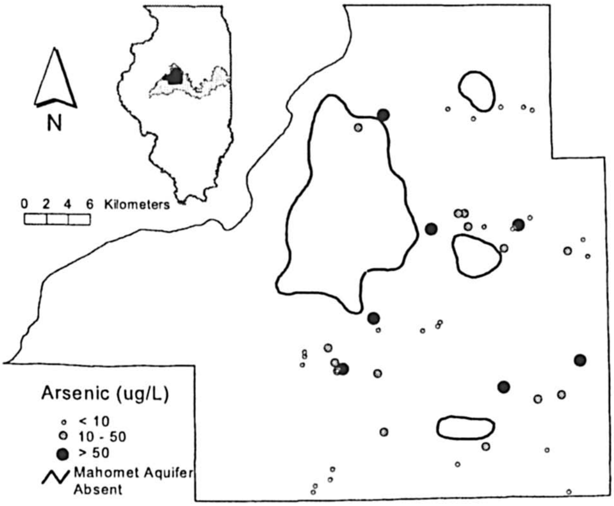

Figure 2. Dissolved arsenic concentrations in Tazewell County wells. The Mahomet Aquifer underlies the entire county except for the outlined areas.

The relationship between manganese, arsenic, and NPOC was similar to that between sulfate, arsenic, and NPOC. Arsenic was undetectable for almost all samples with more than 0.1 mg L^{-1} manganese and detectable for lower manganese concentrations. Manganese concentrations were below 0.1 mg L^{-1} for almost all samples with over 2 mg L^{-1} NPOC and over 0.1 mg L^{-1} for lower NPOC concentrations (Figure 4). A similar relationship between manganese and arsenic was found for groundwater in West Bengal (*8*). It was proposed that MnO_2 may be present where the manganese concentrations are highest and, because MnO_2 reduction is thermodynamically favored, iron oxide reduction is incomplete and arsenic remains sorbed to the remaining iron oxide. In the Mahomet Aquifer, MnO_2 may be depleted where the NPOC concentrations are high.

Downloaded by PENNSYLVANIA STATE UNIV on September 11, 2012 | http://pubs.acs.org
Publication Date: October 3, 2005 | doi: 10.1021/bk-2005-0915.ch011

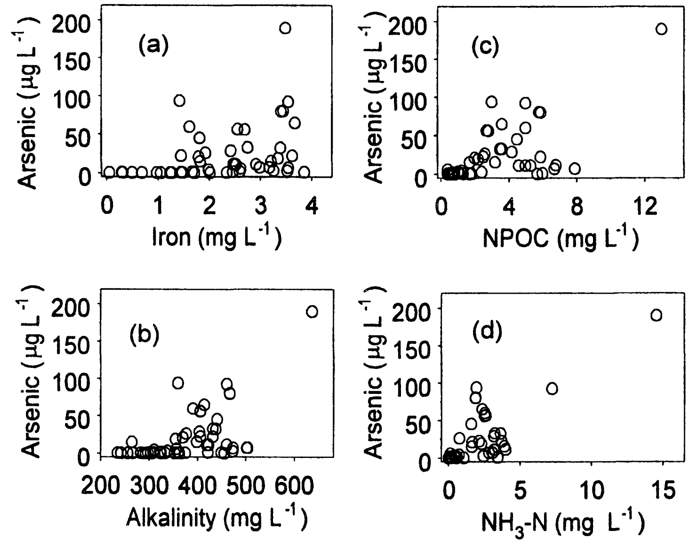

Figure 3. Dissolved arsenic as a function of iron (a), non-purgeable organic carbon (b), alkalinity (c), and ammonia-N (d). Tazewell County.

There were no apparent differences in arsenic concentrations among the different depth classes in both Champaign and Tazewell Counties. Also, the samples with the highest arsenic concentrations had the lowest chloride concentrations, while most samples with high chloride concentrations had low arsenic concentrations (Figure 5). These results differ from those of Warner (*3*), who found that for DeWitt, Logan, and McLean Counties in the central part of the aquifer, arsenic was correlated with chloride and generally increased with depth. Clearly, the bedrock is not a significant arsenic source in the eastern and western areas of the aquifer, although it may be a source in the central area.

In most samples As(III) was the main arsenic species (Figure 6). For total arsenic concentrations less than 8 µg L^{-1} As(III) was usually the only detectable species, while for samples with over 8 µg L^{-1} As(III) usually accounted for more than 90% of the dissolved arsenic. The arsenic speciation was consistent with the redox conditions in the aquifer, i.e., no detectable DO or nitrate and moderately high iron. The speciation results generally agree with those for the central part of the aquifer (*3*).

Downloaded by PENNSYLVANIA STATE UNIV on September 11, 2012 | http://pubs.acs.org
Publication Date: October 3, 2005 | doi: 10.1021/bk-2005-0915.ch011

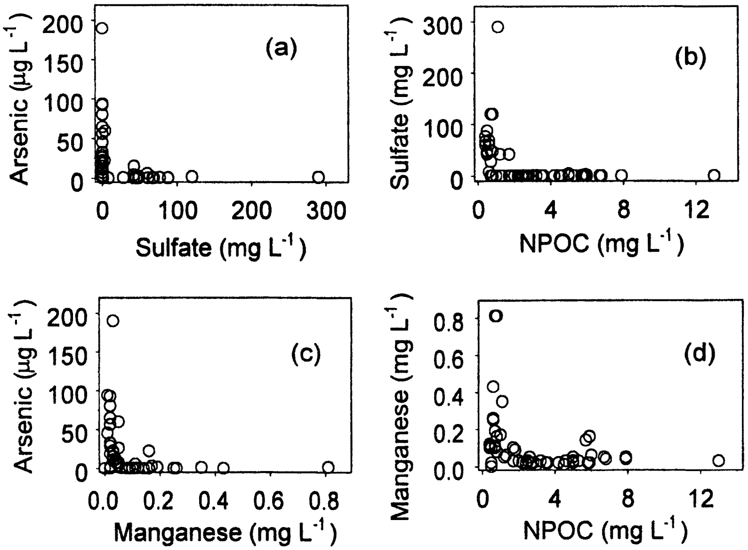

Figure 4. Dissolved arsenic as a function of sulfate (a) and manganese (c). Sulfate (b) and manganese (d) as a function of non-purgeable organic carbon. Sulfate concentration units mg L^{-1} as SO_4^{2-}.

The arsenic Eh-pH diagram (Figure 7) was constructed for 14EC, the typical aquifer temperature, using a recent thermodynamic data compilation (*27*). The ranges of pH and potential include the measured pH and ORP values. Most of the measurements lie in a band near the line for equal concentrations of As(III) and As(V) regardless of the dissolved arsenic concentration. This agrees qualitatively with the measured arsenic speciation because both species were detected in many samples with over 8 μg L^{-1}. This may, in turn, indicate that arsenic speciation was somehow related to the redox couples the ORP probe responded to. However, only one point is near the theoretical potential for an As(V):As(III) ratio of 1:10, even though the results shown in Figure 6 suggest that most of the points should lie near this line if the system were in redox equilibrium. Most measured potentials were in the range for which the As(V) concentrations would be expected to be up to 100 times greater than the As(III) concentrations. Other researchers have also found that their pH-ORP data plot completely in the As(V) field (*17, 28-32*). Smedley (*33*) reported groundwater analyses for which As(III) made up 3-39% of the total arsenic, the ORP values were 221-469 mV, and the pH values were between 5.4 and 7.2. Although both arsenic species were detectable, many of these data would be off the top of the scale of Figure 7. Clearly, arsenic speciation is not always quantitatively related to measured ORP values.

Downloaded by PENNSYLVANIA STATE UNIV on September 11, 2012 | http://pubs.acs.org
Publication Date: October 3, 2005 | doi: 10.1021/bk-2005-0915.ch011

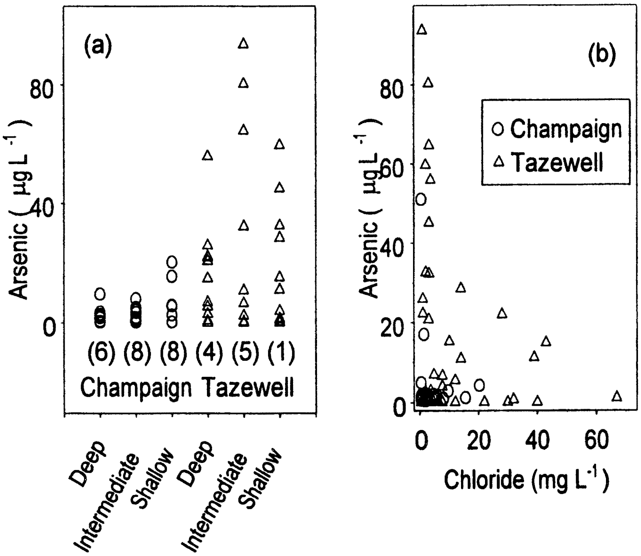

Figure 5. Dissolved arsenic concentrations for different well depths (a). Dissolved arsenic as a function of chloride for all wells (b). Mahomet aquifer only, no Glasford wells.

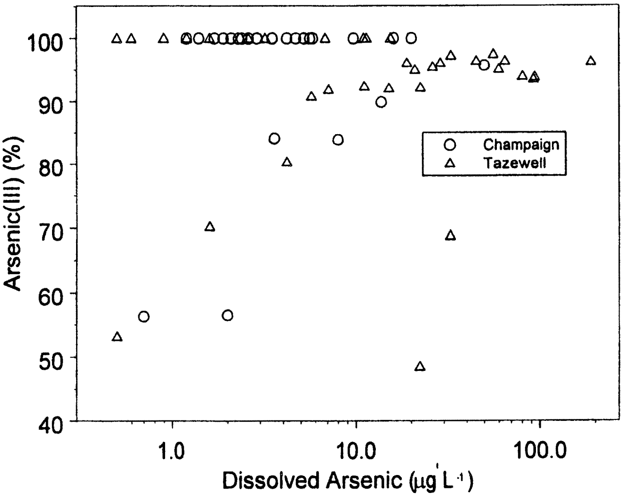

Figure 6. Arsenic(III) as a percentage of dissolved arsenic in all samples with detectable arsenic.

No samples had any detectable methylated arsenic species, which is consistent with some published studies (*34-37*). Other authors (*38-41*) have found one or more methylated species at low levels (<2 μg L^{-1}) in some groundwaters, but in those studies the inorganic arsenic (As(III)+As(V)) concentrations were over 300 μg L^{-1}.

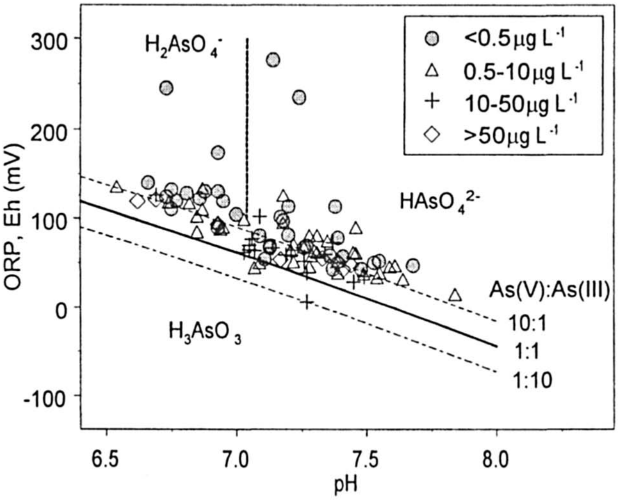

Figure 7. Arsenic Eh-pH diagram for all samples, 14EC.

Acknowledgements

This work was supported by the Illinois Waste Management and Research Center (WMRC). Joe Karny, Matthew Kirk, Bryan Coulson, Brian Dunneback, Sean Sinclair, Yu-Feng Lin, and Jung-Ho Park assisted with well selection and sample collection. All analyses besides total/dissolved arsenic, arsenic speciation, and metals determinations were performed by chemists at WMRC (Teresa Chow, Monte Wilcoxon) and ISWS (Sofia Lazovsky, Ruth Ann Nichols). ISWS and WMRC are agencies of the Illinois Department of Natural Resources.

Downloaded by PENNSYLVANIA STATE UNIV on September 11, 2012 | http://pubs.acs.org
Publication Date: October 3, 2005 | doi: 10.1021/bk-2005-0915.ch011

References

1. Panno, S. V.; Hackley, K. C.; Cartwright, K.; Liu, C. L. *Ground Water.* **1994**, *32*, 591-604.
2. Holm, T. R. *Ground-Water Quality in the Mahomet Aquifer, McLean, Logan, and Tazewell Counties*; Contract Report 579; Illinois State Water Survey:Champaign, IL, 1995.
3. Warner, K. L. *Ground Water.* **2001**, *39*, 433-442.
4. Nickson, R. T.; McArthur, J. M.; Ravenscroft, P.; Burgess, W. G.; Ahmed, K. M. *Appl. Geochem.* **2000**, *15*, 403-413.
5. McArthur, J. M.; Ravenscroft, P.; Safiulla, S.; Thirlwall, M. F. *Water Resour. Res.* **2001**, *37*, 109-117.
6. Horberg, L. *Pleistocene deposits below the Wisconsin drift in northeastern Illinois.* Report of Investigations 165, Illinois State Geological Survey:Champaign, IL, 1953.
7. Islam, F. S.; Gault, A. G.; Boothman, C.; Polya, D. A.; Charnock, J. M.; Chatterjee, D.; Lloyd, J. R. *Nature.* **2004**, *430*, 68-71.
8. McArthur, J. M., Banerjee, D. M., Hudson-Edwards, K. A., Mishra, R.,; Purohit, R., Ravenscroft, P., Cronin, A., Howarth, R. J., Chatterjee, A.,; Talukder, T., Lowry, D., Houghton, S., Chadh, D. K. *Appl. Geochem.* **2004**, *19*, 1255-1293.
9. Harvey, C. F.; Swartz, C. H.; Badruzzaman, A. B. M.; Keon-Blute, N.; Yu, W.; Ali, M. A.; Jay, J.; Beckie, R.; Niedan, V.; Brabander, D.; Oates, P. M.; Ashfaque, K. N.; Islam, S.; Hemond, H. F.; Ahmed, M. F. *Science.* **2002**, *298*, 1602-1606.
10. Herzog, B. L.; Wilson, S. D.; Larson, D. R.; Smith, E. C.; Larson, T. H.; Greenslate, M. L. *Hydrogeology and Groundwater Availability in Southwest McLean and Southeast Tazewell Counties. Part 1: Aquifer Characterization.* Cooperative Groundwater Report 17, Illinois State Geological Survey, Illinois State Water Survey:Champaign, IL, 1995.
11. Barcelona, M. J.; Gibb, J. P.; Helfrich, J. A.; Garske, E. E. *Practical Guide for Ground-Water Sampling.* Contract Report 374, Illinois State Water Survey:Champaign, IL, 1985.
12. Clesceri, L. S.; Greenberg, A. E.; Eaton, A. D., Eds. *Standard Methods for the Examination of Water and Wastewater, 20th ed.* A.P.H.A., A.W.W.A., W.E.F.: Washington, D.C., 1998.
13. Glaser, J. A.; Foerst, D. L.; McKee, G. D.; Quave, S. A.; Budde, W. L. *Environ. Sci. Technol.* **1981**, *15*, 1426-1435.
14. Holm, T. R., Kelly, W. R., Wilson, S. D., Roadcap, G. R., Talbott, J. L., Scott, J. S. *Arsenic Geochemistry and Distribution in the Mahomet Aquifer, Illinois*; Research Report RR-107, Waste Management and Research

Downloaded by PENNSYLVANIA STATE UNIV on September 11, 2012 | http://pubs.acs.org
Publication Date: October 3, 2005 | doi: 10.1021/bk-2005-0915.ch011

Center:Champaign, IL, 2004. http://www.wmrc.uiuc.edu/main_sections/info_services/library_research_reports.cfm.

15. Schreiber, M. E.; Simo, J. A.; Freiberg, P. G. *Hydrogeol. J.* **2000**, *8*, 161-176.
16. Ayotte, J. D.; Montgomery, D. L.; Flanagan, S. M.; Robinson, K. W. *Envir. Sci. Technol.* **2003**, *37*, 2075-2083.
17. Armienta, M. A.; Villasenor, G.; Rodriguez, R.; Ongley, L. K.; Mango, H. *Environ. Geol.* **2001**, *40*, 571-581.
18. Smedley, P. L.; Nicolli, H. B.; Macdonald, D. M. J.; Barros, A. J.; Tullio, J. O. *Appl. Geochem.* **2002**, *17*, 259-284.
19. Ravenscroft, P.; McArthur, J. M.; Hoque, B. A. (2001) Geochemical and Palaeohydrological Controls on Pollution of Groundwater by Arsenic; In *Arsenic Exposure and Health Effects IV,* W. R. Chappell, C. O. Abernathy, R. Calderon, Eds., Elsevier:Oxford, pp. 1-20.
20. Zachara, J. M.; Girvin, D. C.; Schmidt, R. L.; Resch, C. T. *Environ. Sci. Technol.* **1987**, *21*, 589-594.
21. van Geen, A.; Robertson, A.; Leckie, J. *Geochim. Cosmochim. Acta.* **1994**, *58*, 2073-2086.
22. Holm, T. R. *J. Am. Water Works Assoc.* **2002**, *94*, 174-181.
23. Redman, A. D.; Macalady, D. L.; Ahmann, D. *Envir. Sci. Technol.* **2002**, *36*, 2889-2896.
24. Dowling, C. B.; Poreda, R. J.; Basu, A. R.; Peters, S. L.; Aggarwal, P. K. *Water Resour. Res.* **2002**, *38*, 12-1 - 12-18.
25. Bostick, B. C.; Fendorf, S. *Geochim. Cosmochim. Acta.* **2003**, *67*, 909-921.
26. Rittle, K. A.; Drever, J. I.; Colberg, P. J. S. *Geomicrobiol. J.* **1995**, *13*, 1-11.
27. Nordstrom, D. K.; Archer, D. G. In *Arsenic in Ground Water*; A. H. Welch, K. G. Stollenwerk, Eds., Kluwer:Boston, 2003, 1-25.
28. Bottomley, D. J. *J. Hydrol.* **1984**, *69*, 223-257.
29. Welch, A. H.; Lico, M. S.; Hughes, J. L. *Ground Water.* **1988**, *26*, 333-347.
30. Robertson, F. N. *Envrion. Geochem. Health.* **1989**, *11*, 171-185.
31. Planer-Friedrich, B.; Armienta, M. A.; Merkel, B. J. *Environ. Geol.* **2001**, *40*, 1290-1298.
32. Kim, M. J.; Nriagu, J.; Haack, S. *Environ. Poll.* **2002**, *120*, 379-390.
33. Smedley, P. L. *J. African Earth Sci.* **1996**, *22*, 459-470.
34. Irgolic, K. *Speciation of Arsenic in Water Supplies*; EPA 600/1-82-010; USEPA:Washington, D.C., 1982.
35. Chen, S. L.; Dzeng, S. R.; Yang, M. H.; Chiu, K. H.; Shieh, G. M.; Wai, C. M. *Environ. Sci. Technol.* **1994**, *28*, 877-881.
36. Chatterjee, A.; Das, D.; Mandal, B. K.; Chowdhury, T. R.; Samanta, G.; Chakraborti, D. *Analyst.* **1995**, *120*, 643-650.

Downloaded by PENNSYLVANIA STATE UNIV on September 11, 2012 | http://pubs.acs.org
Publication Date: October 3, 2005 | doi: 10.1021/bk-2005-0915.ch011

37. Kondo, H.; Ishiguro, Y.; Ohno, K.; Nagase, M.; Toba, M.; Takagi, M. *Water Res.* **1999**, *33*, 1967-1972.
38. DelRazo, L.; Arellano, M.; Cebrian, M. *Environ. Pollution.* **1990**, *64*, 143-153.
39. Lin, T. H.; Huang, Y. L.; Wang, M. Y. *J. Toxicol. Environ. Health.* **1998**, *53*, 85-93.
40. Lin, N. F.; Tang, J.; Bian, J. M. *Environ. Geochem. Health.* **2002**, *24*, 249-259.
41. Shraim, A.; Sekaran, N. C.; Anuradha, C. D.; Hirano, S. *Appl. Organomet. Chem.* **2002**, *16*, 202-209.

Downloaded by PENNSYLVANIA STATE UNIV on September 11, 2012 | http://pubs.acs.org
Publication Date: October 3, 2005 | doi: 10.1021/bk-2005-0915.ch011

Downloaded by STANFORD UNIV GREEN LIBR on September 12, 2012 | http://pubs.acs.org
Publication Date: October 3, 2005 | doi: 10.1021/bk-2005-0915.ch012

Chapter 12

Controls on Arsenic Concentrations in Groundwater near Lake Geneva, Wisconsin

T. L. Root[1], J. M. Bahr[1], and M. B. Gotkowitz[2]

[1]Department of Geology and Geophysics, University of Wisconsin, Madison, WI 53706
[2]Wisconsin Geological and Natural History Survey, Madison, WI 53705

Geochemical and hydrochemical data from Lake Geneva, Wisconsin indicate that arsenic in groundwater may be the result of reductive dissolution of (hydr)oxide minerals. Geologic, hydrogeologic, and geochemical factors create reducing conditions that lead to arsenic mobilization in the deep Quaternary and upper Silurian aquifers, while groundwater in shallow Quaternary sediments is largely unaffected by arsenic. Groundwater chemistry data and the results of a pumping test suggest that there is little groundwater movement between the deeper, arsenic-impacted aquifers, and the shallow, non-impacted aquifer.

Introduction

Approximately 15% of wells open to Quaternary glacial and shallow bedrock aquifers near Lake Geneva, Wisconsin, U.S.A. have As concentrations exceeding the U.S. Environmental Protection Agency standard of 10 μg/l. Because there is no evidence of anthropogenic sources of As in the region, the As is believed to be naturally occurring. However, prior to this study no geologic sources of As had been identified, and little was known about the hydrogeology and geochemistry of the As-impacted aquifers.

Study Area

Lake Geneva is located in southeastern Wisconsin (Figure 1). The surficial deposits in the study area consist of Quaternary glacial sediments that overlie Silurian dolomites (Figure 2). The glacial deposits are more than 150 m thick where glacial materials fill bedrock valleys (*1*). Beneath the Silurian dolomites are Ordovician and Cambrian sedimentary units and Precambrian basement.

The principal aquifers in the study area are the Quaternary glacial, Silurian dolomite, and Cambrian-Ordovician sandstone aquifers (Figure 2). Stratified sand and gravel layers within the Quaternary aquifer are separated by low-permeability fine grained tills, resulting in shallow and deep water-bearing zones within the aquifer. Regional groundwater flow is to the east. The Maquoketa Shale, a regional aquitard, separates the Silurian aquifer from the underlying Cambrian-Ordovician aquifer (*1*). The majority of wells in the study area obtain water from either the Quaternary or Silurian aquifers, and this study only addresses processes occurring in these units.

There is significant spatial variation in As concentrations throughout the study area. Maximum As concentrations in water from wells open to the Silurian aquifer are around 100 μg/l, while maximum As concentrations in water from the deep Quaternary aquifer are around 50 μg/l. Water from wells open to the shallow Quaternary sediments has relatively low As concentrations.

Methods

Two monitoring wells, MW-1 and MW-2, were completed approximately 10 m away from an existing As-impacted well, WS-3, which is open to the bottom of the Quaternary and top of the Silurian aquifers. Arsenic concentrations in groundwater samples taken from WS-3 ranged from 34 μg/l to 85 μg/l during a time span from 1996 to 2004. MW-1 was drilled using the rotosonic method, collecting 100 m of continuous, relatively undisturbed core through the Quaternary deposits and extending 8 m into the Silurian dolomite. MW-1 is screened at the base of the Quaternary deposits, above a clay-filled dissolution opening near the top of the bedrock. MW-2, drilled with air rotary drilling, is completed in the upper Quaternary deposits. Cross sections showing the stratigraphy of the study area are based on the core from MW-1 and existing well construction records.

Approximately 5-cm thick slices were taken from the MW-1 core for whole-rock geochemical analysis. At least one sample was taken from each distinct stratigraphic horizon. Within thick horizons, a sample was taken at least

Downloaded by STANFORD UNIV GREEN LIBR on September 12, 2012 | http://pubs.acs.org
Publication Date: October 3, 2005 | doi: 10.1021/bk-2005-0915.ch012

Downloaded by STANFORD UNIV GREEN LIBR on September 12, 2012 | http://pubs.acs.org
Publication Date: October 3, 2005 | doi: 10.1021/bk-2005-0915.ch012

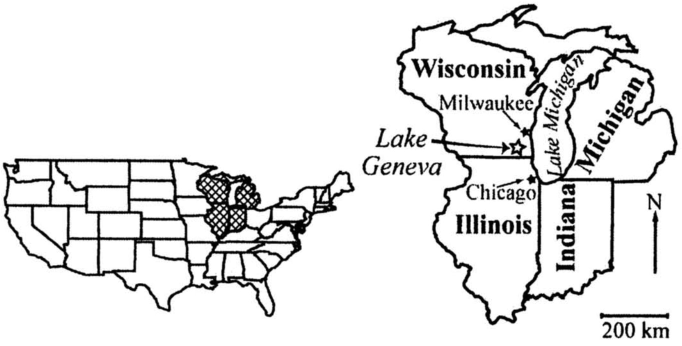
Wisconsin
Milwaukee
Lake Michigan
Michigan
Lake Geneva
Chicago
Illinois
Indiana
N
200 km

Figure 1. Location of study area.

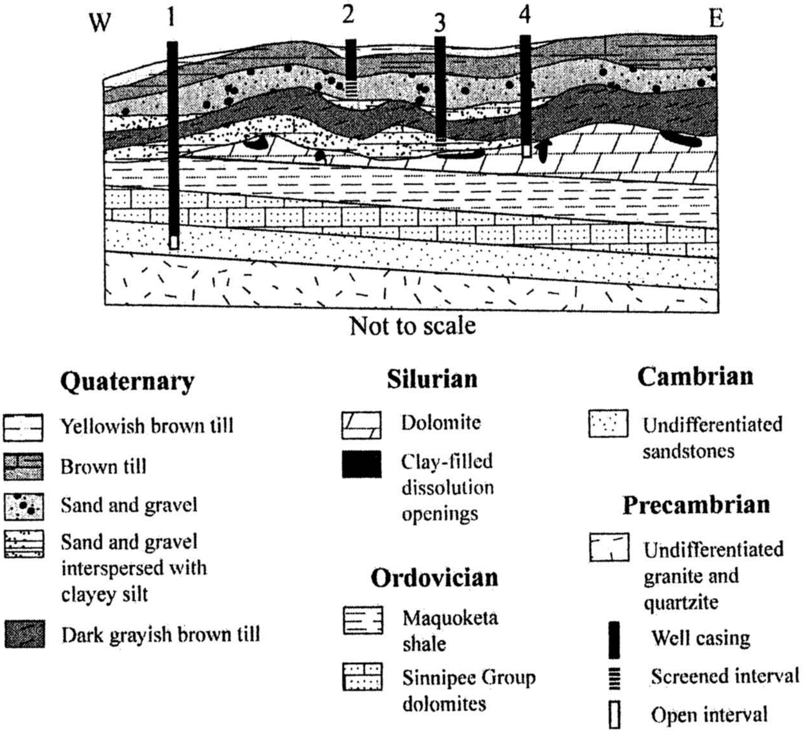
W
1
2
3
4
E
Not to scale
Quaternary
Yellowish brown till
Brown till
Sand and gravel
Sand and gravel interspersed with clayey silt
Dark grayish brown till
Silurian
Dolomite
Clay-filled dissolution openings
Ordovician
Maquoketa shale
Sinnipee Group dolomites
Cambrian
Undifferentiated sandstones
Precambrian
Undifferentiated granite and quartzite
Well casing
Screened interval
Open interval

Figure 2. General geology and typical well construction in the study area. (1. deep sandstone well, 2. shallow Quaternary well, 3. deep Quaternary well, 4. shallow Silurian well.)

every 8 feet. The samples were sent to ALS Chemex (formerly Bondar-Clegg, Inc.) for pulverization, aqua regia digestion, and subsequent analysis by inductively coupled plasma-optical emission spectrometry (ICP-OES). Loss-on-ingnition (*2*), done by the University of Wisconsin Soil and Plant Analysis Laboratory (SPAL), was used to estimate the percent organic matter (OM) in core samples.

Some groundwater chemistry data for the study area are available from previous investigations (*3*). Additional groundwater samples were obtained from residential supply wells. Temperature, pH, redox potential, conductivity, and dissolved oxygen measurements were made in the field. Arsenic species were separated in the field using As speciation cartridges from MetalSoft, Inc. (*4*). Samples for determination of major cations, dissolved metals, and dissolved As were filtered to 0.45 μm and preserved with OPTIMA nitric acid. Filtered (0.45 μm), non-preserved samples were collected for determination of major anions. Non-filtered, non-preserved samples were collected for dissolved organic carbon (DOC) analysis.

The inflection point titration method was used to determine alkalinity *(5)*. Other major anions were determined by ion chromatography at SPAL. Major cations, metals, and As were analyzed by ICP-OES. DOC concentrations were determined using a high-temperature combustion analyzer. Only samples with complete major ion analyses and charge imbalances less than 10% were included in the data analysis. Mineral saturation indices were calculated using The Geochemist's Workbench (*6*).

A 19-hour pumping test provided information about the groundwater flow system in the study area. During this test, approximately 20,000 gallons (73 well volumes) of water were discharged from WS-3. Water chemistry was monitored in the pumped well, and water levels were monitored at MW-1 and MW-2.

Results

Solid-phase Geochemistry

Low As concentrations were found in samples of the yellowish brown and brown tills (<2 mg/kg to 4 mg/kg) (Figure 3). The upper sand and gravel contains very little As; arsenic was at or below the detection limit of 2 mg/kg in 23 out of 25 samples of this unit. The lower sand and gravel unit (Figure 2) was absent at MW-1. Therefore, no data are available for this unit. The highest concentration of As (21 mg/kg) was in an organic-rich horizon at an elevation of 262 m. The clayey silt layers and dark grayish brown till have low to

Downloaded by STANFORD UNIV GREEN LIBR on September 12, 2012 | http://pubs.acs.org
Publication Date: October 3, 2005 | doi: 10.1021/bk-2005-0915.ch012

Downloaded by STANFORD UNIV GREEN LIBR on September 12, 2012 | http://pubs.acs.org
Publication Date: October 3, 2005 | doi: 10.1021/bk-2005-0915.ch012

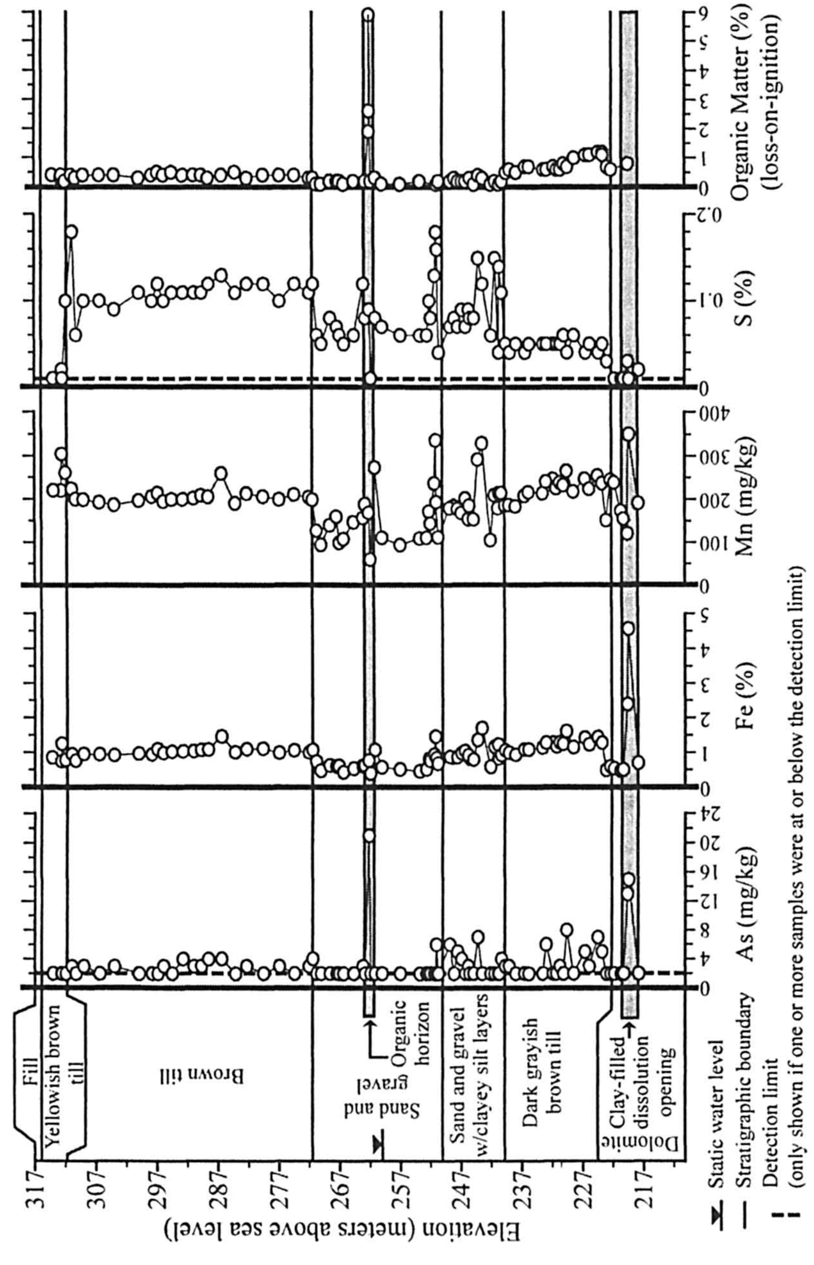

Figure 3. Core description and geochemistry of core samples.

moderate As concentrations ranging from less than detection to 8 mg/kg. Moderately high As (15 mg/kg) was found in an expansive clay filling in a dissolution opening encountered in the dolomite at the bottom of the core. Arsenic concentrations were below the detection limit in all four samples of Silurian dolomite.

The large number of As analyses that were below the detection limit makes it difficult to quantify relationships between As and other elements. However, the overall shape of the profiles (Figure 3) shows definite geochemical differences between the individual stratigraphic horizons. The Fe profile roughly parallels that of As, with moderate concentrations in the yellowish brown and brown tills, lower concentrations in the sand and gravel, moderate concentrations in the clayey silt and dark grayish brown till, and high concentrations in the clay in the dissolution opening. Manganese concentrations are variable but exhibit the same general trends as As and Fe. The OM profile is similar to those of As, Fe, and Mn. OM comprises less than 0.5 weight percent of samples of the yellowish brown till, brown till, sand and gravel, and clayey silt. Samples of the dark grayish brown till and the clay in the dissolution opening contain larger amounts of OM (0.6 to 2 weight percent). The organic-rich horizon contains as much as 6 weight percent OM. In contrast to As, Fe, Mn, and OM, S concentrations are highest in the brown till and lowest in the dark grayish brown till and clay in the dissolution opening.

Downloaded by STANFORD UNIV GREEN LIBR on September 12, 2012 | http://pubs.acs.org
Publication Date: October 3, 2005 | doi: 10.1021/bk-2005-0915.ch012

Groundwater Chemistry

Based on major ion chemistry, wells in the study area can be separated into three distinct groups: 1) wells with As concentrations less than 4 μg/l (low-As), 2) wells with As concentrations between 4 μg/l and 20 μg/l (moderate-As), and 3) wells with As concentrations greater than 20 μg/l (high-As) (Figure 4). With the exception of two outliers, moderate and high-As samples have higher HCO_3^- /(SO_4^{2-} + Cl^-) than low-As samples. This trend is caused by relatively high SO_4^{2-} concentrations (and in a few cases Cl^-) in low-As samples rather than higher HCO_3^- in moderate and high-As samples (Figures 5A and 5B). (Na^+ + K^+)/(Ca^{2+} + Mg^{2+}) increases in the moderate-As samples (Figure 4). The (Na^+ + K^+)/(Ca^{2+} + Mg^{2+}) ratio is relatively high in high-As samples, but there is little variation in this ratio among samples of this group (Figure 4). Low-As samples are more oxidizing and have higher total dissolved solids (TDS) than moderate and high-As samples (Figures 5C and 5D). There is no correlation between As and Fe^{2+} (Figure 5E). Based on a limited number of samples, As and DOC

Downloaded by STANFORD UNIV GREEN LIBR on September 12, 2012 | http://pubs.acs.org
Publication Date: October 3, 2005 | doi: 10.1021/bk-2005-0915.ch012

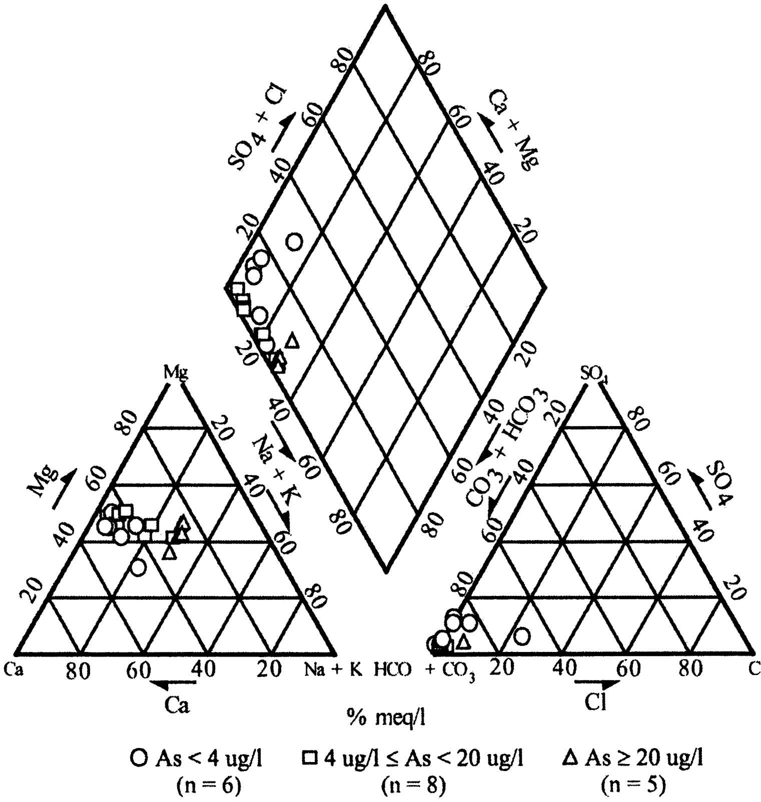

Figure 4. Major ion chemistry and As concentrations in wells in the study area. (For all samples with As < 7 ug/l, detection limit = 0.3 ug/l.)

appear positively correlated (Figure 6). The pH of all the samples ranges from 7.2 to 7.8, and 70%-100% of the As is As(III).

All of the groundwater samples are at or near saturation with respect to dolomite, calcite, and siderite (Figure 7). Most samples are slightly undersaturated with respect to rhodochrosite. $Fe(OH)_3$ saturation indices are variable, but all high-As samples are undersaturated with respect to $Fe(OH)_3$. A lack of S^- data precludes calculation of reliable saturation indices for sulfide minerals.

Results from the pumping test conducted at WS-3 showed 5.2 m of drawdown in MW-1, which is open to the deep Quaternary aquifer. There was no measureable change in water level in MW-2 (completed in the shallow Quaternary aquifer). Arsenic concentrations in the pumped well (WS-3) fluctuated early in the test (48 μg/l to 60 μg/l), but overall there was little change in water chemistry with time.

Downloaded by STANFORD UNIV GREEN LIBR on September 12, 2012 | http://pubs.acs.org
Publication Date: October 3, 2005 | doi: 10.1021/bk-2005-0915.ch012

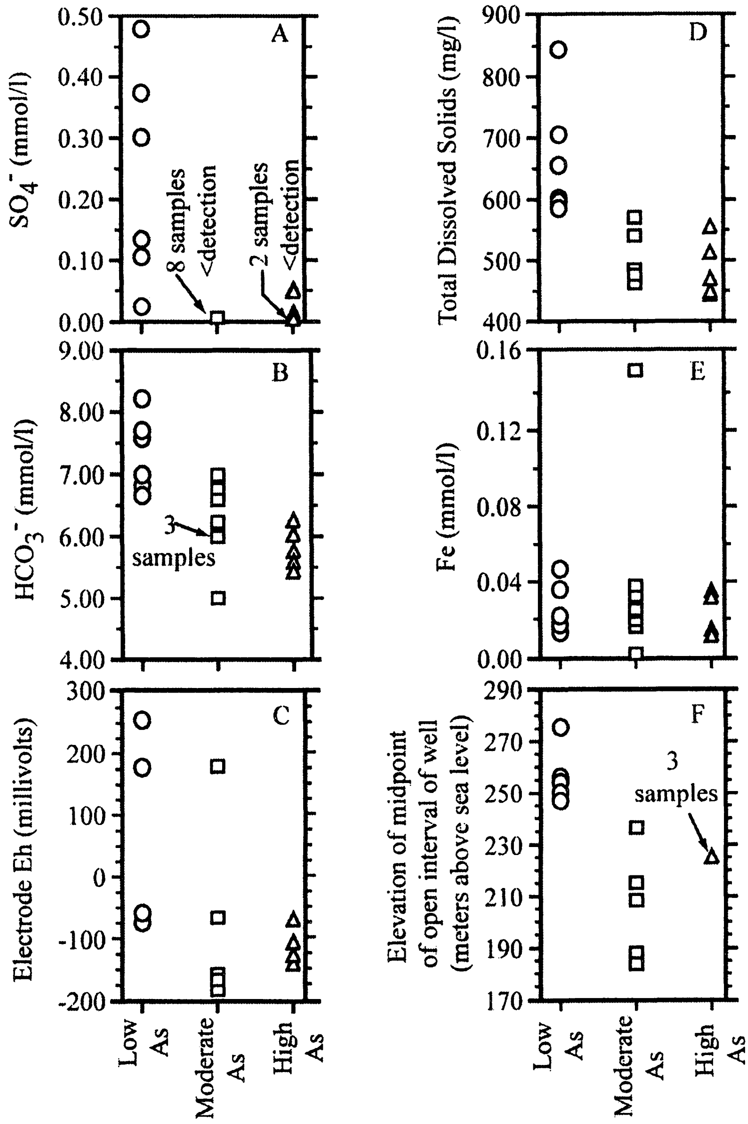

Figure 5. Chemical and physical characteristics of low-As (<4 μg/l), moderate-As (≥4 μg/l to ≤20 μg/l), and high-As (>20 μg/l) samples. (For samples with As <7 ug/l, detection limit = 0.3 ug/l.)

Downloaded by STANFORD UNIV GREEN LIBR on September 12, 2012 | http://pubs.acs.org
Publication Date: October 3, 2005 | doi: 10.1021/bk-2005-0915.ch012

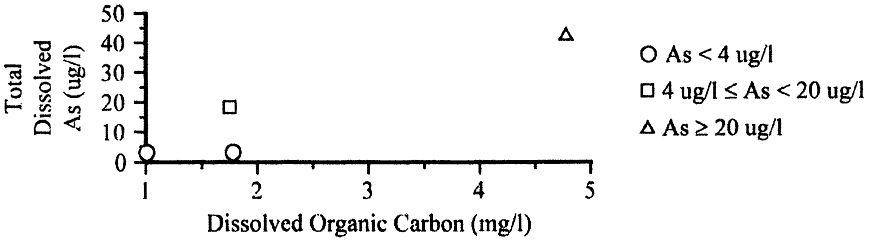

Figure 6. – Relationship between As and dissolved organic carbon in ground water samples.

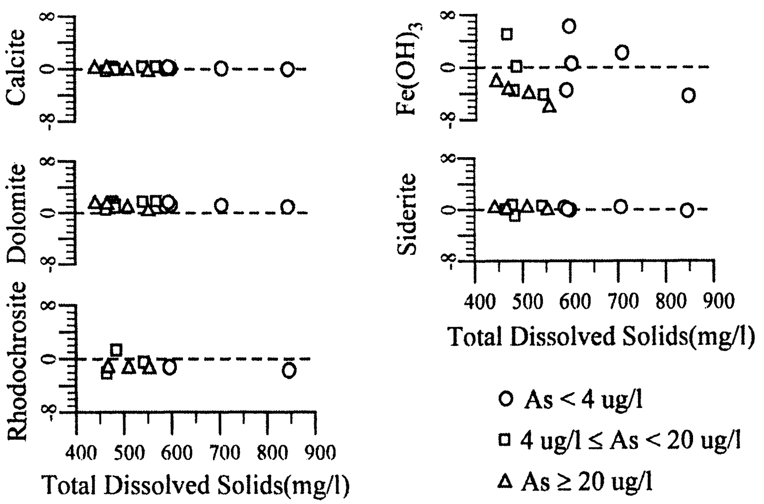

Figure 7. Saturation indices for primary minerals in groundwater samples from the study area.

Comparison of groundwater As concentrations with well construction records revealed a correlation between As and well completion depth. All low-As wells are completed in the shallow sand and gravel above the dark grayish brown till (Figure 5F and well 2 in Figure 2). The moderate and high-As wells are all open beneath the dark grayish brown till in the deep Quaternary and shallow Silurian aquifers (Figure 5F and wells 3 and 4 in Figure 2).

Discussion

Possible Arsenic Sources

Arsenic-rich pyrite is one of the most common As-bearing minerals (*7*). Oxidation of As-rich sulfide minerals is one possible mechanism for releasing As to groundwater (*8*). Arsenic is also found in association with (hydr)oxide minerals, both as sorbed species and incorporated into the mineral structure. Reductive dissolution of (hydr)oxides is another possible mechanism of As mobilization (*8*). Arsenic may also sorb to clay minerals, calcite, and organic matter (*8, 9*). Desorption of As may occur via reductive mechanisms or competition with other species for sites on mineral surfaces (*8*).

Based on the apparent negative correlation between As and S in the MW-1 core samples (Figure 3), solid-phase As is not associated with sulfide minerals. Additionally, the negative correlation between As and Eh (Figure 5C), and the fact that many of the high-As groundwater samples smell strongly of reduced S, indicate that sulfate reduction (rather than sulfide oxidation) occurs in the As-impacted aquifers.

Although limited in extent, zones of sulfide mineralization occur in both the Silurian dolomite and Maquoketa shale, which subcrop in the region. Therefore oxidation of sulfide minerals in the bedrock may occur upgradient from the study area. However, the negative correlation between As and SO_4^{2-} (Figure 5A) in groundwater suggests that sulfide dissolution is not the cause of the observed aqueous As concentrations.

The similarities in the profiles of As, Fe, and Mn in the core (Figure 3) suggest that solid-phase As might be associated with (hydr)oxide minerals. The presence of (hydr)oxides has not been confirmed by X-ray diffraction (XRD); however, poorly crystalline (hydr)oxides present at a few weight percent are not detectable using XRD.

The fact that As concentrations are higher in more strongly reducing waters (Figure 5C) also indicates that As is being mobilized via reductive dissolution of (hydr)oxides. Reduction of (hydr)oxides is often coupled to microbial oxidation of OM (*12*). Thus, the positive correlations between As and OM in the core (Figure 3) and groundwater (Figure 6) also support the reductive dissolution hypothesis. The $Fe(OH)_3$ saturation indices (Figure 7) indicate that dissoluton of ferric hydroxide is thermodynamically favorable in high-As groundwaters.

A positive correlation between As and HCO_3^- has been reported for groundwater in Bangladesh and West Bengal, where As is thought to be mobilized by reductive dissolution of Fe-(hydr)oxides (*12, 13*). The HCO_3^- is produced by the oxidation of OM. We do not observe a correlation between As and HCO_3^- in groundwater samples from our study area (Figure 5B). It is not

Downloaded by STANFORD UNIV GREEN LIBR on September 12, 2012 | http://pubs.acs.org
Publication Date: October 3, 2005 | doi: 10.1021/bk-2005-0915.ch012

Downloaded by STANFORD UNIV GREEN LIBR on September 12, 2012 | http://pubs.acs.org
Publication Date: October 3, 2005 | doi: 10.1021/bk-2005-0915.ch012

clear whether this lack of correlation indicates that elevated As concentrations are not linked to microbial respiration or if weathering reactions involving HCO_3^- overwhelm any microbial HCO_3^- contribution linked to reductive dissolution.

Mobilization of As via reductive dissolution of Fe-(hydr)oxides is expected to yield a positive correlation between aqueous As and Fe^{2+}. However, under reducing conditions Fe^{2+} may be removed from solution via the formation of Fe-sulfide minerals or siderite. Thus, the lack of correlation between As and Fe^{2+} in the groundwater samples (Figure 5E) is not sufficient to rule out the reductive dissolution hypothesis. Most of the groundwater samples are saturated with respect to siderite (Figure 7). However, no siderite has been identified in XRD analysis of core samples.

Because sediments in the study area have high clay and carbonate contents, these materials are possible As sources. Both clays and calcite typically contain much less weight percent As than (hydr)oxide minerals (*8*). However, the relatively high As concentration in the clay-filled dissolution opening in the MW-1 core (Figure 3) suggests that the clay may be an important source of As for some wells.

Relatively high As concentrations are found in the organic-rich horizon in the MW-1 core (Figure 3), but this horizon is not likely a significant regional source of As. The organic material was likely deposited in small wetlands situated in topographic lows that are not laterally extensive. Additionally, the organic-rich horizon at MW-1 is less than 20 cm thick and is above the water table (Figure 3).

Controls on Arsenic Concentrations

The As-depth relationship (Figure 5F) indicates that geologic, hydrogeologic, and geochemical factors create conditions that lead to As mobilization in the deep Quaternary and shallow Silurian aquifers (wells 3 and 4 in Figure 2) but not in the shallow Quaternary aquifer (well 2 in Figure 2). The lower solid-phase As concentrations in the shallower parts of the system (Figure 3) may be at least partially responsible for the observed As-depth relationship. However, the groundwater chemistry data (Figures 4-7) indicate that geochemical conditions in the shallow part of the system are also different than those in the deeper parts of the system.

The higher TDS, HCO_3^-, and SO_4^{2-} (Figure 5) in water from shallow wells are likely the result of unsaturated zone and/or shallow groundwater processes. P_{CO2} is typically elevated in unsaturated zones and shallow groundwater systems leading to enhanced mineral weathering that results in increased concentrations of HCO_3^- and TDS. As noted above, these weathering reactions may overwhelm any HCO_3^- signal resulting from microbial oxidation of OM. The SO_4^{2-} is likely generated by oxidation of sulfide minerals near the water table, where dissolved oxygen concentrations are higher. Sulfide minerals were probably entrained in till as glaciers overrode mineralized zones in underlying bedrock units. Dissolution of gypsum is another documented source of SO_4^{2-} in glacial aquifers (*14*), but we are unaware of previous studies identifying gypsum in glacial deposits in Wisconsin.

The increasing $(Na^+ + K^+)/(Ca^{2+} + Mg^{2+})$ in moderate-As samples (Figure 4) is probably the result of Na^+ and K^+ on the surface of clays exchanging for Ca^{2+} and Mg^{2+} in solution. The dark grayish brown till and clays in the dissolution opening (Figure 3) are the most clay-rich units in the core and the most probable locations for cation exchange to occur. The consistent $(Na^+ + K^+)/(Ca^{2+} + Mg^{2+})$ ratio (Figure 4) among high-As samples indicates that these samples are not influenced by cation exchange. These samples may be influenced more by water-rock interactions in the Silurian dolomite rather than in the clay in the Quaternary aquifer.

The reducing conditions in the deep Quaternary/shallow Silurian play a key role in promoting (hydr)oxide dissolution and As mobility. The reducing conditions are likely brought on by microbial oxidation of OM, which consumes electron acceptors. More oxidizing conditions may persist in the shallow Quaternary due to the lower OM concentrations in those aquifer sediments. The shallow parts of the aquifer are also likely to receive younger, more oxidizing recharge. In addition to contributing directly to the relatively oxidizing conditions, this supply of electron acceptors would enhance rates of OM consumption, and OM would be depleted more quickly in the shallow sediments than in the deeper sediments. Thus the distribution of OM in the aquifer sediments and the redox state of the groundwater may be greatly influenced by the groundwater flow regime.

The lack of response in water level in the shallow Quaternary well (MW-2) during the pumping test indicates that there is little hydraulic connection between the shallow Quaternary aquifer (low-As) and the deeper Quaternary and shallow Silurian (high-As) aquifers. The groundwater chemistry data lend further credence to the hypothesis that shallow, low-As wells are on a different groundwater flow path than deeper, As-impacted wells. Vertical groundwater gradients are downward; yet, shallower, low-As wells have higher TDS than deeper, high-As wells (Figure 5D). Thus, the relatively high TDS in the low-As wells is more likely the result of water-rock interaction within the shallow flow system than water-rock interaction along a flow path between the deep and shallow systems. These observations suggest that the dark grayish brown till is an aquitard separating the upper, non-As-impacted system from the deeper, As-impacted system. If the upper system is recharged locally with relatively young and oxygenated water and the lower system lies along a regional flow path further from the recharge area, the hydrogeology of the study area may

Downloaded by STANFORD UNIV GREEN LIBR on September 12, 2012 | http://pubs.acs.org
Publication Date: October 3, 2005 | doi: 10.1021/bk-2005-0915.ch012

contribute significantly to the different geochemical conditions and As concentrations observed in the two flow systems.

Conclusions

Depth profiles of As, Fe, Mn, and OM concentrations in core collected from the study area show similar patterns, and As appears more mobile at lower elevations where conditions are relatively reducing and SO_4^{2-} concentrations are negligible. These observations support the hypothesis that As is associated with (hydr)oxide minerals and is mobilized via reductive dissolution of those (hydr)oxides.

Geologic, hydrogeologic, and geochemical factors create conditions where As is mobile in the deep Quaternary and upper Silurian aquifers but not in the shallow Quaternary aquifer. Given our present understanding of the problem, the only viable mitigation measure for existing As-impacted wells is treatment to remove As from the water. New wells should be completed in the shallow flow system, if possible.

Acknowledgements

This work has been supported by the U.S. Geological Survey, the University of Wisconsin System, the Wisconsin Department of Natural Resources, the Wisconsin Geological and Natural History Survey, the U.S. Department of Energy, and the Geological Society of America. We would also like to thank the staff at Woods Elementary School in Lake Geneva, Katie Thornburg, and Nita Sahai.

References

1. Borman, R.G. *Ground-Water Resources and Geology of Walworth County, Wisconsin*; Wisconsin Geological and Natural History Survey Information Circular 34: Madison, WI, 1976.
2. Ben-Dor, E.; Banin, A. *Commun. in Soil Sci. Plant Anal.,* **1989,** 20, 1675-1695.
3. Gotkowitz, M. *Report on the Preliminary Investigation of Arsenic in Groundwater near Lake Geneva, Wisconsin*; Wisconsin Geological and Natural History Survey Open File Report 2000-02: Madison, WI, 2000.
4. Meng, X.; Wang, W. Speciation of Arsenic By Disposable Cartridges. In *Third International Conference on Arsenic Exposure and Health Effects*: Society of Environmental Geochemistry and Health, University of Colorado at Denver: Denver, CO, 1998.

Downloaded by STANFORD UNIV GREEN LIBR on September 12, 2012 | http://pubs.acs.org
Publication Date: October 3, 2005 | doi: 10.1021/bk-2005-0915.ch012

5. Wilde, F.D.; Radtke, D.B. Alkalinity and Acid Neutralizing Capacity. In *National Field Manual for the Collection of Water-Quality Data*; Techniques of Water-Resources Investigations, Book 9, Chap. A6.6; U.S.G.S: Accessed on-line at http://pubs.water.usgs.gov/twri9A1 (10/4/03).
6. Bethke, C. M. *The Geochemist's Workbench Release 3.0, A Users' Guide To Rxn, Act2, Tact, React, And Gtplot*; Craig Bethke: Urbana-Champaign, IL, 1998.
7. Nordstrom, D. K. Overview Of Arsenic Occurrences And Processes Controlling Arsenic Mobility In Groundwater. In *Institute on Lake Superior Geology Proceedings, 47th Annual Meeting*: Madison, WI, 2001, 47-1, 73.
8. Smedley, P.L.; Kinniburgh, D.G. *Appl. Geochem.* **2002**, 17, 517-568.
9. Stollenwerk, K.G. Geochemical Processes Controlling Transport of Arsenic in Groundwater: A Review of Adsorption. In *Arsenic in Groundwater, Geochemistry and Occurrence*; Welch, A.H.; Stollenwerk, K.G.; Ed.; Kluwer Academic Publishers: Boston, MA, 2003, pp 67-100.
10. Attig, J. *Personal Communication*; Wisconsin Geological and Natural History Survey: Madison, WI.
11. Eaton, T.T.; Bradbury, K.R. Hydraulic Properties and Porewater Geochemistry in the Maquoketa Shale, Southeastern Wisconsin. In *Geological Society of America Annual Meeting Abstracts with Programs*: 1998.
12. Nickson, R. T.; McArthur, J. M.; Ravenscroft, P.; Burgess, W. G.; Ahmed, K. M. *Appl. Geochem.* **2000**, 15, 406-413.
13. Zheng, Y.; Stute, M.; van Geen, A.; Gavrieli, I.; Dhar, R.; Simpson, H.J.; Schlosser, P.; Ahmed, K.M. *Appl. Geochem.* **2004**, 19, 210-214.
14. Swanson, K.D. Chemical Evolution of Groundwater in Clay Till in a Prairie Wetlands Setting in the Cottonwood Lake Area Stutsman County, North Dakota. M.S. Thesis, University of Wisconsin, Madison, WI, 1990.

Downloaded by STANFORD UNIV GREEN LIBR on September 12, 2012 | http://pubs.acs.org
Publication Date: October 3, 2005 | doi: 10.1021/bk-2005-0915.ch012

Downloaded by PENNSYLVANIA STATE UNIV on September 11, 2012 | http://pubs.acs.org
Publication Date: October 3, 2005 | doi: 10.1021/bk-2005-0915.ch013

Chapter 13

Arsenic Occurrence, Sources, Mobilization, and Transport in Groundwater in the Newark Basin of New Jersey

M. E. Serfes, S. E. Spayd, and G. C. Herman

New Jersey Geological Survey, P.O. Box 427, Trenton, NJ 08625

Arsenic concentrations as high as 215 ug/L in ground water occur in bedrock aquifers of the Newark Basin in New Jersey. This basin is a Mesozoic aged half graben containing red, gray and black mudstone, shale and sandstone with basic igneous intrusions and flows. In 2000-01, random sampling of 94 domestic wells in a 200 square mile study area revealed that 15 percent have arsenic concentrations exceeding 10 ug/L. Those wells generally have low dissolved oxygen concentrations, < 3 mg/L, and pH values range from 7.5 to 8.2. Analyses of red, gray and black mudstone and shale yielded maximum As concentrations of 13, 50 and 240 ppm respectively. Pyrite (FeS_2) in the black shale contains up to 40,000 ppm As. A spatial association between high As in ground water and black shale is observed. Hematite and clays in red mudstone are also potential sources of As. Mobilization of As via pyrite oxidation and desorption from hematite and clays are potential mechanisms. Transport of As is aided by competitive adsorption, an alkaline pH, and suboxic aqueous environment.

In Advances in Arsenic Research; O'Day, P., et al.;
ACS Symposium Series; American Chemical Society: Washington, DC, 2005.

Introduction

On February 22, 2002 The United States Environmental Protection Agency (USEPA) lowered the arsenic drinking water standard for public water supplies from 50 micrograms per liter (ug/L) to 10 ug/l with a compliance date of January 2006 *(1)*. Estimated risks of lung or bladder cancers in individuals with lifetime exposure to drinking water with more than 10 ug/L arsenic exceed 1 to 2 in 1000 *(2)*. Human exposure to inorganic As in drinking water has been linked to internal and external cancers and non-cancer related health impacts *(3, 4)*. Arsenic in ground-water supplies is both an international and national issue with countries on all continents being affected *(5)*. The State of New Jersey has proposed to implement a stricter arsenic standard of 5 ug/L.

A spatial analysis of arsenic concentrations in New Jersey ground water was conducted in 1998 by the New Jersey Geological Survey (NJGS); New Jersey Department of Environmental Protections (NJDEP) in anticipation of the new drinking water standard. Concentrations of arsenic from wells sampled in the cooperative NJDEP/United States Geological Survey (USGS) Ambient Ground Water Quality Network (AGWQN) and other studies in New Jersey were analyzed as a function of Physiographic Province *(6, 7, 8, 9)*. The initial assessment showed that arsenic concentrations are generally less than the reporting limit of 1 μg/L in all provinces except in that part of the Piedmont Province that is underlain by bedrock of a Mesozoic aged tectonic extension produced half graben called the Newark Basin (NB). There, 25 out of 45 wells sampled had arsenic detections that ranged from 1 to 19 μg/L (Figure 1). A subsequent analysis of public supply well data from the NJDEP Bureau of Safe Drinking Water showed a similar pattern. Most notably, a public supply well in the western NB in New Jersey had a consistent arsenic concentration of ~ 45 ug/L since it's installation in 1995. In January 1999 a private well sampled as part of the AGWQN in the western NB in New Jersey was found to have 57 ug/L arsenic. Together, these results prompted research studies that focused on assessing the occurrence, sources, mobilization, transport and treatment of arsenic in ground water in the western NB in New Jersey *(10, 11, 12, 13)*.

This paper mainly summarizes our findings concerning the occurrence and geologic sources of arsenic in a 200 square mile study area in the central NB, where the highest arsenic concentrations in ground water had been found (Figure 1). Also, hypotheses concerning the mobilization and transport of arsenic in this hydrogeologic setting are proposed and discussed.

Downloaded by PENNSYLVANIA STATE UNIV on September 11, 2012 | http://pubs.acs.org
Publication Date: October 3, 2005 | doi: 10.1021/bk-2005-0915.ch013

Background

Arsenic Aqueous Chemistry

Arsenic is a heavy metalloid element with atomic number 33 and has only one natural isotope with atomic mass 75. It has four valence states in the natural environment: -3, 0, +3 and +5. However, in ground water it generally forms inorganic oxyanions of arsenite As (III), [$H_3AsO_3^o$ below pH 9.2], and arsenate As (V), [$H_2AsO_4^-$ at pH < 6.9 and $HAsO_4^{2-}$ at higher pH values] *(5)*. Although not significant in most natural ground water, organically bound arsenic such as the methylated species monomethylarsonic acid (MMA) and dimethylarsinic acid (DMA) may be produced where arsenic and organic contaminants occur together. Arsenic is particularly mobile within the pH range 6.5 to 8.5 that is commonly found in ground water. It can be present under both reducing and oxidizing conditions. The species of arsenic occurring at a particular location are mainly controlled by the pH, Eh and possibly microbiological activity *(15)*.

Potential Arsenic Sources in the Newark Basin

Potential sources of arsenic in ground water in the NB are arsenical pesticides and the decomposition of minerals containing arsenic. Arsenical pesticides were widely used in this country, including New Jersey, from the late 1800s until the mid- to late 1900s *(16)*. The greatest use in New Jersey was in fruit orchards *(17)*. Arsenical pesticides are not very water soluble and bind tightly to soil particles. Studies in North Dakota, South Dakota, Wisconsin and Minnesota all conclude that ground water is largely unaffected by past arsenical pesticide use *(15)*. Therefore, arsenic from arsenical pesticide use in agricultural areas is generally not very mobile in soils and not considered a major source in ground water. The application of phosphate fertilizers can however release slugs of arsenic via competitive adsorption where they are applied *(15)*. However, sulfide oxidation and iron oxide reduction are considered the most important mechanisms for As being released into groundwater *(15)*.

Newark Basin Hydrogeology

In New Jersey, the Piedmont Physiographic Province is mostly underlain by a Triassic and Jurassic aged (195-225 million year old) half graben, a tectonic depression produced in a tensional environment, called the Newark Basin (NB) (Figure 1).

Downloaded by PENNSYLVANIA STATE UNIV on September 11, 2012 | http://pubs.acs.org
Publication Date: October 3, 2005 | doi: 10.1021/bk-2005-0915.ch013

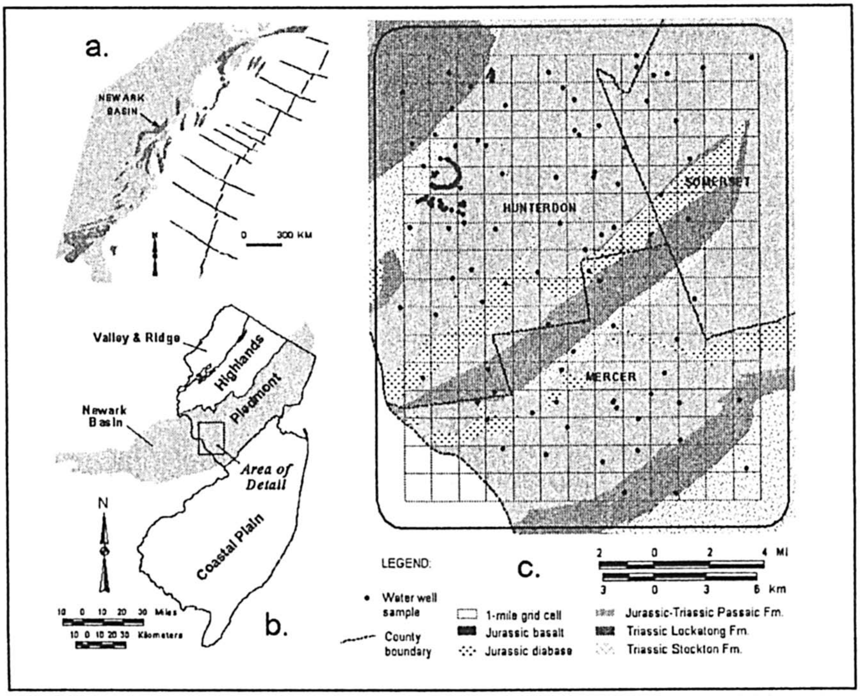
a.
NEWARK BASIN
0 300 KM
Valley & Ridge
Highlands
Piedmont
Newark Basin
Area of Detail
Coastal Plain
N
10 0 10 20 30 Miles
10 0 10 20 30 Kilometers
b.
HUNTERDON
SOMERSET
MERCER
LEGEND:
● Water well sample
County boundary
1-mile grid cell
Jurassic basalt
Jurassic diabase
Jurassic-Triassic Passaic Fm.
Triassic Lockatong Fm.
Triassic Stockton Fm.
c.
2 0 2 4 MI
3 0 3 6 km

Figure 1. Rift basins of eastern North America and the Newark Basin (modified from 14) are shown in (a). (b) is a map of New Jersey showing the Newark Basin and area of detail, and (c),is the area of detail showing the 200 square mile study area and location of wells sampled. Fifteen percent of wells sampled had greater than 10 ug/L arsenic. The Passaic and Lockatong Formations had highest occurrence and concentratiions of As.

Downloaded by PENNSYLVANIA STATE UNIV on September 11, 2012 | http://pubs.acs.org
Publication Date: October 3, 2005 | doi: 10.1021/bk-2005-0915.ch013

The NB contains coarse to fine grained non-marine sedimentary rocks associated with igneous diabase intrusions and basalt flows. These geologic materials have been faulted and gently folded, with strata generally dipping 15 degrees to the northwest, perpendicular to major normal fault trends. Four lithic groups are, from youngest to oldest:

1. Basalt interlayered with sedimentary rock (early Jurassic), mudstone, siltstone, sandstone and conglomerate.
2. The Passaic Formation (Triassic), mainly cyclical sequences of red mudstone, siltstone and sandstone with intermittent gray mudstone and black shale.

3. The Lockatong Formation (Triassic), black (organic rich), gray and red cyclical sequences of argillitic mudstone, siltstone and shale containing lenses of pyrite and calcite.
4. The Stockton Formation (Triassic), mainly comprised of arkosic sandstone, siltstone and shale derived from fluvial sediments.

The Lockatong and Passaic Formations were mostly deposited in deep (black), transitional (gray) and shallow (red) lake environments. Detailed stratigraphic relationships, including the identification of specific members in the Newark Basin, are reported from the Newark Basing Coring Project *(18)*.

The unweathered Passaic and Lockatong Formations in the Newark Basin are generally characterized as anisotropic, leaky, multi-layered aquifer systems (LMAS) with bed-parallel water-bearing zones (WBZs) sandwiched between thicker nonconductive zones *(19, 20)*. Flow between WBZs occurs as leakage via fractures that cross-stratigraphic layering or as cross flow in well boreholes. Hydraulic conductivity, and therefore preference for flow, is greatest parallel to bedding strike, somewhat less in the dip direction and least perpendicular to bedding *(21, 22)*. Weathered bedrock near the surface is more hydraulically isotropic and possesses greater storage, but is considered less permeable than that in the deeper parts of the aquifer *(19)*. Hydrogeologic investigations in shallow weathered sedimentary rock with dipping beds at the Oak Ridge National Laboratory (ORNL) facility yielded a comprehensive understanding of contaminant transport in that setting *(23, 24)*. In the shallow weathered zone there, near surface-storm flow and deeper water-table flow are largely controlled by topography with permeable weathered WBZs acting as conduits between the two. Recharge to the deeper unweathered bedrock aquifer mainly occurs where deep WBZs intersect the shallow weathered zone. Although uncertainties still exist, the conceptual flow model used here for the Passaic and Lockatong Formations is based on the shallow weathered and deeper unweathered bedrock models described above. Work to better understand ground-water flow characteristics in the Newark Basin continue to be conducted by the NJGS and others.

Arsenic Investigation and Results

Detailed Spatial Analysis of Arsenic Occurrence in the Central Newark Basin

In 1999-2000, the NJGS used a Geographic Information System to conduct a detailed spatial analysis and investigation on the occurrence of arsenic in ground water as a function of bedrock lithology. The study was concentrated in

Downloaded by PENNSYLVANIA STATE UNIV on September 11, 2012 | http://pubs.acs.org
Publication Date: October 3, 2005 | doi: 10.1021/bk-2005-0915.ch013

a 200 square mile area in the western NB in New Jersey where high concentrations of arsenic in well water were found (Figure 1). A grid-based approach using square mile cells, and random selection within blocks, was used to assure that the sampling was spatially distributed within the study area rather than being mainly clustered in high population areas if a simple random approach was used *(25)*. The goal was to collect a representative well-water sample and field parameter data: pH, dissolved oxygen, specific conductivity, and temperature from at least one domestic well per cell. Untreated samples were collected mainly from outside taps after water had flowed for at least 15 minutes and field parameters stabilized. All samples were analyzed using ICP-MS at Environmental Health Laboratories, a New Jersey certified laboratory, in Indiana using EPA Method 200.8 - Determination of Trace Elements by Inductively Coupled Plasma - Mass Spectrometry. Three well records per cell for a total of 600 well records total were obtained by conducting a well record search using the New Jersey Department of Environmental Protection Division of Water Supply database. Generally the most recent well records in each cell were used to simplify the determination of the property owner. Letters requesting volunteers for this project were sent out to the well owners and the first to respond was the one sampled. Out of the 200 cells, volunteers were found in 94. Cluster sampling in two areas where at least one well had an arsenic concentration greater than 40 ug/L was also conducted.

Downloaded by PENNSYLVANIA STATE UNIV on September 11, 2012 | http://pubs.acs.org
Publication Date: October 3, 2005 | doi: 10.1021/bk-2005-0915.ch013

Sample Results

Of the 94 wells sampled, 15 percent have arsenic concentrations exceeding 10 ug/L. Well water from the Passaic and Lockatong Formations have the highest arsenic concentrations and frequency of occurrence *(10, 11, 12)*. The Passaic Formation is the more aerially extensive of the two. Arsenic concentrations greater than 10 ug/L generally have low dissolved oxygen (DO) concentrations (DO < 3 mg/L) and pH values range from 7.5 to 8.2 (Figure 2). Arsenic concentrations greater than 40 ug/L are associated with suboxic (DO < 1.0 mg/L) ground water and a pH of about 8. Subsequent sampling also identified several areas in the NB where some wells have even higher concentrations than found in the original reconnaissance. Several wells in diabase near the contact with sedimentary rock in the southwestern NB in New Jersey have up to 95 ug/L arsenic. Approximately 10 miles east of those wells, a well in the Lockatong Formation has up to 150 ug/L arsenic. Also, wells drawing water from a sulfide mineralized zone in the Passaic Formation under a basalt flow in the north-central NB in New Jersey have arsenic concentrations that vary up to 215 ug/L.

Downloaded by PENNSYLVANIA STATE UNIV on September 11, 2012 | http://pubs.acs.org
Publication Date: October 3, 2005 | doi: 10.1021/bk-2005-0915.ch013

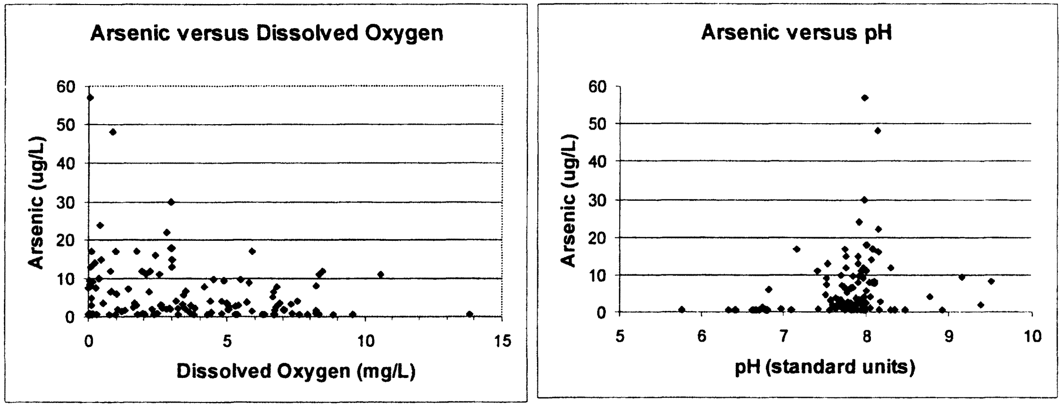

Figure 2. Arsenic versus dissolved oxygen and pH in ground water in the western NB in New Jersey. This is a compilation of data from the 94 wells sampled there. Note that a DO < 3 mg/L and a pH between 7.5 and 8.2 are the optimal range for arsenic greater than 10 ug/L.

Table I. Arsenic speciation in 9 private residential wells in the Passaic Formation. Concentrations in μg/L.

Species	*Well 1*	*2*	*3*	*4*	*5*	*6*	*7*	*8*	*9*
As total	22.3	31.8	61.9	39.8	19.5	5.2	40.5	9.7	22.7
As + 3	0.3	0.1	0.5	1.6	<0.1	<0.1	0.3	<0.1	0.2
As + 5	22.0	31.4	59.6	37.9	19.2	4.9	39.9	9.3	22.5
MMA	<0.1	0.1	0.4	<0.1	0.1	<0.1	0.1	0.2	<0.1
DMA	<0.1	0.2	0.4	0.2	0.2	0.2	0.2	0.2	<0.1

Downloaded by PENNSYLVANIA STATE UNIV on September 11, 2012 | http://pubs.acs.org
Publication Date: October 3, 2005 | doi: 10.1021/bk-2005-0915.ch013

Samples were also collected for the analysis of arsenic species at select wells using opaque containers and an EDTA preservative to minimize metal oxyhydroxide precipitation as described in *(26)*. These samples were analyzed at the U.S. Geological Survey in Denver Colorado. Species results showed that arsenic in ground water in the Passaic Formation is predominantly arsenate even under suboxic conditions (Table 1). One explanation for the occurrence of the oxidized arsenic species in the Passaic could be reactive contact with Mn-oxide coatings that were identified by the investigators on a bedrock fracture surface in the Passaic Formation using energy dispersion spectroscopy (EDS). Manganese oxides are known to rapidly oxidize arsenic from As (III) to As (V) *(27, 28)*. A similar analysis of 23 public supply wells in the Passaic Formation known to have elevated arsenic concentrations showed the same. However, Arsenite (As III) was the dominant species in 2 private and 2 public wells in the Lockatong Formation where it comprised over 63 percent of total arsenic concentrations that ranged from 11.9 to 45.0 ug/L in the 4 wells. Water from those wells also had a hydrogen sulfide odor indicating strong reducing conditions. The methylated arsenic species monomethylarsonic acid (MMA) and dimethylarsinic acid (DMA) were all less than 0.5 ug/L.

Arsenic Sources

Arsenic ranks fifty-second in crustal abundance and has an average crustal concentration of 1.8 mg/Kg or parts per million (ppm), (29). Arsenic concentrations from whole rock geochemical analyses of rocks from the Stockton, Lockatong and Passaic Formations are shown in Figure 3. Black shale and gray mudstone from the Passaic and Lockatong Formations can have high arsenic concentrations with some pyrite rich portions of black shale exceeding 200 ppm *(30)*. The Stockton Formation and red mudstone and siltstone of the Passaic Formation generally have much lower concentrations of arsenic. Electron microprobe analysis of the black shale identified the mineral pyrite (FeS_2) as the major source of arsenic. Two separate black shale members from

Downloaded by PENNSYLVANIA STATE UNIV on September 11, 2012 | http://pubs.acs.org
Publication Date: October 3, 2005 | doi: 10.1021/bk-2005-0915.ch013

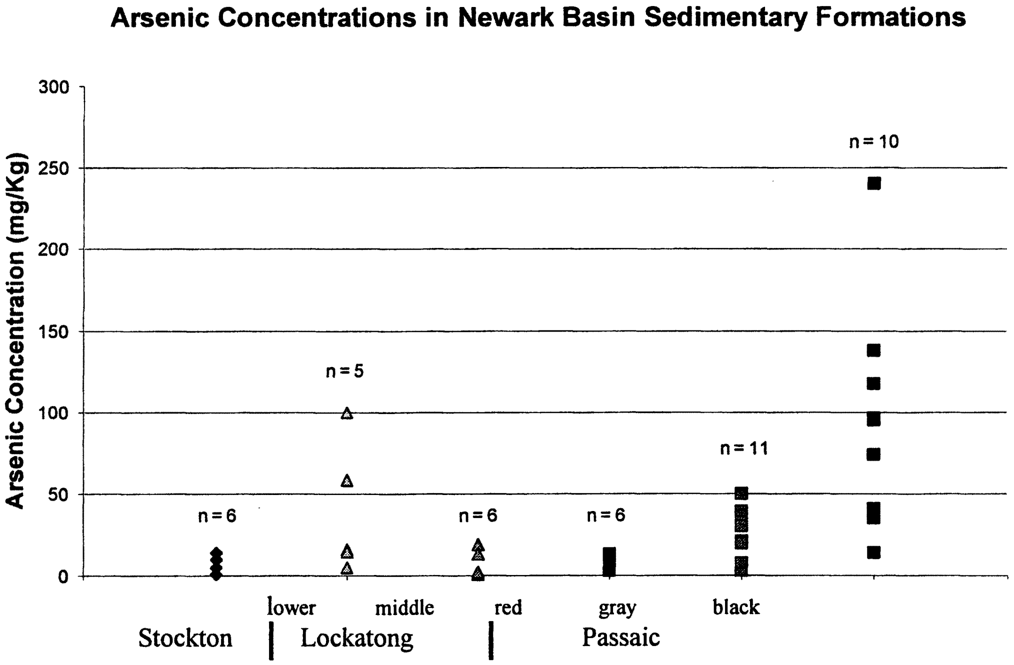

Figure 3. Arsenic whole rock concentration (mg/Kg) data from: (9, 10, 11 and 30) and other NJGS data. The Ukranian and Cedar Grove Member data in the Passaic Formation is from Malinconico, M.L., Personal Communication, Lamont-Doherty Earth Observatory, 10/30/2000.

the lower and middle part of the Passaic Formation have maximum arsenic concentrations measured in pyrite of 40,000 and 3,000 ppm (Figure 4). Arsenic concentrations varied considerably within and between pyrite grains and smaller grains generally had higher concentrations than larger grains. For example, the pyrite grain with 4 weight percent arsenic was less than two microns in diameter. A spatial relationship between high arsenic concentrations in ground water and black shale in both the Lockatong and Passaic Formations was observed.

Although black and gray shale have the highest concentrations of arsenic, red mudstone and siltstone are volumetrically the most abundant lithologies in the Passaic Formation. Therefore, red mudstone and siltstone are also being investigated as a potential source of arsenic to ground water. Red mudstone and siltstone contain abundant hematite (Fe_2O_3), which can be a significant arsenic source mineral. Clay minerals are also a potential source. Hematite in these rock units has been suggested as the source of hydrothermally mobilized copper and other metals making up the stratabound red-bed copper deposits found in the NB *(31)*. It is believed that as these metal rich fluids migrated, the metals precipitated out of solution as sulfide minerals in reducing environments, which would have existed in and near the organic-rich black shales. A portion of the arsenic in pyritic black shales may have been derived from this source.

Arsenic Mobilization and Transport

Processes controlling the mobilization of As in ground water include mineral precipitation and dissolution, adsorption and desorption, chemical transformations, ion exchange and biological activities *(5, 15)*. Assessment of potential mobilization mechansims active in the NB are based on identified natural sources and geochemical observations associated with well water containing elevated arsenic concentrations. First, arsenic concentrations in individual wells that have been sampled mutiple times over periods of months and years have generally varied by less than 10 percent indicating a steady state geochemical condition. Ground water with arsenic concentrations greater than 40 ug/L in the Passaic Formation in the NB is characterized by: [1] dissolved oxygen concentrations < 1.0 mg/L, [2] pH range between 7.5 to 8.2, [3] arsenate > 95 % arsenic total, [4] generally low iron and manganese concentrations, [5] average sulfate and total dissolved solids concentrations for the Passaic, [6] a significant direct correlation between arsenic and strontium concentrations at two locations having multi-element data, three wells in one location and four in the other, and [7] the upgradient occurrence of black and gray shale. It must also be noted that in the Passaic Formation the volume of black and gray shale is far exceeded by the red, and that the water bearing zones found to contain the higher

Downloaded by PENNSYLVANIA STATE UNIV on September 11, 2012 | http://pubs.acs.org
Publication Date: October 3, 2005 | doi: 10.1021/bk-2005-0915.ch013

Downloaded by PENNSYLVANIA STATE UNIV on September 11, 2012 | http://pubs.acs.org
Publication Date: October 3, 2005 | doi: 10.1021/bk-2005-0915.ch013

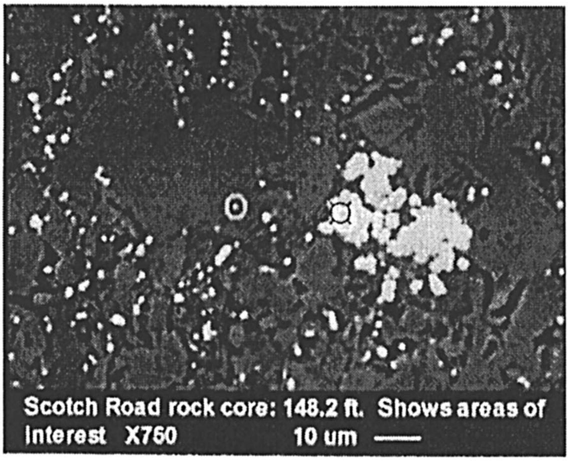
Scotch Road rock core: 148.2 ft. Shows areas of Interest X760
10 um ——
o
¤

Figure 4. Scanning electron micrograph of black shale from the Newark Basin in New Jersey. Pyrite (bright) in a calcite matrix (dark). Arsenic concentrations in pyrite, 11,500 (o) and 15,860 (¤) mg/Kg. Analyses by NJGS at the Department of Geological Sciences, Rutgers University. Core samples collected and donated by Zoltan Szabo, USGS (30).

arsenic concentrations are in the red mudstones and siltstones. Mobilization and transport hypotheses must account for these observations.

To better understand the possible mobilization mechanisms a leach study using pulverized rock from the Passaic Formation and doubly deionized water was conducted under abiotic conditions following a procedure described in *(32)*. Preliminary leach results from black (~ 52 mg/Kg arsenic), gray (~ 13 mg/Kg arsenic) and red (~ 4 mg/Kg arsenic) shale and mudstone showed that after completion of the 20 week procedure, arsenic concentrations remained nearly temporally consistent with red (~ 6 ug/L) > black (~ 3 ug/L) > gray (~ 1 ug/L) in the leachate. Microscopic examination of pyrite in the pulverized black shale showed that it had not oxidized after 20 weeks and therefore presumably was not contributing arsenic to the leachate. Molybdenum concentrations in leachate from the black shale were consistently reported in the mg/L range and were 2 orders of magnitude higher than that in the gray and red. The oxyanion molybdate is known to successfully compete with arsenate for sorption sites on iron oxides under pH conditions < 6.0 *(33)*. A study using *Thiobacillus ferrooxidans* inoculants on the same geologic material is being conducted cooperatively with the Biotechnology Center, for Agriculture and the Environment at Rutgers University. A subsequent but modified leach experiment using red shale with ~ 13 mg/kg yielded 39 ug/L arsenic

The fact that a rock or mineral contains arsenic does not necessarily mean that it is released in significant quantities or is mobile enough along the groundwater flow path to exceed drinking water standards. The mobilization and transport mechanisms discussed below are based on observations made in the Passaic Formation, however, they may also be applicable in the Lockatong Formation where black shale dominates. Based on the arsenic source and mobilization background above, three possible arsenic mobilization source zones impacting ground water are proposed. They are: [1] black shale dominant, such as in the Lockatong Formation, [2] black shale semi-equilibrated water as an arsenic source and mobilizing agent in red mudstones and siltstones that are down gradient from it, such as in the Passaic and Lockatong Formations, and [3] red mudstones and siltstones as dominant arsenic sources. Figure 5 illustrates the three source zone possibilities, which are combined with shallow and deep ground-water flow characteristics into a conceptual model of arsenic mobilization and transport in the NB.

Black shale in the Passaic Formation contains the highest whole rock arsenic concentrations but is less than a few feet thick and sandwiched between much thicker red sequences. The highest arsenic concentrations in ground water are found in the water bearing zones in the red mudstones and sitltones. The dominant mineral source of arsenic in black shale is pyrite and therefore the decomposition of pyrite is necessary to mobilize it. The primary oxidizer of pyrite is O_2, however secondary oxidants such as Fe^{3+} and NO_3^- can also play a role and microorganisms such as Thiobacillus Ferrooxidans can catalyze the oxidation process *(34)*. Pyrite oxidation is therefore expected to be most significant at or above the water table where O_2 is readily available and continually supplied. Arsenic mobilized in the black shale in the shallow weathered zone would have to flow downslope and recharge WBZs in the red mudstones and siltstones to account for the arsenic laden and lower DO water found there. In order to maintain elevated arsenic concentrations, geochemical mechanisms that would limit arsenic adsorption during transport would have to be active along the flow path. The pH of water flowing from the black shale mobilization zone is expected to be low, probably acidic. Newly formed and possibly existing iron oxide phases would act as strong adsorbents of arsenic under those conditions. However, competition with oxyanions such as molybdate may limit arsenic adsorption and maintain elevated concentrations in the critical area within and just downgradient and outside of the source zone. Mineral-water reactions that consume hydrogen ions, such as reactions with calcite, would increase the aqueous pH along the flow path thereby limiting the adsorption of arsenic onto existing iron oxides such as hematite. Whole rock geochemistry shows that arsenic and strontium concentrations are much higher in black shale than in gray and red units. Geochemical evidence supporting the hypothesis that black shale is a major source of high arsenic concentrations in ground water include: [1] the upgradient occurrence of black shale associated with impacted wells, [2] the direct correlation between strontium and arsenic in ground water, [3] the low DO in ground-water containing elevated arsenic concentrations, and [4] the occurrence of elevated concentrations of arsenic in the Lockatong Formation which is dominantly black shale.

Downloaded by PENNSYLVANIA STATE UNIV on September 11, 2012 | http://pubs.acs.org
Publication Date: October 3, 2005 | doi: 10.1021/bk-2005-0915.ch013

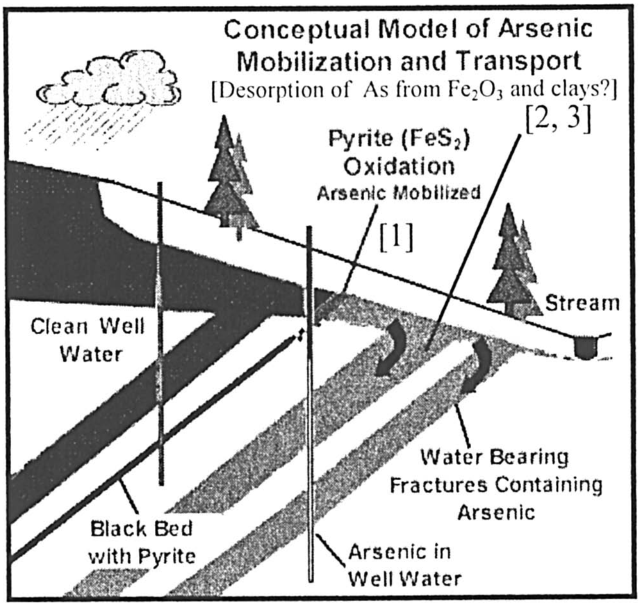
Conceptual Model of Arsenic Mobilization and Transport
[Desorption of As from Fe_2O_3 and clays?]
[2, 3]
Pyrite (FeS_2) Oxidation
Arsenic Mobilized
[1]
Stream
Clean Well Water
Water Bearing Fractures Containing Arsenic
Black Bed with Pyrite
Arsenic in Well Water

Figure 5. A 2-D conceptual model showing possible arsenic mobilization and transport in the Newark Basin. [1, 2, 3] As source zones described in text. Shallow and deep flow zones are after (23) and (19).

In addition to arsenic being released to ground water from the oxidation of pyrite in the black shale mobilization zone, specific geochemical characteristics of that water may facilitate the mobilization of arsenic outside that zone in red mudstones and siltstones (Figure 5). Black shale-water interactions are expected to decrease the aqueous dissolved oxygen concentration, potentially producing sub-oxic water, and increase concentrations of dissolved organic carbon and oxyanions such as molybdate. When this water interacts with minerals in the red strata, such as hematite, reductive destabilization and competitive adsorption may release additional arsenic into solution. An increasing pH along the flow path would further initiate arsenic desorption and maintain concentrations. Interestingly, bedding confined dissolution zones associated with evaporite filled and interconnected root cavities in red mudstones and siltstones can be significant WBZs and are observed to carry water with high arsenic concentrations at several locations *(20)*. It is possible that as these networks grow, more hematite and clay surface area would continually become available. The elevated and steady state arsenic concentrations found in ground water in the NB are likely the result of a combination of hydrogeochemical variables.

Downloaded by PENNSYLVANIA STATE UNIV on September 11, 2012 | http://pubs.acs.org
Publication Date: October 3, 2005 | doi: 10.1021/bk-2005-0915.ch013

Conclusions

1. Hydrogeochemical evidence supports the hypothesis that pyrite bearing black shale in the Lockatong and Passaic Formations are sources of arsenic to ground water in some settings. The oxidation of pyrite is the necessary trigger for arsenic release and is expected to occur in the shallow unsaturated and saturated zones.
2. Leach experiments and field evidence support the possibility that certain red strata in the Passaic Formation can be significant sole sources of arsenic to ground water. Hematite and possibly clay minerals are the likely ultimate sources there. Optimum aqueous geochemical conditions, such as a pH range between 7.5 to 8.2, are believed to act as triggers by promoting the desorption of arsenic and/or hindering adsorption. Wells intersecting significant WBZs associated with these strata are predicted to yield water with elevated arsenic concentrations.
3. More work to better understand the mobilization and transport of arsenic in the NB is needed and is ongoing at the NJDEP and Rutgers University.

Acknowledgements

We would like to thank all of the individuals from the New Jersey Department of Environmental Protection, Rutgers University and the United States Geological Survey who provided support, advice and assistance.

References

1. USEPA, Implementation Guidance for the Arsenic Rule, Drinking Water Regulations for Arsenic and Clarifications to Compliance and New Source Contaminants Monitoring , EPA-816-K-02-018, 2002; pp 1-83.
2. National Academy of Sciences National Research Council (NAS), Arsenic in Drinking Water, National Academy Press, 1999; pp 1-330.
3. International Agency for Research on Cancer (IARC), Arsenic and arsenic compounds: IARC Monograph on the Evaluation of Carcinogenic Risks to Humans-Overall Evaluations of Carcinogenicity: an Update of the IARC Monographs 1 to 42, IARC, Lyon, France, Suppl. 7, 1987, 100-106.
4. NRC, National Academy of Sciences National Research Council (NAS), 2001, Arsenic in Drinking Water: 2001 Update, National Academy Press.
5. Smedley, P.L.; Kinniburgh, D.G. *Appl. Geochem.* **2002**, *17*, 517 – 568.

Downloaded by PENNSYLVANIA STATE UNIV on September 11, 2012 | http://pubs.acs.org
Publication Date: October 3, 2005 | doi: 10.1021/bk-2005-0915.ch013

6. Fusillo, T.V.; Hochreiter, J.J.; and Grant, D.L. Water-Quality Data for the Potomic-Raritan-Magothy Aquifer System Southwestern New Jersey, 1923-83: USGS, Open File Report 84-734, 1984; pp 1-127.
7. Serfes, M. S., Natural ground-water quality in bedrock of the Newark Basin, New Jersey, New Jersey Geological Survey Report GSR 35, 1994; pp 1-28.
8. Kozinski, J.; Szabo, Z.; Zapecza, O.S.; Barringer, T.H. Natural Radioactivity in, and Inorganic Chemistry of, Ground Water in the Kirkwood-Cohansey Aquifer System, Southern New Jersey, 1983-89: USGS.WRI Report 92-4144, 1995; pp 1-130.
9. Serfes, M.E. in press, Ground Water Quality in the Bedrock Aquifers of the Highlands and Valley and Ridge Physiographic Provinces of New Jersey: New Jersey Geological Survey Report GSR 39, 2004.
10. Serfes, M.E.; Spayd, S.E.; Herman, G.C.; Monteverde, D.E. Arsenic Occurrence, Source and Possible Mobilization Mechanisms in Ground Water of the Piedmont Physiographic Province in New Jersey: Poster, in EOS, Transactions of the American Geophysical Union Fall Meeting, v. 81, no. 48, November 28, 2000, p. F525-H210-08.
11. Serfes, M.E.; Spayd, S.E.; Herman, G.C.; Monteverde, D.E. Arsenic Occurrence, Source and Possible Mobilization Mechanisms in Ground Water of the Newark Basin in New Jersey: Poster given at the Arsenic in Drinking Water: An International Conference at Columbia University on November 26-27, 2001.
12. Serfes, M.E.; Spayd, S.E.; Herman, G.C. Arsenic in New Jersey Ground Water: Presentation with abstract given at the American Chemical Society national meeting in NYC, NY, Advances in Arsenic Research, September 7 - 9, 2003.
13. Spayd, S.E.; Sites, A.; Serfes, M.E.; Murphy, E. NJDEP, Treating Residential Home Well Water to Reduce Arsenic Levels in New Jersey - Preliminary Data, Poster prepared for presentation at Arsenic in Drinking Water: An International Conference at Columbia University, New York, November 26-27, 2001.
14. Schlische, R.W.; Withjack, M.O.; Olsen, P.E. Relative timing of CAMP, rifting, continental breakup, and inversion: tectonic significance, in Hames, W.E., McHone, G.C., Renne, P.R., and Ruppel, C.R., eds.; The Central Atlantic Magmatic Province: Insights from Fragments of Pangea: American Geophysical Union Monograph 136, 2002, 33-59.
15. Welch, A.H.; Westjohn, D.B.; Helsel, D.R.; Wanty, R.B. *Groundwater* **2000**, *38*, 589-604.
16. Murphy, E.A.; Aucott, M. *Sci. Total Environ.* **1998**, *218*, 89-101.
17. NJDEP, Findings and Recommendations for the Remediation of Historic Pesticide Contamination - Final Report March 1999.

Downloaded by PENNSYLVANIA STATE UNIV on September 11, 2012 | http://pubs.acs.org
Publication Date: October 3, 2005 | doi: 10.1021/bk-2005-0915.ch013

18. Olsen, P.E.; Kent, D.V.; Cornet, B.; Witte W.K.; Schlische, R.W. *GSA Bulletin* **1996**, *108*, 40-77.
19. Michalski, A.; Britton, R. *Groundwater* **1997**, *35*, 318-327 .
20. Herman, G.C. Hydrogeologic framework of bedrock aquifers in the Newark Basin, New Jersey: Field Guide and Proceedings, Geology in Service to Public Health, 18th Annual Meeting, Geologic Assoc. of NJ, 2001; p 6–45.
21. Morin, R.H.; Carlton, G.B.; Poirier, S. *Groundwater* **1997**, *35*, 328-338.
22. Morin, R.H.; Senior, L.A.; Decker, E.R. *Groundwater* **2000**, *38*, 182-192.
23. Soloman, D.K.; Moore, G.K.; Toran, L.E.; Dreier, R.B.; McMaster, W.M. Status report: a hydrologic framework for the Oak Ridge Reservation: Oak Ridge National Laboratory (ORNL/TM-12026), Environmental Sciences Division, Publication no. 3815, 1992; pp 1-23.
24. Driese, S.G.; McKay, L.D.; Penfield, C.P. *J. Sed. Res.* **2001**, *71*, 843-857.
25. Alley, W.M.; Regional Ground-Water Quality: Van Nostrand Reinhold, New York, NY, 1993; pp 1-634.
26. Bednar, A. J.; Garbarino, J. R.; Ranville, J. F.; Wildeman, T. R. *Environ. Sci. Technol.* **2002**, *36*, 2213 -2218
27. Driehaus, W.; Seith, R.; Jenkel, M. *Water Res.* **1995**, *1*, 297-305.
28. Scott, M.J.; Morgan, J.J. *Environ. Sci. Technol.* **1995**, *29*, 1898–1905.
29. Demayo, A. Elements in the Earths Crust, Weast, Robert C, CRC Handbook of Chemistry and Physics, 66th Edition, Ed., CRC Press Inc., Boca Ratan, Fl, 1985; p F145.
30. Szabo, Z.; Taylor, T.A.; Payne, D.F.; Ivahnenko, T. Relation of Hydrogeologic Characteristics to Distribution of Radioactivity in Ground Water, Newark Basin, New Jersey: USGS, WRIR, 95-4136, 1997; p 1-134.
31. Rose, A.W.; Bianchi-Mosquera, G.C. *Econ. Geol.* **1993**, *88*, 1226-1236.
32. Standard Test Method for Accelerated Weathering of Solid Materials Using a Modified Humidity Cell American Society for Testing and Materials, ASTM, Designation: D 5744 – 96 (2001), ASTM, West Conshohocken, PA, 2001; pp 1-13.
33. Manning, B.A.; Goldberg, S. *Soil Sci. Soc. Am. J.* **1996**, *60*, 121-131.
34. Schreiber, M.E.; Simo, J.A.; Freiberg, P.G. *Hydrogeology* **2000**, *8*, 161-176.

Downloaded by PENNSYLVANIA STATE UNIV on September 11, 2012 | http://pubs.acs.org
Publication Date: October 3, 2005 | doi: 10.1021/bk-2005-0915.ch013

Downloaded by UNIV OF GUELPH LIBRARY on September 12, 2012 | http://pubs.acs.org
Publication Date: October 3, 2005 | doi: 10.1021/bk-2005-0915.ch014

Chapter 14

Groundwater Geochemistry, Microbiology, and Mineralogy in Two Arsenic-Bearing Holocene Alluvial Aquifers from the United States

J. A. Saunders[1,*], S. Mohammad[1], N. E. Korte[2], M.-K. Lee[1], M. Fayek[3], D. Castle[4], and M. O. Barnett[5]

[1]Department of Geology and Geography, Auburn University, Auburn, AL 36849
[2]Consultant, Grand Junction, CO 81506
[3]Oak Ridge National Laboratory, P.O. Box 2008, Oak Ridge, TN 37831
[4]Center for Environmental Biotechnology, University of Tennessee, Knoxville, TN 37996
[5]Department of Civil Engineering, Auburn University, Auburn, AL 36849

Groundwaters in two Holocene alluvial aquifers containing elevated dissolved arsenic in the USA have similar geochemical characteristics and microbiology. These include: 1) near-neutral pH and moderately reducing redox state where reactive organic matter is present; 2) significant dissolved iron and manganese; 3) presence of both iron- and sulfate-reducing bacteria of the genera *Geobacter* and *Desulfovibrio*, respectively; and 4) evidence that precipitation of authigenic minerals (e.g., carbonates and sulfides) limits concentrations of dissolved metal(loid)s. This study indicates that heterotrophic anaerobic bacteria directly mediate both the dissolution of detrital iron and manganese minerals in the aquifers, which leads to release of As and other trace elements, and also indirectly leads to supersaturation with respect to authigenic minerals such as siderite ($FeCO_3$) and rhodochrosite ($MnCO_3$). Locally, conditions suitable for metabolism of sulfate-reducing bacteria may prevail, leading to precipitation of As-bearing biogenic pyrite enriched in ^{32}S.

In Advances in Arsenic Research; O'Day, P., et al.;
ACS Symposium Series; American Chemical Society: Washington, DC, 2005.

Precipitation of As-poor siderite and As-bearing pyrite will affect earlier dissolved As/Fe ratios of groundwaters, perhaps masking the original effect of concomitant As and Fe release by bacterial-mediated reductive dissolution of As-bearing hydrous ferric oxide. Comparison of the results of this study to data from Bangladesh and India suggest that these groundwater geochemical and microbiologic processes may be universal to Holocene alluvial aquifers in many places around the world. If so, then release of arsenic to these young river flood-plain sediments is an expected consequence of common biogeochemical processes.

Downloaded by UNIV OF GUELPH LIBRARY on September 12, 2012 | http://pubs.acs.org
Publication Date: October 3, 2005 | doi: 10.1021/bk-2005-0915.ch014

Introduction

The metalloid arsenic is highly toxic and can contaminate groundwater by a variety of biogeochemical processes. Although anthropogenic sources are common as arsenic has a number of industrial uses, the natural sources currently pose the biggest human health risk worldwide. Arsenic is a common constituent in a number of base- and precious-metal and coal deposits where it is released by oxidation of iron sulfide minerals such as As-bearing pyrite (FeS_2) and much less commonly, arsenopyrite (FeAsS) (*1,2*). Similarly, a number of anoxic marine sedimentary rocks may contain sulfide sources of As and their weathering can also release As (*3-6*). *In situ* weathering of glacial deposits (*7*), loess and volcanic ash (*8*), and crystalline "basement" rocks (*9*) are some continental sources that have been proposed as origins of As contamination of groundwater. The aforementioned processes typically lead to elevated dissolved concentrations close to their rock sources. Recent research has shown that Holocene alluvial floodplain deposits, such as in Bangladesh, India, etc., are most problematic from the human health standpoint (*10-13*). These floodplains may form far from the ultimate As source and appear to derive dissolved As from stream sediments that were physically transported to the floodplain (*9*). In this paper, we discuss the geochemistry and geomicrobiology of groundwater in two Holocene alluvial aquifers with locally elevated As in the USA and compare them to groundwaters from Bangladesh. The comparisons indicate that similar geochemical, microbiologic, mineralogic, and hydrogeologic conditions occur in young alluvial floodplains and that toxic levels of dissolved As can be produced.

Korte was the first in the USA to document natural elevation of arsenic in shallow Holocene alluvial floodplain deposits at Kansas City, Missouri (*14,15*). Korte (*14*) proposed that arsenic was released by reduction of As-bearing HFO's

Downloaded by UNIV OF GUELPH LIBRARY on September 12, 2012 | http://pubs.acs.org
Publication Date: October 3, 2005 | doi: 10.1021/bk-2005-0915.ch014

by co-deposited organic matter. At about the same time, Lovley and coworkers (*16*) documented the importance of dissimilatory iron-reducing bacteria (FeRB) on iron geochemical cycling in groundwaters. Similarly, geochemical studies indicated that FeRB and sulfate-reducing bacteria (SRB) had a major control on the fate and transport of Fe and Mn in groundwater from Mississippi (*17*). In an extension of Korte's model for As release to alluvial aquifers, FeRB and SRB were also implicated in controlling the geochemical behavior of arsenic and other trace metals such as Co, Ni, V, U, Ba, and REE's in Holocene alluvial floodplain deposits in east-central Alabama (*9*). In that study, it was proposed that sorption of As and other trace metals on Fe-Mn oxyhyroxides in stream sediments concentrated these dissolved elements, and was the source of the same elements in the adjoining floodplain deposits (9).

Since the mid 1990's reports of As contamination of Holocene aquifers from the Indian subcontinent (*10-13* and references therein) and Hungary (*18*) began to be published. Two competing hypotheses about the source of As in Holocene alluvial aquifers were proposed (*2, 19*): 1) oxidation of As-bearing pyrite (FeS_2); and 2) reductive dissolution of As-bearing hydrous ferric oxides (HFO). Recent research supports the latter hypothesis (*9, 20-27*), although the ultimate As source, and the mechanism for its introduction into Holocene alluvial aquifers have not been addressed. In this paper, we document for the first time from field microbiology studies that FeRB apparently cause elevated dissolved As in Holocene alluvial aquifers. Further, geochemical data and modeling indicate that the often-observed lack of a statistically significant correlation between dissolved As and Fe is probably due to precipitation of authigenic iron minerals such as siderite and pyrite.

Materials and Methods

Two field areas were selected for this investigation: 1) Korte's (*14*) original discovery area of natural As contamination at Kansas City, Missouri; and 2) a field site in Alabama where As and other trace elements in aquifer waters and minerals have been described (*9*). Groundwater at the Kansas City site was collected from monitoring wells with a >20-year history of water analyses showing no anthropogenic effects and also was representative of the varying geochemical conditions at the site. Three splits of water samples were collected in the field: 1) one split that was filtered using 0.45µm teflon filters and acidified with ultra pure nitric acid; 2) another sample was collected and not filtered or acidified; and 3) an additional sample was collected in sterile glass bottles for bacterial culturing. Specific electrical conductance, alkalinity, Eh, pH, temperature, and sulfide were all measured in the field. In addition, several liters of groundwater were pressure filtered in the field to collect bacteria for

DNA analysis. Laboratory analyses for cations and As were done by ICP-MS, and anions were determined using ion chromatography. Geochemical modeling was accomplished using Geochemist's Workbench (*28*) and PHREEQC (*29*).

Samples with viable bacteria were refrigerated and transported directly to the lab where culture media were set up to evaluate for the presence or absence of FeRB and SRB in each of the 8 monitoring well groundwaters. Filters containing bacteria were frozen at -80°C and were ultimately analyzed by using kits to extract the DNA from the filters, PCR to amplify the DNA, and the 16S rDNA was sequenced in order to identify important bacterial strains. At the Alabama field area, solid samples of auger cuttings were collected in sterile plastic bags for chemical and microbiologic analyses. Fe and As were extracted using 0.5N HCl and were measured in the lab. Bacteria were identified by culturing and enumerated using the most probable number (MPN) technique.

Samples of authigenic pyrite from the Alabama field site were polished and etched using a solution of $KMnO_4$ and HCl to bring out textural and chemical features. In particular, As-rich zones in pyrite were enhanced and identified by this procedure. Polished sections were then analyzed by a JEOL electron microprobe, which confirmed that etch-enhanced portions of pyrite were enriched in As. To examine the relationship between pyrite arsenic content and possible connections to metabolism of sulfate-reducing bacteria, three pyrite samples were investigated in detail using the ion microprobe (secondary ion mass spectrometry, SIMS) at Oak Ridge National Laboratory. In SIMS, a high energy "primary" ion beam bombards a surface, triggering release of secondary ions whose mass/charge ratios are measured using mass spectrometers. The technique is useful for *in situ* isotopic and trace-element analyses, and As/S ratios and $\partial^{34}S$ values were measured in 20μm spots in traverses of up to 15 analyses in single crystals.

Results and Discussion

Location of Study Areas

The Kansas City study area is at the U.S. Department of Energy's (DOE) Kansas City Plant (KCP) located in floodplain deposits of the Blue River, a tributary of the Missouri River (Figure 1). The aquifer at the KCP site consists mainly of Holocene stream-valley alluvial deposits that unconformably overlie Pennsylvanian strata of limestone and shale (*14*). Alluvial deposits typically consist of sand and gravel deposits and locally intermittent lenses of sand, silt, and clay. Groundwater at the KCP site is unconfined but locally can exist under confined conditions where clay layers are present (*14*). Water level depths in wells at the KCP typically are <7 m. The Alabama study area is located along two streams in extensive Holocene floodplain deposits (Figure 2) that C-14 age

Downloaded by UNIV OF GUELPH LIBRARY on September 12, 2012 | http://pubs.acs.org
Publication Date: October 3, 2005 | doi: 10.1021/bk-2005-0915.ch014

dating have shown to be <7000 years old (*30*). These alluvial deposits consist primarily of silty sand containing erratic but common macro wood fragments up 0.5m in size (*9,31*). The alluvium unconformably overlies the Cretaceous Tuscaloosa Group of the Alabama Coastal Plain in the study area (*9*). Groundwater is unconfined with depths to the water table typically <2m.

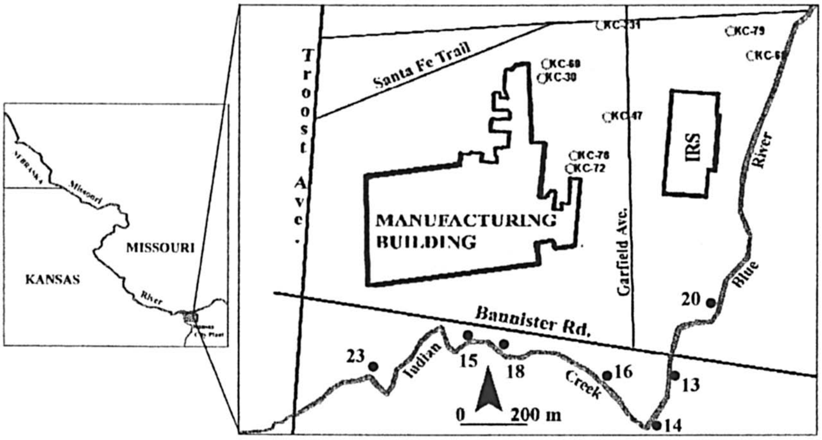
KANSAS
MISSOURI
Missouri
River
Troost Ave.
Santa Fe Trail
KC-60
KC-30
KC-31
KC-79
KC-6
KC-47
KC-78
KC-72
MANUFACTURING BUILDING
IRS
Garfield Ave.
Blue River
Bannister Rd.
20
23
15
18
16
13
14
Indian Creek
0 200 m

Figure 1. Location map for the DOE Kansas City Plant and monitoring wells used in this study. Also shown are concentrations for total arsenic in stream sediment samples (in mg/kg) from adjacent streams.

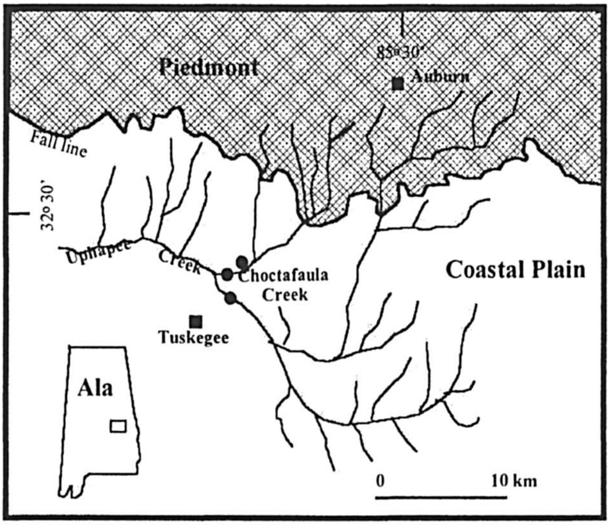
Piedmont
85°30'
Auburn
Fall line
32° 30'
Uphapee Creek
Choctafaula Creek
Tuskegee
Coastal Plain
Ala
0 10 km

Figure 2. Location map for the Alabama study area.

Downloaded by UNIV OF GUELPH LIBRARY on September 12, 2012 | http://pubs.acs.org
Publication Date: October 3, 2005 | doi: 10.1021/bk-2005-0915.ch014

Groundwater Geochemistry and Microbiology

Groundwater at the Kansas City Plant is highly variable in redox state, iron, and manganese content, but has near-neutral pH (Table I). Arsenic was significantly elevated (e.g., >50µg/L) in three of the eight samples, which also happened to have the lowest Eh values (Table I). Dissolved Fe ranged from 0.2 to 17.1 mg/L, Mn from 0.5 to 7.9 mg/L, and alkalinity ranging from 175 to 350 mg/L (as $CaCO_3$). Geochemical modeling with PHREEQC indicates that groundwater samples have positive saturation indices (SI) for siderite ($FeCO_3$) in two of the three As-elevated wells and supersaturated SI values for rhodochrosite ($MnCO_3$) in all three elevated-As samples (Table 1). Similarly, all eight groundwater samples are supersaturated with respect to goethite (FeOOH) and understaurated with respect to ferrihydrite ($Fe(OH)_3$), suggesting that an iron oxyhydroxide phase with a solubility between those two might have been the source of iron in groundwaters.

Table I. Selected Geochemical Data from the Kansas City Field Area

Well ID	*KC-30*	*KC-47*	*KC-60*	*KC-68*	*KC-72*	*KC-76*	*KC-79*	*KC-231*
pH	7.03	6.74	6.99	6.53	7.30	7.09	6.88	7.03
Eh (mV)	114	22	113	-139	-110	-114	-90	32
Alkalinity (mg/L)*	300	290	245	350	250	185	175	270
Mn^{2+} (mg/L)	0.46	2.96	5.71	7.89	0.51	4.94	5.53	4.28
Fe^{2+} (mg/L)	0.79	1.62	0.24	17.10	0.23	5.09	0.40	2.68
As_{total} (µg/L)	12	1	2	78	167	131	8	33
*as $CaCO_3$								
Saturation indices (SI)								
Calcite	0.39	-0.38	-0.07	-0.39	0.15	-0.22	-0.29	0.02
Ferrihydrite	-0.41	-2.77	-0.81	-4.78	-3.65	-3.10	-4.45	-1.14
Goethite	5.48	3.12	5.08	0.11	2.24	2.79	1.44	4.75
Rhodochrosite	-0.11	0.54	1.06	0.78	0.33	0.95	0.74	0.93
Siderite	-0.13	0.00	-0.56	0.84	-0.24	0.70	-0.66	0.47

Additional geochemical modeling was conducted with the Geochemist's Workbench to compare groundwaters from the Kansas City study area to groundwaters from As-contaminated areas of Bangladesh, using published data from the British Geological Survey's (BGS) "Special Study" in which Eh was also measured in the field (*32*). An Eh-pH plot for the KCP waters indicates that they plot in the stability fields of both arsenate (As-V, $HAsO_4^{2-}$) and arsenite (As-III, $As(OH)_3^0$ or $H_3AsO_3^0$), although the most As-enriched samples

Downloaded by UNIV OF GUELPH LIBRARY on September 12, 2012 | http://pubs.acs.org
Publication Date: October 3, 2005 | doi: 10.1021/bk-2005-0915.ch014

plot in the arsenite field (Figure 3a) and even into the narrow stability fields of solid mineral phase orpiment (As_2S_3). The BGS data plot in the same general area in Eh-pH space (Figure 3a) with a shift to slightly higher Eh values when the much larger data set is plotted. Similarly, Eh-pH plots were made for average geochemical conditions (with respect to Fe, Mn, carbonate, and S species) for both the KCP site groundwaters and those from Bangladesh (Figure 3b). KCP groundwaters plot near the Fe^{2+}-siderite and Mn^{2+}-rhodochrosite boundary, suggesting that they are approaching local equilibrium with both mineral phases (consistent with siderite SI values discussed previously). The most As-rich groundwater samples from the KCP study area plot close to the stability field of pyrite (Figure 3b). As before, KCP and Bangladesh groundwaters plot in the same approximate areas in Eh-pH space (Figure 3b). Similarly, groundwaters from Bangladesh appear to be close to equilibrium (or are supersaturated with) with respect to siderite and rhodochrosite.

Several researchers have proposed that Fe- and possibly Mn-reducing bacteria may have been important in producing As-contaminated groundwater in Holocene alluvial aquifers. However, this has only been inferred from the high Fe(Mn) contents of groundwaters with elevated As, its moderately reducing state, and a general correlation between dissolved Fe, As, and alkalinity (*9,21,22,24,26*). To evaluate this hypothesis, we conducted reconnaissance microbiologic investigations at our two field sites. At the Kansas City site, we collected two different types of samples for microbiologic investigations: 1) groundwater samples for culturing of viable bacteria; and 2) (frozen) filters that contained the bacteria removed from several liters of groundwater in the field for microbial analyses. In the former case, each of eight well samples was used to inoculate anaerobic culture media designed to grow either FeRB or SRB. Only in groundwater samples from wells KC-68, KC-72, and KC-76 could FeRB and SRB be cultured. These wells also have the lowest field Eh values and the highest As content (Table I). In the other five wells, neither class of bacteria could be cultured. We would argue that this presence/absence data is proof that FeRB are at least *available* to catalyze Fe-reduction in the As-enriched wells and is the first direct field indication of their involvement in producing arsenic contamination in groundwater.

Similar to the culturing experiments, cloning and sequencing of the 16S rDNA genes extracted from bacteria filtered from groundwater at the KCP site also indicated the presence of FeRB and SRB from the high-As samples. Clones with sequences similar to known FeRB (e.g., *Geobacter* sp.) were also abundant in two the high-As samples (KC-68, KC-72; Table II). In particular, *Geobacter sulfurreducens* was found in two samples (KC-60, KC-68; Table II). *G. sulfurreducens* is not a strict anaerobe (consistent with oxidizing Eh of KC-60, Table I) but does couple organic-matter oxidation to several possible terminal electron acceptors, notably HFO (*33*). Clones similar to known SRB within the delta-proteobacteria (e.g., *Desulfovibrio* sp.) group were also present in two low Eh samples (KC-76, KC-79; Table II). In contrast, very few of the clones from

Downloaded by UNIV OF GUELPH LIBRARY on September 12, 2012 | http://pubs.acs.org
Publication Date: October 3, 2005 | doi: 10.1021/bk-2005-0915.ch014

Downloaded by UNIV OF GUELPH LIBRARY on September 12, 2012 | http://pubs.acs.org
Publication Date: October 3, 2005 | doi: 10.1021/bk-2005-0915.ch014

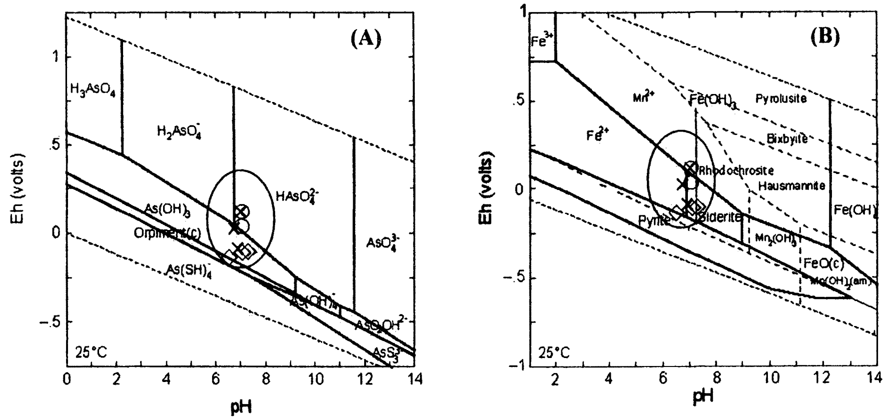

Figure 3. Eh-pH diagram calculated for average geochemical conditions at the Kansas City Plant in (a) As-S-H_2O and (b) As-Fe-Mn-S-H_2O system. Total As concentration of KCP samples: cross = As <10 μg/L; circle = 10-50 μg/L and; diamond = >50 μg/L. Also shown is the field where groundwater data from the BGS "Special Study" (32) plot on same diagram (large oval).

Table II. Frequency of known FeRB and SRB in Kansas City samples. Frequency was determined as percentage of all clones sequenced.

Wells	Closest Relative	Similarity (%)	Accession Number	Frequency (%)
KC-30	None	–	–	–
KC-47	None	–	–	–
KC-60	*Geobacter sulfurreducens*	98	U13928	13
KC-68	*Geobacter sulfurreducens*	99	U13928	20
KC-72	*Geobacter* sp. ENN1	98	AY034485	27
	Uncultured delta proeobacterium n14r	95	AF194203	20
	Uncultured *Geobacter* sp. strain NS1	97	AF404348	13
KC-76	*Desulfovibrio* sp. HS2	99	AY274444	13
	Desulfovibrio sp. JG1	98	AJ295678	13
	Desulfovibrio sp. Met 82	98	AY062930	20
	Desulfovibrio longus	99	X63623	13
KC-79	*Desulfovibrio* sp. HS2	98	AY274444	27
KC-231	None	–	–	–

Downloaded by UNIV OF GUELPH LIBRARY on September 12, 2012 | http://pubs.acs.org
Publication Date: October 3, 2005 | doi: 10.1021/bk-2005-0915.ch014

low-As samples were related to known FeRB or SRB bacteria. Thus the molecular biological data generally corroborate the bacterial culturing results.

Groundwater chemistry for the Alabama field site is generally similar to groundwater from the KCP site. It contains elevated Fe and Mn (up to 1 and 3 mg/L respectively, consistent with its moderately reducing nature), pH 6.6 to 6.8, 1-10 μg/L each of As, Co, Ni, Zn, total REEs, and 50-175 μg/L of Ba. Because bacterial studies were conducted only on groundwater samples at the KCP site, we wanted to evaluate if *solid* aquifer materials might yield similar results as seen at KCP. We used a truck-mounted auger to advance a borehole into the alluvial aquifer at the Alabama field site and collected samples below the water table for microbiologic and chemical analyses. As at the KC site, both FeRB and SRB were cultured from the aquifer, and enumeration indicated that FeRB were most abundant (Figure 4). Data on extractable Fe(II), Fe(III), and As, are also shown in Figure 4. Extractable As is relatively constant with depth (4-5 mg/kg) but extractable Fe(III) predominates at shallow depths, giving way to more abundant Fe(II) below a depth of 12 feet (3.7 m). This data are consistent with As present in HFO, and the observed more reducing conditions (more sulfidic) with depth.

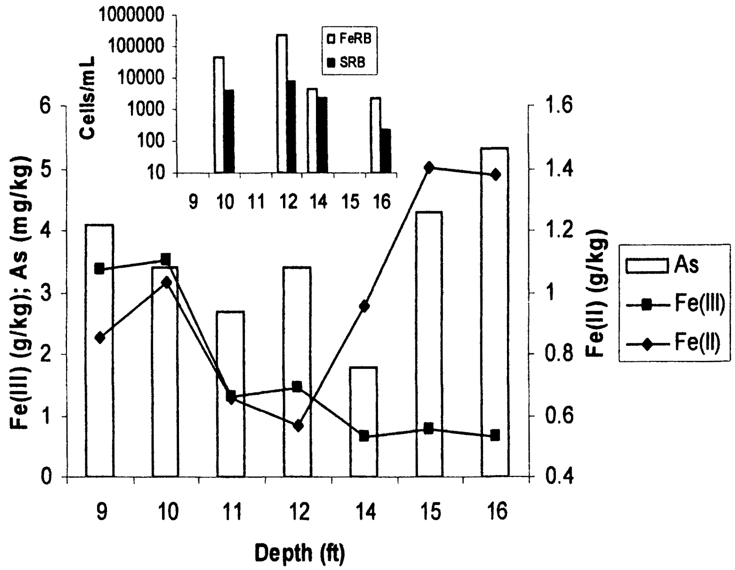

Figure 4. Analysis of extractable Fe and As (by 0.5M HCl), and relative abundance of common bacteria groups in solid aquifer samples from a borehole from the Alabama field area. Note iron-reducing bacteria predominate at all depths samples.

In the Alabama field site, pyrite replaces wood fragments up to 0.5 m in diameter and the organic matter appears to support localized sulfate-reducing conditions near the base of the alluvial aquifer (*9*). Electron microprobe analyses indicate that pyrite contains up to 0.62 wt. % As, even though present-day groundwaters contain less than 10 μg/L As. Ion microprobe analyses of pyrite grains from the aquifer show a finger-print of SRB metabolism (Figure 5). Individual pyrite crystals are zoned with respect to $\partial^{34}S$, typically exhibiting isotopically lighter cores and becoming progressively heavier toward the rims. Two such cycles of >45‰ enrichment of ^{34}S are evident in Figure 5, which are classic Rayleigh fractionation patterns consistent with S-isotopic fractionation under closed system conditions with respect to S (due to S depletion of a finite supply of dissolved sulfate). Arsenic also appears to be preferentially removed from groundwaters in the early stages of bacterial sulfate reduction as pyrite first begins to grow (Figure 5).

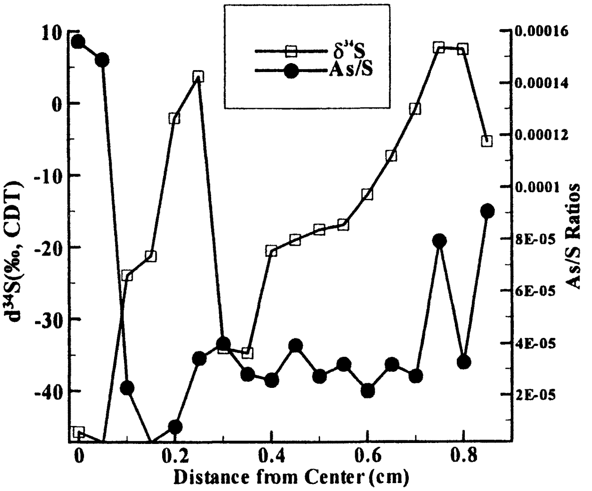

Figure 5. Ion microprobe (SIMS) analyses (As/S atomic ratio, $\partial^{34}S$) of a single pyrite crystal from the Alabama study area from a core-to-rim traverse. Each data point represents an analysis of a 20μm "spot". Two sulfate-reduction cycles representing ~45‰ fractionation of sulfur isotopes are apparent, and note that As is most enriched at the start of the first cycle.

Previous studies (e.g., 10-13 and references therein) have noted that groundwaters with elevated arsenic in alluvial floodplain deposits also have elevated iron (typically 1-50 mg/L). Because the U.S. EPA secondary drinking water standard (not health-based) for iron is 0.5 mg/l, use of this water in the

Downloaded by UNIV OF GUELPH LIBRARY on September 12, 2012 | http://pubs.acs.org
Publication Date: October 3, 2005 | doi: 10.1021/bk-2005-0915.ch014

United States and other "developed" nations has largely been for irrigation of crops and not human consumption. We believe the high iron content has led to the under-appreciation of the fact that elevated As is common in alluvial aquifers in the developed nations of the world as well as countries such as a Bangladesh, India, Pakistan, etc. The major difference of course is that rivers in the developed nations are kept clean enough for drinking water purposes because of the investment in expensive infrastructure, and rivers in developing nations may be polluted and thus not fit for drinking. This has driven the use of the iron- and locally As-rich groundwaters of Holocene river floodplains.

Saunders et al. (*9*) and Pritchett (*31*) observed that trace-elements found in elevated amounts in groundwater in the Alabama study are similar to those (e.g., Co, Ni, Ba, V, Zn, REEs) enriched in ferromanganese coatings from stream-sediments from the present-day adjacent stream. Trace metals and As are generally concentrated in the silt-size and finer particle sizes of stream sediments, corresponding to the enrichment of Fe-oxyhydroxides in this size fraction (*34*). Bulk stream sediments from Indian Creek and the Blue River adjacent to the KCP contain 10-22 ppm As (Figure 1), leading Korte (*35*) to suggest such sediments were the ultimate source of As in the KCP groundwaters.

Results of our study support the general concept that As occurs in reducing and typically Fe- ± Mn-enriched groundwaters. Anaerobic heterotrophic bacteria mediate the reductive dissolution of Fe and Mn minerals as illustrated by the following chemical reactions:

$$2MnO_2 + CH_2O + 3H^+ \rightarrow 2Mn^{2+} + HCO_3^- + 2H_2O \qquad (1a)$$
$$4FeO(OH) + CH_2O + 7H^+ \rightarrow 4Fe^{2+} + HCO_3^- + 6H_2O \qquad (1b)$$

Figure 3 shows that reduction on Mn(IV) minerals occurs under more oxidizing conditions than Fe(III) minerals, and consequently Mn-reducing bacteria will out-compete Fe-reducers as long as reactive solid Mn phases are available (*16*). Reaction 1b illustrates reductive dissolution of a common hydrous ferric oxides (HFO) phase and is the basis for the so-called "As-HFO" hypothesis for As release from host As-bearing HFO. The presence and abundance of FeRB such as *Geobacter* in our two study areas provide the first field evidence supporting the hypothesized bacterial reduction of HFO and As release to groundwater.

Moderately reducing, As-enriched groundwaters from the Kansas City site are generally superaturated with respect to rhodochrosite and siderite (Table I), although KC-72 is an exception. KC-72 has a $SI_{siderite}$ of -0.24 which is within the usual analytical uncertainty of the SI calculations for waters in equilibrium with the mineral phase (*36*). Saunders and Swann (*17*) proposed that Fe- and Mn-reducing bacteria metabolism could facilitate precipitation of both carbonate phases in aquifers because the *products* of reactions 1a and 1b become the *reactants* for Fe- and Mn-carbonate precipitation:

Downloaded by UNIV OF GUELPH LIBRARY on September 12, 2012 | http://pubs.acs.org
Publication Date: October 3, 2005 | doi: 10.1021/bk-2005-0915.ch014

$$Mn^{2+} + HCO_3^- \rightarrow MnCO_3\text{ (rhodochrosite)} + H^+ \qquad (2a)$$
$$Fe^{2+} + HCO_3^- \rightarrow FeCO_3\text{ (siderite)} + H^+ \qquad (2b)$$

Further, Saunders and Swann (*17*) observed that authigenic carbonate phases often had inclusions of sulfide minerals such as pyrite and proposed that biogenic sulfate reduction probably occurred at the site of carbonate deposition. Because biogenic sulfate reduction raises pH and produces alkalinity as well as H_2S (reaction 3a), then this could explain both carbonate precipitation and iron sulfide formation (e.g., reaction 3b):

$$SO_4^{2-} + 2CH_2O + 2H^+ \rightarrow H_2S\text{ (aq)} + 2H_2CO_3^{o} \qquad (3a)$$
$$Fe^{2+} + H_2S\text{ (aq)} \rightarrow FeS\text{ (am)} + 2H^+ \qquad (3b)$$

Recently, authigenic siderite and rhodochrosite have been documented in alluvial aquifers in As-enriched areas of India and Bangladesh (*37-40*). Thus we propose that if Fe- and Mn-reducing bacteria are producing the moderately reducing, metal- and As-rich waters observed in this study and elsewhere in river floodplain deposits, then siderite and rhodochrosite are going to be important phases controlling the solubility of iron and manganese in these waters. As discussed by Dowling et al. (*41*), precipitation of siderite will preferentially remove iron relative to As in groundwater, then that can explain the often-observed poor statistical correlation for Fe and As in many similar groundwaters. By the same token, precipitation of iron sulfides could preferentially remove As relative to iron (by coprecipitation) and also affect the remaining As/Fe ratio in groundwater (e.g., *14*). Several researchers (e.g., *21*) have observed As-bearing pyrite as an authigenic phase in alluvial aquifers, which has led some to propose that it was the source of As in alluvial aquifer groundwaters. This is highly unlikely due to the low redox state of the water and the general lack of dissolved sulfate that would result from sulfide mineral oxidation. We propose that SRB have removed whatever limited sulfate was initially in solution in these terrestrial waters and removed a small amount of iron and As in the process (e.g., reactions 3a and 3b along with As coprecipitation in Fe-sulfide). Thus As-bearing pyrite is a *sink* for As in these conditions and not a source. Similarly, Zheng et al. (*27*) observed that some groundwaters from Bangladesh contain significant dissolved As under sulfate-reducing conditions and proposed that lack of appreciable sulfate limited the capacity of SRB to remove all of the As from groundwaters. Thus sulfate-limited SRB metabolism, acting on groundwaters occurring previously under Fe-reducing conditions likely explains the observed inverse relationship between As and sulfate typically observed in As-contaminated Holocene alluvial aquifers worldwide. Recently Kirk et al. (*42*) presented a similar conclusion in their Illinois study area that arsenic mobility is largely controlled by FeRB and SRB metabolism under anaerobic conditions.

Downloaded by UNIV OF GUELPH LIBRARY on September 12, 2012 | http://pubs.acs.org
Publication Date: October 3, 2005 | doi: 10.1021/bk-2005-0915.ch014

Conclusions

Stream sediments adjacent to the As-bearing groundwater at the KCP plant contain 10-20 ppm As, which is elevated over the crustal abundance of ~2 ppm for As. Leaching experiments indicate that As is apparently associated with hydrous ferric oxides (HFO) in alluvial aquifer sediments from the Alabama study area. These data support the concept that sorption of As dissolved in stream waters by HFO in the active stream sediments is the likely As-concentration process in the linked stream-alluvial aquifer groundwater systems. When stream sediments are physically transported and deposited in adjacent flood-plain deposits along with organic matter, then anaerobic conditions are established and FeRB such as *Geobacter* (identified in As-rich waters in this study) cause the release of Fe and As from HFO by reductive dissolution. Similarly, Mn-reducing bacteria may release Mn and other trace metals (e.g., Co, Ni, Ba, V, etc.) preferentially adsorbed on (or coprecipitated in) Mn-rich oxyhydroxide phases. Thus, these metal-reducing bacteria cause the elevated levels of Fe and Mn, as well as As and other trace elements in the study areas. The same bacteria may also cause the precipitation of authigenic siderite and rhodochrosite, which limit the mobility of Fe and Mn (respectively) in these groundwaters. Although SRB are also present in aquifers of both study areas and locally cause As-bearing pyrite to precipitate, the general lack of sulfate in these and most terrestrial aquifers limit their ability to remove significant amounts of As from these systems. Comparison of aquifer geochemistry, mineralogy, and microbiology from the USA study areas to India and Bangladeshi groundwaters with elevated As indicate similar processes apparently occur in many Holocene alluvial aquifers around the world. Further, precipitation of authigenic siderite and iron sulfide can greatly affect As/Fe ratios of remaining dissolved constituents.

Downloaded by UNIV OF GUELPH LIBRARY on September 12, 2012 | http://pubs.acs.org
Publication Date: October 3, 2005 | doi: 10.1021/bk-2005-0915.ch014

Acknowledgements

We thank Joe Baker of DOE's Kansas City Plant for facilitating field studies during a time of security alerts at most US government installations. Thanks also to Eric E. Roden for help with microbiologic culturing experiments and iron measurements.

References

1. Welch, A.H.; Lico, M.S. *Appl. Geochem.* **1998**, *13*, 521-539.
2. Welch, A.H.; Westjohn, D.B.; Helsel, D.R.; Wanty, R.B. *Ground Water* **2000**, *38*, 589-604.

Downloaded by UNIV OF GUELPH LIBRARY on September 12, 2012 | http://pubs.acs.org
Publication Date: October 3, 2005 | doi: 10.1021/bk-2005-0915.ch014

3. Belzille,. N. *Geochim. Cosmochim. Acta.* **1998,** *52,* 2293-2302.
4. Huerta-Diaz, M.A.; Morse, J.W. *Geochim. Cosmochim. Acta.* **1992**, *56*, 2681-2702.
5. Sullivan, K.A.; Aller, R.C. *Geochim. Cosmochim. Acta* **1996**, *60*, 1465-1477.
6. Schreiber, M.E.; Simo, J.A.; Freiberg, P.G. *Hydrogeol. J.* **2000,** *8*, 161-176.
7. Yan, X.-P.; Kerrich, R.; Hendry, M.J. *Geochim. Cosmochim. Acta* **2000**, *62*, 2637-2648.
8. Smedley, P.L.; Nicolli, H.B.; Macdonald, D.M.J. Barros, A.J.; Tullio, J.O. *Appl. Geochem.* **2002**, *17*, 259-284.
9. Saunders, J.A.; Pritchett, M.A.; Cook, R.B. *Geomicrobiol. J.* **1997**, *14*, 203-217.
10. Chatterjee, A.; Dipankar D.; Mandal, B.K.; Chowdhury, T.R.; Samanta, G.; Chakraborti, D.A. *The Analyst* **1995**, *120*, 643-650.
11. Bhattacharya, P.; Chatterjee, D.; Jacks, *G. Int. J. Water Resour. Devel.* **1997,** *13*, 79-87.
12. Acharyya, S.K.; Chakraborty, P.; Lahiri, S.; Raymahashay, B.C.; Guha, S.; Bhowmik, A.; Chowdhury, T.R.; Basu, G.K.; Mandal, B.K.; Biswas, B.K.; Samanta, G.; Chowdhury, U.K.; Chanda, C.R.; Lodh, D.; Roy, S.L.; Saha, K.C.; Roy, S.; Kabir, S.; Quamruzzaman, Q.; Chakraborti, D.; and McArthur, J.M. *Nature* **1999**, *401*, 545-547.
13. McArthur, J.M., Banerjee, D.M., Hudson-Edwards, K.A., Mishra, R., Purohit, R, Ravenscroft, P., Cronon, A., Howarth, R.J., Chatterjee, A., Talukder, T. *Appl. Geochem.* **2004**,*19*, 1255-1293.
14. Korte, N.E *Environ. Geol. Water Sci.* **1991**, *18*, 137-141.
15. Korte, N.E.; Fernando, Q. *Crit. Rev. Environ. Contro.* **1991**, *21*, 1-39.
16. Lovley, D.R.; Chapelle, F.H.; Phillips, E.J.P. *Geology* **1990**, *18*, 954-957.
17. Saunders, J.A.; Swann, C.T. *Appl. Geochem.* **1992**, *7*, 361-374.
18. Hungarian Geological Survey, *Ann. Rept.1996,* **1996,** 23-24.
19. Smedley, P.L. Kinniburgh, D.G. *Appl. Geochem.* **2002**, *17*, 517-568.
20. Nickson, R.T.; McArthur, J.M.; Burgess, W.G.; Ahmed, K.M.; Ravenscroft, P.; Rahman, M. *Nature* **1998**, *395*, 338.
21. Nickson, R.T.; McArthur, J.M.; Ravenscroft, P.;
22. McArthur, J.M.; Ravenscroft, P.; Safiullah, S.; Thirlwall, M.F. *Water Resour. Res.* **2001**, *37*, 109-118.
23. Harvey, C.F.; Swartz, C.H.; Badruzzaman, A.B.M.; Keon-Blute, N.; Yu, W.; Ali, M.A.; Jay, J.; Beckie, R.; Niedan, V.; Brabander, D.; Oates, P.M.; Ashfaque, K.N.; Islam, S.; Hemond, H.F.; Ahmed, M.F. *Science* **2002**, *298*, 1602-1606.
24. Anawar, H.M.; Akai, J.; Komaki, K.; Terao, H.; Yoshioka, T.; Ishizuka, T.; Safiullah, S.; Kato, K. *J. Geochem. Explor.* **2003**, *177*, 109-131.
25. Stuben, D.; Berner, Z.; Chandrasekharam, D.; Karmakar, J. *Appl. Geochem.* **2003**, *18* , 1417-1434.

26. van Geen, A.; Zheng, Y.; Versteeg, R.; Stute, M.; Horneman, A.; Dhar, R.; Steckler, M.; Gelman, A.; Small, C.; Ahsan, H.; Graziano, J.; Hussain, I.; Ahmed, K.M. *Wat. Resour. Res.* **2003**, *39*, 1140-1150.
27. Zheng, Y.; Stute, M.; van Geen, A.; Gavrieli, I.; Dhar, R.; Simpson, J.; and Ahmed, K.M. *Appl. Geochem.* **2004**, *19*, 201-214.
28. Bethke, C.M. *The Geochemist's Workbench: A users guide to Rxn, Act2, React, and Gtplot:*; University of Illinois, 1994.
29. Parkhurst, D.L., and Appelo, C.A.J. *User's guide to PHREEQC (Version 2)-a computer program for speciation, batch-reaction, one-dimensional transport, and inverse geochemical calculations*; U.S. Geological Survey Water-Resources Investigations Report 99-4259: USGS: Denver, CO, 1999.
30. Markewich, H.W.; and Christopher, R.A. *Pleistocene (?) and Holocene Fluvial History of Uphapee Creek, Macon County, Alabama;* U.S. Geological Survey Bulletin 1522: USGS: Denver, CO, 1982.
31. Pritchett, M.A. M.S. thesis, Auburn University, Auburn, AL, 1997.
32. BGS and DPHE, *Arsenic contamination of groundwater in Bangladesh*, Technical Report, WC/00/19: British Geol. Survey: Keyworth, U.K., 2001.
33. Methe, B.A. et al., *Science* **2003**, *302*, 1967-1969.
34. Levinson, A.A. *Introduction to exploration geochemistry*, Applied Publishing; Maywood, Illinois, 1974.
35. Korte, N.E *Naturally occurring arsenic in the groundwater at the Kansas City Plant*: Oak Ridge National Laboratory Publication No. 3501, 1990.
36. Langmuir, D. *Aqueous and environmental geochemistry*; Prentice Hall: New York, 1997.
37. Mukherjee, P.K.; Pal, T.; Sengupta, S.; Shome, S. *J. Geol. Soc. India,* **2001**, *58*, 173-176.
38. Pal, T.; Mukherjee, P.K.; Sengupta, S.; Bhattacharyya, A.K.; and Shome, S. *Gondwana Research,* **2002**, *5*, 501-512.
39. Sengupta, S., Mukherjee, P.K., Pal, T., Shome, S. *Environ. Geol.,* **2004**, *45*, 1071-1081.
40. Sikder, A.M. *pers. Com.* **2004**.
41. Dowling C.B.; Poreda, R.J.; Peters, S.L.; Basu, A.R.; Agarwaal, P.K.; *Water Resour. Res.* **2002**, *38*, 109-118.
42. Kirk, M.F.; Holm, T.R.; Park, J.; Jin, Q.; Sanford, R.A.; Fouke, B.W.; Bethke, C.M. *Geology*, **2004**, *32*, 953-956.

Downloaded by UNIV OF GUELPH LIBRARY on September 12, 2012 | http://pubs.acs.org
Publication Date: October 3, 2005 | doi: 10.1021/bk-2005-0915.ch014

Downloaded by UNIV MASSACHUSETTS AMHERST on September 11, 2012 | http://pubs.acs.org
Publication Date: October 3, 2005 | doi: 10.1021/bk-2005-0915.ch015

Chapter 15

Oxidation of Groundwater Arsenic and Iron

A. R. Keimowitz[1,2], H. J. Simpson[1,2], S. N. Chillrud[1], M. Stute[1-3], M. Tsang[1], S. Datta[1,3], and J. Ross[1]

**[1]Lamont Doherty Earth Observatory of Columbia University,
Palisades, NY 10964
[2]Department of Earth and Environmental Sciences, Columbia University,
New York, NY 10027
[3]Department of Environmental Science, Barnard College,
New York, NY 10027**

The behaviors of dissolved arsenic and iron are significantly decoupled in groundwaters beneath a closed landfill in southern Maine and in laboratory experiments using these groundwaters. At this site naturally-occurring arsenic is mobilized from the glacial sediments under reducing conditions induced and promoted by landfill leachate. Differences in arsenic and iron behavior were seen in laboratory titration experiments which progressively oxidize groundwater from this site and in field data for groundwater composition in the area surrounding this former landfill. The persistence of elevated levels of dissolved arsenic in groundwaters where dissolved iron is relatively low provides direct indication of the difficulty of preventing transport of arsenic from this type of site.

In Advances in Arsenic Research; O'Day, P., et al.;
ACS Symposium Series; American Chemical Society: Washington, DC, 2005.

Mobilization of arsenic under reducing conditions has been demonstrated in many countries *(1,2)*, including Vietnam *(3)*; Bangladesh and West Bengal, India *(4,5)*; and a number of regions in the USA, including New England *(6,7)* and the northern Mid-West *(8-10)*. Detailed mechanisms of mobilization have been debated *(11,12)* and probably vary in both space and time. The role of iron has been of particular interest *(13)*: an association is often observed between high concentrations of dissolved arsenic and high concentrations of dissolved iron and other redox-sensitive species *(1,5,13)*. Arsenic is often sorbed to iron oxyhydroxides in oxidized sediments *(14-16)*, and elevated dissolved arsenic in groundwaters has often been attributed to reductive dissolution of iron compounds *(17,18)*.

Recent investigations, however, report significant groundwater arsenic mobilization decoupled from dissolution of iron hydroxides *(19-21)*. These studies indicate that in Bangladesh significant mobilization of arsenic may occur concurrently with iron(III) reduction but without appreciable iron(II) dissolution.

Removal of arsenic from groundwaters via oxidation has been proposed and/or implemented as an important water treatment and site remediation strategy. For example, groundwater extraction and treatment, the most common method of removal of dissolved arsenic, usually relies on oxidation and precipitation/co-precipitation of arsenic with oxidized iron species *(22)*; simple systems for in-home oxidation of water supplies are sometimes introduced to decrease drinking water arsenic in Bangladesh *(23-25)*; and pilot field studies of *in situ* aquifer oxidation have been conducted *(26,27)*. Oxidative removal of arsenic from solution via sorption to iron oxyhydroxides is well established as a removal strategy for public water supplies *(14,15)*, but its application to field environments has only recently begun to be investigated *(28)*. It has been proposed that natural *in situ* oxidants remove arsenic from natural waters via sorption to iron oxyhydroxides in Bangladesh groundwaters *(12)* and in a polluted New England lake *(29)*. Senn and Hemond *(29)* reported analogous removal of dissolved arsenic and iron mediated by NO_3^- reduction.

In this study, we observe significant decoupling in removal of dissolved arsenic and iron from groundwaters as conditions become progressively more oxic beneath and near a closed landfill in southern Maine. It has previously been reported for this site that landfill leachate has contributed to the evolution of reducing conditions in the subsurface, causing natural arsenic to be released from the sediment and resulting in groundwater with ~4 μmol L^{-1} (~300 μg L^{-1}) arsenic *(26,30)*.

Data discussed here are of two types: field data from groundwater monitoring and laboratory data from a batch titration experiment. These data are examined to explore differential removal of dissolved iron and arsenic as conditions become more progressively more oxic.

Downloaded by UNIV MASSACHUSETTS AMHERST on September 11, 2012 | http://pubs.acs.org
Publication Date: October 3, 2005 | doi: 10.1021/bk-2005-0915.ch015

Methods

The unconsolidated aquifer beneath the landfill consists of poorly sorted sediment classified as glacial till and outwash deposits. Its thickness varies appreciably, but averages ~10 meters above crystalline bedrock. The hydraulic gradient slopes approximately eastward towards a nearby lake (Figure 1). The initial contaminants of concern at the site were volatile organic compounds such as dimethyl formamide *(31-33)*. These contaminants, as well as arsenic, have been detected outside the landfill perimeter in one well in the eastern region, in a plume extending throughout the southern region, and in a plume extending throughout the northern region (Figure 1). A groundwater extraction and treatment system was installed at this site in 1995, and the groundwater extraction well is located near the middle of the central region *(26,30)*. Treated groundwater is reinjected at the northern-most and southern-most points of the landfill perimeter.

Downloaded by UNIV MASSACHUSETTS AMHERST on September 11, 2012 | http://pubs.acs.org
Publication Date: October 3, 2005 | doi: 10.1021/bk-2005-0915.ch015

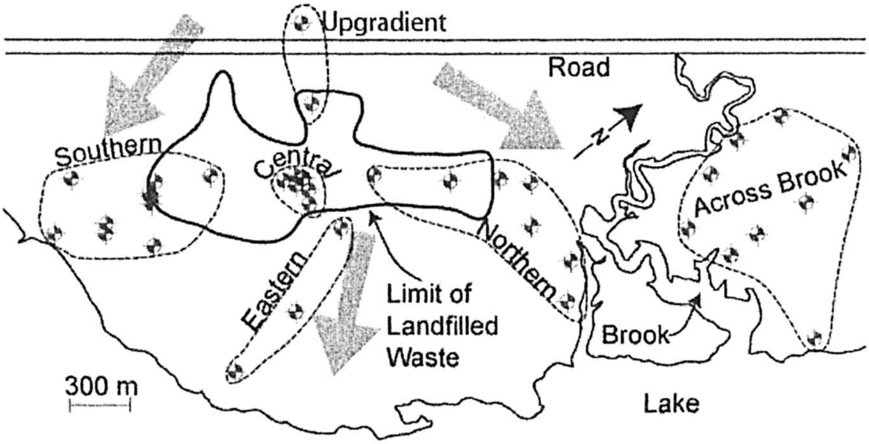

Figure 1. Map of the closed landfill site in southern Maine, showing the landfill perimeter, nearby surface waters, and the regions into which wells have been grouped. Monitoring and observation wells are shown in gray; the extraction well in the center of the landfill is shown in black.

The wells discussed here have been grouped into five regions (Figure 1). Field data were obtained during July-August 2000 (all regions) and November-January 2001 (central and upgradient regions). Examination of data from long-term monitoring for the period from 1989 to 1995 indicates small temporal variability. Groundwater samples collected from 42 monitoring and observation wells were analyzed for a number of components, including total dissolved arsenic and iron, at the University of Connecticut Environmental Research Institute with EPA method 6010 *(34)* or at Lamont-Doherty Earth Observatory. Limits of detection were 0.07 μM (5 μg L^{-1}) for arsenic and 9 μM (0.5 mg L^{-1}) for iron. When presenting arsenic/iron ratios here, all samples for which arsenic and/or iron were not detected are omitted.

Groundwater used for titration experiments was obtained from a sampling port on a closed pipe connected to the extraction well in the center of the landfill. This groundwater was used immediately after collection while it was highly reducing (oxidation-reduction potential, or ORP, was approximately -170 mV). The titration experiments took place in a 10 L PVC reaction vessel which contained integrated ORP and dissolved oxygen electrodes, syringe ports, and an equilibration piston. The movement of the piston in this system allowed withdrawal of contained fluids and/or injection of reagents without appreciable leakage of air or loss of water.

During the titration experiment highly reducing groundwater from the landfill site was placed in the titration vessel where it was oxidized with periodic injections of 0.5-2.0 mL aliquots of 1-3% H_2O_2, while being continuously stirred with a Teflon-coated magnetic stir-bar and while readings from both electrodes were automatically recorded at regular intervals. Aqueous samples withdrawn during titration were filtered with 0.45 μm ion chromatography filters, acidified to 1% with trace-metal grade HCl, and then analyzed on a Hitachi Z-8200 Polarized Zeeman Atomic Absorption Spectrophotometer (AAS) in flame ionization mode for iron and in graphite furnace ionization mode for arsenic. Analytical detection limits are identical to those listed above.

Groundwater Titration Experiment

When ~9 L reducing groundwater (ORP≈-170 mV) from the landfill site was titrated with hydrogen peroxide, 6.6±0.7 mmol of dissolved, presumably ferrous, iron were removed from solution, likely by oxidation and rapid precipitation. This would require ~3.3 mmol H_2O_2, assuming 2:1 Fe(II):H_2O_2 reaction stoichiometry *(35,36)*. A total of 3.6±0.4 mmol of H_2O_2 was injected before the equivalence point of the redox titration, when the ORP increased rapidly from −13 mV to 157 mV and dissolved iron concentrations dropped below the detection limit (Figure 2). These data indicate that dissolved iron(II) was the major redox buffering species in this experiment.

Consumption of H_2O_2 during the titration appears to have occurred at much higher rates during the first eight hours, when Fe(II) was present and small aliquots (~0.02 mmoles L^{-1}) of H_2O_2 titrant were added. Each H_2O_2 addition resulted in an immediate rise in ORP within the three minute interval of ORP

Downloaded by UNIV MASSACHUSETTS AMHERST on September 11, 2012 | http://pubs.acs.org
Publication Date: October 3, 2005 | doi: 10.1021/bk-2005-0915.ch015

Downloaded by UNIV MASSACHUSETTS AMHERST on September 11, 2012 | http://pubs.acs.org
Publication Date: October 3, 2005 | doi: 10.1021/bk-2005-0915.ch015

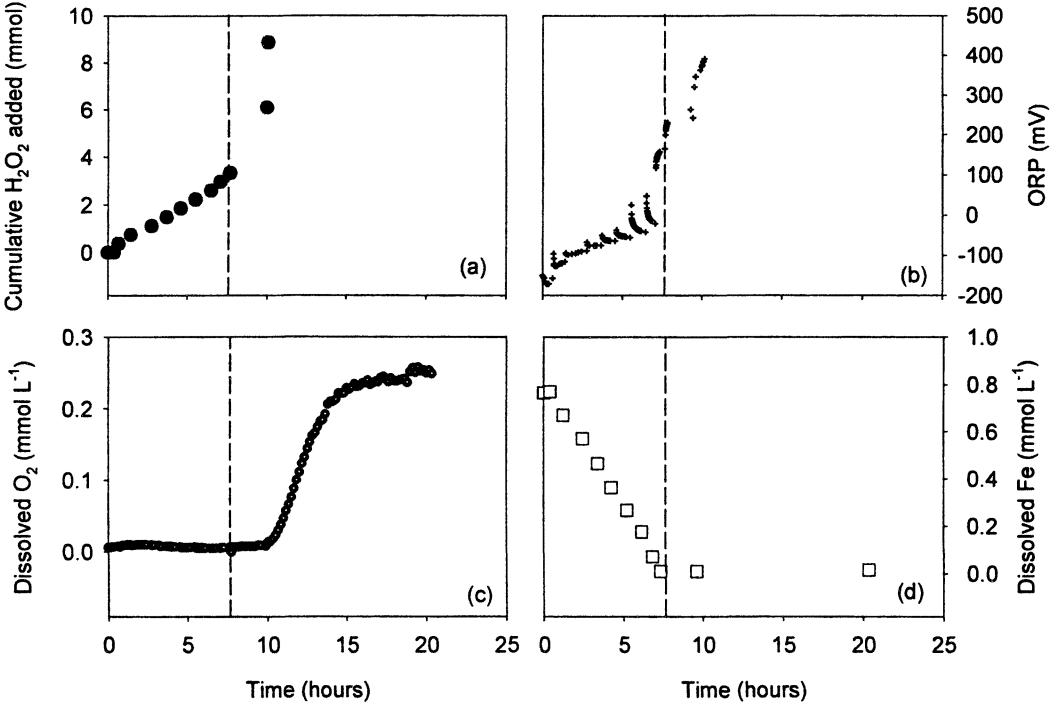

Figure 2. Redox titration of strongly reducing groundwater with hydrogen peroxide. The dashed vertical lines show the approximate equivalence point as determined from (b). Iron oxidation can account for >95% of the redox buffering of this system.

measurements, followed by about 45 minutes of gradual decrease in ORP values. The first rapid increase most likely represents rapid homogenous reaction of H_2O_2 with Fe(II); Millero and Sotolongo found that this reaction required less than 30 seconds *(37)* and this reaction has been shown to be yet faster in the presence of sulfate at concentrations similar to those in this experiment *(38)*. The second, slower decrease in ORP is likely indicative of formation of iron oxide precipitate. After about 8 hours, at which point (ferrous) iron was no longer in solution, H_2O_2 disproportionated very slowly to O_2. Dissolved O_2 increased from 0 to ~250 μM over a period of about five hours.

Iron and arsenic are removed from solution to different relative extents as peroxide titrant is added (Figure 3). This implies that the removals of arsenic and iron from solution probably proceed via different mechanisms. Iron is most likely removed from solution via precipitation as amorphous iron hydroxides *(39)*; orange iron flocs were observed to form during the titration. The removal of arsenic, on the other hand, may proceed via one or more mechanisms, including precipitation, co-precipitation, adsorption, or some combination thereof. During the course of the H_2O_2 titration, changes in pH, ORP, dissolved iron concentration and speciation, solid iron concentration and morphology, and arsenic speciation and concentration may influence the relative extent of these removal mechanisms *(40)*. Several studies have shown that arsenic oxidation with H_2O_2 is significantly facilitated by the presence of ferrous iron *(40-42)*, and this mechanism is presumably occurring to a significant extent during the removal of dissolved arsenic.

Arsenic adsorption on iron hydroxides can be assumed to be the main mechanism of arsenic removal *(42)*. Pierce and Moore *(15)* observed that adsorption of arsenic to iron hydroxide occurs on the time scale of hours, which is consistent with the time scale of arsenic removal in this peroxide titration. The initial maximum concentration for arsenic in this experiment was ~3 μmol L^{-1}, which is in the range for which a Langmuir isotherm has been shown *(15)* to best describe the sorption of arsenic to amorphous iron hydroxides, i.e. that arsenic is sorbed to a limited number of specific sites on amorphous iron hydroxides. At pH 7, the approximate initial pH of the groundwater, $\Gamma_{A,max}$ = 513 μmol g^{-1}, where $\Gamma_{A,max}$ is the specific sorption capacity of the iron oxides for arsenite that best fits the observed Langmuir isotherm *(15)*. Therefore, removal of the ~27 μmol arsenic in solution via sorption would require ~0.9 mmol (~53

Downloaded by UNIV MASSACHUSETTS AMHERST on September 11, 2012 | http://pubs.acs.org
Publication Date: October 3, 2005 | doi: 10.1021/bk-2005-0915.ch015

Downloaded by UNIV MASSACHUSETTS AMHERST on September 11, 2012 | http://pubs.acs.org
Publication Date: October 3, 2005 | doi: 10.1021/bk-2005-0915.ch015

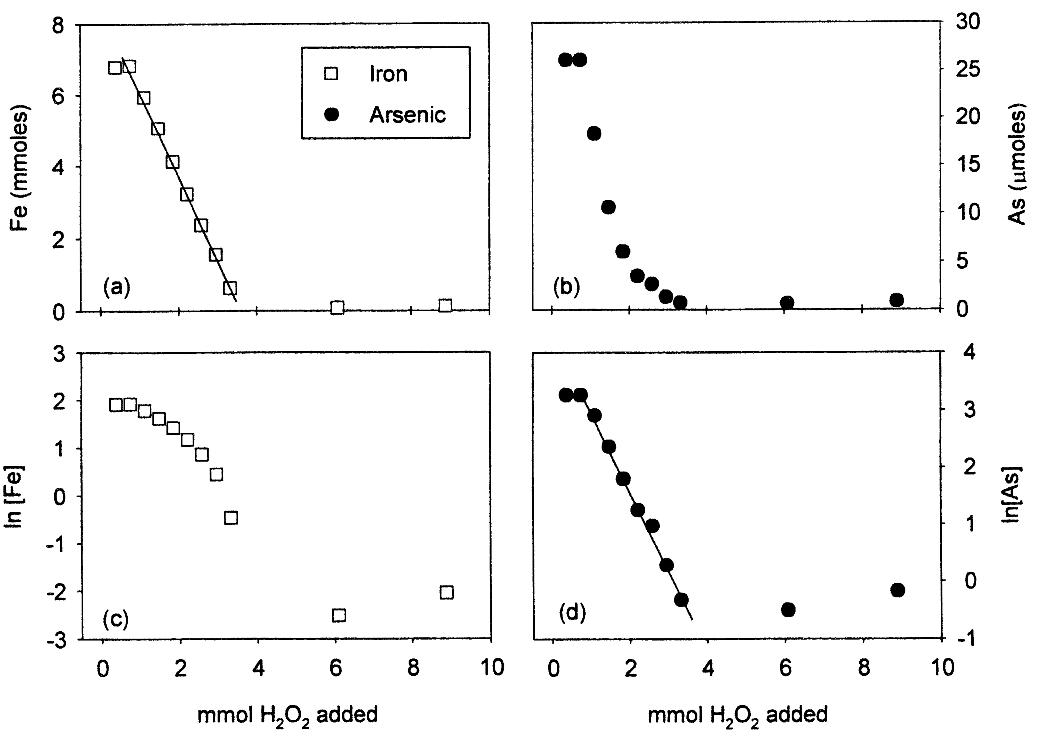

Figure 3. Amounts of (a) iron and (b) arsenic in solution as a function of the amount of hydrogen peroxide added in a groundwater peroxide titration. The difference in shapes of these curves is also evident in semi-log plots of (c) iron concentration and (d) arsenic concentration versus peroxide added.

mg) iron. The ~0.9 mmol iron removed from solution by the first peroxide aliquot added was therefore sufficient to remove all the initial dissolved arsenic via sorption. $\Gamma_{A,max}$ for arsenate at pH 7 is 454 μmol g^{-1} *(15)*. The ~7 mmol iron removed over the course of the experiment was certainly enough to adsorb all arsenic present using either the arsenite or arsenate value for sorption capacity, and this experiment did not approach saturation of the strong arsenic sorption sites.

Phosphate in this water was below the detection limit of ~4.5 μM, and was therefore not likely competing for surface sorption sites. Sulfate, however, was 2.5 mM, but Pierce and Moore *(15)* indicate that its sorption competes with arsenic sorption when sulfate is adsorbed prior to arsenic addition, which was not the case in this experiment. Although sulfate and arsenic were presumably sorbed to the iron oxides concurrently, arsenic sorption does not appear limited in peroxide titration.

Arsenic was removed from solution initially very quickly and later more slowly, for reasons that have not yet been adequately explained. Because each aliquot of H_2O_2 reacted quickly and stoichiometrically with ferrous iron, iron was removed from solution at a relatively constant rate until its concentration fell to below the detection limit. Therefore over the course of the experiment, the dissolved arsenic/iron ratio decreased from 4×10^{-3} to 9×10^{-4} (all arsenic/iron ratios are reported in moles/moles) from the start of the titration until analytical detection limits for arsenic and/or iron were reached.

Groundwater Monitoring and Sediment Leaching Data

Arsenic/iron ratios varied in field groundwater data from 1×10^{-3} to 1.2×10^{-1}. The arsenic/iron ratios for individual sampling events are plotted as a function of distance from the extraction well, which is assumed for these purposes to be the approximate center of the landfill (Figure 4a). Several data points at the same distance usually indicate a multi-level well nest at that location. This figure shows that relatively low arsenic/iron ratios are observed at all distances from the extraction well. High As/Fe ratios, however, are only observed at larger distances from the landfill center. Upgradient wells were not plotted because arsenic was below detection limits.

It has been reported *(26,30)* that dissolved arsenic at this site is mobilized primarily beneath the landfill and it is plausible that it is subsequently transported elsewhere in groundwater. This is consistent with the site hydrogeology because arsenic was not detected in any upgradient wells and

Downloaded by UNIV MASSACHUSETTS AMHERST on September 11, 2012 | http://pubs.acs.org
Publication Date: October 3, 2005 | doi: 10.1021/bk-2005-0915.ch015

because groundwater has been shown to flow from the landfill towards the lake (Figure 1), flowing through the northern, southern, and eastern regions. This groundwater flow regime has been demonstrated with hydraulic head gradients and by detection of volatile organic compounds originating within the landfill in the eastern, northern, and southern regions.

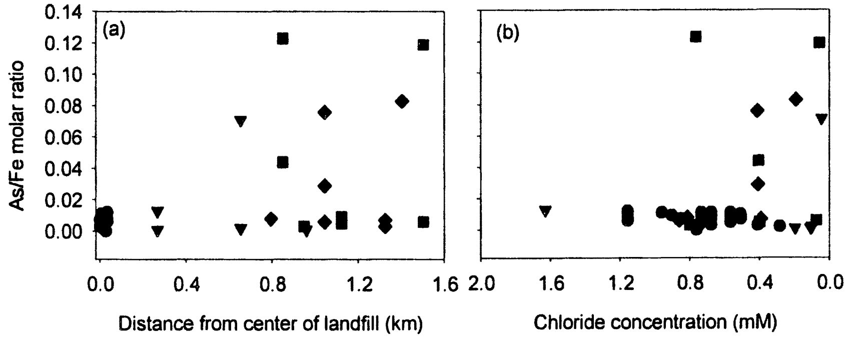

Figure 4. Arsenic/iron molar ratios as a function of (a) distance from the center of the landfill and (b) chloride concentration. The wells are grouped by regions shown in Figure 1: ● central; ▼eastern; ■ northern; ◆southern. The x-axis in panel (b) is reversed to display similar trends in (a) and (b).

It has previously been shown that arsenic is also mobilized to some extent in the eastern region *(26)*, a natural swamp with typically anoxic groundwaters. This could potentially alter our interpretation of Figure 4a, although removal of the eastern data (triangle symbols) from this figure does not strongly alter the overall pattern. Chloride can generally be used as a tracer of landfill leachate *(43)*. Because background chloride concentrations at this site are ~0.04 mM and maximum chloride concentrations beneath the landfill are ~2.0 mM (50:1 variability), chloride should be a sensitive tracer of landfill leachate proportions in the groundwaters near the landfill. When arsenic/iron ratios are plotted as a function of chloride concentration (Figure 4b), a pattern similar to Figure 4a appears. At all chloride concentrations, low arsenic/iron ratios are seen, but high arsenic/iron ratios are only observed at low chloride concentrations, i.e. with significantly diluted leachate.

If we therefore assume that the groundwater in the central region acts as a source of chloride, arsenic, and iron to the general area, the increase in the arsenic/iron ratio with decreasing chloride concentration could be explained either by a relative increase in arsenic concentrations or relative decrease in the iron concentrations. Because both arsenic and iron concentrations decrease with decreasing chloride concentrations (Figure 5), the trend in arsenic/iron ratios

Downloaded by UNIV MASSACHUSETTS AMHERST on September 11, 2012 | http://pubs.acs.org
Publication Date: October 3, 2005 | doi: 10.1021/bk-2005-0915.ch015

must be explained at least partially by a preferential decrease in iron concentration as groundwaters highly influenced by leachate are diluted.

In Figure 5 there are two samples with the highest chloride concentrations and low dissolved iron and arsenic. These samples were obtained from wells very near the treated groundwater reinjection points, and therefore do not fit the general trend because groundwater treatment accomplished almost total removal of arsenic and iron, but left chloride relatively unaffected. Removal of these two points does not significantly alter the pattern in figure 4.

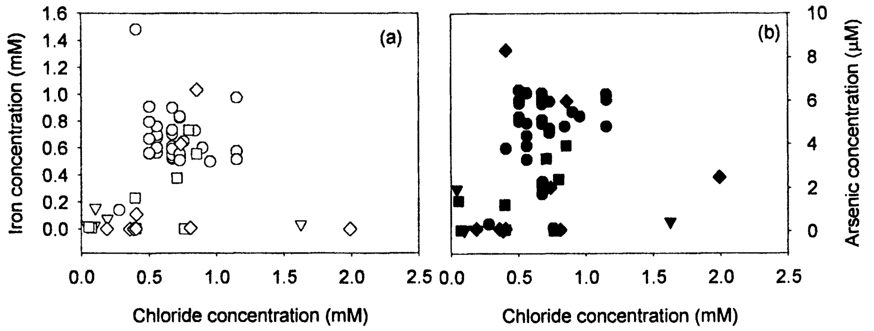

Figure 5. (a) Iron and (b) arsenic as a function of chloride concentration in groundwater. Open symbols represent iron and closed symbols represent arsenic, and symbolo shapes represent region, as in Figure 4.

Is it possible that dilution of contaminated water with uncontaminated water could explain the arsenic/iron variation observed? A simple conservative end-member mixing model was used to examine this question. The endmembers chosen were central waters with typical values of 3.8 μM arsenic and 0.8 mM iron and un-contaminated up-gradient waters with 0.06 μM arsenic and 0.03 mM iron. The only upgradient sample with iron above the detection limit contained 0.03 mM iron, so this value was used in the mixing model. Arsenic was not detected in any upgradient well, so an "uncontaminated" value of 0.06 μM of arsenic was used. This value represents the detection limit, and therefore the upper bound on the arsenic concentration. Ayotte et al *(44)* also found that 93% of groundwaters in New England in unconsolidated sediments fell below this value.

Mixing of these two endmembers gives arsenic/iron ratios <0.005, as compared with ≤0.123 observed for field data (Figure 4). Therefore, some processes must be occurring to alter concentrations of arsenic and/or iron in the advected groundwaters. We conclude that these processes must involve preferential removal of dissolved iron, presumably as it is oxidized and

Downloaded by UNIV MASSACHUSETTS AMHERST on September 11, 2012 | http://pubs.acs.org
Publication Date: October 3, 2005 | doi: 10.1021/bk-2005-0915.ch015

precipitates, since both iron and arsenic concentrations are decreasing as chloride concentration decreases and the arsenic/iron ratio increases.

Conclusions

As conditions became more oxic in the reaction vessel, the arsenic/iron ratio *decreased* from 4×10^{-3} to 9×10^{-4}; more oxic conditions in the field were associated with *increasing* arsenic/iron ratios from 2×10^{-3} to 1.2×10^{-1}. The difference in both trend and range between the laboratory and field data requires examination. One plausible explanation is that the presence of sediment facilitates iron removal or inhibits arsenic removal, thereby increasing the arsenic/iron ratio. Laboratory equilibrations and titrations of sediment and water do permit higher arsenic/iron ratios than equilibrations and titrations of water alone; with sediment present, the arsenic/iron ratio reaches $\sim2\times10^{-2}$, still nearly an order of magnitude below the maximum field values of arsenic/iron observed.

It is not altogether surprising that the presence of complicated mineral phases, as opposed to only amorphous iron oxides, results in different mechanisms of arsenic and iron removal. Recent work *(19,20)* has indicated somewhat decoupled release of iron and arsenic from sediment. We have presented data that the inverse process, removal of iron and arsenic from solution, also shows significant decoupling in behavior of these two elements, particularly in the presence of sediment. Kinetic limitations appear to prevent dissolution of reduced iron in Bangladesh and could also prevent precipitation of arsenic in Maine groundwater. Although arsenic and iron are often considered fellow geochemical travelers *(1,5,13)*, these studies show that arsenic tends to enter and to remain in solution more readily than iron. Our data are thus consistent with the persistence of elevated dissolved arsenic in groundwaters from aquifers containing arsenic of natural sedimentary origin. It has been proved quite difficult to prevent transport of arsenic beyond the landfill boundaries at this site *(26)*, and data presented here helps explain this difficulty.

Downloaded by UNIV MASSACHUSETTS AMHERST on September 11, 2012 | http://pubs.acs.org
Publication Date: October 3, 2005 | doi: 10.1021/bk-2005-0915.ch015

Acknowledgements

The authors would like to thank United Technologies Corporation for providing access to the field site, Mactec for assistance in the field, Richard Post and Nikolaos Nikolaidis for help with monitoring data, and Dave Witham for assistance with sampling activities. This work was supported by National Institutes of Health Grant 1 P42 ES10349, National Institutes of Environmental Health Sciences Grant P30 ES09089, National Science Foundation Graduate

Research Traineeship in Hydrology DGE9554573, and United Technologies Corporation. This is LDEO contribution #6682.

References

1. Smedley, P. L.; Kinniburgh, D. G. *Appl. Geochem.* **2002**, *17*, 517-568.
2. Nordstrom, D. K. *Science* **2002**, *296*, 2143-2145.
3. Berg, M.; Tran, H. C.; Nguyen, T. C.; Pham, H. V.; Schertenleib, R.; Giger, W. *Environ. Sci. Technol.* **2001**, *35*, 2621-2626.
4. Acharyya, S. K.; Chakraborty, P.; Lahiri, S.; Raymahashay, B. C.; Guha, S.; Bhowmik, A. *Nature (London)* **1999**, *401*, 545.
5. Nickson, R.; McArthur, J.; Burgess, W.; Ahmed, K. M.; Ravenscroft, P.; Rahman, M. *Nature (London)* **1998**, *395*, 338.
6. Stollenwerk, K. G.; Colman, J. A. In *Arsenic in Ground Water*; Kluwer Academic Publishers: Norwell, MA, 2003.
7. Mayo, M. J.; Hon, R.; Brandon, W. C.; Ford, R. *Proc. Am. Chem. Soc.* **2003**, *226*, U594-U594.
8. Kolker, A.; Haack, S. K.; Cannon, W. F.; Westjohn, D. B.; Kim, M. J.; Nriagu, J.; Woodruff, L. G. In *Arsenic in Ground Water*; Kluwer Academic Publishers: Norwell, MA, 2003.
9. Korte, N. *Environ. Geol. Water. Sci.* **1991**, *18*, 137-141.
10. Root, T. L.; Bahr, J. M.; Gotkowitz, M. *Proc. Am. Chem. Soc.* **2003**, *226*, U584-U585.
11. Zheng, Y.; Stute, M.; Geen, A. v.; Gavrieli, I.; Dhar, R.; Simpson, H. J.; Ahmed., K. M. *Appl. Geochem.* **2004**, *19*, 201-214.
12. Harvey, C. F.; Swartz, C. H.; Badruzzaman, A. B. M.; Keon-Blute, N.; Yu, W.; Ali, M. A.; Jay, J.; Beckie, R.; Niedan, V.; Brabander, D.; Oates, P. M.; Ashfaque, K. N.; Islam, S.; Hemond, H. F.; Ahmed, M. F. *Science* **2002**, *298*, 1602-1606.
13. Bose, P.; Sharma, A. *Water Res.* **2002**, *36*, 4916-4926.
14. Raven, K. P.; Jain, A.; Loeppert, R. H. *Environ. Sci. Technol.* **1998**, *32*, 344-349.
15. Pierce, M. L.; Moore, C. B. *Water Res.* **1982**, *16*, 1247-1253.
16. Goldberg, S.; Johnston, C. T. *J. Colloid. Interf. Sci.* **2001**, *234*, 204-216.
17. Nickson, R. T.; McArthur, J. M.; Ravenscroft, P.; Burgess, W. G.; Ahmed, K. M. *Appl. Geochem.* **2000**, *15*, 403-413.
18. Stuben, D.; Berner, Z.; Chandrasekharam, D.; Karmakar, J. *Appl. Geochem.* **2003**, *18*, 1417-1434.
19. van Geen, A.; Rose, J.; Thoral, S.; Garnier, J. M.; Zheng, Y. *Geochim. Cosmochim. Acta.* **2004**, *68,* 3475-3486.

Downloaded by UNIV MASSACHUSETTS AMHERST on September 11, 2012 | http://pubs.acs.org
Publication Date: October 3, 2005 | doi: 10.1021/bk-2005-0915.ch015

20. Horneman, A.; van Geen, A.; Kent, D.; Mathe, P. E.; Zheng, Y.; Dhar, R.; O'Connell, S.; Hoque, M.; Aziz, Z.; Shamsudduha., M.; Seddique, A.; Ahmed, K. M. *Geochim. Cosmochim. Acta* **2004**, *68*, 3459-3473.
21. Islam, F. S.; Gault, A. G.; Boothman, C.; Polya, D. A.; Charnock, J. M.; Chatterjee, D.; Lloyd, J. R. *Nature (London)* **2004**, *430*, 68-71.
22. EPA *Arsenic Treatment Technologies for Soil, Waste, and Water*, EPA 542-R-02-004, 2002.
23. Yuan, T.; Luo, Q. F.; Hu, J. Y.; Ong, S. L.; Ng, W. J. *J. Env. Sci. Health A* **2003**, *38*, 1731-1744.
24. Meng, Z. G.; Korfiatis, G. P.; Christodoulatos, C.; Bang, S. *Water Res.* **2001**, *35*, 2805-2810.
25. Cheng, Z.; van Geen, A.; Jing, C.; Meng, Z.; Seddique, A.; Ahmed, K. M. *Environ. Sci. Technol.* **2004**, *38*, 3442-3448.
26. Keimowitz, A. R.; Simpson, H. J.; Stute, M.; Datta, S.; Chillrud, S. N.; Ross, J.; Tsang, M. *Appl. Geochem.* **2004,** *In press.*
27. *Final ORC Pilot Study Report*, **2002,** Harding ESE/Mactec, Portland, ME.
28. Sharma, A. K.; Tjell, J. C.; Mosbaek, H. *Journal De Physique Iv* **2003**, *107*, 1223-1226.
29. Senn, D. B.; Hemond, H. F. *Science* **2002**, *296*, 2373-2376.
30. Lackovic, J. A.; Nikolaidis, N. P.; Dobbs, G. M. *Hazardous and Industrial Wastes* **1999**, *31*, 451-459.
31. EPA, "Winthrop Landfill." http://yosemite.epa.gov/r1/npl_pad.nsf/51dc4f173ceef51d85256adf004c7ec8/4cb08d6f0665d8438525691f0063f705?OpenDocument, 2003.
32. EPA, "Third Five-Year Review Report." http://www.epa.gov/region01/superfund/sites/winthrop/35539.pdf, 2002.
33. EPA, "NPL Site Narrative for Winthrop Landfill, NPL, Superfund." http://www.epa.gov/superfund/sites/npl/nar36.htm, 1983.
34. EPA, "Index to EPA Test Methods." http://www.epa.gov/region01/oarm/testmeth.pdf, 2001.
35. Stumm, W.; Morgan, J. J. In *Aquatic Chemistry* 3rd Ed.; John Wiley & Sons, Inc.: New York, 1996; pp 425-515.
36. Buxendale, J. H. *Advances in Catalysis* **1952**, *4*, 31-86.
37. Millero, F. J.; Sotolongo, S. *Geochim. Cosmochim. Acta* **1989**, *53*, 1867-1873.
38. Le Truong, G.; De Laat, J.; Legube, B. *Water Res* **2004**, *38*, 2384-2394.
39. Stumm, W.; Morgan, J. J. In *Aquatic Chemistry* 3rd Ed.; John Wiley and Sons: New York, 1996; p 273.
40. Hug, S. J.; Leupin, O. *Env. Sci. Technol.* **2003**, *37*, 2734-2742.

Downloaded by UNIV MASSACHUSETTS AMHERST on September 11, 2012 | http://pubs.acs.org
Publication Date: October 3, 2005 | doi: 10.1021/bk-2005-0915.ch015

41. Pettine, M.; Campanella, L.; Millero, F. J. *Geochim. Cosmochim. Acta* **1999**, *63*, 2727-2735.
42. Pettine, M.; Millero, F. J. *Mar. Chem.* **2000**, *70*, 223-234.
43. Christensen, T.H.; Kjeldsen, P.; Bjerg, P.L.; Jensen, D.L.; Christensen, J.B.; Baun, A.; Albrechtsen, H.J.; Heron, G. *Appl. Geochem.* **2001**, *16*, 659-718.
44. Ayotte, J. D.; Montgomery, D. L.; Flanagan, S. M.; Robinson, K. W. *Environ. Sci. Technol.* **2003**, *37*, 2075-2083.

Downloaded by UNIV MASSACHUSETTS AMHERST on September 11, 2012 | http://pubs.acs.org
Publication Date: October 3, 2005 | doi: 10.1021/bk-2005-0915.ch015

Downloaded by UNIV OF GUELPH LIBRARY on September 12, 2012 | http://pubs.acs.org
Publication Date: October 3, 2005 | doi: 10.1021/bk-2005-0915.ch016

Chapter 16

Arsenic Diagenesis at the Sediment–Water Interface of a Recently Flooded Freshwater Sediment

Stephanie S. Chow and Martial Taillefert*

School of Earth and Atmospheric Sciences, Georgia Institute of Technology, Atlanta, GA 30332

In a previous study, elevated dissolved arsenic concentrations were detected in the Chattahoochee River (GA) and decreased in concentration with increasing distance from a suspected point-source, suggesting that arsenic could be scavenged by particles and settle to the sediment-water interface (SWI). In this study, the distribution of arsenic in sediments was determined to assess its biogeochemical cycling close to the SWI following a high deposition event. A combination of analytical techniques - ICP-MS and voltammetry - was used to measure the speciation of dissolved arsenic in two sediment cores. In addition, the porewater distribution of O_2, Fe(II), Mn(II), and ΣH_2S was measured with Au/Hg voltammetric microelectrodes to obtain high resolution profiles of the redox species involved in arsenic cycling. Our data show that dissolved arsenic is in the form of As(V) only and accumulates directly below the SWI. The significant correlation between Fe(II) and As(V) indicates that As(V) is released from iron oxides during their microbial reduction. These results suggests that sedimentation of As(V) occurring after storm events is followed by remobilization of As(V) in porewaters and upward diffusion, thus recycling arsenic into the overlying water.

In Advances in Arsenic Research; O'Day, P., et al.;
ACS Symposium Series; American Chemical Society: Washington, DC, 2005.

Introduction

The adverse human health effects of arsenic have been known for several centuries. The biochemical behavior and toxicity of arsenic depend on its chemical form. In natural environments, arsenite (As(III)) is not only more mobile but can be greater than 60 times more toxic than arsenate (As(V)), or organoarsenic compounds (*1, 2*).

Most environmental arsenic problems are a result of mobilization under natural conditions (*3*). The mobilization of arsenic in natural waters is mainly controlled by solid-solution interactions with iron oxides primarily (*1, 4-7*) because their charge, in contrast to manganese and aluminum oxides, is slightly positive at circumneutral pH (*7*). Under oxic conditions, As(V) is negatively charged and readily adsorbs onto iron oxides (*5, 8-10*) limiting its mobility and bioavailability. In anoxic conditions, however, it may be released during the reductive dissolution of these oxides (*3*) and simultaneously reduced (*11*), thus turning arsenic-contaminated sediments into a continuous source of As(III). As(V) may be reduced to As(III) microbially (*12-14*) or chemically by dissolved sulfide (*15*) and Fe(II) (*16, 17*) though both chemical reactions are usually slow. As(III) is neutral at circumneutral pH and is less susceptible to adsorption onto metal oxides (*5, 8, 9*). In the presence of dissolved sulfide, As(III) may form thioarsenite complexes (*18*) and eventually precipitate as arsenosulfide minerals (*19, 20*) or, alternatively, adsorb onto iron sulfide minerals (*20*). Organoarsenic species are formed biochemically as a detoxification mechanism (*4*) but are generally in low concentration in aquatic systems (*3*). Finally, As(III) can be rapidly reoxidized in the presence of dissolved oxygen (*21, 22*) or manganese oxides (*22-25*). Thus, desorption and remobilization of arsenic from sediments is influenced by pH, the activity of microorganisms, and the concentrations of dissolved oxygen, sulfide, and iron in interstitial waters (*6, 8, 20, 26-29*). In addition, phosphate, bicarbonate, silicate, and organic matter all compete with arsenic for adsorption sites, thus enhancing arsenic mobility (*29*).

The biogeochemical cycling of arsenic in aquatic systems has been largely derived from laboratory studies in well-defined conditions (e.g., *5, 8, 15-25*) and mainly examined in groundwater aquifers (*3*). In contrast, the spatial distribution of arsenic in sediments is rarely investigated (*6, 9, 10, 26, 28, 30*) and its redox speciation almost never determined (*26, 30*). The objective of this study is to examine the likely factors controlling arsenic early diagenesis in freshwater sediments with a high spatial resolution. The biogeochemical processes regulating the cycling of arsenic in the sediment of a major river impoundment in Georgia were investigated using a combination of Au/Hg voltammetric microelectrodes (O_2, Fe(II), Mn(II), ΣH_2S), voltammetry with Hanging Mercury Drop Electrode (HMDE) (As(III)), and Inductively Coupled Plasma-Mass

Downloaded by UNIV OF GUELPH LIBRARY on September 12, 2012 | http://pubs.acs.org
Publication Date: October 3, 2005 | doi: 10.1021/bk-2005-0915.ch016

Spectrometry (ICP-MS) (total dissolved As). The influence of iron, manganese, and sulfur cycling on the mobilization of arsenic is discussed in this paper.

Study Location

West Point Lake (inset Figure 1) is a 25,900-acre mainstream Chattahoochee River impoundment located 90 km southwest of Atlanta (GA). West Point Lake lies on a 50 km stretch of the Chattahoochee River between Franklin and West Point (GA). The lake has a shoreline of more than 800 km and runs along and across the Georgia/Alabama State line. The lake is controlled by the Army Corps of Engineers and was impounded in 1974 to provide drinking water, flood control, hydroelectric power, navigation, wildlife development, and general recreation for Southwest Georgia.

Five freshwater sediment cores (Figure 1) were collected from the outfall of the Chattahoochee River north of the drinking water reservoir of West Point Lake in LaGrange (GA) based on elevated total dissolved arsenic concentrations detected in the water column (*31*). There are no recorded geothermal or mining activities located in the surrounding area (*32*), but a suspected anthropogenic source has been identified (*31*) The sediment cores were collected in July, 2003 three weeks after the excessive precipitation attributed to Tropical Storm Bill brought approximately 10 foot crests through the study location. In this paper, we present the results from CR-4 and CR-5 only, which are approximately 60 km away from the suspected arsenic source (*31*), in an area where dissolved arsenic was depleted from the water column.

Methods

Sediment Core Collection and Porewater Extraction

Sediment samples were collected with 60 cm long and 10 cm diameter polycarbonate core liners. Approximately 10 cm of overlying water was collected with each core to maintain the integrity of the sediment-water interface and minimize exposure to the atmosphere during transport to the laboratory. High resolution voltammetric and potentiometric profiles of $O_{2(aq)}$, Fe^{2+}, Mn^{2+}, ΣH_2S (H_2S, HS^-, S^0, S_x^{2-}), $FeS_{(aq)}$, and pH were obtained by lowering an Au/Hg voltammetric microelectrode (*33*) and a pH minielectrode (Diamond General Corp.), in millimeter increments, into each sediment core with a micromanipulator (Analytical Instrument Systems, Inc.).

Downloaded by UNIV OF GUELPH LIBRARY on September 12, 2012 | http://pubs.acs.org
Publication Date: October 3, 2005 | doi: 10.1021/bk-2005-0915.ch016

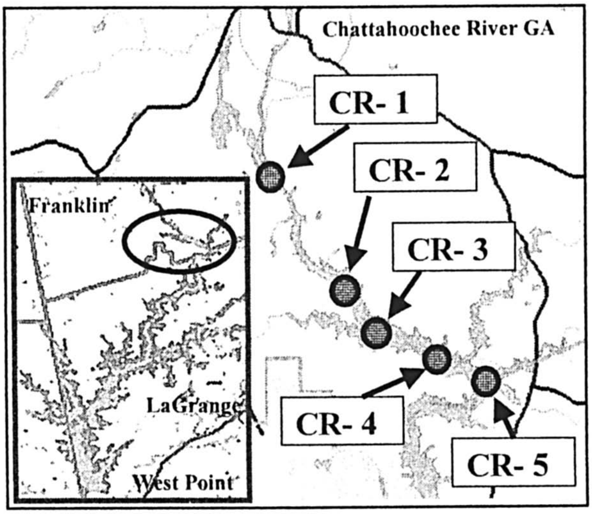

Figure 1. Study Location, Chattahoochee River and West Point Lake GA. Five sediment cores, numbered CR-1 to CR-5, were collected along the Chattahoochee River for this study. Their locations are provided on the map.

Voltammetric and pH measurements were conducted with a DLK-100A potentiostat that includes a voltmeter for combination measurements (Analytical Instrument Systems, Inc.). Dissolved oxygen was measured cathodically by linear sweep voltammetry, while Fe^{2+}, Mn^{2+}, ΣH_2S, and $FeS_{(aq)}$ were detected by cathodic square wave voltammetry. Prior to each scan, a conditioning step was applied at -0.1 V for 10 s to clean the microelectrode. Scan rates of 200 mV/s were used for all measurements (*33, 34*). The pH was calculated using the Nernst Law after recording the potential and sample temperature at the minielectrode (*34*). By using microelectrodes, a suite of constituents could be measured with a high spatial resolution without sediment handling, thus minimizing contamination while maximizing the volume of porewater for other analyses. Immediately following completion of the electrochemical profiles, the sediments were sectioned and centrifuged under $N_{2(g)}$ atmosphere, and porewaters were filtered (Norm-Ject sterile Teflon syringe and Puradisc 0.2μm Whatman filter) and acidified with Trace Metal Grade HCl or HNO_3 (Fisher) as needed for preservations and analysis. All porewaters were extracted and maintained in a $N_{2(g)}$ atmosphere and kept at 4°C until analysis of As(III), total dissolved arsenic

Downloaded by UNIV OF GUELPH LIBRARY on September 12, 2012 | http://pubs.acs.org
Publication Date: October 3, 2005 | doi: 10.1021/bk-2005-0915.ch016

(As$_d$), chloride, nitrate, sulfate, total dissolved orthophosphate, and total dissolved silica within 24 hours.

Analytical Methods

All solutions were prepared with 18 MΩ-cm Reverse Osmosis (RO) water (Barnstead). All plasticware and glassware used for trace metal analyses were acid-washed in 2% Trace Metal Grade HNO_3 (Fisher) for one week and rinsed thoroughly with RO water. For As(III) analysis, standards were made from an As(III) stock solution prepared daily by dissolving As(III) oxide (Alfa Aesar) in NaOH then acidifying with 12 N HCl (*35*).

Voltammetric measurements for As(III) were performed with a HMDE using the VA 663 multi-mode mercury drop electrode stand (Metrohm) coupled to the PGSTAT 12 Autolab potentiostat (Ecochemie) The reference electrode was an Ag/AgCl/KCl (3 M) with a 0.2 M NaCl glass bridge, and a glassy carbon rod acted as the counter electrode. The solutions were thoroughly degassed with ultra high purity $N_{2(g)}$ in between each As(III) measurement to prevent reoxidation by dissolved oxygen. As(III) concentrations were determined by amending the sample with 0.7 mM Cu(II) ($CuCl_2 \cdot 2H_2O$ Aldrich) and 1 M HCl. A potential was applied at -0.4 V for 10 seconds to form an arseno-copper complex (Eq. 1 - deposition step) (*35*).

$$yH_3As^{(III)}O_3 + xCu(Hg) + 3yH^+ + 3ye^- \rightarrow Cu_x^{(I/II)}As_y^{(-III)} + 3yH_2O \qquad (1)$$

The potential was then scanned cathodically (from -0.4 V to -1.2 V) at 300 Hz using square wave voltammetry to reduce $Cu^{(I/II)}$ from the arseno-complex to Cu^0 and allow the indirect measurement of As(III) (Eq. 2 - stripping step).

$$Cu_x^{(I/II)}As_y^{(-III)} + 3yH^+ + 3ye^- \rightarrow xCu(Hg) + yAs^{(-III)}H_3 \qquad (2)$$

Figure 2 shows a triplicate raw data scan of a 1 nM As(III) standard. The detection limit of the method was 0.25 nM As(III) (at 3σ of the blank).

Total dissolved arsenic concentrations (As$_d$) were determined in triplicate with a Hewlett Packard HP-4500 ICP-MS. Standards were prepared from a 1,000 ppm in 5% HNO_3 As stock solution (Aldrich). An internal standard of 1 ppb yttrium, prepared from 1,000 ppm stock solution (Aldrich) was added to standards and samples to correct for internal drift of the instrument. For quality control, As$_d$ standards were inserted every 10 samples. The detection limit of As$_d$ was found to be 0.25 nM.

Downloaded by UNIV OF GUELPH LIBRARY on September 12, 2012 | http://pubs.acs.org
Publication Date: October 3, 2005 | doi: 10.1021/bk-2005-0915.ch016

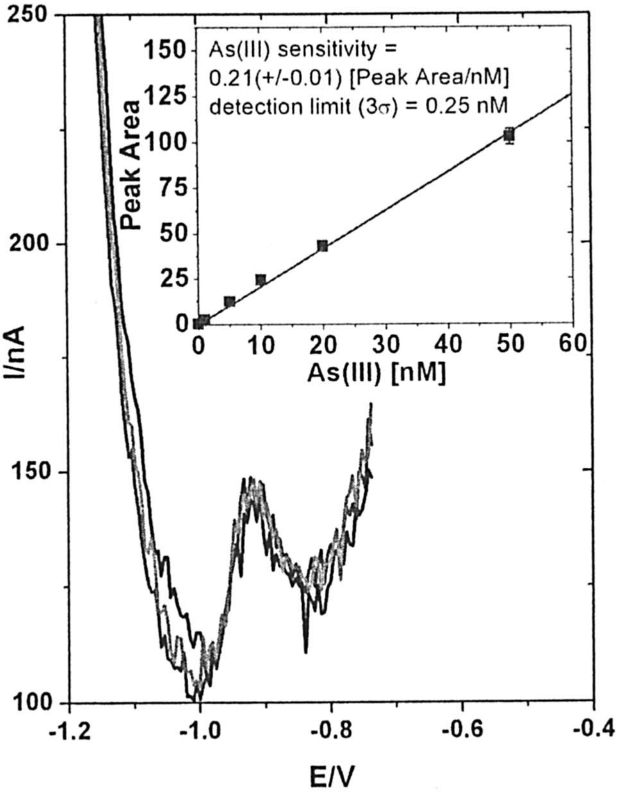

Figure 2. Reproducibility of triplicate HMDE voltammetric measurements of a 1 nM As(III) standard. The inset shows a typical calibration curve. The method has a detection limit of 0.25 nM at three standard deviations from the blank.

Total dissolved phosphate and silica were determined by spectrophotometry (*36, 37*). Sulfate, nitrate, and chloride were measured by Ion Chromatography (Dionex Model 300X) with a bicarbonate buffer as eluent. Amorphous iron oxides were extracted in triplicate in selected samples using ascorbate reagent (38). Fe(II) produced during the extraction was analyzed with the Ferrozine Method (39).

Results

Both cores were anoxic with dissolved oxygen decreasing from approximately 280 μM in the overlying water to undetectable levels just below

Downloaded by UNIV OF GUELPH LIBRARY on September 12, 2012 | http://pubs.acs.org
Publication Date: October 3, 2005 | doi: 10.1021/bk-2005-0915.ch016

the sediment-water interface (Figure 3a and 4a). As illustrated on Figure 3b, the pH decreased from 6.4 just below the SWI to 6.1 at 20 mm, then stabilized until 50 mm where it decreased again to reach 5.8 at 80 mm. Fe(II) rose from undetectable levels (< 5 μM) within 10 mm from the SWI to a maximum of 940 μM in CR-4 (Figure 3a) and 540 μM in CR-5 (Figure 4a). It then stabilized around these values until 40 mm in both CR-4 and CR-5. While Fe(II) abruptly increased in CR-5 to a maximum of 550 μM before decreasing regularly to a minimum of 100 μM at 80 mm, it oscillates between 500 and 900 μM below 40 mm in CR-4. Mn(II) concentrations displayed similar behaviors in both CR-4 and CR-5, except that Mn(II) was produced at 5 mm below the SWI in CR-4 and directly at the interface for CR-5. It increased to reach a maximum of 590 μM between 45 and 55 mm in CR-4 (Figure 3a) and 470 μM between 20 and 30 mm in CR-5 (Figure 4a). Below these depths, Mn(II) decreased in both cores to approximately 100 μM. No ΣH_2S (detection limit < 0.2 μM) were detected in these sediments.

Figure 3c illustrates the depth profiles of chloride, nitrate and sulfate. Chloride concentrations were approximately 130 μM in the first 10 cm of the sediment then slightly decreased to 100 μM. Nitrate (Figure 3c) was detected in the overlying water only, at a concentration of 27 μM. Sulfate concentrations were highest at 47 μM in the overlying water then diminished regularly to below the detection limit of 2 μM at 43 mm in CR-4 (Figure 3c). Total dissolved phosphate and total dissolved silica (data not shown) were below detection limit in both cores.

The concentration of amorphous iron oxides, as determined by the ascorbate extraction, decreased with depth in CR-4, from 108 ±6 μmol/g in the top 8 mm to 95 ±8 μmol/g between 15 and 25 mm (the depth depicting the highest dissolved As(V) in the porewaters - Figure 3d), and to 36 ±2.5 μmol/g between 88 and 98 mm. CR-5 results displayed a more stable profile with concentrations of amorphous iron oxides ranging between 56 ±2 μmol/g at the surface and 52 ±4 μmol/g between 58 and 71 mm (depth depicting the highest As(V) concentration - Figure 4b), and with a slight increase to 71 ±4 μmol/g between 104 and 114 mm.

As(III) was not detected in the extracted porewaters using HMDE, even after increasing the deposition time from 60 to 600 s to improve the detection limit. We therefore conclude that total dissolved arsenic (As_d) profiles (Figure 3d and 4b) are indicative of arsenate only. In both cores, the concentration of As(V) was significant at the sediment-water interface, 25 nM in CR-4 and 75 nM in CR-5, and increased deeper to a maximum of 156 nM between 15 and 25 mm in CR-4 and 107 nM between 55 and 68 mm in CR-5. As(V) then decreased to a minimum of 15 nM between 125 and 135 mm in CR-4 and 20 nM between 95 and 105 mm in CR-5.

Downloaded by UNIV OF GUELPH LIBRARY on September 12, 2012 | http://pubs.acs.org
Publication Date: October 3, 2005 | doi: 10.1021/bk-2005-0915.ch016

Downloaded by UNIV OF GUELPH LIBRARY on September 12, 2012 | http://pubs.acs.org
Publication Date: October 3, 2005 | doi: 10.1021/bk-2005-0915.ch016

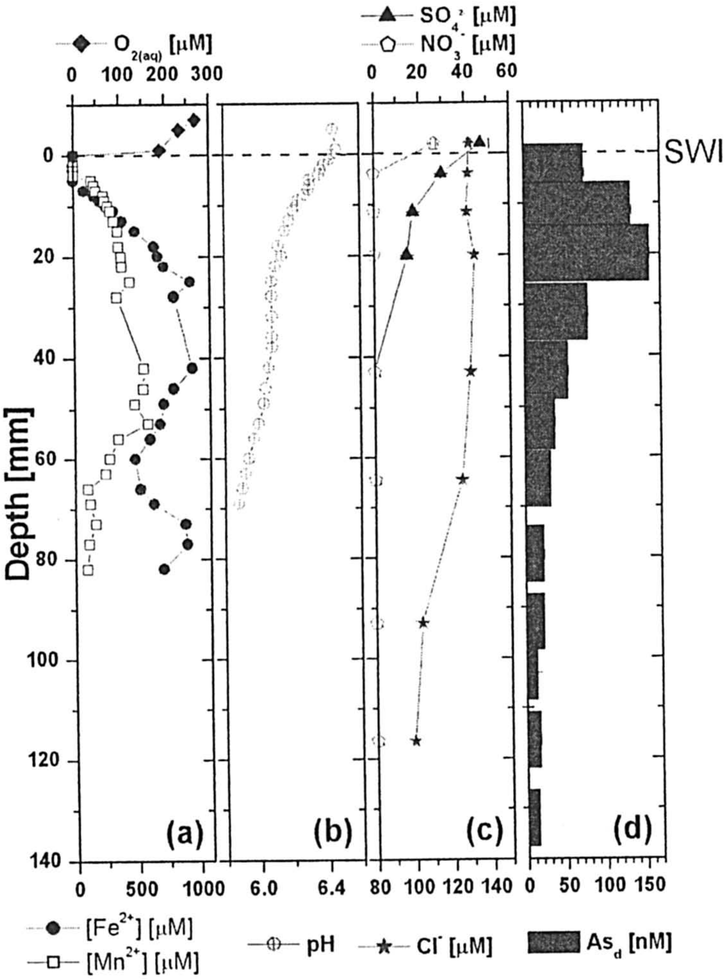

Figure 3. Depth Profile of dissolved oxygen, Fe(II), and Mn(II) by voltammetric microelectrode (to 80 mm) (a); pH by minielectrode (to 80 mm) (b); sulfate, nitrate and chloride by ion chromatography (c); and As_d by ICP-MS with error bars (d) in CR-4 collected in July 2003 in the Chattahoochee River.

Downloaded by UNIV OF GUELPH LIBRARY on September 12, 2012 | http://pubs.acs.org
Publication Date: October 3, 2005 | doi: 10.1021/bk-2005-0915.ch016

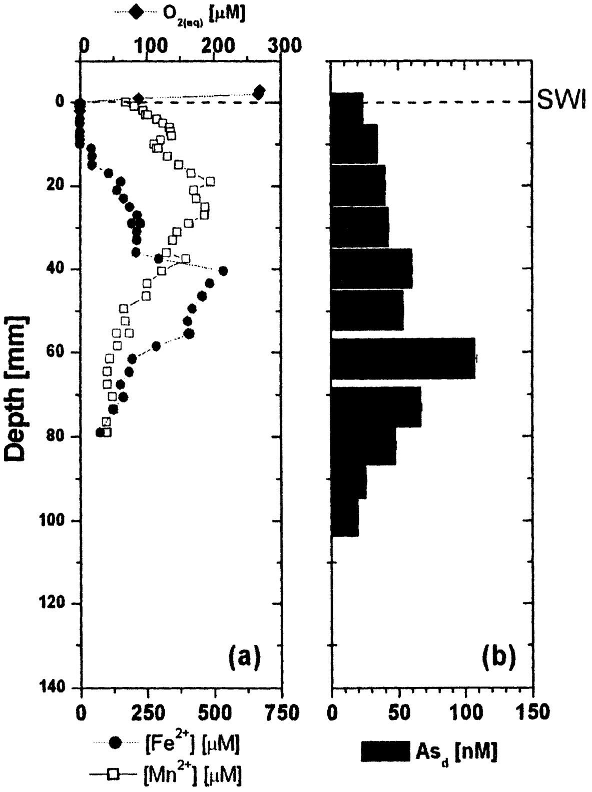

Figure 4. Depth Profile of dissolved oxygen, Fe(II), and Mn(II) by voltammetric microelectrode (to 80 mm) (a); and As_d by ICP-MS with error bars (b) of CR-5 collected in July 2003 in the Chattahoochee River.

Discussion

Altogether, these chemical profiles provide a clear picture of the processes regulating the cycling of arsenic near the sediment-water interface. The rapid decrease in dissolved oxygen close to the SWI (Figure 3a and Figure 4a) indicates that both sediments are anoxic. The low concentration of Fe(II), the absence of NO_3^-, and the decrease in pH near the SWI suggest that a combination of aerobic respiration (Eq. 3), denitrification (Eq. 4), and chemical oxidation of Fe(II) (Eq. 5) occur within the first centimeter of these sediments:

$$CH_2O + O_2 \rightarrow HCO_3^- + H^+ \quad (3)$$

$$5CH_2O + 4NO_3^- \rightarrow 5HCO_3^- + 2N_2 + H^+ + 2H_2O \quad (4)$$

$$4Fe^{2+} + O_2 + 10H_2O \rightarrow 4Fe(OH)_{3(s)} + 8H^+ \quad (5)$$

Iron oxidation is confirmed by the high concentration of amorphous iron oxides detected in the upper sediment of CR-4 and CR-5. Additionally, manganese and iron oxide reduction is demonstrated with the production of Mn(II) and Fe(II) within the first 3 to 4 cm of these sediments (Figure 3a and Figure 4a). The occurrence of metal reduction leads to a subsequent stabilization of the pH in the sediment porewaters (Figure 3b) because these reactions consume protons (*34*). Chemical reduction of manganese and iron oxides by dissolved sulfide (Eq. 6 and 7) may occur in sediments. However, the maximum concentration of dissolved sulfide available from the sulfate present in these freshwater sediments (i.e. 50 μM) is not high enough to account for all the Mn(II) and Fe(II) produced (compare maximum sulfate to maximum Mn(II) and Fe(II) concentrations in Figure 3 and 4).

$$MnO_2 + H_2S + 2H^+ \rightarrow Mn^{2+} + S^{(0)} + 2H_2O \quad (6)$$

$$2Fe(OH)_{3(s)} + H_2S + 4H^+ \rightarrow 2Fe^{2+} + S^{(0)} + 6H_2O \quad (7)$$

Similarly, the chemical reduction of manganese oxides by Fe(II) is also possible (Eq. 8) but is usually slow above pH 4 (*40*).

$$MnO_2 + 2Fe^{2+} + 4H_2O \rightarrow Mn^{2+} + 2Fe(OH)_{3(s)} + 2H^+ \quad (8)$$

It can therefore be concluded that most of the reduction of manganese and iron oxides is microbial in these sediments. Interestingly, Mn(II) reaches the sediment-water interface in core CR-5, suggesting that it diffuses out of the sediment at this location. This feature is well known and due to the slow oxidation kinetics of Mn(II) at circumneutral pH in the presence of oxygen (*41*). The disappearance of sulfate within the first 40 mm of CR-4 (Figure 3c) suggests that sulfate reduction proceeds in these sediments. Dissolved sulfide was not detected in the porewaters suggesting that it was removed by precipitation with FeS. However, MINEQL+ calculations using an average pH of 6.1, Fe(II) concentration of 800 μM and assuming 50 μM H_2S (i.e. the maximum sulfate measured) produced in these sediments indicate that the solubility product of FeS_{am} and mackinewite are not exceeded. At this point, it is not clear if the system is not at equilibrium or if the thermodynamic database is inaccurate.

Downloaded by UNIV OF GUELPH LIBRARY on September 12, 2012 | http://pubs.acs.org
Publication Date: October 3, 2005 | doi: 10.1021/bk-2005-0915.ch016

Nevertheless, the sulfate profile suggests that H_2S is produced episodically in these sediments.

Arsenic is thought to enter the Chattahoochee River upstream of the study location and is transported in the oxic river water in the form of As(V) (*31*). As As(V) flows downstream, it may adsorb onto colloidal and particulate matter contained in the river and settle to the sediment-water interface. The data indicate that this sediment is not a natural source of arsenic, since the concentration of dissolved arsenic is high near the SWI and depleted at depth, and support earlier hypothesis that the anthropogenic input of arsenic is significant in the Chattahoochee River (*31*).

The role of manganese and iron on the arsenic cycle has been investigated extensively (*6, 8, 9, 15-17, 20, 22-24, 28*). In these sediments, adsorption of arsenic should dominate in the upper sediments which contain the highest concentration of amorphous iron oxides. The adsorption of arsenic is also affected by the degree of crystallization of the iron oxides because the density of adsorption sites decreases as the minerals are more crystallized (*42*). To determine the extent of adsorption of As(V) onto iron oxides in the first centimeters of these sediments, we implemented a double-layer surface adsorption model with MINEQL+ using parameters from the literature (*42*). The model assumes a specific surface area of 600 m^2/g for amorphous iron oxides and two types of binding sites: high affinity sites with a density of 5 mmol/mol Fe and low affinity sites with a density of 0.2 mol/mol Fe. The input concentrations used in the model are based on the data of Figure 3 and 4 (pH = 6.4; $[AsO_4^{3-}]$ = 150 nM; $[Cl^-]$ = 130 μM; $[Fe^{2+}]$ = 10 μM; $[SO_4^{2-}]$ = 50 μM) or are estimated from previous work in the area (i.e. DIC = 300 μM). Assuming a sediment density varying between 0.98 and 0.87 g/cm^3 clayey and silty sediments(*43*), the molar concentration of amorphous iron oxides is ca. 0.05 M. The model calculation predicts that 97% of the arsenate in our system is adsorbed onto iron oxides.

As(V) is produced simultaneously with Fe(II) in the first few centimeters of both sediments (Figure 3 and 4). A positive correlation exists between Fe(II) and As(V) in both cores, though with different slopes (Figure 5). From the slopes, a As:Fe(II) ratio of 3:10,000 in the top 25 mm of CR-4 and 6:100,000 in the top 40 mm of CR-5 were found. These data indicate that adsorbed arsenic may be released during the reduction of iron oxides, thus confirming the significant role of iron in the arsenic cycle. These data also indicate that more arsenate is scavenged onto iron oxides in CR-4 than in CR-5. Silicates and phosphate were below the detection limit in both cores, suggesting they probably do not significantly effect arsenic mobilization in this system.

Mn(II) depth profiles indicate that the reduction of manganese oxides occurs in these sediments, however their involvement with arsenic is not evident. First, adsorption is not favored because at circumneutral pH, manganese oxides are

Downloaded by UNIV OF GUELPH LIBRARY on September 12, 2012 | http://pubs.acs.org
Publication Date: October 3, 2005 | doi: 10.1021/bk-2005-0915.ch016

negatively charged (*7*) while As(V) is mainly deprotonated (*41, 42*). It is also known that manganese oxides oxidize arsenite to arsenate (*23-25*) according to:

$$MnO_2 + H_3AsO_3 \rightarrow Mn^{2+} + HAsO_4^{2-} + H_2O \qquad (9)$$

However, there is an inconsistent correlation between Mn(II) and As(V) in both cores (not shown). The lower adsorption affinity of As(V) onto manganese oxides at circumneutral pH along with the poor correlation between Mn^{2+} and As(V) suggest that manganese oxides play a minor role in the arsenic cycle in these sediments.

As previously mentioned, sulfate disappears in these porewaters suggesting that sulfate reduction may occur in these sediments. It has been shown recently that dissolved sulfide may slowly reduce As(V) and complex As(III) in the form of electrochemically inactive AsO_xS_y (*18, 20*) that could then undergo precipitation. Our measurements, however, could not detect any As(III) in solution in these sediments. We ruled out the possible oxidation of our samples after porewater extraction since the sediment cores were sectioned, centrifuged, filtered, acidified, and stored at 4°C under a $N_{2(g)}$ atmosphere until As(III) analysis, which was conducted within 24 hours after collection. In addition, the arsenosulfide complexes, if present, should be dissociated in the acidic conditions of the As(III) analysis (pH 1) and detected electrochemically.

The fact that the sediment is reduced but arsenic is oxidized may be due to the dynamic nature of the system studied. The surficial sediments evaluated in this study were most likely deposited after the passage of Tropical Storm Bill, which impacted the site three weeks prior to this investigation. It is possible that the kinetically slow reduction of As(V) had not occurred so soon after deposition, while microbial iron reduction released As(V) in solution. Finally, the presence of As(V) and Fe(II) at deeper locations in CR-5 as compared to CR-4 is probably due to the more turbulent river flow at CR-5 which may bring dissolved oxygen to the sediment and increase erosion. This process is evidenced by a general decrease in both the Fe(II) and amorphous iron oxide concentrations in the sediment of CR-5 compared to CR-4 (Figure 3 and 4).

Diffusive fluxes were calculated for each core using Fick's Law with the molecular diffusion coefficient of phosphate as a proxy for that of arsenate (9.1 x 10^{-5} cm^2/sec for $H_2PO_4^-$). According to these calculations, approximately 60 to 200 nM/cm^2yr of arsenic may be diffusing into the overlying water column from the sediment. Although the arsenic concentrations detected in the porewaters are not considered high compared to contaminated sites, the data suggest that arsenic is remobilized and may impact the drinking water reservoir located downstream.

Downloaded by UNIV OF GUELPH LIBRARY on September 12, 2012 | http://pubs.acs.org
Publication Date: October 3, 2005 | doi: 10.1021/bk-2005-0915.ch016

Downloaded by UNIV OF GUELPH LIBRARY on September 12, 2012 | http://pubs.acs.org
Publication Date: October 3, 2005 | doi: 10.1021/bk-2005-0915.ch016

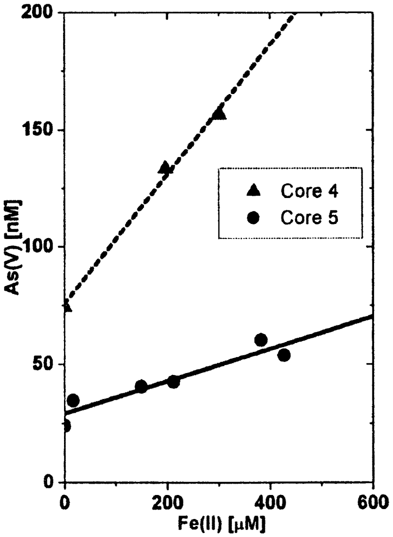

Figure 5. Correlation between Fe(II) and As(V) between 0 and 25 mm in CR-4 (triangles) and between 0 and 40 mm in CR-5 (circles).

Conclusions

This study successfully combined several analytical techniques to determine the profiles of major redox species and the speciation of As(III) and As(V) with a high spatial resolution (i.e., < 10 cm) in two contaminated freshwater sediments. Results provide evidence of a substantial correlation between the diagenetic processes involving iron and arsenic in these sediments. The sediment profiles suggest that iron oxides scavenge arsenic in the form of arsenate in the water column and settle to the sediment-water interface where they are reduced by iron reducing bacteria. As a result of microbial iron reduction, As(V) is released and accumulates in the porewaters near the sediment-water interface, where it can diffuse back to the overlying waters.

Interestingly, As(III) was never found in the porewaters, suggesting that the reduction of As(V) is a slow process that was not occurring in these recently deposited sediments. Future studies will test the hypothesis that microbial and chemical reduction of As(V) are too slow compared to the hydraulic residence time of arsenic in these sediments.

Acknowledgements

The authors express their gratitude to Flip Froelich and Stephany Rubin-Mason for their help with the ICP-MS measurements and Judson Partin, Elizabeth Carey, and Gwendolyn Bristow for their assistance in the field and laboratory. This work was funded by the Georgia Water Resources Institute through a grant from the Department of Interior/Geological Survey (Contract # 01HQGR0139).

Downloaded by UNIV OF GUELPH LIBRARY on September 12, 2012 | http://pubs.acs.org
Publication Date: October 3, 2005 | doi: 10.1021/bk-2005-0915.ch016

Literature Cited

1. Ferguson, F.; Gavis, J. *Wat. Res.* **1972,** *6*, 1259-1274.
2. Ryu, J.; Gao, S.; Dahlgren, R.A.; Zierenberg, R.A. *Geochim. Cosmochim. Acta* **2002**, *66*, 2981-2994.
3. Smedley, P.L.; Kinniburgh, D.G. *Appl. Geochem.* **2002**, *17*, 517-568.
4. Cullen, W.; Reimer, K.J. *Chem. Rev.* **1989,** *89,* 713-764.
5. Jain, A.; Raven, K.P.; Loeppert, R.H. *Environ. Sci. Technol.* **1999**, *33*, 1179-1184.
6. Kneebone, P.E.; O'Day, P.A.; Jones, N.; Hering, J.G. *Environ. Sci. Technol.* **2002**, 3*6*, 381-186.
7. Stumm, W. *Chemistry of the Solid-Water Interface*; John Wiley and Sons, Inc.; New York, 1992.
8. Pierce, M.L.; Moore, C.B. *Wat. Res.* **1982,** *16*, 1247-1253.
9. Belzile, N.; Tessier., A. *Geochim. Cosmochim. Acta* **1990,** 5*4,* 103-1039.
10. Mucci, A.; Boudreau, B.; Guignard, C. *Appl. Geochem.* **2003**, *18,* 1011-1026.
11. Guo, T.; DeLaune, R.D.; Patrick Jr., W.H. *Environ.Intern.* **1997**, *23*, 305-316.
12. Ahmann, D.; Krumholz, L.R.; Hemond, H.F.; Lovley, D.R.; Morel, F.M.M. *Environ. Sci. Technol.* **1997**, *31*, 2923-2930.
13. Harrington, J.M.; Fendorf, S.E.; Rosenzweig, R.F. *Environ. Sci. Technol.* **1998**, *32*, 2425-2430.
14. Oremland, R.S.; Dowdle, P.R.; Hoeft, S.; Sharp, J.O.; Schaffer, J.K.; Miller, L.G; Blum, J.S; Smith, R.L; Bloom, N.S; Wallschlaeger, D. *Geochim. Cosmochim. Acta* **2000**, *64*, 3073-3084.
15. Rochette, E.A.; Bostick, B.C.; Li, G.C.; Fendorf, S. *Environ. Sci. Technol.* **2000**, *34*, 4714-4720.
16. Appelo, C.A.J.; Van Der Weiden, M.J.J.; Tournassat, C.; Charlet, L. *Environ. Sci. Technol.* **2002,** *36*, 3096-3103.
17. Charlet, L.; Bosbach, D.; Peretyashko, T. *Chem. Geol.* **2002,***190*, 303-319.
18. Wilkin, R.T.; Wallschlager, D.; Ford, R.G. *Geochem. Trans.* **2003**,*4*, 1-7.

19. Sadiq, M. *Mar. Chem.* **1997**, *31*, 285-297.
20. Bostick. B.C.; Fendorf, S. *Geochim. Cosmochim. Acta* **2003**, *67*, 909-921.
21. Johnson, D.L.; Pilson, M.E.Q. *Environ. Lett.* **1975**, *8*, 157-171.
22. Scott, M.J.; Morgan, J.J. *Environ. Sci. Technol.* **1995**, *29*, 1898-1905.
23. Manning, B.A.; Fendorf, S.E.; Goldberg S. *Environ. Sci. Technol.*. **1998**, *32*, 2383-2388.
24. Chiu, V.Q.; Hering, J.G. *Environ. Sci. Technol.* **2000**, *34*, 2029-2034.
25. Driehaus, W.; Seith, R.; Jekel, M. *Wat. Res.* **1995**, *29*, 297-305.
26. Andreae, M.O. *Limnol. Oceanogr.* **1979**, *24*, 440-452.
27. Xu, H.; Allard, B.; Grimvall, A. *Water Air Soil Pollut.* **1988**, *57*, 269-278.
28. Mok, W. A.; Wai, C.M. *Environ. Sci. Technol.* **1990**, *24*, 102-108.
29. Meng, X.K.; Guo. P.; Bang, S.; Bang, K.W. *Toxicol. Letters* **2002**, *133*, 103-111.
30. Yan, X.-P.; Kerrich, R.; Hendry, M.J. *Geochim. Cosmochim. Acta* **2000**, *62*, 2637-2648.
31. Lesley, M.P.; Froelich, P.N. Proceedings of 2003 Georgia Water Resources Conference, April 2003.
32. Huddlestun, P.F. *A revision of the lithostratigraphic units of the coastal plain of Georgia - The Miocene Through Holocene.* Department of Natural Resources, Environmental Protection Division, Georgia Geological Survey; Atlanta, GA, 162, 1988.
33. Brendel, P.J.; Luther, G.W. *Environ. Sci. Technol.* **1995**, *29*, 751-761.
34. Taillefert, M.; Rozan, T.F.; Glazer, B.T.; Herszage, J.; Trouwborst, R.E.; Luther III. G.W. In: *Environmental Electrochemistry: Analyses of Trace Element Biogeochemistry*, M. Taillefert and T.F. Rozan, Eds. American Chemical Society Symposium Series; American Chemical Society: Washington, D.C., **2002**, Vol. 811, 247-264.
35. Li, H.; Smart, R.B. *Anal. Chim. Acta* **1996**, *325,* 25-32.
36. Murphy J.R.; Riley J.P. *Anal. Chim. Acta* **1962**, *27*, 31-36.
37. Strickland, J.D.H. *J. Amer. Chem. Soc.* **1952**, *74*, 862-876.
38. Kostka, J.E.; Luther III, G.W. *Geochim. Cosmochim. Acta* **1994**, *58*, 1701-1710.
39. Stookey, L.L. *Anal. Chem.* **1970**, *42*, 779-782.
40. Postma, D. *Geochim. Cosmochim. Acta* **1985**, *49*, 1023-1033.
41. Stumm, W.; Morgan, J.J. *3rd Ed. Aquatic Chemistry Chemical Equilibria and Rates in Natural Waters*, John-Wiley and Sons, Inc.; New York; 1996.
42. Dzombak, D.A.; Morel, F.M.M. *Surface Complexation Modeling: Hydrous Ferric Oxide.* John Wiley and Sons, Inc.; New York; 1990.
43. Kastler, J.A.; Wilberg, P.L. *Estuar. Coastal Shelf Sci.* **1996**, *42*, 683-700.

Downloaded by UNIV OF GUELPH LIBRARY on September 12, 2012 | http://pubs.acs.org
Publication Date: October 3, 2005 | doi: 10.1021/bk-2005-0915.ch016

Downloaded by UNIV MASSACHUSETTS AMHERST on September 11, 2012 | http://pubs.acs.org
Publication Date: October 3, 2005 | doi: 10.1021/bk-2005-0915.ch017

Chapter 17

Natural Attenuation of Arsenic in Semiarid Soils Contaminated by Oxidized Arsenic Wastes

Margarita Gutiérrez-Ruíz, Mario Villalobos*, Francisco Romero, and Pilar Fernández-Lomelín

Environmental Bio-Geochemistry Group, LAFQA, Instituto de Geografía, National Autonomous University of Mexico (UNAM), Circuito Exterior, Ciudad Universitaria, México, Coyoacán, 04510, D.F., México

This work presents experimental evidence for the natural attenuation of arsenic in semi-arid soils contaminated by wastes containing oxidized arsenic species. This evidence was obtained through measurements of water-soluble As in aqueous soil extracts of extensive soil sampling sets, and by comparing them with the solubility of the original As species in the wastes. Additionally, wet chemical analyses of total As, Pb, Zn, Cd, Cu, Mn, Fe, Ca, and pH, were conducted on these samples. Selected fine soil fractions of high total As content but low water-soluble As content were analyzed by Scanning Electron Microscopy coupled with Energy Dispersive X-ray Fluorescence Spectroscopy, and revealed predominant associations between As, Pb, and Zn, and little to none of As with Fe. This evidence suggests attenuation is due to formation of very low-solubility heavy metal-like arsenates as arsenic-containing wastes equilibrate with the soil media. Thermodynamic solubility calculations, using total elemental contents and data from pure heavy metal arsenates, further support this hypothesis.

In Advances in Arsenic Research; O'Day, P., et al.;
ACS Symposium Series; American Chemical Society: Washington, DC, 2005.

Introduction

Arsenic is a toxic element to plants and animals because of its affinity for proteins, lipids and other cell components *(1,2)*. It has been associated with a number of different cancers, as well as to cardiovascular and neurological effects, depending on the mode and level of exposure *(1,3)*.

Arsenic is commonly found in parent rock and mineral environments in low oxidation states [usually 0, -1 and –2 *(4,5)*], appearing associated to sulfidic minerals, typically as arsenopyrite [FeAsS] or arsenical pyrite [$Fe(As,S)_2$], and to analogous sulfides and arsenides of other transition metals (e.g., of Pb, Zn and Cu) *(3,4)*. In oxidized environments a number of different arsenite [of As(III)] and arsenate [of As(V)] minerals of transition metals exist *(3-5)*. Consequently, As is a natural component of Pb, Cu, Zn and Au ores *(6)* and inevitably enters metallurgical processing *(3)*. Arsenic and other trace metals accompanying the original parent mineral ores appear in the mining wastes. Thus, As is ubiquitous in mineral wastes and the soil environments in which they are disposed of.

The bioavailability of heavy metals in general depends on their reactivity and solubility. The mobility of As in soils is inextricably linked to its speciation because a considerable range of mobility behaviors is observed for the stable chemical species under ambient conditions *(4,5)*. The present work is concerned with aerated semi-arid contaminated soil environments where the stable As species are the higher oxidation states, namely As(III) and As(V), which are the most mobile chemical forms in aqueous environments *(6,7)*. These two chemical forms are readily interchangeable under variable redox conditions in soils, such as those that exist during alternating saturated and unsaturated regimes *(5,7,8)*.

Iron oxides have been identified to reduce the mobility of oxidized As species through a range of mechanisms from adsorption to coprecipitation *(9-16)*. However, some evidence suggests that under certain conditions, this control may be exerted by the lower solubility of mixed Fe-metal arsenates *(10,14,17,18)*. For example, Beudantite (Pb-Fe arsenate-sulfate-hydroxide mineral) has been detected by X-ray diffraction (XRD) in acid sulfide-rich tailings from gold mining *(10,14)*. Morin et al. *(18)* detected a secondary iron arsenate containing barium (pharmacosiderite) in a natural soil developed from weathering of arsenopyrite and other reduced As minerals that originate from hydrothermal processes. In contrast, Lumsdon et al. *(19)* inferred that adsorption to hydrous ferric oxides, and not arsenate mineral formation, was controlling As availability in similar As-contaminated soil environments, by performing thermodynamic calculations and modeling using concentration values of species extracted from the soils. However, they did not consider thermodynamic solubility constants of metal arsenates other than those of Ca and Fe(III), which

Downloaded by UNIV MASSACHUSETTS AMHERST on September 11, 2012 | http://pubs.acs.org
Publication Date: October 3, 2005 | doi: 10.1021/bk-2005-0915.ch017

Downloaded by UNIV MASSACHUSETTS AMHERST on September 11, 2012 | http://pubs.acs.org
Publication Date: October 3, 2005 | doi: 10.1021/bk-2005-0915.ch017

show much higher As solubilities at circumneutral pH values *(7)*, despite the high concentrations of first-row transition metals in the soils studied.

The role of iron oxides in As retention has been amply demonstrated in the literature, however, few studies have been conducted on industrial residues rich in heavy metals, which may provide under specific conditions, available fractions of these elements. Davis et al. *(17)* identified, using electron microprobe analysis and wavelength dispersive spectroscopy, as major As-bearing liberated particles in smelter-impacted soils and house dusts, a complex solid substitution series described as heavy metal – As oxides, with very low contributions from Fe – As oxides.

The present work is part of an investigation to seek remediation strategies of soils contaminated with As and other heavy metals. Here, we show evidence of natural As attenuation in the soil environments studied as due to insolubilization processes through formation of heavy metal arsenate compounds. Two different semi-arid sites in Mexico where soils have been contaminated with As(III) and As(V) wastes were studied. Wet chemical analyses of total and water-soluble As contents, total metal contents and other soil parameters, as well as electron microscopy coupled with energy dispersive spectroscopy were performed.

Materials and Methods

Study Area

Sampling sites are located in semi-arid regions in north and central Mexico (Fig. 1) on terrain surrounding smelting complexes located in Monterrey (MONT) and San Luis Potosi (SLP) cities. The MONT plant operated 107 years producing Pb, Ag, Au, Sb, Bi alloys and Se. Mainly two wastes were produced: "paspurrias" (a white mixture of Ca-carbonates with Ca-arsenates, at high pH) and slag (a black vitrified solid with As and heavy metals). The wastes are stored in a superficial disposal site (Fig. 1), but traces of paspurrias are still visible in the surrounding soils. The study area (≅ 60 Ha) in MONT is underlain by brown, clayey, alkaline soils with calcareous nodules (caliche). The annual average temperature (AAT) is 22 °C, average rainfall (AAR) is 638.5 mm, and average evaporation rate (AAER) is 1941 mm.

In the SLP site a smelter has operated since 1890, producing Cu (Cu- Plant), As_2O_3 (As- Plant) and "calcinas" (a subproduct rich in Pb and As). This site is located in the NE of the city. The wastes (melt slag) are deposited in two places (Fig. 1). A residential area is located East of the As- Plant (Morales Distric 8,800 inhabitants ≅ 100 Ha,). The AAT is 24.5 °C, the AAR is 351 mm, and the AAER is 2072 mm. Two different sites were sampled (Fig. 1): the Morales

Downloaded by UNIV MASSACHUSETTS AMHERST on September 11, 2012 | http://pubs.acs.org
Publication Date: October 3, 2005 | doi: 10.1021/bk-2005-0915.ch017

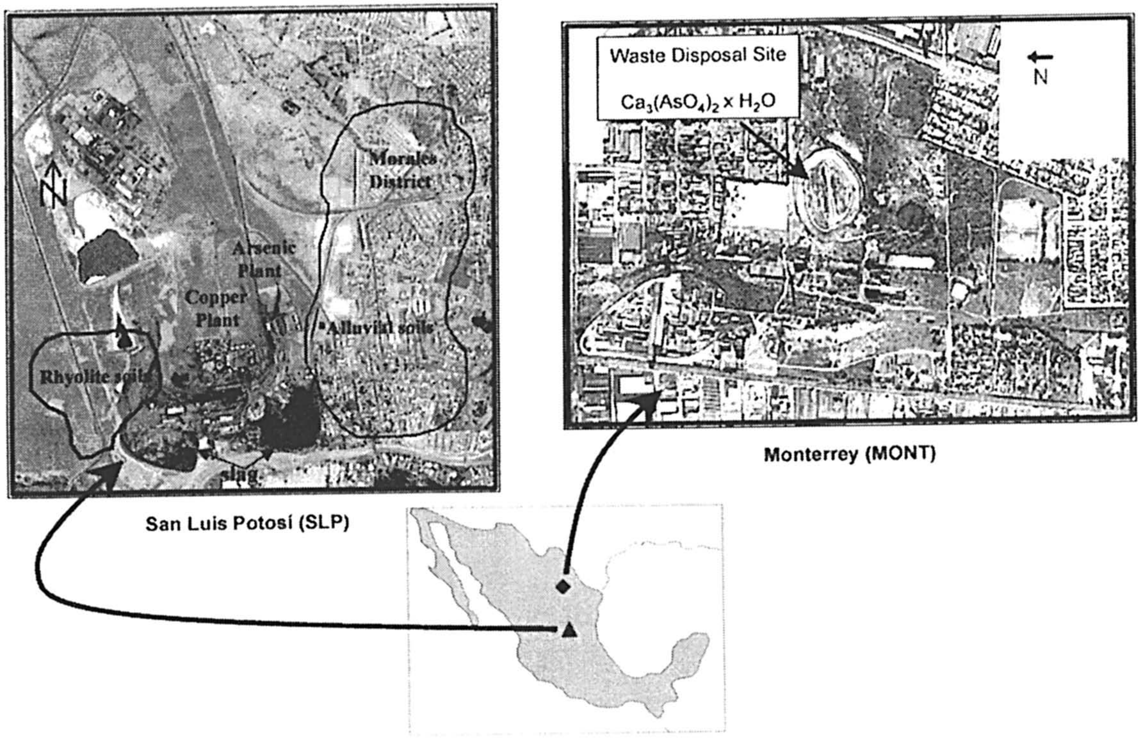
N
Morales District
Arsenic Plant
Copper Plant
Alluvial soils
Rhyolite soils
slag
San Luis Potosí (SLP)
Waste Disposal Site
$Ca_3(AsO_4)_2 \times H_2O$
N
Monterrey (MONT)

district, composed of alluvial soils rich in calcareous nodules; and an uninhabited field composed of rhyolite soils (≅ 28 Ha).

Soil and waste sampling and storage

Forty two test pits were dug to a depth of 2.50 m in the MONT site, collecting samples approximately every 15 to 25 cm to obtain 162 soil samples. In the SLP site, 100 soil samples were collected (0-15 cm). Each sample was a composite of 5–10 sub samples taken from 1 Ha grid squares. Thirty subsurface soil samples were collected from 6 cores of total depths of 80 to 120 cm, by taking samples every 15 – 30 cm depth intervals. Product and sub-product samples were collected: Black As (high content of As_2O_3), Furnace Dusts (rich in Pb and As), Dust of Converters (rich in Cu), and "Calcinas".

Chemical and physical analysis

Air-dried samples were disaggregated, sieved (<2 mm), homogenized, ground and sieved (<70 μm), and stored. Total heavy metals and As concentrations were determined by US-EPA method 3051 *(20)*. Water-soluble As determinations were performed by suspending the solid samples in water in equilibrium with the atmosphere (1:20, solid:water) *(21)* in batch polyethylene reactors and continuously shaking for 18 hr. (above 90% of total water-extractable As). While this extraction may not be sufficient to remove As fractions possibly sorbed to surface-active minerals, the procedure with HCO_3^- to determine available As *(22)* may liberate As from potential calcium arsenate solids (*cf.* Fig. 4 and later discussion) and thus, was not used. After equilibration, the suspensions were centrifuged for 15 min at 3000 rpm; the leachates were filtered through a 0.45 μm membrane, transferred to polyethylene vials, and stored in the dark at 4°C until analysis for pH and dissolved As. Total Cd, Cu, Pb, Zn, Fe, and Ca were quantified by flame AAS [US-EPA method 7000B *(23)*], and As by HG-AAS [US-EPA method 7062 *(24)*]. Soluble metals were analyzed in SLP soil samples. Fine fractions of soil were processed with a JEOL JXA-8900R superprobe scanning electron microscope coupled with energy dispersive X-ray spectrometry (SEM-EDS).

Results and Discussion

MONT Site

The pH of superficial soils varied considerably, from neutral to very alkaline (Fig. 2a), although most were found between 8 and 10. Soils were impacted by the high pH of "paspurrias" (pH>10), but it is expected that upon reaction with

Downloaded by UNIV MASSACHUSETTS AMHERST on September 11, 2012 | http://pubs.acs.org
Publication Date: October 3, 2005 | doi: 10.1021/bk-2005-0915.ch017

Downloaded by UNIV MASSACHUSETTS AMHERST on September 11, 2012 | http://pubs.acs.org
Publication Date: October 3, 2005 | doi: 10.1021/bk-2005-0915.ch017

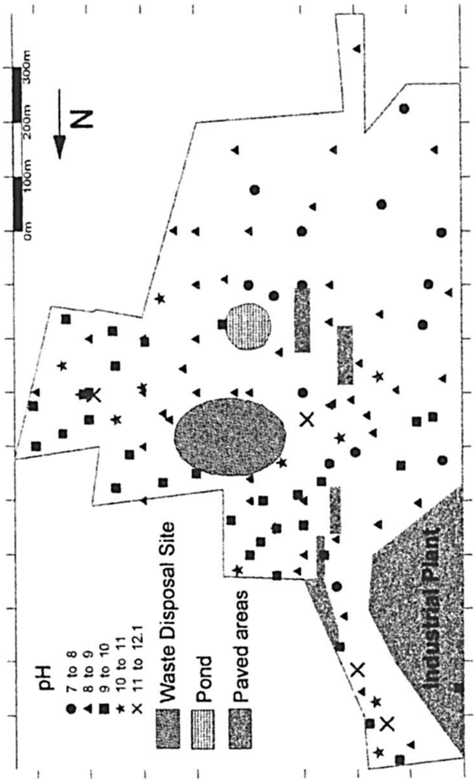
pH
● 7 to 8
▲ 8 to 9
■ 9 to 10
★ 10 to 11
✕ 11 to 12.1
Waste Disposal Site
Pond
Paved areas
Industrial Plant
0m
100m
200m
300m
N

Downloaded by UNIV MASSACHUSETTS AMHERST on September 11, 2012 | http://pubs.acs.org
Publication Date: October 3, 2005 | doi: 10.1021/bk-2005-0915.ch017

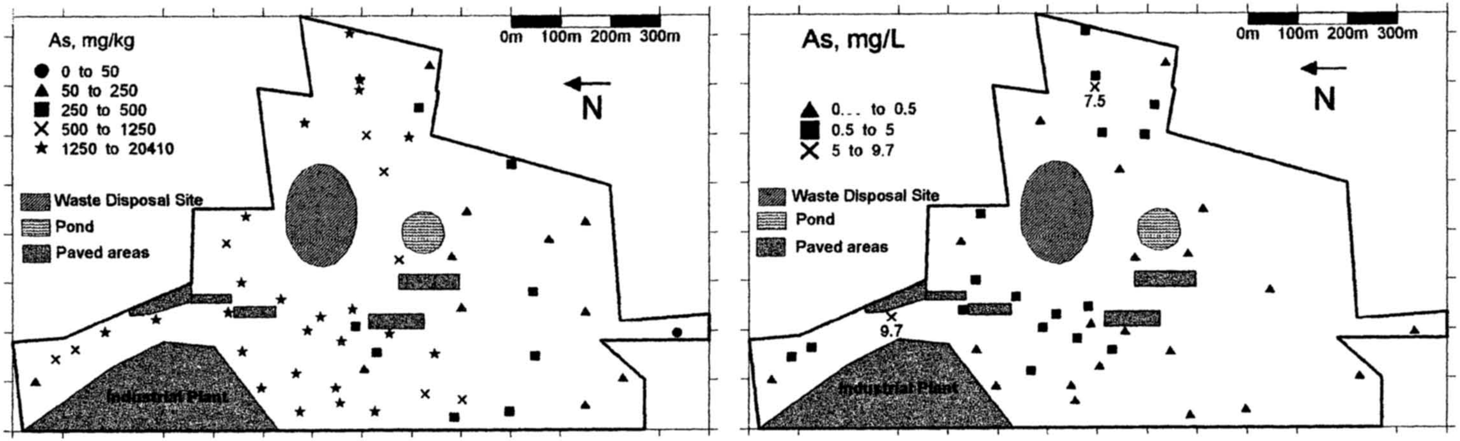
As, mg/kg
● 0 to 50
▲ 50 to 250
■ 250 to 500
✕ 500 to 1250
★ 1250 to 20410
Waste Disposal Site
Pond
Paved areas
0m 100m 200m 300m
N
Industrial Plant
As, mg/L
▲ 0... to 0.5
■ 0.5 to 5
✕ 5 to 9.7
7.5
9.7
Waste Disposal Site
Pond
Paved areas
0m 100m 200m 300m
N
Industrial Plant

Figure 2. pH values (a); and arsenic contents in superficial soils overlaid on map of MONT study site, (b) total concentrations (mg/kg); (c) water-soluble concentrations (mg/L) in 1:20 ratio solid:liquid.

atmospheric CO_2 and through the soil buffering capacity, their pH will be lowered as they equilibrate with soil. Thus, a positive correlation is expected between pH and the presence of fresh paspurrias in soils. From the pH distribution (Fig. 2a), the industrial section, in the North part of the site, seems to contain higher amounts of fresh paspurrias than the southern sections. Total As was extremely variable (Fig. 2b), reaching values in some samples of *ca.* 2% As by weight (Table I). Most samples in the industrial section showed values above 250 mg/kg, which is the soil cleanup level considering a target cancer risk level of 10^{-4} for residential soil use, while the limit for industrial soil use is 500 mg/kg *(25,26)*. Samples in the southern area showed values below 250 mg/kg in general. In Fig. 2b, 50 mg/kg is taken as a background As value for Mexican semi-arid soils *(8,26)*. Total concentrations both of As and metals decreased rapidly with depth (results not shown), tending towards their background values. Of the potentially toxic elements, Pb and Zn showed the highest average concentrations (Table I) followed by Mn and Cu, and Cd with the lowest values. Soluble As in the industrial section (North) showed values in general below 5 mg/L (Fig. 2c), which is the Mexican limit to defines a waste as toxic *(27)*, but higher than 0.5 mg/L, which is the criterion limit for cleanup of polluted soils in Mexico *(28)*. In the southern section of the site, soluble values found were below this limit (Fig. 2c). In Fig. 2c, the USEPA As limit in drinking waters (0.05-mg/L) was used as reference *(29)*.

A positive linear correlation between total and soluble As was found for total As values above 1,250 mg/kg (not shown), which suggests these samples are composed mostly of residues not reacted with soil, and thus are difficult to equilibrate under the extraction conditions. Below 1,250 mg/kg total As, soluble As was independent of total As (Fig. 3), and instead an empirical correlation was found showing it directly dependent both on total calcium and pH. This behavior may be explained considering that the original wastes contained high concentrations of Ca solids at high pH. At lower pH after reacting with soil, soluble calcium increases and may leach downwards, decreasing total calcium contents in the upper horizons, while soluble As decreases (Figs. 2c, 3).

A comparison of the experimental aqueous As concentrations with the theoretical solubilities of two predominant calcium arsenates (Fig. 4) (which are likely the main As source of the original wastes in soils) shows that samples with high pH are close to the solubility lines of systems closed to CO_2. Aqueous As concentrations for open systems are predicted to be much higher at pH values above 8 (Fig. 4) because carbonate ions substitute arsenate ions in binding and precipitating calcium, and thus liberate the former to the aqueous phase. However, since the wastes already contain high concentrations of $CaCO_3$ to begin with, their behavior at high pH seems to follow in effect that of closed CO_2 systems, despite their being open to the atmosphere (Fig. 4). As pH decreases,

Downloaded by UNIV MASSACHUSETTS AMHERST on September 11, 2012 | http://pubs.acs.org
Publication Date: October 3, 2005 | doi: 10.1021/bk-2005-0915.ch017

aqueous As concentrations are orders of magnitude lower than those predicted by the simple solubility of Ca-arsenates even in the closed systems (Fig. 4).

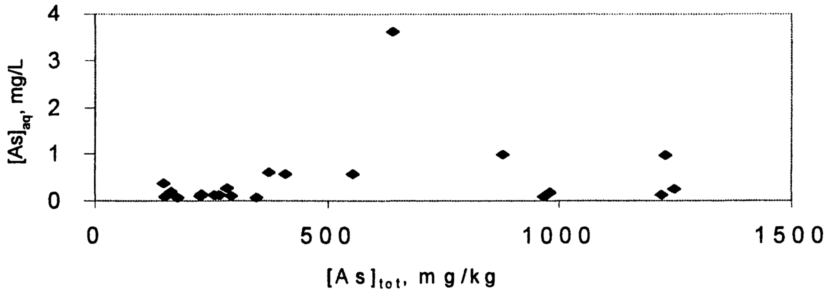

Figure 3. Relation between total [<1250 mg/kg)] and soluble As in MONT samples.

Table I. Total Element Content (mg/kg) Statistics for all Soils of Each Study Site

	As	*Pb*	*Zn*	*Cd*	*Cu*	*Mn*	*Fe*	*Ca*
SLP site (rhyolite soils)								
Median	995 (187)*	1467 (488)*	604	42	1183	nd#	nd#	Nd#
Interval	405-9340 (35-2420)*	903-24615 (67-3180)*	177-5267	5-594	102-15099			
MONT site								
Median	981	6750	3029	23	244	592.5	38550	119500
Interval	<1-20400	194-111000	191 - 51500	<3-573	5-594	107-2875	7000-171100	60000-278000

*These data correspond to the alluvial soils.
#nd = not determined

We modeled the final predicted equilibrium in the system by including thermodynamic solubility constants of pure heavy metal arsenates. For this, we considered for each sample the total As and metals concentrations, individually, as well as all other total components, and let the final state be dictated by the most insoluble phases at equilibrium. The underlying assumption was the availability of all species to react with each other (i.e., kinetic and other constraints were ignored). Predictions yielded As solubilities controlled by metal arsenates other than those of Ca and Fe(III), depending on the pH region (Fig. 5), with values much closer to those found experimentally.

Downloaded by UNIV MASSACHUSETTS AMHERST on September 11, 2012 | http://pubs.acs.org
Publication Date: October 3, 2005 | doi: 10.1021/bk-2005-0915.ch017

Downloaded by UNIV MASSACHUSETTS AMHERST on September 11, 2012 | http://pubs.acs.org
Publication Date: October 3, 2005 | doi: 10.1021/bk-2005-0915.ch017

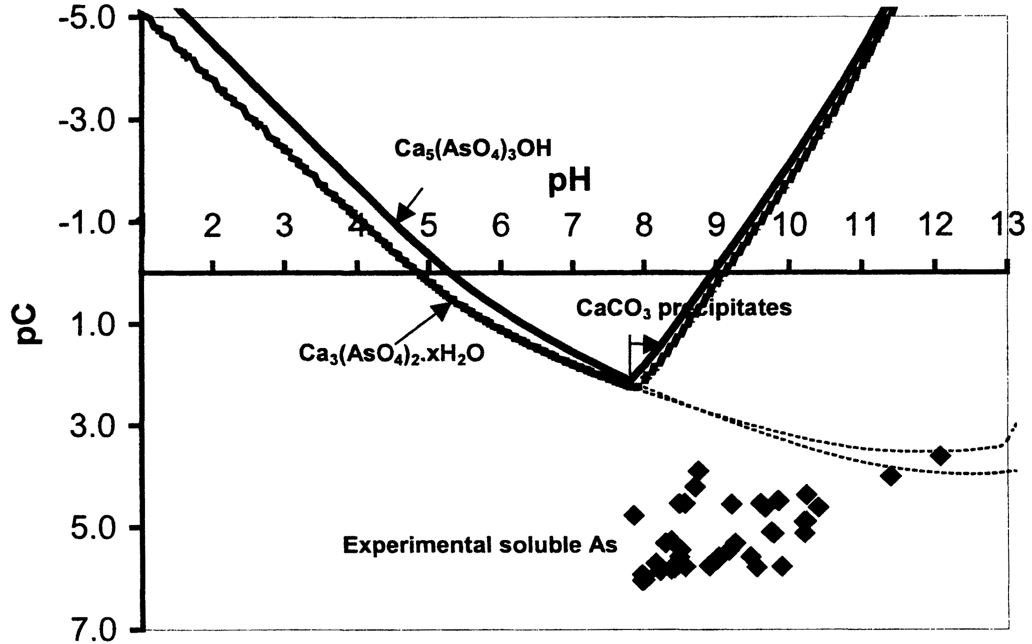

Figure 4. Solubility diagram of two common calcium arsenates in open (thick lines) and closed (dashed lines) atmospheric CO_2 systems, and comparison with aqueous concentrations in superficial soils of MONT study site. Thermodynamic data taken from (31) and (34). $I=0.01M$.

Downloaded by UNIV MASSACHUSETTS AMHERST on September 11, 2012 | http://pubs.acs.org
Publication Date: October 3, 2005 | doi: 10.1021/bk-2005-0915.ch017

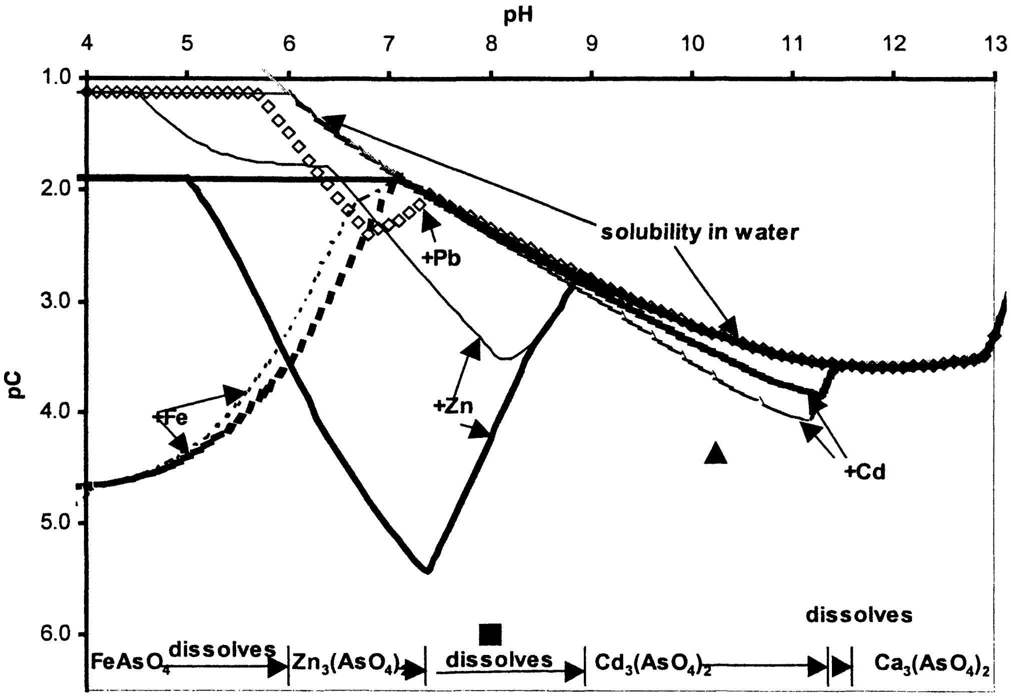

Figure 5. Solubility of calcium arsenates in the presence of $CaCO_3$ *and the total metal concentrations of two MONT sampling points, experimental data (symbols) and thermodynamic predictions for each metal individually (lines): square (As tot = 967mg/kg) – thick lines; triangle (As tot = 5620 mg/kg) – thin lines. The description of arsenate formation tendencies in the lower part applies to the thick lines. Thermodynamic data taken from (31,34,35). I=0.01M.*

Figure 5 shows examples for two sampling points with different total As and metals concentrations. Arsenic solubility is predicted to be controlled sequentially, as pH increases, by Fe(III) at low pH, by Zn at circumneutral pH, by Cd at high pH, and finally by Ca at the highest pH values. Lead arsenates may play a small role in the circumneutral region if the total Zn concentration decreases sufficiently, as is shown for the conditions of the sampling point represented by the thin lines (triangle, Fig. 5). The two experimental aqueous As values (symbols – Fig. 5) are still found below the predicted values, but lie much closer than when compared to the predicted Ca- arsenate solubility. The actual solids controlling As solubility in the soil samples are probably mixed-metal arsenates, for which no solubility data is available, but which likely show solubilities that are close to those of pure metal arsenates [probably intermediate between those of the pure individual components *(17)*]. The results shown in figure 5 suggest that As solubility is controlled in these specific points by Zn-containing arsenates in one case, and Cd-containing arsenates in the other.

Further evidence using a SEM coupled with EDS elemental analysis on selected As-rich soil particles of low As solubility showed the following results in mole%: 18.6 Ca, 5.5 Zn, 5.0 As, 1.6 Si, 1.5 Mg, 0.9 Al, 0.8 Pb, confirming the possibility of associations of these elements (especially Ca, Zn, and As) in highly insoluble, probably mixed metal-calcium arsenates. Preferential association of As with Zn has been confirmed by μ-X-ray fluorescence mapping work on soil particles of this site using a synchrotron source *(30)*, although associations with Pb were also found, as well as some with Fe.

SLP Site

Alluvial soils (Morales District) showed very homogeneous pH values (8.1 ±0.25), while the rhyolite soils showed pH values from 4 to 8 (Fig. 6a). Regarding total and water-soluble As (Fig. 6b and c), alluvial soils showed a considerable range of concentrations with no obvious significant correlation with location, nor between total and soluble values. The rhyolite soils showed higher values of total As than the alluvial soils, but within the high range of the soluble values found in the latter (Fig. 6c). The highest soluble As concentrations found were 5 mg/L, but a considerable number of samples showed values below 0.5 mg/L. These values are orders of magnitude lower than the theoretical solubility of As_2O_3 (considered the source pollutant from the smelter) of 28,000 mg As/L. Also, they are one to two orders of magnitude lower than the experimental As solubility values obtained under the same extracting conditions for product and sub-product samples of the smelting plant, considered the contaminant sources (Table II, Fig. 7). Although soluble As was found in higher concentrations than the other metals (except in dusts of converters – Table II), metal solubility in general was high, suggesting relatively high availability for reaction with As(V) after As(III) oxidation.

Downloaded by UNIV MASSACHUSETTS AMHERST on September 11, 2012 | http://pubs.acs.org
Publication Date: October 3, 2005 | doi: 10.1021/bk-2005-0915.ch017

The considerably lower solubility of As in contaminated soils, compared to that in the original sources (sub-products, Fig. 7) suggests that equilibration processes occurring in soils promote a decrease in the mobility of the As source, as observed in the MONT site. Although sorption processes to surface-active soil minerals are possible, we hypothesize the formation of highly insoluble most likely mixed heavy metal arsenates after oxidation of the original As(III) source through prolonged contact with air.

Downloaded by UNIV MASSACHUSETTS AMHERST on September 11, 2012 | http://pubs.acs.org
Publication Date: October 3, 2005 | doi: 10.1021/bk-2005-0915.ch017

Table II. pH and Water-Soluble Concentrations (mg/L) of Elements in Smelter Products and subproducts of SLP Site (1:20 solid:liquid)

Product	*pH*	*As*	*Pb*	*Cd*	*Zn*	*Cu*
Black As	3.92	1421.5	6.7	21.9	68.4	0.2
Furnace Dusts	6.21	878	4.2	102	105	< 0.04
Dusts of Converters	5.13	43.9	4.3	56.3	193	147
Calcines	6.24	67.2	0.26	2.5	0.6	< 0.04

Thermodynamic calculations support this hypothesis because the solubilities of divalent Pb, Cu, Zn and Cd arsenates are predicted to be in the range of those observed experimentally (Fig. 7). Additionally, in rhyolite soils high negative correlations were found between soluble metals (results not shown) and soluble As (except with Zn). This supports metal arsenate solubility as controlling As availability from the generic solubility equilibrium: $M_3(AsO_4)_2\ _{(s)} = 3M^{2+} + 2AsO_4^{3-}$, where an increase in one of the ions causes a decrease in the other, even in the case of mixed-metal arsenates. However, in the alluvial soils very high positive correlations were found between soluble As and soluble Zn and Cu. This behavior would disagree with the hypothesis of metal arsenate precipitation, and suggests that other additional mechanisms may be taking place.

Results using SEM-EDS show an enrichment of high As-containing particles (24%) with Pb (27%) and Zn (11.3%), in addition to Si (23.8%), and lower concentrations of Ca (7.3%), Fe (4.3%), Cd (2.1%) and Cu (0.3%). This suggests As associations with the former metals in secondary minerals. This was confirmed by µ-X-ray fluorescence mapping work using a synchrotron source *(30)*, where a preferential association of As with Zn and Pb was found, although Fe was present in all particles analyzed. While it is possible that simultaneous but independent associations of these elements to a Si- or Fe-containing mineral is being manifested in these observations, it is hard to imagine a surface with similar affinity for anions (arsenate) as for cations (metals) at a fixed pH value, except perhaps for the occurrence of ternary

Downloaded by UNIV MASSACHUSETTS AMHERST on September 11, 2012 | http://pubs.acs.org
Publication Date: October 3, 2005 | doi: 10.1021/bk-2005-0915.ch017

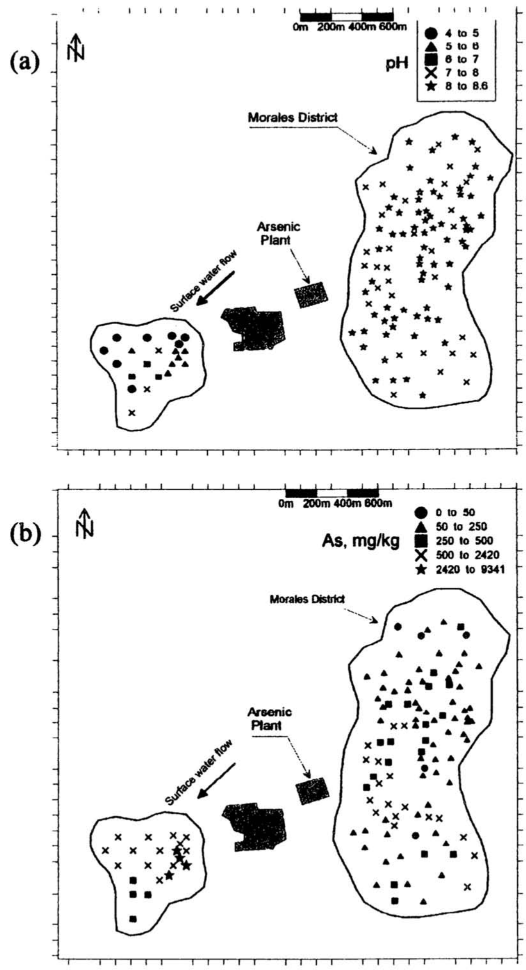
(a)
N
0m 200m 400m 600m
pH
● 4 to 5
▲ 5 to 6
■ 6 to 7
✕ 7 to 8
★ 8 to 8.6
Morales District
Arsenic Plant
Surface water flow
(b)
N
0m 200m 400m 600m
As, mg/kg
● 0 to 50
▲ 50 to 250
■ 250 to 500
✕ 500 to 2420
★ 2420 to 9341
Morales District
Arsenic Plant
Surface water flow

Figure 6. pH values (a); and arsenic contents in superficial soils overlaid on map of SLP study site, (b) total concentrations (mg/kg); (c) water-soluble concentrations (mg/L) in 1:20 ratio solid:liquid.

Downloaded by UNIV MASSACHUSETTS AMHERST on September 11, 2012 | http://pubs.acs.org
Publication Date: October 3, 2005 | doi: 10.1021/bk-2005-0915.ch017

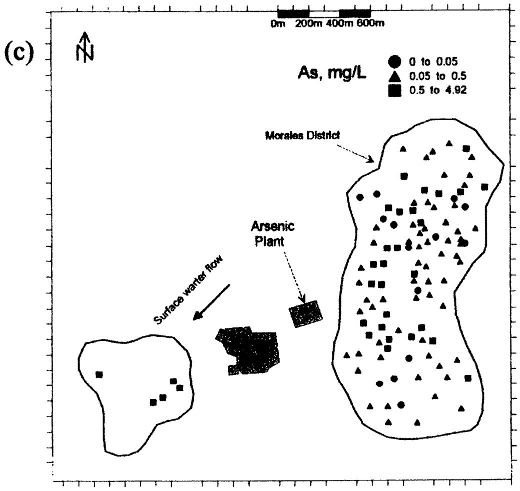
(c)
N
0m 200m 400m 600m
As, mg/L
● 0 to 0.05
▲ 0.05 to 0.5
■ 0.5 to 4.92
Morales District
Arsenic Plant
Surface warter flow

Figure. 6. Continued.

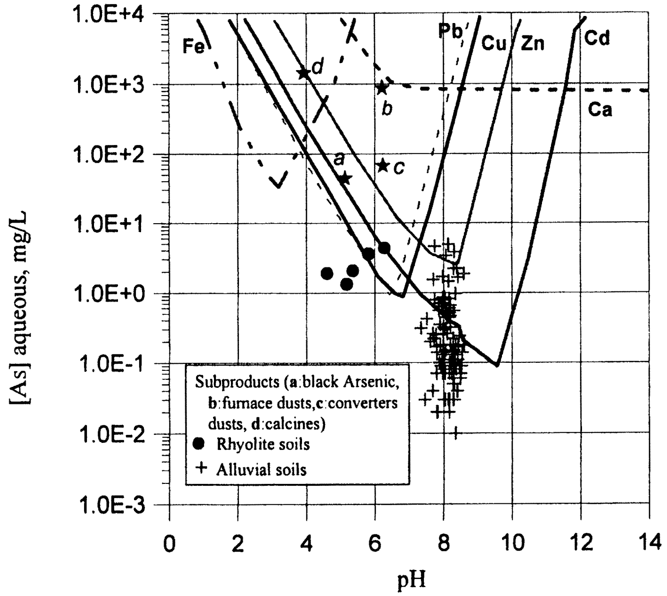

Figure. 7. Experimental values of aqueous As in soil samples and sub products of SLP site, and comparison to theoretical solubilities of different heavy metal arsenates. Thermodynamic data taken from (31,34,35). I=0.01M.

sorption complexes. This latter process would explain the positive correlations found between soluble elements in the alluvial soils.

Conclusions

Experimental evidence has been presented for heavy metal As-like solids controlling the solubility and likely mobility of As in soils impacted by oxidized As-containing wastes. Pure divalent heavy metal arsenate phases show thermodynamically much lower solubility than the Fe(III) and Ca counterparts, and a comparison with the experimental solubility observed in soil samples shows much closer values of dissolved As to the former rather than the latter arsenates. Additional evidence was obtained by SEM-EDS spectra, where As-containing particles were found enriched with heavy metals such as Zn and Pb, to the exclusion of Fe, identified in other studies as a major As sorbent. The actual phases responsible for the decrease in As solubility observed may include solid solutions of arsenates with varying proportions of Zn, Pb, and maybe other metals, such as Ca, Cu, Fe, etc. These heavy metals accompany As in the original contaminant sources. We propose the following mechanisms of arsenate phase formation after contact with soil: in the case of SLP, the As(III)-containing residues are oxidized in the presence of soil moisture and air; Fe is preferentially accumulated in slag after oxidation to Fe oxides at high temperatures in the smelter plants, as opposed to in As-containing atmospheric dusts. Thus, Fe oxides are not available to sorb As in non-slag wastes and emissions after air oxidation. In the MONT case a pH buffering action of the soil reduces the initial high pH of the residues deposited. Lead and Zn are amphoteric metals more soluble than Fe at the high pH of the process, forming negatively charged hydroxy species, which convert to neutral hydroxy and carbonated species as pH decreases *(31)*, and which in turn may interact with the arsenate ions. Additionally, the precipitated (hydr)oxides of these metals are expected to show higher pH values of points of zero charge, especially PbO, than those of Fe oxides *(32,33)*, and thus may interact with arsenate ions at higher pH values than Fe oxides. This way, quantitative arsenate sorption to small metal oxide particles may be a preceding mechanism for solid heavy metal arsenate formation. Currently, we are performing x-ray absorption studies to confirm the formation and to determine the exact molecular configurations and mechanisms of As–heavy metal formation in soil settings.

Acknowledgments

We would like to thank Carlos Briseño at the Institute of Geophysics, and Ivan Puente Lee, at the Chemistry School, both at UNAM, for the technical aid in electron microscope measurements. Also, to Dr. José Luz González at the Chemistry School, UNAM, for the valuable discussions in data analysis. For

Downloaded by UNIV MASSACHUSETTS AMHERST on September 11, 2012 | http://pubs.acs.org
Publication Date: October 3, 2005 | doi: 10.1021/bk-2005-0915.ch017

help in soil sampling and pre-treatment we thank Gerardo Martínez Jardines, Heriberto Rosas and José Santos Jallat, and technicians from LAFQA, UNAM. This work was funded by Industrial Minera México, and by the GTZ, Germany.

Downloaded by UNIV MASSACHUSETTS AMHERST on September 11, 2012 | http://pubs.acs.org
Publication Date: October 3, 2005 | doi: 10.1021/bk-2005-0915.ch017

References

1. Naqvi, S.M., Vaishnavi, C., and Singh, H. In: *Arsenic in the environment. Part II: Human health and ecosystem effects;* J.O. Nriagu, Eds.; Advances in Environmental Science and Technology; John Wiley: New York, NY, 1994; Vol. 27, chapter 4, pp. 55-91.
2. Harrington, J.M.; Fendorf, S.E.; and Rosenzweig, R.F. *Environ. Sci. Technol.* **1998,** *32,* 2425-2430.
3. Riveros, P.A.; Dutrizac, J.E.; and Spencer, P. *Can. Metall. Quart.* **2001,** *40,* 395-420.
4. Brown Jr., G.E., Foster, A.L., and Ostergren, J.D., *Proc. Natl. Acad. Sci. USA.* **1999,** *96,* 3388-3395.
5. Meng, X.; Jing, C.; and Korfiatis, P. In: *Biogeochemistry of environmentally important trace elements;* Y. Cai, O.C. Braids, Eds. American Chemical Society: Washington, D.C., 2003; pp. 70-83.
6. Smith, E.; Naidu, R.; and Alston, A.M. *Adv. Agron.* **1998,** *64,* 149-195.
7. Sadiq, M. *Water Air Soil Poll.* **1997,** *93,* 117-136.
8. Yan-Chu, H. In: *Arsenic in the environment. Part I: Cycling and characterization*; J.O. Nriagu, Ed. John Wiley: New York, NY, 1994; pp. 17-49.
9. Foster, A.L.; Brown Jr., G.E.; Tingle, T.N.; and Parks, G.A. *Am. Mineral.* **1998,** *83,* 553-568.
10. Roussel, C.; Neel, C.; and Bril, H. *Sci. Total Environ.* **2000,** *263,* 209-219.
11. Savage, K.S.; Tingle, T.N.; O'Day, P.A.; Waychunas, G.A.; and Bird, D.K. *Appl. Geochem.* **2000,** *15,* 1219-1244.
12. Craw, D.; Koons, P.O.; and Chappell, D.A. *J. Geochem Explor.* **2002,** *76,* 13-29.
13. Tye, A.M.; Young, S.D.; Crout, N.M.J.; Zhang, H.; Preston, S.; Bailey, H.; Davison, W.; McGrath S.P.; Paton G.I.; and Kilham K. *Environ. Sci. Technol.* **2002,** *36,* 982-988.
14. Neel, C.; Bril, H.; Courtin-Nomade, A.; and Dutreuil, J.-P. *Geoderma* **2003,** *111,* 1-20.
15. Paktunc, D.; Foster, A.; and Laflamme, G. *Environ. Sci. Technol.* **2003,** *37,* 2067-2074.
16. Paktunc, D.; Foster, A.; Heald, S.; and Laflamme, G. *Geochim. Cosmochim. Acta* **2004,** *68,* 969-983.
17. Davis, A.; Ruby, M.V.; Bloom, M.; Schoof, R.; Freeman, G.; and Bergstrom, P.D. *Environ. Sci. Technol.* **1996,** *30,* 392-399.

18. Morin, G.; Lecoq, D.; Juillot, F.; Calas, G.; Idelfonse, P.; Belin, S.; Briois, V.; Dillmann P.; Chevallier P.; Gauthier C.; Sole A.; Petit P.-E.; and Borensztajn S. *Bull. Soc. Geol. Fr.* **2002,** *3,* 281-291.
19. Lumsdon, D.G.; Meeussen, J.C.L.; Paterson, E.; Garden, L.M.; and Anderson, P. *Appl. Geochem.* **2001,** *16,* 571-581.
20. US-EPA, *Microwave assisted acid digestion of sediments, sludges, soils, and oils* Method 3051, USEPA, 1994.
21. ASTM, *Standard test method for shake extraction of solid waste with water* ASTM designation 03987-85, ASTM, 1985.
22. Loeppert, R.H.; Jain, A.; Abd El-Haleem, M.A.; and Biswas, B.K. *ACS Sym. Ser.* ACS: Washington, D.C., 2003; pp. 42-56.
23. US-EPA, *Atomic Absorption Methods* Method 7000B, USEPA, 1992.
24. US-EPA, *Antimony and Arsenic Atomic Absorption, Borohydride Reduction.* Method 7062, USEPA, 1994.
25. Valberg, P.A.; Beck, B.D.; Bowers, T.S.; Keating, J.L.; Bergstrom, P.D.; and Boardman, P. *Regul. Toxicol. Pharm.* **1997,** *26,* 219-229.
26. Gutiérrez-Ruiz, M.*20 collaborators. Diagnostico ambiental de la planta de Monterrey. Grupo Mexico - Industrial Minera Mexico.* Project report "Residuos Peligorsos-UNAM.GTZ y CIMA, SC", LAFQA, Instituto de Geografia, UNAM: Mexico, 2000, 389 pp.
27. Nom-052-ECOL-1993, *Que establece las caracteristicas de los residuos peligrosos, el listado de los mismos y los límites que hacen a un residuo peligroso por su toxicidad al ambiente.* Diario Oficial de la Federación, 22 de Octubre de 1993, México.
28. Anteproyecto, *de Norma Oficial Mexicana que establece criterios para determinar niveles de limpieza para la remediación de suelos contaminados por metales y metaloides.* México, 2004.
29. USEPA, *Code of Federal Regulations* 1999, 40 CFR 141.11
30. Marcus, M.A.*Unpublished* Advanced Light Source, Lawrence Berkeley National Laboratory, Berkeley, California.
31. Schecher, W.D.; and McAvoy, D.C. *MINEQL+. A chemical equilibrium modeling system. Version 4.0 for windows;* Environmental Research Software: Hallowell, ME, 1999.
32. Kosmulski, M.*J. Colloid Interface Sci.* **2002,** *253,* 77-87.
33. Kosmulski, M.*J. Colloid Interface Sci.* **2004,** *275,* 214-224.
34. Bothe, J.V., Jr.; and Brown, P.W. *Environ. Sci. Technol.* **1999,** *33,* 3806-3811.
35. Papelis, C.; Hayes, K.F.; and Leckie, J.O. *Hydraql: A program for the computation of chemical equilibrium composition of aqueous batch systems including surface-complexation modeling of ion adsorption at the oxide/solution interface* Technical Report No. 306, Stanford University, Dept. of Civil Engineering: Stanford, CA, 1988, 130 pp.

Downloaded by UNIV MASSACHUSETTS AMHERST on September 11, 2012 | http://pubs.acs.org
Publication Date: October 3, 2005 | doi: 10.1021/bk-2005-0915.ch017

Downloaded by PENNSYLVANIA STATE UNIV on September 12, 2012 | http://pubs.acs.org
Publication Date: October 3, 2005 | doi: 10.1021/bk-2005-0915.ch018

Chapter 18

Modeling Seasonal Arsenic Behavior in the Waikato River, New Zealand

Jenny G. Webster-Brown and Vincent Lane

SGES Environmental Science, University of Auckland, P.O. Box 92019, Auckland, New Zealand

Abstract

Significant seasonal variations occur in As concentrations in the Waikato River, a major lowland river in New Zealand. The As is of geothermal origin, and an acceptable explanation for the seasonal change has proved elusive. Data for As and Li concentrations from a monthly river water quality monitoring program, together with data from a recent study of suspended particulate material (SPM) and As in the lower catchment, have provided the basis for a new hypothesis; that the summer maximum in As concentration represents conservative behavior of the geothermal As from the upper catchment, and the winter minimum is due to the combined effects of greater dilution of geothermal fluid flow in river waters, and a greater degree of As adsorption onto Fe oxide-rich, winter SPM. To test this hypothesis, in-river and experimental As adsorption onto SPM has been modeled using a diffuse layer, surface complexation model, assuming Fe oxide to be the only adsorbing surface present. The model was able to reproduce the summer and winter seasonal variations in the degree of As adsorption onto SPM. However, during algal blooms in late summer and autumn, biological uptake by diatoms may also result in As removal from the water column.

In Advances in Arsenic Research; O'Day, P., et al.;
ACS Symposium Series; American Chemical Society: Washington, DC, 2005.

Introduction

The Waikato River is New Zealand's longest river, and is extensively used for industry, domestic, pastoral and agricultural water supply. The upper catchment includes a large area of natural geothermal activity, together with several geothermal power stations and 8 hydroelectric lakes (Figure 1). In the middle reaches of the river, near Hamilton city, the concentration of As in the Waikato River water typically ranges from 0.02 to 0.06mg/L (*1*). In the lower river, near Tuakau, the concentrations typically range from 0.01- 0.03mg/L (*2*). The As is predominantly present in dissolved form (73-100%; *2*), as inorganic As^V (*3*), and is entirely of geothermal origin (*4*).

A number of research studies have been undertaken into the behavior, toxicity and bioavailability of As in this river system (e.g., *1, 2, 3, 5, 6, 7, 8*). One aspect of As behavior that has so far defied conclusive explanation is the distinct seasonal trend, which shows a broad maximum in As concentration in summer and a minimum in winter (Figure 2). Various hypotheses have been proposed for this seasonal trend, including;

a) Desorption of As from sediments and suspended particulate matter (SPM) during the summer months, as a direct effect of temperature on the As^V adsorption process (e.g., *1*). The temperature typically ranges from 10-25°C. This direct effect has been effectively disproved in adsorption experiments (*2*), where little difference was observed in As^V adsorption onto SPM over the temperature range 5 - 30°C.

b) Abiotic or biotic reduction of sedimentary As^V to As^{III}, which is not as readily adsorbed onto sediment, resulting in As release into the water column (e.g., *1*). A review of thermodynamic data for As redox reactions indicated that a temperature increase of ~15°C would be unlikely to significantly increase abiotic reduction of As^V. However, bacteria capable of reducing As^V have been previously identified in the Waikato River and their activity was observed to be notably higher in summer (*12*). High concentrations of As^{III} in the water column have been detected periodically in the upper reaches of the river (e.g., *3*, *13*). However, fortnightly monitoring of dissolved AsV and AsIII throughout the lower catchment (at Tuakau) in 2003 by the authors showed that As^{III} did not exceed 10% of the dissolved As at any time, and was in fact lowest (0.7%) during the As maximum (0.038 mg/L), which occurred in May in 2003.

c) Periodic release of the As^{III} present in the anoxic basal layer of the stratified hydroelectric lakes, when the lake turnover occurs in autumn (*7*). This would result in a very short-term pulse of high As concentration in the water column, but does not appear to constitute an explanation for the consistently higher As concentrations throughout summer and autumn.

Downloaded by PENNSYLVANIA STATE UNIV on September 12, 2012 | http://pubs.acs.org
Publication Date: October 3, 2005 | doi: 10.1021/bk-2005-0915.ch018

Downloaded by PENNSYLVANIA STATE UNIV on September 12, 2012 | http://pubs.acs.org
Publication Date: October 3, 2005 | doi: 10.1021/bk-2005-0915.ch018

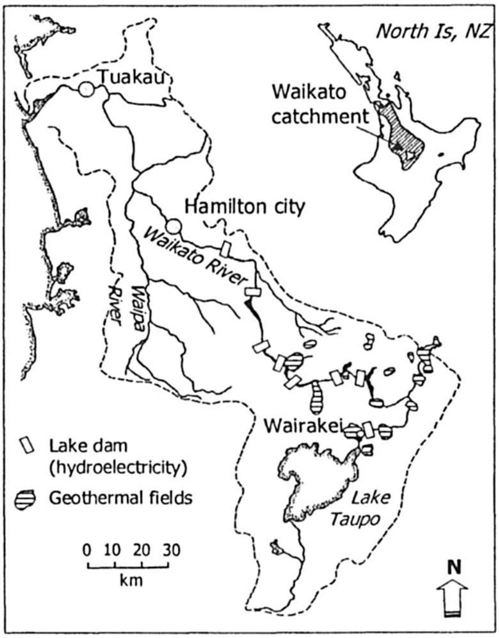
North Is, NZ
Waikato catchment
Tuakau
Hamilton city
Waikato River
Waipa River
Wairakei
Lake Taupo
Lake dam (hydroelectricity)
Geothermal fields
0 10 20 30
km
N

Figure 1. The Waikato River catchment, North Island, New Zealand, showing the positions of major geothermal fields and hydroelectric dams.

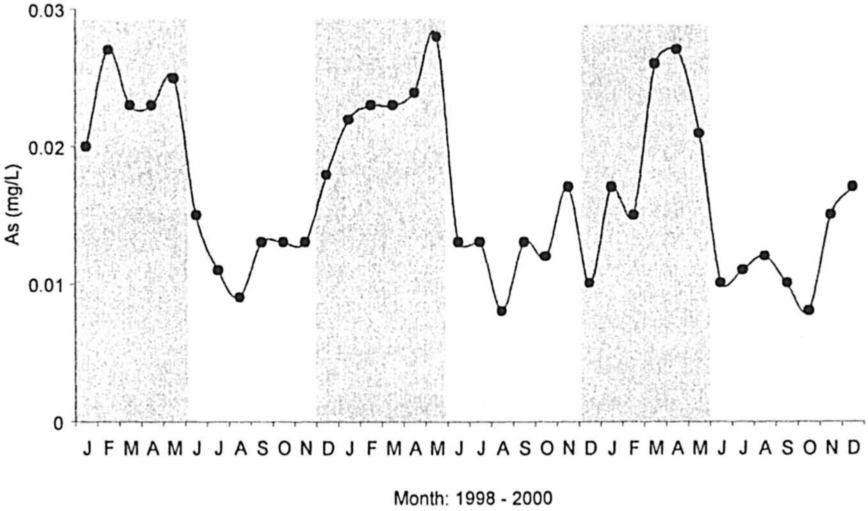

Figure 2. Seasonal changes in total As concentration in the lower Waikato River at Tuakau (9, 10, 11). Shaded areas = summer and autumn months.

Given the inability of each of these proposed hypothesis to fully explain As seasonal behaviour, a re-evaluation of As behavior in this river system has been undertaken using monthly chemical monitoring data for the Waikato River, collected over the last 10 years by the regional council "Environment Waikato" (e.g., *10*), and the results of a more detailed study of As and SPM at Tuakau (*2*). The assumption inherent in all of the previous hypotheses, that the summer maximum is in some way due to As release from the river sediments, is challenged. Instead it is proposed that the summer maximum represents conservative behavior of dissolved As at this time of year. The winter minimum is caused by a greater degree of geothermal fluid dilution in the higher river flows of winter, combined with greater As adsorption onto the more Fe oxide-rich SPM which occurs after the algal growth in summer and autumn has ended. To test this hypothesis, in-river and experimental As adsorption onto SPM has been modeled using a diffuse layer, surface complexation model, assuming Fe oxide to be the only adsorbing surface present.

Downloaded by PENNSYLVANIA STATE UNIV on September 12, 2012 | http://pubs.acs.org
Publication Date: October 3, 2005 | doi: 10.1021/bk-2005-0915.ch018

Seasonal changes in As concentrations and SPM composition

Arsenic concentration

Monthly water quality monitoring data for Li and "total" As concentration have been used in this analysis of seasonal variability. Sampling and analytical methods are outlined in detail in Wilson (*10*); Li has been determined on an unfiltered water sample by ICP-mass spectrometry (ICP-MS) and "total" As on an unfiltered water sample subjected to a nitric acid digestion, also by ICP-MS.

Some degree of seasonal variation in As concentration might be expected as a direct consequence of changing river flow rate, with greater dilution of the geothermal fluid input in winter when there is a higher rainfall. Indeed, monitoring data for other geothermal chemicals such as Li and B, which are known to behave conservatively, do show summer maxima and winter minimum due to dilution (e.g., data in *10*). However, the variation in As concentration is more extreme. This is evident in the seasonal change in the ratio of total As:Li (Figure 3). The weight ratio of total As:Li immediately downstream of the largest geothermal fluid input (at Wairakei) is relatively constant at 0.29 ± 0.02 (average and standard deviation for combined monthly data for 1998, 1999 and 2000). As shown in Figure 3, in summer this ratio persists into the lower reaches of the river (at Hamilton and Tuakau), with neither As nor Li being preferentially removed from or added to the water column. Similar trends in the As:Li ratio were evident in the data for every year since monitoring data collection commenced in 1993. Consequently, in summer the concentrations of As reflect conservative behavior.

Dilution of geothermal fluid in higher river flows in winter would affect both ions to the same degree. Therefore, if higher rainfall and higher river flow were responsible for the winter minimum, the As:Li ratio would remain more-or-less unchanged from summer to winter. However, this is clearly not the case, as the As:Li ratio decreases significantly over winter (Figure 3), suggesting a greater degree of removal of As from the water column. Chemical conditions in the river do not favour precipitation of As-bearing minerals, so the most likely mechanisms for As removal are uptake by biota or adsorption onto particulate material. Arsenic accumulation by aquatic plants has been reported from this river (*5*, *8*). However, the maximum growth period for plants, when they can remove dissolved As most effectively, is in spring and summer, rather than in winter. Arsenic uptake by phytoplankton is also a recognized phenomenon (e.g., *14*), but once again diatom growth occurs predominantly in summer and autumn, rather than in winter.

Therefore As removal by adsorption onto abiotic particles, particularly adsorption onto the reactive SPM in the water column, appears to be the most viable option. Significantly, there appears to be no consistent seasonal change in factors affecting As adsorption such as pH (typically within the range 7.2-7.9 at Tuakau; *10*) or major ion concentrations (*15*).

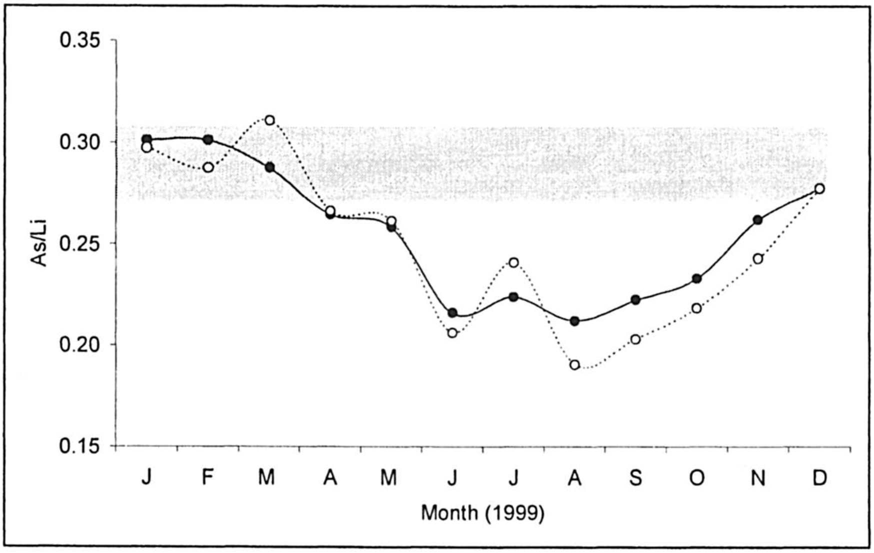

Figure 3. The weight ratio of total As:Li in the lower Waikato River, at Tuakau (○) and Hamilton (●) in 1999 (data from (10)). The shaded area shows the ratio (±SD) present in the upper Waikato River, immediately below Wairakei but upstream of the hydroelectric lakes.

Downloaded by PENNSYLVANIA STATE UNIV on September 12, 2012 | http://pubs.acs.org
Publication Date: October 3, 2005 | doi: 10.1021/bk-2005-0915.ch018

Composition of SPM

A more detailed study of Waikato River chemistry, including As, other trace element and SPM concentrations, and SPM characterization, was undertaken at Tuakau from November 1998 - November 1999. Details of sampling and analytical methods are given in Webster-Brown et al., (*2*). The standard, arbitrary definitions of "dissolved" as measured on a water sample after field filtration through a 0.45µm membrane, "acid-soluble" as measured in an unfiltered water sample acidified to pH<2 at the time of collection, and SPM as the particulate retained on the 0.45 µm membrane, have been used. Arsenic analysis was by hydride-generation AAS. The characteristics of the SPM which are most likely to influence its ability to adsorb As include mineralogy (particularly the amorphous oxide phases present), organic content and surface area. Therefore SPM retained on the filter membrane was digested in nitric acid to dissolve amorphous oxide phases, and analyzed by ICP-MS for Fe, Mn, Al and trace elements. Freeze-dried SPM was analyzed for TOC using a CHN analyzer and for surface area using *p*-nitrophenol adsorption.

Results of the Tuakau study indicated no consistent seasonal trend in SPM concentration in the water column, due to short-term responses to rainfall and surface run-off conditions. However, the TOC, Mn, Fe and Al content showed consistent, significant seasonal change (Figure 4).

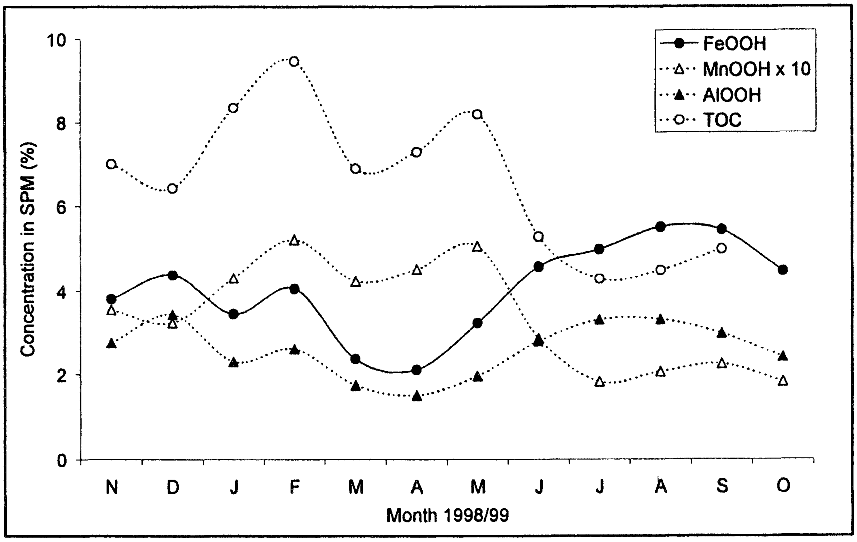

Figure 4. Seasonal variation in the Fe-, Al- and Mn-oxide (calculated as MeOOH) and TOC content of Waikato River SPM at Tuakau.

Downloaded by PENNSYLVANIA STATE UNIV on September 12, 2012 | http://pubs.acs.org
Publication Date: October 3, 2005 | doi: 10.1021/bk-2005-0915.ch018

The periods of highest TOC and Mn concentration in the SPM corresponded to diatom blooms of *Asterionella formosa* (in February) and *Melosira granulata* (in April/May), as identified by scanning electron microscopy. Diatoms are significantly greater than 0.45 μm in size and are consequently included in the SPM separated by filtration. The Fe and Al concentration of the SPM was generally low through this period, but increased after May, peaking in July - September when TOC was at its lowest concentration. In-river K_D calculations has shown a greater degree of As partitioning into the SPM at Tuakau during the winter months, with an average log $K_D = 3.79 \pm 0.05$ in late summer-early autumn, compared to 4.12 ± 0.13 in winter-early spring (*2*). No relationship between K_D and the amount of SPM in the water column was apparent, indicating that the observed variation in As concentration can not be attributed to the "particle concentration effect", as has been proposed to explain seasonal variation in As concentration in Moira Lake in Canada (*14*).

Experimentally determined adsorption of As^V onto SPM collected from January, April and July (*2*) confirmed the ability of the July SPM to adsorb more As (up to 50% As adsorbed over a 24hr period), compared to January SPM (up to 30%) or April SPM (up to 20%). A direct relationship between the Fe or Al content and the ability of SPM to adsorb As was therefore evident. Arsenic has a strong affinity for Fe oxide (e.g., *16*) and previous identification of Fe oxide as the principal binding surface for As in Waikato River bed sediments (*17*), indicates that Fe oxide is the principal adsorbing surface for As in the SPM.

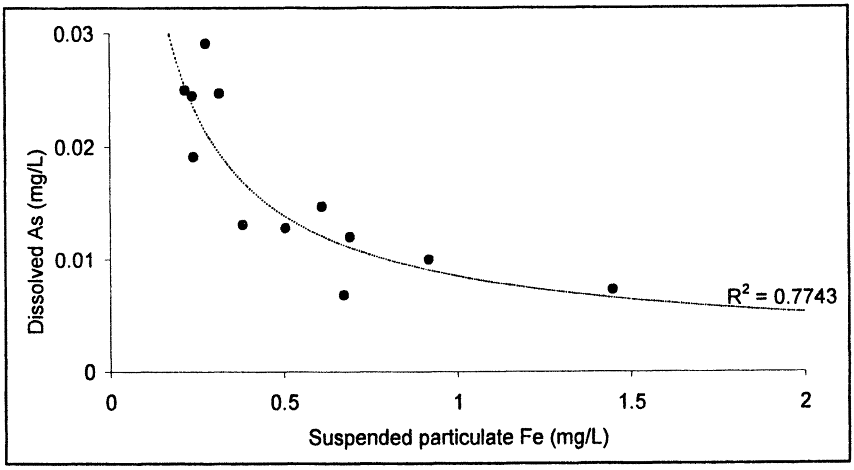

Figure 5. The relationship between dissolved As and the concentration of particulate Fe in the water column at Tuakau, between Nov 1998 - Nov 1999

Downloaded by PENNSYLVANIA STATE UNIV on September 12, 2012 | http://pubs.acs.org
Publication Date: October 3, 2005 | doi: 10.1021/bk-2005-0915.ch018

The negative correlation observed between dissolved As and the concentration of particulate Fe in the water column (Figure 5) provides further support for this association.

Modeling As adsorption onto SPM

In order to test the hypothesis that the seasonal variations in the Fe oxide content of the SPM influence As concentrations in the lower Waikato River, As adsorption onto Fe oxide in the SPM was modeled using surface complexation and the diffuse layer model. The MINTEQA2 code (*18*) was used, incorporating Dzombak and Morel's (*19*) surface complexation constants for hydrous ferric oxide adsorption (HFO), with the exception of As and Si adsorption constants which were taken from Swedlund and Webster (*16*). It was initially assumed that all Fe oxide was present as HFO, and that the surface characteristics for HFO, such as site density and surface area, were as defined by Dzombak and Morel (*19*). The suspended particulate Fe concentration was calculated in two different ways:

a) For adsorption edge modeling, the suspended particulate Fe concentration has been calculated from the Fe content of the SPM, and the SPM concentration.

b) For in-river modeling, the previous method led to high errors in river waters with low SPM concentrations. Consequently, the difference between dissolved and acid-soluble Fe was instead used to calculate suspended particulate Fe concentration. Good agreement between these two calculation methods of was observed for river waters with relatively high SPM concentrations.

Downloaded by PENNSYLVANIA STATE UNIV on September 12, 2012 | http://pubs.acs.org
Publication Date: October 3, 2005 | doi: 10.1021/bk-2005-0915.ch018

Experimental As adsorption edge modeling

The methods used for adsorption edge determination were those reported in Swedlund and Webster (*16*). Adsorption edges were measured on summer and winter freeze-dried SPM, using an inert 0.1M $NaNO_3$ electrolyte to reduce the effects of solution chemistry on ion activity. The allowed reaction time was 24 hrs, which has previously been shown to be sufficient for equilibrium As adsorption onto HFO (*16*). The SPM concentration was 100 mg/L, and (initial) As concentrations were 0.1, 0.5 and 1.0 mg/L. A concentration of 0.1mg/L As, corresponds to a weight ratio of As:SPM of 1:1000 which is closest to the mean in-river ratio of 1:1400 measured at Tuakau in 1998/99 (range: 1:370 to 1: 2800).

The pH range for As adsorption was correctly modeled, but the degree of adsorption was over-estimated (not shown), particularly at lower As:Fe ratios. The adsorption edges for 0.1mg/L As were better modeled if it was assumed that only 4-5% of the suspended particulate Fe was available to adsorb As (Figure 6). At higher As concentrations of 0.5mg/L and 1.0 mg/L, corresponding to As:SPM ratios of 1:200 and 1:100 respectively, the data was best modeled assuming 20% of the measured suspended particulate Fe concentration was available to adsorb As.

Downloaded by PENNSYLVANIA STATE UNIV on September 12, 2012 | http://pubs.acs.org
Publication Date: October 3, 2005 | doi: 10.1021/bk-2005-0915.ch018

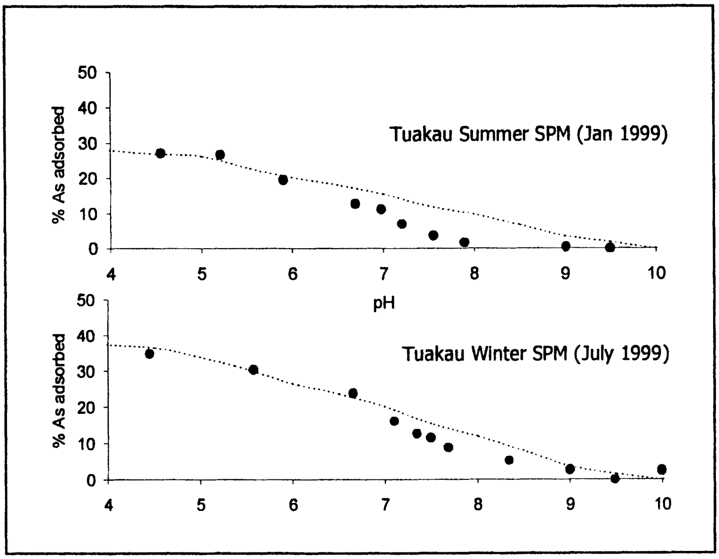

Figure 6. Experimental adsorption edges (•) for As (0.1mg/L) adsorption onto SPM (100mg/L), with modeled edges (---) shown for adsorption onto 0.11mg/L Fe for summer SPM (4% of total particulate Fe concentration) and 0.16mg/L Fe for winter SPM (5% of total particulate Fe concentration).

This suggests that the initial assumption that all Fe oxide in the SPM is present as, or is as reactive as, HFO may be incorrect. Possible explanations include the following:

a) The Fe oxide in the SPM is not entirely present as amorphous HFO, but includes other less reactive Fe oxide minerals or organic-bound Fe.

b) The Fe oxide is predominantly present as HFO, but is less reactive than the freshly-prepared amorphous HFO for which the surface complexation data in the model have been derived. This could be due to the effects of aging such as reduced surface area and site density due to particle aggregation and/or site occupation by adsorbed species. No attempt was made to remove any adsorbed species prior to the adsorption experiments, as their occupation of sites is a natural limitation on As adsorption, which must be considered.

Downloaded by PENNSYLVANIA STATE UNIV on September 12, 2012 | http://pubs.acs.org
Publication Date: October 3, 2005 | doi: 10.1021/bk-2005-0915.ch018

Notably when the Fe-rich winter SPM was acid-soaked (pH 3.5) for 48 hrs to remove adsorbed cations, acid-base titration data (not shown) indicated a similar adsorption site density (~ 0.003 mol/g Fe) to that of HFO (0.0037 mol/g Fe; *19*). This suggests that site occupation by adsorbed species, rather than mineralogical differences or aging effects, might be responsible for the reduced As adsorption.

In-River modeling

For modeling As behavior in the Waikato River at Tuakau, pH, dO_2, major ion and trace element data were all included in the MINTEQA2 geochemical speciation model so that competitive adsorption and solution complexing processes could be taken into account as far as possible. It was particularly important to include H_4SiO_4, which strongly competes with As for adsorption sites on Fe oxide (*16*). The lower Waikato River is relatively Si-rich (20-30 mg/L measured as H_4SiO_4), due to geothermal fluid inputs in the upper catchment. The MINTEQA2 model predicted that 40-60% of the adsorption sites on the Fe oxide could be occupied by Si under these conditions.

As might have been expected from the experimental adsorption modeling results, the model overestimated the degree of As adsorption in the Waikato River at Tuakau. The amount of As adsorbed to SPM, determined as the difference between dissolved and acid-soluble As, constituted between 1.5% and 27% of the As present in the water column (Figure 7). Assuming all of the suspended particulate Fe present in the water column was present as HFO and available to adsorb As, the model generally overestimated the degree of As adsorption. However, the model again provided a better fit to the observed data if it was assumed that ≤20% of the suspended Fe oxide was available to adsorb As (Figure 7).

The months of autumn, particularly April, appeared to be an exception. The inability of the model to reproduce the degree of As binding to SPM observed for April (and to a lesser extent for the other months of autumn), might be explained by considering processes other than adsorption. The April sample collection at Tuakau coincided with a *Melosira granulata* diatom bloom (*2*), and very high diatom concentrations were observed in March and May also. It is likely that As uptake by these diatom species contributed more to the As-SPM association observed at this time, than inorganic adsorption processes.

Downloaded by PENNSYLVANIA STATE UNIV on September 12, 2012 | http://pubs.acs.org
Publication Date: October 3, 2005 | doi: 10.1021/bk-2005-0915.ch018

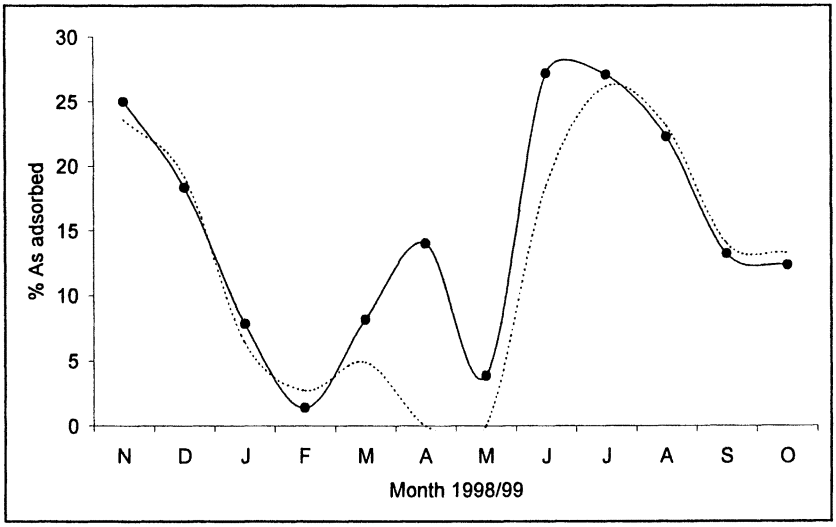

Figure 7. Observed As adsorption in the Waikato River at Tuakau (●), compared to As adsorption modeled (----) allowing the % reactive Fe oxide to vary between 5% and 20% to achieve the best fit to observed As adsorption for each month.

The predictive capability of these adsorption modeling results were tested by attempting to reproduce the summer maximum/winter minimum trend observed for dissolved As (Figure 8). For this exercise it was necessary to take dilution effects into account, so as a first step a theoretical total As concentration was calculated from the Li concentrations measured at Tuakau in 1998/99 (*10*) and the As:Li ratio of 0.29. Then a dissolved As concentration was calculated from this value, based on modeled adsorption for each month as shown in Figure 7.

General agreement with the measured dissolved As concentrations suggests that this model could be used to reliably estimate dissolved As concentrations in the lower Waikato River catchment for the purposes of environmental impact assessment, specifically assessment of As toxicity and bioavailablity. A slightly greater degree of As removal than could be modeled using dilution and adsorption is apparent in autumn, winter and spring. This is likely to be due to upstream removal of As bound to SPM, which will settle out of the water column in the more quiescent regions of the river, particularly in the lakes dammed for hydroelectricity generation. Measured dissolved As concentrations at Tuakau in January and February were, on the other hand, somewhat higher than predicted by the model. Arsenic concentrations measured 6 days later at this site (*10*) were in better agreement with the model (~0.023 mg/L) indicating that the values measured by the authors may be due to short-term fluctuations in As concentration.

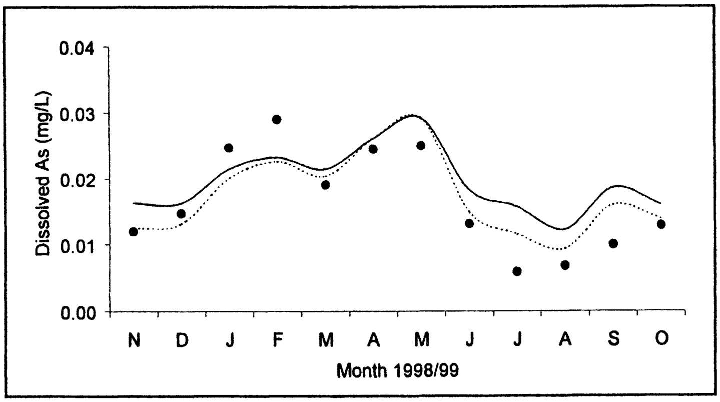

Figure 8. Measured dissolved As concentrations at Tuakau (•), theoretical total As based on Li concentrations (—), and dissolved As modeled (---) using this theoretical total As concentration and the adsorption parameters derived previously for Figure 7.

Summary

The proposed hypothesis; that the summer maximum in As concentrations in the Waikato River represents conservative behavior of dissolved As at this time of year, appears to be correct. This contradicts previous hypotheses, which attributed the summer maximum to As release, in various ways, from river sediments. The winter minimum is caused by the combined effects of dilution of geothermal fluid in higher river flows and a greater degree of As adsorption

Downloaded by PENNSYLVANIA STATE UNIV on September 12, 2012 | http://pubs.acs.org
Publication Date: October 3, 2005 | doi: 10.1021/bk-2005-0915.ch018

Downloaded by PENNSYLVANIA STATE UNIV on September 12, 2012 | http://pubs.acs.org
Publication Date: October 3, 2005 | doi: 10.1021/bk-2005-0915.ch018

onto the more Fe oxide-rich winter SPM. The latter effect can be modeled using a diffuse layer, surface complexation model, and allowing only part (5-20%) of the Fe oxide present in the water column to be available to adsorb As. The percentage of available, reactive Fe oxide was derived by modeling experimental adsorption data for As and SPM. This modeling approach was simple but effective, and well supported by surface complexation data for HFO. Further refinement of the model is anticipated. However, due to the high affinity of Fe oxide for As, there appears to be no need to invoke the more complex models proposed for trace element binding to SPM, such as the assemblage model (*20*), in which the individual adsorptive capacities of different mineral and organic surfaces in the SPM are combined, or the composite model (*21*), where surface complexation data are generated for the composite SPM surface without recourse to individual components.

However, application in other As-rich catchments has not yet been tested. It is likely that the portion of reactive Fe oxide in the SPM would need to be re-determined for new catchments, before this model could be more widely used in the study of As behaviour.

Acknowledgements

The help of Environment Waikato in providing access to their monitoring data is gratefully acknowledged, as is the contribution of Kerry Webster in the collection of data at Tuakau. This work has been funded by the Foundation for Research Science and Technology, and the University of Auckland, New Zealand.

Literature Cited

1. McLaren, S.J.; Kim, N.D. *Environmental Pollution,* **1995**, *90*, 67-93.
2. Webster-Brown J.G.; Lane V.; Webster K.S. *Proc. 22nd Geothermal Workshop, NZ,* **2000**, 63-68.
3. Aggett J.; Aspell A.C. *NZ J. Science,* **1980,** *23*, 77-82.
4. Timperley M.H.; Huser B.A. *NZ J. Marine & Freshwater Res.,* **1996**, *30*, 525-535.
5. Reay P.F. *J. Applied Ecology* **1972**, *9*, 557-565
6. Aggett J.; Kreigman M.R. *Water Research,* **1988**, *22*, 407-411.
7. Aggett J.; O'Brien G. *Env. Sci. Technol.,* **1985**, *19*, 231-238.
8. Robinson B.; Duwig C.; Bolan N.; Kannathasan M.; Saravan A. *Sci. Tot. Env.*, **2003**, *301*, 67-73.
9. Wilson B. *Env. Waikato Tech. Report,* **1999,** *14.*
10. Wilson B. *Env. Waikato Tech. Report,* **2000,** *7.*

11. Wilson B. *Env. Waikato Tech. Report,* **2001,** *6.*
12. Freeman M.C. *NZ J. Marine & Freshwater Res.,* **1985**, *19*, 277-282.
13. Polya D.A.; Lythgoe P.R.; Abou-Shakra F.; Gault A.G.; Brydie J.R.;Webster J.G.; Brown K.L.; Nimfopoulos M.K.; Michailidis K.M. *Min. Mag.*, **1998**, *67*, 247-261.
14. Faye M.S.; Diamond M.L. *Hydrobiologia*, **1996**, *324*, 117-123.
15. Webster-Brown J.G.; Webster K.S. *ESR/UoA Tech. Report.* **2000,** *10*
16. Swedlund P.J.; Webster J.G. *Water Res.,* **1999**, *33*, 3413-3422.
17. Aggett J.; Roberts L.S. *Env. Sci. & Technol.,* **1986**, *2*0, 183-186.
18. Allison J.D.; Brown D.S.; Novo-Gradac K.J. *US EPA Report,* **1991**, *EPA/600/3-91/021.*
19. Dzombak, D.A.; Morel, F.M.M. *Surface Complexation Modeling: Hydrous Ferric Oxide.* John Wiley & Sons, NY, 1990.
20. Lofts S.; Tipping E. *Geochim. Cosmochim. Acta,* **1998**, *62*, 2609-2625.
21. Davis J.A.; Coston J.A.; Kent D.B.; Fuller, C.C. *Env. Sci. & Technol.,* **1998**, 32, 2820-2828.

Downloaded by PENNSYLVANIA STATE UNIV on September 12, 2012 | http://pubs.acs.org
Publication Date: October 3, 2005 | doi: 10.1021/bk-2005-0915.ch018

Downloaded by UNIV OF GUELPH LIBRARY on September 11, 2012 | http://pubs.acs.org
Publication Date: October 3, 2005 | doi: 10.1021/bk-2005-0915.ch019

Chapter 19

The Application of Rapid Small-Scale Column Tests in Iron-Based Packed Bed Arsenic Treatment Systems

Mohammad Badruzzaman and Paul Westerhoff

Civil and Environmental Engineering Department, Arizona State University, Tempe, AZ 85287–5306

The rapid small-scale column test (RSSCT) is applicable to simulate pilot-scale performance for arsenate adsorption onto porous iron-based adsorbents. Commercially available granular ferric hydroxide (GFH) and Bayoxide Sorb33 (E33) have been evaluated for arsenate removal in this study. The BET surface area of GFH is 236 m^2/g and for E33 is 129 m^2/g. Both GFH and E33 possess identical pore size distribution. Proportional diffusivity (PD) and constant diffusivity (CD) based RSSCTs have been conducted with GFH and E33 and compared against corresponding pilot column performance. PD-RSSCTs simulated pilot column breakthrough curves reasonably well, but CD-RSSCTs failed to correspond pilot scale performance. The column arsenate adsorption density (q_{column}) varies from 0.3 – 0.4 μg arsenate/mg dry GFH and 0.3-1.53 μg arsenate/mg dry E33 for GFH and E33 respectively depending upon water quality.

In Advances in Arsenic Research; O'Day, P., et al.;
ACS Symposium Series; American Chemical Society: Washington, DC, 2005.

Introduction

Arsenic contamination of drinking water is a global problem. Arsenic is present in the aquatic environment in both organic (i.e. methylated) and inorganic forms caused by weathering and dissolution of arsenic bearing minerals, rocks and ores (*1*). Arsenic usually occurs as arsenate (As(V)) or arsenite (As(III)) in surface and ground waters used as raw potable water supplies. Arsenate (H_3AsO_4, $H_2AsO_4^-$, $HAsO_4^{2-}$, or AsO_4^{3-}) occurs in anionic form over the pH range of 5 to 12. Arsenite (H_3AsO_3, $H_2AsO_3^-$, and $HAsO_3^{2-}$) occurs in a lower Eh waters. Arsenic is classified as a Class A human carcinogen because of carcinogenic (prone to cancer of the bladder, lungs, skin, kidney, liver, and prostate) and non-carcinogenic (harmful to neurological and cardiovascular systems) effects (*2*). The USEPA lowered the maximum contaminant level (MCL) for arsenic in drinking water from 50 μg/L to 10 μg/L in 2002, which will be enforced in 2006. The WHO, European Union and several counties have also recently lowered the recommended or required arsenic limit to 10 μg/L. The reduced MCL has increased the research need for arsenic treatment processes in the potable water supply systems and industrial discharges.

Arsenic treatment technologies include adsorption on metal hydroxides during coagulation or by adsorptive packed-beds, removal by ion exchange resins or membrane systems (*3-13*). But coagulation, membranes and ion exchange technologies might not be the feasible choices because of pretreatment requirements, high volume of waste brine handling and water loss associated with sewer disposal of waste brine. On the other hand, metal oxides/hydroxides packed adsorption systems are advantageous as the spent media is non hazardous and can be disposed to any municipal landfill (*14*).

Many forms of adsorbents have been emerged recently for arsenic removal, but iron-based minerals have a high affinity for arsenic (*15-17*). Several porous/nonporous adsorbents such as granular ferric hydroxide (GFH), Bayoxide E33, zero valent iron, sulfur modified iron, activated alumina, iron modified activated alumina, magnesium impregnated activated alumina, TiO_2 etc. have been investigated for arsenic removal efficiency and adsorption mechanisms either through conventional batch isotherms or kinetic studies and using advanced electrochemical and spectroscopic instruments (*14, 18-20, 22*). Isotherms yield useful information on comparison of the adsorbents and the magnitude of competitive effects, but as a static equilibrium test, the extension of isotherm data is limitedly applicable to estimate important operational parameters. Moreover, batch experiments do not simulate the hydrodynamic condition of full-scale system. So the application of packed bed column experiments generating the breakthrough curves or the operation life of the adsorbents is very critical. But pilot tests are costly and could delay implementation of full-scale treatment systems design and construction. So there

Downloaded by UNIV OF GUELPH LIBRARY on September 11, 2012 | http://pubs.acs.org
Publication Date: October 3, 2005 | doi: 10.1021/bk-2005-0915.ch019

is a need to develop a mini-column test to shorten the duration of pilot-column tests.

Rapid small-scale column tests (RSSCTs) have been applied over the last two decades for simulating pilot-scale performance of organic micropollutants and natural organic matter (NOM) removal by granular activated carbon (GAC) (*23-29*). The adsorption mechanisms of inorganic compounds (arsenic) onto metal oxides are different from organic compounds adsorption onto porous activated carbon, as inorganic ions form inner-sphere complexes whereas organic compounds are adsorbed due to hydrophobic (van der waals) interaction. However, in both cases intraparticle diffusion appears to be rate the limiting mass transport process (*30*, *37)*. Therefore, the authors hypothesize that RSSCTs developed for organic compounds and activated carbon would be applicable to simulate full/pilot plant performance of arsenic adsorption onto metal hydroxides such as GFH and E33 with fraction of water, time and cost required to conduct field testing. The rationale of this research is to extend the theory and experimental methodologies of RSSCTs. The specific objectives of this study are: a) physical characterization of GFH and E33, b) evaluation of different approaches of RSSCTs through mini-column experiments, c) comparison of RSSCTs to pilot column performance and to determine appropriate scaling approach, and d) comparative evaluation of the performance of GFH and E33. This paper concentrates on arsenate removal from groundwater of the southwestern parts of the Unites States, primarily Arizona.

Downloaded by UNIV OF GUELPH LIBRARY on September 11, 2012 | http://pubs.acs.org
Publication Date: October 3, 2005 | doi: 10.1021/bk-2005-0915.ch019

Scaling Procedure

The dispersive flow pore surface diffusion model (DFPSDM) has been considered as the closest mathematical formulation of the performance of full-scale adsorber, as it considers three important mass transfer mechanisms such as - film diffusion, pore and surface diffusion (*36*). Analytical solution of the DFPSDM was successful in a very limited basis for simulating the behavior of full-scale performance due to the variability of model parameters from the real systems. But the RSSCT, designed from the dimensionless parameters obtained from the DFPSDM, was successful for scaling down a full-scale adsorber to bench-scale for organics adsorption onto GAC.

Assumptions: First, boundary conditions for the full-scale and small-scale process must occur at the same dimensionless coordinate values in the dimensionless differential equations. Second, dimensionless parameters in the dimensionless differential equations must be equal for the full-scale and small-scale process. Finally, no change in mechanism can occur when reducing the size of the process.

Scaling Approach: The dimensionless groups, that are used in the DPSDM to describe the relative importance of different transport mechanisms, are -

Downloaded by UNIV OF GUELPH LIBRARY on September 11, 2012 | http://pubs.acs.org
Publication Date: October 3, 2005 | doi: 10.1021/bk-2005-0915.ch019

surface solute distribution parameter (D_g) or Capacity factor (C_f), Peclet number (Pe), Stanton number (St), surface diffusion modulus (Ed_s), and pore diffusion modulus (Ed_p). Equating the dimensionless quantities for small and large column dimensions, the operational design parameters for the RSSCT such as empty bed contact time (EBCT), loading rate, etc have been developed. Regarding intraparticle diffusion, the adsorption of organic compounds by activated carbon demonstrated that surface diffusion typically dominates over pore diffusion (*33, 34*). The adsorption of metal cations by porous iron oxide has also been reported as surface diffusion dominating adsorption process *(32)*. Therefore, the authors assumed that intraparticle transport of arsenate onto porous sorbents is also controlled by surface diffusion. Therefore, equating the surface diffusion modulus (Ed_s) for small (SC) and large (LC) column the equation 1 can be generated:

$$\frac{EBCT_{LC} * D_{s,LC} * D_{g,S,LC}}{R^2_{LC}} = \frac{EBCT_{SC} * D_{s,SC} * D_{g,SC}}{R^2_{SC}} \qquad (1)$$

As the pore solute distribution parameter (Dg) of large-column may be equal to the small- scale, the equation 1 can be re-written as equation 2:

$$\frac{EBCT_{LC}}{EBCT_{SC}} = \left(\frac{R_{LC}}{R_{SC}}\right)^2 * \left(\frac{D_{s,SC}}{D_{s,LC}}\right) \qquad (2)$$

Considering that surface diffusivity of arsenate (D_s) onto porous sorbents is dependent on the adsorbent particle size according to equation 3:

$$\frac{D_{S,SC}}{D_{L,LC}} = \left(\frac{R_{LC}}{R_{SC}}\right)^X \qquad (3)$$

From equation 2 and 3, the general equation for empty bed contact time (EBCT) and particle radius (R) can be expressed as the equation 4.

$$\frac{EBCT_{SC}}{EBCT_{LC}} = \left(\frac{R_{SC}}{R_{LC}}\right)^{2-X} \qquad (4)$$

Two different approaches of the RSSCT scaling can be established, as - constant (CD) diffusivity based RSSCT (CD-RSSCT) and proportional (PD) diffusivity based RSSCT (PD-RSSCT). The two approaches differ if D_s values are independent (for CD) or a linear function (for PD) of adsorbent radius. In other words, for CD-RSSCT and PD-RSSCT design, the values for X are zero and one, respectively should be used in equation 4.

Considering similar breakthrough spreading for small and large column, the Reynolds number of a small column would be equal to that of a large column along with other dimensionless parameters such as St and Pe. Consequently, following operational design equation for the RSSCT can be developed:

$$\frac{V_{F,SC}}{V_{F,LC}} = \frac{R_{P,LC}}{R_{P,SC}} \tag{5}$$

Where, $V_{F,SC}$ and $V_{F,LC}$ are loading rates of the small and large columns respectively. Experience with organic adsorption onto GAC suggests that for PD-RSSCT, equation 5 yields a long column and consequently generates an excessive pressure drop (*39*). As film diffusion is not important, the flowrate of mini-column can be reduced by the ratio of the product of the Reynolds and Schmidt number (Sch) in equation 5 until the dispersion does not become important. The modified form of equation 5 can be expressed as equation 6:

$$\frac{V_{F,SC}}{V_{F,LC}} = \frac{R_{P,LC}}{R_{P,SC}} * \frac{Re_{SC}.Sch}{Re_{LC}.Sch} \tag{6}$$

However, to ensure the similar dispersion effect for large and small-scale columns, the product of Reynolds number and the Schmidt number was mentioned in the mechanical range of 200-200,000 (*35*). The authors have experimented PD-RSSCTs for different values of the product of Re and Sch (Re_{sc}*Sch) and concluded that a value of 2000 can simulate full-scale performance reasonably well (*30, 37*). All PD-RSSCTs of this study have been conducted using the value of 2000 as Re_{SC}*Sch.

Downloaded by UNIV OF GUELPH LIBRARY on September 11, 2012 | http://pubs.acs.org
Publication Date: October 3, 2005 | doi: 10.1021/bk-2005-0915.ch019

Materials and Methods

Water Samples

Natural groundwater (DOC< 0.5 mg/L) from three different well sites of Arizona, USA was used in the column studies. W1 contained ~ 50 µg/L of arsenic at ambient pH of 8.9 and associated water quality data are: alkalinity ~ 156 mg $CaCO_3$/L, TDS of ~ 420 mg/L, and silica 22 mg/L. W2 contained 10 µg/L of arsenic with ambient pH of 7.8, alkalinity ~ 215 mg $CaCO_3$/L, and silica 31 mg/L. W3 contained 16.5 µg/L of arsenic, ambient pH of 8.27 and associated important water quality parameters are: TDS ~ 291mg/L, alkalinity ~ 214 mg $CaCO_3$/L, and silica ~52 mg/L, sulfate ~12mg/L, fluoride ~ 0.5mg/L, nitrate ~ 1.5mg/L.

Experiments

BET Surface Area. BET surface areas and pore size distributions of "virgin" GFH and E33 were determined from N_2 isotherm data collected at 77°K (Autosorb-1-MP, Quantachrome Corporation, Boynton Beach, FL). Prior to analysis particles were outgassed overnight at 423°K. The density functional theory (DFT) was used to calculate micropore volumes, mesopore volumes and micropore size distributions from the N_2 adsorption data (Vulcan kernel, PC software version 1.19, Quantachrome, Boynton Beach, FL). Standard methods were employed for the determination of moisture content (ASTM D2216) and packed bed porosity (ASTM D854-58) (*31*).

RSSCT Experiments. Laboratory columns consisted of 1.1 cm (Ace Glass, Vineland, NJ) diameter glass columns approximately 30.5 cm in length with Teflon end caps. Teflon tubing (3.2 mm) was used. Piston pumps with stainless steel heads were used (Fluid Metering Inc. Syosset, NY). Schematic of the set up is shown is Figure 1. Columns were backwashed to remove fine particles, by operating the column in upflow mode with distilled water until the effluent water ran clear. The typical backwashing flow rate for the RSSCT columns was in the ranges of 10-20mL/min and resulted in bed expansion of approximately 40%.

Pilot Columns. PVC pilot columns containing as-received media were operated by consulting (W1, W3) personnel and arsenic breakthrough data provided to the authors. Pilot columns were backwashed approximately every 3 to 4 weeks to prevent excessive pressure development. Temperatures of the pilot columns influent water were similar to raw water of the RSSCT column experiments.

Arsenic Analysis. All samples collected for arsenic analysis were preserved using nitric acid (JT Baker ultra pure reagent grade Ultrex II Nitric, Phillipsburg, NJ). A Varian SpectrAA-400 atomic absorption spectrometer (Palo Alto, CA) with a Varian Graphite Furnace Tube Atomizer, Zeeman background correction, and auto-sampler was used for analyzing the samples for dissolved arsenic.

Results and Discussion

Physical Characterization of GFH and E33

The BET surface area of GFH media was 231 m^2/g for 100x140 mesh size and 240 m^2/g for 10x30 mesh size, on an average 236 m^2/g. On the other hand,

Downloaded by UNIV OF GUELPH LIBRARY on September 11, 2012 | http://pubs.acs.org
Publication Date: October 3, 2005 | doi: 10.1021/bk-2005-0915.ch019

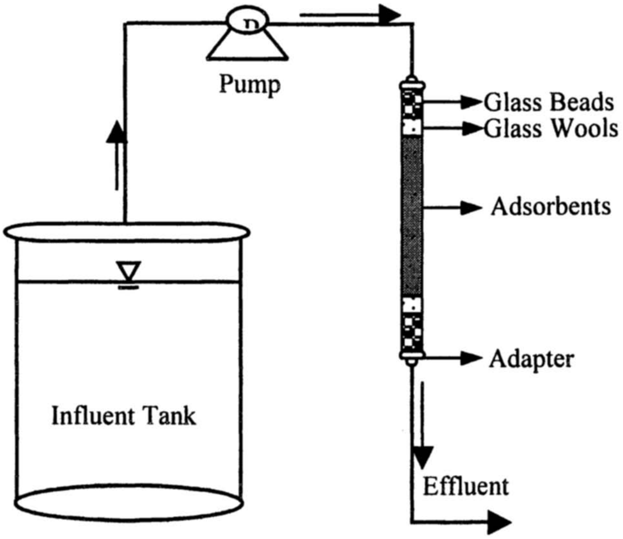

Figure 1. Schematic of the experimental set-up for Rapid Small Scale Column Tests (RSSCTs).

the BET surface area of E33 media was 128 m^2/g for 100x140 mesh size and 129 m^2/g for 10x30 mesh size, on an average 127 m^2/g. The BET surface area of "as received" medias were 227m^2/g for GFH and 129 m^2/g for E33. The variation of surface area as a function of media size is negligible. The pore volume distributions for the 100x140 mesh sizes of GFH and E33 are presented in Figure 2. Two major pore widths were detected such as - the micropore (<20Å) and mesopore (20 to 500Å) ranges. E33 particles are slightly more micro- porous than GFH particles. Pore size distributions of GFH and E33 for 10x30 mesh size, not presented here, also showed the similar trend of 100x140 mesh size.

CD-RSSCTs vs PD-RSSCTs

Figures 3 and 4 compare the breakthrough curves generated from CD-RSSCTs and PD-RSSCTs for GFH and E33 respectively. The breakthrough curves generated from PD-RSSCTs exert an initial lag period (i.e. undetectable

Downloaded by UNIV OF GUELPH LIBRARY on September 11, 2012 | http://pubs.acs.org
Publication Date: October 3, 2005 | doi: 10.1021/bk-2005-0915.ch019

Downloaded by UNIV OF GUELPH LIBRARY on September 11, 2012 | http://pubs.acs.org
Publication Date: October 3, 2005 | doi: 10.1021/bk-2005-0915.ch019

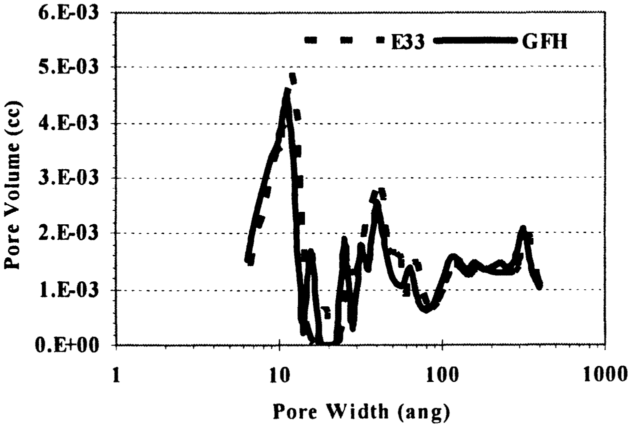

Figure 2. Pore size distribution of GFH and E33 for 100x140 mesh size particles.

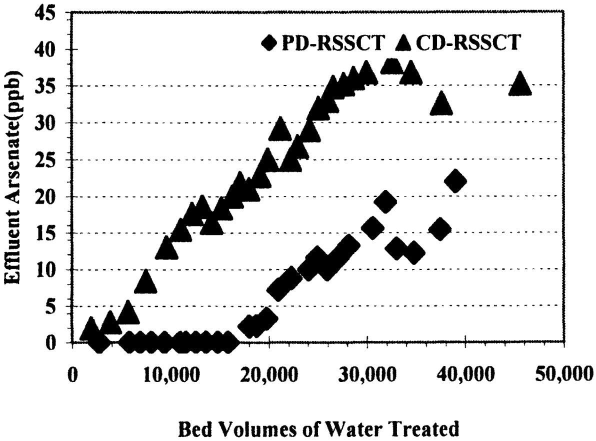

Figure 3. Comparison of the breakthrough curves of GFH for proportional diffusivity (PD-RSSCT) and constant diffusivity (CD-RSSCT) based approaches.

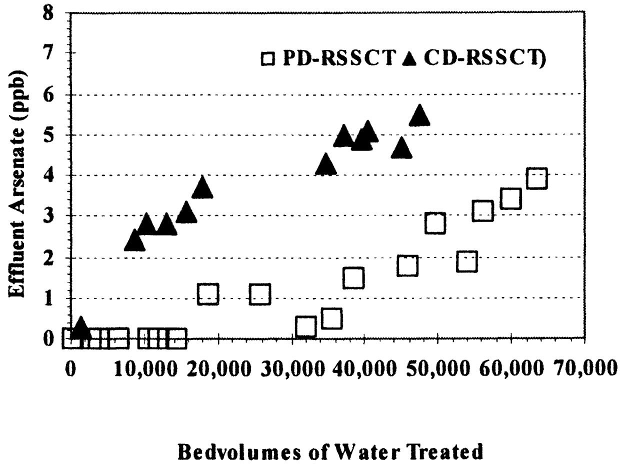

Figure 4. Comparison of the breakthrough curves of E33 for proportional diffusivity (PD-RSSCT) and constant diffusivity (CD-RSSCT) based approaches.

Downloaded by UNIV OF GUELPH LIBRARY on September 11, 2012 | http://pubs.acs.org
Publication Date: October 3, 2005 | doi: 10.1021/bk-2005-0915.ch019

arsenic concentration) up to 15-17 thousands of bed volumes, but arsenate concentration was detected in the effluent of CD-RSSCTs from 1-2 thousands of bed volumes (Figures 3 and 4). Moreover, the slope of breakthrough curves in the mass transfer zones for CD-RSSCTs is steeper than that of the PD-RSSCTs for both GFH and E33 (Figures 3 and 4). Adsorption density, q_{column} (i.e. the area above the breakthrough curve divided by the dry mass of the media) calculated for both CD-RSSCTs and PD-RSSCTs breakthrough curves (Table I). Table I shows that the adsorption density of CD-RSSCT (i.e. 0.12 μg arsenate/mg dry GFH) with GFH is only 35% of the adsorption density obtained from PD-RSSCT (i.e. 0.34 μg arsenate/mg dry GFH) for water 3. For E33 column CD-RSSCT could achieve the arsenate adsorption density (i.e. 0.83 μg arsenate/mg dry E33) only 50% of the PD-RSSCTs (i.e. 1.53 μg arsenate/mg dry E33) for water 1. Overall, the shape and the adsorptive capacity suggest that CD-RSSCTs generates faster breakthrough curves with lower arsenate adsorption than PD-RSSCTs. This discrepancy is might be due to adsorption kinetics. As arsenate transport into porous sorbents is limited by intraparticle diffusion, the faster flow-rate in CD-RSSCT does not allow sufficient time for arsenate molecule to travel to the innermost adsorption site.

Downloaded by UNIV OF GUELPH LIBRARY on September 11, 2012 | http://pubs.acs.org
Publication Date: October 3, 2005 | doi: 10.1021/bk-2005-0915.ch019

Table I. Dimensions and Operational Configurations of Pilot and Mini-columns.

Water Type	*Media Used, Scaling Type*	*As Con.(ppb), pH*	*Dimension (Diameter, Depth)cm*	*Simulated EBCT (min)*	*Mesh size*	*Re*Sch*	*Dry Mass (gm)*	*Loading Rate (m/h)*	*q_{Column} (μg/mg)*
W1	GFH, Pilot	50, 7.6	(19.2,101.6)	2.6	As received	30,304	31399.00	23.50	NA
W1	GFH, CD-RSSCT	50, 7.6	(1.05, 4.3)	2.6	140X170	15,000	2.20	137.70	0.12
W1	GFH, PD-RSSCT	50, 7.6	(1.1, 6.7)	2.6	140X170	2,000	3.9	30.60	0.34
W1	E33, Pilot	50, 7.6	(30.48, 85.34)	2.5	As received	26,053	42561.0	20.21	0.38
W1	E33, CD-RSSCT	50, 7.6	(1.05, 6.5)	2.5	140X170	26,053	2.10	239.70	0.17
W1	E33, PD-RSSCT	50, 7.6	(1.1, 6.5)	2.5	140X170	2,000	2.8	18.4	0.38
W2	E33-Pilot	10, 7.8	(30.48, 85.34)	2.5	As received	26,053	42561.0	20.2	NA
W2	E33, CD-RSSCT	10, 7.8	(1.05, 6.5)	2.5	140X170	26,053	2.8	239.7	0.83
W2	E33, PD-RSSCT	10, 7.8	(1.1, 6.5)	2.5	140X170	2,000	2.8	18.4	1.74
W3	GFH	16.5, 8.27	(30.48, 85.34)	2.5	As received	26,053	42561.0	20.2	0.4
W3	GFH, PD-RSSCT	16.5, 8.27	(1.1, 6.5)	2.5	140X170	2,000	3.6	18.4	0.33
W3	E33, PD-RSSCT	16.5, 8.27	(1.1, 6.5)	2.5	140X170	2,000	2.8	18.4	0.74

Comparison of RSSCTs and Pilot Columns

The breakthrough curves of RSSCTs using both CD and PD scaling approach have been compared against pilot column performance in Figure 5 and 6. Pilot column dimensions and operating conditions and scaled down RSSCTs configurations and operating conditions are summarized in the Table 1. Figure 5 illustrates the comparison of breakthrough curves of pilot column against CD-RSSCT and PD-RSSCT conducted with E33 with water 1. Up to 19 thousands of BVs the PD-RSSCT simulated the pilot column reasonably well, beyond that PD-RSSCT generated steeper breakthrough than pilot column. In terms of duration, PD-RSSCT reached an effluent concentration of 10μg As/L about 50% earlier than the pilot column. Table 1 depicts and indicates that the arsenate adsorption density calculated PD-RSSCT (i.e. 0.35 μg arsenate/mg dry E33) is very comparable to that of pilot column (i.e. 0.38 μg arsenate/mg dry E33) upto effluent arsenate concentration of 10μg/L. Figure 5 also illustrates that CD-RSSCT does not correspond to pilot column performance. Arsenate adsorption density of CD-RSSCT (i.e. 0.17 μg arsenate/mg dry E33) is only 50% of the adsorption density of the pilot column (i.e. 0.38 μg arsenate/mg dry E33). As the shape of the breakthrough curve of CD-RSSCTs using GFH and E33 are similar, it is expected that CD-RSSCT with GFH will not simulate pilot column performance. Westerhoff et al. (*37*) also concluded that CD-RSSCT with GFH did not simulate the pilot column. Figure 6 compares the performance of pilot column to the corresponding PD-RSSCT with GFH for water 3. Upto 30 thousands of BVs the breakthrough curve of RSSCT was right at the top of that of the pilot-scale, but beyond 30 thousands of BVs RSSCT showed a steeper media utilization rate than pilot column. According to Figure 6, PD- RSSCT reached effluent concentration of 10 μg-As/L about 25% earlier than the pilot column. As mentioned in Table 1, the arsenate adsorption density of PD-RSSCT (i.e. 0.33 μg arsenate/mg dry GFH) is very comparable to the adsorption density of pilot column (0.40 μg arsenate/mg dry GFH). The possible explanation for the tail-end mismatch of pilot columns and RSSCTs is the slight change in water chemistry (i.e. pH) of raw water of mini-columns from field sites due to transportation and storage or the limitation of scaling.

Overall, RSSCT designed by PD approach is a close approximation to the pilot-scale. Recent studies of the authors with GFH also justified that PD-RSSCT simulate pilot column performance (*37*). More over, model water kinetic experiments simulated with homogeneous surface diffusion model (HSDM) using GFH have showed the dependency of surface diffusivity on the adsorbent particle size and hypothesized a fundamental basis of the application of PD-RSSCTs for arsenate adsorption onto metal oxides (*38*).

Downloaded by UNIV OF GUELPH LIBRARY on September 11, 2012 | http://pubs.acs.org
Publication Date: October 3, 2005 | doi: 10.1021/bk-2005-0915.ch019

Downloaded by UNIV OF GUELPH LIBRARY on September 11, 2012 | http://pubs.acs.org
Publication Date: October 3, 2005 | doi: 10.1021/bk-2005-0915.ch019

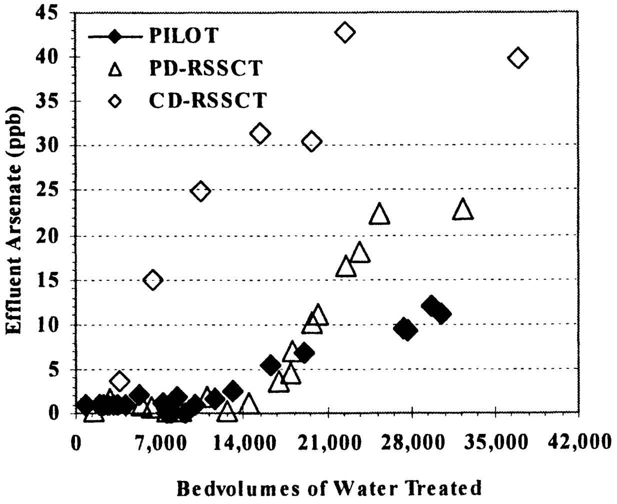

Figure 5. Comparison of breakthrough curves of pilot column against PD-RSSCT and CD-RSSCT for E33.

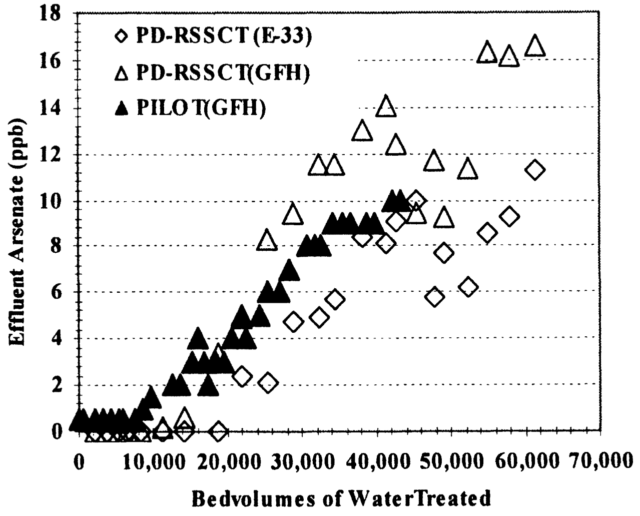

Figure 6. Comparison of breakthrough curves of pilot column (GFH) against PD-RSSCT with GFH and PD-RSSCT with E33.

Performance Evaluation of GFH and E33

Figure 6 shows the comparison of breakthrough curves generated from PD-RSSCT using GFH and E33 for water 3. Up to 15 thousands of BVs both GFH and E33 mini-columns generated an initial lag period and beyond that GFH column showed steeper mass utilization profile than E33 column. As shown in Figure 6, E33 can treat about 10,000 BVs of raw water than GFH for the water 3 until the effluent of the column reaches 10μg/L. As mentioned in Table 1 arsenate adsorption density of E33 column (i.e. 0.74 μg arsenate/mg dry E33) is twice much more that the adsorption density of GFH column (i.e. 0.34 μg arsenate/mg dry GFH). Westerhoff et. al. *(40)* also demonstrated the side-by-side comparison of the breakthrough curves of GFH and E33 for five different water from southwest parts of US, and concluded that E33 and GFH are quite comparable for arsenic removal, although occasional water quality condition can lead to a large difference (*40*).

To investigate the difference in performance of GFH and E33, breakthrough profiles of fluoride, vanadium and silica etc. are also monitored in effluents from RSSCTs columns. The authors hypothesize that silica contributes primarily to inhibit arsenate adsorption on GFH resulting less treatability than E33. Breakthrough profiles of silica for water 3 (data not included here) suggested that complete breakthrough of silica in E33 column occurred at about 2,000BVs whereas in GFH column at about 7,500BVs, equating about 2-3 times more amount of silica adsorption in GFH column.

Downloaded by UNIV OF GUELPH LIBRARY on September 11, 2012 | http://pubs.acs.org
Publication Date: October 3, 2005 | doi: 10.1021/bk-2005-0915.ch019

Conclusion

Commercially available GFH and Bayoxide E33 can treat 20,000~ 70,000 BVs while treating Arizona groundwater before the effluent arsenate concentration reaches MCL value of 10μg/L depending upon ancillary water quality conditions. Proportional diffusivity based RSSCTs (PD-RSSCTs) appear valid to simulate the pilot-scale performance for both GFH and E33. In the tail end PD-RSSCT generated steeper slope of the breakthrough curve, which might be a limitation of the RSSCT scaling approach. The breakthrough curves of only two PD-RSSCTs have been compared against pilot column performances in this study, but similar studies of the authors with several other water sources and pilot column configurations confirm that PD-RSSCT is a close approximation to the pilot column performance. On other hand, constant diffusivity based RSSCTs can be conducted in shorter duration than PD-RSSCTs, but generates different shape of the breakthrough curve than PD-RSSCTs and fail to correspond the pilot-scale performance. Overall, the application of RSSCTs might be extendable to evaluate existing and emerging

Downloaded by UNIV OF GUELPH LIBRARY on September 11, 2012 | http://pubs.acs.org
Publication Date: October 3, 2005 | doi: 10.1021/bk-2005-0915.ch019

innovative porous sorbents (i.e. GFH, E33, Metasorb G, etc), impact of water qualities (initial arsenate concentration, pH, temperature) and operational regimes (e.g., EBCTs, on-off pump cycling, series vs parallel arrangement) and the effect of competing irons (i.e. silica, calcium, vanadium, etc) on arsenate removal. This work also provides an evidence to expand the use of RSSCTs to investigate adsorption of a wide range of inorganic ions (e.g., selenium, chromium, cadmium, perchlorate, vanadium) onto porous metal oxides/hydroxides (e.g., iron, aluminum).

Acknowledgements

Financial support for this work was provided the National Science Foundation Water Quality Center at Arizona State University. Help from Dr. Detlef Knappe (North Carolina State University) and input from Prof. Dr.-Ing. Martin Jekel (Technical University Berlin) and Dr.-Ing. Wolfgang Driehaus (GEH Wasserchemie GmbH & Co. KG, Osnabrueck, Germany) are acknowledged. Any opinions, findings, conclusions or recommendations expressed in this publication are those of the authors and do not necessarily reflect the view of supporting organizations.

References

1. Smedley, P. L.; Kinniburgh, D. G. *Applied Geochem.* **2002**, *17(5),* 517-568.
2. NRC. (2002). "NRC subcommittee to update the 1999, Arsenic in drinking water, committee on toxicology." Washington DC.
3. Chen, H. W.; Frey, M. M.; Clifford, D.; McNeill, L. S.; Edwards, M. *JAWWA* **1999**, *91(3)*, 74-85.
4. Chen, A. S. C.; Fields, K. A.; Sorg, T. J.; Wang, L. L. *JAWWA* **2002**, *94(9)*, 64-77.
5. Brandhuber, P.; Amy, G. *Desalination* **1998**, *117(1-3)*, 1-10.
6. Brandhuber, P.; Amy, G. *Desalination* **2001**, *140(1)*, 1-14.
7. Cheng, R. C.; Wang, H. C.; Beuhler, M. D. *JAWWA* **1994**, *86(9)*, 79-90.
8. McNeill, L. S.; Edwards, M. *JAWWA* **1995**, *87(4)*, 105-113.
9. McNeill, L. S.; Edwards, M. *J. Env. Eng.-ASCE* **1997a**, *123(5)*, 453-460.
10. McNeill, L. S.; Edwards, M. *JAWWA* **1997b**, *89(1)*, 75-86.
11. Scott, K. N.; Green, J. F.; Do, H. D.; McLean, S. J. *JAWWA* **1995**, *87(4)*, 114-126.
12. Wang, L.; Chen, A. S. C.; Sorg, T. J.; Fields, K. A. *JAWWA* **2002**, *94(4)*, 161-173.
13. Wingrich, H.; Wolf, C. *J. Water Sup. Res. Tech.-AQUA* **2002**, *51(5)*, 273-281.

14. Chowdhury, Z.; Kommineni, S.; Narashimhan, R.; Brereton, J.; Amy, G.; Sinha, S. AWWA Research Foundation, 2002.
15. Goldberg, S.; Johnston, C. T. *J. Colloid Interface Sci.* **2001**, *234(1)*, 204-216.
16. Raven, K. P.; Jain, A.; Loeppert, R. H. *Evniron. Sci. Technol.* **1998**, *32(3)*, 344-349.
17. Wilkie, J. A.; Hering, J. G. *Colloids and Surfaces a-Physicochemical and Engineering Aspects* **1996**, *107*, 97-110.
18. Melitas, N.; Wang, J. P.; Conklin, M.; O'Day, P.; Farrell, J. *Environ. Sci. Technol.* **2002**, *36(9)*, 2074-2081.
19. Driehaus, W.; Jekel, M.; Hildebrandt, U. *J. Water Services Res. Tech.-AQUA*, **1998**, *47(1)*, 30-35.
20. Meng, X.; Jing, M.; Pena, E. *ACS National Meeting*, 2003. New York, NY.
21. Jekel, M.; Seith, R. *AWWA Inorg. Conf.* 2001, Albuquerque, NM.
22. DeMarco, M. J.; Sengupta, A. K., and Greenleaf, J. E. *Water Res.* **2003**, *37(1)*, 164-176.
23. Crittenden, J. C.; Berrigan, J. K.; Hand, D. W. *J. Water Pollut. Control Fed.* **1886**, *58(4)*, 312-319.
24. Crittenden, J. C.; Berrigan, J. K.; Hand, D. W.; Lykins, B. *J. Env. Eng-ASCE* **1987**, *113(2)*, 243-259.
25. Crittenden, J. C.; Reddy, P. S.; Arora, H.; Trynoski, J.; Hand, D. W.; Perram, D. L.; Summers, R. S. *JAWWA* **1991**, *83(1)*, 77-87.
26. Crittenden, J. C.; Vaitheeswaran, K.; Hand, D. W.; Howe, E. W.; Aieta, E. M.; Tate, C. H.; McGuire, M. J.; Davis, M. K. *Water Res.* **1993**, *27(4)*, 715-721.
27. Crozes, G., Hagstrom, J.; Suffet, I. H.; Young, C. *Water Sci Technol.* **1999**, *40(6)*, 39-44.
28. Cummings, L.; Summers, R. S. *JAWWA* **1994**, *86(6)*, 88-97.
29. Knappe, D. R. U.; Snoeyink, V. L., Roche, P.; Prados, M. J.; Bourbigot, M. M. *Water Res.* **1997**, *31(11)*, 2899-2909.
30. Badruzzaman, M. MS Thesis, Arizona State University, Tempe, AZ, 2002
31. *Annual Book of ASTM Standards*, American Society for Testing and Materials, West Conshohocken, PA; 2001.
32. Axe, L.; Trivedi, P. *J. Colloid Interface Sci.* **2002**, *247(2)*, 259-265.
33. Komiyama, H.; Smith, J. M. J. *AIChe* **1974**, *20(6)*, 1110-1117.
34. Noll, K. E.; Gounaris, V.; Hou, W. S. *Adsorption Technology for air and water pollution control*, Lewis Publication, Chesea, MI, 1992.
35. Sanjay, P. MS Thesis. Michigan Technological University, MI, 1988.
36. Sontheimer, H.; J., C. C.; Summers, R. S. *Activated Carbon for Water Treatment*, DVGW-Forschungsstelle, Karlsruhe. 1998.
37. Westerhoff, P. K.; Highfield, D. E.; Badruzzaman, M.; Yoon, Y. *J. Env. Eng.- ASCE* (Expected Feb. 2005).

Downloaded by UNIV OF GUELPH LIBRARY on September 11, 2012 | http://pubs.acs.org
Publication Date: October 3, 2005 | doi: 10.1021/bk-2005-0915.ch019

38. Badruzzaman, M.; Westerhoff, K. P.; Knappe, D. *Water Res.* **2004**, *38(18)*, 4002-4012.
39. Summers, R. S.; Crittenden, J. C. A Tech. Trans. Conf. AWWA & EPA, 1989, 67-95.
40. Westerhoff, P.; Badruzzaman, M. *ACS National Meeting*, 2003. New York, NY.

Downloaded by UNIV OF GUELPH LIBRARY on September 11, 2012 | http://pubs.acs.org
Publication Date: October 3, 2005 | doi: 10.1021/bk-2005-0915.ch019

Downloaded by PENNSYLVANIA STATE UNIV on September 12, 2012 | http://pubs.acs.org
Publication Date: October 3, 2005 | doi: 10.1021/bk-2005-0915.ch020

Chapter 20

Arsenic Removal by Activated Carbon-Based Materials

Baolin Deng[1,*], Mendy Caviness[2], and Zhimang Gu[1]

[1]Department of Civil and Environmental Engineering, University of Missouri, Columbia, MO 65211
[2]Lovington High School, Lovington, NM 88260
[*]Corresponding author: dengb@missouri.edu

Eight different types and brands of household filtration systems were purchased at area stores and assessed for their efficiency to remove arsenic from drinking water. These systems were using primarily activated carbon as filter media. The results showed the arsenic removal by the activated carbon in these household filtration systems was minimal. A new procedure was developed to impregnate iron onto granular activated carbon based on treatment of virgin activated carbon with ferrous chloride, followed by oxidation of ferrous to ferric iron. The iron impregnation onto activated carbon significantly enhanced the material's ability for arsenic uptake. In a test with tap water containing 518 μg/L of arsenic, hardness of 260.3 mg/L (as $CaCO_3$), alkalinity of 110 mg/L (as $CaCO_3$), and pH 7.85, arsenic can be removed to below 10 μg/L for 2,950 empty bed volumes, and at saturation, total amount of arsenic removed reached 3.92 mg As per g of adsorbent.

In Advances in Arsenic Research; O'Day, P., et al.;
ACS Symposium Series; American Chemical Society: Washington, DC, 2005.

Introduction

In recognition of the risk associated with the long-term exposure of arsenic (As) from drinking water, the United States Environmental Protection Agency has recently revised the maximum contaminant level of arsenic from 50 to 10 ppb [*1*]. This standard revision has a major impact on some US public water supply systems, in particular, thousands of small water systems serving a population of less than 10,000 [*2-3*]. Additionally, many private homes and businesses in rural areas are served by individual wells. While these private water supplies may not be under the EPA regulation for public water system, the health concern still exists. The problem with As is even worse in some other places in the world, notably Bangladesh, India, and China. For example, arsenic in drinking water is expected to cause 200,000 to 270,000 deaths from cancer in Bangladesh alone [*4*].

Arsenic occurs primarily as arsenate and arsenite in water [*5*]. Arsenite is more prevalent in anaerobic systems while arsenate more prevalent in aerobic environments[*6*]. Many treatment technologies are available for arsenic removal, including coagulation/filtration, lime softening, activated alumina adsorption, iron adsorption, ion exchange, and membrane processes [*1*]. Most of these approaches are, however, expensive and only suitable for large water systems [*7-8*]. For some small communities where the problem with As is the greatest, much more cost-effective technologies are needed.

Household filtration systems, a common type of "point-of-use" (POU) water purification device, have been widely used in the United States, primarily for aesthetic reasons such as odor and taste removal. It is of interest to see whether these household filtration systems also posses certain capacity for removing arsenic. The objective of this study is to assess the possible removal of arsenic by store bought household filtration systems and explore whether activated carbon, the primary filter media used in those systems, can be modified with ferric compounds to enhance arsenic removal. Ferric compounds are known to have strong affinity to arsenic, including amorphous hydrous ferric oxide [*9-12*], goethite (α-FeOOH) [*13-14*], and other granular iron-containing materials [*15-18*]. Activated carbon has been widely used for trace organic and inorganic contaminant treatment in water. A key attribute for activated carbon (GAC) is its porous structure with high specific surface areas ranging from several hundred to around two thousand m^2/g [*19*], making it a great adsorbent. Granular activated carbon is most suitable for fixed bed application due to its good mechanical and hydraulic properties. By impregnating ferric iron into granular activated carbon, we may take advantages of high arsenic affinity of iron and highly porous structure of carbon and develop an adsorbent highly efficient for arsenic removal from drinking water supplies and wastewater streams [*20*].

Downloaded by PENNSYLVANIA STATE UNIV on September 12, 2012 | http://pubs.acs.org
Publication Date: October 3, 2005 | doi: 10.1021/bk-2005-0915.ch020

Experimental Section

Eight household filtration systems were purchased at area stores. The types of filtration systems were pitcher, faucet mount, countertop, and under the sink systems, as shown in Table 1. Information on the recommended water flow rate, maximum and minimum water pressures, treatment capacity, and the nature of filter material was provided by the manufacturers for each apparatus.

Table 1. Filtration systems assessed.

Brand	*Type*	*Water Flow Rate*	*Water Pressure (max./min. psi)*	*Capacity*	*Filter Material*
Brita	Pitcher	7.6 L/day	Not available	151 L	Activated carbon/ ion exchanger
Brita	Faucet Mount	2.8 L/min	100/20	378 L	Activated carbon
GE Single	Undersink	2.3 L/min	125/40	4725 L	Activated carbon
GE Dual	Undersink	2.3 L/min	125/20	4725 L	Activated carbon
PUR	Pitcher	7.6 L/day	Not available	151 L	Activated carbon
PUR Select	Faucet Mount	2.5 L/min	100/20	378 L	Activated carbon
PUR Ultimate	Faucet Mount	2.5 L/min	100/20	378 L	Activated carbon
PUR Plus	Countertop	3 L/min	125/20	756 L	Activated carbon

The household filtration systems were assessed using groundwater from the City of Socorro, New Mexico. The City of Socorro water supplies were provided by six groundwater wells with arsenic concentrations ranging from 6 to 37 µg/L and hardness from 66 to 327 mg/L (as $CaCO_3$). Primary arsenic species was arsenate [*21*]. The well water was distributed directly to consumers after disinfection with chlorine. The water used in this study was primarily from the School of Mines Well and the Olsen Well, with possible mixing with other well waters. For the Brita Pitcher and the PUR Pitcher filtration systems, tap water

Downloaded by PENNSYLVANIA STATE UNIV on September 12, 2012 | http://pubs.acs.org
Publication Date: October 3, 2005 | doi: 10.1021/bk-2005-0915.ch020

Downloaded by PENNSYLVANIA STATE UNIV on September 12, 2012 | http://pubs.acs.org
Publication Date: October 3, 2005 | doi: 10.1021/bk-2005-0915.ch020

was spiked with sodium arsenate to reach an influent arsenic concentration close to 50 ppb. The remaining filters were directly attached to the faucet in the water quality laboratory at the New Mexico Bureau of Mines on the New Mexico Tech campus. For each of these directly-attached filtration tests, four samples of influent were analyzed prior to the filtration process and averaged to obtain the influent As concentration. The values were all within the range from 34 to 40 μg/L, essentially constant during the testing time period. Effluent arsenic concentration was analyzed as a function of filtration volume. The filter manufactures recommended running water through the filters prior to use in order to flush any loose carbon particles from the filter. In this study, effluent samples were taken after the first liter of water. A total of 282 water samples were taken and analyzed for the filtration experiments. All samples were acidified to pH 2.0 with ultra high purity nitric acid. Arsenic levels were determined by graphite furnace atomic absorption spectrophotometry (GFAA) using nickel nitrate matrix modifier. Standard quality control procedures were followed. Duplicate samples were included in each batch. A certified reference sample from National Institute of Standards and Testing (NIST #1643d) was included in each batch along with a 10 ppb standard.

Preparation of iron-impregnated activated carbon was based on diffusion of ferrous iron into internal pores of granular activated carbon, followed by oxidation with sodium hypochlorite [*22*]. After testing with various types of granular activated carbon, Dacro 20×40Li from American Norit Co. was chosen as the primary porous medium for iron impregnation. The sample prepared in this study (As-GAC) was then examined by scanning electron microscope (SEM) (AMRAY 1600) to determine the surface morphology and iron distribution. A working distance of 5-10 mm, spot size of 2-3, secondary electron (SE) mode, and an accelerating voltage of 5 KeV were used to view the samples. SEM Images and energy dispersive spectroscopy (EDS) analyses at various parts of the granular activated carbon was collected using a digital data acquisition system. The performance of the As-GAC was evaluated by column tests. Groundwater from the University of Missouri-Columbia was used as source water for the assessment. The main chemical components in the water were (mg/L): Ca = 57.4, Mg = 28.0, Na = 52.0, K = 6.4, Cu = 0.064, Fe = 0.029, S = 11.7 and B = 0.5, determined by inductively-coupled plasma – mass spectroscopy (ICP-MS). The water was spiked with arsenate to an initial concentration of 518 μg/L. The column size was 250×ϕ6mm, so the column has a length-to-diameter ratio of about 40:1. A total of 3.60 g of As-GAC adsorbent was used to fill the column. Empty bed contact time (EBCT) was controlled at 10 min. The selected EBCT was significantly longer than those of typical POU devices but comparable to those of conventional water treatment plant GAC absorbers, which had EBCTs in the range of 7-20 min [*23*]. That was because large As-GAC particles (0.42 – 0.84 mm) were used in the testing and our primary objective was to assess the adsorption capacity. The corresponding flow rate of arsenic solution was about 0.75ml/min.

Results and Discussion

Assessment of household water filters

The performance of various filters for arsenic removal was evaluated based on their breakthrough curves, as shown in Figures 1-3. The breakthrough curves were plotted by the empty bed volume (EBV) versus the ratio of the effluent to the influent concentrations. Since As concentration in the influent water was near or less than 50 μg/L, a C/C_0 ratio of 0.2 corresponded to a concentration equal or less than 10 μg/L in the effluent, the permitted level of arsenic. The result indicated that in no case, the detected amount of arsenic was lower than 10 μg/L, after the first liter of water was used for flushing of loose carbon particles. For Brita Pitcher filter (Figure 1), the effluent concentration reached near 80% of the influent value at 40 EBV but the filter still showed some arsenic removal up to 330 EBV; while for Brita Faucet Mount, it reached saturation at around 120 EBV. For both GE Single and GE Dual filters, they reached saturation at around 90 EBV (Figure 2). Two of the PUR filters, the pitcher type and PUR Select, demonstrated some adsorption up to around 300 EBV, and the other two types reached saturation at around 100 EBV (Figure 3). To summarize, arsenic removals by these household filtration systems were all minimal. This, of course, was well expected because they were primarily designed for taste and odor removal, not for arsenic.

Iron-impregnated granular activated carbon

Iron impregnated granular activated carbon was examined by scanning electron microscopy (SEM), revealing the porous structures of the granular adsorbents. Representative micrographs of the adsorbent (As-GAC) are presented in Figure 4. The SEM imaging indicated that the distribution of iron in As-GAC was uniform when the iron content in As-GAC was 5-7% (Figure 4a). For the sample with higher iron content (> 7%), there was an iron band on the outer edge of the GAC particles (Figure 4b). Iron impregnation decreased the BET specific surface area from 528 for the virgin granular activated carbon to 350 m^2/g for the material with 7.8% of iron, measured by nitrogen adsorption using PMI Automated BET Sorptometer (Porous Materials, Inc.).

Downloaded by PENNSYLVANIA STATE UNIV on September 12, 2012 | http://pubs.acs.org
Publication Date: October 3, 2005 | doi: 10.1021/bk-2005-0915.ch020

Downloaded by PENNSYLVANIA STATE UNIV on September 12, 2012 | http://pubs.acs.org
Publication Date: October 3, 2005 | doi: 10.1021/bk-2005-0915.ch020

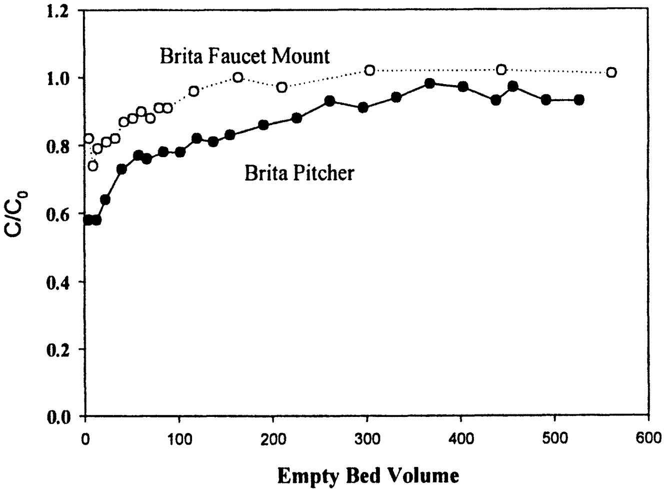

Figure 1. Breakthrough curves of arsenic for Brita filtration systems with C_0 = 50 μg/l

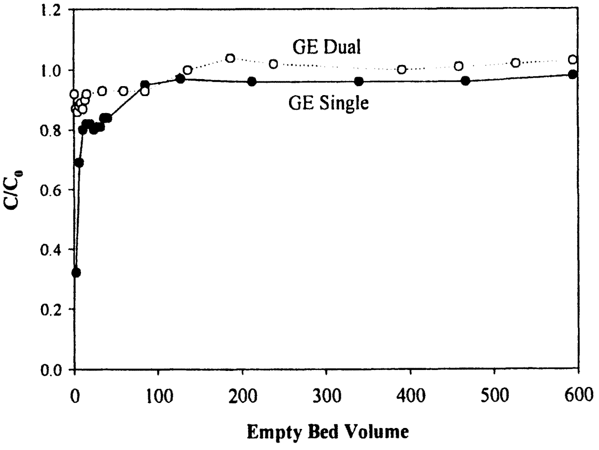

Figure 2. Breakthrough curves of arsenic for GE filtration systems with C_0 = 50 μg/l

Downloaded by PENNSYLVANIA STATE UNIV on September 12, 2012 | http://pubs.acs.org
Publication Date: October 3, 2005 | doi: 10.1021/bk-2005-0915.ch020

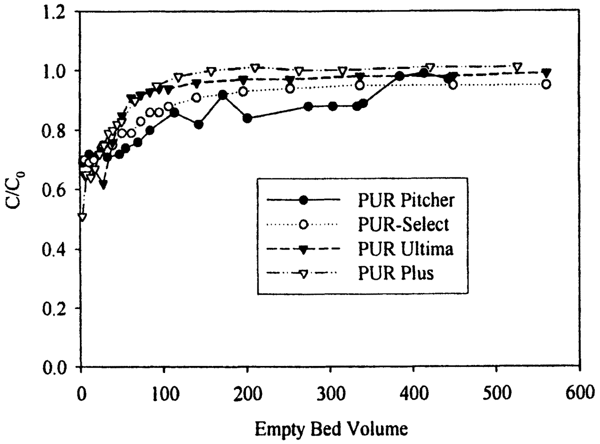

Figure 3. Breakthrough curves of arsenic for PUR filtration systems with C_0 = 50 μg/l

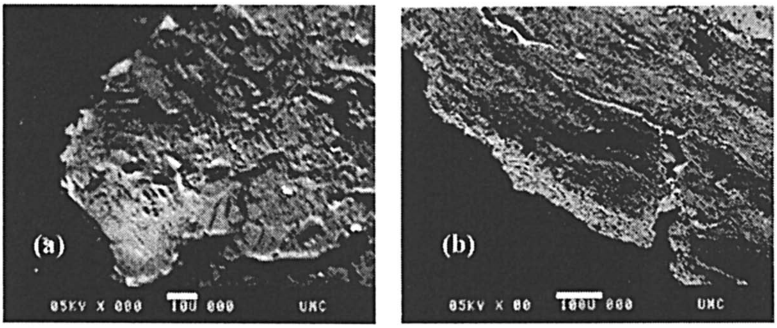

Figure 4. SEM micrographs of As-GAC samples treated with 0.15M (a), and 0.40M (b) of iron chloride.

Column test of arsenic removal by the iron-impregnated granular activated carbon

The efficiency of As-GAC for arsenic treatment was investigated in a column study lasting for a total of 31 days. A relatively high influent concentration of arsenic (518 µg/L) was used in this test. While this concentration was likely to be higher than most of drinking water supplies, it could better show the adsorption capacity of the material and allow the test be completed in a reasonable time frame. As shown by the arsenic breakthrough curve (Figure 5), the breakthrough started at 2,950 EBV. At this time, the total amount of arsenic adsorbed was 3.10 mg As/g adsorbent. Arsenic concentration increased after the breakthrough and reached 500 µg/L at approximately 4,500 EBV.

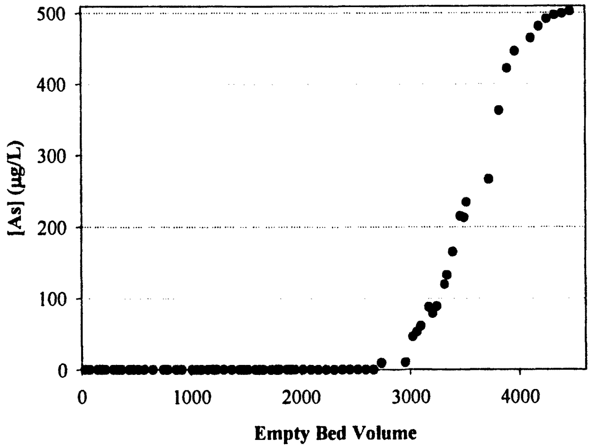

Figure 5. Arsenic concentration in the effluent as a function of empty bed volume

This result clearly demonstrated that the iron-impregnated activated carbon (As-GAC) examined in this study had much higher adsorption capacity than the commercial household filtration units tested. There is a potential to use the material in the POU devices for arsenic removal when ground into fines or in municipal water treatment systems in the granular form.

Downloaded by PENNSYLVANIA STATE UNIV on September 12, 2012 | http://pubs.acs.org
Publication Date: October 3, 2005 | doi: 10.1021/bk-2005-0915.ch020

Conclusions

The store bought filters examined in this study are ineffective for arsenic removal. Impregnation of iron into the granular activated carbon can dramatically enhance the material's ability for arsenic treatment. At 518 µg/L of arsenic influent concentration, the breakthrough began at approximately 3000 empty bed volumes. The impregnation process does not significantly change the granular and porous nature of the carbon so it should be suitable for large scale packed bed applications. Additional work is underway to assess whether the iron-impregnated activated carbon still maintains its ability for other inorganic and organic contaminant treatment.

Downloaded by PENNSYLVANIA STATE UNIV on September 12, 2012 | http://pubs.acs.org
Publication Date: October 3, 2005 | doi: 10.1021/bk-2005-0915.ch020

Acknowledgments

Analytical support by Lynn Brandvold, Terry Thomas, and Amy Mathis at the New Mexico Bureau of Mines & Mineral Resources and Edward J. Hinderberger at the University of Missouri-Columiba are greatly appreciated. The authors also thank two anonymous reviewers and the editor for their constructive comments. Financial support for this research was provided by the U.S. National Science Foundation (No. BES-0093848).

References

1. U. S. EPA, *Federal Register* 40 CFR Parts 141 and 142, *65* (121). June 2000.
2. National Research Council, *Arsenic in Drinking Water*, National Academy Press, Washington, D.C., 1999.
3. National Research Council, *Arsenic in Drinking Water: 2001 Update*, National Academy Press, Washington, D.C., 2001.
4. WHO (World Health Organization), *Arsenic in Drinking Water,* Fact Sheet No 210. Revised May 2001. (http://www.who.int/inf-fs/en/fact210.html).
5. Kartinen, E. O. Jr; Martin, C. J. *Desalination*, **1995**, *103*, 79-88.
6. Rajakovic, L. J.; Mitrovic, M. M. *Environmental Pollution*, **1992**, *75*, 279-287.
7. Bitner, M. J.; Chwirka, J. D. In *Proceeding of 39th New Mexico Water Conference*, Albuquerque, NM, 1994, pp. 251-255.
8. Viraraghavan, T.; Subramanian, K. S.; Aruldoss, J. A. *Wat. Sci. Tech.*, **1999**, *40* (2), 69-76.
9. Pierce, M. L.; Moore, C. B. *Water Research,* **1982**, *16*, 1247-1253.

10. Shen, Y. S. *Journal AWWA*., **1973**, 543-552.
11. Edwards, M. *Journal AWWA*, **1994**, *86*(9), 64-78
12. Hering, J. G.; Chen, P.; Wilkie, J. A.; Elimelech, M.; Liang, S. *Journal AWWA*, **1996**, 155-167.
13. Matis, K. A.; Zouboulis, A. I.; Malamas, F. B.; Afonso, M. D. R.; Hudson, M. J. *Environmental Pollution*, **1997**, *97*(3), 239-245.
14. Sun, X.; Doner H. E. *Soil Science*, **1998**, *163*, 278-287.
15. Benjamin, M. M.; Sletten, R. S.; Bailey, R. P.; Bennett, T. *Water Res*., **1996**, *30*(11), 2609–2620.
16. Joshi, A.; Chaudhuri, M. *Journal Environ. Engr.*, **1996**, *122*(8), 769-771.
17. Santra, S.; Tapec, R.; Theodoropoulou, N.; Dobson, J.; Hebard, A.; Tan, W. *Langmuir*, **2001**, *17*, 2900-2906.
18. Driehaus, W.; Jekel, M.; Hildevrand, U. *J Water SRP Aqua*, **1998**, *47*, 30-35.
19. Montgomery Consulting Engineers, Inc. *Water Treatment Principles and Design*, Wiley & Sons, New York, NY, 1985.
20. Reed, B.E.; Vaughan, R.; Jiang, L.Q. *J. Environ. Eng-ASCE*. **2000**, *126*, 869-873.
21. Brandvold, L. A.; Frisch, P. L. In *New Mexico Geological Society Proceedings Volume*, 2002 Annual Spring Meeting, p. 9.
22. Gu, Z.; Deng, B. In *Preprints of Extended Abstracts* (Division of Environmental Chemistry) at 226th ACS National Meeting , New York, NY September 7-11, 2003, Vol. *43*(2), 361-365.
23. Droste, R. L. *Theory and Practice of Water and Wastewater Treatment*, Wiley &Sons, New York, NY, 1997.

Downloaded by PENNSYLVANIA STATE UNIV on September 12, 2012 | http://pubs.acs.org
Publication Date: October 3, 2005 | doi: 10.1021/bk-2005-0915.ch020

Downloaded by UNIV OF GUELPH LIBRARY on September 11, 2012 | http://pubs.acs.org
Publication Date: October 3, 2005 | doi: 10.1021/bk-2005-0915.ch021

Chapter 21

Arsenic Removal from Drinking Water Using Clay Membranes

Jun Fang[1], Baolin Deng[1,*], and T. M. Whitworth[2]

[1]Department of Civil and Environmental Engineering, University of Missouri at Columbia, Coumbia, MO 65211
[2]Department of Geological and Petroleum Engineering, University of Missouri at Rolla, MO 65409
[*]Corresponding author: dengb@missouri.edu

While many treatment technologies are available for arsenic removal from drinking water including coagulation/filtration, lime softening, activated alumina adsorption, ion exchange, and membrane processes, most of these approaches are expensive and more suitable for large water systems. In this study, membranes made of low-cost clay minerals were explored for arsenate removal. Montmorillonite, kaolinite, and illite were selected for membrane preparation. Feed water spiked with arsenate was pumped through the compacted clay membranes and the effluent was collected at the lower pressure side for arsenic analysis. The ability of clay membranes to retain arsenic was investigated at different initial arsenic concentrations and ionic strengths controlled by sodium chloride. The influence of applied pressure and the permeate flux on arsenic removal efficiency was also examined. The results indicated that a greater than 90% of arsenic rejection could be achieved for water with 50-100 μg/l of arsenate using the clay membranes. The required pressure for clay membrane filtration was, however, significantly higher than that of synthetic organic membranes.

In Advances in Arsenic Research; O'Day, P., et al.;
ACS Symposium Series; American Chemical Society: Washington, DC, 2005.

Introduction

Arsenic is of increasing environmental concern due to increased awareness of its adverse effects to human health. Excessive amounts of arsenic can cause acute gastrointestinal and cardiac damage. Long term exposure to arsenic via drinking water leads to health problems such as vascular disorders and skin cancer *(1-3)*. To minimize the risk, the US Environmental Protection Agency has revised the Maximum Contamination Level (MCL) of arsenic in drinking water from 0.05 mg/l to 0.01 mg/l. Viable water treatment technologies are being reassessed for their efficacy in removing arsenic from drinking water and for their potential applicability to meet the new standard *(4)*. The technologies investigated include coagulation/filtration *(5, 6)*, lime softening *(7)*, ion exchange, activated alumina adsorption *(8)*, and membrane filtration processes *(9-12)*.

A key characteristic of a membrane is its ability to restrict or prevent the passage of some solutes in solution while permitting transport of others. The solute rejection by membranes is based on size and/or electrical restrictions. The membrane would be ideal if it could absolutely retain a solute. Typical membranes used in arsenic removal studies are synthetic polymeric membranes. It has been shown that membrane filtration processes, such as reverse osmosis (RO) and nanofiltration (NF), are capable of arsenic removal, particularly at low influent arsenic concentrations *(13)*. Brandhuber and Amy *(10)* reported As(V) could be effectively treated by RO and NF with rejection rate higher than 95%, and membrane surface charge might be a more important factor in determining the rejection of As(V) than the molecular weight cut-off of the membranes. However, the applications of polymeric membranes are limited by lack of heat, chemicals, and corrosion resistance, as well as their high cost. Development of other low-cost inorganic membranes should be explored for future uses.

Clays are known to have membrane properties and can reject ionic solutes in solution *(14-17)*. Clay mineral surfaces are negatively charged due to the substitution of the lower valence for higher valence cations within the mineral structure, as well as the broken bonds on the mineral surface. The ideality of clay membranes is a function of the membrane's surface charge density and porosity as well as the concentration of ions in solution *(18)*. Clay membrane efficiency increases greatly when the double layer of adjacent clay platelets overlaps under compaction. A possible mechanism for charged compacted clay membranes rejecting ion solutes is that the anions attempting to pass through the clay membranes are repelled by the negative charge on the clay platelets, cations tend to remain with their co-ions in order to maintain the electrical neutrality in the solution, thus their movement across the clay is also restricted *(19)*. For uncharged membranes, like kaolinite, the rejection arises predominantly from their size exclusion properties *(20)*.

Downloaded by UNIV OF GUELPH LIBRARY on September 11, 2012 | http://pubs.acs.org
Publication Date: October 3, 2005 | doi: 10.1021/bk-2005-0915.ch021

Downloaded by UNIV OF GUELPH LIBRARY on September 11, 2012 | http://pubs.acs.org
Publication Date: October 3, 2005 | doi: 10.1021/bk-2005-0915.ch021

Some studies have been previously conducted on the potential uses of clays as practical membranes. Ishiguro et al. *(21)* applied an uncompacted 0.5 mm thick montmorillonite layer as a reverse osmosis membrane to separate salt solutions and non-ionized organics. The clay membrane exhibited characteristics typical of a charged membrane, rejecting sodium chloride solute less effectively with increasing solute concentrations. The rejection rate of non-ionized organics was very low. They also found that the separation of amino acids depended greatly on the net charge carried by the amino acid molecule *(21)*. In another study, Li et al. *(22)* used a compacted bentonite membrane to purify oil-field produced water that contained total dissolved solids (TDS) of 196,250 mg/L. To maximize the flow through the membrane, ultrathin (0.04mm to 0.06 mm thick) bentonite clay membranes were used and results demonstrated that the membrane efficiency for inorganic solutes decreased with increasing solute concentration and with increasing total dissolved solids *(22)*.

Arsenic is considered a metalloid that exists in various forms and oxidation states in the environment. Two species commonly found in drinking water are arsenate and arsenite. Arsenate is the thermodynamically stable form of inorganic arsenic in oxic water, and usually predominates in surface water. Under typical drinking water pH (5.5 - 8.5) conditions, arsenate exists as anionic $H_2AsO_4^-$and $HAsO_4^{2-}$. Clay membranes, which are negatively charged, should be capable of rejecting arsenate from drinking water. To our knowledge, however, this has not been experimentally demonstrated. The objective of this study is to examine the potential arsenic removal by thin compacted clay membranes at different initial arsenate and background electrolyte concentrations.

Experimental Methods

Clay minerals used in this study were obtained from the Clay Minerals Society Source Clay Repository (Department of Geological Sciences, University of Missouri-Columbia). Samples of sodium montmorillonite (SWy-2) from Crook County, WY, poor crystallized kaolinite (KGa-2), and illite (IMt-2) from Silver Hill, MT, were used for membrane preparation. The illite fragments were ground with a mortar and pestle to pass a 75μm sieve before the preparation. To purify the clay minerals, each of the three clay/water slurries was poured into a plastic jar with marble mill media and milled on a mechanic roller for two days. Standard sedimentation technique was then used to obtain the smaller size fraction. Following separation, the clay slurries were dialyzed, freeze dried in a benchtop freeze drier (Labconco, Model 4.5), and finally the freeze dried clays were stored in sealed bags prior to use *(17)*.

Figure 1 is the schematic of the experimental setup, followed a design similar to the one used by Fritz and Whitworth *(23)*. The membrane filtration system consisted of a feedwater reservoir, a high performance liquid chromatographic (HPLC) pump capable of delivering fluid at constant flow rates ranging from 0 to 10 ml/min (Gilson Model 305), pressure gauge, an acrylic cell with two caps, and sample collection bottles. The membrane area in this cell was 15.52±0.01 cm^2.

Downloaded by UNIV OF GUELPH LIBRARY on September 11, 2012 | http://pubs.acs.org
Publication Date: October 3, 2005 | doi: 10.1021/bk-2005-0915.ch021

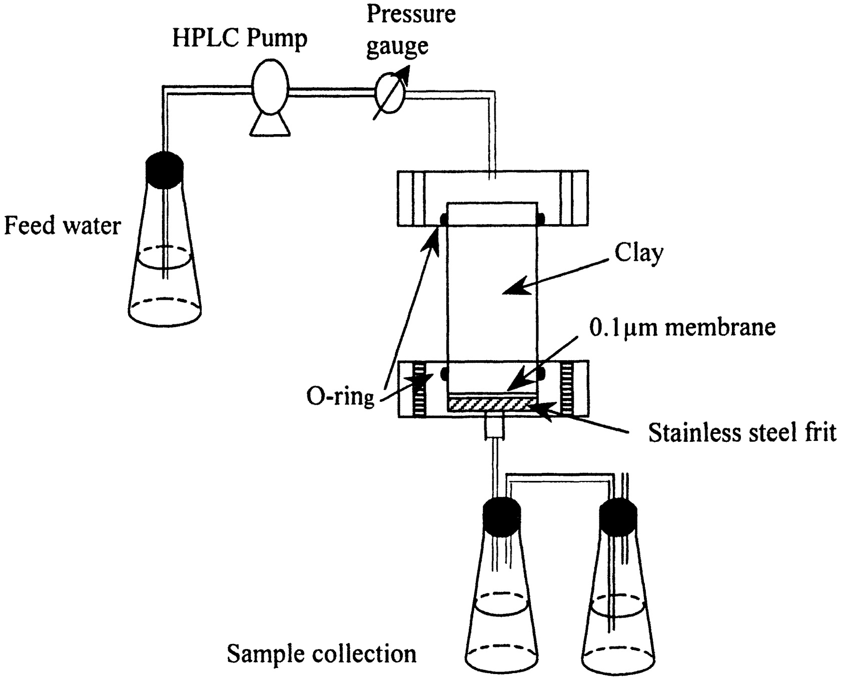

Figure 1. Schematic of the experimental setup.

The clay membrane was prepared in the experimental setup. A 316 stainless steel porous frit was first set into the lower cap, then two pieces of membrane filter papers (Millipore, 0.1 μm) were placed on top of the frit. The acrylic cell was carefully inserted into the lower cap without wrinkling the filter papers, with an O-ring installed for leak prevention. A clay suspension, formed by mixing 0.30 g of freeze-dried sodium montmorillonite with 120 ml deionized water, was transferred to the cell. The cell was then sealed with the upper cap and O-ring, followed by bolting the cell and caps tightly with threaded steel rods. Using this typical down- flow filtration system, deionized water was pumped through the port in the center of upper cap into the cell to compact the clay suspension, forming a thin layer of membrane on the top of the filter paper. An Ashcroft pressure gauge ranging from 0 to 2000 psi was installed in front of the cell to measure the applied pressure to the cell. The time period used for membrane formation usually lasted for two to four days. The internal pressure of the cell depended on the flow rate of the system. Since the acrylic cell used in the system could only endure a maximum continuous pressure around 1500 psi, the flow rate of the system was set no more than 0.2 ml/min to maintain the pressure at approximately 1100 psi.

Permeability (L_p) of the clay membrane to deionized water was measured after the clay membrane formation, when the flow rate and applied pressure reached a steady state. Under this condition, L_p could be calculated from the equation (1):

$$L_p = \frac{J_v}{\Delta P} \qquad (1)$$

where J_v is the water flux at the steady state in cm/s and ΔP is the applied hydraulic pressure in dyn/cm^2. Since $J_v = Q/A$, with Q being the volumetric flow rate (cm^3/s) and A the membrane surface area (cm^2), the permeability can also be represented as:

$$L_p = \frac{Q}{\Delta P * A} \qquad (2)$$

Once the data for permeability calculation were collected, the deionized water in the cell was removed and replaced by the arsenate solution, followed by pumping the solution through the clay membrane at a constant flow rate. The effluent samples were periodically collected from the lower pressure side of the membrane, and analyzed to assess possible arsenic rejection. An evaporation control system, as detailed in the literature *(22, 24)*, was used to prevent water evaporation during the sampling process.

Filtration experiments with montmorillonite, kaolinite and illite were also conducted in an experimental system following a design by Whitworth and Fritz *(25)*, slightly different from the system shown in Figure 1. Here clay membranes were compacted between two stainless steel frits by a hydraulic press, using 0.50 g montmorillonite, kaolinite or illite. The compaction pressure was up to 34.8 Mpa. The tests were conducted under a flow rate of 0.63 ml/min, background NaCl concentration of 0.010 M, initial arsenate of 100.4 ppb, and pH 7.05.

Total arsenic concentration in samples were determined by hydride generation atomic fluorescence spectroscopy *(26)*, using a PSA millennium analytical system (PSA Analytical Ltd). A calibration curve, with a concentration ranging from 0 to 50 μg/L, was obtained using arsenate reference solution (1000

Downloaded by UNIV OF GUELPH LIBRARY on September 11, 2012 | http://pubs.acs.org
Publication Date: October 3, 2005 | doi: 10.1021/bk-2005-0915.ch021

ppm ±1%, Fisher certified). The correlation coefficient (R^2) was always higher than 99.9%. The method detection limit was approximately 50 parts per trillion (ppt). High arsenic samples outside the linear calibration range were diluted before analysis. The arsenic detector could be concurrently connected to a HPLC system for arsenic speciation *(26)*. In this study, no arsenate transformation was detected.

Results and Discussion

Reverse osmosis experiments were conducted under various operational conditions (flow rate and applied pressure) and types of clay minerals. Water permeability coefficients were determined right after the formation of the membranes. Solutions for testing solute rejection were prepared with deionized water containing 50 µg/L or 100 µg/L of arsenate (As(V)) and various concentrations of NaCl (0, 0.005, 0.010, 0.050, 0.25M). The solution pH was adjusted to 7.0 ± 0.2 using 0.10 M NaOH or HCl. Experimental parameters and results were summarized in Table 1.

To better understand the relationship between the flow rate and applied pressure and membrane properties, different flow rates were applied in the experiments. Results indicated that in general, the higher the flow rate, the greater the water permeability coefficient. Experiments DF030405 and DF030613 were designed to examine the effect of flow rate on arsenate rejection.

Table I. Experimental Parameters and Results

Experiment#	*Flow rate (ml/ min)*	*[NaCl] (M)*	*Initial As Conc (mg/l)*	*Exp. Duration (days)*	*Avg As rejection after steady state (%)*	*Avg As rejection for first 500 ml effluent (%)*	*Permeability Coefficient, L_p ($cm^3(dyne*s)^{-1}$)*
DF020827	0.2	0.1	41.26	1.9		89.2	2.83E-12
DF030123	0.15	0	99.78	5.09	40.3	50.1	2.58E-12
DF030218	0.15	0.005	98.41	3.38	45.9	58.9	2.32E-12
DF030405	0.08	0.01	113.95	4.96		94.9	1.10E-12
DF030613	0.1	0.01	101.27	3.3		89.2	2.29E-12
DF031023	0.04	0.01	96.04	11.9	55.0		5.18E-13
DF030805	0.04	0.05	101.79	24.07	68.0		5.94E-13
DF030804	0.04	0.25	101.12	20.06	64.0		5.83E-13
DF030825-M*	0.63	0.01	113.57	13.67			N/A
DF030825-K*	0.63	0.01	100.44	5.95			N/A
DF030825-I*	0.63	0.01	100.44	3.07			N/A

Downloaded by UNIV OF GUELPH LIBRARY on September 11, 2012 | http://pubs.acs.org
Publication Date: October 3, 2005 | doi: 10.1021/bk-2005-0915.ch021

The results (Figure 2) showed that arsenate rejection was slightly decreased with increasing flow rate from 0.08 to 0.10 ml/min, as well as with the elapsed time. The corresponding increase in pressure was much more significant, from 200 to 400 psi.

For a down-flow membrane filtration system, the solution flux, defined as the ratio of the influent volumetric flow rate to the membrane surface area, is related to the applied pressure across the membrane. Higher flow rate could result in: i) an increase of solute concentration at the membrane surface due to enhanced concentration polarization; ii) an increase of total solute mass flux due to the increased solution flux; and iii) more compaction of membranes as the result of increasing overlying fluid pressure. These effects may all impact arsenic removal. It is expected that the first process will decrease the arsenic rejection. The effect of the second process on the relative arsenic rejection depends upon the ratio of solute to water flux. The third process would increase the arsenic rejection. This is because the degree of solute rejection of reverse osmosis is controlled by the membrane porosity and charge *(27)*. More compaction would lead to smaller pore sizes of membrane and more overlapping of electrical double layers, consequently increased arsenic rejection. In the experiments DF030405 and DF030613, a small decrease in arsenic rejection with increasing solution flux was observed, which may reflect the total effects of these different factors. Fritz and Marine reported that more salt was retained on high- pressure side of the membrane with decreasing solution flux *(16)*, i.e., the rejection efficiency was increased. This agreed with our observation.

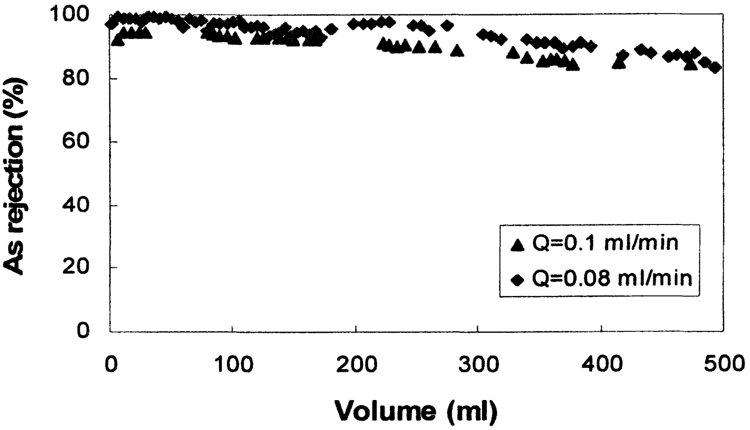

Figure 2. Effects of the flow rate on the As (V) rejection (background solution concentration[NaCl] = 0.01M).

Downloaded by UNIV OF GUELPH LIBRARY on September 11, 2012 | http://pubs.acs.org
Publication Date: October 3, 2005 | doi: 10.1021/bk-2005-0915.ch021

Effects of ionic strength on arsenate rejection were investigated in various NaCl background solutions. Two sets of experiments with different flow rates were conducted. As shown in Figure 3, arsenic rejection was slightly increased with increasing NaCl concentration from 0.0 to 0.0050 M at a constant flow rate of 0.15 ml/min (DF030123 and DF030218). To better visualize the effect, average arsenate rejections after reaching steady state were calculated. The results, as listed in Table 1, showed that the rejections were 40.3% at 0.0M NaCl and 45.9% at 0.0050M NaCl. At a flow rate of 0.04 ml/min (DF031023, DF030804, and DF030805), the rejection increased from 55.0% to 68.0% when NaCl concentration was increased from 0.010 to 0.050M. When NaCl concentration was further increased to 0.25 M, however, the rejection was slightly decreased to 64.0%.

Hodgson suggested that in multiple solute solutions, the rejection of a given ion is improved by the presence of a more permeable ion of like charge *(28)*. Compared with the chloride anion (Cl^-), anionic arsenate were a less permeable ion, which had a larger molecular weight and a much lower concentration. Herein, arsenate rejection increased with increasing ionic strength (I), as observed in this study at the flow rate of 0.15ml/min when the ionic strength was increased from 0.0 to 0.005M, as well as at the flow rate of 0.04 ml/min when the ionic strength was increased from 0.010 to 0.050M. This trend, however, is not extended to the system with I=0.25 M. A probable explanation was that the double layer of clay platelets was dramatically compressed at this high ionic

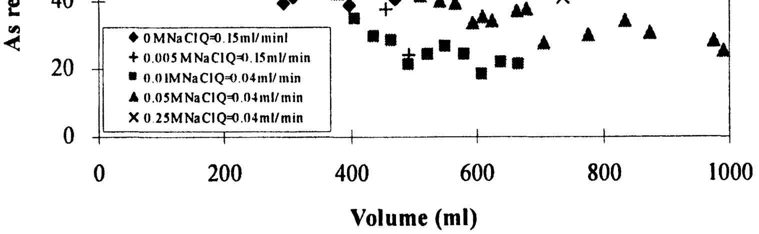

Figure 3. Effects of Ionic strength on arsenate rejection by montmorillonite membranes.

Downloaded by UNIV OF GUELPH LIBRARY on September 11, 2012 | http://pubs.acs.org
Publication Date: October 3, 2005 | doi: 10.1021/bk-2005-0915.ch021

strength, so the negative electrical potential in membrane pathway was not high enough to repel the arsenate anions. Nevertheless, by comparing the arsenic rejection at different flow rates, it appeared that a lower flow rate would lead to a higher rejection even when the electrical double layer was compressed at I=0.25 M.

Figure 4 showed the relative arsenic rejections at two initial arsenic concentrations: 41.3 ppb (DF020827) and 98.26 ppb (DF030218). The flow rates were 0.2 ml/min in the low arsenic system and 0.15 ml/min in the high arsenic system, and the ionic strengths were 0.10M and 0.005M, respectively. It was clear that percentage arsenic rejection was much higher when a lower initial arsenate concentration was applied. This was observed under the unfavorable flow rate and ionic strength conditions for the low arsenic system. The result was consistent with the concept that in the presence of more permeable co-occurring ions, the smaller the relative concentration of the less permeable ion (i.e., arsenate), the greater is its rejection by the membrane.

Downloaded by UNIV OF GUELPH LIBRARY on September 11, 2012 | http://pubs.acs.org
Publication Date: October 3, 2005 | doi: 10.1021/bk-2005-0915.ch021

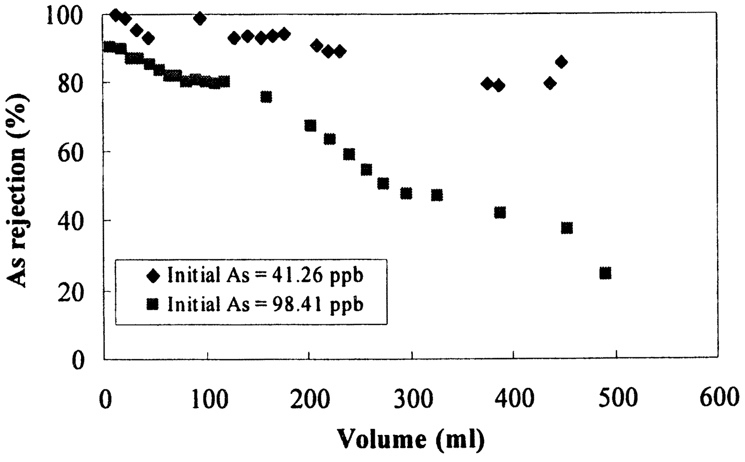

Figure 4. Effects of the initial arsenate concentration on the arsenic rejection.

Arsenic rejection by montmorillonite (DF082503-M*), kaolinite (DF082503-K*) and illite (DF082503-I*) membranes were shown in Figure 5. Montmorillonite had the highest overall rejection. The rejection of the kaolinite membrane was higher than that of the illite membrane. The result was somewhat unexpected because the charge density of the illite membrane was much higher than that of the kaolinite membrane, and should have higher rejection. The mechanisms responsible for differing solute rejection on these two clay membranes were unclear. A possible reason was that larger sizes of illite particles might exist in illite membrane. Our grinding and milling processes may have not resulted in homogeneous illite particles suitable for membrane preparation. It is known that the electrical double layer thickness is on the order of tens of nanometers or less *(29)*. When particle sizes in the clay membrane were not fine enough, the electrical double layer thickness is insignificant compared to the pore sizes, so the rejection due to the electrical double layer repulsion might not be the dominant mechanism. Should this be true, the observed arsenic rejection for kaolinite and illite must mainly be due to size exclusion. Further research is needed to illustrate the solute rejection mechanisms.

Downloaded by UNIV OF GUELPH LIBRARY on September 11, 2012 | http://pubs.acs.org
Publication Date: October 3, 2005 | doi: 10.1021/bk-2005-0915.ch021

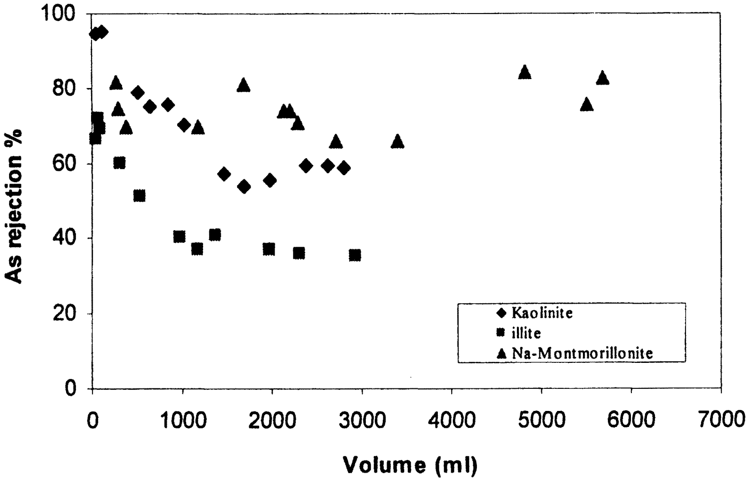

Figure 5. Influence of clay types on arsenate rejection.

Conclusions

This study has demonstrated that a thin layer of clay can serve as a reverse osmosis membrane for arsenic rejection. The rejection efficiency of montmorillonite membranes is over 90% for low concentration of arsenate under suitable ionic strength conditions. The flow rate and applied pressure has small impacts on the membrane removal efficiency. Arsenate rejection of the clay membrane deteriorated after obtaining 500 ml of effluents. Decreasing rejection efficiency with time is expected because a concentration polarization layer forms in this type of experimental setup. Application of clay membranes for practical uses generally employs cross-flow systems. Kaolinite and illite also show membrane properties for arsenic rejection, although the overall efficiency is lower than montmorillonite membranes. In addition to electrical double layer repulsion being an important mechanism for arsenate rejection by the clay membranes, size exclusion may also play a role since less charged kaolinite still demonstrates membrane properties.

Downloaded by UNIV OF GUELPH LIBRARY on September 11, 2012 | http://pubs.acs.org
Publication Date: October 3, 2005 | doi: 10.1021/bk-2005-0915.ch021

Acknowledgements

The authors thank Ms. M. Hart at the University of Missouri-Rolla and Mr. L. Li at New Mexico Tech for their invaluable inputs to this study, and two anonymous reviewers for their constructive comments. Financial support provided by the US National Science Foundation (No. BES-0093848) was greatly appreciated.

References

1. Chen, C. J.; Lin, L. J. *Adv. Environ. Sci. Technol.* **1994**, *27,* 109-31.
2. WHO, *Environmental Health Criteria, 18: Arsenic.* World Health Organization, Geneva, 1981.
3. Pontius, F. W.; Brown, K. G.; Chen, C. J. *JAWWA* **1994**, *86*(9), 52-63.
4. Viraraghavan, T.; Subramanian, K.S.; Aruldoss, J.A. *Water Sci. Technol.* **1999**, *40*(2), 69-76.
5. Hering, J. G.; Chen, P. Y.; Wilkie, J. A.; Elimelech, M.; Liang, S. *JAWWA* **1996**. *88*(4), 155-167.
6. Scott, K. N.; Green, J. F.; Do, H. D.; Mclean, S. J. *JAWWA*, **1995**, *87*(4) 114-126.
7. McNeill, L. S.; Edwards, M. *J. Env. Eng-ASCE* **1997**, *123*, 453-460.
8. Clifford, D. A.; Ghurye, G.; Tripp, A.R. In *Proceedings of the International Conference on Arsenic Exposure and Health Effects,* 3rd, San Diego, CA, July 12-15, 1998, pp. 379-387.
9. Chang, S. D.; Ruiz, H.; Bellamy, W. D.; Spangenberg, C. W.; Clark, D. L. In *Proceedings of the 1994 National Conference on Environmental Engineering*. Boulder, CO. ASCE: New York, NY, 1994, pp. 632-639.
10. Brandhuber, P.; Amy, G. *Desalination* **1998**, *117*, 1-10.
11. Seidel, A.; Waypa, J. J.; Elimelech, M. *Environmental Engineering Science* **2001**, *18*, 105-113.

12. Kang, M.; Tamada, S.; Kamei, T.; Magara, Y. *Desalination* **2000**, *131*, 293-298.
13. Hering, J. G.; Elimelech, M. *Arsenic Removal by Enhanced Coagulation and Membrane Processes.* AWWA Research Foundation and American Water Works Association. 1997; 188 pp.
14. Milne, I. H.; McKelvey, Jr. J. G.; Trump, R. P. *Bull. Amer. Ass. Petrol. Geol.* **1964**, *48,* 103-5.
15. Hanshaw, B. B.; Coplen, T. B. *Geochim. Cosmochim. Acta* **1973**, *37*, 2311-27.
16. Fritz, S. J.; Marine, I. W. *Geochim. Cosmochim. Acta* **1983**, *47*, 1515-22.
17. Whitworth, T. M.; Fritz, S. J. *Appl. Geochem.* **1994**, *9*, 533-46.
18. Hanshaw, B. B. *Membrane properties of compacted clays*; Harvard University: Cambridge, MA, 1962, p 113.
19. Fritz, S. J. *Clays Clay Miner.* **1986**. *34(2)*, 214-23.
20. Keijzer, T. J. S.; Kleingeld, P. J.; Loch, J. P. G. In Proceedings of the Conference on Geoenvironmental Engineering: Contaminated Ground: Fate of Pollutants and Remediation, Cardiff, UK, Sept. 16-18, 1997, pp. 199-204.
21. Ishiguro, M.; Matsuura, T.; Detellier, C. *J. Membrane Sci.* **1995**, *107,* 87-92.
22. Li, L.; Whitworth, T. M.; Lee, R. *J. Membrane Science* **2003**. *217*, 215-225.
23. Fritz, S. J.; Whitworth, T. M. *Water Resources Research* **1994**, *30,* 225-35.
24. Whitworth, T. M. Ph.D. Dissertation, Purdue Univrrsity, West Lafayette, IN, 1993.
25. Whitworth, T. M.; Fritz, S. J. *Appl.Geochem.* **1993**, *9*, 533-546.
26. Le, X. C.; Ma, M.; Wong, N. A. *Anal. Chem.* **1996**, *68*, 4501-4506.
27. Marine, I. W.; Fritz, S. J. *Water Resour. Res.* **1981**, *17,* 73-82.
28. Hodgson, T. D. *Desalination* **1970**, *8*, 99-138.
29. Helfferich, F. *Ion Exchange*, McGraw-Hill, New York, NY, 1962, p 642.

Downloaded by UNIV OF GUELPH LIBRARY on September 11, 2012 | http://pubs.acs.org
Publication Date: October 3, 2005 | doi: 10.1021/bk-2005-0915.ch021

Chapter 22

Zeolite Performance as an Anion Exchanger for Arsenic Sequestration in Water

Siddhesh Shevade* and Robert G. Ford

National Risk Management Research Laboratory, U.S. Environmental Protection Agency, Ada, OK 74820
***Corresponding author: siddhesh_shevade@yahoo.com**

Zeolites are well known for their use in ion exchange and acid catalysis reactions. The use of zeolites in anion or ligand exchange reactions is less studied. The NH_4^+ form of zeolite Y (NY6, Faujasite) has been tested in this work to evaluate its performance for arsenic removal from water in continuous-flow reactions. Zeolite NY6 performed well for arsenate removal under simple and complex inlet chemistries. The results from column studies indicate that contact time and zeolite particle size can be varied to optimize both the physical and chemical performance of the continuous-flow process. Evaluation of a physical mixture of NY6 and the NH_4^+ form of zeolite ZSM-5 indicate the potential for treatment of complex contaminant streams containing As, Cd, Pb and MTBE. Overall, these experimental results indicate that synthetic zeolites offer significant flexibility in designing continuous-flow treatment processes for the removal of inorganic and organic contaminants in aqueous waste streams.

In Advances in Arsenic Research; O'Day, P., et al.;
ACS Symposium Series; American Chemical Society: Washington, DC, 2005.

Introduction

Arsenic is of environmental concern due to its toxicity and carcinogenicity (*1,2*). Its presence in water is due to the dissolution of minerals from subterranean strata or from an anthropogenic origin such as the leaching of man-made arsenic compounds from smelting of metal ores, agricultural pesticides, desiccants and wood preservatives. It causes arsenical dermatitis, skin cancer (*3*), neurological effects, enlargement of liver, heart disease and internal cancers (*4*). Techniques such as adsorption (*5,6*), anion exchange (*7*), reverse osmosis (*8*) and coagulation processes (*9,10*) are commonly used for arsenic removal from water. Alumina (*5*) and iron oxide/hydroxides (*10*) are commonly employed for arsenic removal in adsorption and coagulation methods. Iron oxide coated polymer (*11*), and silica containing iron oxides (*12*) have also been tested for arsenic removal from drinking water.

Zeolites are well known for their ion exchange capacity (*13,14,15*). Due to the negative structural charge in zeolites, they are most commonly employed as cation exchangers. The role of zeolites in the conversion of solid and liquid hazardous wastes into environmentally acceptable products has also been successfully evaluated (*16,17*). Several zeolites, namely clinoptilolite (*18*), chabazite (*18*), SZP1 (*19,20*), 13X (*21*) and 5A (*21*) have been identified for arsenic removal from water. Synthetic zeolites Faujasite Y, ZSM-5 and Beta also showed very good arsenic removal properties in our earlier studies (*22*). In published reports on arsenic removal using activated alumina, adsorption via ligand exchange has been identified as the removal mechanism (*5,23*). A similar reaction has been postulated for arsenic sorption onto Al-rich zeolites (*22,24*).

The focus of this study was to examine arsenic removal in continuous-flow column applications. Factors that were examined included pH, empty bed contact time, and the influence of competing ions on arsenic uptake. The main aim was to screen synthetic zeolite Faujasite Y for arsenic removal with short contact time over a wide pH range, which may be a potential water treatment process for drinking water purification and industrial effluent treatment. Zeolite performance was assessed relative to the current and proposed arsenic MCL of 50 and 10 ppb, respectively (*25*).

Experimental

Zeolites Faujasite Y [NY6] (Si:Al = 6) and ZSM-5 [NZ] (Si:Al = 40) were procured in NH_4^+ form (ZEOLYST International, USA). Arsenate solutions were prepared by dissolving sodium arsenate [Na_2HAsO_4 $7H_2O$ (J.T. Baker)] into de-ionized water (Millipore 18 MΩ). Zeolite NY6 was chosen for study, since our previous research demonstrated this material performed well for arsenate removal in batch systems. Zeolite ZSM-5 was employed in this study to evaluate the use of zeolite mixtures for treatment of complex waste streams containing both inorganic and organic contaminants. Companion studies in our laboratory have indicated that ZSM-5 is capable of degrading methyl tert-butyl ether (MTBE). Due to the geochemical conditions that develop in ground water plumes resulting from gasoline spills, MTBE and redox sensitive metals such as arsenic are often encountered as co-contaminants.

Reactions

The continuous-flow reactions were carried out in up-flow, fixed-bed glass column reactors (Kontes Flex-Column, 1.0 cm ID). Zeolite samples of different particle size (0.125-2 mm [120-10 mesh sizes]) were loaded into the column to achieve an equivalent bed volume of 1.8-2.2 ml. Different size fractions of zeolite NY6 were generated by pelletizing the initial fine-grained material and crushing the resultant pellet. Size fractions were subsequently isolated from the crushed material by sieving. Solutions containing 1000 ppb As^V were passed through the column using a peristaltic pump. The pH of inlet and outlet solutions were measured throughout each experiment. Reaction parameters that were tested included empty bed contact time (EBCT), inlet pH, zeolite particle size and the affect of competing ions including nitrate ($Ca(NO_3)_2$) and phosphate (Na_2HPO_4).

A column study was also carried out to assess the capability to treat complex waste streams using a zeolite mixture. For this test, an inlet solution containing 1000 ppb Pb, 1000 ppb Cd and 1000 ppb MTBE along with 1000 ppb As was passed through a mixture of NY6 and NZ (1.0 g of each).

Analysis and Characterization

Chemical analysis of dissolved As, Cd and Pb in aqueous samples was carried out using a Perkin Elmer Optima 3300DV inductively coupled plasma optical emission spectrometer (ICP-OES) or a Perkin Elmer 5100ZL graphite furnace atomic absorption spectrophotometer (GFAAS). MTBE analysis was carried out by gas chromatography using a Tekmar 2000 purge and trap system coupled to an Hewlett-Packard 5890 GC with a flame ionization detector. The limits of arsenic quantitation for ICP-OES and GFAAS were 33 ppb and 2 ppb, respectively.

Results and Discussion

In recent work (*22*) we have studied arsenic removal from pollutant water by using synthetic zeolites. Arsenic removal was examined in batch reaction experiments as a function of pH to assess zeolite performance and stability. The inferences from our previous work are: zeolites achieve arsenic removal via a ligand exchange mechanism; high aluminum containing zeolites showed better arsenic removal capacity; structural stability and pH buffering capacity of zeolites enabled arsenic removal from waste streams with initial pH varying from 2 to 12. Arsenic removal to desired levels was achieved on zeolites within 15 min of reaction time in batch studies (*22,24*), which leads us to the continuous-flow reaction studies presented in this paper.

Effect of Empty Bed Contact Time (EBCT)

In continuous-flow reactions, the time for interaction between the sorbate and sorbent is a critical factor in determining performance for contaminant removal. We investigated the influence of interaction time by varying EBCT, a design parameter required for process scale-up. The results of arsenate removal on zeolite NY6 for three EBCTs (0.36, 1.5 and 4.5 min) are shown in Figure 1. It was observed that the effectiveness of arsenate removal increased with increasing EBCT. For an EBCT of 0.36 min, removal of arsenate below the current EPA MCL (50 ppb) was only achieved through 50 bed volumes (BV). Increase of the EBCT to 1.5 min and 4.5 min resulted in an increase of the number of bed volumes effectively treated to approximately 250 and greater than 300 BV, respectively. Arsenate was removed to a concentration of <10 ppb for an EBCT of 1.5 min, whereas outlet concentrations were greater for an EBCT of 4.5 min. However, there is currently insufficient data to confirm whether there is an optimal EBCT that maximizes both the extent (outlet concentration) and capacity (bed volumes treated) for treatment.

Effect of pH

In the batch reaction studies (*22*) zeolite NH_4^+/Y (NY6) showed arsenate removal over a wide initial pH range 2-12. The capacity to remove arsenate under these conditions was realized due to the ability of the zeolite to buffer pH within a range where ligand exchange was optimal. Arsenic removal capacity decreased significantly outside of this initial pH range due to zeolite instability resulting in transformation to a poorly crystalline aluminosilicate incapable of buffering the reaction pH. The capacity for zeolite NY6 to buffer pH in continuous-flow studies was also examined in this work.

Results of arsenate removal as a function of inlet pH are shown in Figure 2. The reaction was carried out using 1.0 g of zeolite NY6 with a particle size range of 0.125-0.18 mm resulting in a bed volume of 1.8 ml. The EBCT was maintained between 1.4-1.7 min. For an inlet pH of 6.47, arsenate removal

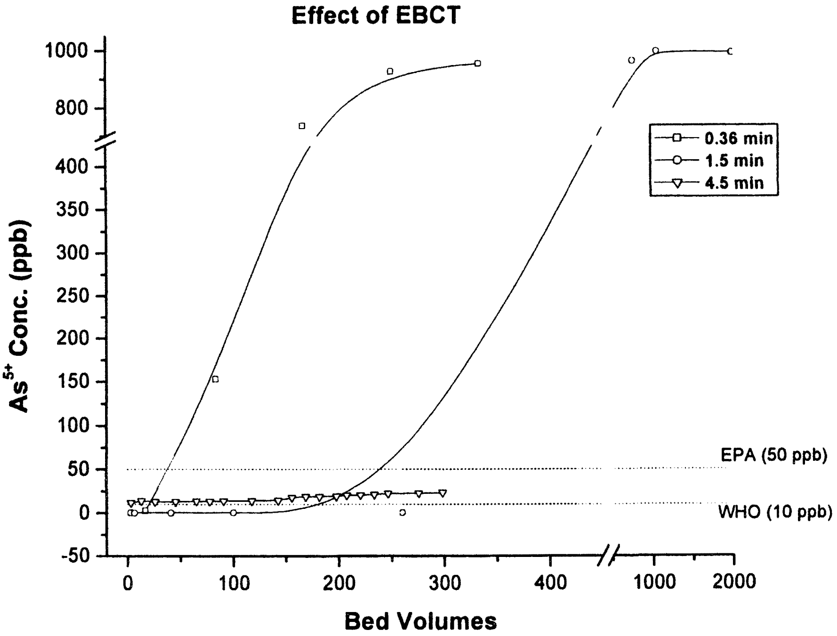

Figure 1. Removal of arsenate as a function of empty bed contact time (EBCT) on NH_4^+/Y (NY6). Reaction conditions: 1.0 g zeolite (1.8 ml bed volume); 1000 ppb As^V; inlet pH ~ 6.5; outlet pH ~ 6.5; zeolite particle size = 0.125-0.18 mm.

below 10 ppb was observed for over 250 BV. When inlet pH was decreased to 2.04, arsenate removal below 10 ppb and 50 ppb was observed for 200 BV and 250 BV, respectively. However, arsenate removal below 50 ppb was achieved for less than 80 BV when the inlet pH was increased to 11.07 (EBCT = 1.5 min), and outlet arsenate concentration exceeded inlet concentration after approximately 125 BV. This decrease in performance may have resulted from an inability of the zeolite to buffer the reaction pH within an optimal range due to the short contact time. Increasing the EBCT to 4.7 min slightly improved performance (in excess of 50 ppb after 120 BV), but these results demonstrate that there are limits to the ability of zeolite NY6 to buffer pH in a continuous-flow reaction.

This observation can be explored in more detail based on results shown in Figure 3. Outlet pH as well as incremental and cumulative arsenate removal are shown as a function of bed volumes treated for the experiments documented in Figure 2. For all experiments the outlet pH was initially buffered within a pH range of approximately 4 to 6. However, there is a transition starting after approximately 100 BV where the outlet pH begins converging to the inlet pH (Figure 3A). This demonstrates a limitation in the ability of the zeolite to buffer the reaction pH under the conditions of these column experiments. The impact of this phenomenon on arsenate removal is shown in Figures 3B and 3C. Incremental arsenate removal was calculated based on the measured loss of solution As for the BV (1.8 ml for all column experiments) during which the sample was collected. These results show that arsenate was removed at a rate of approximately 1.8 (mg As/kg zeolite)/BV for up to 100 BV under all conditions. This apparent rate of removal was maintained for the entire period of observation for column experiments receiving inlet solutions at pH 2.04 and 6.47. For the pH 2.04 experiment, zeolite performance eventually dropped off as indicated by an increase in As^V outlet concentration (0.9 ppb at 189 BV, 42.0 ppb at 263 BV). Complete column failure occurred for experiments conducted at pH 11.07 as indicated by net desorption of arsenate from the zeolite after approximately 125 BV. Increasing the EBCT from 1.7 to 4.7 min did not improve zeolite performance, and calculation of cumulative arsenate removal suggests that zeolite performance was further degraded. This observation is consistent with previous results shown in Figure 1, suggesting that there are non-beneficial reactions within the column that become more important with increasing residence time in these column experiments.

Effect of zeolite particle size

Investigation of the effect of particle size on zeolite performance was considered important for development of a continuous-flow treatment process. In general, particle reactivity is expected to increase with decreasing particle size

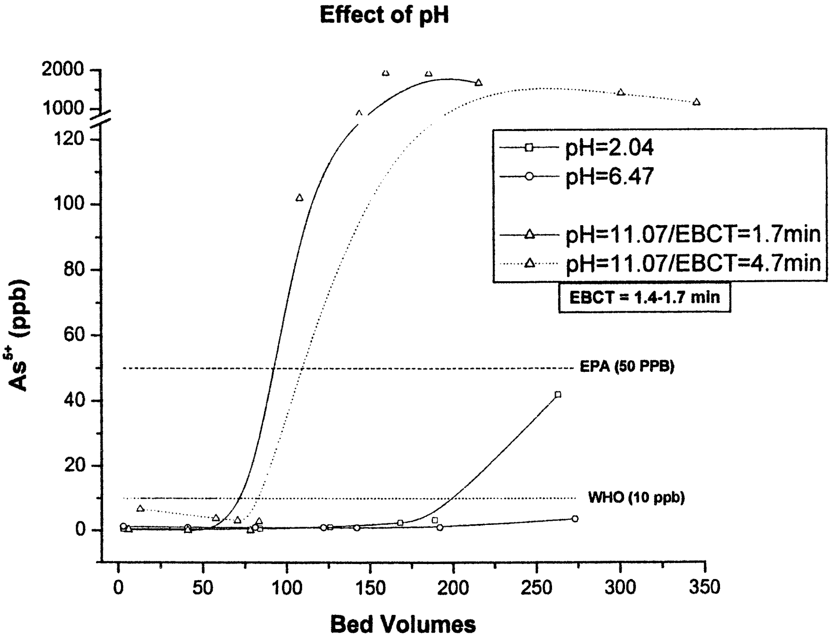

Figure 2. The effect of pH on arsenate removal by NH_4^+/Y (NY6). Reaction conditions: 1000 ppb initial As^V; EBCT = 1.4-1.7 min; zeolite = 1.0 g (bed volume = 1.8 ml, zeolite particle size = 0.125-0.18 mm.

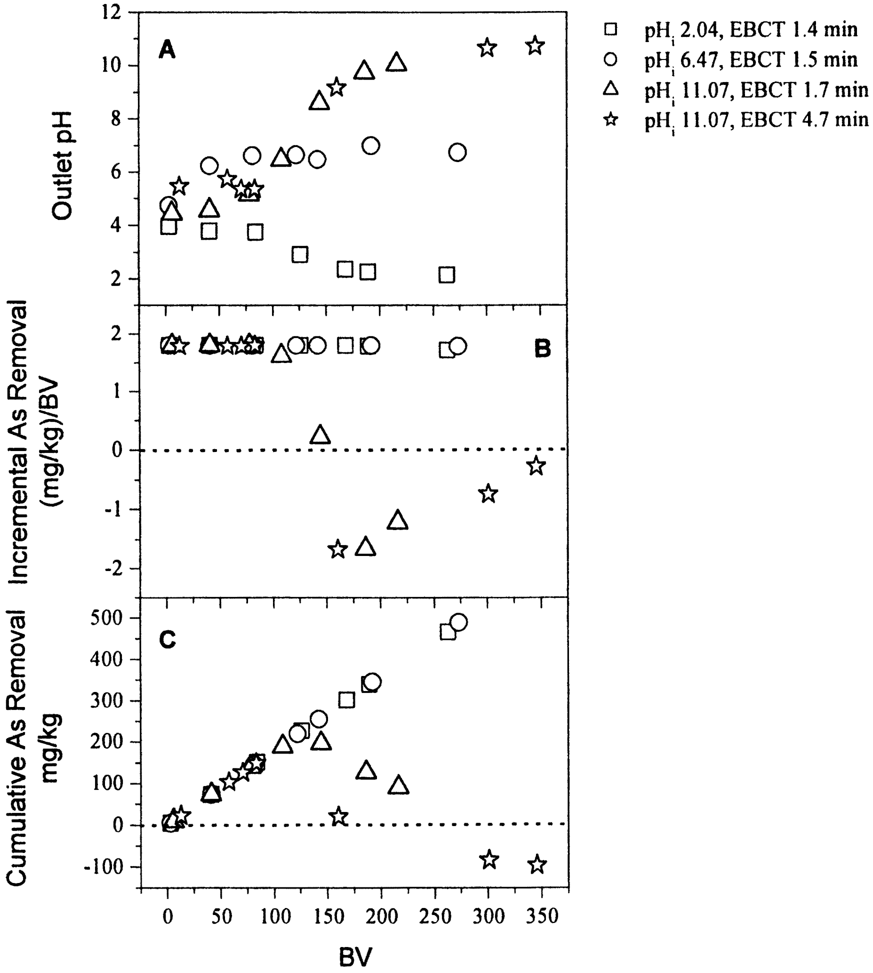

Figure 3. Outlet pH (A), incremental (B) and cumulative (C) arsenate removal patterns for column experiments documented in Figure 2. Arsenate removal expressed as mg As per kg zeolite. Column conditions: 1.0 g zeolite NY6; BV = 1.8 ml; 1000 ppb As.

due to concurrent increase in reactive surface area. However, fine-grained solids can cause performance problems in column applications due to the development of back pressure. To address this issue, we isolated a range of zeolite size fractions (0.125-2 mm overall size range [120-10 mesh sizes]) by sieving and tested column performance using a fixed mass of zeolite (1 g dry material) in all experiments. Results of these experiments are shown in Figure 4. It was observed that with larger particles, zeolite performance decreased significantly as referenced to the currently enforced EPA MCL. This may be because of the short-circuiting effect caused by the larger zeolite particles and comparatively smaller column dimensions. With particle size 0.85-2 mm (10-20 mesh), the zeolite was not at all effective. This may be because of the short-circuiting effect. Reduction of zeolite particle size within the range of 0.425-0.85 mm (20-40 mesh) improved performance, but only through approximately 60 bed volumes. With the smallest particle size range (0.125-0.18 mm [80-120 mesh]), the zeolite was effective through ~350 bed volumes. These results point toward the possibility of tailoring the zeolite particle size to optimize both physical and chemical performance of the system in order to optimize process operation.

Effect of competing anions

Since ligand exchange is proposed as the mechanism of arsenate sorption to zeolite NY6, the influence of competing anions was tested to evaluate the influence on zeolite performance. Competing anions nitrate and phosphate were tested. In these experiments the concentrations of these impurities were maintained in the range of their MCL for EPA regulated chemicals or SMCL (suggested maximum contaminant level) for EPA unregulated chemicals (i.e., $NO_3^- = 331$ ppm; $PO_4^{3-} = 2$ ppm).

Arsenate removal is shown in Figure 5. These results indicate that zeolite performance did not differ significantly in the absence or presence of nitrate in single competing anion experiments. There was reduction in arsenate sorption in the presence of phosphate. In arsenate removal experiment with nitrate impurity, the zeolite NY6 was effective below EPA limits through 160 bed volumes as compared to 200 bed volumes in the blank experiment. The phosphate ions reduced the zeolite effectiveness to 110 bed volumes. Further investigation examining the influence of potential determining ions on zeolite surface charge will be an important component towards process optimization.

Effect of complex inlet solution

Overall zeolite performance will depend on the chemical composition of the inlet solution. Most contaminated waters resulting from industrial processes or

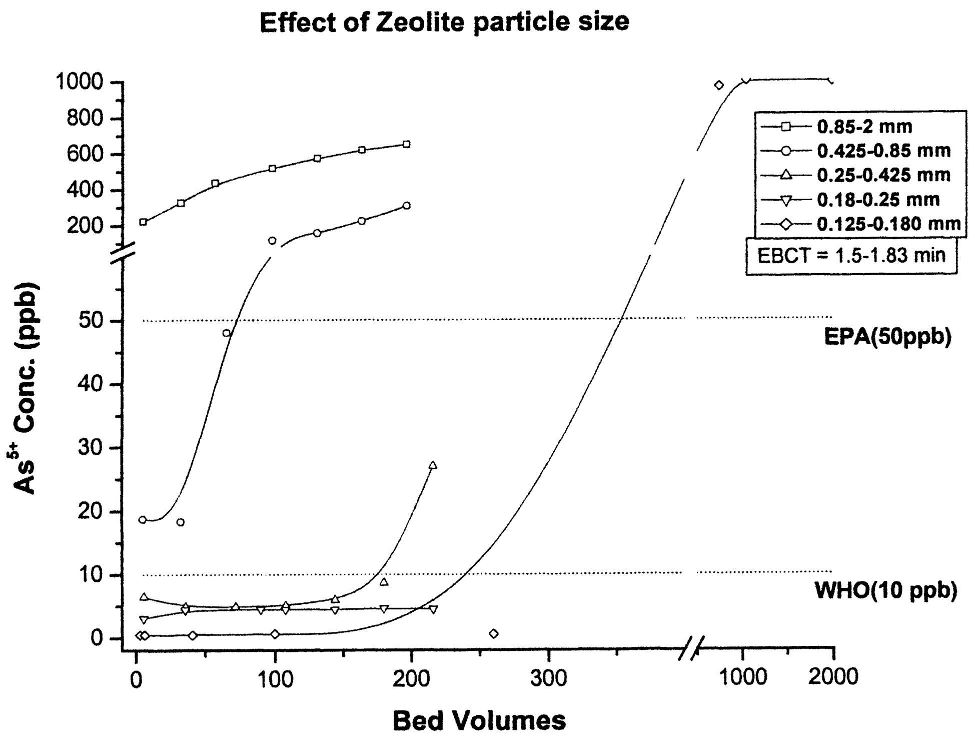

Figure 4. The effect of zeoliteparticle size on arsenate removal by NH_4^+/Y (NY6). Reaction conditions: 1000 ppb initial As^V; zeolite =1.0 g; EBCT = 1.5-1.83 min; inlet pH ~ 6.5.

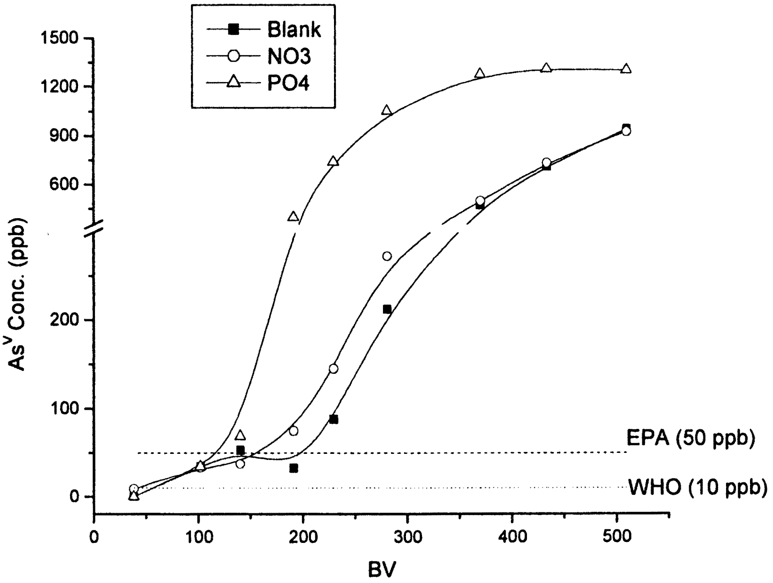

Figure 5. The effect of inorganic impurities on arsenate removal by NH_4^+/Y (NY6). Reaction conditions: ~1000 ppb initial As^V; zeolite=1.0 g; inlet and outlet pH ~7.0; EBCT = 1.4-1.7 min; impurity conc.: NO_3^{2-} (331 ppm), PO_4^{3-} (2 ppm).

environmental contamination will possess a mixture of inorganic and organic contaminants at varying concentrations. Since zeolites possess beneficial properties for cation/anion exchange and organic compound degradation, we tested the performance of select zeolite materials for the simultaneous removal of As, Cd, Pb and MTBE in an aqueous system. Our previous work has demonstrated that zeolite NH_4^+/Y (NY6) performed well for the removal of As, Cd and Pb, while zeolite NH_4^+/ZSM-5 (NZ) could be used to degrade MTBE.

A physical mixture of zeolites NY6 and NZ with particle size in the range of 0.125-0.85 mm were loaded into a column as previously described. Contaminant removal was assessed using an EBCT of 3.8 min (BV = 3.1 ml). The results of this experiment are shown in Figure 6. The zeolite mixture successfully removed arsenate below the EPA (50 ppb) and WHO (10 ppb) MCL for 250 and 200 BV, respectively. The zeolite mixture also resulted in Cd removal through 1200 BV below the EPA MCL (5 ppb) and Pb removal through 1800 BV below the EPA MCL (15 ppb). The mixture showed MTBE removal through 4200 BV below the EPA advisory limit (20 ppb). These results indicate that component additivity may be used as a basis for preparing tailored zeolite mixtures to optimize performance for complex waste streams. The use of physical zeolite mixtures may preclude the need to synthesize alternative zeolites for the treatment of complex mixtures, warranting further investigation.

Conclusion

In column studies, the NH_4^+/Y zeolite performed well for arsenate removal under a range of inlet conditions. As observed for batch reactions (*22*), zeolite performance was very good over a wide pH range, although there is an apparent limitation in the zeolite's pH buffering capacity in a continuous-flow system. The presence of competing anions may degrade or enhance zeolite performance apparently through modifying the capacity to buffer the reaction pH. However, experiments testing contaminant removal in complex aqueous streams indicate that all competing effects may balance out, resulting in no net loss in zeolite performance. This research also demonstrates the possibility of applying physical mixtures of zeolites possessing the desired properties for treatment of waste streams containing mixtures of inorganic and organic contaminants. These results are promising for the use of synthetic zeolites to treat contaminated ground water and industrial waste effluents, since these materials possess the triple capacity for cation/anion exchange and organic compound degradation.

Acknowledgement

The analytical support of Dr. Ning Xu and Ms. Sandra Saye from ManTech Environmental Research Services, Inc. is acknowledged. The U. S.

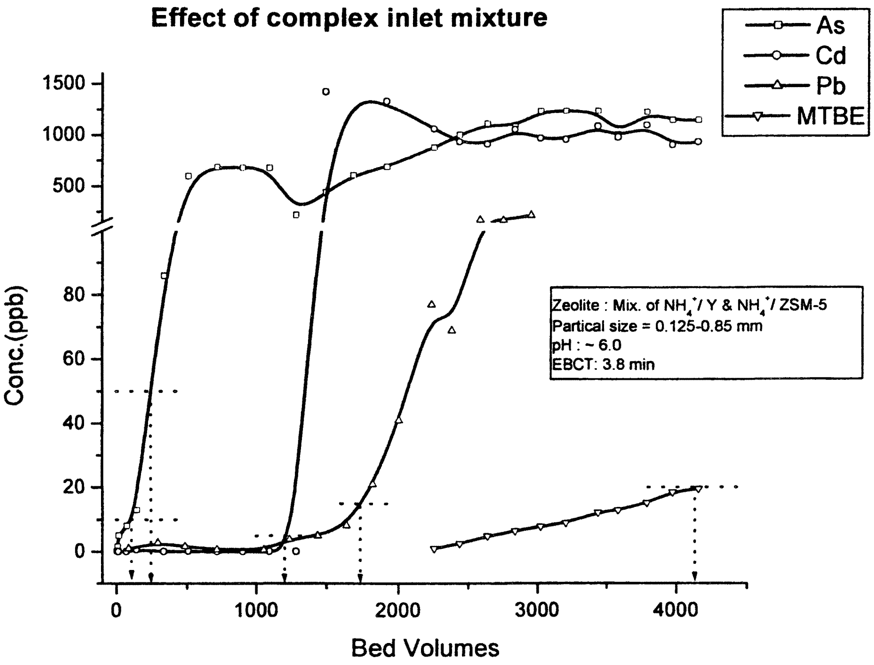

Figure 6. Effect of complex inlet mixture; reaction conditions: inlet conc. = ~ 1000 ppb of As, Cd, Pb and MTBE; zeolite: mixture of 1.0 g NH_4^+/Y (NY6) and 1.0 g NH_4^+/ZSM-5 (NZ); particle size = 0.125-0.85 mm; bed vol. = 3.1 ml; inlet pH: ~ 6.0; EBCT: 3.8 min.

Environmental Protection Agency through its Office of Research and Development funded and managed the research described here. The work was performed while Dr. Siddhesh Shevade held a National Research Council, National Risk Management Research Laboratory, Ground Water and Ecosystems Division Research Associateship. This document has not been subjected to Agency review and therefore does not necessarily reflect the views of the Agency, and no official endorsement should be inferred.

References

1. World Health Organization *Toxic effects of arsenic in humans*, URL http://www.who.int/peh-super/0th.lec/Arsenic/series4/002.html.
2. U.S. Environmental Protection Agency *Arsenic in drinking water: health effects research*, URL http://www.epa.gov/OGWDW/ars/ars10.html.
3. Dutta, A.; Chaudhuri. M. *Aqua.* **1991**, *40(1)*, 25-29.
4. Pontius, F.W. *J. Am. Water Works Assoc.* **1994**, *86(*9), 6.
5. Stumm, W.; Morgan, J.J. *Aquatic Chemistry: Chemical Equilibria and Rates in Natural Waters*, 3rd edition, Wiley: New York, NY, 1996.
6. Clifford, D.A.; Ghurye, G.L. in *Environmental Chemistry of Arsenic;* Frankenberger, W.T., Ed.; Marcel Dekker, New York, NY, 2002.
7. Ghurye, G.L.; Clifford, D.L.; Tripp, A.R. *J. Am. Water Works Assoc.* **1999**, *91*, 85-96.
8. Sorg, T.J.; Logsdon, G.S. *J. Am. Water Works Assoc.* **1978**, *70*, 379-392.
9. Hering, J.G.; Elimelech, M. *Am. Water Works Assoc. Research Foundation,* Report 90706: Denver, CO, 1996.
10. Driehaus, W.; Jekal, M.; Hildebrand, U. *J. Water.* **1998**, *47*, 30-35.
11. Katsoyiannis, I.A.; Zouboulis A.I. *Water Res.* **2002**, *36(20)*, 5141-5155.
12. Zeng, L. *Water Res.* **2003**, *37(18)*, 4351-4358.
13. Barrer, R.M. *Hydrothermal Chemistry of Zeolites*, Academic Press,: New York, NY, 1982.
14. Breck, D.W. *Zeolites Molecular Sieves;* Wiley: New York, NY 1974.
15. Nishino, A. *Catal. Today* **1991**, *10*, 107-112.
16. Weitkamp, J. Karge, H.G. *Proc. Inter. Symp. Environ. Catal.*, Tokyo, 1993, 292-310

17. Iwamoto, M. *Stud. Surf. Sci. Catal.* **1994**, *84*, 1395-1400.
18. Bonnin, Dagmar . *Proc. Annu. Conf., Am. Water Works Assoc.*, **1997**, 421-425.
19. Xu, Y.; Ohki, A.; Maeda, S. *Chemistry Letters* **1998**, *10*, 1015-1020.
20. Xu, Y.; Ohki, A.; Maeda, S. *Toxi. & Env. Chem.* **2000**, *76 (1,2)*, 111-115.
21. Abdel-Fattah, M. Tarek, Ansari, Z. Ahsan , Voice, C. Thomas. ACS National meeting: Div. Env. Chem **2000**, *40(1)*, 422-425.
22. Shevade, S.; Ford, R. *Water Res.* **2004**, *38*, 3197-3204.
23. Goldberg S.; Johnston. C. *J. Colloid Int. Sci.* **2001**, *234(1)*, 204-216.
24. Shevade, S.; Ford, R.; Puls, R. ACS Natl. meet: Div. Env. Chem; **2001**, *41(2)*; 131-134
25. U.S. Environmental Protection Agency *Drinking Water Standard for Arsenic*, EPA Report 815-F-00-015: Washington, DC, 2001.

Chapter 23

Characterization of Arsenic-Containing Water Treatment Residuals

Hun-Young Wee and Timothy A. Kramer

Department of Civil Engineering, Texas A&M University, 3136 TAMU,
College Station, TX 77843–3136

The characterization of water treatment residuals containing arsenic was examined and arsenic desorption and leachability from the residuals were focused. Solution pH is a critical variable in controlling arsenic stability in the residuals. The release of arsenic from the residuals was elevated at low and high pH due to the increase dissolution of the adsorbents such as Fe and Al hydroxides. The negatively charged surfaces of the adsorbents at high pH reduced arsenic anion adsorption. Competition with phosphate can play a significant role for the arsenic leaching from residuals because phosphate tends to compete with As(V) on the sorption sites. The cooperative effects of calcium can help to bind arsenic on metal hydroxides. Arsenic leaching from water treatment residuals was found to be underestimated by the toxicity characteristics leaching test (TCLP) due to the pH of the leachates being favorable for As(V) adsorption.

In Advances in Arsenic Research; O'Day, P., et al.;
ACS Symposium Series; American Chemical Society: Washington, DC, 2005.

Introduction

Arsenic is commonly recognized as a toxic and carcinogenic metal compound *(1)*. The adverse health effects when humans are exposed to arsenic compounds are well documented *(2)*. Arsenic contamination of groundwater and/or drinking water has been reported as a critical water quality issue in Vietnam, Bangladesh, and West Bengal, India *(3, 4, 5)*. In particular, 70 million people in Bangladesh have been poisoned due to naturally occurring arsenic in wells used for drinking water sources *(6)*, and highly elevated concentrations of arsenic (greater than 1 mg/L) have been commonly detected.

The U.S. Environmental Protection Agency (USEPA) has lowered the maximum contaminant level (MCL) of arsenic from 50 to 10 µg/L, effective in 2006 *(2)*. Numerous treatment technologies have been developed and applied to arsenic removal from various contaminated waters. Theses technologies may be grouped to four major categories: precipitative processes, membrane processes, adsorptive processes, and ion exchange *(7, 8)*. Most arsenic compounds are physically separated from waters and condensed. In addition, appreciable volumes of arsenic-contaminated residuals are expected to be produced to match the revised MCL.

The overall objective of this paper is to discuss the arsenic desorption characteristics depending on the pH and the presence of solutes such as phosphate, sulfate, and calcium. Arsenic leaching by the toxicity characteristic leaching procedure (TCLP) is also studied.

Arsenic in Water Treatment Residuals

Limited work has been conducted on the characterization of arsenic containing residuals. Amy et al. *(8)* investigated arsenic leachability in various water treatment plant (WTP) residuals using the TCLP. The results showed that the arsenic concentration in the residuals generated from WTPs was vastly different and soluble arsenic concentrations in the leachates also varied depending on residuals. However, the concentrations of arsenic in the leachates were not over the limit of 100 times of MCL for arsenic (5 mg/L). Thus, the landfill disposal alternative was recommended for arsenic containing WTP residuals. Soluble arsenic concentrations in residuals generated from iron-based precipitation treatment were studied depending on the redox conditions *(9)*. They divided three redox zones: adsorption, mobilization, and reductive fixation. In the mobilization zone, soluble arsenic concentration was great due to the reductive dissolution of iron oxides and oxidative dissolution of arsenic containing minerals such as arsenian pyrite ($Fe(S,As)_2$) and arsenopyrite (FeAsS). To minimize arsenic mobility, the maintenance of high redox and neutral pH was suggested when arsenic leaching behaviors in municipal sewage sludge were investigated depending on the redox conditions and pH *(10)*.

Arsenic Desorption Studies

Effects of pH on Arsenic Desorption

Solution pH is a critical variable in controlling arsenic stability in solid matrices due to the ionization characteristics of As(III) and As(V) being significantly different. The pK_a values of inorganic arsenic species are As(III) ($pK_1 = 9.2$ and $pK_2 = 12.1$) and As(V) ($pK_1 = 2.2$, $pK_2 = 6.96$, and $pK_3 = 11.5$) (11). At normal natural pH environments (pH 4-9), $HAsO_4^{2-}$ and $H_2AsO_4^-$ are the dominant species for As(V) and $H_3AsO_3^0$ for As(III) *(12)*.

The six different residuals were collected from different water treatment plants. These residuals represent granular ferric oxy-hydroxide (Residual 1 and 3), granular activated alumina (Residual 2), ferric chloride addition (Residual 5), alum addition (Residual 6), and lime softening (Residual 4). The concentrations of major metals obtained from the residuals are shown in Table I.

Table I. Concentrations of major metals in residuals.

Residual	*Total As (mg/kg)*	*Total Fe (mg/kg)*	*Total Al (mg/kg)*	*Total Ca (mg/kg)*	*Total Mn (mg/kg)*
1	2700	520000	210	1500	740
2	33	21000	300000	5600	10
3	2300	500000	990	5700	850
4	15	24000	18000	36000	430
5	150	50000	30000	18000	710
6	400	20000	46000	1900	1400

Figure 1 shows the soluble As(III) and As(V) concentrations in the residuals as pH changes. Higher arsenic concentrations were observed at low and high pH. As(III) concentrations were highest at pH 4, and soluble As(V) concentrations were highest at pH 10. The maximum adsorption for As(V) and As(III) on iron and aluminum hydroxides usually occurs around pH 5 and pH 9, respectively *(13, 14)*. Results of soluble Fe and Al concentrations were similar to those of

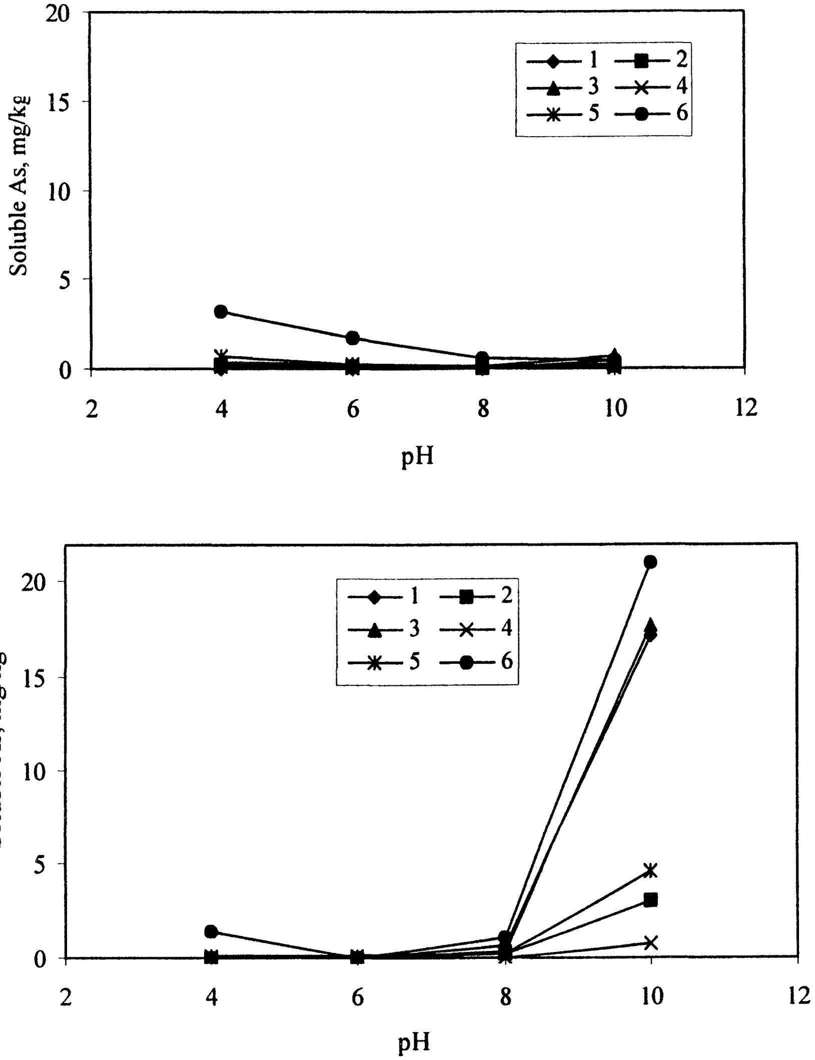

Figure 1. Effect of pH on arsenic leaching: (A) As(III), and (B) As(V). NOTE: Unit of soluble As is based on the dry solids.; Weight ratio of dry solids to extract solution (DI water titrated to a desired pH) was 1:20.

arsenic (data not shown). Interestingly, higher leached Fe and As(V) concentrations in residuals samples 1 and 3, both a granular ferric hydroxide, were observed simultaneously at pH 10 due to the dissolution of the Fe hydroxides and, subsequent, As(V) release.

The As(III) and As(V) desorption trends can be explained by the dissolution of Fe and Al hydroxides (i.e., increase of solubility) and the charge of the arsenic species. The solubility diagrams of the Fe hydroxides and Al hydroxides as a function of pH are shown in Figure 2 and Figure 3, respectively *(15)*. Activity coefficients for the species were ignored, so activities and concentrations were assumed to be equal.

By the amphoteric behavior, the solids, such as Fe and Al hydroxides, are dissolved to form cationic species at low pH and to form anionic species at high pH *(15)*. During the dissolution of Fe and Al hydroxides, surface arsenic species can also be dissolved. At pH 4, the predominant As(III) species is $H_3AsO_3^0$, which has a neutral charge. The surfaces of Fe and Al hydroxides are positively charged at low pH. Therefore, the dissolution of metal hydroxides and a positively charged surface of the metal hydroxides and a neutral charge of dominant As(III) species facilitate the release of bound arsenic, and readsorption of leached As(III) cannot readily occur. At pH 4, the prevalent species for As(V) is $H_2AsO_4^-$, which can be easily adsorbed onto the metal hydroxides. Thus, soluble As(V) concentration in the leachate was lower than that of As(III) at low pH.

The surfaces of Fe and Al hydroxides are negatively charged at high pH. Therefore, the increasingly negative surface potential with increasing pH makes for unfavorable conditions for the adsorption of anionic arsenic species such as $HAsO_4^{-2}$ for As(V) and $H_2AsO_3^-$ for As(III) at pH 10. In brief, the increasing negative surface charge of the metal hydroxides with increasing pH promote the desorption of As(V). The neutrally and negatively charged species of As(III) are predominant at pH 10 and thus, As(III) should be released due to repulsion from the negatively charged surface of metal hydroxides. It is hypothesized that, at pH 10, the reason why leached As(III) concentrations were less than As(V) might be the lower concentrations of As(III) contained in the residuals and the presence of neutrally charged species of As(III).

At neutral pH (pH 6 and 8), the released arsenic, soluble Fe, and Al concentrations were very low due to the insolubility of the Fe and Al hydroxides and the predominant arsenic species. When the disposal of arsenic tainted residuals is planned without any post-treatment, the neutral pH condition of the system should be maintained to minimize arsenic solubility and mobilization.

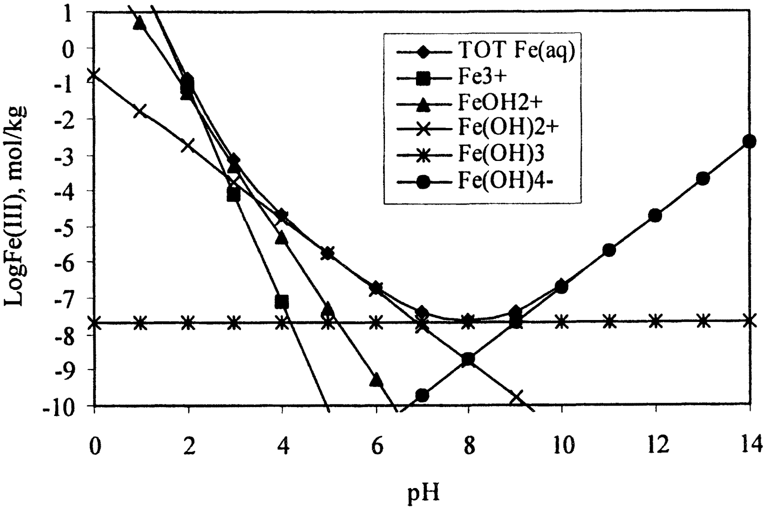

Figure 2. Solubility of amorphous $Fe(OH)_3$, $K_{sp} = 10^{-37.1}$, *as a function of pH at 25°C.*

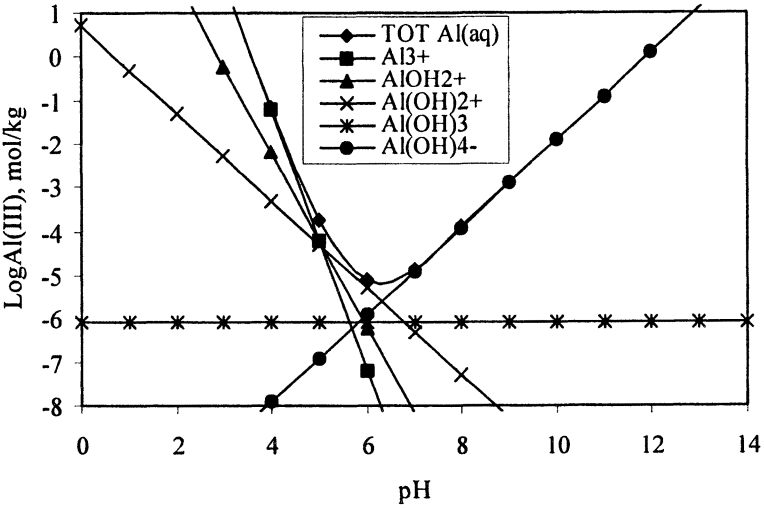

Figure 3. Solubility of amorphous $Al(OH)_3$, $K_{sp} = 10^{-31.2}$, *as a function of pH at 25°C.*

Effects of Phosphate on As Desorption

The mobilization of bound arsenic on adsorbents is strongly influenced by the presence of ligands that can compete with arsenic for surface sorption sites. In particular, phosphate tends to compete with As(V) for sorption sites on the surface of the metal hydroxides (equation 1) and thus, tends to extract the As(V) compounds *(16, 17, 18)*. The adsorption behavior of phosphate and As(III) are vastly different and a significantly higher concentration of bound As(III) compared to As(V) was observed on iron minerals in the presence of 0.1M sodium phosphate *(19, 20)*.

$$\text{Fe-oxide-AsO}_4\text{H} + \text{HPO}_4^{2-} \rightarrow \text{Fe-oxide-PO}_4\text{H} + \text{HAsO}_4^{2-} \qquad (1)$$

As(III) and As(V) concentrations released by the competition with phosphate are shown in Figure 4. The results indicated that As(V) was the dominant arsenic species extracted by phosphate. The granular ferric hydroxide residuals, 1 and 3, contained high concentrations of total arsenic (data not shown) and thus, the concentration of As(V) released in the two residuals was much higher than that in the other residuals samples.

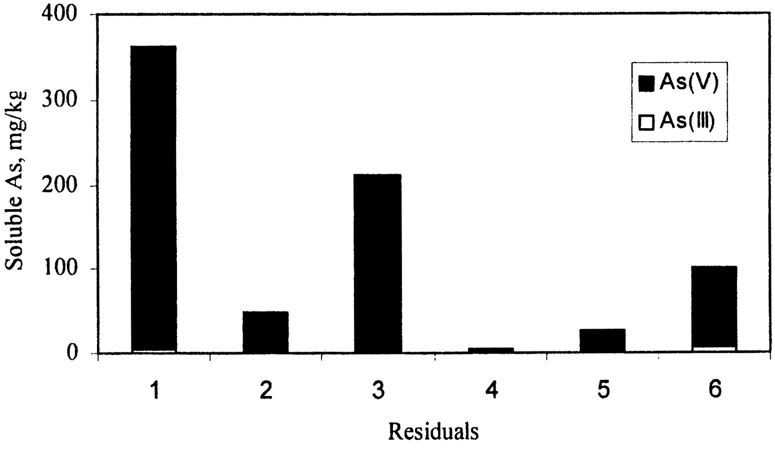

Figure 4. Competitive desorption of arsenic with phosphate. Note: Unit of soluble As is based on the dry solids.; Weight ratio of dry solids to extract solution (0.1M phosphate, pH 7) was 1:20.

Effects of Calcium on As Desorption

Calcium can play an important role to stabilize the bound arsenic compounds on metal hydroxides at high pH *(21)*. Figure 5 shows that arsenic leaching from the residuals which were prepared with the addition of calcium hydroxide as a neutralizing agent is less than release from the residuals with the addition of sodium hydroxide.

The negatively charged surface of iron hydroxides changes to positive by sorption of calcium (equation 3 and 4) so that favorable conditions for negatively charged arsenic sorption exists *(22)*.

$$\equiv Fe^{w}OH^{0} + Ca^{2+} = \equiv Fe^{w}OCa^{+} + H^{+} \qquad (3)$$

$$\equiv Fe^{s}OH^{0} + Ca^{2+} = \equiv Fe^{s}OHCa^{2+} \qquad (4)$$

The cooperative effect of calcium was found in the phosphate adsorption on goethite in seawater, i.e. the enhancement of phosphate adsorption was observed in the presence of calcium at high pH *(23)*. The addition of calcium shows that a less leachable arsenic containing residual can be generated by desorption studies in the presence of phosphate (Figure 6). The formation of solid phase calcium-phosphate and calcium-arsenate compounds may also be responsible for the reduced arsenic desorption in the presence of calcium.

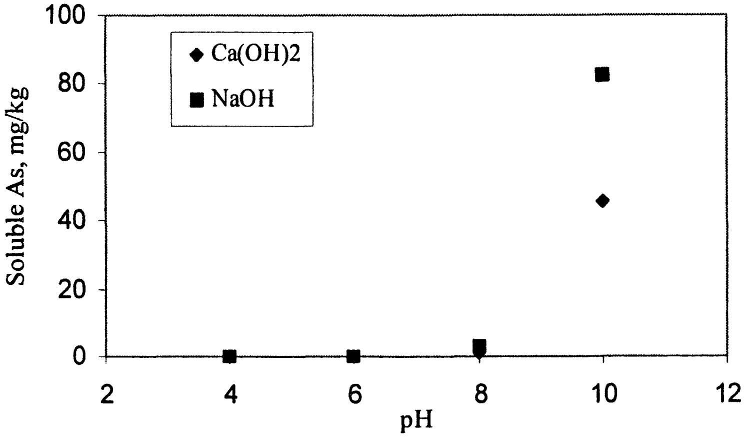

Figure 5. Desorption of As(V) at different pHs in the two residuals. NOTE: Unit of soluble As is based on the dry solids.; Weight ratio of dry solids to extract solution (DI water titrated to a desired pH) was 1:20.

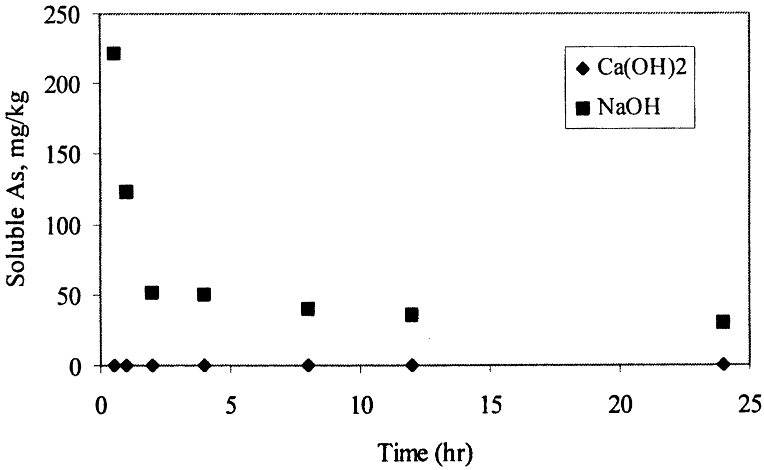

Figure 6. Desorption kinetics of As(V) in the two residuals in the presence of 0.1 M phosphate. Note: Unit of soluble As is based on the dry solids.; Weight ratio of dry solids to extract solution (0.1M phosphate, pH 7) was 1:20.

Consequently, the addition of calcium is very helpful to prevent arsenic desorption at high pH and in the presence of phosphate. However, various experiments, surface analyses, and supporting data are required to identify the cooperative roles of calcium.

Toxicity Characteristic Leaching Procedure (TCLP)

The *toxicity characteristics leaching procedure* (TCLP), a regulatory test, is employed to determine whether a particular contaminant can be disposed in a landfill *(24)*. Evaluation of stabilization techniques has been broadly conducted using the TCLP method *(25)*. In the leaching test, target solid materials are crushed to small size, mixed with an extraction liquid, and agitated in a rotary reactor for 18 hours. Subsequently, insoluble and soluble phases are separated through a filter. However, it was reported that the TCLP would not be a suitable leaching test to predict the release of contaminants (oxoanion-forming elements) from municipal solid wastes *(26)*. The pH values of TCLP extraction solutions (type I = 4.93 and type II = 2.88) are favorable for As(V) adsorption on adsorbents so arsenic leaching could be underestimated by the test *(16)*.

Two field residuals were subjected two types of leaching solution for the TCLP. Results of TCLP type I (0.1M acetic acid & 0.064M NaOH, pH 4.93) and type II (0.1M acetic acid, pH 2.88) are presented in Table II and Table III, respectively.

Table II. Results of TCLP extraction solution type I.

Residual	*Final pH*	*As(III) (mg/kg)*	*As(V) (mg/kg)*	*Fe (mg/kg)*	*Al (mg/kg)*	*Ca (mg/kg)*
1	5.44	< 0.02	0.37	< 1	< 20	1070
2	5.18	0.10	0.07	0.60	160	5300
3	5.14	0.29	0.15	< 1	< 20	8400
4	6.61	0.06	0.24	< 1	< 20	11000
5	5.94	0.31	0.79	3.10	< 20	8500
6	5.48	2.50	6.10	48	150	820

Table III. Results of TCLP extraction solution type II.

Residual	*Final pH*	*As(III) (mg/kg)*	*As(V) (mg/kg)*	*Fe (mg/kg)*	*Al (mg/kg)*	*Ca (mg/kg)*
1	3.50	< 0.02	0.62	130	< 20	1400
2	4.01	0.16	< 0.02	6.40	3600	3500
3	3.76	0.33	< 0.02	2.80	< 20	5800
4	4.93	0.07	0.20	290	< 20	28000
5	4.30	0.72	1.70	3400	200	12000
6	3.97	5.0	14	920	4500	880

From these data, it is concluded that pH is critical for the release of As, Fe, Al, and Ca. In oxidized systems, the solubility, adsorption and movement of arsenic (As(III) and As(V) both) are controlled predominantly by adsorption reactions with oxide minerals such as Fe and Al oxides (12, 16). At low pH (3-5), solubility of the Fe and Al oxides increases and thus, the concentration of inorganic arsenic released in the leachates is expected to be also increased. However, maximum As(V) adsorption on Fe and Al oxides is usually achieved at low pH (4-5) (13, 27). Comparing to these two data to the results of arsenic desorption at high pHs (Figure 1) and competitive desorption with phosphate (Figure 4), arsenic leaching might be underestimated through the use of TCLP.

Conclusions

Various environmental factors may affect arsenic desorption. In high and low solution pHs, soluble concentrations of As(V) and As(III) were increased respectively. Phosphate can compete with As(V) on sorption sites. Thus, in the presence of phosphate, the release of As(V) was enhanced. Under aerobic conditions, effects of sulfate on arsenic desorption were minor but an important role of sulfur compounds should be considered in the anaerobic conditions. The cooperative action of calcium for arsenic binding on metal hydroxides was observed. These findings indicate that the TCLP test may not be suitable to predict arsenic leaching in residuals.

Acknowledgements

The authors would like to acknowledge the financial support for this research from the AWWA Research Foundation (AWWARF), Denver, Colorado.

References

1. Bates, M. N.; Smith, A. H. *Am. J. Epidemiol.* **1992,** *135*, 462-476.
2. USEPA. *National Primary Drinking Water Regulations; Arsenic and Clarifications to Compliance and New Source Contaminants Monitoring; Final Rule.* **2001,** Federal Register, 66:6975.
3. Berg, M.; Tran, H. C.; Nguyen, T. C.; Pham, H. V.; Schertenleib, R.; Giger, W. *Environ. Sci. Technol.* **2001,** *35*, 2621-2626.
4. Chakraborti, D.; Biswas, B. K.; Chowdhury, T. R.; Basu, G. K.; Mandal, B. K.; Chowdhury, U. K.; Mukherjee, S. C.; Gupta, J. P.; Chowdhury, S. R.; Rathore, K. C. *Curr. Sci. India* **1999,** *77*, 502-504.
5. Nickson, R.; McArthur, J.; Burgess, W.; Ahmed, K. M.; Ravenscroft, P.; Rahman, M. *Nature* **1998,** *395*, 338.
6. Lepkowski, W. *Chem. Eng. News* **1998,** *76*, 27-29.
7. USEPA. *Arsenic Treatment Technologies for Soil, Waste, and Water. Solid Waste and Emergency Response.* **2002,** EPA-542-R-02-004.
8. Amy, G.; Edwards, M.; Benjamin, M.; Carlson, K.; Chwirka, J.; Brandhuber, P.; McNeil, L.; Vagliasindi, F. *Arsenic Treatability Options and Evaluation of Residuals Management Issues.* **2000,** Denver, CO: AWWARF and AWWA.
9. Meng, X.; Korfiatis, G. P.; Jing, C.; Christodoulatos, C. *Environ. Sci. Technol.* **2001,** *35*, 3476-3481.

10. Carbonell-Barrachina, A. A.; Jugsujinda, A.; Burlo, F.; Delaune, R. D.; Patrick, W. H. *Water Res.* **1999,** *34,* 216-224.
11. Cherry, J. A.; Shaikh, A. U.; Tallman, D. E.; Nicholson, R. V. *J. Hydrol.* **1979,** *43,* 373-392.
12. Sadiq, M. *Water Air Soil Poll.* **1997,** *93,* 117-136.
13. Raven, K. P.; Jain, A.; Loeppert, R. H. *Environ. Sci. Technol.* **1998,** *32,* 344-349.
14. Goldberg, S.; Johnston, C. T. *J. Colloid Interf. Sci.* **2001,** 234, 204-216.
15. Langmuir, D. *Aqueous Environmental Geochemistry*; Prentice-Hall: Upper Saddle River, NJ, 1997; pp 231-265.
16. Loeppert, R. H.; Jain, A.; El-Haleem, M. A. A.; Biswas, B. K. *Biogeochemistry of Environmentally Important Trace Elements* **2003,** ACS Sym. Ser. 835, 42-56.
17. Hongshao, Z.; Stanforth, R. *Environ. Sci. Technol.* **2001,** *35,* 4753-4757.
18. Hiemstra, T.; Van Riemsdijk, W. H. *J. Colloid Interf. Sci.* **1999,** *210,* 182-193.
19. Jackson, B. P.; Miller, W. P. *Soil Sci. Soc. Am. J.* **2000,** 64, 1616-1622.
20. Jain, A.; Loeppert, R. H. *J. Environ. Qual.* **2000,** 29, 1422-1430.
21. Wilkie, J. A.; Hering, J. G. *Colloid Surface A.* **1996,** *107,* 97-110.
22. Dzombak, D. A.; Morel, F. M. M. *Surface Complexation Modeling: Hydrous Ferric Oxide*; John Wiley & Sons: New York, NY, **1990;** pp 173-178.
23. Hawke, D.; Carpenter, P. D.; Hunter, K. A. *Environ. Sci. Technol.* **1989,** *23,* 187-191.
24. USEPA. *Test Methods for Evaluating Solid Waste, Physical/Chemical Methods*, 3rd edition; SW-846, Method 1311; U.S. Government Printing Office: Washington, DC, **1992.**
25. LaGrega, M. D.; Buckingham, P. L.; Evans, J. C. *Hazardous Waste Management*; McGraw-Hill: New York, NY, **1994;** pp 641-704.
26. Hooper, K.; Iskander, M.; Sivia, G.; Hussein, F.; Hsu, J.; Deguzman, M.; Odion, Z.; Ilejay, Z.; Sy, F.; Petreas, M.; Simmons, B. *Environ. Sci. Technol.* **1998,** *32,* 3825-3830.
27. Anderson, M. A.; Ferguson, J. F.; Gavis, J. *J. Colloid Interf. Sci.* **1976,** *54,* 391-399.

Chapter 24

The Roles of Hydroxyl Radical, Superoxide Anion Radical, and Hydrogen Peroxide in the Oxidation of Arsenite by Ultrasonic Irradiation

Tielian Xu[1], Yong Cai[1], Stephen P. Mezyk[2], and Kevin E. O'Shea[1,*]

[1]Department of Chemistry and Biochemistry, Florida International University, Miami, FL 33199
[2]Department of Chemistry and Biochemistry, California State University, Long Beach, CA 90840

The ultrasonically induced oxidation of arsenite, As(III), in aqueous media is effective over a range of concentrations and may be applicable as a pretreatment step for the removal of arsenic from water. We have conducted detailed studies on the conversion of arsenite in aqueous media by ultrasonic irradiation, focusing on the roles of •OH, $O_2^{-\bullet}$ and H_2O_2 formed during the irradiation. The rate of the H_2O_2 induced transformation of As(III) is much slower than under hydroxyl radical generating ultrasonic conditions. The addition of superoxide dismutase does not change the rate of disappearance of As(III) under ultrasonic irradiation. The conversion of As(III) is very slow under selective generation of superoxide anion radical and its protonated form using gamma radiolysis, indicating that superoxide anion radical does not play a significant role in the conversion of As(III). In summary, hydroxyl radical plays the key role in the conversion of As(III), while hydrogen peroxide plays a minor role and superoxide anion radical has little or no role in the conversion of arsenite during ultrasonic irradiation.

Introduction

Arsenic is one of the most problematic water contaminants in the world and approximately 100 million people are at health risks world-wide due to drinking arsenic contaminated water *(1)*. Consumption of arsenic contaminated water is linked to negative health effects, including increased risk of diabetes, cardiovascular problems, hormonal disruption, cancer, DNA damage, and vascular diseases *(2)*. The visible symptoms include the discoloration of skin, roughness in palms and feet, warts, gangrene and cancer. The contamination of drinking water with this element is an unique environmental issue because the major source of arsenic is natural, a result of weathering of minerals in rocks and soils. While there has been considerable debate about an appropiate Maximum Contaminant Level (MCL) for arsenic in drinking water, it is generally agreed the maximum level should be no higher than 10 ppb, with the understanding that lower levels may significantly decrease the associated health risks *(3)*.

Arsenic present in groundwater and drinking water is typically found in the inorganic forms, arsenite, As(III) and arsenate, As(V). As(III) is prevalent in anoxic groundwater, being more toxic and more mobile and having a lower affinity for absorbents than As(V). The oxidation of As(III) to As(V) is highly desirable for enhancing the immobilization of arsenic and is required for most arsenic removal technologies. The removal processes typically involve the addition of chemical oxidants followed by co-precipitation/adsorption of As(V) on metal oxyhydroxides *(4)*.

The use of Advanced Oxidation Technologies (AOTs) is attractive for the treatment of arsenic contaminated water. AOTs generate powerful oxidants, including hydroxyl radicals, which have been shown to be effective for the remediation of a variety of organic pollutants *(5-7)*. A variety of methods, i.e., photochemical and radiolytic methods, are employed in AOTs to generate hydroxyl radicals, but these methods often require the addition of chemical oxidants, metals and/or catalysts, which can be expensive. The use of photochemical processes is limited to solutions, which are not turbid and can be costly because of expenses related to the production of UV light. Ultrasonic irradiation, an AOT, does not require the addition of chemical oxidants and can be employed for the treatment of turbid solutions and slurries.

A limited number of reports have appeared on the conversion of As(III) using AOTs including TiO_2 photocatalysis *(8)* and a previous report by our group on the oxidation of As(III) by ultrasonic irradiation *(9)*. Ultrasonic irradiation of oxygenated aqueous solutions leads to a number of different radicals, $\bullet OH$, $H\bullet$, $HO_2^{\bullet}$, $O_2^{-\bullet}$, as well as the chemical oxidant, H_2O_2, which can also promote oxidative degradation *(10)*. In our previous study, ultrasonic irradiation was used to effectively and readily oxidize As(III) to As(V) in oxygenated aqueous solutions. However, additional experiments were required to develop a more complete understanding of detailed mechanism of arsenite oxidation. We report herein our studies to assess the role of hydroxyl radical, superoxide anion radical, and hydrogen peroxide during the ultrasonic induced conversion of As(III) in aqueous media.

Experimental section

Materials and chemicals

$Na_2HAsO_4 \cdot 7H_2O$ and As_2O_3 were purchased from Aldrich and used for preparation of 1 ppm stock solutions of arsenate and arsenite. NaOH, $NaBH_4$ and formate were reagent grade and used as received from Fisher. HCl was trace metal grade from Fisher. Catalase, CAT (EC 1.11.1.6) and Superoxide dismutase, SOD (EC 1.15.1.1) were obtained from Sigma and stored in the freezer. The water used was ultrapure and prepared by milli-pore filtration (US Filter Co.) of deionized water followed by distillation. Gases (Oxygen and Argon) were zero grade obtained from Air Products.

Sonolysis

Ultrasonic irradiation was conducted with a high frequency, high intensity ultrasonic irradiator (UES Model 15-660), equipped with an aluminum-faced transducer and a specially designed focusing-reactor glass vessel. Initial solution volumes were 500 mLs aqueous solution with a 80 mLs of headspace. The ultrasonic instrument was operated in continuous mode at 500 W and a frequency of 665 kHz. Five hundred mLs of arsenite solution were added to the reaction vessel and rigorously purged with a saturating gas (O_2 or Ar) for 5 minutes prior to irradiation. The samples were taken at given time intervals. An equal volume O_2 or Ar gas was added to the reaction vessel when each sample was removed for analysis. The temperature of the cooling bath was maintained at 12 ± 3°C throughout the reaction process by the addition of ice and constant circulation.

Arsenic analysis

As(III) and As(V) were determined by a PS Analytical Millenium Excalibur Atomic Fluorescence System (PSA 10.055) coupled to a HPLC (anion exchange column, PRP X-100, 250mm × 4.6mm × 10μm). Details of the analytical procedures used are descrided elsewhere (9).

Gamma radiolysis

Steady state ^{60}Co experiments were performed at the Radiation Laboratory, University of Notre Dame, Indiana, to study the ability of $HO_2{}^\bullet/O_2{}^{-\bullet}$ to convert As(III). These irradiations were performed at a dose rate of 8.0 Gy/min on 40.0 mLs of solution in 47.0 mLs capped vials. These experiments were done under O_2 saturation in the presence of formate (0.01M) to scavenge •OH, and quantitatively create the superoxide species, as indicated by equations 1-5.

$$H_2O \rightsquigarrow {}^{\bullet}OH,\ H^{\bullet},\ e^- \qquad (1)$$

$${}^{\bullet}OH + HCO_2{}^- \rightarrow {}^{\bullet}CO_2{}^- + H_2O \qquad (2)$$

$${}^{\bullet}CO_2{}^- + O_2 \rightarrow CO_2 + O_2{}^{-\bullet} \qquad (3)$$

$$e^-/H^\bullet + O_2 \rightarrow O_2{}^{-\bullet}/HO_2{}^\bullet \qquad (4)$$

$$HO_2{}^\bullet \rightarrow H^+ + O_2{}^{-\bullet} \qquad (5)$$

Catalase (CAT, EC 1.11.1.6) 380U/mL was added to the solutions immediately after irradiation to catalyze the decomposition of H_2O_2 into H_2O and O_2. The vials were then kept in ice until analyzed.

Results and discussion

Ultrasonic cavitation

To better understand the role of the different reactive species and oxidants formed during caviation, it is important to briefly discuss the cavitation process. The growth, contraction, and collapse of the gas bubble (cavitation) leads to extreme conditions and three different reaction zones, gas phase (extreme conditions), interface (supercritical conditions) and bulk solution (mild conditions) (11). Given the low volatility of arsenite and arsenate, the reactions involved with these substrates are not expected to occur in the gas phase but rather in solution or at the interface near the site of cavitation. Hence the conversion of arsenite is expected to be the result of reactions involving the reactive species generated during ultrasonic irradiation and not from the direct pyrolytic transformation of As(III) in the gas phase as can occur with volatile compounds (7). Under our experimental conditions ultrasonic irradiation leads to the pyrolysis of water, generating hydroxyl radicals and hydrogen atoms, as illustrated in eq 6. In the presence of oxygen, the hydrogen atom rapidly reacts to form superoxide anion radical as a predominant reaction pathway, eq 7. In the absence of oxygen, the hydrogen atom can recombine with H• or HO•, but does not significantly react with substrates dissolved in the solution. The hydroxyl radical can react with substrates at or near the site of cavitation or with another hydroxyl radical to form hydrogen peroxide, eq 8 (11).

$$H_2O \rightarrow H\bullet + \bullet OH \qquad (6)$$

$$H\bullet + O_2 \rightarrow HO_2^{\bullet} \qquad (7)$$

$$\bullet OH + \bullet OH \rightarrow H_2O_2 \qquad (8)$$

In the following sections we discuss the roles of hydroxyl radical, hydrogen peroxide and superoxide anion radical during ultrasonic treatment of As(III).

Role of O_2 and hydroxyl radicals in ultrasonic treatment of As(III)

To assess the roles of hydroxyl radicals and oxygen, experiments were performed in the presence and absence of oxygen (argon saturation). The removal of O_2 from the reaction vessel minimizes the formation of $O_2^{-\bullet}$ and also allows for the assessment of the reactions of hydrogen atom which in the presence of oxygen is readily consumed by oxygen. Arsenite is readily transformed upon irradiation with ultrasound (665 kHz) over a range of concentrations (0.67 to 6.70μM) under oxygen and argon saturation as illustrated in Figure 1. The degradation is consistent with a pseudo-first-order process as reported previously (9). Our measured rate constants under both conditions agree within experimental error over the concentration range studied, as summarized in Table 1. The slight difference between these rate constants and previous values (9) may be due to the slight differences in the reactor design and experimental setup. We were unable to confirm the presence of AsH_3, the most likely product from the reaction of hydrogen atom with As(III). The slight increase in the rate constant under argon saturation is consitent with the explanation that the conditions generated during cavitation are more extreme and hence lead to more radicals and greater rates of conversion. It is clear that oxygen is not required for the initial transformation of As(III).

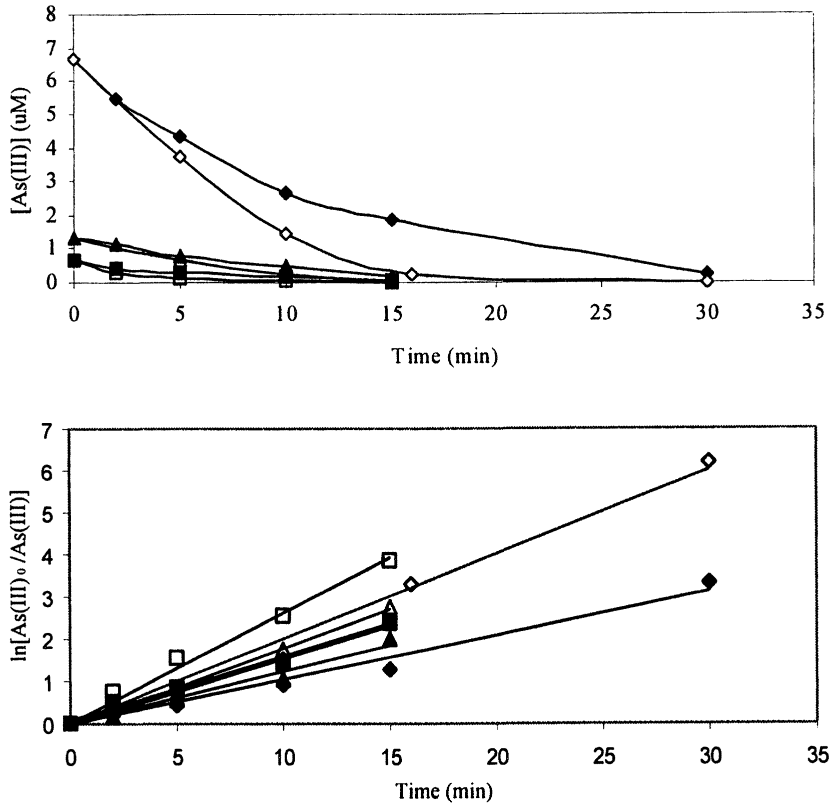

Figure 1. Ultrasonic irradiation of As(III) under oxygen saturation (solid symbol) and under argon saturation (open symbol) (□:6.70μM; ▲:1.34μM; ■: 0.67μM).

Table 1. Pseudo-first-order rate constants for conversion of As(III)

Initial As Conc. (μM))	*O_2 Saturation*		*Ar Saturation*	
	k (min^{-1})^a	*R^2*	*K (min^{-1})^a*	*R^2*
0.67	0.15	0.98	0.25	0.99
1.34	0.13	0.98	0.19	0.99
6.70	0.11	0.99	0.22	0.99

a: Duplicate runs indicate the results are reproducible, with less than 15% error.

The mass balance between As(III) and As(V) is complete within experimental error at low arsenic concentration but drops to 70-75 % at the highest concentrations studied, as illustrated in Figure 2. The total arsenic in solution measured using ICP-MS gave excellent mass balance among starting materials and reaction products, indicating the presence of an unidentified arsenic species, not As(III) or As(V), in the treated solutions. Mauro *at. el.* found that As(III) is reduced to arsine (AsH_3) by ultrasonic irradiation in the presence of zinc (12). While these authors attribute the formation of AsH_3 to reduction by hydrogen atom, it is also plausible that the zinc metal is activated by the ultrasound so that it may be directly involved in the reduction of As(III). We have conducted a number of experiments to detect the presence of AsH_3 in the headspace, involving oxidation by $HClO_4$ or chelation by NaDDTC (sodium diethyldithiocarbamate). All of which indicate that AsH_3 is not formed at detectable levels under our reaction conditions.

Based on the previous results and the rapid reaction of hydroxyl radicals with arsenite, it appears that hydroxyl radicals may play an important role in the conversion of arsenite during ultrasonic irradiation.

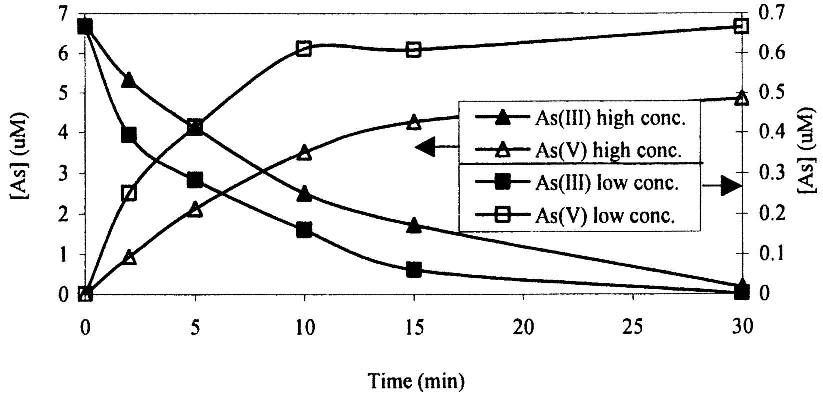

Figure 2. As(III) conversion to As(V) by ultrasonic irradiation under O_2.

Role of H_2O_2 produced during ultrasound irradiation

Arsenite can be also oxidized by H_2O_2 which is produced under our ultrasonic conditions. Hydrogen peroxide, formed primarily by the reaction of two hydroxyl radicals, was produced at a rate of 0.01 mM/min under our experimental conditions as determined using the I_3^- method (13). The production of hydrogen peroxide by ultrasound irradiation under oxygen saturation is similar in the presence and absence of 0.67 uM As(III). These results indicate that the amount of •OH lost to react with As(III) is insignificant compared to total •OH and hence does not appreciably affect the formation of hydrogen peroxide. These results are consistent with expectations, given the relatively high concentration of H_2O_2 (mM) vs low As(III) concentration (μM). To assess the extent of H_2O_2 induced oxidation of arsenite during ultrasonic irradation, we prepared a solution of 0.15 mM H_2O_2 (similar to the level of H_2O_2 produced after 15 min of ultrasonic irradiation) and 0.67 μM As(III). The solution was kept in the dark at room temperature and the concentration of As(III) was monitored as a function of time.

The rate of As(III) reaction with H_2O_2 is consistent with that of Maurizio *et. al.* (14). The concentration of hydrogen peroxide used in our experiments was significantly higher than what is produced during the early stages of ultrasonic irradiation. Only about 35% As(III) was oxidized by H_2O_2 in 30 min, yet As(III) was almost completely converted in the same time period under ultrasound irradiation (Figure 3). The conversion of As(III) by ultrasonic irradiation compared to the conversion by H_2O_2, illustrates that ultrasound induced conversion is much faster and must involve additional non-hydrogen peroxide reaction pathways.

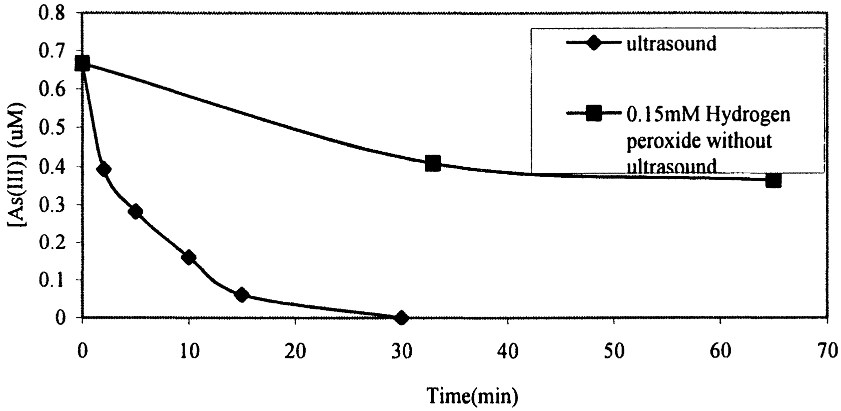

Figure 3. Comparison of transformation of As(III) by H_2O_2 and ultrasound irradiation.

Role of $O_2^{-\bullet}$ on oxidation of As(III)

Superoxide anion radical (SO) has been proposed as the major oxidant for the oxidation of arsenite by TiO_2 photocatalysis, another AOT (8). Ultrasonic irradiation under oxygen saturation leads to $HO_2^{\bullet}$ radical (pKa = 4.8) as illustrated in eq 7 , which is readily deprotonated at neutral pH. Superoxide dismutase (SOD) has been used in semicondutor photocatalysis systems to assess the role of superoxide (15). SOD can catalyze the destruction of $O_2^{-\bullet}$ free radical, which follows eq 9.

$$2O_2^{-\bullet} + 2H^+ \rightarrow O_2 + H_2O_2 \qquad (9)$$

To test the role of $O_2^{-\bullet}$ and its protonated form $HO_2^{\bullet}$ during the ultrasonic irradiation of As(III), SOD was added to the solution to quench the reactions of the superoxide anion radical. If superoxide anion plays a role in the conversion of As(III) during ultrasonic irradiation, the presence of SOD, which has specific action against SO, should reduce the conversion of As(III). The presence of SOD did not affect the rate of As(III) conversion by ultrasonic irradiation at concentrations from 0.67 to 6.70 μM, despite the high activity of SOD employed (2,500 or 10,000U), as illustrated in Figure 4. The effect of SOD suggests that $O_2^{-\bullet}$ is not significant in the conversion of As(III).

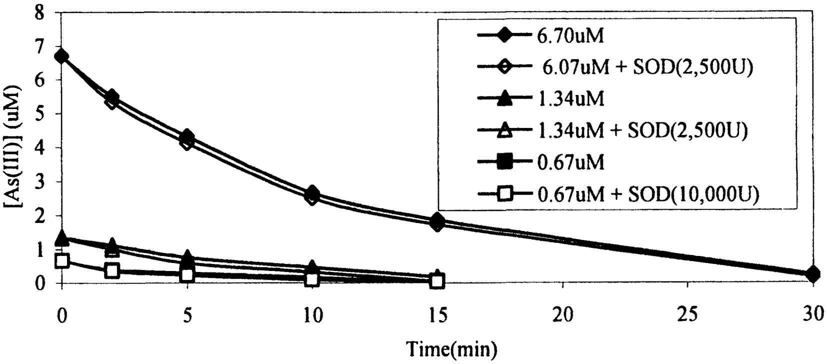

Figure 4. Effect of SOD on As(III) conversion by ultrasonic irradiation under O_2 saturation.

To further assess the ability of SO to convert As(III) in aqueous media, experiments were also conducted using gamma radiolysis, employing a ^{60}Co irradiation source, to generate SO. The solution pH was adjusted to investigate the neutral and anionic forms of SO.

The calculated $O_2^{-\bullet}$ production rate was 5.10 μM/min. After 15 min irradiation, approximately 76.5 μM $O_2^{-\bullet}$ is generated, which is in considerable excess relative to the initial As(III) concentration (~ 13 μM). The reaction rate of As(III) with $O_2^{-\bullet}$ appears to be quite slow, as illustrated by Figure 5, further supporting our conclusion that SO is not an important oxidant in the conversion of As(III) during ultrasonic irradiation.

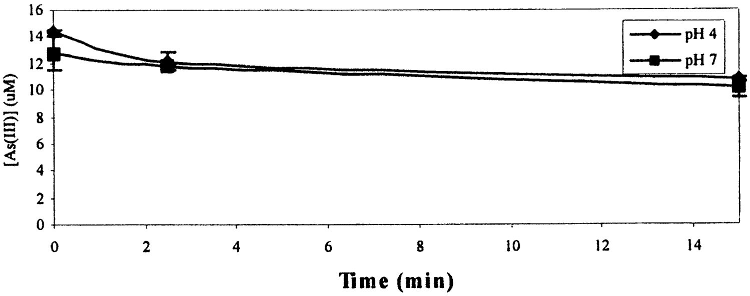

Figure 5. Conversion of As(III) by radiolytically generated $O_2^{-\bullet}$.

These results indicated that the dominant species responsible for the conversion of As(III) is not H_2O_2, nor $O_2^{-\bullet}$, but the •OH radical produced during ultrasound irradiation. The initial step of the conversion of As(III) to As(V) by ultrasound irradiation is illustrated below, eq 10. The rate for this reaction is nearly diffision-controlled to form As(IV) (16).

$$\text{As(III)} + \text{HO}\bullet \rightarrow \text{As(IV)} + \text{HO}^- \qquad k = 10^9\ \text{M}^{-1}\text{s}^{-1} \qquad (10)$$

As(IV) is short lived under the reaction conditions and can be oxidized to As(V) by a number of competing reactions (16), including disproportionation of As(IV) to As(III) and As(V), reaction of As(IV) with O_2 to give As(V) and superoxide anion radicals.

Conclusions

At concentrations 0.67 to 6.70 μM (50 to 500 ppb), a rapid decrease in the initial concentrations of As(III) was observed with half lives of less than 30 minutes, and concentrations of less than 10 ppb (~ 1-2 ppb) were easily obtained at extended irradiation time. The conversion of As(III) is consistent with pseudo-first-order kinetics. Under oxygen saturation, As(III) is degraded at a slower rate than under argon saturation. The faster rate of As(III) disappearance under argon saturation is consistent with the observation that hydroxyl radical yields are higher under argon relative to oxygen saturation. H_2O_2 is produced during ultrasound irradiation of water and As(III) solution, but the reaction of As(III) with H_2O_2 is much slower than that observed from ultrasound irradiation of As(III). Studies involving SOD and radiolysis indicate that $O_2^{-\bullet}$ is not important in the conversion of As(III). The dominant species in the conversion of As(III) appears to be the hydroxyl radical, which is formed during the cavitation process, and can rapidly convert As(III) to As (IV), which can be subsequently oxidized to As(V).

Acknowledgements

KEO gratefully appreciates the support from the NIH/NIEHS (Grant # S11ES11181) and the Dreyfus foundation. We thank the Radiation Laboratory, University of Notre Dame, for the use of their ^{60}Co facilities.

References

1. Smith, A. H.; Lingas, E. O.; Rahman, M. B. *World Health Org.* **2001**, *78*, 1093.
2. Chriesten, K. *Environ. Sci. Technol.* **2001**, *35(13)*, 286A.
3. Drinking Water Standard for Arsenic, USEPA, Office of Water: Washington DC, 2001, EPA-815-F-00-015.
4. Jekel, M. R. In *Arsenic in the Environment, Part I: Cycling and Characterization*; Jerome, O. Nriagu., Eds.; John Wiley& Sons Inc: NY, 1994; pp 119-131.
5. Cooper, W. J.; Mezyk, S. P.; O'Shea, K. E.; Kim, D. K.; Mincher, B.; Hardison, R. D. *Rad. Phys. Chem,* **2003**, *67*, 523.
6. O'Shea, K. E.; Beightol, S.; Garcia, I.; Kalen, D. V.; Cooper, W. J. *J. Photochem. Photobiol. A: Chem.* **1997**, *107*, 221.
7. Kim, D. K.; O'Shea, K. E.; Cooper, W. J. *J. Environ. Eng.* **2002**, *9*, 806.
8. Hyunjoo, L.; Wonyong, C. *Environ. Sci. Technol.* **2002**, *36*, 3872.
9. Motamedi, S.; Cai Y.; O'Shea, K. E. In *ACS symposium Sciences. 835,* Cai, Y.; Braids, O. C. American Chemical Society, Washington, DC, 2003; pp 84-94.
10. von Sonntag, C.; Mark, G.; Tauber, A.; Schuchmann H. P. *Adv. Sonochemistry* **1999**, *5*, 109.
11. Suslick K. S. *Sci. Am.* **1989**, 80.
12. Mauro, K.; Andrude, V. M.; Bovges, S. S.; Sousa, C. S.; Oliveriva, F. S. *J. Braz. Chem. Soc.* **2003**, *14(2)*, 254.
13. Fang, X.; Wu, J.; Schuchmann, H. P.; von Sonntag, C. *Int. J. of Radiat. Biol.* **1995**, *68(5)*, 459.
14. Maurizio, P.; Luigi, C.; Frank, J. M. *Geochim. Cosmochim. Acta.* **1999**, *63(18),* 2727.
15. Amalric, L.; Guillard, C.; Pichat, P. *Res. Chem. Intermed.* **1994**, *20(6),* 579.
16. Kläning, U. K.; Benon, H. J. B.; Sehested, K. *Inorg. Chem.* **1989**, *28*, 2717.

Chapter 25

Arsenic Removal by Zero-Valent Iron: A Field Study of Rates, Mechanisms, and Long-Term Performance

Dimitrios Vlassopoulos[1], Nelson Rivera[2], Peggy A. O'Day[2], Michael T. Rafferty[1], and Charles B. Andrews[1]

[1]S.S. Papadopulos and Associates, Inc., 815 SW 2nd Avenue,
Portland, OR 97204
[2]School of Natural Sciences, University of California, Merced, CA 95344

Zero-valent iron (ZVI) is an effective medium for removal of arsenic (As) from water. A performance evaluation was conducted at a field site where shallow groundwater is contaminated by As at mg/L levels. Field column tests show that As removal follows pseudo first-order kinetics, with a half-life on the order of 5 minutes. Steady-state column effluent concentrations decreased with increasing retention time for retention times shorter than 45 minutes, but were independent of retention time for longer retention times, indicating a steady-state uptake reaction. Spectroscopic and microscopic characterizations of unreacted and reacted material show that metallic iron is partially oxidized to maghemite (γ-Fe_2O_3) in the unreacted material and that arsenic is incorporated into an Fe(III) oxyhydroxide structure during reaction with groundwater. These results suggest that As uptake is controlled by the rate of incorporation of arsenic into Fe(III) oxyhydroxide as it forms during oxidation of maghemite. To evaluate long-term performance, a prototype in-ground reactor (1.8 m^3 iron bed) was built and operated over a one-year period (~4,400 pore volumes) to treat groundwater with ~3 mg/L As. Initially, effluent As concentrations were less than 10 μg/L, but gradually increased over time as As accumulated on the reactive media. Between

In Advances in Arsenic Research; O'Day, P., et al.;
ACS Symposium Series; American Chemical Society: Washington, DC, 2005.

~1,600 and 2,200 pore volumes, preferential pathways began to develop within the reactor, resulting in significant flow channeling and incomplete As removal.

Introduction

In recent years, ZVI has received considerable attention as a reactive medium for removal of a variety of contaminants from water (*1*, and references therein). Technologies based on ZVI for As removal are of particular interest, in view of the strong chemical affinity of Fe for As, and potential reduction in treatment costs relative to existing alternatives such as chemical precipitation/coagulation and ion exchange. Numerous studies (*2-7*) have demonstrated As removal by ZVI in batch and flow-through systems. These studies have shown that the arsenic removal mechanism is closely linked to the formation of iron corrosion products.

Aqueous corrosion of elemental iron is an oxidative dissolution process, and proceeds both aerobically (coupled to oxygen consumption):

$$Fe^{0} + \tfrac{1}{2}O_2 + 2H^{+} = Fe^{++} + H_2O \qquad (1)$$

as well as anaerobically (coupled to hydrogen evolution):

$$Fe^{0} + 2H^{+} = Fe^{++} + H_{2(g)} \qquad (2)$$

These reactions produce an increase in pH and dissolved iron concentration and a decrease in redox potential. Depending on water chemistry, Fe(II) can be further oxidized to Fe(III). With increasing degree of oxidation, solid corrosion products can include $Fe(OH)_2$, mixed Fe(II/III) oxides or hydroxides (magnetite, green rusts), and FeOOH polymorphs. Arsenic exhibits a strong affinity for sorption on green rusts (*8,9*), which are intermediate products of iron oxidation. Under oxidizing conditions, green rust will transform to ferric oxyhydroxide phases (*8*), in which arsenic can ultimately be sequestered by adsorption or co-precipitation (*10,11*). Furthermore, solid-phase spectroscopic and solution-phase speciation evidence indicates that As(V) does not directly participate as an oxidant in iron corrosion and therefore reduction of As(V) to As(III) is not expected to be significant (*4,9*).

Here we present results of an *in situ* groundwater treatment study conducted at a former pesticide manufacturing site in New Jersey where shallow groundwater in a perched zone is affected by arsenic at concentrations of up to several mg/L. Column tests were performed in the field to develop design and operating parameters for a prototype in-ground reactor. The reactor was initially operated and monitored over a one-year period to evaluate long-term performance. Characterization of reaction products and evaluation of uptake rates in the field are discussed in terms of a proposed reaction mechanism.

Materials and Mehtods

The granular ZVI used in this study was obtained from Connelly-GPM (Chicago, IL). The ZVI is fairly uniform in grain size (-8 to +20 mesh, or 0.84 to 2.38 μm) and has a relatively high specific surface area (1.8 m^2/g). A typical analysis yields (% by weight): Fe 89.8, C 2.85, Mn 0.6, S 0.107, P 0.132, Si 1.85, Ni 0.21, Cr 0.17, Mo 0.15, Ti 0.004, Cu 0.2, Co 0.003, and O content up to 3.9 % (by difference).

ZVI was mixed 50% by weight (approximately 1:3 by volume) with coarse quartz sand. The porosity of the mixture was measured at ~50%.

Field Column Tests

Three flow-through vessels were used: a 57-L canister, a 75-L canister, and a 10-cm diameter by 60-cm long (~4 L) PVC column. A known volume of the ZVI/sand mixture was packed between layers of pea gravel and the vessels were sealed. Groundwater was pumped to an equalization tank, and from there it was pumped to the reactor vessel. Each of the tests consisted of pumping groundwater through the vessel in upflow mode at a constant flow rate, which was varied between tests (0.07 – 2 L/min). This allowed the hydraulic residence time within the ZVI layer to be varied between 1 minute and 5 hours. Each test was run for between one and several days, depending on the flow rate.

Influent and effluent water temperature, pH, and specific conductance were monitored continuously with multi-parameter sensor/datalogger systems equipped with flow-through cells. Redox potential and dissolved oxygen in both influent and effluent were also measured periodically. Automatic samplers were used to collect influent and effluent water samples at regular intervals. Water samples were analyzed for As by inductively coupled plasma-optical emission spectroscopy (ICP-OES) and graphite furnace-atomic absorption (GF-AAS) (detection limits of 50 and 2 μg/L, respectively) and Fe by ICP-OES (detection limit of 20 μg/L).

Solid Phase Characterization

Following completion of the field column tests, reactive media samples were recovered for solid phase and spectroscopic studies. Since surface reactions were of interest, the reacted ZVI was sonified for an hour to collect the fine fraction from the surface. The fine material was recovered using a 0.45 μm filter. Subsamples of the fines were digested in *aqua regia* and analyzed by GF-AAS for As and Fe.

For X-ray absorption spectroscopy (XAS) analysis, samples were mounted wet into a teflon sample holder, and sealed with mylar tape. Bulk Fe K-edge XAS data were collected at the Stanford Synchrotron Radiation Laboratory to determine Fe phases based on the local atomic coordination around Fe atoms. Samples were run on beamline 2-3 at room temperature and on wiggler beamline 4-1 at cryogenic temperatures (15-20 K). All XAS data were collected using a Si(220) monochromator crystal and a vertical beam size of 1 mm. Energy was calibrated using the first inflection on the absorption edge of iron metal foil, which was set at 7112 eV. X-ray Absorption Near Edge Structure (XANES) and Extended X-ray Absorption Fine Structure (EXAFS) to $k = 13\ \text{Å}^{-1}$ were collected and analyzed using EXAFSPAK (*12*) with theoretical phase shift and amplitude functions calculated with FEFF (*13*). XANES spectra were least-squares fit with linear combinations of reference iron compounds from a previously analyzed library (*14*). Energy was treated as an adjustable parameter; fits with energy shifts of greater than 1 eV were rejected. EXAFS spectra were analyzed by background subtraction and non-linear least-squares fits on a shell-by-shell basis by methods described previously (*14-16*).

The particle size and morphology of the iron media before and after reaction were examined by scanning electron microscopy (SEM) and energy dispersive spectrometry (EDS) for spot elemental analysis. Samples were mounted on aluminum alloy stub mounts with double-stick carbon tape. The SEM used was an FEI XL-30sFEG housed at the University of California, Davis. The microscope was operated at 20 kV with a working distance of 6 mm, a beam diameter of 2.6 nm, and 617 pA for the EDS analysis.

In-Ground Reactor

Design and Construction. Rate constants for As removal derived from the field column tests were used to design the full-scale prototype, which was intended to treat up to 40 L/min of water containing dissolved As at an average concentration of 3 mg/L. Figure 1 is a schematic diagram of the reactor. Contaminated groundwater is collected in a perforated drain pipe and is piped to the reactor through an in-ground, gravity flow system that isolates the flow stream from surrounding groundwater. Water flows through a totalizing flow meter into the reactor and is discharged from the reactor into a limestone gravel trench. The reactor, constructed from a 3.5 m^3 concrete vault, was installed between 2.1 and 3.4 meters below ground surface. Treatment occurs within a 1.8 m^3 bed containing approximately 3400 kg of the ZVI/sand mixture. Gravel chambers are located at each end of the concrete vault to distribute the flow across the iron bed. Sampling ports are installed in the influent and effluent piping, and multilevel monitoring points are also installed at four locations within the reactor.

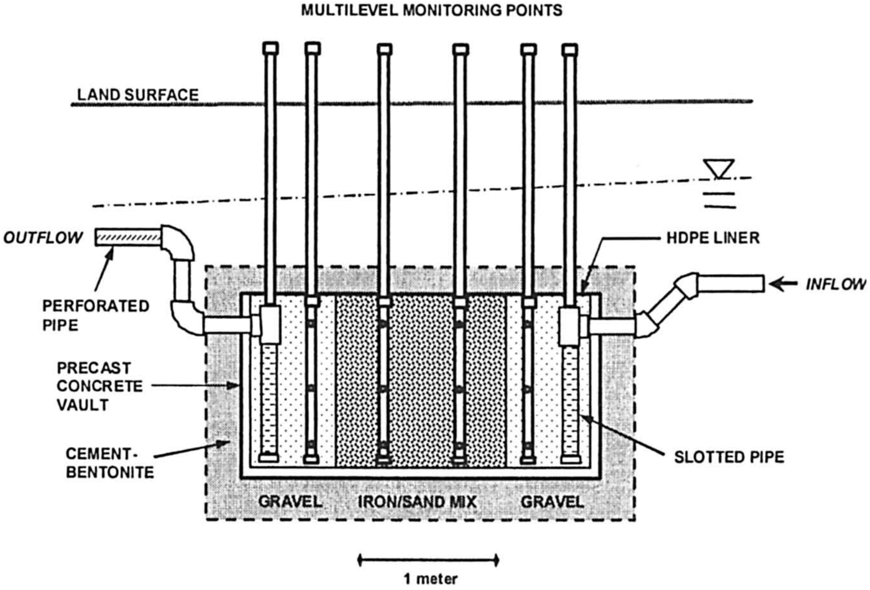
MULTILEVEL MONITORING POINTS
LAND SURFACE
OUTFLOW
PERFORATED PIPE
PRECAST CONCRETE VAULT
CEMENT-BENTONITE
HDPE LINER
INFLOW
SLOTTED PIPE
GRAVEL
IRON/SAND MIX
GRAVEL
1 meter

Figure 1. Schematic cross-section of in-ground reactor. The general location of the water table at time of construction is indicated by the sub-horizontal dot-dash line.

Monitoring. Samples from the influent, effluent, and interior monitoring points were collected periodically using a peristaltic pump fitted with disposable polyethylene tubing and operating at a low flow rate (<100 mL/min). Water temperature, specific conductance, pH, dissolved oxygen, redox potential (ORP) turbidity, and ferrous iron were measured in the field. Samples from influent, effluent and interior sampling ports were analyzed for total and dissolved As and Fe, major ions, Al, Mn, SiO_2 and H_2S. Water levels were also measured at each of the sampling ports to monitor hydraulic changes in the system.

Results

Field Column Tests

Influent As concentrations remained fairly constant over the duration of the tests, with a mean of 3.0 mg/L. Figure 2 shows steady-state effluent concentration as a function of retention time. Effluent As concentrations were generally less than 10 µg/L for tests with residence times longer than 47 minutes, but longer residence times did not appear to further decrease effluent As concentrations. For residence time tests shorter than ~45 minutes, higher effluent As concentrations were generally observed. The relationship between effluent arsenic and retention time is consistent with a combination of a first-order kinetic process (mass transfer) and an equilibrium partitioning as proposed in (7). Although there is some scatter in the short retention time data which may be attributed to differences between the reactors used and/or to aging of the ZVI over the duration of the tests, a first-order rate constant of 0.13 minute^{-1} is conservatively estimated, which corresponds to a half-life of arsenic in the column of approximately 5.3 minutes.

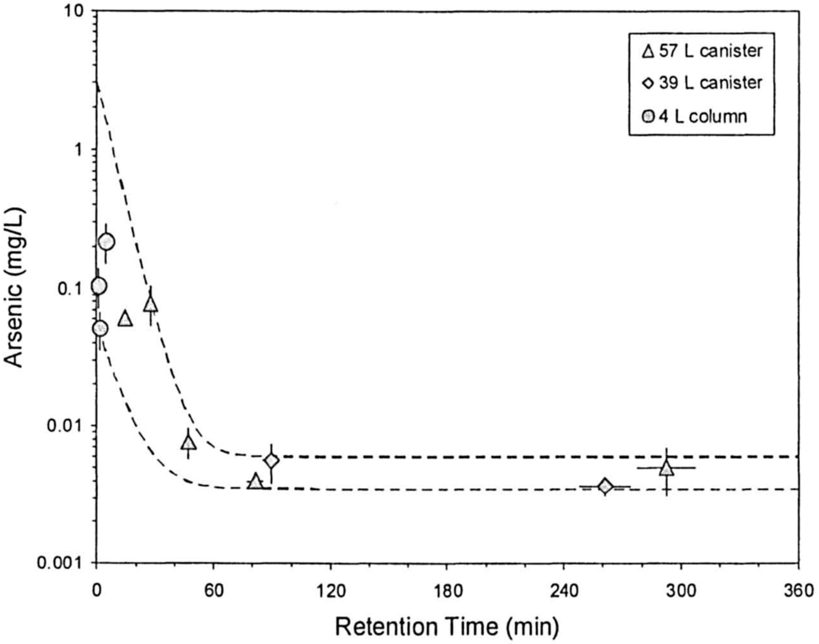

Figure 2. Steady-state column effluent arsenic concentration as a function of retention time. Dashed lines are upper and lower bound calculations assuming a combination of 1st-order removal rate and equilibrium partitioning.

Solid Phase and Spectroscopic Studies

Samples from the field column tests were analyzed by XANES and EXAFS spectroscopy at the Fe K-edge to examine iron phases before and after reaction with the groundwater. XANES analyses of unreacted ZVI and two samples of reacted material recovered from column tests showed differences in their spectral features, which are best seen in first-derivative spectra (Figure 3(a)). A distinct difference in the spectra occurs around 7130 eV where the unreacted ZVI exhibits a shoulder, wheareas the reacted ZVI has no such feature. This shoulder is also seen in the maghemite reference spectrum but not in iron oxyhydroxide reference spectra. There is no evidence in the unreacted iron spectrum for the presence of magnetite or iron metal, which were detected by XAS in a previous study (*5*), probably because fine surface material rather than bulk material was analyzed in this study. The unreacted iron spectrum was well fit with two components – maghemite (γ-Fe_2O_3), which contains both Fe(II) and Fe(III), as the dominate phase (81%), and a smaller component (19%) of an Fe(III) oxyhydroxide phase (Table 1). Because of the similarity in XANES spectral features among the Fe(III) oxyhydroxide compounds ferrihydrite (amorphous $Fe(OH)_3$), goethite (α-FeOOH), and lepidocrocite (γ-FeOOH), these phases cannot be distinguished by XANES analysis alone (*14*). Fits to the reacted iron spectra with maghemite were poor. Reacted iron spectra were well fit with a single Fe(III) oxyhydroxide component, as shown in Figure 3(b). Addition of a second component did not improve the fit significantly, and similar fits to the XANES spectra were obtained using ferrihydrite or goethite as the reference compound.

Table 1. XANES fit results for unreacted and reacted ZVI

Sample	*Reference compound*	*Fraction*	*Energy shift (eV)*	*[As]*[a] *(mg/kg)*
Unreacted	Maghemite	81 %	0.65	
	Lepidocrocite	19 %	0.24	
Reacted #1	Lepidocrocite	100 %	0.05	450
Reacted #2	Lepidocrocite	100 %	0.09	250

[a] Concentrations of As by acid digestion, analysis by GF-AAS; detection limits for As were 6.25 mg/kg.

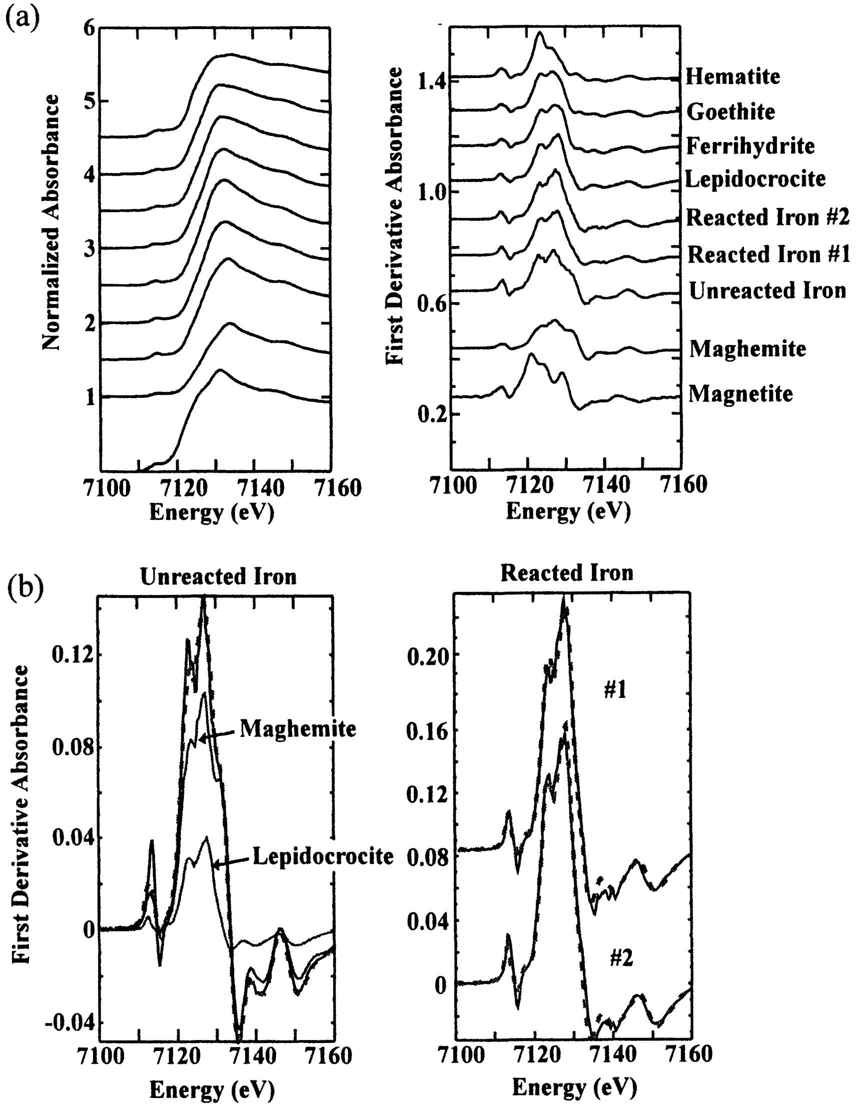

Figure 3. (a) Iron K-edge XANES spectra of reacted and unreacted column samples compared with reference compounds; (b) Fits of 1st-derivative spectra with maghemite and Fe(III) oxyhydroxide (lepidocrocite) reference spectra. Solid lines are data; dashed lines are least-squares fits.

Figure 4 shows the EXAFS spectra and best fits of unreacted and reacted column samples compared to the reference compounds identified in the XANES analysis. Numerical fit results are summarized in Table 2. The reacted sample has distinct differences in its EXAFS when compared to the unreacted sample spectrum. In the unreacted iron spectra, there is a small shoulder on the first peak at k = 5.5 Å^{-1} which matches maghemite and is not present in the reacted iron #1 spectra. Also, oscillations from k = 9-11.2 Å^{-1} are weaker in unreacted iron. Although similar, the unreacted sample spectrum does not exactly match the reference maghemite spectrum, consistent with the XANES fit result that indicated a second, small component of Fe(III) oxyhydroxide.

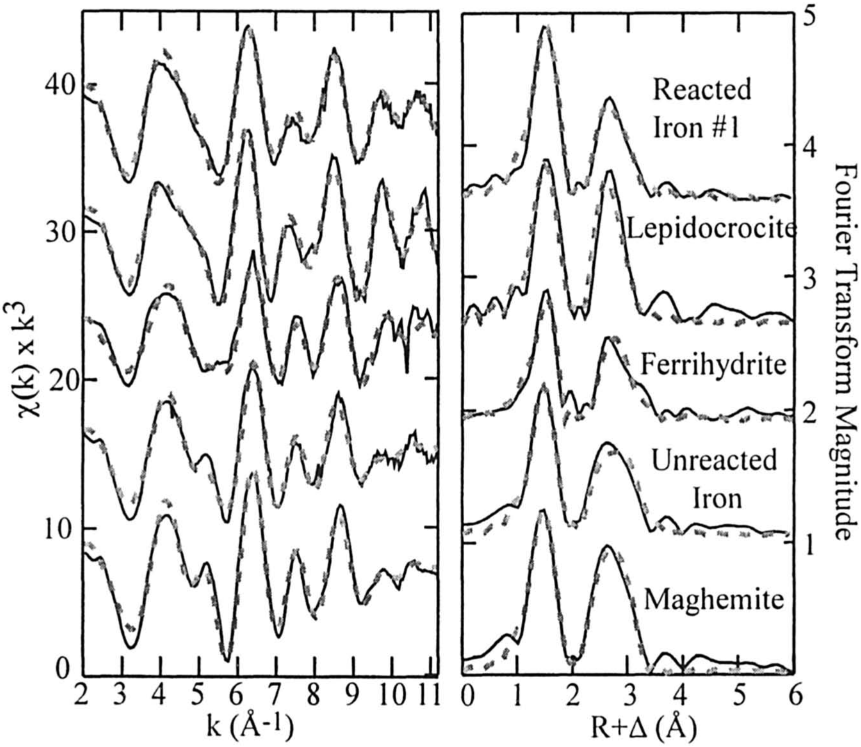

Figure 4. Iron K-edge EXAFS spectra. EXAFS spectra and corresponding Fourier transforms for reacted and unreacted column samples compared with reference compounds. Solid lines are data; dashed lines are least-squares fits.

The EXAFS spectrum of the reacted sample was fit assuming interatomic distances that were consistent with an Fe(III) oxyhydroxide local structure. However, fits assuming only the local structure of either lepidocrocite or ferrihydrite did not adequately fit the spectrum (note that the EXAFS spectrum of goethite is nearly identical to that of ferrihydrite, see *14*). Bulk analysis of the reacted samples for As (Table 1) suggest that a relatively high concentration of As was associated with the reacted iron. Thus, the fit model was modified to include As in the local atomic structure. Least-squares refinement of the EXAFS indicated a small fraction of backscattering from arsenic ($N \sim 0.8$) at a mean distance of 3.34 (±0.02) Å (Table 2). The Fe-Fe interatomic distances determined in the fit are more similar to the local structure of lepidocrocite than ferrihydrite, with two distances resolvable at 2.97 Å and 3.08 Å. The Fe-As interatomic distance from the EXAFS fit is slightly longer than the distance reported in laboratory studies of arsenate sorbed to lepidocrocite ($R = 3.34 \pm 0.02$ Å vs. $R = 3.29$ Å from (*11*)) but within error of the Fe-As distance in the mineral scorodite ($FeAsO_4 \cdot 2H_2O$) as determined by EXAFS ($R = 3.35$-3.36 Å from (*11*) and (*17*)). This interatomic distance indicates a local geometry in which an arsenate tetrahedron forms a bridging bidentate complex to two iron octahedra (*11,18,19*). Based on the amount of As in the reacted sample and the local geometry determined by EXAFS, we postulate that new reactive sites are produced as the material reacts with the water, maghemite is oxidized, and an Fe(III) solid precipitates, incorporating sorbed As into the local structure. Incorporation of As into the newly formed Fe(III) oxyhydroxide would cause local disorder of the ideal structure, and therefore explain why the observed spectrum of the reacted sample does not match the local atomic structure of either lepidocrocite or ferrihydrite.

SEM imaging of reacted media showed precipitates forming on both ZVI particles and quartz grains (Figure 5). Silicon (from quartz sand) and Fe were detected by EDS spot analyses but As was not, probably because EDS is not particularly surface sensitive, and As may not be uniformly distributed in the reacted iron particles.

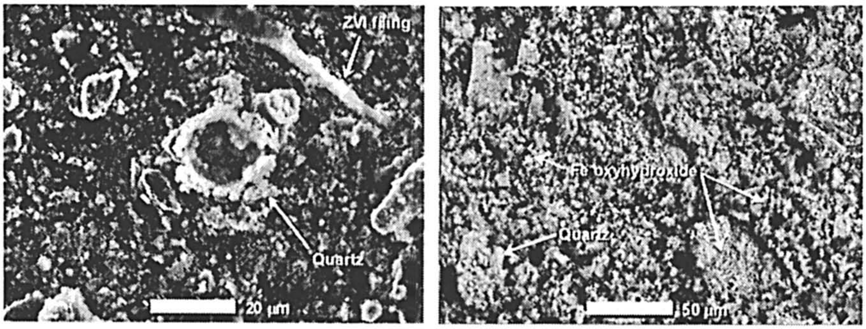

Figure 5. SEM images of ZVI/quartz media. Left: unreacted media showing ZVI filings and quartz particles. Right: reacted media showing extensive formation of iron-oxyhydroxides both as discrete particles and as surface precipitates on quartz.

Table 2. EXAFS fit results for unreacted and reacted iron compared to reference compound fits.

Sample	*A-B*	N_B	*R (Å)*	σ^2 *(Å²)*	ΔE_0 *(eV)*	χ^2	
Unreacted Iron	Fe-O	2.2*	1.91*	0.0045*	0.3*	0.23	
	Fe-O	2.9*	2.02*	0.0088*			
	Fe-Fe	3.1*	2.99*	0.0099*			
	Fe-Fe	4.2*	3.47*	0.0110*			
	Fe-Fe	1.0*	3.71*	0.0027*			
Reacted Iron #1	Fe-O	6	1.98*	0.0094*	-0.3*	0.23	
	Fe-Fe	1.6*	2.97*	0.0094*			
	Fe-Fe	2.6*	3.08*	0.0070*			
	Fe-As	0.8*	3.34*	0.0060*			
Reference Compounds	*A-B*	N_B	*R (Å)*	σ^2 *(Å²)*	ΔE_0 *(eV)*	χ^2	*Crystallographic R (Å)*
Lepidocrocite[a]	Fe-O	6	1.99*	0.0069*	1.0*	0.55	2.01
	Fe-Fe	4	3.03*	0.0094*			2.94
	Fe-Fe	2	3.07*	0.0030*			3.07
	Fe-Fe	2	3.98*	0.0080*			3.88
Ferrihydrite[b]	Fe-O	3	1.93*	0.0023*	-1.3*	0.11	
	Fe-O	3	2.05*	0.0058*			
	Fe-Fe	2	3.02*	0.0030*			
	Fe-Fe	2	3.24*	0.0015*			
	Fe-Fe	4	3.41*	0.0088*			
Maghemite[c]	Fe-O	1.3	1.92*	0.0046*	-0.35*	0.31	1.92, 1.98
	Fe-O	4	2.08*	0.0088*			2.08
	Fe-Fe	4	2.98*	0.0096*			2.96
	Fe-Fe	6	3.46*	0.0110*			3.42, 3.47
	Fe-Fe	1.3	3.69*	0.0030*			3.53

Notes: A-B is the absorber-backscatterer atom pair; N_B = number of backscatterers at interatomic distance R; σ^2 is the Debye-Waller factor; ΔE_0 is the difference in photoelectron threshold energy between reference functions and data; χ^2 is a reduced least-squares goodness-of-fit parameter. The amplitude reduction factor (S_o^2) was fixed at 0.70 for all samples except for ferrihydrite (varied value = 0.26, see (*14*)) and lepidocrocite (varied value = 0.74 with N fixed). Crystalline reference compounds lepidocrocite and maghemite are compared to interatomic distances determined independently by X-ray diffraction.

*Parameter varied in least squares fit; for fits with large number of shells, parameters not all varied simultaneously.

[a] Crystallographic distances calculated from the structure determination of (*20*).

[b] Reference compound fit from (*14*).

[c] The two crystallographic R values represent tetrahedral Fe^{IV} and octahedral Fe^{VI} in maghemite (21).

In-Ground Reactor

The prototype reactor treated nearly 4,000,000 L or approximately 4,400 pore volumes (PV) of contaminated groundwater over the course of the one-year test period at flow rates typically between 5 and 12 L/min. The reactor was not operated between days 109 (~1,180 PV) and 197 due to lack of groundwater flow to the reactor caused by declining groundwater levels.

A typical profile of changes in water chemistry inside the reactor is shown in Figure 6. Dissolved oxygen and arsenic are rapidly depleted within the first 30 cm of the ZVI bed, and dissolved iron increases. A significant increase in pH is also noted but was found to be inversely related to flow rate. Dissolved iron concentrations are highest within the ZVI bed and decrease again within the downstream gravel chamber due to continuing oxidation and precipitation.

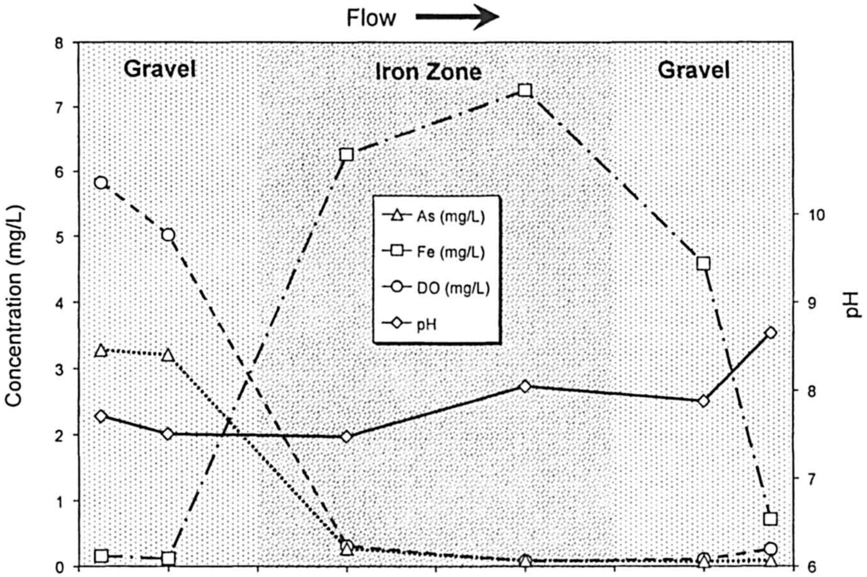

Figure 6. Cross-section of reactor showing typical profiles for dissolved arsenic, iron, and oxygen, and pH along the flowpath.

Influent dissolved As concentrations ranged from 2.26 to 3.46 mg/L with an average of 2.86 mg/L. Effluent dissolved As concentrations ranged from below analytical detection limits (2 μg/L) and increased over time to greater than 1 mg/L (Figure 7). Dissolved As concentrations in monitoring points within the iron bed also increased over time but remained lower than the effluent.

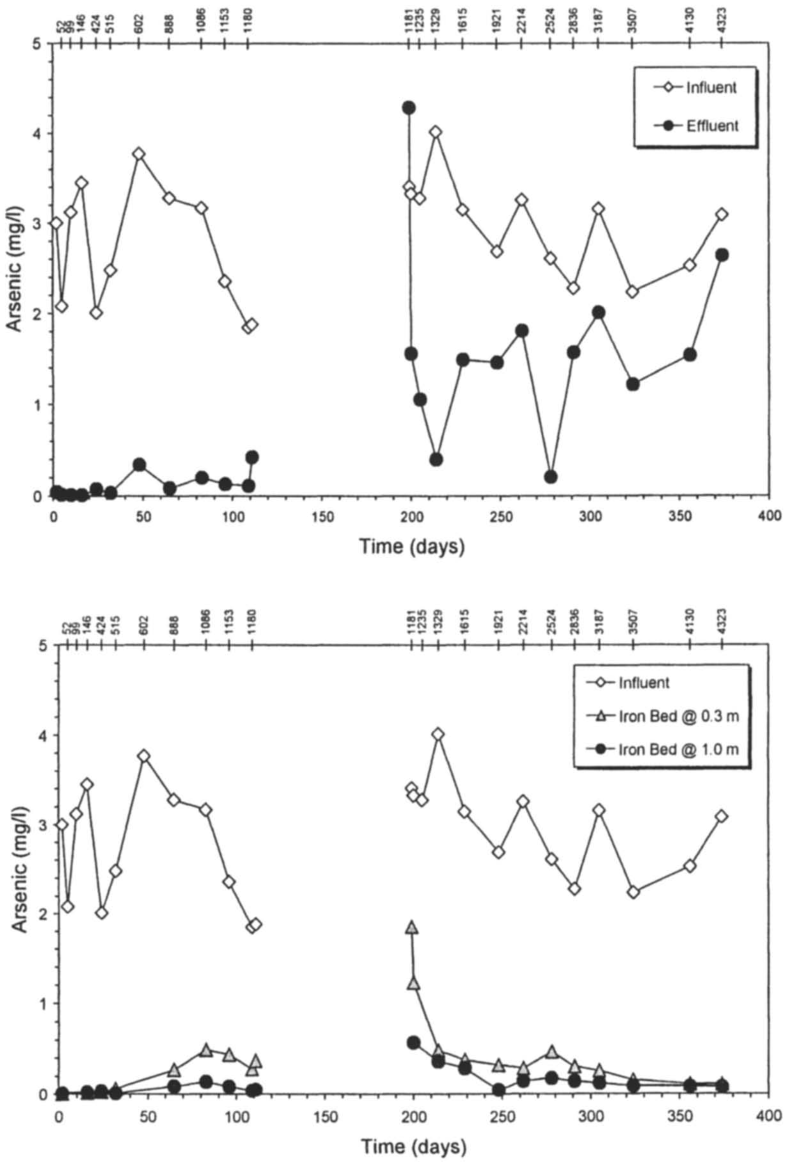

Figure 7. Time series of dissolved arsenic concentrations in influent, effluent (top), and interior monitoring points (bottom) of prototype reactor. Numbers across tops of graphs indicate number of pore volumes.

For a short time after the no-flow period ended (at day 198), elevated dissolved As concentrations and pH (10-12) were observed, both in the effluent and within the iron bed. This is explained by the prolonged contact time of the ZVI with stagnant water trapped in the reactor during the no-flow period (~88 days). Iron corrosion reactions progressed, creating a very high pH condition within the reactor. Arsenic adsorption on iron oxides and oxyhydroxides has a strong pH dependence (*22*), with the greatest adsorption occurring at near neutral to slightly basic pH and decreasing with increasing pH above 8-9. Therefore, high pH within the stagnant reactor caused temporary desorption of previously adsorbed As. After the stagnant water was flushed by new groundwater, arsenic concentrations within the iron bed again decreased to levels observed prior the no-flow period (Figure 7).

Following ~1,300 PV, effluent concentrations became more erratic, and began to approach influent concentrations. This was accompanied by a gradual increase in the hydraulic head gradient across the upstream front of the iron bed over time. It was hypothesized that preferential flow pathways had formed within the reactor. A tracer test subsequently confirmed that part of the flow was bypassing the iron bed. Examination of monitoring data indicated significant flow bypassing had started between approximately 1,600 and 2,200 PV.

Measured Eh-pH conditions within the reactor fall into the stability fields of Fe(III) oxyhydroxide and As(V) (Figure 8), which have also been confirmed by XANES and EXAFS spectroscopy (arsenic spectroscopic data not presented here).

Conclusions

The combination of field test results as a function of flow rate and spectroscopic characterization indicate molecular-level reactions that influence the performance of iron reactive barriers for arsenic removal. Our observations are consistent with a mechanism of arsenic uptake that is not limited by the surface sorption capacity of the solid, but instead reflects a balance between the rate of oxidation of maghemite to Fe(III) oxyhydroxide, and the rate of As incorporation into the newly formed oxyhydroxide. Flow rate is important in determining the extent of As uptake because it determines the loading rate of arsenic, the rate of supply of oxidants (dissolved oxygen), and the residence time for reaction with iron media. Although the initial arsenic adsorption step is relatively fast, sufficient residence time is needed to achieve a particular effluent concentration. Long residence times, however, can also lead to higher pH and less efficient As adsorption onto Fe(III) oxyhydroxide. This is a particularly important consideration for passive (*in situ*) applications where natural variations in flow rate may be significant.

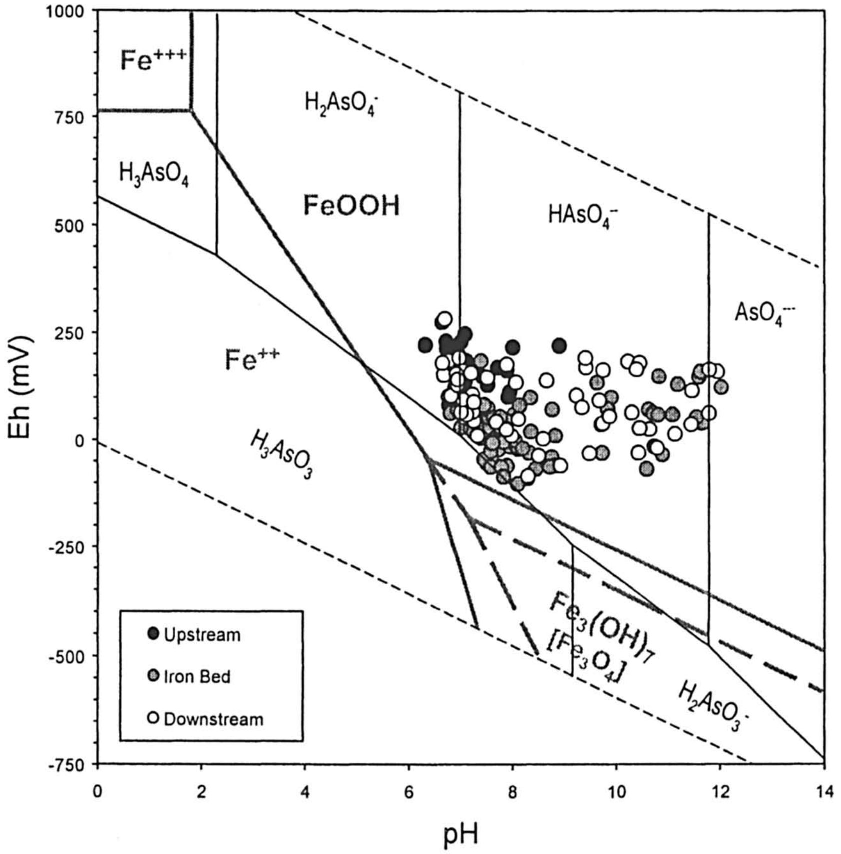

Figure 8. Measured Eh-pH relations within the iron bed and in the upstream and downstream gravel chambers plotted on an Eh-pH diagram showing stability regions of dissolved arsenic species (black lines) and iron oxide/hydroxides (thick gray lines). Green rust ($Fe_3(OH)_7$) field shown by solid gray lines and magnetite (Fe_3O_4) field shown by dashed lines. Thermodynamic data for arsenic species from (23), and for green rust and other iron species from (24).

References

1. *Handbook of Groundwater Remediation Using Permeable Reactive Barriers;* Naftz, D; Morrison, S.J.; Fuller, C.C.; Davis, J.A., Eds.; Academic Press: San Diego, CA, 2002, 539 p.
2. Lackovic, J.A.; Nikolaidis, N.P.; Dobbs, G.M. *Environ. Eng. Sci.* **2000**, *17*, 29-39.
3. Su, C.; Puls, R.W. *Environ. Sci. Technol.* **2001**, *35*, 1487-1492.
4. Farrell, J.; Wang, J.; O'Day, P.; Conklin, M. *Environ. Sci. Technol.* **2001**, *35*, 2026-2032.
5. Melitas, N.; Wang, J.; Conklin, M; O'Day, P.; Farrell, J. *Environ. Sci. Technol.* **2001**, *35*, 2074-2081.
6. Vlassopoulos, D.; Pochatila, J.; Lundquist, A.; Andrews, C.B.; Rafferty, M.T.; Chiang, K.; Sorel D.; Nikolaidis, N.P. In *Remediation of Chlorinated and Recalcitrant Compounds—2002*; Gavaskar, A.R.; Chen, A.S.C., Eds.; Battelle Press: Columbus, OH, 2002; Paper 2H-05.
7. Nikolaidis, N.P.; Dobbs, G.M.; Lackovic, J.A. *Water Research* **2003**, *37*, 1417-1425.
8. Randall, S.R.; Sherman, D.M.; Ragnarsdottir, K.V. *Geochim. Cosmochim. Acta* **2001**, *65*, 1015-1023.
9. Su, C.; Wilkin, R.T. **2005**, In *Advances in Arsenic Research*; O'Day, P.; Vlassopoulos, D.; Meng, X.; Benning, L., Eds.; ACS Symposium Series; American Chemical Society: Washington, DC, 2002; this volume.
10. Fuller, C.C.; Davis, J.A.; Waychunas, G.A. *Geochim. Cosmochim. Acta* **1993**, *57*, 2271-2282.
11. Waychunas, G.A.; Rea, B.A.; Fuller, C.C.; Davis, J.A. *Geochim. Cosmochim. Acta* **1993**, *57*, 2251-2269.
12. George, G.N.; Pickering, I.J. *EXAFSPAK: A suite of computer programs for analysis of X-ray absorption spectra*; Stanford Synchrotron Radiation Laboratory: 2000.
13. Rehr, J.J.; Albers, R.C.; Zabinsky, S.I. *Phys. Rev. Lett.* **1992**, *69*, 3397–3400.
14. O'Day, P.A., Rivera, N., Root, R. & Carroll, S.A. *Am. Mineral.* **2004**, *89*, 572–585.
15. Brown, G.E.; Calas, G.; Waychunas, G.A.; Petiau, J. In *Spectroscopic Methods in Mineralogy and Geology*; Hawthorne, F. C., Ed.; Mineralogical Society of America: Washington, DC, 1988; Vol. 18, p 431-512.
16. O'Day, P.A., Rehr, J.J., Zabinsky, S.I.; Brown, G.E., Jr. *J. Am. Chem. Soc.* **1994**, *116*, 2938–2949.
17. Foster, A.L.; Brown, G.E., Jr.; Tingle, T.N.; Parks, G.A. *Am. Mineral.* **1998**, *83*, 553-568.

18. Savage, K.E.; Tingle, T.N.; O'Day, P.A.; Waychunas, G.A.; Bird, D.K. *App. Geochem.* **2000,** *15*, 1219-1244.
19. Foster, A.L; In *Arsenic in Goundwater;* Welch, A.H.; Stollenwerk, K.G., Eds.; Kluwer: Boston, MA, 2003; pp. 27–65.
20. Christensen, A.N.; Lehmann, M.S.; Convert, P. *Acta Chem. Scan. Ser. A* **1982**, *36*, 303-308.
21. Greaves, C. *J. Solid State Chem.* **1983,** *30*, 257-263.
22. Dixit, S.; Hering, J. *Environ. Sci. Technol.* **2003,** *37*, 4182-4189.
23. Nordstrom, D.K.; Archer, D.G. In *Arsenic in Goundwater;* Welch, A.H.; Stollenwerk, K.G., Eds.; Kluwer: Boston, MA, 2003; pp. 1–25.
24. Bourrié, G.; Trolard, F.; Genin, J.M.R.; Jaffrezic, A.; Maitre, V.; Abdelmoula, M. *Geochim. Cosmochim. Acta* **1999,** *63*, 3417–3427.

Downloaded by NORTH CAROLINA STATE UNIV on September 12, 2012 | http://pubs.acs.org
Publication Date: October 3, 2005 | doi: 10.1021/bk-2005-0915.ch026

Chapter 26

Removal of Arsenic from Bangladesh Groundwater with Zero-Valent Iron

Nikolaos P. Nikolaidis[1], Zhongqi Cheng[2], and Alexander van Geen[2]

[1]**Department of Environmental Engineering, Technical University of Crete, Chania, Greece**
[2]**Lamont-Doherty Earth Observatory of Columbia University, Palisades, NY 10964**

Cartridges containing zero-valent iron filings mixed with sand were tested in Bangladesh to evaluate their effectiveness in removing arsenic from groundwater. The experiments were conducted by pumping, respectively, 1830 and 1140 L of groundwater over the course of a week from two wells containing 560 and 290 μg/L As. The set-up included two cartridges connected in series for As removal, and a downstream aeration vessel followed by a nylon filter to reduce Fe concentrations in the effluent. After conditioning the cartridges for 3-4 days, As concentrations in the effluent consistently remained at or below the WHO guideline of 10 μg/L. Groundwater treatment with iron filings may therefore be a viable technology for arsenic mitigation in Bangladesh.

Dissolved arsenic concentrations in groundwater that are higher than the recommended WHO 10 μg/L guideline for drinking water have been reported in many parts of the world, notably Bangladesh, West Bengal of India, Taiwan, Argentina, Mexico as well as the United Staes (*1-8*). Poorly-understood natural processes contribute to elevated groundwater As levels across a wide range of geological settings, for example, alluvial floodplains and deltas in Bangladesh

In Advances in Arsenic Research; O'Day, P., et al.;
ACS Symposium Series; American Chemical Society: Washington, DC, 2005.

and West Bengal, loess aquifers in Central Argentina, glacial tills in the northeastern and midwestern US, and hydrothermal systems in California and New Mexico.

The reliance on groundwater for human water supply in many parts of the world requires the development of reliable and affordable methods for removing As. One method, coined "Arsenic Remediation Technology" (AsRT, US Patent 6,387,276 B1), which is based on iron filings mixed with sand has been developed at the University of Connecticut (*9*). Field tests conducted in the US (Maine, and New Jersey) (*10,11*), Greece (*12*), Argentina and Switzerland (unpublished data) have demonstrated that iron filings can reduce As concentrations to below 10 μg/L for groundwaters of very different composition. The mechanisms of As removal by iron-filings are only partially understood; likely processes include surface precipitation, coprecipitation, and surface complexation (*9,10,13*).

The present study describes the performance of two household-scale As removal units that were deployed in Bangladesh. A significant potential advantage of this approach over other methods for removing As from well water at the household-level (*14-16*) is that little labor would be required for routine use. The experiments were conducted as part of an interdisciplinary program to determine the causes for elevated As concentrations in Bangladesh groundwater, evaluate various mitigation options, and quantify the health impact of past exposure (http://superfund.ciesin.columbia.edu).

Methodology

Two units were deployed for about a week each at two different wells in January 2001. Each unit consisted of two cartridges connected in series, followed by an aeration vessel and a filtration cartridge (Figure 1). The first two cartridges each contained 1.9 kg of sand and 2.4 kg of iron filings (1:1 by volume); the third cartridge contained a nylon filter. The total volume of the iron-filing/sand media in each cartridge was 2.7 L; the estimated porosity ~0.45. Iron filings were purchased from Connelly-GPM, Inc. of Chicago, IL (stock number CC-1004). The silica sand was a #4 Q-Rok mined by U.S. Silica in Berkley Springs, WV. Well water was pumped through each system at 130-150 mL/min (residence times of 8-9 minutes in the media) by a portable peristaltic pump with three heads (Masterflex). One head pumped water from the well through the first two cartridges and into the aeration vessel. The second head continuously bubbled air into the aeration vessel through a glass frit to oxidize and precipitate ferrous iron released by the filings. The third head pumped the water containing high levels of Fe-oxyhydroxide particles flocs, from the aeration vessel through the last cartridge containing a standard 5-μm nylon filter.

Downloaded by NORTH CAROLINA STATE UNIV on September 12, 2012 | http://pubs.acs.org
Publication Date: October 3, 2005 | doi: 10.1021/bk-2005-0915.ch026

Samples were collected daily at the inlet of the system, the outlet of the second iron filing column (i.e. before the aeration vessel), and the outlet of the nylon filter. Temperature, pH, conductivity, the oxidation-reduction potential (ORP), and dissolved oxygen were also measured daily at the inlet and outlet with an ORION meter. All samples were acidified to 1% HCl (OPTIMA) on site. Phosphate concentrations for all samples were measured by colorimetry in the field using colorimetric molybdate-blue method (*17*). Samples from the inlet and outlet were analyzed for both P and Fe by inductively coupled plasma atomic emission spectrometry with coupled plasma Perkin Elmer Optima 3300XL instrument two months later at the University of Connecticut (UConn). Arsenic was measured at Uconn by hydride generation flame atomic adsorption spectrometry (HG-FAA) using a Perkin-Elmer Model 5100 atomic adsorption spectrometer equipped with an electrodeless discharge lamp (EPA method 6010), with detection limit at 4 µg/L. Inlet and outlet samples collected on January 11 and 18 were also analyzed by high resolution inductively coupled plasma-mass spectrometry (HR ICP-MS) in December 2001 at Lamont Doherty Earth Observatory for a broad suite of inorganic constituents (Na, Mg, Si, K, Ca, Mn, Mo, Se, Al, S, Zn, Sr, Sb, Ba, Cd, Cr, Cu, Pb, Zn, Ni and Cu), some of which are of potential health concern. The detection limit of this method for As is ~0.1 µg/L (*18*). The composition of the mixed iron-filing/sand mixture was also determined with HR ICP-MS after disgestion with mixed HF-HNO_3 acid.

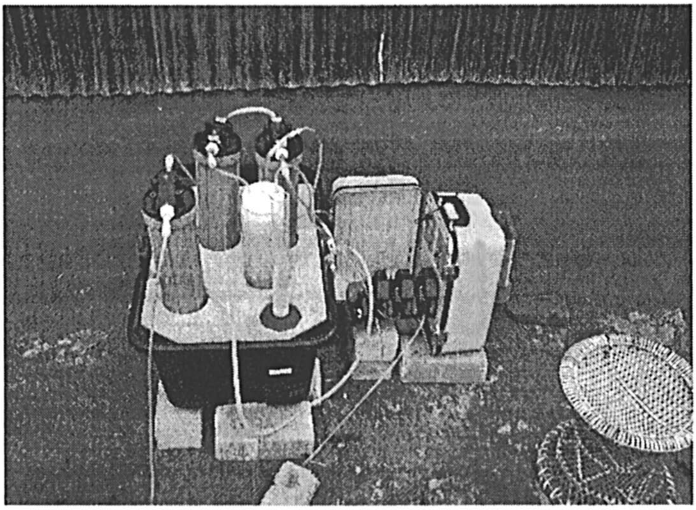

Figure 1. AsRT unit setup.

Downloaded by NORTH CAROLINA STATE UNIV on September 12, 2012 | http://pubs.acs.org
Publication Date: October 3, 2005 | doi: 10.1021/bk-2005-0915.ch026

Results

The inlet As, Fe and P concentrations of the two AsRT units did not vary significantly during the deployment period (Figures 2, 3). Arsenic inflow concentrations of 560 and 290 μg/L for AsRT units A and B, respectively, were also not significantly different from concentrations obtained for the same wells (IDs 4133 and 4146) as part of a large survey conducted a year earlier (*18*). ORP measurements suggest that unit B was tapping a more reducing aquifer; dissolved Fe and P concentrations were significantly higher and S levels were lower compared to water at the inlet of unit A (Table I). Of all the inorganic constituents other than As that were analyzed for the inflow of both units, only Mn concentrations exceeded the corresponding WHO guideline value for drinking water of 0.5 mg/L (Table I).

AsRT units A and B treated 1,830 L and 1,140 L of well water over 8 and 6 days, respectively. During the first few days of the deployment, HG FAA and HR ICP-MS measurements indicated detectable (>4 μg/L) As in the outflow from unit A and concentrations of ~100 μg/L in the outflow from unit B (Figures 2, 3). However, both units became very effective during the second half of the deployment when As concentrations in the effluent remained consistently below 10 μg/L (Table I). Although the dissolution of iron-filing/sand media could have released many elements of potential health concern, their levels at the outlet were all below respective WHO guideline limits (Table II), with the exception of Mn (Tables I and II). Mn concentrations were reduced by about one third for both units relative to the inflow, but remained above 0.5 mg/L.

The corrosion of iron filing material releases significant quantities of Fe, which was confirmed by the orange-colored precipitate formed in the aeration vessel. Despite its simplicity, the combination of aeration and filtration effectively removed excess Fe in the solutions. Iron concentrations in the effluent were maintained below 1 mg/L, the secondary WHO criterion for Fe in drinking water which is based on taste and esthetics rather than health (Figures 2, 3). The time series data indicate that P was also removed by the AsRT units, although the removal was not as effective as for As and declined over the course of the deployments. In the case of unit A, which treated a larger volume of water than unit B, P concentrations at the intermediate sampling point (just before the aeration vessel) gradually increased to reach the level of the inflow over the course of the deployment (Figure 2). For both AsRT units, the precipitation and removal of Fe oxides contributed to the removal of As and P from the effluent.

Downloaded by NORTH CAROLINA STATE UNIV on September 12, 2012 | http://pubs.acs.org
Publication Date: October 3, 2005 | doi: 10.1021/bk-2005-0915.ch026

Downloaded by NORTH CAROLINA STATE UNIV on September 12, 2012 | http://pubs.acs.org
Publication Date: October 3, 2005 | doi: 10.1021/bk-2005-0915.ch026

Table I. Performance of AsRT at Two Wells in Bangladesh (January 2001)

	Unit A-4133		*Unit B-4146*	
	Inflow	*Outflow*	*Inflow*	*Outflow*
pH	6.8	7.1	7.1	7.4
Temp (°C)	23.8	21.2	24.7	22.3
Cond. (μS/cm)	653	612	724	650
DO (mg/L)	2.1	7.3	1.1	7.6
Eh (mV)	-20.9	109.8	-130.4	67.1
As (μg/L)	560	<4	290	8
Fe (mg/L)	1.2	0.4	7.2	0.4
P (μg/L)	280	130	580	96
Na (mg/L)	25	23	38	40
Mg	26	24	25	25
Si	20	15	17	13
K	9.0	8.0	6.2	6.5
Ca	81	71	65	64
Mn	6.2	5.0	3.4	2.5
S	7.4	7.1	2.4	2.6
Mo (μg/L)	4.4	9.8	6.2	7.4
Se	3.1	3.2	2.4	2.2
Al	20	18	20	17
Zn	19	18	18	18
Sr	150	270	120	160
Sb	<0.1	<0.1	<0.1	0.2
Ba	1	43	16	21
Cd	<0.1	<0.1	<0.1	<0.1
Cr	2.5	2.4	2.6	2.4
Cu	8.4	0.4	0.3	0.3
Pb	0.2	0.2	0.1	0.2
Hg	0.2	0.2	0.2	0.2
Ni	2.4	2.9	2.5	2.3
U	1.1	0.2	<0.1	<0.1

All data obtained by HR ICP-MS, except for As (HG FAA) and Fe and P (ICP-AES).

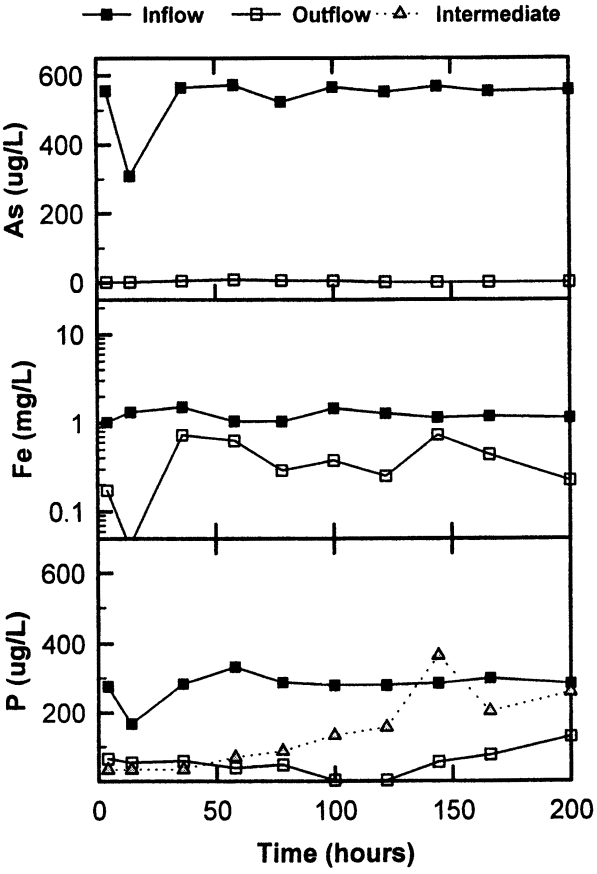

Figure 2. AsRT performance at Well 4133 in Bangladesh: Comparison of influent and effluent arsenic, iron, and phosphate concentrations.

Downloaded by NORTH CAROLINA STATE UNIV on September 12, 2012 | http://pubs.acs.org
Publication Date: October 3, 2005 | doi: 10.1021/bk-2005-0915.ch026

Downloaded by NORTH CAROLINA STATE UNIV on September 12, 2012 | http://pubs.acs.org
Publication Date: October 3, 2005 | doi: 10.1021/bk-2005-0915.ch026

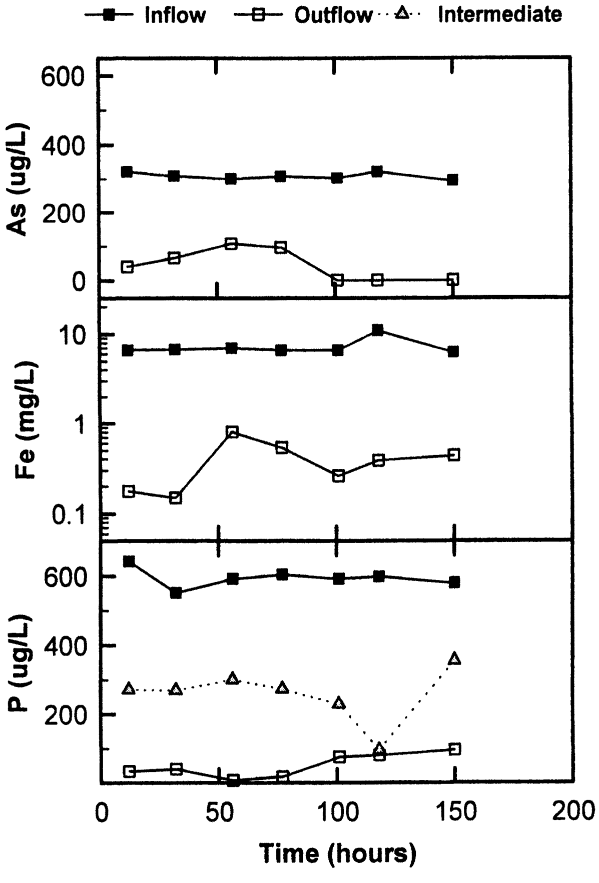

Figure 3. AsRT performance at Well 4146 in Bangladesh: Comparison of influent and effluent arsenic, iron, and phosphate concentrations

Downloaded by NORTH CAROLINA STATE UNIV on September 12, 2012 | http://pubs.acs.org
Publication Date: October 3, 2005 | doi: 10.1021/bk-2005-0915.ch026

Table II. Composition of the Iron Filing and Sand Mixture

Element	*Concentration (mg/kg)*	*Element*	*Concentration (mg/kg)*
Na	87	Mo	200
Mg	98	Ni	390
Si	8900	Al	78
K	107	P	213
Ca	114	S	188
As	25	Ti	86
Ba	1	V	63
Cr	870	Co	41
Cu	1240	Zn	15
Mn	3990	Fe	~50%

Discussion

A variety of methods have been developed to remove arsenic from drinking water but these are usually only effective for arsenate and required a pre-oxidation step for arsenite removal (*19-22*). The technologies also suffer from interferences by P in the water because of strong competition of P(V) with As(V) arsenate for surface sorption sites. In Bangladesh, arsenic is present in groundwater predominantly as As(III) (*23*). As observed in the past, AsRT very effectively removes both As(V) and As(III). The limited removal of P(V) at comparable concentration in the inflow suggests that AsRT may actually remove As(III) more effectively than As(V) (*9, 24*). One of the keys to effective As(III) removal by AsRT may therefore precisely be the relatively poor retention of P(V). This is an important feature in the case of Bangladesh since groundwater P levels are frequently an order of magnitude higher than As.

Most existing As-removal technologies cannot be applied on a wide range of scales that extends from home-based units to large scale water treatment plant and industrial waste treatment. In the case of AsRT, field tests at a landfill in Maine, U.S.A.,with elevated groundwater As concentrations demonstrated a removal capacity of ~ 7 g As per kg of iron filing media (*10*). A larger unit deployed at the same site effectively treated 5500 L/day of groundwater for 8 months essentially without maintainance (*10*). The results of the deployments presented in this study show that AsRT could also be applied at the household level in rural Bangladesh.

Additional factors have to be considered for evaluating the potential for widespread use of AsRT in Bangladesh. The initial breakthough of As from an AsRT unit has been observed in the past (*10*). It is probably due to the limited surface area available for arsenate and arsenite adsorption at the initial stages of the iron filing corrosion process. The rate at which this process occurs depends on the corrosiveness of the water, which may vary significantly between wells.

Downloaded by NORTH CAROLINA STATE UNIV on September 12, 2012 | http://pubs.acs.org
Publication Date: October 3, 2005 | doi: 10.1021/bk-2005-0915.ch026

The implication is that proper training and monitoring of effluent water quality is required before a unit is used to produce water for human consumption. The sensitivity of the capacity of an AsRT system to potential variations in groundwater composition over time also needs to be evaluated with long-term deployments. Periodic monitoring will be required to determine when an AsRT cartridge needs to be replaced. The main complication of this technology is the significant export of iron which requires a separate removal step. Long-term deployments elsewhere suggest that clogging of Fe and sand-containing cartridges should not be a problem. Clogging significantly limits the applicability of the 3-kolshi system, which also relies on Fe filings (*25*). The ample supply of a reactive media, on the other hand, overcomes the problem of limited As removal when insufficient Fe is naturally present in groundwater. Another potential concern faced by all water treatment technologies is bacterial growth within the system. Although the initial setup cost of AsRT could be relatively higher than the 3-kolshi system, it is easier to maintain and can be used for much longer periods continuously (which reduces cost over the long run).

The AsRT technology is fairly unique in that it requires relatively little maintenance for a long time and is cost effective. Household-level As-removal units that require considerably more effort such as daily additions of ferric chloride, filtration through a sand bed, and periodic washing of the sand have been used by hundreds of households in Bangladesh for extended periods (*14-16*). Our experiments in Bangladesh suggest that an AsRT-based system similar to the ones tested could produce continuously 6 L/hour of clean water, i.e. enough to meet the drinking and cooking needs of several families. Due to the relatively low cost of iron filing and sand that can both be produced in Bangladesh, the operating and maintenance cost per unit of a household is estimated to be below US$1 per year. In addition, the system can be scaled-up easily and can be used as a mini-water treatment plant for a group of people or a small village. Toxicity Leaching Characteristic Procedure tests (*10*) on the spent filter material produced As concentrations in the leachate three orders of magnitude less than the criteria, which renders the material safe for disposal in a municipal landfill in the US.

Conclusions

This pilot study demonstrates that iron filings can reduce As concentrations in Bangladesh groundwater to the level of the WHO guideline value for drinking water, without the addition of other elements of potential health concern. No reagents need to be routinely added. AsRT may become useful in areas where As-safe groundwater is not easily available.

Acknowledgements

This project was funded by grant P42ES10349 of the US NIEHS/Superfund Basic Research Program. The authors thank Phillip Larese-Casanova from the University of Connecticut and the staff at the University of Connecticut Environmental Research Institute for their help in the planning and execution of the project. Valuable support was also provided by Kazi Matin Ahmed and his students in the Geology Department of the University of Dhaka. This is Lamont Doherty Earth Observatory contribution #6631.

Downloaded by NORTH CAROLINA STATE UNIV on September 12, 2012 | http://pubs.acs.org
Publication Date: October 3, 2005 | doi: 10.1021/bk-2005-0915.ch026

References

1. Azcue, J. M.; Nriagu, J. O. In: *Arsenic in the Environment, Part I: Cycling and Characterization*, Nriagu, J. O. Ed.; John Wiley & Sons, New York, 1994; p 1-15.
2. Dhar, R. K., Biswas, B. Kr.; Samanta, G.; Mandal, B. Kr.; Chakraborti, D.; Roy, S.; Jafar, A.; Islam, A.; Ara, G.; Kabir, S.; Khan, A. W.; Ahmed, S. A.; Hadi S. A. *Current Sci.* 1997, 73, 48-58.
3. Mandal B. K.; Chowdhury, T. R.; Samanta, G.; Basu, G. K.; Chowdhury, P. P.; Chanda, C. R.; Lodh, D.; Karan, N. K.; Dhar, R. K.; Tamili, D. K.; Das, D.; Saha, K.C.; Chakraborti D. *Current Sci.* 1996, 70, 976-986.
4. Smedley, P.L.; Nicolli, H.B.; Macdonald, D.M.J.; Barros, A.J.; Tullio J.O. *Appl. Geochem.* 2002, 17, 259-284.
5. Chen, S.L.; Dzeng, S. R.; Yang, M. H.; Chiu, K. H.; Shieh, G. M.; Wai, C. M. *Environ. Sci. Technol.* 1994, 28, 877-881.
6. Del Razo, L. M.; Arellano, M. A.; Cebrian, M. E. *Environ. Pollut.* 1990, 64, 143-153.
7. Welch, A. H.; Lico, M. S.; Hughes, J. L. *Groundwater* 1988, 26, 333-347.
8. Ryker, S.J. *Geotimes* 2001, 11, 34-36.
9. Lackovic, J. A.; Nikolaidis, N. P.; Dobbs, G. M. *Environ. Eng.. Sci.* 2000, 17, 29-39.
10. Nikolaidis N.P.; Dobbs, G.M.; Lackovic J.A. *Water Res.* 2003, 37 (6), 1417-1425.
11. Vlassopoulos, D.; Pochatila, J.; Lundquist, A.; Andrews, C.B.; Rafferty, M.T.; Chiang, K.; Sorel D.; Nikolaidis, N.P. Proceedings of 3rd International Conference on Remediation of Chlorinated and Recalcitrant Compounds, May 20-23, Monterey, CA, 2002.

12. Meladiotis I.; Veranis N. S.; Nikolaidis N.P. Proceedings of Conference on Protection and Restoration of the Environment VI, 1-5 July, Skiathos Island, Greece, 2002.
13. Farley J.; Wang J.; O'Day, P; Conklin, M., *Environ. Sci. Technol.* 2001, 35, 2026-2032.
14. Meng X.G.; Korfiatis G.P.; Christodoulatos C.; Bang S. T. *Water Res.* 2001, 35(12), 2805.
15. Hug S.J.; Canonica L.; Wegelin M.; Gechter D.; von Gunten U. *Env. Sci. Technol.* 2001, 35 (10), 2114.
16. Cheng, Z.; van Geen, A.; Jing, C.; Meng, X.; Seddique, A.; Ahned, K., *Environ. Sci. Technol.* 2004, 38(12), 3442-3448.
17. SMWW, Standard methods for the examination of water and wastewater. Phosphorous by ascorbic acid: Method 4500-P-F. 20th edition, 1998.
18. Cheng, Z.; Zheng, Y.; Mortlock, R.; van Geen, A. Rapid multi-element analysis of groundwater by high-resolution inductively coupled plasma mass spectrometry, 2004. *Anal. Bioanal. Chem.* 379(3), 512-528.
19. Hering J. G.; Chen, P. Y.; Wilkie, J. A.; Elimelech, M.; Liang, S. *J. Am. Water Works Assoc.* 1996, 88 (4), 155-167.
20. Joshi, A.; Chaudhuri, M. *J. Environ. Eng.* 1996, 122, 769-771.
21. Maeda, S.; Ohki, A.; Tsurusaki, Y.; Takeshita, T. *Separ. Sci. Technol.* 1990, 25, 547-555.
22. Huang, C. P.; Vane, L. M. *J. Water Pollut. Control Fed.* 1989, 61, 1596-1603.
23. BGS/DPHE, Arsenic contamination of groundwater in Bangladesh: 2001. British Geological Survey, Keyworth, UK, 2001.
24. Su, C.; Puls, R.W. *Environ. Sci. Technol.* 2001, 35 (7), 1487-1492.
25. Munir, A.K.M.; Rasul, S.B.; Habibuddowla, M.; Alauddin, M.; Hussam, A.; Khan, A.H., In: Technologies for Arsenic Removal from Drinking Water. Ahmed, E.; Feroze, Ali; Ashraf, M.; Adeel, Z. eds. BUET and United Nations University, Dhaka, 2001.

Downloaded by NORTH CAROLINA STATE UNIV on September 12, 2012 | http://pubs.acs.org
Publication Date: October 3, 2005 | doi: 10.1021/bk-2005-0915.ch026

Downloaded by NORTH CAROLINA STATE UNIV on September 11, 2012 | http://pubs.acs.org
Publication Date: October 3, 2005 | doi: 10.1021/bk-2005-0915.ch027

Chapter 27

Assessment of Safe Water Options for Villages in Bangladesh

Phillip T. Crisp[1], Ahmedul Hye Chowdhury[1], Andrew Lau[2], Quazi Quamruzzaman[3], and Mahmuder Rahman[3]

[1]School of Chemical Engineering and Industrial Chemistry, University of New South Wales, Sydney, New South Wales 2052, Australia
[2]GHD Group, 180 Lonsdale Street, Melbourne, Victoria 3000, Australia
[3]Dhaka Community Hospital, 190/1 Bara Moghbazar, Wireless Railgate, Dhaka-1217, Bangladesh

The most promising options for safe high-volume water supplies are: dugwells (with floating intake), sand filters (clean pond or river), and deep tubewells (if safe aquifer known). For convenience and acceptance, each requires a supply system, preferably a pump (hand or electric), an elevated tank and reticulation (in-ground plastic pipes, concrete aprons and taps). Low-volume supply options are: rainwater harvesting (optimized for size and elimination of first-flush; expensive), very-shallow tubewells (to dugwell depth) and air/iron treatment systems (for arsenic-affected tubewells). All options, except deep tubewells, can be constructed by villagers using local equipment/materials. Dugwells with supply systems may be economically viable without external aid and suitable for more than half the affected villages.

In Advances in Arsenic Research; O'Day, P., et al.;
ACS Symposium Series; American Chemical Society: Washington, DC, 2005.

Any successful system for providing safe water must be simple, cheap, use local materials and local knowledge, and fit within the social and educational constraints of village life. Most affected people live in small villages that are not suited to large-scale water treatment systems. Conventional urban treatment methods are not appropriate, even if scaled down, since expensive materials and chemicals are required, and proper maintenance is difficult to arrange.

Villagers currently take water from conveniently located tubewells, sometimes in their homes. Most people in affected villages have only a general idea that arsenic is a poison. For social, cultural or time-management reasons, villagers may not even take water from safe tubewells located nearby. Any new water system must be able to compete with existing tubewells in terms of convenience, especially in areas where people are only beginning to show symptoms of arsenicosis. In badly affected areas, convenience is not the major consideration, since people are desperate for any safe water source.

Many wealthy, educated people leave the villages and migrate to the cities. Only the lowest technology devices, requiring minimal maintenance, have a chance of widespread success in villages. Most people in villages live on less than 60 Tk ($US1) per day. Agricultural laborers in poor areas of the country earn 30-50 Tk per day, providing the principal income for a family of 4-10 people. This imposes a severe limit on the cost of any successful water system. There are, however, some wealthy individuals in villages who could fund safe-water systems, if they were clearly profitable. Groups of families could also co-operate to pool resources or borrow money to fund safe water systems, once the benefits were evident and the methods established.

Simple technologies based on iron, concrete and, to a lesser extent, plastic are available. Galvanized iron sheet is ubiquitous, having largely replaced thatch as a roofing material. Welding and riveting are common. Reinforced concrete is used in villages for important buildings, such as mosques, and for durable items such as bridges. Bricks are widely manufactured and commonly smashed by hand to provide aggregate for concrete. Plastic is mostly used in pipes. There is a general lack of non-ferrous metals and modern materials. Safe-water systems using iron, reinforced concrete and plastic pipes lie within current capabilities. Hand pumps are common. Electricity is available in some villages, usually for a few hours morning and night.

Villagers should be encouraged to solve the arsenic problem themselves. Gifts of safe water systems improve the condition of only a tiny fraction of the affected people. Such gifts often have a negative effect in villages, since people do little, while hoping to be the next recipient of a free water system. Ion-exchange, membrane filtration and chemical treatment systems for removing arsenic that have been donated to villages have failed once the donors have departed, due to lack of understanding, training or continued funding. Community involvement, understanding and commitment are essential for any successful safe-water system.

Downloaded by NORTH CAROLINA STATE UNIV on September 11, 2012 | http://pubs.acs.org
Publication Date: October 3, 2005 | doi: 10.1021/bk-2005-0915.ch027

At present, rich and poor people in villages are drinking water with similar arsenic concentrations. Provided options are developed for large groups of families, there is an incentive for the more wealthy, educated and influential villagers to be involved in solving the arsenic problem. If single-family options are pursued, rich families will acquire safe-water systems and become less interested in solving the problems of their poor neighbors.

Safe water sources and supply systems

Downloaded by NORTH CAROLINA STATE UNIV on September 11, 2012 | http://pubs.acs.org
Publication Date: October 3, 2005 | doi: 10.1021/bk-2005-0915.ch027

Water-borne diseases remain a major problem, currently causing far more deaths each year than arsenic-related diseases (10560 arsenic patients identified by 2002 *(1)*, whereas 9% of all deaths and 20% of deaths of children aged 1-4 due to diarrhoea and dysentery in 1999 *(2)*). Safe water, sanitation, hygiene and health are inter-related. Pathogens may be introduced into all "safe" water systems by poor hygiene practices. It is crucial that new water sources introduced into villages do not increase the rate of water-borne diseases.

The best sources of safe water are those intrinsically free from both pathogens and arsenic (dugwells, very shallow tubewells and deep tubewells in suitable sediments; rainwater systems). If such sources are not available, the choice is to remove pathogens from low-arsenic pond or river water (using a sand filter) or remove arsenic from pathogen-free tubewell water (using an air/iron system). Safe water is only required for drinking and cooking; contaminated water can still be used for washing and other purposes.

Safe water sources are conveniently classified by the volume of water that they produce, since this indicates the number of families able to be supplied and hence the level of social organization. Dugwells, sand filters and deep tubewells are high-volume sources, capable of providing 4 m^3 or more per day, sufficient for at least 50-100 families. Very shallow tubewells, dug to the same depth as dugwells, have a supply capacity related to the porosity of the soil and the arrangement of the intake; one to several families may be supplied. Rainwater harvesting generally provides for only one family; collection is limited by the guttered roof area, and storage is limited by the size of the tank. Air/iron treatment systems currently provide for only one family, but it is possible that large-scale systems could be developed to provide for many families.

High-volume sources can be connected to supply systems. In the simplest system, women carry containers to the source, fill them, and return home. Alternatively, a system for home delivery of pots of safe water could be set up. Villagers could jointly acquire a source by borrowing capital, as a profit-making activity, a similar arrangement to the micro-loan scheme offered by Grameen Bank to rural women for cottage industries and mobile phones. Another option is for a rich individual to set up a safe-water supply system as a business. However, the most convenient supply system is a reticulated water supply, with pump, elevated tank and underground plastic pipes to taps. Prosperous villagers or business groups may be able to afford the shared cost of such a system. Organized supply systems, involving payment, are most likely to succeed in villages, since benefits are valued and maintenance occurs. The sustainable output of every high-volume source should be measured, since this determines the number of families that can be provided with safe water and critically affects the cost per family, and hence the economics of the supply system.

Supply systems for ~100 families appear to be economically viable in the context of a Bangladeshi village. A high-volume source, e.g. dugwell, can be constructed for 35,000-45,000 Tk (*1,3*), or less if villagers do the digging themselves, resulting in a capital cost ~400 Tk or less per family. A source with reticulation system can be constructed for a capital cost of ~90,000 Tk (*3*), requiring a contribution per family of ~900 Tk, which is comparable to the cost of galvanized iron roofing for a house.

A reticulated water supply system comprises an elevated tank, typically 2 m^3 in volume and constructed from sheet galvanized iron, with hot riveted angle iron on the corners. The tank is supported by concrete pillars on a concrete platform, so that the bottom of the tank is at least 3 m above the ground. Water is pumped from a high-volume source into the tank by means of a hand pump, or electric pump if electricity is available. Pedal-powered water pumps are also possible in villages without electricity. The water flows by gravity from the tank through underground plastic pipes to a number of taps in the village. Reticulated water systems, each supplying 40-100 families, are currently operating at sites in Pabna, Laksham and Shirajdekhan, using dugwell sources, and in Shirajdekhan, using a river sand filter. Villagers did not contribute to the capital cost, but pay for maintenance of the system (~20 Tk per family per month).

For thousands of years, water was obtained in Bangladesh from protected ponds and from dugwells. Then, the tubewell introduced an unprecedented level of convenience, rapidly supplanting traditional water sources. A tap provides an even higher level of convenience, which can be appreciated in areas where arsenic is not yet a major problem. Reticulated water supply systems, with taps at multiple points in a village, have many advantages: capital and running costs are shared, women save time and effort in carrying water, a tap can be placed in the area of each family cluster to overcome cultural restrictions on travel, and the separation of water source from points of water use reduces the chance of source contamination by wastewater.

Dugwells

A dugwell (*1*) is essentially a hole in the ground, typically 10 m deep and 1.5 m in diameter, lined with concrete rings, with the upper half cemented in order to reduce permeability. The rings extend to a depth 1.5 m below the surface of the aquifer at its lowest level (dry season: April). Traditional

Downloaded by NORTH CAROLINA STATE UNIV on September 11, 2012 | http://pubs.acs.org
Publication Date: October 3, 2005 | doi: 10.1021/bk-2005-0915.ch027

dugwells, using a bucket on a rope or on a cantilevered bamboo pole, typically provide water for 1-5 families. An improved design of dugwell uses a hand pump (as for a tubewell) to extract water, thus reducing the likelihood of contamination from buckets; even better is a dugwell with a reticulation system.

Both physical and chemical factors are responsible for the low concentration of arsenic in dugwell water, depending on the type of dugwell, the geochemistry of the local sediments and the rate of water extraction (*1*). A dugwell takes water from the surface layer of the shallow aquifer. This water largely comprises rain and floodwater (containing virtually no arsenic) that has percolated down through the surface sediments. Water extracted from a dugwell has been in contact with soil minerals for only a short time (generally less than one year), during which time the quantity of dissolved arsenic is usually low. Dugwells with low water-extraction rates allow reaction of dissolved iron(II) in the water with atmospheric oxygen to form iron(III). This precipitates as hydrated iron(III) hydroxide, adsorbing and removing some dissolved arsenic species. Similarly, annual variation of aquifer height may allow penetration of oxygen from the air into sediments near the dugwell, forming hydrated iron(III) hydroxide which acts as a chemical trap for arsenic species.

A dugwell has the advantage of being a known technology, which has been used and trusted for thousands of years. A dugwell is relatively cheap to construct (*1,3*), since it requires only a digging team (4 men for about 4 days), approximately 30 concrete rings (300 mm high, 1500 mm diameter, 150 mm thick), cement, sand, a metal cover and equipment comprising shovels, buckets and bamboo poles. Only a small area (5 m radius circle) of valuable high ground is required for a dugwell, an important factor in crowded villages.

Not all villages have soils suitable for dugwells. Some dugwells yield water high in arsenic *(4)*. Near the coast, the shallow aquifer is saline and dugwell water is undrinkable. Some soils contain a high proportion of clay minerals and this reduces the rate of recharge of the water at the bottom of a dugwell. Some unstable soils require modified construction techniques to avoid hazards to diggers. Other soils are sufficiently fluid to flow into the open bottom of the dugwell, requiring a concrete plug to be placed at the bottom of the dugwell to force the water to flow into the pool through the gaps between the lower uncemented rings. Some aquifers fall below the 7 m suction limit during the dry season (*5*) and would require a subsurface or submersible electric pump for water extraction. It is likely that more than half of the arsenic-affected areas of Bangladesh are suitable for dugwell construction.

Construction of a successful dugwell requires attention to a number of details. Latrines and contaminated ponds must be located far from the dugwell. A concrete apron should extend at least 1.5 m around the top of the dugwell to prevent penetration of water down around the outside of the dugwell through unconsolidated materials remaining from the backfilling of the dugwell hole. The

Downloaded by NORTH CAROLINA STATE UNIV on September 11, 2012 | http://pubs.acs.org
Publication Date: October 3, 2005 | doi: 10.1021/bk-2005-0915.ch027

top half of the dugwell should be cemented to reduce permeability through the inter-ring spaces. The top of the dugwell must be covered to prevent animals such as frogs and lizards falling into the dugwell, then dying and rotting. A floating intake pipe should be used to minimize turbidity. Water should not be extracted using a bucket, due to the chance of contamination; a hand pump or, preferably, a reticulation system should be used.

The polluting activities in the area around the dugwell should be carefully controlled, e.g. defecation by humans (especially children) and animals (especially cows) and mixing of pesticides. If application of pesticides and fertilizers on nearby agricultural land is not well managed, there may be long-term problems with chemical infiltration.

Downloaded by NORTH CAROLINA STATE UNIV on September 11, 2012 | http://pubs.acs.org
Publication Date: October 3, 2005 | doi: 10.1021/bk-2005-0915.ch027

Dugwell operation at Iruaien, Laksham

A dugwell was constructed at Iruaien, Laksham in April 2003 (10 m deep, 1.5 m internal diameter; Figure 1) by the Bangladesh-Australia Centre for Arsenic Mitigation (BACAM). It provides 2 m^3 of water morning and evening by means of an electric pump. The water is transferred to a 2 m^3 tank, with its base situated 5 m above the ground on a concrete platform. Water is reticulated from the tank by plastic pipes to eight sites in the village. Each time the tank is filled, a water column ~1 m is removed from the dugwell. Thus, the rate of water movement up the dugwell is ~2 m per day. The concentration of arsenic in the water was <30 ppb during construction in April, and 9 ppb in November (c.f. Bangladesh limit: 50 ppb). Turbidity was initially a problem but, with continued pumping, the clarity of the water improved and in December was considered excellent. The water tastes like slightly mineralized rainwater. In December 2003, 50 families (~300 people) were each contributing 20 Tk/month to maintenance of the dugwell and were being supplied with water. In addition, ~45 families were being provided with water from the dugwell at no cost.

During the wet season in 2003, water penetrated through the surface layer of the soil (3-8 m) in the vicinity of the dugwell, and settled on top of the aquifer (Figure 2). The early rain/floodwater formed the lower part of the annual layer in the aquifer and the late rain/floodwater formed the upper part. After the wet season, water in the surface layer of the aquifer near the dugwell migrated laterally to canals and rivers, thinning the annual layer of floodwater in the surface aquifer. In summer, agricultural pumping of water from deep layers of the aquifer, caused the annual layer of the aquifer to move downwards, as a unit.

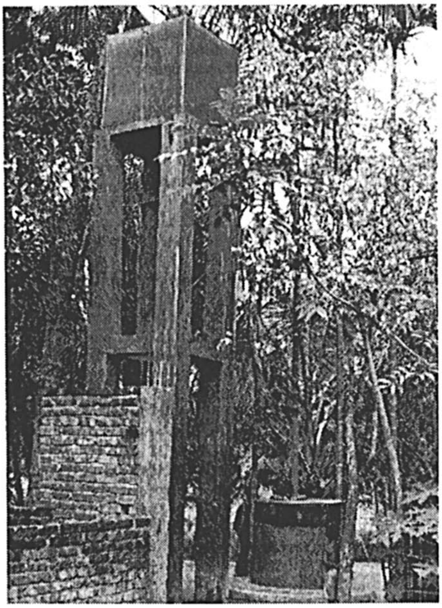

Figure 1. The BACAM dugwell and reticulation system at Iruaien, Laksham, 4 October 2003.

Downloaded by NORTH CAROLINA STATE UNIV on September 11, 2012 | http://pubs.acs.org
Publication Date: October 3, 2005 | doi: 10.1021/bk-2005-0915.ch027

Water is extracted from a high-volume dugwell at such a rapid rate (~2 m water column each day at Iruain, Laksham) that there is little opportunity for water constituents, such as iron(II) or arsenic(III) to react with oxygen in the air. Most particles of iron(III) hydroxide, formed at the surface of the water column, are pumped from the well before sedimentation becomes significant. This implies that the water extracted from the dugwell is closely similar to the pore water in the sediment. As the quantity of water extracted from the dugwell increases, pore water will be drawn from more distant parts of the subsurface sediment. More distant pore water may contain a higher or a lower concentration of arsenic. Every dugwell is expected to behave differently as the rate of water extraction increases. Some dugwells may support very high extraction rates, without exceeding the allowable arsenic concentration. Since subsurface chemistry is not known, the performance limits of each dugwell should be independently tested.

The infiltrated rain and floodwater forming the annual layer on top of the surface aquifer (Figure 2) initially contains little arsenic. It is expected to slowly accumulate arsenic dissolving from arseniferous minerals, especially in the vicinity of organic matter, with the arsenic concentration in pore water

Downloaded by NORTH CAROLINA STATE UNIV on September 11, 2012 | http://pubs.acs.org
Publication Date: October 3, 2005 | doi: 10.1021/bk-2005-0915.ch027

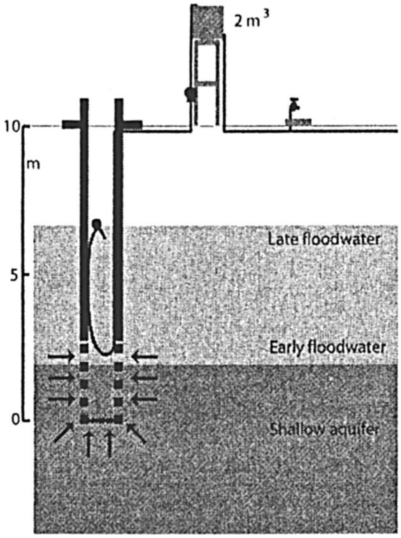

Figure 2. Cross-section of the aquifer and dugwell at Iruaien, Laksham. Water levels are based on 2003 data.

increasing with contact time. The arsenic concentration in dugwell water is expected to be higher during the dry season than the wet season.

The maximum pumping rate is limited by the recharge of the water at the bottom of the dugwell through the uncemented rings around the sides and through the bottom. When the dugwell was constructed in April, the bottom was pumped dry, and the villagers estimated that it took around 2 hours for the pool to refill to its full height of 1.5 m. If it is assumed that continuous pumping would increase the flow rate, by lowering the level of water and increasing the hydrostatic gradient, ~1 m^3 could be pumped from the dugwell every hour during the dry season. In the wet season, the maximum recharge rate should be greater, since a larger interior well surface is available and a larger hydrostatic gradient is possible. At present, a pumping rate of 4 m^3 per day is sufficient for 50-100 families. In theory, sufficient water could be pumped from the dugwell in summer for >600 families, if the dugwell was pumped continuously. As the pumping rate increases, the concentration of suspended particles in the water is expected to increase, especially when the dugwell is new. Turbidity, not arsenic, may limit the pumping rate from the dugwell. If this proves to be the case, it may be possible to deal with turbidity by means of a sand filter.

Sand Filters

Sand filters purify low-arsenic water from a pond or river by removing suspended particles and pathogens by slow filtration through sand in a concrete tank approximately 4 m square and 2 m high, containing chambers filled with crushed bricks, sand of different porosities and a storage reservoir for purified water. This type of sand filter is not backwashed to clean the sand; fine particles accumulate on the upper layer of sand until the layer is periodically scraped off and replaced. Sand filters produce safe water, provided the system is well maintained and pathogen levels are not excessively high (*1*). Sand filters do not remove arsenic unless minerals containing iron, or other transition metals, are present in the sand.

It is important that the flow of water down through the sand bed is uniform, since this reduces flow velocity, increasing the retention of particles including pathogenic organisms. Channeling is to be avoided. Two grades of sand (coarse, then fine) are desirable. The collection of water after passage through the sand bed is best achieved by means of layers of crushed brick of increasing particle size, containing a network of plastic pipes embedded in the coarsest (bottom) brick layer. Current designs of sand filters can probably be improved by adding an elevated storage reservoir for untreated water with a tap to maintain a slow uniform flow of water through the system. In addition, the efficiency of the crushed-brick pre-filter, which removes silt, can probably be improved.

The main problem with a sand filter is microbial contamination of the water, either due to inadequate maintenance, or to an increased concentration of pathogens as a result of a pollution episode in the pond or river supplying water. The flow of water through a sand filter is slow, and the top layer of sand may need frequent removal to eliminate blockage by silt. A pump, either hand or electric, is required to transport water to the sand filter. There are problems in finding suitable sites for sand filters, since clean permanent ponds are now mostly used for commercial fish culture (*5*) and many rivers are heavily polluted. If fish ponds are converted to water sources for sand filters on a large scale, fish production will decline. There may be opportunity for long-term reorganization of ponds in villages by reducing the number of latrine ponds.

Downloaded by NORTH CAROLINA STATE UNIV on September 11, 2012 | http://pubs.acs.org
Publication Date: October 3, 2005 | doi: 10.1021/bk-2005-0915.ch027

Deep Tubewells

Deep-tubewell water is generally used for agricultural purposes, but may be safe and palatable (low in arsenic, salt, hydrogen sulfide and toxic metals). Safe deep aquifers exist beneath many arsenic-affected areas of Bangladesh (*5*). Aquifers of the Plio-Pleistocene age or older are low in arsenic, as are most aquifers of the Late Pleistocene-Early Holocene, though the latter may not remain so (*6*).

Downloaded by NORTH CAROLINA STATE UNIV on September 11, 2012 | http://pubs.acs.org
Publication Date: October 3, 2005 | doi: 10.1021/bk-2005-0915.ch027

There are a number of problems with the use of deep aquifers. If care is not taken to seal the bore-hole during construction, water may descend to the deep aquifer from the surface aquifer, transporting arsenic. Clay layers between aquifers are thinner in the north of the country (*7*), making it harder to achieve a natural seal between aquifers, increasing cross-aquifer contamination. There are long-term issues concerning the viability of deep aquifers as a result of heavy water usage for agriculture and transport of arsenic in the saturated zone, especially ingress of water from other aquifers. Aquifers are best considered on the basis of their geological age rather than depth (*8*).

An aquifer suitable for a safe deep tubewell is sometimes known as a result of deep tubewells already sunk for agricultural purposes. If not, test drilling to locate a suitable aquifer is relatively time-consuming and expensive. Tubewells (to all depths) are dug by pumping water under pressure through a plastic tube held vertically and allowed to bore into the ground, eroding soil particles that are carried up to the surface by the flowing water. Shallow tubewells can be dug manually by holding the descending plastic tube by hand. Deep tubewells, however, require heavy rigs to support the weight of the descending plastic tube. Such rigs are owned by construction companies that may charge inflated fees for digging deep tubewells.

Very Shallow Tubewells

Where a high-volume dugwell is providing low-arsenic water, it is likely that a very shallow tubewell sunk to the same depth will also provide safe water. A very shallow tubewell (*1*) provides water from the annually-renewed surface layer of the shallow aquifer without opportunity for reaction with air. A very shallow tubewell is cheap to construct, but has a number of potential problems. Care must be taken to drill the tubewell to the correct depth. There may be problems with the rate of recharge in clay soils, especially during the dry season, and there is suspicion from villagers about new tubewells that look the same as the ones that are currently poisoning them.

In Iruain, Laksham, one anomalous green tubewell (12 ppb arsenic) in a large area of red tubewells (200-800 ppb arsenic) was tested and found to be only 8.3 m deep. This indicates a role for very shallow tubewells in Iruain.

The best use of very shallow tubewells is probably in areas where high-volume dugwells have been shown to succeed and the depth of the aquifer surface is known. In this case, very shallow tubewells may be used to provide water to families that are remote from areas where safe water is available.

Downloaded by NORTH CAROLINA STATE UNIV on September 11, 2012 | http://pubs.acs.org
Publication Date: October 3, 2005 | doi: 10.1021/bk-2005-0915.ch027

Air-Iron Systems

Treatment systems using air and iron to remove dissolved iron(II) ions from tubewell water have been used for a decade in order to improve water flavor and reduce the amount of brown food-staining (e.g. rice), when the water is used for cooking. The traditional system, known as the 3-kalshi (*1*), uses three pots in series. The first stores water and supplies it slowly to the second, via a hole in its base. The second exposes the water to air, iron turnings and filter cloths. The third collects the purified water. Iron(II) ions present in the tubewell water are oxidised to iron(III) ions, which then precipitate as hydrated iron(III) hydroxide, which is retained on the filter cloths. Additional hydrated iron(III) hydroxide adsorbant is provided by rusting of the iron metal. Arsenic(III) species in the tubewell water are partially adsorbed on the iron hydroxide materials. In addition, some arsenic(III) is oxidised to arsenic(V) which is both less poisonous than arsenic(III) and more readily adsorbed on iron hydroxide surfaces.

The 3-kalshi is labor-intensive for women, and only partially effective. Nevertheless, it demonstrates an effective chemistry for arsenic removal and is the only chemical treatment system for tubewell water that has proven successful in villages to date. Its attractions are simple design and cheap materials. It may be possible to develop a large-scale 3-kalshi system for purification of tubewell water (*9*). A laboratory pilot version consists of a tank with the following features: baffles that force the water repeatedly to the surface to expose it to air, crushed brick at the bottom to trap precipitated materials, and a bed of scrap iron to remove remaining arsenic. Such a system has performed well in laboratory trials (*10*), but remains to be tested in the field.

Rainwater Harvesting

Rainwater harvesting technology (*1*) currently used in Bangladesh is not optimal and rainwater systems have generally experienced difficulties. The standard system, following IDE-UNICEF guidelines, uses a 6 m channel gutter to collect water from a galvanized iron roof, directing it via a manual first-flush device to a 3.2 m^3 concrete tank, shaped like a minaret. There are many problems. The collecting area is too small to capture enough water as the dry season approaches, increasing the periods when the tank is empty. The tank is too small to provide sufficient reserves for the dry season. The first flush device requires manual operation that may not be carried out. Screening is not always adequate to prevent frogs, lizards, etc, entering the tank. Overflow of water is arranged from the top of the tank, rather than from the bottom (to remove anoxic water, and decaying organic particles). As only ~20 mm (or less) of mortar is applied to the chicken-wire reinforcing during construction, water and oxygen can penetrate the mortar and react with the wire, resulting in rusting, expansion and cracking of the concrete. Sometimes, chicken-wire reinforcing is not used and tanks have been known to "explode".

According to rainfall calculations, the minimum size of a rainwater tank for an average family is 4 m^3, with the volume preferably much larger (*1*). The tank itself is the most expensive item in a rainwater harvesting system. There is an economy in scale as the tank is made larger, but the problem is that stored water is difficult to share between families. Conflicts are likely to arise if one family uses more than its share, or wastes water by leaving a tap running. There is opportunity for rainwater collection on shared buildings such as schools, using large tanks, but there are then problems with equitable distribution of water, and security outside normal working hours.

Householders find the flavor of tank water too heavily mineralized and alkaline for the first few months, while the concrete completes its setting and leaches calcium salts. Later, householders may find the taste of rainwater unpalatable, since they are used to the more mineralized flavor of tubewell water. Inadequate training of householders in relation to possible hazards sometimes results in contamination, e.g. by pigeons defecating on the roof, or by animals (e.g. frogs) entering the tank, dying and decaying. Most importantly, rainwater harvesting is so expensive (6200 Tk per family (*1*); 1500 Tk per person (*3*)) that it is beyond the means of most villagers; reliance must therefore be placed on external aid organizations. The cost of a well-designed and long-lasting rainwater harvesting system for a family is comparable to that of a dugwell. Whereas a dugwell can provide 4 m^3 of water per day all year round, a rainwater tank may store less than that 4 m^3 of water, which must last a family during the 3 months of the dry season.

There is a long history of successful rainwater collection in Australia and other dry countries, but the cost of durable systems is beyond the means of most Bangladeshi families. The standard material for tank construction in villages is currently concrete, but there are possibilities of building tanks from galvanized iron sheet with bamboo frames. Such tanks could be cemented in sections as they corrode near the base, thus spreading the capital cost of a tank over several years. Alternatively, plastic tanks could be made in sections for assembly in villages.

Conclusion

A dugwell, with a reticulation system serving ~100 families, appears to be the best option in arsenic affected villages, since the technology is simple, cheap and relatively well proven. It is also sufficiently desirable for its convenience and modernity that families may be willing to allocate the resources needed for

Downloaded by NORTH CAROLINA STATE UNIV on September 11, 2012 | http://pubs.acs.org
Publication Date: October 3, 2005 | doi: 10.1021/bk-2005-0915.ch027

construction. If high-flow dugwells succeed, very shallow tubewells to the same depth should provide smaller amounts of water for outlying families.

If a relatively clean pond or river is available, a sand filter is a good option, again best combined with a reticulation system. A deep tubewell with reticulation is an appropriate choice, if a deep aquifer is known to provide safe water. High-volume systems reticulated to ~100 families may be economically viable in villages without external financial assistance. Systems without reticulation are cheaper to construct, but are less attractive to villagers, and require a higher level of hygiene understanding and motivation.

There are still options to consider in circumstances where the soil is not suitable for dugwells, there is no clean pond or river, and there is no knowledge of a safe deep aquifer in the area. Rainwater harvesting systems can be installed, but are relatively expensive. A test drilling program can be commenced to search for a suitable deep aquifer, but this is also expensive. Home-based 3-kalshi systems can be established, but these require high maintenance. A large-scale 3-kalshi system may prove successful, and cheap water tanks constructed from metal or plastic may be possible.

Every water system should be tested before use and monitored biannually (before and after the wet season), taking into account all likely contaminants, not just arsenic and pathogens. Fluoride, heavy metals and pesticides should also be considered. A major increase in the capacity of analytical facilities in Bangladesh is needed to meet these requirements.

Many important factors need to be considered in building and maintaining a safe water system. These can make the difference between success and failure. These factors often relate to hygiene issues that are not obvious to villagers, e.g. pigeons defecating on the roof of a rainwater system, a dirty bucket lowered into a dugwell, or contaminated pond water used to prime a hand pump with a worn seal. It is important that such matters be documented, communicated and updated as more information becomes available. Provision of safe water needs to be integrated with education and health programs to be successful.

Downloaded by NORTH CAROLINA STATE UNIV on September 11, 2012 | http://pubs.acs.org
Publication Date: October 3, 2005 | doi: 10.1021/bk-2005-0915.ch027

Acknowledgements

This project was funded by the Australian Government through AusAID (Bangladesh-Australia Centre for Safe Water and Food Project, Component 2: Clean Water Program). The project was managed by GHD Pty Ltd and the Commonwealth Research Centre for Waste Management and Pollution Control (CRCWMPC), with funding to University of New South Wales and Dhaka Community Hospital (Bangladesh-Australia Centre for Arsenic Mitigation, BACAM). The views expressed are those of the authors and not necessarily those of AusAID. The authors thank the staff of Dhaka Community Hospital for assistance with this work, and the family of Md. Abdul Hye Chowdhury for their generosity and insights into technology and society. The authors thank David Garman (CRCWMPC), Alison Baker and Peter Nadebaum (GHD), Wahidul Biswas and Eva Crisp for their valuable comments and assistance.

References

1. *Arsenic Mitigation in Bangladesh;* Feroze Ahmed, M; Mufad Ahmed, C., Eds; Local Government Division, Government of Bangladesh: Dhaka, 2002; pp 81-174.
2. Caldwell, B.K.; Caldwell, J.C.; Mitra, S.N.; Smith, W. *IUSSP Regional Population Conference on Southeast Asia's Population in a Changing Asian Context*, Bangkok, 2002; pp 1-27.
3. Dhaka Community Hospital *Report on Dug Wells Implemented by DCH, 2nd Phase: Drinking Water Supply through Pipelines at the Household Level for the Rural Community*, 2003; http://phys4.harvard.edu/~wilson/arsenic/ remediation/dugwells.
4. Arsenic Research Group, School of Environment, Jadavpur University, Scientific Studies on Dug Wells; http://www.sos-arsenic.net/english/dugwell.
5. Faruque, H.S.M.; Huq, I.; Abdullah, S.K.M.; Nishar, A.; Farooque, M.K.; Mustofa, K.G.; Alam, S.; Ruzzaman, M. *Report of the Committee on Surface Water Development and Management for Drinking Water Supply in Arsenic affected areas of Bangladesh;* Local Government Division, Government of Bangladesh: Dhaka, 2003; p 19.
6. Abdullah, S.K.M.; Islam, M.N.; Faruque, H.S.M.; Chowdhury, L.R.; Halim, M.A.; Chowdhury, A.Q.; Hossain, A; Huq, I.; Hussain, M.M. *Report on the Ground Water Task Force;* Local Government Division, Government of Bangladesh: Dhaka, 2002; pp 33-47.
7. British Geological Survey; Department of Public Health Engineering, Government of Bangladesh *Arsenic Contamination in Bangladesh, Final Report;* 2001; Vol. 2, p 267.
8. Islam, M.N.; Uddin, M.N. *International Workshop on Arsenic Issue in Bangladesh;* Local Government Division, Government of Bangladesh: Dhaka, 2002; p 16.
9. Crisp, P.T.; Chowdhury, A.H. *BUET-UNU International Workshop on Technologies for Arsenic Removal from Drinking Water;* Dhaka, 2001; pp 85-98.
10. Chowdhury, A.H.; Crisp, P.T. *Advances in Arsenic Research;* O'Day, P.A.; Vlassopoulos, D.; Meng, X.; Benning, L.G., Eds; American Chemical Society: Washington, DC, 2004; pp 386-397.

Downloaded by NORTH CAROLINA STATE UNIV on September 11, 2012 | http://pubs.acs.org
Publication Date: October 3, 2005 | doi: 10.1021/bk-2005-0915.ch027

Downloaded by NORTH CAROLINA STATE UNIV on September 12, 2012 | http://pubs.acs.org
Publication Date: October 3, 2005 | doi: 10.1021/bk-2005-0915.ch028

Chapter 28

Two-Year Operation of an Air–Iron Treatment System for the Removal of Arsenic from Simulated Bangladeshi Tubewell Water

Ahmedul Hye Chowdhury and Phillip T. Crisp

School of Chemical Engineering and Indutrial Chemistry, University of New South Wales, Sydney, New South Wales 2052, Australia

A model system for As(III) removal from simulated Bangladeshi tubewell water (in mg/L: As(III) 0.2, Fe(II) 5, Ca^{2+} 40, Na^{+} 50, SO_4^{2-} 9, Cl^- 70, HCO_3^- 133, PO_4^{3-} 6, SiO_3^{2-} 20) was operated indoors for a period of 2 years at the rate of 8 L per day. The system comprised: 1. water storage tank with tap regulator, 2. tank with internal baffles which forced water repeatedly down through crushed brick and up to the surface, 3. tank containing scrap iron (fire-burnt tin-plated steel cans), 4. water lock to maintain water level, and 5. storage tank. In tank 2, particles of $Fe(OH)_3.nH_2O$ (I) were retained in the crushed brick, while As was partially precipitated with I and partially oxidized to As(V). Arsenic removal in tank 2 varied from 95% to 30% (in the presence of PO_4^{3-} & SiO_3^{2-}). The arsenic concentration in the output water was <5 µg/L for two years. The design of a pilot system for safe agricultural water is presented.

In Bangladesh, approximately 49 million people are drinking water with an arsenic concentration >10 ppb (World Health Organization limit), 29 million are drinking water with arsenic >50 ppb (Government of Bangladesh limit) and 10 million are drinking water with arsenic >200 ppb (*1*). Symptoms of arsenicosis have already reached epidemic proportions, and the largest mass poisoning in human history is predicted if the majority of people in affected areas are not soon provided with safe drinking water.

Water purification techniques using coagulation-flocculation, membranes (*2,3*) and other advanced systems (*4*) are used in large-scale water treatment for towns and cities, but are not appropriate to the treatment needs of the majority of the Bangladeshi population, who live in small villages. Due to widespread poverty amongst the affected people, arsenic removal from groundwater must be accomplished at very low cost, using materials that are either widely available or capable of being produced with only minor modifications to existing production techniques. Materials that can be made using few resources other than human labor are preferred. For popular acceptance, especially in areas where arsenic-related health problems are not yet epidemic, any new system should provide a level of convenience as great or greater than the tubewells in current use.

Treatment of tubewell water to remove arsenic has been assessed as one of the available safe-water options for villages (*5*). The 3-kalshi method (*1*), which uses only air, light, scrap iron and charcoal to purify heavily mineralized water, while simultaneously removing arsenic, is the only system that has achieved widespread success. Small-scale systems for purifying the water for a single household, based on the 3-kalshi method, have been demonstrated (*6,7*). However, all these systems have two common disadvantages. Firstly, they are time-consuming, reducing time available for family care and education, especially for women. Secondly, they are expensive, especially for initial purchase of equipment (typically 450-2500 Tk *(1)*). These two disadvantages can be reduced if water treatment is accomplished on a larger scale: construction and running costs can then be shared between a number of families, and maintenance activities can be efficiently shared. Men in the village (or a paid "water worker") could be responsible for maintenance activities, and a large-scale system (~50000 Tk, based on cost of sand filters) could purify as much water each day as a hundred domestic 3-kalshi systems.

Earlier papers by the authors (*8,9*) proposed a design for a low-cost treatment system for tubewell water based on the same chemistry as the 3-kalshi method, but on a large scale (similar to a sand filter) and optimized for chemical efficiency. This paper describes two years of operation of a laboratory-scale model of this treatment system. This paper also proposes the design of the next development stage: a pilot system for purifying tubewell water to supply safe low-arsenic water for agriculture.

Downloaded by NORTH CAROLINA STATE UNIV on September 12, 2012 | http://pubs.acs.org
Publication Date: October 3, 2005 | doi: 10.1021/bk-2005-0915.ch028

Construction of the treatment system

A water treatment system (Figures 1 & 2) was constructed following the design proposed by the authors in earlier papers (*8,9*). The structure was constructed from 12 mm Perspex sheet, held together with 3/16 BSW 304-stainless-steel bolts drilled and tapped into the edges at 50 mm intervals. Holes (1/4") were drilled at 50 mm intervals in the base of every second section of the precipitation tank and at the base of the adsorption tank. Black neoprene gasket (1 mm) was placed between all surfaces before tightening bolts and all seams were sealed with silicone sealant (Dow Corning 747) after tightening.

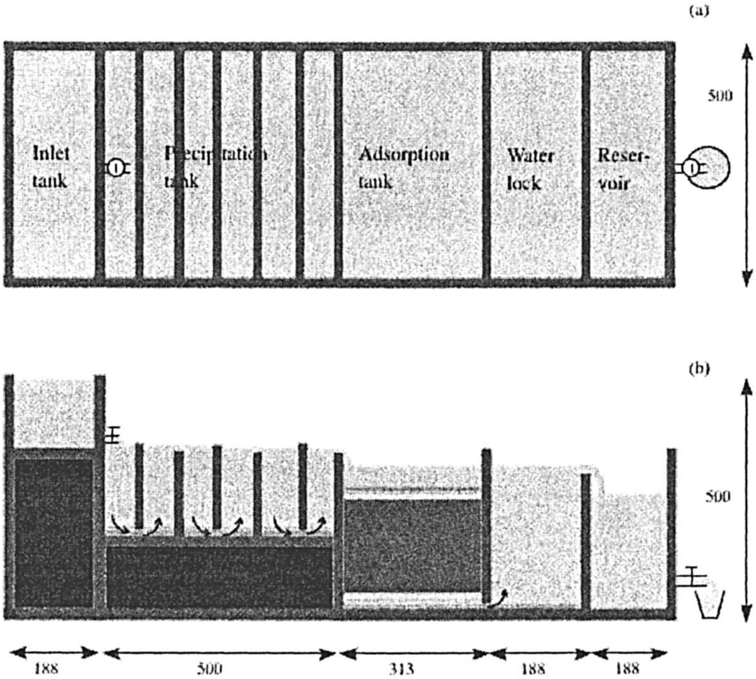

Figure 1. Water treatment system constructed in the laboratory in plan view (a) and cross-sectional view (b). Dimensions are in mm.

Brass taps were inserted at the base of the inlet tank and the reservoir, and coarse crushed brick (5-10 mm) was placed to a depth of 50 mm in the base of each section of the precipitation tank. The adsorption tank was filled, in order, with coarse crushed brick (5-10 mm diameter; 50 mm layer), medium crushed

Downloaded by NORTH CAROLINA STATE UNIV on September 12, 2012 | http://pubs.acs.org
Publication Date: October 3, 2005 | doi: 10.1021/bk-2005-0915.ch028

Downloaded by NORTH CAROLINA STATE UNIV on September 12, 2012 | http://pubs.acs.org
Publication Date: October 3, 2005 | doi: 10.1021/bk-2005-0915.ch028

brick (2-5 mm diameter; 50 mm layer), fine crushed brick (1-2 mm diameter; 50 mm layer), burnt tin-plated steel cans (Gadsden Pty Ltd; burnt >10 min in open wood fire; cut into ~15 mm squares; 4 kg; ~300 mm layer), fine crushed brick (50 mm layer), medium crushed brick (50 mm layer) and coarse crushed brick (50 mm layer).

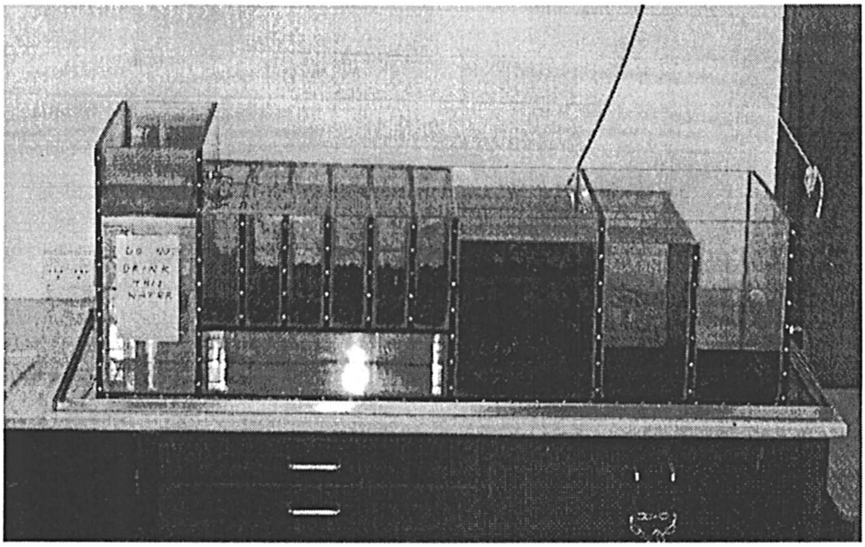

Figure 2. Side view of the air-iron treatment system in the laboratory.

Method

After construction, water (Sydney tap water; pH 7.5, total As <0.003 mg/L) was run through the tank for 6 days. The components of simulated Bangladeshi tubewell water were then added one at a time, so the effect of each could be observed. Components were added in the order: As (III) 0.2 mg/L (Day 7); Fe (II) 5.0 mg/L (Day 14); Na^+ 50 mg/L, HCO_3^- 133 mg/L, Ca^{2+} 40 mg/L and Cl^- 70 mg/L (Day 28), PO_4^{3-} 6 mg/L (Day 90); SiO_3^{2-} 20 mg/L (Day 180). The concentrations chosen were the average values reported for tubewell water, except for PO_4^{3-} and SiO_4^{3-}, which were the maximum allowable values in drinking water, selected to test the limits of the treatment system (*10,11,12*).

Each day, except during weekends after the first month, a volume of 8 L of solution, comprising initially water, then containing also the ingredients described above, was allowed to run into the system during a period of approximately 4 h, by adjustment of the brass tap on the inlet tank. Residence time for water in the system was approximately 15 days.

During the first month of operation, arsenic concentrations were measured in the inlet tank, the first stage of the precipitation tank, the last stage of the precipitation tank, the adsorbent bed and the reservoir. In addition, arsenic was measured in the middle precipitation stage on days 12-14. After the first month, arsenic measurements were limited to the last precipitation stage and the reservoir.

Arsenic concentrations were measured using a silver diethyldithiocarbamate colorimetric method (*13*), modified to enhance sensitivity and eliminate fragile components of equipment (*14*), with a 2σ limit of detection of 5 ppb.

Downloaded by NORTH CAROLINA STATE UNIV on September 12, 2012 | http://pubs.acs.org
Publication Date: October 3, 2005 | doi: 10.1021/bk-2005-0915.ch028

Results

When 200 ppb arsenic(III) was initially passed through the system, the concentrations of total arsenic measured at points in the treatment system were substantially less than 200 ppb (Figure 3). The concentration dropped to 180-100 ppb in the stages of the precipitation tank, and to ~25 ppb in the reservoir. Approximately 80% of the arsenic was removed, presumably through adsorption on surfaces of brick and burnt steel cans. Since the bricks were rich in iron (same red color as Bangladeshi bricks) and the steel cans were beginning to rust, it is likely that adsorption on iron oxide/hydroxide surfaces was primarily responsible for the initial adsorption of arsenic.

When Fe(II) ions were added to the system on Day 14, $Fe(OH)_3.nH_2O$ precipitated in the inlet tank and in the first stages of the precipitation tank. Approximately 80% the total arsenic was removed by adsorption on the surfaces of $Fe(OH)_3.nH_2O$ particles. The bed of rusting tin-plated steel cans became increasingly effective at trapping arsenic with time, presumably due to increasing formation of rust particles on the metal surfaces. By Day 40, the iron bed reduced the arsenic concentration from 40 ppb to10 ppb.

Addition of the ions Na^+, HCO_3^-, Ca^{2+} and Cl^- at Day 28 had little apparent effect on the removal of arsenic (Figures 3 & 4). Adsorption of arsenic on $Fe(OH)_3.nH_2O$ particles in the precipitation stage remained approximately constant and the efficiency of the bed of rusting iron continued to improve. By Day 90, the concentration of total arsenic in the reservoir had dropped to <5 ppb, the detection limit of the analytical method.

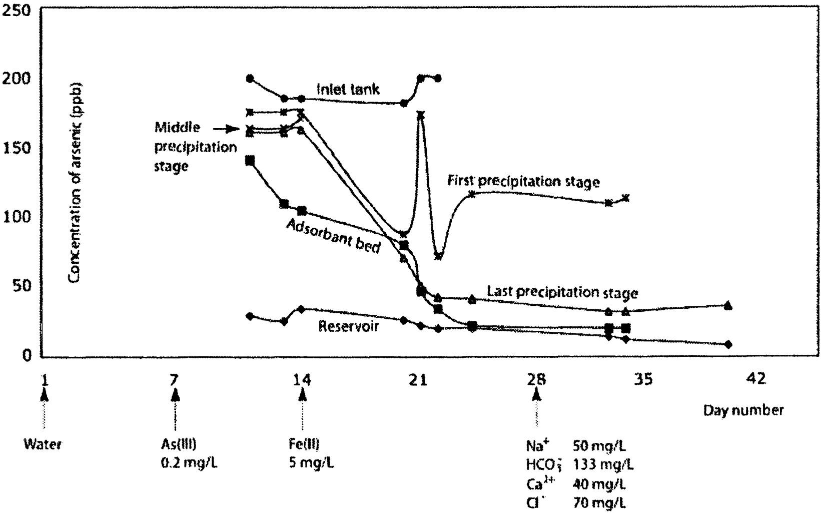

Figure 3. Variation in total arsenic concentration in different sections of the treatment system during the first month of the study.

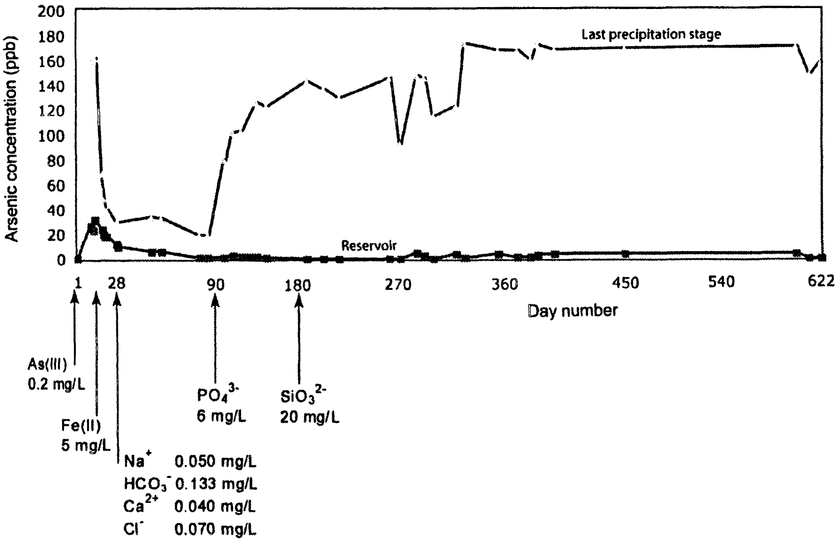

Figure 4. Variation in total arsenic concentration in the last stage of the precipitation tank and in the reservoir over the two years of the study. Additions of chemical species are indicated.

Downloaded by NORTH CAROLINA STATE UNIV on September 12, 2012 | http://pubs.acs.org
Publication Date: October 3, 2005 | doi: 10.1021/bk-2005-0915.ch028

Phosphate ions, added at Day 90, had a dramatic effect in reducing the efficiency of the precipitation stage. Arsenic concentrations rose to 140 ppb, equivalent to only 30% removal on particles of precipitating $Fe(OH)_3.nH_2O$. Addition of silicate ions at Day 180 had little, if any, effect on the efficiency of the precipitation stage, the decline in efficiency continuing to 20%. The bed of rusting iron cans was able to trap the arsenic that passed the precipitation stage. Concentrations of arsenic remained at or below the detection limit of 5 ppb until Day 622, when the experiment was terminated. This is below the Australian standard (7 ppb), the WHO and USA standard (10 ppb), and well below the Bangladeshi water standard (50 ppb). The pH of the effluent water was in the range 6.5-7.5 throughout the two-year period and remained at pH 6.9 after addition of all reagents on Day 180.

Algae and bacteria grew in all chambers of the treatment tank, forming a layer on top of the crushed bricks, on the tank walls and on the surface, especially after addition of phosphate. Biological layers were removed at regular intervals. Mosquito larvae also grew in the reservoir and the water lock, but not in earlier sections of the treatment system containing higher arsenic concentrations.

During the second year of operation, an additional experiment was conducted to test the effect of increasing the light intensity. Ultra-violet light, which would normally be present in sunlight, but absent from the glass-enclosed space of the laboratory, was also provided. A double fluorescent light (4 ft) fitted with GrowPlus natural sunlight tubes (used in hydroponics) was placed above the tank for a period of 4 weeks (*15*). No effect was observed on the concentration of arsenic either in the last stage of the precipitation tank or in the reservoir. Speciation of arsenic in the last precipitation stage using a modified silver diethyldithiocarbamate method (*16*) indicated that the arsenic was largely (>80%) in the form of arsenic(V), both before and during the period of increased light intensity.

During the two-year experiment, 800 mg of dissolved arsenic were added. When the bed of tin-plated steel cans was examined at the end of the two-year experiment, it was found that little rusting had taken place. Only a tiny fraction of the iron was consumed. Most of the capacity of the iron bed remained at the end of the experiment. All the pieces of tin-plated steel retained their structural strength and were coated with rust over only ~30% of their surface. This indicates that the tin plating continued to protect the metal. When the wet tin cans were allowed to stand in air after the experiment, they rapidly rusted. This indicates that atmospheric oxygen was unable to reach the metal in the bed and that the rusting of iron was limited by dissolved oxygen in the water.

Downloaded by NORTH CAROLINA STATE UNIV on September 12, 2012 | http://pubs.acs.org
Publication Date: October 3, 2005 | doi: 10.1021/bk-2005-0915.ch028

Discussion

The inclusion of baffles in the precipitation tank brings about efficient aeration of the water, oxidation of iron(II) to iron(III) and precipitation of $Fe(OH)_3.nH_2O$. This precipitate adsorbs and removes some of the arsenic(III) from the water. Treatment systems that have passed tubewell water through a bed of scrap iron without pretreatment have become blocked with precipitated $Fe(OH)_3.nH_2O$ and the systems have failed. By using crushed brick at the bottom of the tank, the precipitate is effectively removed, preventing particles from reaching the iron bed where they would clog the crushed bricks and iron pieces. In the precipitation tank, some of the arsenic(III) is oxidized to arsenic(V); the process apparently does not benefit from UV radiation or additional light. Arsenic(V) is easier to remove by adsorption on iron(III) surfaces than arsenic(III) and is also less toxic. Conversion of arsenic(III) to arsenic(V) may contribute to the high efficiency of the treatment system. The conversion of arsenic(III) to arsenic(V) may be due to aerobic biological activity or reactions on $Fe(OH)_3.nH_2O$ particles.

The water lock maintains the level of water in the adsorbant bed, ensuring that water moves uniformly through the bed without channeling. The importance of uniform migration of dissolved species through adsorption media is understood in the chromatographic separation of compounds on particle adsorbants. The adsorption bed in the treatment system neither dries out, nor allows ready access to atmospheric oxygen, which would promote rapid oxidation of iron. The iron rusts slowly, continuously forming small amounts of fresh $Fe(OH)_3.nH_2O$ adsorbant. The iron hydroxide is fully hydrated, maximizing its porosity and adsorptive power. The utilization of iron is better than in the 3-kalshi method, where water is allowed to drip on iron filings (*1*). Uniform flow of water through the iron bed is assisted by the use of crushed brick of different porosities, large to small as the bed is approached from above and from below. This is especially important at the base of the adsorption bed, in order to prevent preferential migration of water down the side of the bed nearest the holes to the water lock.

Downloaded by NORTH CAROLINA STATE UNIV on September 12, 2012 | http://pubs.acs.org
Publication Date: October 3, 2005 | doi: 10.1021/bk-2005-0915.ch028

Design and operation of a pilot system for agriculture

A pilot system (5 m^3 per day; Figure 6), based on our laboratory model, is planned for construction in Bangladesh. In order to avoid the possibility of harm to villagers during the testing and optimization of the system, it is planned to provide low-arsenic water for irrigation of crops. Crops containing low levels of arsenic are a priority for reducing arsenic in food eaten by villagers and no systems are currently available for reducing arsenic in irrigation water. There are no disadvantages in trialing the system for irrigation water. At worst, the arsenic levels in crops will not be reduced by the treatment. If the pilot system performs well, it can be comprehensively tested and may later be developed as a safe system for drinking water.

The proposed pilot system will be constructed from reinforced concrete in the shape of a rectangle, as though the laboratory model had been folded in half. The design is similar to sand filters in common use in Bangladesh, but with a more complicated arrangement of internal sections. The empty water lock will be replaced with a mixed bed of charcoal and coarse sand, to remove any organic contaminants in groundwater or any bacterial/algal toxins which might have formed in the iron bed or in earlier stages of the system.

Downloaded by NORTH CAROLINA STATE UNIV on September 12, 2012 | http://pubs.acs.org
Publication Date: October 3, 2005 | doi: 10.1021/bk-2005-0915.ch028

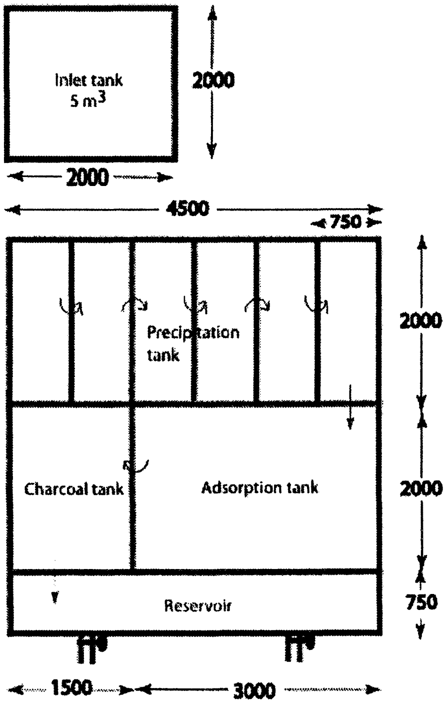

Figure 5. Proposed water treatment system for construction in villages in Bangladesh (plan view). Dimensions are in mm. Depths are: inlet tank, 1200 mm; precipitation tank, 1500 mm; other chambers, 2000 mm.

It is proposed that a small electric pump will transfer water to the inlet tank, from which it flows by gravity through the treatment system and into an irrigated field. The size of the irrigated field must be determined, based on the water needs of the crop. The 5 m^3 daily capacity can supply 10 mm of water over an area of 500 m^2. Crops that are known to accumulate arsenic will be tested.

Each stage of the precipitation tank will have a 300 mm layer of crushed brick on the bottom. The iron bed will contain scrap iron free from contaminants; iron turnings from a machine shop, or burnt tin-plated steel off-cuts from a sheet-metal shop, should be suitable. The charcoal bed will be a mixture of coarse sand (or fine crushed brick) mixed with rice-husk charcoal. Iron and charcoal beds will be supported above and below by layers of crushed brick of increasing particle size. The system will be covered, like a sand filter, in order to minimize algal growth and to prevent access by mosquitos or animals.

Charcoal is particularly good for adsorbing organic compounds from aqueous solution and has a long history of use for this purpose. Rice-husk charcoal can be readily produced in Bangaldesh and should be ideal, provided it is heated to a high temperature in order to remove polyaromatic hydrocarbons and other volatile compounds.

It is expected that the iron bed will function for at least two years. When it is necessary to replace the iron bed, the rusted iron will contain the same amount of arsenic as that which would have been applied to the fields. The rusted iron should be removed, dried and mixed with cement, sand and crushed bricks to make concrete for use in reinforced concrete. Rust materials containing trapped arsenic have been shown to pass standard leaching tests. If the rust is further immobilized in cement, the leaching from such an alkaline material is expected to be below current detection limits. Since leaching from waste materials is an issue of great importance, the disposal of all wastes should be carefully considered and their leaching properties tested.

Conclusion

The treatment system described in this paper is particularly efficient for removing arsenic from water since it makes optimal use of air, natural iron(II) ions and time, allowing spontaneous reactions to go virtually to completion. Remaining traces of arsenic are eliminated by means of the simple adsorbant, iron(III) hydroxide, produced by rusting iron.

Construction of a treatment tank will be similar to construction of a pond-sand filter, except that more care will be required in adjusting levels of internal walls, and skill will be required in manipulating bulk materials. The cost of materials for a treatment tank should be relatively modest, if shared between a community of users. Most materials are available locally: cement, reinforcing,

Downloaded by NORTH CAROLINA STATE UNIV on September 12, 2012 | http://pubs.acs.org
Publication Date: October 3, 2005 | doi: 10.1021/bk-2005-0915.ch028

crushed bricks, sand, scrap iron and rice-husk charcoal. Once skilled workers develop the necessary techniques, rapid construction of treatment tanks should be possible. Groups of families could fund and supervise construction. Only contaminated tubewells that provide water for drinking and cooking need to be fitted with treatment tanks. Contaminated wells can continue to be used for washing and other purposes.

The retention times required in the treatment system for tubewell waters with different iron(II), phosphate, silicate, calcium and hydrogencarbonate ion concentrations are not known. The efficiency and long-term performance of adsorbant beds also must be assessed. Extensive practical testing of the design is needed to identify optimum construction techniques and maintenance procedures. For this reason, it is recommended that a pilot system to produce agricultural water be constructed as the next development step.

Removal of arsenic from contaminated tubewell water is a method of last resort (5, *9*). If a high-volume water source is available from a dugwell, deep tubewell or sand filter, it should be used in preference to an air/iron treatment system. However, there will be villages where dugwells fail due to arsenic contamination, unstable soil or saline aquifer; where an arsenic-free and palatable deep aquifer cannot be found; and where a clean pond or unpolluted river is not available. Large-scale arsenic removal from tubewell water may prove cheaper than rainwater harvesting systems. Large-scale removal of arsenic offers social benefits over the domestic purification of tubewell water using a 3-kalshi, since women save time that could be used for better purposes.

The treatment system described in this paper is not patented and contains no patented components. If the system is developed as a source of drinking water, no royalties will be payable and no expensive materials need be imported.

Downloaded by NORTH CAROLINA STATE UNIV on September 12, 2012 | http://pubs.acs.org
Publication Date: October 3, 2005 | doi: 10.1021/bk-2005-0915.ch028

Acknowledgements

The authors would like to thank Prof. M. Feroze Ahmed (Bangladesh University of Engineering and Technology, Dhaka), David Garman (Commonwealth Research Centre for Waste Management and Pollution Control; CRCWMPC) and Alison Baker (GHD Pty Ltd) for their valuable comments and assistance. The authors would like to thank the family of Md. Abdul Hye Chowdhury for their generosity and insights into technology and society, and Eva A. Crisp for her support and helpful editorial comments. The authors thank the Australian Government for financial assistance during the later stages of the research through AusAID (Bangladesh-Australia Centre for Safe Water and Food Project, Component 2: Clean Water Program), with program management by GHD Pty Ltd and the CRCWMPC.

References

1. *Arsenic Mitigation in Bangladesh;* Feroze Ahmed, M; Mufad Ahmed, C., Eds; Local Government Division, Government of Bangladesh: Dhaka, 2002; pp 81-174.
2. Sancha, A.M. *Int. Water Assoc.* **2000**, *18*, 621-624.
3. Karcher, S.; Caceres, L.; Jekel, M. *Water Environ. Management* **1999**, *13*, 164-169.
4. Jeckel, M.; Seith, R. *Int. Water Assoc.* **2000**, *18*, 628-632.
5. Crisp, P.T.; Chowdhury, A.H.; Lau, A.; Quamruzzaman, Q.; Rahman, M. *Advances in Arsenic Research;* O'Day, P.A.; Vlassopoulos, D.; Meng, X.; Benning, L.G., Eds; American Chemical Society: Washington, DC, 2004; pp. xxx-xxx.
6. Khoe, G.H.; Emett, M.T.; Zaw M.; Prasad, P. Arsenic removal from tubewell water in Bangladesh. AusAID Report, Australian Nuclear Science and Technology Organization and CRC for Waste Management, AusAID, Canberra ACT, 1999.
7. BAMWSP; DFID; WaterAid. Rapid assessment of household level arsenic removal technologies. Phase 1–Final Draft Report. BAMWSP, 2001.
8. Crisp, P.T.; Chowdhury, A.H. Design of a low-cost purification system for the removal of arsenic from groundwater in Bangladesh and India. Nirmal Bangladesh Conference, Sydney, 2000.
9. Crisp, P.T.; Chowdhury, A.H. *BUET-UNU International Workshop on Technologies for Arsenic Removal from Drinking Water;* Dhaka, 2001; pp 85-98.
10. Meng, X.; Bang, S.; Korfiatis, G.P. *Water Res.* **2000,** *34,* 1255-1261.
11. Meng, X.; Korfiatis, P.G.; Christodoulatos, C.; Bang, S. *Water Res.* **2001,** *35,* 2805-2810.
12. Nickson, R.T.; McArthur, J.M.; Ravenscroft, P.; Burgess, W.G.; Ahmed, K.M. App. Geochem. **2000**, *15*, 403-413.
13. *Standard Methods for the Examination of Water and Wastewater.* 3500-As B. silver diethyldithiocarbamate method. American Public Health Association, AHPA, 20th ed, 1998.
14. Chowdhury, A.H.; Cahyadi, B; Crisp, P.T. Manuscript in preparation.
15. O'Connor, M. Honors Thesis, University of New South Wales, 2002.
16. Brett, C. Honors Thesis, University of New South Wales, 2002.

Downloaded by NORTH CAROLINA STATE UNIV on September 12, 2012 | http://pubs.acs.org
Publication Date: October 3, 2005 | doi: 10.1021/bk-2005-0915.ch028

Downloaded by NORTH CAROLINA STATE UNIV on September 11, 2012 | http://pubs.acs.org
Publication Date: October 3, 2005 | doi: 10.1021/bk-2005-0915.ch029

Chapter 29

Geochemical Modeling of Arsenic Speciation and Mobilization: Implications for Bioremediation

Ming-Kuo Lee[1], James A. Saunders[1], Richard T. Wilkin[2], and Shahnewaz Mohammad[1]

[1]Department of Geology and Geography, Auburn University, Auburn, AL 36849
[2]Office of Research and Development, National Risk Management Research Laboratory, U.S. Environmental Protection Agency, Ada, OK 74820

Geochemical modeling techniques were used to examine the biogeochemical linkages between Fe, S, and As in shallow alluvial aquifers. We modeled: 1) the adsorption and desorption of As onto the surface of hydrous ferric oxides (HFO's) in stream beds under aerobic conditions; 2) reductive dissolution of HFO by iron-reducing bacteria in anaerobic conditions; and 3) precipitation and sorption of As under sulfate-reducing conditions. The modeling results indicate that reductive dissolution of HFO, rather than desorption, is the main trigger leading to the release of As under near-neutral pH conditions. Dissolved arsenic may be removed by co-precipitation or precipitation with iron or arsenic sulfides under reducing conditions. However, the formation of soluble thioarsenite species at high H_2S/Fe ratios would enhance As mobility. Moreover, As concentrations would remain high in Fe-free solutions when the precipitation of arsenic sulfide solids such as orpiment (As_2S_3) or realgar (AsS) is kinetically prohibited or when their amorphous precursors are formed. Geochemical modeling of sulfate reduction shows the Eh effect on mineral precipitation and pH controls on the sorption of As in acidic waters. As(V) sorbs strongly onto the protonated sites of HFO over the pH range of 3 to 6. As(III) sorption is also favored by increasing pH, however, As(III) desorbs and becomes mobilized at very low oxidation state as it reacts with reduced sulfur to form thioarsenite complexes. This study demonstrates the importance of using geochemical modeling techniques to evaluate the transport and mobility of As in natural waters.

In Advances in Arsenic Research; O'Day, P., et al.;
ACS Symposium Series; American Chemical Society: Washington, DC, 2005.

Introduction

A widespread *natural* groundwater As contamination has been identified in Holocene alluvial aquifers. Such As-contaminated groundwater is being used for drinking, cooking, or irrigation at a number of populated places around the world, with tragic human consequences. Nowhere is the scope of As-poisoning a bigger human health problem than in West Bengal, India and Bangladesh (WBB), where tens to hundreds of millions of people drink As-contaminated groundwaters (*1*). The health effects and mortalities related to drinking As in the WBB region are well documented, and this crisis has been dubbed one of the biggest environmental disaster in the history of the Earth (*2*). Similar problems have been identified in Vietnam, Hungary, and China (*3*).

Recent studies have linked the natural biogeochemical cycles of Fe and As to the widespread As contamination of shallow groundwater resources (*4-5*). The primary source of As is believed to be the weathering of As-rich minerals in the basin headwaters. Under aerobic conditions Fe(III) and Mn(IV) oxides remove As from surface water, but subsequent development of anaerobic conditions in alluvial deposits can reverse this process, leading to high levels of As in groundwater. Under progressively more reducing conditions, sulfate reducing bacteria (SRB) can also remove As by sequestering it in Fe-sulfides (*6-7*). Thus, bacterially-mediated redox reactions involving organic carbon, Fe, Mn, and S may lead to cycling of As between solid minerals and groundwater. The biogeochemical linkages between Fe, Mn, S, and As in alluvial aquifers have not been tested rigorously through theoretical geochemical modeling. Thermodynamic data for many As species required for geochemical modeling have been compiled by several investigators (*8,9*). The main objective of this study is to use new thermodynamic data for thioarsenite speciation (*10*) and solubility of amorphous arsenic sulfides (*11-12*) to model arsenic reactivity and mobility under various geochemical environments. Our modeling efforts first characterized the speciation and solubility of arsenic in Fe-S-As-H_2O systems. A series of reaction path modeling were then conducted to investigate the biogeochemical cycling of As and its sources and sinks, including: 1) the adsorption of As onto HFO in stream beds under aerobic conditions; 2) the desorption of As in response to pH and Eh changes; 3) reductive dissolution of HFO by Fe reducing bacteria under moderately reducing conditions; and 4) precipitation and sorption of As under sulfate-reducing conditions.

A better understanding of the speciation and mobility of As in natural environments is also important for groundwater bioremediation. Bioremediation methods that precipitate arsenic *in situ* as solid (mineral) phases are considered as the most promising technologies because they provide cost-effective options for As removal (*13*). Recent studies indicate that SRB have removed As, Co, and Ni from shallow groundwater in an alluvial aquifer in central Alabama, USA, by coprecipitating them in biogenic pyrite (*14*). Our modeling results

Downloaded by NORTH CAROLINA STATE UNIV on September 11, 2012 | http://pubs.acs.org
Publication Date: October 3, 2005 | doi: 10.1021/bk-2005-0915.ch029

show that bioremediation of As-contaminated groundwater using SRB can be complicated by the formation of soluble thioarsenites as well as the solubility of As sulfide solids under sulfate reducing conditions (*10*).

Methods - Geochemical Modeling

In general, a reaction path model traces how a fluid's chemistry evolves and which minerals precipitate or dissolve over the course of geochemical processes. Construction of geochemical models for metals reactivity at near-surface conditions requires the inclusion of surface complexation theory (*15,16*) to account for metal adsorption and desorption. General mathematical models for tracing water-rock interactions and sorption of dissolved metals onto mineral surfaces are well described by a number of investigators (*13,17*). In addition, a geochemical model can trace the effect of microbial metabolism and growth in aqueous environments using generalized kinetic rate laws (*18*). In this paper we demonstrated how surface complexation theory and microbial-mediated reactions can be integrated into multicomponent geochemical systems. Geochemists Workbench 4.0 (GWB, *17*) was used to investigate speciation, sorption, and precipitation of As. Thermodynamic data for thioarsenite species and amorphous As and Fe sulfide phases were compiled (Table I) into a revised GWB database *Thermo04-As* which can be obtained from Auburn University.

Table I. Equilibrium constants (at 25°C) for the formation of thioarsenites, arsenic sulfides, and iron sulfides used in geochemical modeling.

Reactions	log K_{25}	Refs.
Thioarsenite species		
$As(OH)_4^- + HS^- + 2H^+ \Leftrightarrow As(OH)_2(SH) + 2H_2O$	17.92	*10*
$As(OH)_4^- + HS^- + H^+ \Leftrightarrow As(OH)_2S^- + 2H_2O$	12.77	*10*
$As(OH)_4^- + 2HS^- + H^+ \Leftrightarrow As(OH)S_2^{2-} + 3H_2O$	17.83	*10*
$As(OH)_4^- + 3HS^- + 2H^+ \Leftrightarrow AsS_3H^{2-} + 4H_2O$	29.61	*10*
$As(OH)_4^- + 4HS^- + 4H^+ \Leftrightarrow As(SH)_4^- + 4H_2O$	45.77	*10*
$As(OH)_4^- + 3HS^- + H^+ \Leftrightarrow AsS_3^{3-} + 4H_2O$	21.72	*10*
Arsenic sulfides and iron sulfides		
$2As(OH)_4^- + 3HS^- + 5H^+ \Leftrightarrow As_2S_3$ (Orpiment) $+ 8H_2O$	65.60	*12*
$2As(OH)_4^- + 3HS^- + 5H^+ \Leftrightarrow As_2S_{3\,(am)} + 8H_2O$	63.27	*12*
$As(OH)_4^- + HS^- + 2H^+ \Leftrightarrow AsS$ (Realgar) $+ 3.5H_2O + .25\ O_{2(aq)}$	14.68	*17*
$Fe^{2+} + 2HS^- + .5\ O_{2(aq)} \Leftrightarrow FeS_2$ (Pyrite) $+ H_2O$	59.29	*19,20*
$.875\ Fe^{2+} + HS^- + .0625\ O_{2(aq)} \Leftrightarrow FeS_{.875}$(Pyrrhotite) $+ .75\ H^+ + .125\ H_2O$	9.88	*19,20*
$Fe^{2+} + HS^- \Leftrightarrow FeS$ (Mackinawite) $+ H^+$	3.10	*11*
$Fe^{2+} + As(OH)_4^- + HS^- \Leftrightarrow AsFeS$ (Arsenopyrite) $+ 2.5H_2O + .75\ O_{2(aq)}$	-47.84	*17*

Downloaded by NORTH CAROLINA STATE UNIV on September 11, 2012 | http://pubs.acs.org
Publication Date: October 3, 2005 | doi: 10.1021/bk-2005-0915.ch029

Modeling Results

Speciation of As

Redox potential (Eh), pH, and S activity are the most important factors controlling As speciation. Phase diagrams for As speciation in the presence of S were calculated using the ACT2 sub-program of GWB with added thermodynamic data for thoiarsenite species and amorphous As_2S_3. Figure 1 shows that under oxidizing conditions $H_2AsO_4^-$ and H_3AsO_4 are dominant at low pH (< 7) while $HAsO_4^{2-}$ and AsO_4^{3-} become dominant at higher pH. Under reducing conditions H_3AsO_3 predominate over a wide range of pH values. Under even more reducing conditions, solid arsenic sulfides (orpiment) or thioarsenite aqueous complexes become the dominant phases.

Downloaded by NORTH CAROLINA STATE UNIV on September 11, 2012 | http://pubs.acs.org
Publication Date: October 3, 2005 | doi: 10.1021/bk-2005-0915.ch029

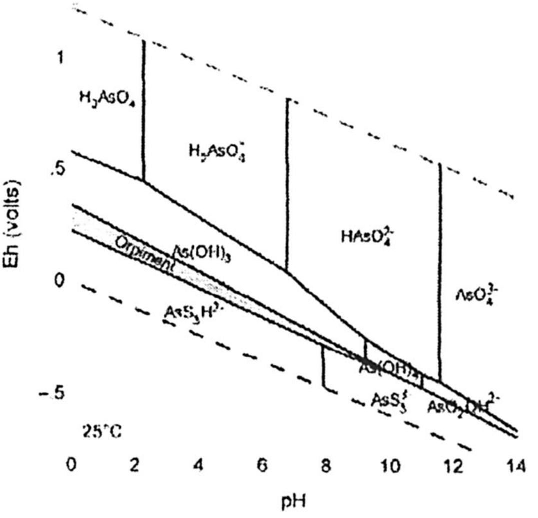

Figure 1. Redox-pH diagrams for arsenic drawn at 25 ℃ and fixed As and SO_4^{2-} activities of 10^{-2}. Dashed lines show stability limits of water at 1 bar pressure. Realgar, $As(SH)_4^-$, $As(OH)_2(SH)$, and $As(OH)_2^{2-}$ are suppressed (not considered in the calculation).

Figure 2 illustrates the effects of variable activities of H_2S on speciation and solubility of As at fixed redox (Eh = 100 mV) and neutral pH (7) conditions. Arsenic solubility reaches a minimum value at log $H_2S(aq)$ activity ≈ -4.5 and becomes relatively soluble with further increase or reduction in $H_2S(aq)$ activity. The solubility of less stable amorphous As_2S_3 (dashed phase boundary) is about 1 log units above the more stable orpiment. This implies that As concentrations would be higher if the system deviates significantly from equilibrium with thermodynamically stable arsenic sulfide phases (i.e., orpiment or realgar). Pure orpiment rarely forms in natural waters because its precipitation is kinetically inhibited at near-neutral pH conditions (*12*). Figure 2 also shows that thioarsenites dominate arsenic speciation at $aH_2S > 10^{-4.5}$ under neutral pH conditions. Thioarsenites are conservative compared to other arsenic species and do not appreciably sorb onto mineral surfaces. Thus the formation of soluble thioarsenites (e.g., AsS_3H^{2-}) would enhance As mobility at high activity of H_2S. It should be noted that As has higher solubility at higher pH conditions (not demonstrated) as the stability fields of solid arsenic sulfide shrinks.

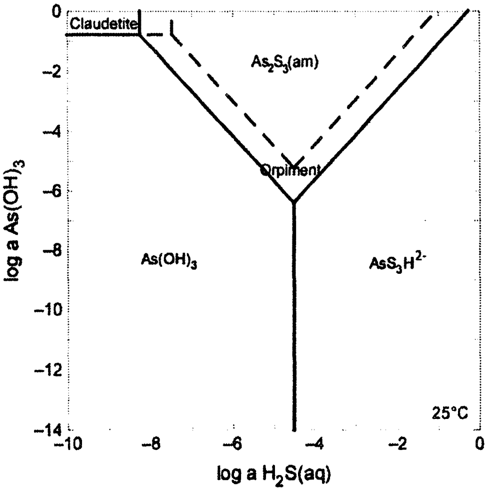

Figure 2. Stability diagram versus aH_2S for arsenic at 25 ℃. Solid lines separate As sulfide minerals and aqueous species. Dashed lines show metastable boundaries (with orpiment, realgar, and $As(SH)_4^-$ suppressed) for amorphous As_2S_3.

Figure 3a shows the stability fields of various iron sulfide phases for the Fe-S-As system at fixed redox (Eh = -200 mV) and pH (5) conditions. In Fe-rich systems, dissolved As can be removed by co-precipitation or sorption with amorphous or crystalline iron sulfides. The stability field of arsenopyrite is very limited but could expand as As content increases or Eh decreases. Arsenopyrite is replaced by more stable iron oxides or sulfides at relatively neutral pH conditions (Figure 3b). The phase boundaries (dashed lines) for pyrrhotite and iron monosulfide (mackinawite) were calculated by suppressing the most stable phase pyrite. Mackinawite is the kinetically favored amorphous precursor to the very common mineral pyrite (*19,20*). The precipitation of mackinawite is important as arsenic can be strongly sorbed onto its surfaces at relatively neutral pH conditions (*11*). The solubility of Fe sulfides generally decreases as pH rises (Figure 3b), thus bacterial sulfate reduction could promote the precipitation of Fe sulfide by increasing pH and enhance As sorption and removal from solution.

Downloaded by NORTH CAROLINA STATE UNIV on September 11, 2012 | http://pubs.acs.org
Publication Date: October 3, 2005 | doi: 10.1021/bk-2005-0915.ch029

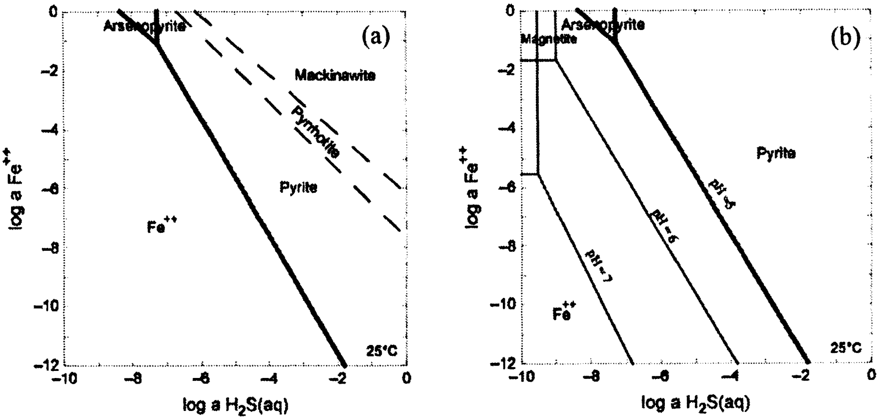

Figure 3. Solubility diagrams versus aH_2S for iron sulfide minerals at 25 °C. Solid lines separate iron sulfide minerals and aqueous species. As species activity=$10^{-1.5}$. Dashed lines in (a) show metastable boundaries for intermediate phases pyrrhotite and iron monosulfide (mackinawite) at pH = 5. Effects of pH values on mineral solubility are shown in (b).

Adsorption and desorption of As

We modelled the adsorption of As species by oxide minerals under aerobic conditions and then their desorption as pH changes using GWB and the surface complexation model (*15*). The initial system contains 1 kg of river water and a small amount (1 g) of $Fe(OH)_3$ at pH 7. The river water contains 1 ug/kg of As(III), 1 ug/kg of As(V), and 0.05 molal of NaCl. The calculation prevents the redox coupling between As(III) and As(V). More stable ferric minerals hematite, goethite, and jarosite are suppressed as they are unlikely to reach equilibrium with river water at surface temperatures. Ferric hydroxides used in the simulation have high specific surface areas (600 m^2/g) for sorption reactions. The surface of HFOs is composed of weakly sorbing sites (density = 0.4 mol/mol mineral) and strongly sorbing sites (density = 0.01) (*13,17*).

The modeling results show that the initial As sorbed onto $Fe(OH)_3$ is about 10.68 mg/kg (10.53 mg/kg as As(V) and 0.15 mg/kg as As(III)) in equilibrium with a river containing 2 ug/kg of total dissolved As at pH 7. This result suggests that As is strongly adsorbed by iron oxyhydroxides under aerobic, near-neutral pH conditions. It should be noted that concentrations of As in alluvial sediments depend on mineralogy (the amounts of Fe oxides and sulfides), texture, and sorbing competition from other ions. For example, the sorbed As contents in Holocene alluvial sediments are in the range 10-22 mg/kg and 1.2-

Downloaded by NORTH CAROLINA STATE UNIV on September 11, 2012 | http://pubs.acs.org
Publication Date: October 3, 2005 | doi: 10.1021/bk-2005-0915.ch029

5.9 mg/kg in part of USA (*21*) and Bangladesh (*22*), respectively. The amounts of sorbed As would decrease if it competes with other ions for the sorbing sites (*22*). Our modeling results show that significant desorption of As(V) and minor desportion of As(III) occur as pH increases from 7 to 10 in a sliding activity path (Figure 4a-b). The final As concentration in the fluid increases to 1800 ug/kg while the As sorbed onto $Fe(OH)_3$ drops to 8.85 mg/kg (8.70 mg/kg of As(V) and 0.15 mg/kg of As(III)). A sharp increase in As concentrations (> 100 ug/kg) does not occur until pH > 8.5 (Figure 4a-b). Most As-rich groundwaters from Holocene alluvial aquifers in Bangladesh and USA have near-neutral pH values less than 8 (*21*), implying that As contents in the alluvial aquifers could not have been derived solely from desorption, and that alternative mechanisms such as bacterial dissolution of HFOs are more important.

Using the same neutral starting conditions as in Figure 4a-b, a model for sliding pH from 7 to 3 predicted that As concentrations would increase from 1 to about 25 ug/kg (Figure 4c-d). This is in response to the lower sorption affinity of As(III) at acidic pH conditions (Figure 4c). This result implies that dissolved As concentrations would also increase when strongly adsorbed As(V) is replaced by less strongly adsorbed As(III) under reducing conditions.

A third model simulated the desorption of arsenic from HFO under reducing conditions. An analysis of a typical Bangladesh groundwater was used to set the fluid's initial composition. To simulate the effect of bacterial Fe(III) reduction (*23*), the fluid redox potential Eh decreases linearly from its initial value of 0 mV to -180 mV at the end of the reaction path. In the model, pH is a free constraint and increases from 7 to 7.15 in response to a drop in Eh. In this natural system the presence of other ions such as SO_4 and Ca would compete with As for sorption sites. The modeling results show that, with various amounts of HFO present in the system, an Eh drop would result in the release of a few to a few tens of μg As kg^{-1} (Figure 5), which is far more than that predicted in the system free of competitive ions (Figure 4c-d) under similar near-neutral pH conditions. The predicted level of As release, however, is far less than many reducing, As-contaminated groundwaters from Bangladesh, which contain up to several hundreds of $\mu g/kg$ of As (*24*). This suggests that the actual mechanisms releasing As from HFOs are far more complex than the simple desorption reactions predicted by the surface complexation model.

Bacterial Reduction of Fe(III) and Mn(IV) Oxides

GWB was used to trace the sequence of biogeochemical reactions that occurs during the bacterial Fe (III) and Mn(IV) oxide reduction, the major trigger for As release in alluvial aquifer systems. The purpose of the modeling

Downloaded by NORTH CAROLINA STATE UNIV on September 11, 2012 | http://pubs.acs.org
Publication Date: October 3, 2005 | doi: 10.1021/bk-2005-0915.ch029

is to provide insights on the precise sequence of mineral reactions during the reductive dissolution of Fe and Mn oxides. Since the precise reactions involving reductive dissolution of HFOs containing adsorbed As on HFOs are complex and have not been studied in detail, the model is not aimed at quantifying As release. We begin by equilibrating an Alabama coastal plain groundwater up-gradient of an iron reduction zone at 25°C. The calculation used the water chemical data collected from the Eutaw aquifer in Moundville (*23*) and assumes the initial concentrations of Fe and Mn reflecting equilibrium with hematite (Fe_2O_3, a proxy of Fe(III) oxyhydroxides) and pyrolusite (MnO_2, a proxy for Mn(IV) oxyhydroxides) in the aquifer under aerobic conditions. The model then simulates the biogeochemical effects of titration of organic matter into the system. The accompanying bacteria growth and metabolism processes are also calculated. We consider the biotransformation of hematite as follow:

$$4\ Fe_2O_3\ (\textit{hematite}) + CH_3COO^- + 15\ H^+ \rightarrow 8\ Fe^{2+} + 2HCO_3^- + 8H_2O \quad (1)$$

Here, Fe(III)-reducing bacteria grow by utilizing acetate as the limiting organic substrate to reduce hematite (as electronic acceptor) in the system. In the simulation, fluid reactants containing 3000 μmol of CH_3COO^- displace existing fluid from the system over the course of reaction path. The initial biomass concentration is assumed to be 0.01 mg/kg. Since the analytical data of microbial kinetic parameters are seldom collected under natural conditions, the rate constant k and half-saturation constant K_D are arbitrarily set to be 0.0003 mol mg^{-1} sec^{-1} and 10^{-5} in the model We further specify the growth yield Y and the decay constant D to be 900 mg mol^{-1} and 10^{-6} sec^{-1}, respectively.

The results show significant biomass growth from 0.01 to 2,500 mg/kg in 100 simulation days. The predicted mineral reactions of Mn and Fe oxides (Figure 6) follow the Ostwald's step rule (*25,26*). Pyrolusite in the initial system first becomes unstable during bacterial reduction and transforms over time to a sequence of progressively more stable Mn minerals (Figure 6) at lower Eh values:

$$\text{Pyrolusite}(MnO_2) \rightarrow \text{Bixbyite}\ (Mn_2O_3) \rightarrow \text{Hausmannite}(Mn_3O_4) \rightarrow Mn(OH)_2 \quad (2)$$

Once the reduction of Mn minerals has nearly completed, the iron redution starts (Figure 6) and hematite (Fe_2O_3) begins to dissolve to form more stable magnetite (Fe_3O_4) at very low oxidation states. This result is consistent with the theoretical redox sequence that Fe reduction proceeds after the Mn reduction reactions. At the later stage of the reaction, reduced metal species also combine with HCO_3^- released from organic sources to form minerals such as rhodochrosite ($MnCO_3$), siderite ($FeCO_3$), and strontianite ($SrCO_3$). Fe- and Mn-rich groundwaters downstream from Moundville are actually saturated with siderite and strontianite (*23*). Moderately reducing, As-rich groundwaters from the Kansas City (*21*) are also saturated with respect to rhodochrosite and siderite. The modeling results

Downloaded by NORTH CAROLINA STATE UNIV on September 11, 2012 | http://pubs.acs.org
Publication Date: October 3, 2005 | doi: 10.1021/bk-2005-0915.ch029

Downloaded by NORTH CAROLINA STATE UNIV on September 11, 2012 | http://pubs.acs.org
Publication Date: October 3, 2005 | doi: 10.1021/bk-2005-0915.ch029

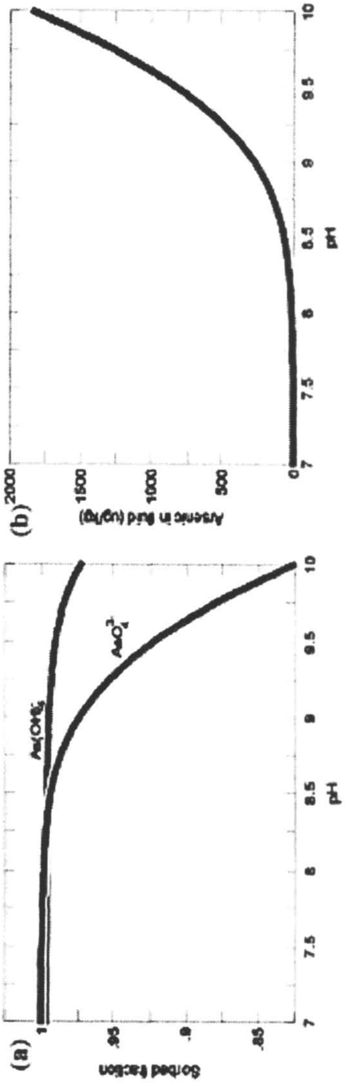

Downloaded by NORTH CAROLINA STATE UNIV on September 11, 2012 | http://pubs.acs.org
Publication Date: October 3, 2005 | doi: 10.1021/bk-2005-0915.ch029

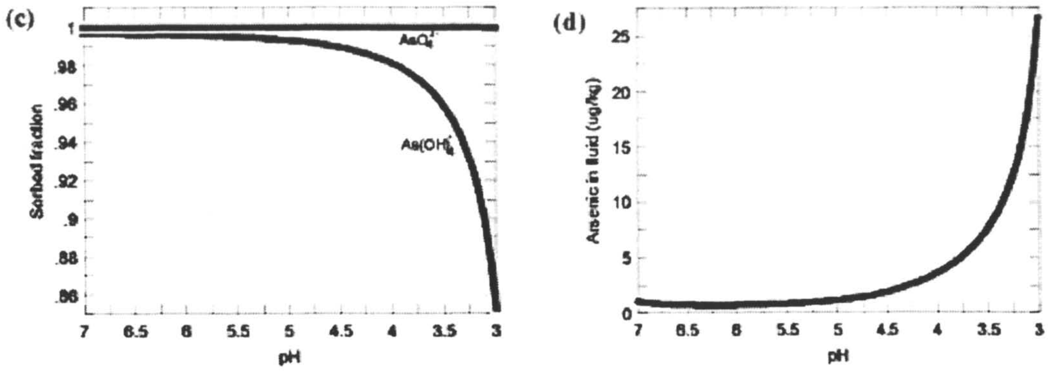

Figure 4. Sorbed fraction (a) and dissolved As concentrations (b) versus pH calculated by HFO desorption simulations with pH sliding from 7 to 10. (c) and (d) are results of a model with pH sliding from 7 to 3.

Downloaded by NORTH CAROLINA STATE UNIV on September 11, 2012 | http://pubs.acs.org
Publication Date: October 3, 2005 | doi: 10.1021/bk-2005-0915.ch029

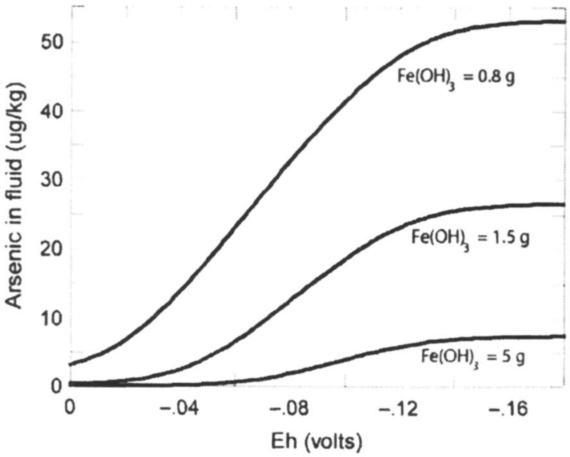

Figure 5. Dissolved As concentrations versus Eh calculated by desorption simulations with Eh sliding from 0 to -180 mV. The initial Bangladesh groundwater (pH = 7, Eh = 0 mV) contains Na^+ (24.9 mg/kg), Cl^- (13.4 mg/kg), Ca^{2+} (78.3 mg/kg), Mg^{2+} (12.8 mg/kg), K^+ (2.35 mg/kg), Fe^{2+} (0.23 mg/kg), HCO_3^- (304.9 mg/kg), SO_4^{2-} (31.9 mg/kg), and NO_3^- (0.1 mg/kg). As is nearly completed sorbed at the beginning. Each curve shows calculated As concentrations for a given HFO mass in reacting with 1 kg of fluids.

Downloaded by NORTH CAROLINA STATE UNIV on September 11, 2012 | http://pubs.acs.org
Publication Date: October 3, 2005 | doi: 10.1021/bk-2005-0915.ch029

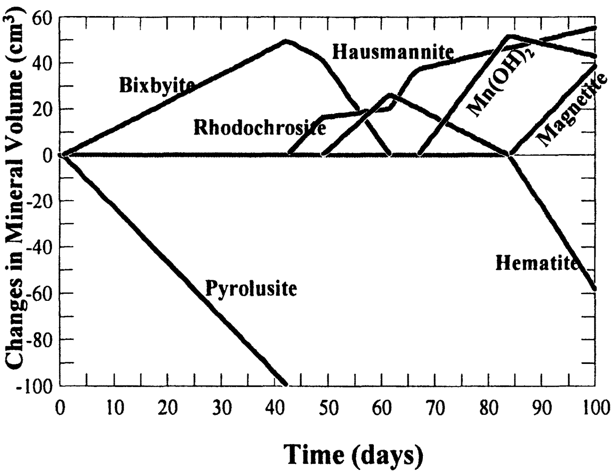

Figure 6. Predicted sequence of mineralogic reactions resulting from bacterial reduction of Fe and Mn oxides in equilibrium with Moundville groundwater near the Eutaw aquifer outcrop. The plot shows changes in mineral volume as acetate is titrated into the system with time. Positive changes indicate precipitation, and negative changes show dissolution.

indicate that the biotransformation of iron and manganese minerals could control As release in coastal plain aquifers and requires continued investigation.

Arsenic Precipitation and Sorption under Reducing Conditions

In the final model, we investigated how bacterial sulfate reduction induces the precipitation of metal sulfides and sorption of arsenic from a contaminated groundwater. Nanafalia aquifer at study site in southeastern Alabama was initially contaminated by heavy metals in the 1980s from a large car-battery recycling operation. Bioremediation experiments involved the stimulation of naturally-occurring SRB to remediate the metals-contaminated groundwater *in situ* (*13*). The chemical compositions of contaminated groundwater at the site (*13*) were used as the initial condition in the simulation. To model the effect of SRB metabolism, the fluid Eh decreases linearly from its initial values of +400 mV to -150 mV, as observed during field bioremediation (*13*). The values of pH vary from 3.2 to 6 in the same sliding path.

The modeling results show how the mobility of metals is affected by the geochemical changes (i.e., a drop in Eh and an increase in pH) associated with bacterial sulfate reduction. Sulfide produced by sulfate reduction reacts with metals to form minerals including pyrite (FeS_2), galena (PbS), sphalerite (ZnS), covellite (CuS), orpiment (As_2S_3) and other precipitates at Eh below -50 mV (Figure 7). The precipitation of minerals significantly lowers the concentrations of corresponding metals in solution. The calculation also shows that various metals are sorbed over a wide range of pH during sulfate reduction (Figure 8).

Most metal ions remain in solution as long as the pH is below 3.5. As the pH value increases over the reaction path, sorption of metals on HFOs becomes significant in the reacting geochemical system. As(V) sorbs strongly onto the protonated weak sites of ferric hydroxide over the entire range of calculation (Figure 8). Arsenite dominates at lower oxidation potentials and low pH conditions and its sorption is also favored by increasing pH according to

$$(w)FeOH_2^+ + As(OH)_3 \rightarrow (w)FeH_2AsO_3 + H_2O + H^+ \qquad (3)$$

Modeling results indicate that As is increasingly sorbed onto the ferric hydroxide surface as pH increases under acidic condition. The results imply that high As concentrations are not expected in S-rich, acidic reducing system since such geochemical environments favor As precipitation (i.e., as orpiment or realgar) or sorption. However, at very low oxidation potentials as pH increases to about 5.8, As desorbs and becomes mobilized as it reacts with dissolved sulfide to form thioarsenite complexes (Figure 9). This result is consistent with the As speciation models (Figures 1 and 2) and indicates that the formation of thioarsenite species may enhance As mobility in S-rich, reduced aquifers.

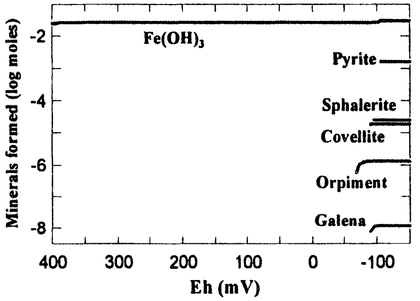

Figure 7. Predictive cumulative mineral assemblage precipitated as Eh decreases as a result of bacterial sulfate reduction.

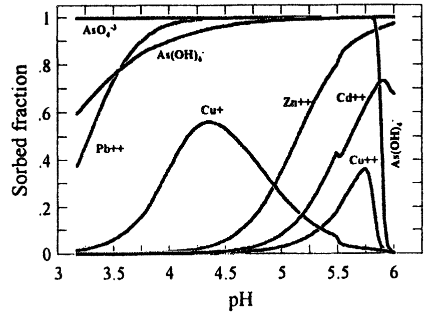

Figure 8. Predictions of the amounts of metals sorbed onto HFO as a function of pH.

Biogeochemical Linkage of As, Fe, and S

To evaluate As geochemical behavior under sulfate-reducing conditions, we investigated As-bearing pyrite from the drainage basin of Choctafaula Creek in east-central Alabama. At this site, SRB use macro wood fragments in Holocene alluvium to fuel sulfate reduction (*14*). Pyrite locally fossilizes the wood and the individual growth bands contain up to 6200 mg/kg As. Ion microprobe

Downloaded by NORTH CAROLINA STATE UNIV on September 11, 2012 | http://pubs.acs.org
Publication Date: October 3, 2005 | doi: 10.1021/bk-2005-0915.ch029

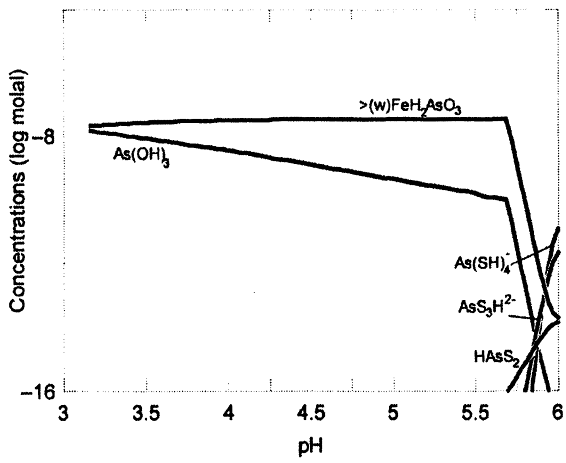

Figure 9. Calculated molality of predominant arsenic species of a reaction path in which arsenite sorbs onto ferric hydroxide to form FeH_2AsO_3 complexes as pH increases. The value of pH increases as a result of bacterial sulfate reduction. Arsenite later desorbs to form thioarsenite complexes under reducing, neutral-pH conditions.

analyses were conducted for As content and $\delta^{34}S$ across single pyrite crystals. Results (see Figure 5 in Saunders et al., this volume) show two cycles of the depletion of ^{34}S (with $\delta^{34}S$ values as low as -50‰), characteristic of the kinetic isotope fractionation of SRB (*27*). However, the trend of moving toward isotopically heavier $\delta^{34}S$ values from core to rim (e.g., over time) in each cycle is definitive evidence of SRB metabolism.

The ion microprobe data indicate that As tends to be preferentially incorporated into pyrite (*6,28*) and removed from groundwater at the start of a sulfate-reduction cycle. The subsequent decline of As levels in pyrite for the remainder of a cycle illustrates (Figure 5 in Saunders et al., this volume) that As reacts with H_2S generated by sulfate reduction to form aqueous thioarsenic complexes (Figures 1 and 2). A relatively flat As pattern in the second cycle suggests that As reactivity declines as Fe contents in solution drop after initial precipitation. It appears that the dissolved H_2S/Fe ratios control whether As is incorporated into pyrite or remains in solution. Our data suggest that As coprecipitates in pyrite from Fe-rich fluids at the beginning of a sulfate-reduction cycle (Figure 10). When iron is depleted by pyrite precipitation during SRB metabolism, As apparently forms stable thioarsenite complexes that compete with the growing pyrite surfaces for As. The overall effect of SRB is to remove As from groundwater enriched in dissolved iron, however the reaction product H_2S can enhance arsenic solubility when dissolved Fe is exhausted. Thus for the groundwaters that have elevated iron contents, SRB will effectively remove arsenic as pyrite is formed.

Conclusions

This study utilized numerical modeling techniques to link the natural biogeochemical reactions among of Fe, S, and As to the widespread As

Downloaded by NORTH CAROLINA STATE UNIV on September 11, 2012 | http://pubs.acs.org
Publication Date: October 3, 2005 | doi: 10.1021/bk-2005-0915.ch029

contamination of shallow groundwater resources. Our modeling results are consistent with the hypothesis (*29,30*) that As is strongly sorbed by HFO under oxidized conditions and the subsequent bacterial reductive dissolution mechanism might be an important process for releasing As. Geochemical models suggested that deposition of stream sediment HFOs and organic matter in alluvial deposits ultimately triggers the activity of Fe(III) reducing bacteria, resulting in the release of sorbed As to groundwater. High As concentrations are not expected in S-rich, reducing systems because such environments favor the precipitation of arsenic sulfides (e.g., orpiment, realgar) or iron sulfides (e.g., pyrite, mackinawite). Modeling results have implications for remediating As contamination in groundwater. Attention should be given to the formation of thioarsenite species in Fe-depleted, reduced aquifers since thioarsenites are less readily adsorbed compared to arsenite. Our study indicates that dissolved H_2S/Fe ratios control whether As can be incorporated into pyrite or remains in solution. We propose that bioremediating As-contaminated groundwater is possible by adding Fe-bearing solids (or solutions) and a carbon electron donor (e.g., sucrose, molasses, methanol, acetate, methanol, etc.) through injection wells. Injection of soluble Fe(II) into groundwater: 1) insures the availability of Fe for SRB metabolism; 2) limits the buildup of potentially toxic levels of H_2S; 3) keeps the H_2S/Fe ratio low enough to prevent thioaresenites from occurring to significant extent, and 4) provides Fe needed for the As-"encapsulating" FeS phases. This approach can be effective in treating As-contaminated groundwater as the conditions for As-coprecipitation in FeS are optimized.

Downloaded by NORTH CAROLINA STATE UNIV on September 11, 2012 | http://pubs.acs.org
Publication Date: October 3, 2005 | doi: 10.1021/bk-2005-0915.ch029

Acknowledgments

We thank M. Fayek and L. Riciputi of Oak Ridge National Laboratory for help with the ion microprobe analysis of pyrite. The research described here does not necessarily reflect the views of the EPA, and no official endorsement should be inferred. Mention of the trade names or commercial products does not constitute endorsement or recommendation for use.

References

1. Chatterjee, A.; Das, D.; Mandal, B.K.; Chowdhury, T.R.; Samanta, G.; Chakraborty, D. *The Analyst*, **1995**, *120*, 643-650.
2. Bagla, P.; Kaiser, J. *Science*, **1996**, *274*, 174-175.
3. Berg, M.; Tran, H.C.; Nguyen, T.C.; Pham, H.V.; Schertenleib, R.; Giger, W. *Environ.l Sci. Technol.* **2001**, *35*, 2621-2626.
4. Korte, N.E. *Environ. Geol. Water Sci.* **1991**, *18*, 137-141.
5. Welch, A.H.; Lico, M.S. 1998, *Geochemistry*, **1998**, *13*, 521-539.

6. Huerta-Diaz, M.A.; Morse, J.W. *Geochim. Cosmochim. Acta*, **1992**, *56*, 2681-2702.
7. Saunders, J.A.; Swann, C.T. *Econ. Geol.* **1994**, *89*, 381-390.
8. Norstrom, D.K.; Archer, D.G. In Welch, A.H. and Stollenwerk, K.G. (eds.), *Arsenic in Groundwater*; Kluwer Academic Publishers: Boston, 2003.
9. Cleverley, J.S.; Benning, L.G.; Mountain, B.W. *Appl. Geochem.* **2003**, *18*, 1325-1345.
10. Wilkin, R.T.; Wallschlaeger, D.; Ford, R.G. *Geochem. Trans.* **2003**, *4*, 1-7.
11. Wilkin, R.T.; Ford, R.G. *Environ. Sci. Technol.* **2002**, *36*, 4921-4927.
12. Webster J. *Geochim. Cosmochim. Acta*, **1990**, *54*, 1009-1017.
13. Lee, M.-K.; Saunders, J. A. *Vadose Zone J.* ***2003***, 2, 177-185.
14. Saunders, J.A.; Pritchett, M.; Cook, R. *Geomicrobiol. J.* **1997**, *14*, 203-217.
15. Dzombak, D.A.; Morel, F.M.M. *Surface Complexation Modeling:Hydrous ferric oxide*; John Wiley & Son: New York, 1990.
16. Stumm, W. *Chemistry of the Solid-Water Interface*; John Wiley & Son: New-York, 1992.
17. Bethke, C.M. *Geochemical Reaction Modeling*; Oxford University Press: New York, 1996.
18. Jin, Q.; Bethke, C.M. *Appl. Environ. Microbiol.* **2003**, *69*, 2340-2348.
19. Wilkin, R.T.; Barnes, H.L. *Geochim. Cosmochim. Acta*, **1996**, *60*, 4167-4179.
20. Schoonen, M.A.A.; Barnes, H.L. *Geochim. Cosmochim. Acta*, **1991**, *55*, 1495-1504.
21. Saunders, J.A., Mohammad, S; Korte, N.E., Lee, M.-K.; Castle, D; Barnnet, M.O. **2004**, this volume.
22. Smedley, P.L.; Kinniburgh, D.G. *Appl. Geochem.* **2002**, *17*, 517-568.
23. Penny, E.A.; Lee, M. -K.; Morton, C. *Water Resour. Res.* **2003**, *39*, 1320, 10.1029/2003WR001963.
24. Zheng, Y.; Stute, M.; van Geen, A.; Gavrieli, I.; Dhar, R.; Simpson, H.J.; Schlosser, P.; Ahmed, K.M. *Appl. Geochem.* **2003**, 19, 201-214.
25. Morse, J.W.; Casey, W.H. *Amer. J. Sci.* **1988**, *288*, 537-560.
26. Norden, S. H.; Sibley, H. *Geochim. Cosmochim. Acta* **1994**, 58, 191-196.
27. Faure, G. *Principles of Isotope Geology*; John Wiley: New York, 1986.
28. Sullivan, K.A.; Aller, R. *Geochim. Cosmochim. Acta* **1996**, *60*, 1465-1477.
29. Nickson, R.T.; McArthur, J. M.; Ravenscroft, P.; Burgess, W. G.; Ahmed, K. M. *Appl. Geochem.* **2000**, *15*, 403-414.
30. McArthur, J. M.; Ravenscroft, P.; Safiulla, S.; Thirlwall, M. F. *Water Resour. Res.* **2001**, *37*, 109-117.

Downloaded by NORTH CAROLINA STATE UNIV on September 11, 2012 | http://pubs.acs.org
Publication Date: October 3, 2005 | doi: 10.1021/bk-2005-0915.ch029

Downloaded by 217.66.152.135 on September 11, 2012 | http://pubs.acs.org
Publication Date: October 3, 2005 | doi: 10.1021/bk-2005-0915.ap001

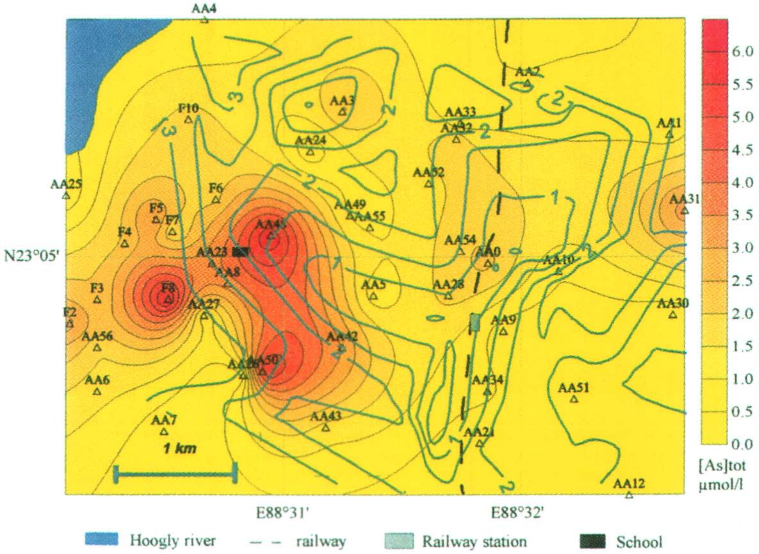
AA4
AA2
AA3
F10
AA33
AA32
AA1
AA24
AA52
AA25
F6
F5
F7
AA49
AA55
AA31
F4
AA45
N23°05'
AA23
AA54
AA0
AA10
AA8
F3
F8
AA5
AA28
AA27
AA30
F2
AA9
AA56
AA42
AA50
AA34
AA6
AA51
AA7
AA43
AA21
1 km
AA12
E88°31'
E88°32'
6.0
5.5
5.0
4.5
4.0
3.5
3.0
2.5
2.0
1.5
1.0
0.5
0.0
[As]tot
µmol/l
3
2
1
Hoogly river
railway
Railway station
School

Plate 4.1. Water table drawdown contour with well positions and groundwater total arsenic concentration at the study site, Chakdaha Block, Nadia district, 65 km north of Calcutta in West Bengal, India (data from (19)). The railway runs through the middle of the city. The black box outlines the 4 km x 5 km study area, located on the Hoogly River East bank.

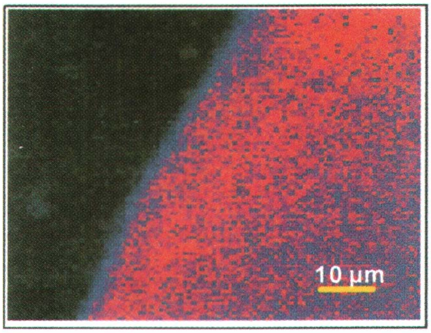

Plate 4.6. PIXE elemental map of a muscovite particle reacted with arsenic (V). Blue pixel: 16 mg kg^{-1} and pink pixel denoteAs concentration below detection limit (d.l. = 10 mg kg^{-1}). Reaction conditions: $[As(V)]_o$ = 1.3 mM, pH 8.6, I = 10^{-3} M $NaNO_3$.

Downloaded by 217.66.152.135 on September 11, 2012 | http://pubs.acs.org
Publication Date: October 3, 2005 | doi: 10.1021/bk-2005-0915.ix001

Author Index

Andrews, Charles B., 344
Badruzzaman, Mohammad, 268
Bahr, J. M., 161
Barnett, Mark O., 91, 191
Benning, Liane, 1
Butler, B., 60
Cai, Yong, 333
Castle, D., 191
Caviness, Mendy, 284
Chakraborty, S., 41
Charlet, L., 41
Chatterjee, D., 41
Cheng, Zhongqi, 361
Chillrud, S. N., 206
Chow, Stephanie S., 220
Chowdhury, Ahmedul Hye, 372, 386
Crisp, Phillip T., 372, 386
Datta, S., 206
Deng, Baolin, 284, 294
Dixit, Suvasis, 8
Fang, Jun, 294
Fayek, M., 191
Fendorf, Scott, 77
Fernández-Lomelín, Pilar, 235
Ford, Robert G., 306
Gotkowitz, M. B., 161
Gu, Zhimang, 284
Gutiérrez-Ruíz, Margarita, 235
Herbel, Mitchell, 77
Hering, Janet G., 8
Herman, G. C., 175
Hilliard, Jeremiah C., 91
Holm, Thomas R., 148
Jacks, Gunnar, 132
Keimowitz, A. R., 206
Kelly, Walton R., 148
Korte, N. E., 191
Kramer, Timothy A., 321
Kubicki, James D., 104
Lane, Vincent, 253
Lau, Andrew, 372
Lee, Ming-Kuo, 191, 398
Mason, P. R. D., 60
Meng, Xiaoguang, 1
Mezyk, Stephen P., 333
Mohammad, Shahnewaz, 191, 398
Nag, Sisir Kanti, 132
Nikolaidis, Nikolaos P., 361
O'Day, Peggy A., 1, 344
O'Shea, Kevin E., 333
Quamruzzaman, Quazi, 372
Radu, Tanja, 91
Rafferty, Michael T., 344
Rahman, Mahmuder, 372
Ray, S. P. Sinha, 132
Rickard, D., 60
Rivera, Nelson, 344
Roadcap, George S., 148
Romero, Francisco, 235
Root, T. L., 161
Ross, G. Roman, 41
Ross, J., 206
Routh, Joyanto, 132
Saraswathy, Ambujom, 132
Saunders, James A., 191, 398
Scott, John S., 148
Serfes, M. E., 175

Shevade, Siddhesh, 306
Simpson, H. J., 206
Spayd, S. E., 175
Stute, M., 206
Su, Chunming, 25
Taillefert, Martial, 220
Talbott, Jonathan L., 148
Tossell, J. A., 118
Tournassat, C., 41
Tsang, M, 206
van Geen, Alexander, 361
Varma, S., 41
Villalobos, Mario, 235
Vlassopoulos, Dimitrios, 1, 344
Webster-Brown, Jenny G., 253
Wee, Hun-Young, 321
Westerhoff, Paul, 268
Whitworth, T. M., 294
Wilkin, Richard T., 25, 398
Wilson, Steven D., 148
Wolthers, M., 41, 60
Xu, Tielian, 333
Yang, Jae K., 91

Downloaded by 217.66.152.135 on September 11, 2012 | http://pubs.acs.org
Publication Date: October 3, 2005 | doi: 10.1021/bk-2005-0915.ix001

Subject Index

A

Ab initio hybrid MO/DFT calculations, arsenic complexation onto aluminum and iron hydroxides, 104–117
Acinetobacter johnsonii, 138, 141*f*
Activated carbon-based materials, arsenic removal, 284–293
Adsorption, arsenic, and desorption, by oxide minerals, modeling results, 403–404, 406–408*f*
Adsorption, arsenic, and heterogeneous reduction at phyllosilicate-water interface, 41–59
Adsorption, arsenic, and precipitation under reducing conditions, modeling results, 409–410, 411*f*
Adsorption, arsenic, and sorption
  aluminum and iron hydroxides, reaction free energies, 111–113
  aluminum oxyhydroxide, modeling, 16–19
  goethite-coated sand column, arsenic, pH variation experiments, 98–101, 102*f*
  iron and aluminum oxyhydroxides, 8–24
  iron oxides, sediment-water interface, model calculation, 230–231
  micas, 50–51
  suspended particulate material, modeling, 259–264
  time, pH, and arsenic concentration effects, carbonate green rust, 28–35
  See also Desorption, arsenic; Langmuir adsorption isotherm
Adsorption, bicarbonate ion interaction, aluminum hydroxide, Gibbs free energies, 126, 128*t*
Adsorption data modeling, constant capacitance model, 49–50
Adsorption edge modeling, arsenic, experimental, 260–262
Adsorption isotherms for As(III) and As(V) on ferrihydrite, 81*f*
Advanced Oxidation Technologies (AOTs), treatment arsenic-contaminated water, overview, 334
Aerobic respiration in sediment-water interface, 228–229
Agriculture, pilot water treatment system, design and operation, 393–395
Air-iron treatment, arsenic removal from tubewell water, 386–397
Air-iron water treatment systems, 382
Alabama (US)
  groundwater geochemistry and microbiology, 199–202
  Holocene floodplain deposits, physical description, 194–195*f*
Algae and bacteria growth removal from treatment tank, 392
Alum, arsenic removal from potable water, 9
Aluminum and iron hydroxides, arsenic complexation models, 104–117
Aluminum hydroxide, amorphous, As(III) and As(V) sorption, compared, 11
Aluminum hydroxide surface, bicarbonate ion interaction, Gibbs free energies, 126, 128*t*
Aluminum hydroxide surface site, model, 108*f*

Downloaded by 217.66.152.135 on September 11, 2012 | http://pubs.acs.org
Publication Date: October 3, 2005 | doi: 10.1021/bk-2005-0915.ix002

Downloaded by 217.66.152.135 on September 11, 2012 | http://pubs.acs.org
Publication Date: October 3, 2005 | doi: 10.1021/bk-2005-0915.ix002

Aluminum oxyhydroxide, As(III) and As(V), sorption behavior, surface complexation modeling, 15–21
Ambient Ground Water Quality Network, 176
Ambikanagar, West Bengal (India), arsenic reduction by indigeneous bacteria in shallow aquifers, 132–147
Anaerobic heterotrophic bacteria, reductive dissolution, iron and manganese minerals, 198*f*, 201
Anion exchanger for arsenic sequestration, zeolite, 306–320
AOTs. *See* Advanced Oxidation Technologies
Aqueous chemistry, arsenic, 177
Aqueous corrosion, elemental iron, reactions, 345
Aqueous species, bicarbonate ion interaction with arsenites, Gibbs free energies, calculations, 120–125, 127*t*
Aquifer, silty sand, field site in Chakdaha, West Bengal, India, 44–50
Aquifers, shallow, arsenic reduction by indigeneous bacteria in shallow aquifers, Ambikanagar, West Bengal, India, 132–147
Arizona (US), natural groundwater samples, 272–273
Arsenic(III) and As(V) transport in experimental subsurface systems 91–103
Arsenic(III) effect and fate modeling with LA-ICP-MS data, 72–73
Arsenic(III) interaction with bicarbonate ion in aqueous solution, calculations, 118–130
Arsenic(III) oxidation, 36–37*f*, 333–343
Arsenic(III) removal by water treatment system for tubewell water, based on 3-kalshi method, 390–393
Arsenic(III) sorption on aluminum oxyhydroxide, modeling, 16–19*f*
Arsenic(IV) production by ultrasound irradiation, 342
Arsenic(V) adsorption onto iron oxides, sediment-water interface, model calculation, 230–231
Arsenic(V) compound formation with mixed heavy metals, 247, 249*f*, 250
Arsenic(V) heterogeneous reduction, 51–56
Arsenic(V) reduction experiments, 46–47
Arsenic(V) reduction rate and microbial growth, 138, 140–143*t*
Arsenic(V) rejection with clay membranes, influences on, 299–304
Arsenic(V) removal in zeolite anion exchanger, influences on, 309–318
Arsenic adsorption. *See Adsorption, arsenic entries*
Arsenic adsorption edge modeling, experimental, 260–262
Arsenic and iron and sulfur, biogeochemical linkage, modeling results, 410–411
Arsenic and iron ratios in field groundwater data, 213–216
Arsenic and iron release with respiratory reduction of Fe(III) and As(V), 82–85*f*
Arsenic-bearing groundwaters, Holocene alluvial aquifers from U.S., 191–205
Arsenic complexation onto aluminum and iron hydroxides, models, 104–117
Arsenic concentration, geologic, hydrogeologic, and geochemical factors, 171–173
Arsenic diagenesis at sediment-water interface, 220–234

Arsenic mobilization and transport, 184–187, 213–214
Arsenic occurrence and transport in groundwater in Newark Basin, 175–190
Arsenic Remediation Technology (AsRT), deployment and results, 362–369
Arsenic removal with zero-valent iron, 361–371
Arsenic sequestration, zeolite as anion exchanger, 306–320
Arsenic speciation and mobilization, geochemical modeling for bioremediation, 398–413
Arsenic transformation and transport in ferric hydroxide coated sands, 77–90
Arsenic treatment systems, iron-based packed bed, rapid small scale column tests, 268–283
Arsenical pesticides, 177
Arsenopyrite, 192, 236
AsRT units. *See* Arsenic Remediation Technology
Asterionella formosa, diatom bloom, 259
Atomic fluorescence spectroscopy, hydride generation, in arsenic determination, 298–299

B

Bacteria
  activity in ferric hydroxide coated sands, 77–90
  arsenate reduction rates, 138, 140–143*t*, 144
  enzymes in dissimilatory arsenate reduction, 88
  iron reducing, 197–199
  mobilization processes, iron oxide-complexed arsenic, 79*f*
  reduction processes, 132–147, 399–400, 404–405, 409*f*
Baffles in precipitation tank, 393
Bangladesh
  arsenic limit in drinking water, 386
  arsenic-poisoning, human health hazard, 399
  Arsenic Remediation Technology performance at two wells, 364–369
  dugwell operation at Iruaien, Laksham, 377–379
  safe water options for villages, 372–385
Bangladesh-Australia Centre for Arsenic Mitigation, 377
Bangladesh groundwater
  arsenic removal with zero-valent iron, 361–371
  Kansas City area groundwaters, comparison, Eh-pH plot, 196–198*f*,
Bangladeshi tubewell water, simulated, air/iron treatment, 386–397
Basis sets, HF/3-21G(d,p) and B3LYP/6-31G(d), 107
Bayoxide Sorb33, 273–280
Bengal Delta Plain shallow aquifer, arsenic occurrence, 41–59
Beudantite, 236
Bicarbonate ion interaction with arsenites in aqueous solution, 118–130
Bidentate binuclear configuration, As(V) onto aluminum and iron hydroxides, 105–106*f*
Binuclear and mononuclear complex formation, As(III) on aluminum oxyhydroxide, 18–19*f*
Binuclear bidentate configuration, As(V) onto aluminum and iron hydroxides, 105–106*f*
Binuclear complexes, surface species, 12

Downloaded by 217.66.152.135 on September 11, 2012 | http://pubs.acs.org
Publication Date: October 3, 2005 | doi: 10.1021/bk-2005-0915.ix002

Biochemical pathway, bacterial reduction, As(V), 143–144
Biogeochemical cycles, iron and arsenic, 399
Biogeochemical linkage, arsenic, iron and sulfur, modeling results, 410–411
Biological effects, dependence on arsenic speciation, 42
Bioremediation, geochemical modeling, arsenic speciation and mobilization, 398–413
Black shale, arsenic concentration and mobilization, 183–187
Blue River (US), bulk stream sediments, 201
Blue River floodplain, physical description 194–195*f*
Breakthrough curves, CD-RSSCTs vs PD-RSSCTs, 274–276
British Geological Survey "Special Study", 196–198

C

^{13}C NMR shifts for carbonates and As(III) oxide-carbonate complexes, 124*t*
Calcium arsenates, solubility, metal concentrations, Monterey, Mexico, 242–246
Calcium effects on arsenic desorption, 328–329
Cambrian-Ordovician sandstone aquifers, Lake Geneva, Wisconsin (US), 162, 163*f*
Carbon-based materials in arsenic removal, 284–293
Carbonate green rust
  arsenic sorption, affected by time, pH, and arsenic concentration, 30–35
  arsenite oxidation, 36–37*f*
  synthesis and characterization, 27–30, 31*f*, 32*f*
Carbonate interaction with arsenic(III) hydroxide species, calculated energetics, 121*t*
CD. *See Constant diffusivity entries*
Chakdaha, West Bengal (India), silty sand aquifer, field site, 44–50
Champaign County, Illinois (US), well sampling results, 150–157
Chattahoochee River mainstream impoundment, Georgia (US), physical description, 222, 223*f*
Chemical oxidation in sediment-water interface, 228–229
Chloride, 214–215, 226, 227*f*
Citrobacter freundii, 138
City of Socorro, New Mexico (US), water supplies, 286
Clay membrane preparation, 297–298
Clay membranes in arsenic removal from drinking water, 294–305
Clay reverse osmosis membrane in arsenate rejection, 303–304
Clay suspensions, heterogeneous reduction of As(V), 51–54
Column comparisons, quantitative techniques, 95, 96*t*
Column outlet concentration, schematic diagram, 93–94*f*
Column test with iron-impregnated granular activated carbon, arsenic removal, 291
Comamonas testosteroni, 138
Competing anions, effect on arsenate removal, 314, 316*f*
Complex inlet solution, effect on arsenate removal, 314, 317, 318*f*
Conductor-like Screening MO method (COSMO), 119–127
Constant capacitance model, adsorption data modeling, 49–51
Constant diffusivity (CD)-based RSSCT, 271–272

Downloaded by 217.66.152.135 on September 11, 2012 | http://pubs.acs.org
Publication Date: October 3, 2005 | doi: 10.1021/bk-2005-0915.ix002

Downloaded by 217.66.152.135 on September 11, 2012 | http://pubs.acs.org
Publication Date: October 3, 2005 | doi: 10.1021/bk-2005-0915.ix002

Constant diffusivity (CD)-RSSCTs versus PD-RSSCTs, comparison, 274–277*t*

Continuous flow reaction method, description, 62*f*, 63–65

Continuous flow reaction system, arsenic uptake by pyrite, 60–76

Continuous flow reactions, zeolite, anion exchangers for arsenic sequestration, 306–320

Corrosion, iron filing materials, 364

Corrosion products, iron, arsenate and arsenite interactions, 25–40

COSMO. *See* Conductor-like Screening MO method

Coupled cluster theory, 119

Crook County, Wyoming (US), sodium montmorillonite, 296

D

Deep tubewells, 380–381

Denitrification in sediment-water interface, 228–229

Department of Energy (US) Kansas City plant, 194

Deprotonation reactions, calculated energetics, 126*t*

Desorption, arsenic
  remobilization from sediments, influences, 221
  sorption-desorption hysteresis, ferrihydrite-coated sands, 81, 82*f*
  studies, 323–331
  See also Adsorption, arsenic; Langmuir adsorption isotherm

Desulfovibrio sp. 197

Detection limits, arsenic, 150

Determination of Trace Elements by Inductively Coupled Plasma – Mass Spectrometry, EPA Method 200.8, 180

Diatom blooms, effect on total organic carbon, 259

Dispersive flow pore surface diffusion model, 270–271

Dissimilatory arsenate reduction, bacterial, 88

Dissolved organic carbon and arsenic, relationship, 166–167, 169*f*

Dissolved oxygen, 180–181*f*, 225–226, 227*f*–228*f*

Drinking water, arsenic removal
  activated carbon-based materials, 284–293
  clay membranes, 294–305

Drinking water standards
  Bangladesh government, arsenic limit, 386
  State of New Jersey, arsenic, 176
  U.S. arsenic, 1, 176, 269, 285, 295, 322
  U.S. iron, secondary, 200
  WHO guideline for arsenic, 361
  WHO secondary criterion for iron, 364

Dugwells, applications, 375–379, 383–384

Dynamic column experiments, arsenic transport, 91–103

E

EDX analysis, pyrite formation on pyrite blocks, 67–68*f*

Empty bed contact time, 287–288, 309, 310*f*

End-member mixing model in arsenic/iron ratio, 214, 215–216

Enrichment bacterial cultures, 135, 137–138, 139*t*

Enterobacter cloacae, 138

"Environment Waikato," 256

Environmental impact, carbonate green rust stability, 38

Environmental implications, arsenic(V) reduction by microbial processes, 144

Environmental Protection Agency (US EPA)
  arsenic standard, 161, 176, 322
  iron secondary drinking water standard, 200
  Method 200.8, 180
Equilibrium constants, extraction for surface complexation modeling, 15–16
EPA. *See* Environmental Protection Agency
EXAFS spectroscopy
  adsorbed As(V) and As(III), 14
  results compared to calculated interatomic distances, 109–111
  solid phase characterization, iron K-edge spectra, 347, 352–354*t*
Extended X-ray Absorption spectroscopy. *See* EXAFS spectroscopy

F

Faujasite Y, synthetic zeolite, 307
Ferric hydroxide coated sands with reducing bacterial activity, arsenic transformation and transport, 77–90
Ferrihydrite, adsorption isotherms for As(III) and As(V), 81*f*
Ferrihydrite-coated sands, sorption-desorption hysteresis, As(III) and As(V), 81, 82*f*
Fick's Law in diffusive flux calculations, 231
Field column tests, arsenic removal by zerovalent iron, 346, 349
Flow rate, effect on arsenate rejection, 300–302

G

Gamma radiolysis, 336
Ganga-Brahmaputra delta, West Bengal, India, field site, 44–45
GAUSSIAN98, 119–120
Geobacter sulfurreducens, 197
Geochemical modeling, arsenic speciation and mobilization, bioremediation, 398–413
Geochemist's Workbench, Kansas City study area compared to Bangladesh, 196–198
Georgia, (US), West Point Lake, Chattahoochee River mainstream impoundment, 222, 223*f*
Geothermal fluid inputs, silicon-rich, 262
Gibbs free energies
  arsenic absorption onto aluminum and iron hydroxide surfaces, 108–113
  bicarbonate ion interaction with arsenites in aqueous solution, 120–125, 127*t*
GIXAFS. *See* Grazing Incidence X-ray Absorption Fine Structure
Glasford and Mahomet Aquifers, arsenic distribution, 148–160
Glasford Aquifer, physical description, 149
Goethite-coated sand, adsorbent, 92
Granular ferric hydroxide, 273–280
Graphite furnace atomic absorption spectrophotometry in arsenic determination, 287
Grazing Incidence X-ray Absorption Fine Structure (GIXAFS), 105
Green rusts, description, 26
Groundwater
  arsenic and iron, oxidation, 206–219
  arsenic mobilization and transport, 184–187
  Bangladesh, zero valent iron in arsenic removal, 344–360
  Lake Geneva, Wisconsin (US), arsenic concentration controls, 161–174
  Moundville (US), predicted mineralogic reactions, 409*f*

Downloaded by 217.66.152.135 on September 11, 2012 | http://pubs.acs.org
Publication Date: October 3, 2005 | doi: 10.1021/bk-2005-0915.ix002

natural arsenic contamination, overview, 399
Newark Basin, New Jersey (US), arsenic occurrences, 175–190

Groundwater chemistry, core samples, Lake Geneva, Wisconsin (US), 166–169

Groundwater flow from landfill, 208*f*, 213–214

Groundwater geochemistry and microbiology, 196–202

Groundwater monitoring and sediment leaching data, 213–216

Groundwater titration experiment, Maine landfill site, 209–213

Groundwaters, arsenic-bearing in Holocene alluvial aquifers from U.S., 191–205

H

Hartree-Fock method calculations, 119, 124*t*, 125*t*

Heavy metal arsenates, mixed, formation, 247, 249*f*, 250

Hematite. *See* Iron(III) oxides, bacterial reduction

Heterogeneous oxidation, arsenic by manganese oxide minerals, 37

Heterogeneous reduction, arsenic with and without iron(II), 51–56

Heterotrophic plate counts and identification, 136

HFO. *See* Hydrous ferric oxide

Holocene alluvial aquifers from U.S., arsenic-bearing groundwaters, 191–205

Hoogly River, (India), 44, 133

Household filtration systems, description, 285–286*t*

Household-level arsenic removal units, 368, 369

Household water filters, assessment and breakthrough curves, 288, 289*f*–290*f*

Human health effects, arsenic, 221, 236, 269, 295, 307, 334, 399

Hydride generation atomic fluorescence spectroscopy in arsenic determination, 298–299

Hydrogen peroxide, 209–213, 339–340

Hydrogen sulfide, effects of activities on arsenic speciation, modeling results, 401–402

Hydrous ferric oxide (HFO), pH effects, sorption As(III) and As(V), 10*f*

Hydroxide minerals, arsenic mobilization via reduction dissolution, 170–171

Hydroxyl radicals, role in ultrasonic treatment, As(III), 337–339, 342–343

Hygiene issues in safe water systems, 376–377, 382–383, 384

Hysteresis, sorption-desorption As(III) and As(V) on ferrihydrite-coated sands, 81, 82*f*

I

ICP-AES (Inductively Coupled Plasma-Atomic Emission Spectrometry), total arsenic determination, 47

ICP-MS (Inductively Coupled Plasma-Mass Spectrometry), metals and other elements detection, 151

Illinois (US), Mahomet and Glasford aquifers, arsenic distribution, 148–160

Illinois State Water Survey, 150

Illite clay type, arsenate rejection, 303–303*f*

Downloaded by 217.66.152.135 on September 11, 2012 | http://pubs.acs.org
Publication Date: October 3, 2005 | doi: 10.1021/bk-2005-0915.ix002

Illite sample from Silver Hill, Montana (US), membrane preparation, 296
In-ground reactor, full-scale prototype, arsenic removal by zerovalent iron, 347–348, 355–357
In-river arsenic behavior modeling, 262–264
India. *See* West Bengal
Indian Creek (US), bulk stream sediments, 201
Inductively Coupled Plasma-Atomic Emission Spectrometry. *See* ICP-AES
Inductively Coupled Plasma-Mass Spectrometry. *See* ICP-MS
Initial arsenic concentration effect on arsenate rejection, 302
Integrated Equation Formalism Polarized Continuum Model, 108
Interatomic distances, calculated, compared to EXAFS for inner-sphere arsenic complexation, 109–111
Ion chromatography, anion determination, 151
Ionic strength, effect on arsenate rejection, 301–302
Iron(0). *See* Zero valent iron
Iron(II) and arsenic correlation, 166, 168*f*
Iron(II) containing suspensions, heterogeneous arsenic reduction, 51–54
Iron(II) depth profile, 226, 227*f*, 228*f*
Iron(II)-free suspensions, heterogeneous arsenic reduction, 54–56
Iron(II) ions, addition effect on arsenic removal, 390–391*f*
Iron(II,III) hydroxycarbonate green rust, arsenate and arsenite sorption, 25–40
Iron(III) oxides, bacterial reduction, modeling results, 404–405, 409*f*
Iron and aluminum hydroxides, arsenic complexation models, 104–117
Iron and dissolved arsenic correlation, 152, 154*f*
Iron-arsenic-sulfur system
  biogeochemical linkage, modeling results, 410–411
  stability fields, iron sulfide phases, modeling results, 402–403*f*
Iron-carbonate precipitation, 201–202
Iron-coated sand, experimental subsurface systems, As(III) and As(V) transport, 91–103
Iron fillings mixed with sand in AsRT units for arsenic removal, 362–369
Iron-hydroxides
  reduction, anaerobic heterotrophic bacteria mediation, 198*f*, 201
  reductive dissolution, in arsenic mobilization, 170–171
Iron-impregnated granular activated carbon, 287–291
Iron in drinking water, secondary standards, 200, 364
Iron oxidation/reduction at sediment-water interface, 229
Iron oxides, As(III) and As(V) sorption onto Fe oxides, 10–11
Iron reducing bacteria, 197–199
Iron removal in hydrogen peroxide titration with landfill site groundwater, 211–213
Iron role in arsenic cycle in sediments, 230, 232*f*
Iron suspended particulate, relation to dissolved arsenic, 259–260
Iruaien, Laksham (Bangladesh), dugwell operation, 377–379

K

3-Kalshi method-based tubewell water treatment system, construction and operation, 388–390

Downloaded by 217.66.152.135 on September 11, 2012 | http://pubs.acs.org
Publication Date: October 3, 2005 | doi: 10.1021/bk-2005-0915.ix002

Downloaded by 217.66.152.135 on September 11, 2012 | http://pubs.acs.org
Publication Date: October 3, 2005 | doi: 10.1021/bk-2005-0915.ix002

3-Kalshi water treatment system, 382, 387
Kansas City, Missouri (US)
  floodplain deposits of Blue River, physical description, 194–195*f*
  shallow Holocene alluvial floodplain, arsenic elevation, 192–193
  USDOE plant, groundwater geochemistry and microbiology, 196–198
Kaolinite clay type, arsenate rejection, 303–303*f*
Kaolinite sample for membrane preparation, 296

L

LA-ICP-MS. *See Laser-ablation entries*
Lactate to acetate conversion in bacterial respiration, ferrihydrite-coated sand column, 83*f*, 84–85*f*
Lagrange, Georgia (US), West Point Lake, physical description, 222, 223*f*
Lake Geneva, Wisconsin (US)
  arsenic groundwater controls, 161–174
  arsenic sources in groundwater, 170–171
  physical description, 162, 163*f*
Laksham, Iruaien (Bangladesh), dugwell operation, 377–379
Landfill in Maine (US)
  closed, groundwater flow from, 208*f*, 213–214
  field tests for AsRT technology, 368
  groundwater arsenic and iron, oxidation in unconsolidated aquifer, 206–219
  physical description, unconsolidated aquifer, 208–209
Landfill leachate tracer, chloride, 214–215
Langmuir sorption isotherm, arsenic sorption on carbonate green rust and arsenic equilibrium relationship, 30–31, 33–34*t*
  See also Adsorption, arsenic; Desorption, arsenic
Laser-ablation craters on surface, reacted pyrite block, 67–69*f*
Laser-ablation ICP-MS depth analysis, 67–68, 70*f*
Leaching. *See* Desorption, arsenic
Lockatong formation, 179

M

Mackinawite, nanoparticulate, 61
Macroscopic sorption experiments, surface species in modeling, 11–14
Mahomet and Glasford Aquifers, arsenic distribution, 148–160
Mahomet Aquifer, 148–149
Maine (US) landfill
  closed, groundwater flow from, 208*f*, 213–214
  field tests for AsRT technology, 368
  groundwater arsenic and iron, oxidation in unconsolidated aquifer, 206–219
  physical description, unconsolidated aquifer, 208–209
Major ion chemistry and arsenic concentrations, Lake Geneva, Wisconsin (US), 167*f*
Manganese(II), depth profile, 226, 227*f*, 228*f*
Manganese(IV) minerals, reduction, anaerobic heterotropic bateria, 198*f*, 201
Manganese(IV) oxides, bacterial reduction, modeling results, 404–405, 409*f*

Downloaded by 217.66.152.135 on September 11, 2012 | http://pubs.acs.org
Publication Date: October 3, 2005 | doi: 10.1021/bk-2005-0915.ix002

Manganese
  arsenic and non-purgeable organic carbon, relationship, 153–155*f*
  reduction at sediment-water interface, 229
  role in arsenic cycle in sediments, 230–231
Manganese-carbonate precipitation, 201–202
Manganese oxide minerals in heterogeneous oxidation, As(III), 37
Maximum contaminant level, arsenic. *See* Drinking water standard
Melosira granulata, diatom bloom, 259
Membrane filtration processes, capabilities, 295
Membrane filtration system, experimental setup, 296–297
Metal oxyhydroxides, As(III) andAs(V) surface species, sets, 13*t*
Metal release, respiratory reduction, Fe(III) and As(V), *Sulfurosprillum barnesii*, 82–89
Metals in water treatment residuals, concentrations, 323*t*
Mexico, arsenic in semi-arid soils near Monterey and San Luis Potosi, physical description, 237–239
Micas, arsenic adsorption on, 50–51, 54
Microbial growth and reduction processes. *See Bacterial entries*
MINEQL+ calculations, FeS_{am} solubility product, 229–230
MINTEQA2 geochemical speciation model, 262
Missouri (US)
  Kansas City, floodplain deposits of Blue River, physical description, 194–195*f*
  shallow Holocene alluvial floodplain, arsenic elevation, 192–193
  USDOE plant, groundwater geochemistry and microbiology, 196–198
MO/DFT. See Molecular orbital/density field theory
Mobilization and transport, arsenic in Newark Basin, 184–187
Mobilization capability for arsenic, bacterial, 136–137
Modeling adsorption data, constant capacitance model, 49–50
Modeling arsenic adsorption, 16–19, 260–264
Modeling arsenic speciation and mobilization, 401–412
Modeling geochemical methods, 400
Modeling pH effects, difficulty, 115
Modeling seasonal arsenic behavior, 253–266
Molecular orbital/density field theory (MO/DFT) calculations, arsenic complexation onto aluminum and iron hydroxides, 104–117
Molecular quantum mechanics methods, 119–120
MØller-Plessett many body perturbation theory method to 2nd order, 119, 120–127
Molybdenum in leachate from black shale, Newark Basin, 185
Mononuclear complexes, surface species, 12
Montana (US), Silver Hill, illite sample for membrane preparation, 296
Monterey (Mexico)
  calcium arsenates, solubility, metal concentrations, 242–246
  semi-arid soils contaminated with arsenic, physical description, 237–239
Montmorillonite
  As(V) reduction experiments in suspension, 51–54

clay type, arsenate rejection, 303–303*f*
reverse osmosis membrane in layer, 296
Moundville (US) groundwater, predicted mineralogic reactions, 409*f*
Muscovites, 50*f*, 54, 55

N

Naturally occurring arsenic mineral environments, 236
New Jersey (US)
  arsenic occurrences in Newark Basin groundwater, 175–190
  former pesticide manufacturing site, 346
  proposed arsenic drinking water standard, 176
  See also Newark Basin, New Jersey (US)
New Mexico (US), City of Socorro, water supplies, 286
New Zealand, Waikato River, modeling seasonal arsenic behavior, 253–266
Newark Basin, New Jersey (US)
  arsenic occurrences in groundwater, 175–190
  hydrogeology, 177–179
  sources, arsenic, 177, 182–184, 185*f*
  spatial analysis, arsenic occurrence, 179–180
  See also New Jersey (US)
Nitrate, depth profile, 226, 227*f*
Non-purgeable organic carbon, relationship to dissolved arsenic, 151–155

O

Oak Ridge National Laboratory (US), hydrogeologic investigations, 179
Optical density for As(V) spiked medium inoculated with bacteria, 140*f*
Outer sphere complexes in As(III) modeling, 12
"Oxidation hypothesis" arsenic, 56
Oxidized arsenic waste contaminants, natural attenuation in semi-arid soils, 235–252
Oxyacid condensation with As(III) hydroxide, calculated energetics, 122*t*
Oxygen, role in ultrasonic treatment, As(III), 337–339
Oxygen-sediment-water interface, dissolved, 225–226, 227*f*–228*f*

P

Particle Induced X-ray Emission. *See* PIXE
Passaic Formation, 178–179
Patent, US 6,387,276 B1, Arsenic Remediation Technology, 362
PD-RSSCTs. *See* RSSCTs
Permeability calculation, clay membrane, 298
Permeable reactive barrier applications, 26
pH-arsenic comparisons
  groundwater in western Newark Basin, 180–181*f*
  superficial soils near Monterrey, Mexico, 239–242
pH effects
  As(III) and As(V) adsorption onto muscovite, 50–51
  As(III) and As(V) sorption onto hydrous ferric oxide, 10
  arsenate removal by zeolite, 309, 311–312*f*, 313*f*
  arsenic desorption, 323–326*f*
pH-redox potential

Downloaded by 217.66.152.135 on September 11, 2012 | http://pubs.acs.org
Publication Date: October 3, 2005 | doi: 10.1021/bk-2005-0915.ix002

  geochemical data from Kansas City Field Area, 196
  relationship to arsenic speciation, 155–157*f*
pH values, soil, San Luis Potosi (Mexico), 246, 248*f*
pH variation, arsenic absorption in goethite-coated sand column, 98–101, 102*f*
Phase diagrams for arsenic speciation, 401
Phosphate effects on arsenic desorption and precipitation, 327, 392
Phyllosilicate-water interface, arsenic adsorption and heterogeneous reduction, 41–59
Piedmont Physiographic Province, 177
Pilot columns and RSSCTs, comparison, 278–279
Pilot water treatment system for agriculture, design and treatment, 393–395
PIXE (Particle Induced X-ray Emission) spectroscopy, arsenic determination, 49
Pore water extraction and sediment core collection, 222–223
Pore water velocity effects in goethite-coated sand column, arsenic adsorption, 95–98
Precipitation and sorption under reducing conditions, arsenic, modeling, 409–410, 411*f*
Proportional diffusivity-RSSCTs. *See* RSSCTs
Protonation, surface complexes, As(III) on aluminum oxyhydroxide, 16–18*f*
Pumping rates, dugwell at Iruaien, Laksham, Bangladesh, 379
Pyrite, 60–76, 200
Pyrite formation on pyrite blocks, 67–72

Q

Quaternary glacial aquifier, Lake Geneva, Wisconsin (US), 162, 163*f*

R

Rainwater harvesting, 382–383, 384
Rapid small scale column tests. *See* RSSCTs
Reaction free energies, arsenic adsorption onto aluminum and iron hydroxides, 111–113
Redox potential
  iron(II) containing suspensions, 52–54
  pH relationship, geochemical data from Kansas City Field Area, 196
  pH relationship to arsenic speciation, 155–157*f*
Reducing conditions
  deep Quaternary/shallow Silurian wells, arsenic mobility, 172
  predicted arsenic precipitation and sorption, 409–410*f*, 411*f*
"Reduction hypothesis" arsenic, 56
Reduction rates, bacterial reduction, As(V), 142–143*t*
Reductive dissolution
  iron and manganese minerals, anaerobic heterotrophic bacteria, 198*f*, 201
  iron-(hydr)oxides in arsenic mobilization, 170–171
Respiratory reduction of Fe(III) and As(V) by *Sulfurosprillum barnessi*, 82–89
Retention time, steady-state column effluent arsenic concentration dependence, 349*f*
Rhodochrosite phase in iron and managanese solubility, 202
RSSCTs (Rapid small scale column tests)

Downloaded by 217.66.152.135 on September 11, 2012 | http://pubs.acs.org
Publication Date: October 3, 2005 | doi: 10.1021/bk-2005-0915.ix002

  constant diffusivity and proportional diffusivity based, comparison, 274–277*t*
  iron-based packed bed arsenic treatment systems, 268–283
  pilot columns, comparison, 278–279
  scaling procedure, 270–272

S

Safe water systems, requirements in Bangladesh, 373–374
San Luis Potosi (Mexico)
  semi-arid soils contaminated with arsenic, physical description, 237–239
  soil pH values, 246, 248*f*
Sand filters, microbial contamination, 380, 384
Saturation indices, primary minerals in groundwater samples, 169*f*
Scaling procedure (RSSCTs), 270–272
Scanning electron microscopy (SEM)
  carbonate green rust, 27, 29, 31*f*
  pyrite formation on pyrite blocks, 67–68*f*
  zerovalent iron/quartz media, 353
Seasonal arsenic behavior in Waikato River (New Zealand), 253–266
Sediment core collection and porewater extraction, 222–223
Sediment leaching data and groundwater monitoring, 213–216
Sediment-water interface, arsenic diagenesis, 220–234
SEM. *See* Scanning electron microscopy
Semi-arid soils, attenuation of oxidized arsenic wastes, 235–252
Shallow tubewells, 381
Siderite phase in iron and manganese solubility, 202
Silicon-rich considerations in adsorption modeling, 262
Silty sand aquifer in Chakdaha, West Bengal (India), field site, 44–50
Silurian dolomite aquifer, Lake Geneva, Wisconsin (US), 162, 163*f*
Silver diethyldithiocarbamate modifiled method, 392
Silver Hill, Montana (US), illite sample for membrane preparation, 296
Smelting complexes in Mexico, semi-arid soils, physical description, 237–239
Socorro, New Mexico. *See* City of Socorro
Sodium montmorillonite from Crook County, Wyoming (US), 296
Soil samples, aqueous arsenic, theoretical solubilities, heavy metal arsenates, 246–247, 249*f*, 250
Solid phase and spectroscopic studies, field column test samples, zerovalent iron in arsenic removal, 350–354
Solid phase geochemistry, core samples, Lake Geneva, Wisconsin (US), 164–166
Solubility and speciation, arsenic, modeling results, 401–403*f*
Solvated H_3AsO_3 species, model, 107*f*
Sonolysis equipment, 335
Sorption. *See* Adsorption, arsenic, and sorption; Desorption, arsenic; Langmuir sorption isotherm
Spatial analysis, arsenic occurrence in Newark Basin, 179–180
Sphingobium yanoikuyae, 138
Stretch vibrational frequencies, As–0 and C–O, calculated, 125*t*
Subsurface systems, experimental, As(III) and As(V) transport, 91–103
Sulfate, depth profile, 226, 227*f*

Downloaded by 217.66.152.135 on September 11, 2012 | http://pubs.acs.org
Publication Date: October 3, 2005 | doi: 10.1021/bk-2005-0915.ix002

Sulfate reduction
  biogenic, in carbonate precipitation, 202
  sediment-water interface, 229
Sulfate with arsenic occurrence, relationship, 152–153, 155*f*, 166, 168*f*
Sulfides, arsenic and iron, equilibrium constants, 400*t*
Sulfur, iron, and arsenic, biogeochemical linkage, modeling results, 410–411
Sulfur reducing bacteria, frequency, 197–200, 399–400
Sulfurosprillum barnessi
  arsenic and iron release with respiratory reduction of Fe(III) and As(V), 82–89
  dissimilatory Fe(III) and AS(V) reduction, effect on arsenic transport, 77–90
Superoxide anion radical, role in oxidation, As(III), 340–342
Surface complexation models, 11–21
Suspended particulate material composition, seasonal changes, 258–260
Synthetic zeolites, preparation for arsenic ion exchange, 307–308

T

"Tailing" in arsenic elution, 86–87*t*
Tazewell County, Illinois (US), well sampling results, 150–157
TCLP. *See* Toxicity characteristic leaching procedure
Thioarsenite species, equilibrium constants, 400*t*
Three-kalshi. *See 3-Kalshi entries*
Total dissolved solids and arsenic concentration, relationship, 168*f*, 172
Toxicity, arsenic. *See* Human health effects, arsenic
Toxicity characteristic leaching procedure (TCLP), 329–330
Treatment methodologies for arsenic, overview, 269–270
Tropical Storm Bill, 222, 231
Tuakau (New Zealand), lower Waikato River, 256, 258–259, 262–264
Tubewell water, simulated Bangladesi, air-iron treatment, 386–397
Tubewells in Bangladesh, 373, 375, 380–381, 384

U

U.S. Department of Energy. *See* Department of Energy (US)
U.S. Environmental Protection Agency. *See* Environmental Protection Agency (US EPA)
U.S. Geological Survey, measurement of arsenic speciation, 182
United States sites. *See specific states*
Unresolved issues, arsenic-related investigations, 2–4
Ultrasonic cavitation, overview, 336–337
Ultrasonic irradiation in arsenite oxidation, 333–343
UV absorption energies, As(III) hydroxide and As(III) carbonate complexes, 125*t*
UV light, effect on arsenic removal and concentration, 293

V

Villages in Bangladesh, safe water options, 372–385
Voltammetric measurements for As(III), analytical method, 224–225

Downloaded by 217.66.152.135 on September 11, 2012 | http://pubs.acs.org
Publication Date: October 3, 2005 | doi: 10.1021/bk-2005-0915.ix002

Downloaded by 217.66.152.135 on September 11, 2012 | http://pubs.acs.org
Publication Date: October 3, 2005 | doi: 10.1021/bk-2005-0915.ix002

W

Waikato River (New Zealand)
  modeling seasonal arsenic behavior, 253–266
  physical description, catchment, 254–255*f*
Water chemistry, in-ground reactor during zerovalent iron arsenic removal, 355–357
Water permeability coefficients, 299
Water safety options for Bangladesh villages, 372–385
Water systems in Bangladesh, acceptability, 373–374
Water treatment, extrapolation to relevant conditions, 19–21*f*
Water treatment residuals, arsenic-containing, characterization, 321–332
Water treatment system for tubewell water, based on 3-kalshi method, construction and operation, 388–390
Well classification by water volume, 374–375
Well completion depth and groundwater arsenic, relationship, 168*f*, 169
Well construction, Lake Geneva, Wisconsin (US), 162–164
Well drilling for sediment sample collection, 135
Well treatment, deployment of AsRT units, 364–369
West Bengal (India)
  Ambikanagar, arsenic reduction by indigeneous bacteria in shallow aquifers, 132–147
  arsenic-poisoning, human health hazard, 399
  Chakdaha, aquifer, silty sand, field site, 44–50
West Point Lake, mainstream Chattahoochee River impoundment, Georgia (US), physical description, 222, 223*f*
WHO guideline for drinking water, arsenic, 361, 386
WHO secondary criterion for drinking water, iron, 364
Wisconsin (US), arsenic groundwater concentration controls near Lake Geneva, 161–174
World Health Organization. *See WHO entries*
Wyoming (US), Crook County, sodium montmorillonite, 296

X

X-ray Absorption Near Edge spectroscopy. *See* XANES spectroscopy
X-ray diffraction, carbonate green rust, 28, 29–30, 32*f*
X-Ray Photoelectron Spectroscopy. *See* XPS spectroscopy
XANES spectroscopy
  adsorbed As(III), 14
  solid phase characterization, iron K-edge spectra, 347, 350–351*f*
XPS spectroscopy
  arsenic determination, 47–49
  muscovites, 54, 55

Z

Zeolite, anion exchanger for arsenic sequestration, 306–320
Zeolite particle size, effect on arsenate removal, 311, 314*f*
Zero valent iron in arsenic removal, 344–360
Zero valent iron in arsenic removal from Bangladesh groundwater, 361–371
ZSM-5, synthetic zeolite, 307